

City Research Online

City St George's, University of London

Citation: Westaby, J. (2021). Structure and ventricular composition including innervation of the normal heart and changes in cardiomyopathy: A morphological, histochemical and immunohistochemical study. (Unpublished Doctoral thesis, St. Georges, University of London)

This is the accepted version of the paper.

This version of the publication may differ from the final published version. To cite this item please consult the publisher's version.

Permanent repository link: https://openaccess.city.ac.uk/id/eprint/37151/

Copyright and Reuse: Copyright and Moral Rights remain with the author(s) and/or copyright holders. Copies of full items can be used for personal research or study, educational, or not-for-profit purposes without prior permission or charge, unless otherwise indicated, provided that the authors, title and full bibliographic details are credited, a hyperlink and/or URL is given for the original metadata page and the content is not changed in any way. For full details of reuse please refer to City Research Online policy.

City Research Online: http://openaccess.city.ac.uk/ publications@citystgeorges.ac.uk

Structure and ventricular composition including innervation of the normal heart and changes in cardiomyopathy: A morphological, histochemical and immunohistochemical study.

Student: Dr Joseph Westaby, CRY Cardiac Pathology Clinical Fellow

Department of Cardiovascular Pathology, Cardiology Clinical Academic Group, Molecular and Clinical Sciences Research Institute, St George's University of London, London, SW17 0RE. Tel: 0208725 5112; Email: [redacted]@sgul.ac.uk

Primary Supervisor: Professor Mary N Sheppard

Secondary Supervisor: Professor Elijah Behr

This thesis is submitted in partial fulfilment of the requirements for the degree of Doctor of Philosophy.

Declaration

The work presented within this thesis has been undertaken by Dr Joseph Westaby under the supervision of Professor Mary N Sheppard and Professor Elijah Behr.

Joseph Westaby

10/12/2021

Acknowledgements

I thank my primary supervisor, Professor Sheppard, for the opportunity to undertake this study, your expertise and skill have guided me through this PhD. It has been an absolute privilege to work with you closely on both this project and the analysis of cardiac specimens. I thank my secondary supervisor, Professor Elijah Behr, for his guidance, particularly on the clinical aspects and research methodology. I thank Dr Daniel Meijles for all his aid and advice.

I am immensely grateful to Cardiac Risk in the Young for supporting both myself and the CRY cardiovascular pathology laboratories. Thank you to Pathological Society and British Division of the International Academy of Pathology who have supported the project with grants. Thanks to National Institute of Health Research who previously supported me with the award of an academic clinical fellowship.

I would like to thank Dr Irina Chis Ster for all her statistical guidance on the multilevel modelling. I thank all our laboratory technicians including Emelia Zullo, Susanna Cooper, Luciana Bicalho, and Khari Edwards and our PA Belmira Fernandez for their assistance. I thank the IRF for their help with the slide scanning, particularly Greg Perry. Thank you to Dr Chris Miles for his aid, advice and humour.

A special thanks to both my parents who have supported me unconditionally throughout the process along with my wonderful fiancée.

CONTENTS

List of figures……...…10

List of tables……..…...17

Publications……19

Grants……20

Awards……21

Abbreviations……22

ABSTRACT 23

CHAPTER 1 INTRODUCTION 25

Sudden Cardiac Death..... 25

Autopsy and Specialist Cardiac Examination..... 25

Sudden Cardiac Death is caused by Ventricular Arrhythmia..... 26

Mechanism of Cardiac Contraction 26

Mechanism of heart rate control..... 29

Mechanisms of arrhythmia 33

The cardiac autonomic nervous system..... 37

Cardiac Autonomic Nervous Function and Assessment 48

Myocardial innervation in disease 50

Neuromodulation..... 52

The structurally normal heart 54

The Cardiomyopathies 54

Innervation in Cardiomyopathy..... 58

Conclusion 59

Aims 60

CHAPTER 2 METHODS 62

The Cardiac Risk in the Young Cardiovascular Pathology Laboratories 62

Clinical data collection 64

The CRY national cardiovascular database 64

Data entry 64

Data extraction 67

Gross anatomical methods 69

Macroscopic pathological examination 69

Methods for preparation of microscopic slides 73

Tissue Processing 73

Embedding 73

Sectioning 74

Haematoxylin and Eosin Staining 74

Picrosirius red stain 75

Immunohistochemistry 75

Antibodies 78

Mounting 78

Quality check 79

Staining optimisation 79

Microscopic examination 80

Microscopic analysis and diagnostic categorisation 80

Terminology used to describe the layers of the heart on histology 81

Slide Scanning 83

Morphometric quantification 83

Statistical analysis 87

Bias 88

CHAPTER 3 OVERALL DATABASE 90

Introduction 90

The Cardiac Risk in the Young Cardiovascular Pathology Laboratories 91

Aim 92

Methods 92

Cardiac dissection and examination 92

Cardiac sections 93

Diagnostic criteria 93

Causes of Sudden Cardiac Death from the CRY-CPL National Database 95

Discussion 104

Comparison to worldwide studies 104

Cardiomyopathies 107

Ischaemic heart disease 113

Valve disease 113

Myocarditis and sarcoidosis 114

Aorta 115

Conduction disease 116

Reasons for differences 116

Limitations 117

Concluding remarks 117

CHAPTER 4 THE NORMAL HEART 118

Introduction 118

Methods 119

Statistics 122

Results 123

Cardiac examination 127

Discussion 143

Ventricular wall measurements 145

Cavity size 146

Oval fossa 146

Coronary arterial dominance 147

Valve circumference 148

Subepicardial fat thickness 148

Epicardial adipose tissue associations and role in disease 149

Limitations 151

Concluding remarks 151

CHAPTER 5 COMPOSITION OF THE NORMAL HEART: FAT, COLLAGEN, MUSCLE AND INNERVATION 153

Introduction 153

Methods 153

Statistics 154

Results 154

Compositional analysis 155

Innervation of the normal ventricular myocardium and overlying subepicardial fat 186

Discussion 202

Composition of the ventricular myocardium 202

Innervation of the ventricular myocardium 205

Innervation and functional consequences 207

Limitations 208

Concluding remarks 208

CHAPTER 6 ARRHYTHMOGENIC CARDIOMYOPATHY 210

Introduction 210

Methods 210

Statistics 211

Results 211

Ventricular myocardium compositional analysis 217

Collagen 217

Innervation of the ventricular myocardium and overlying subepicardial fat 241

General innervation 241

Quantitative analysis of all sections 251

Diseased area quantification 254

Discussion 256

Concluding remarks 261

CHAPTER 7 DILATED CARDIOMYOPATHY 263

Introduction 263

Methods 263

Statistics 264

Results 264

Ventricular myocardium compositional analysis 271

Innervation of the ventricular myocardium 286

General innervation 286

Sections showing fibrosis quantification 298

Discussion 300

Concluding remarks 306

CHAPTER 8 HYPERTROPHIC CARDIOMYOPATHY 309

Introduction 309

Methods 309

Statistics 310

Results 310

Ventricular myocardium compositional analysis 319

Collagen 319

Innervation of the ventricular myocardium 338

General innervation 338

Diseased area quantification 351

Discussion 353

Left ventricular fibrosis 354

Right ventricular fibrosis 355

Correlation to imaging studies 356

Correlation to clinical findings 357

Concluding remarks 358

CHAPTER 9 GRAPHICAL SUMMARY AND CONCLUSIONS 360

Aims 360

Summary 361

Clinical Implications 374

References 381

Supplementary Material 419

List of figures

Figure 1.1. The conduction system 28
Figure 1.2. The sinoatrial node action potential 30
Figure 1.3. The effect of the autonomic nervous system on the heart 32
Figure 1.4. Early and late after-depolarisations 33
Figure 1.5. Theoretical model of re-entry 34
Figure 1.6. Heterogeneity of innervation 36
Figure 1.7. A theoretical pathway for ventricular arrhythmia 37
Figure 1.8. Autonomic neural input to the heart 40
Figure 1.9 Appearance of the cardiomyopathies 55
Figure 2.1. The pathway to and through the CRY laboratory 63
Figure 2.2. Database entry point 64
Figure 2.3. Sections 1 and 2 of the database. 65
Figure 2.4. Sections 3a, b and c and section 4 66
Figure 2.5. Cohort manager 67
Figure 2.6. Selection of the parameters for extraction 68
Figure 2.7. A comma separated values excel spreadsheet 68
Figure 2.8. Blocking protocol 72
Figure 2.9. Immunohistochemistry method 77
Figure 2.10. The different layers of the heart. 82
Figure 2.11. The Hamamatsu Nanozoomer 2.0 RS slide scanner 83
Figure 2.12. Picrosirius red stained section highlighted by Visiopharm 85
Figure 2.13. Visiopharm morphometric selection 86
Figure 2.14. Structure of the data within the multilevel model 88
Figure 2.15. The selection of the retained tissue blocks 89

Figure 3.1. The age at death of the individuals 96
Figure 3.2. The age at death and sex of the individuals 97
Figure 3.3. Causes of death broken down by gender 98
Figure 3.4. Sudden cardiac death in those under and over 35 100
Figure 3.5. Cardiovascular conditions underlying sudden cardiac death 101
Figure 3.6. Sudden cardiac death in under and over 35 102
Figure 3.7. Types of cardiomyopathy 103
Figure 3.8. Causes of SCD from around the world 105
Figure 3.9. Percentage of SCD with normal hearts in other worldwide studies 107
Figure 3.10. Percentage of SCD with cardiomyopathy in other worldwide studies. 111
Figure 3.11. The subtypes of cardiomyopathy in other worldwide studies. 112
Figure 4.1. The ventricular measurements 120
Figure 4.2. The right ventricular outflow tract 121
Figure 4.3. The atrial measurements 122
Figure 4.4. Number of deaths by age and gender 124
Figure 4.5. Body surface area broken down into males and females 125
Figure 4.6. Population pyramid for heart weight in males and females. 130
Figure 4.7. Estimated means based upon significant effects 131
Figure 4.8. The normal oval fossa 135
Figure 4.9. The average atrial measurements for females and males 140
Figure 4.10. The average dimensions for females and males 141
Figure 4.11. Differences between female and male hearts 142
Figure 5.1. The right ventricular outflow tract 161
Figure 5.2. The anterior right ventricular wall 162
Figure 5.3. The lateral right ventricular free wall 163

Figure 5.4. The posterior right ventricular wall 164
Figure 5.5. The interventricular septum 165
Figure 5.6. The anterior left ventricle 166
Figure 5.7. The posterior left ventricle 167
Figure 5.8. The epicardial collagen 168
Figure 5.9. Collagen between adipocytes and around capillaries 169
Figure 5.10. Collagen around an artery and a vein 170
Figure 5.11. The different layers of collagen in the nerves 171
Figure 5.12. Collagen around myocytes 172
Figure 5.13. Collagen and fat around large vessels in the myocardium 173
Figure 5.14. Collagen around small vessels 174
Figure 5.15. Complex networks of small vessels in the myocardium 175
Figure 5.16. Patches of collagen where trabeculae arise from the myocardium 176
Figure 5.17. Thick collagen around the vessels in the trabeculae 177
Figure 5.18. Endocardial collagen 178
Figure 5.19. Well-defined divide between fat and myocytes in the left ventricle..... 179
Figure 5.20. Myocytes encased by adipocytes in the right ventricle 180
Figure 5.21. Fat in the endocardium 181
Figure 5.22. The myocytes of the outer myocardium in the right ventricle 182
Figure 5.23. Myocyte arrangement 183
Figure 5.24. Composition of normal ventricular myocardium by fat and collagen . 185
Figure 5.25. Nerve bundles and individual nerve fibrils in the myocardium 189
Figure 5.26. PGP9.5 immunostaining in the subepicardial fat 190
Figure 5.27. PGP9.5 immunostaining of nerve bundles entering the myocardium . 191
Figure 5.28. Nerves with myocytes and vessels. 192

Figure 5.29. Individual nerve fibrils present in the endocardium 193
Figure 5.30. PGP9.5 stained nerve and individual nerve fibrils in the myocardium.194
Figure 5.31. TH stained sympathetic innervation 195
Figure 5.32. CT stained parasympathetic innervation 196
Figure 5.33. Graphic of innervation of the ventricular myocardium 197
Figure 5.34. Innervation in the normal heart. 200
Figure 6.1. The variability in the macroscopic appearance of ACM 212
Figure 6.2. Plot of lateral RV muscle wall against lateral RV epicardial fat 216
Figure 6.3. The right ventricular outflow tract 221
Figure 6.4. The right ventricle 222
Figure 6.5. The septum 223
Figure 6.6. The anterior left ventricular wall 224
Figure 6.7. The posterior left ventricular wall 225
Figure 6.8. The epicardial collagen layer 226
Figure 6.9. Area of transition between normal and fibrosis 227
Figure 6.10. Fat and fibrosis in the outer myocardium 228
Figure 6.11. Fat and fibrosis present in long continuous stretches. 229
Figure 6.12. Abrupt transition between normal myocardium and fat and fibrosis. .. 230
Figure 6.13. Interstitial fibrosis 231
Figure 6.14. Interstitial fibrosis 232
Figure 6.15. Empty spaces in a streak of fibrosis 233
Figure 6.16. Fat and fibrosis around vessels 234
Figure 6.17. The right ventricle transmural involvement. 235
Figure 6.18. Residual islands of myocytes 236
Figure 6.19. The myocytes in arrhythmogenic cardiomyopathy 237

Figure 6.20. Fat and collagen in the arrhythmogenic cardiomyopathy 240
Figure 6.21. Few PGP9.5 stained large and small nerve bundles..... 244
Figure 6.22. Nerve distribution in an anterior left ventricle 245
Figure 6.23. Nerve distribution in a posterior left ventricle..... 246
Figure 6.24. PGP9.5 stained few nerve bundles in replacement fibrosis 247
Figure 6.25. Sympathetic innervation..... 248
Figure 6.26. Few TH stained small bundles and fibrils..... 249
Figure 6.27. Parasympathetic innervation..... 250
Figure 6.28. Percentage and ratio innervation. 253
Figure 7.1. Typical findings in DCM 265
Figure 7.2. Plot of left atrial measurement 2 against left atrial measurement 2..... 270
Figure 7.3. Right ventricular outflow tract..... 273
Figure 7.4. Right ventricle. 274
Figure 7.5. The septum 275
Figure 7.6. The anterior left ventricle..... 276
Figure 7.7. The posterior left ventricle..... 277
Figure 7.8. Fibrosis merges into the perivascular collagen 278
Figure 7.9. Networks of interstitial and replacement fibrosis 279
Figure 7.10. Continuous stretches of involvement. 280
Figure 7.11. The endocardial collagen is thickened 281
Figure 7.12. Myocytes in dilated cardiomyopathy 282
Figure 7.13. Percentage and ratio of fat and collagen..... 285
Figure 7.14. Few PGP9.5 stained large bundles and small bundles 289
Figure 7.15. Nerve distribution in the anterior left ventricle 290
Figure 7.16. Nerve distribution in the anterior left ventricle 291

Figure 7.17. Sympathetic innervation 292
Figure 7.18. TH stains few small nerve bundles and fibrils 293
Figure 7.19. Parasympathetic innervation 294
Figure 7.20. Percentage and ratio of innervation 297
Figure 8.1. Gross findings 312
Figure 8.2. Plots of significant variables which correlate 317
Figure 8.3 Plots of significant variables which correlate 318
Figure 8.4. The right ventricular outflow tract 323
Figure 8.5. The right ventricle 324
Figure 8.6. The septum 325
Figure 8.7. The anterior left ventricle 326
Figure 8.8. The posterior left ventricle. 327
Figure 8.9. Myocyte disarray and hypertrophy 328
Figure 8.10. Myocyte disarray and fibrosis. 329
Figure 8.11. Interstitial fibrosis 330
Figure 8.12. Replacement fibrosis 331
Figure 8.13. Collagen around vessels 332
Figure 8.14. The endocardial collagen 333
Figure 8.15. Nuclear enlargement and splaying 334
Figure 8.16. Percentage and ratio of fat and collagen 337
Figure 8.17. Few PGP9.5 staining large and small nerve bundles 341
Figure 8.18. Nerve distribution in the septum 342
Figure 8.19. Nerve distribution in septum 343
Figure 8.20. Nerve fibres and fibrils within an area of myocyte disarray. 344
Figure 8.21. Sympathetic innervation 345

Figure 8.22. Few TH stained small nerve fibres and fibrils 346
Figure 8.23. Parasympathetic innervation 347
Figure 8.24. Percentage and ratio of innervation. 350
Figure 9.1. *The conditions underlying sudden cardiac death* 363
Figure 9.2. The major differences between male and female hearts 364
Figure 9.3. Proportional compositional analysis of the normal heart 367
Figure 9.4. Ratio of fat and collagen in the cardiomyopathies to normal 372
Figure 9.5. Ratio of innervation in the cardiomyopathies to normal 373
Figure 9.6. Pairwise correlation scatterplot 375

List of tables

Table 1.1. Different heart rate parameters and the autonomic nervous system. 49

Table 2.1. Antibodies..... 78

Table 2.2. Pathological macroscopic and microscopic criteria 80

Table 3.1. Pathological macroscopic and microscopic criteria 95

Table 4.1. Demographics for females and males 126

Table 4.2. The heart weight and cardiac dimensions 129

Table 4.3. Reference table for estimated normal heart weight 132

Table 4.4. The oval fossa and coronary artery dominance..... 133

Table 4.5. Subepicardial fat thickness..... 137

Table 4.6. Valvular and aortic circumferences 139

Table 5.1. Macroscopic heart measurements for controls and normal hearts. 155

Table 5.2. Proportions of collagen, fat and myocytes in the normal heart 185

Table 5.3. Proportions of innervation in the normal heart..... 199

Table 5.4. Proportions of innervation in the entire cohort 201

Table 6.1. Macroscopic heart measurements for ACM 213

Table 6.2. Correlations between variables 215

Table 6.3. Proportion of collagen, fat and myocytes for ACM 239

Table 6.4. Proportion of innervation for ACM 252

Table 6.5. Proportion of innervation in diseased sections for ACM 255

Table 7.1. Macroscopic heart measurements for DCM 266

Table 7.2. Correlations between variables 269

Table 7.3. Proportion of collagen, fat and myocytes for DCM 284

Table 7.4. Proportion of innervation for DCM 296

Table 7.5. Proportion of innervation in diseased sections for DCM..... 299

Table 8.1. Macroscopic heart measurements for HCM 313

Table 8.2. Correlations between variables in HCM 316

Table 8.3. Proportion of collagen, fat and myocytes for HCM 336

Table 8.4. Proportion of innervation for HCM 349

Table 8.5. Proportion of innervation in diseased sections for HCM. 352

Related Publications

Finocchiaro, Gherardo, et al. "Association of Sexual Intercourse With Sudden Cardiac Death in Young Individuals in the United Kingdom." JAMA cardiology (2022).

Finocchiaro, Gherardo, et al. "Sudden Death in Female Athletes: Insights From a Large Regional Registry in the United Kingdom." Circulation 144.22 (2021): 1827-1829.

Miles, Chris, et al. "Biventricular myocardial fibrosis and sudden death in patients with Brugada syndrome." Journal of the American College of Cardiology 78.15 (2021): 1511-1521.

Ng, K. E., et al. "Early inflammation precedes cardiac fibrosis and heart failure in desmoglein 2 murine model of arrhythmogenic cardiomyopathy." Cell and Tissue Research (2021): 1-20.

Westaby, J. D., et al. "Characterisation of hypertensive heart disease: pathological insights from a sudden cardiac death cohort to inform clinical practice." Journal of Human Hypertension (2021): 1-8.

Finocchiaro, Gherardo, et al. "Arrhythmogenic potential of myocardial disarray in hypertrophic cardiomyopathy: genetic basis, functional consequences and relation to sudden cardiac death." EP Europace (2021).

Cooper, Susanna TE, et al. "The role of endocarditis in sudden cardiac death: Highlighting the value of the autopsy, pathological features and cardiac complications." Cardiovascular Pathology 50 (2021): 107292.

Ciliberti, Giuseppe, et al. "Myocardial infarction with nonobstructed coronary arteries and sudden cardiac death: a clinical and pathological perspective." Circulation: Arrhythmia and Electrophysiology 13.7 (2020): e008302.

Miles, Chris, et al. "Morphometric characterization of collagen and fat in normal ventricular myocardium." Cardiovascular Pathology 48 (2020): 107224.

Westaby, Joseph D., et al. "Insights from examination of hearts from adults dying suddenly to the understanding of congenital cardiac malformations." Clinical Anatomy (2019).

Westaby, Joseph, and Mary N. Sheppard. "Letter by Westaby and Sheppard Regarding Article, “Sudden Cardiac Death in Hypertensive Patients”." Hypertension 74.2 (2019): e37-e37.

Mahmod, Masliza, et al. "Histological evidence for impaired myocardial perfusion reserve in severe aortic stenosis." JACC: Cardiovascular Imaging 12.11 (2019).

Miles, Chris, et al. "Sudden death and left ventricular involvement in arrhythmogenic cardiomyopathy." Circulation 139.15 (2019): 1786-1797.

Grants

Glasgow 2020 Educational Fellowship of £2,500 from BDIAP, 2019.

Bursary from the Pathological Society to attend Leeds Pathology 2019.

Cardiac Risk in the Young Clinical Fellowship and Clinical Lectureship, 2019-2024.

Grant of £10,000 from the Pathological Society, 2018.

Bursary from Pathological Society to attend the 10th Joint Meeting of the British Division of the International Academy of Pathology and the Pathological Society of Great Britain & Ireland, Belfast Pathology 20-23rd June 2017.

Bursary from Pathological Society to attend the 6th National Academic Trainee Network Meeting, 18-19th June 2017, Belfast.

Bursary from BDIAP to attend the IAP/ESP meeting, Cologne, Germany, 25-29th September 2016.

Awards

MSc poster prize for poster on “Sudden cardiac death in cardiac transplantation”, Research day, St George’s, University of London, 8th December 2022 (Co-supervision of Emelia Zullo).

Young Investigator Award for presentation on “Sudden cardiac death in Hypertensive heart disease”, The Society for Cardiovascular Pathology at the United States and Canadian Academy of Pathology, Los Angeles - 29th February 2020.

British Academy of Forensic Sciences Medical Prize for presentation on “Commotio Cordis” - 12th December 2018.

Distinction Award for presentation on PhD plan on “Is Cardiac Innervation altered in the Cardiomyopathies?” – National academic trainee network meeting, Cambridge – 15th October 2018.

List of abbreviations

ACM: arrhythmogenic cardiomyopathy

ANS: autonomic nervous system

CRY: Cardiac Risk in the Young

CRY-CPL: Cardiac Risk in the Young Cardiovascular Pathology Laboratories

CT: choline transporter

DCM: dilated cardiomyopathy

HCM: hypertrophic cardiomyopathy

IVS: interventricular septum

LV: left ventricle

PGP9.5: protein gene product 9.5

PNS: parasympathetic nervous system

RV: right ventricle

RVOT: right ventricular outflow tract

SCD: sudden cardiac death

SNS: sympathetic nervous system

TH: tyrosine hydroxylase

VA: ventricular arrhythmia

ABSTRACT

Sudden cardiac death (SCD), mediated by ventricular arrhythmia (VA), is the most common cause of death. The autonomic nervous system (ANS) is important in VA. Little is known about ventricular innervation within the normal heart. There are no previous detailed immunohistochemical studies comparing the ventricles from normal and cardiomyopathy hearts. The aim is to characterise the normal heart and its ventricular innervation and to see whether there are differences in cardiomyopathies.

At St George's, University of London, we have established a unique database with research consented phenotyped normal human hearts and SCD cases. Ventricular fat and collagen is stained using picrosirius red. Distribution of intrinsic ventricular innervation is determined with immunohistochemistry utilising the general marker PGP9.5, tyrosine hydroxylase, sympathetic marker and the choline transporter, parasympathetic marker. Slide scanning, automated and blinded quantification with whole slide digital image analysis is used for collagen, fat, myocytes and innervation analysis.

Sudden arrhythmic death syndrome and cardiomyopathy cause a majority of non-ischaemic SCD. Gender is the most important predictor of heart weight. We provide a predicted heart weight equation and a reference table. Females have smaller atria, ventricles and valves but more subepicardial fat than males. The normal heart shows a greater innervation in the right ventricular outflow tract (RVOT). Dilated cardiomyopathy shows reduced myocytes. Cardiomyopathies show a trend towards

general denervation. Cardiomyopathies demonstrate regional structural denervation in sections showing fibrosis.

Gender differences in cardiac structure should be considered when assessing for pathology. Innervation findings may aid in understanding why VA develops frequently in the RVOT. Denervation may occur as a patchy process with loss of nerve bundles in combination with fibrosis. Within DCM, the loss of myocytes and innervation may explain reduction of ventricular function. Further work is needed to establish the role of structural denervation in arrhythmogenesis.

CHAPTER 1 INTRODUCTION

Sudden Cardiac Death

We have established a unique database of sudden cardiac death (SCD). SCD refers to an unexpected death of cardiovascular cause within one hour of the development of symptoms if witnessed or within 24 hours of last being seen well if unwitnessed ('Sudden cardiac death. Report of a WHO Scientific Group', 1985). In at least 25% of cases, SCD is the first presentation of cardiac disease (Al-Khatib *et al.*, 2018). Over 70% of sudden death is due to cardiac causes (Risgaard *et al.*, 2015). SCD is a leading cause of mortality, with SCD and arrhythmia accounting for 15-20% of all deaths worldwide (Adabag *et al.*, 2010; Srinivasan and Schilling, 2018). The incidence of SCD shows regional variation with those living in Western societies disproportionately affected (Wong *et al.*, 2019). Most is due to ischaemic heart disease but an estimated 10-35% is due to the cardiomyopathies (Hayashi, Shimizu and Albert, 2015; Katritsis, Gersh and Camm, 2016). The normal heart is frequently identified at autopsy in young individuals experiencing SCD (Fabre and Sheppard, 2006).

Autopsy and Specialist Cardiac Examination

Autopsy is essential to determine an accurate cause of death (Nashelsky and Lawrence, 2003). There are many cardiac diseases that underlie SCD and specialist cardiac pathology examination is important to accurately diagnose these cardiac conditions (De Noronha *et al.*, 2014).

Sudden Cardiac Death is caused by Ventricular Arrhythmia

In most cases of SCD, death results from an electrical disturbance in the heart. This is predominantly mediated through ventricular arrhythmia (VA), and ventricular fibrillation, an erratic, disorganised firing of electrical impulses from myocytes within the ventricles (Hayashi, Shimizu and Albert, 2015; Ackerman, Atkins and Triedman, 2016). The occurrence of three or more episodes of sustained VA within 24 hours is denoted as electrical storm (Aliot *et al.*, 2009; Gao and Sapp, 2013). Arrhythmia arises from a disturbance in the cardiac electrical activity that maintains usual cardiac contraction.

Mechanism of Cardiac Contraction

There are two different types of cells which enable the electrical signal to control heartbeat, the conducting cells which carry the electrical signal and the myocytes which cause contraction in response to the electrical signal.

The electrical signal travels through the conduction system pathway and causes both the atria and ventricles to contract. The sinus node which is a small mass of specialised tissue generates an electrical stimulus 60-100 times per minute under normal conditions. This causes activation of the atrial myocytes and contraction of the atria (figure 1.1). The electrical signal then passes to the atrioventricular node where it is slowed for a short period and then passes down the conduction pathway through the bundle of His to the ventricles. The bundle of His divides into left and right bundle branches which activate the myocytes of the left ventricle (LV) and right ventricle (RV) respectively. The sequential passage of the electrical activity through the heart results in an initial short contraction of the atria followed by contraction of the ventricles (figure 1.1).

The heart contracts 60-100 times per minute with each contraction of the ventricles representing one heartbeat. The initial contraction of the atria empties the blood into the relaxed ventricles prior to ventricular contraction which ejects the blood from the heart. Whilst the ventricle contracts the atria relax filling with blood to allow the process to recur.

The electrical signal travels along these pathways by a complex reaction which causes each cell to activate the one next to it resulting in an orderly passage of the signal. As the cells rapidly activate one another, the entire heart contracts in a coordinated fashion resulting in the heartbeat.

The myocyte is an electrically active contractile cell which is the structural and functional unit of the cardiac muscle. Coordination of contraction and maintenance of cardiac rhythm is controlled by a complex network of interconnected cells which communicate via gap junctions between neighbouring cells and through voltage gated ion channels that control intracellular and extracellular ion levels. Electrical impulse propagation is primarily regulated through the gap junctions which synchronise the action potential and hence the contractions.

The generation of myocardial action potentials is due to the activation and inactivation of ion channels. The sodium and calcium channels cause depolarisation by moving into the myocytes whereas the potassium causes repolarisation by moving out of the myocytes. The waveforms of action potentials in different regions of the heart are different (Figure 1.1). This is due to the differences in expression and/or properties of the ion channels. This causes the unidirectional propagation of electrical activity through the myocardium and the generation of normal cardiac contraction.

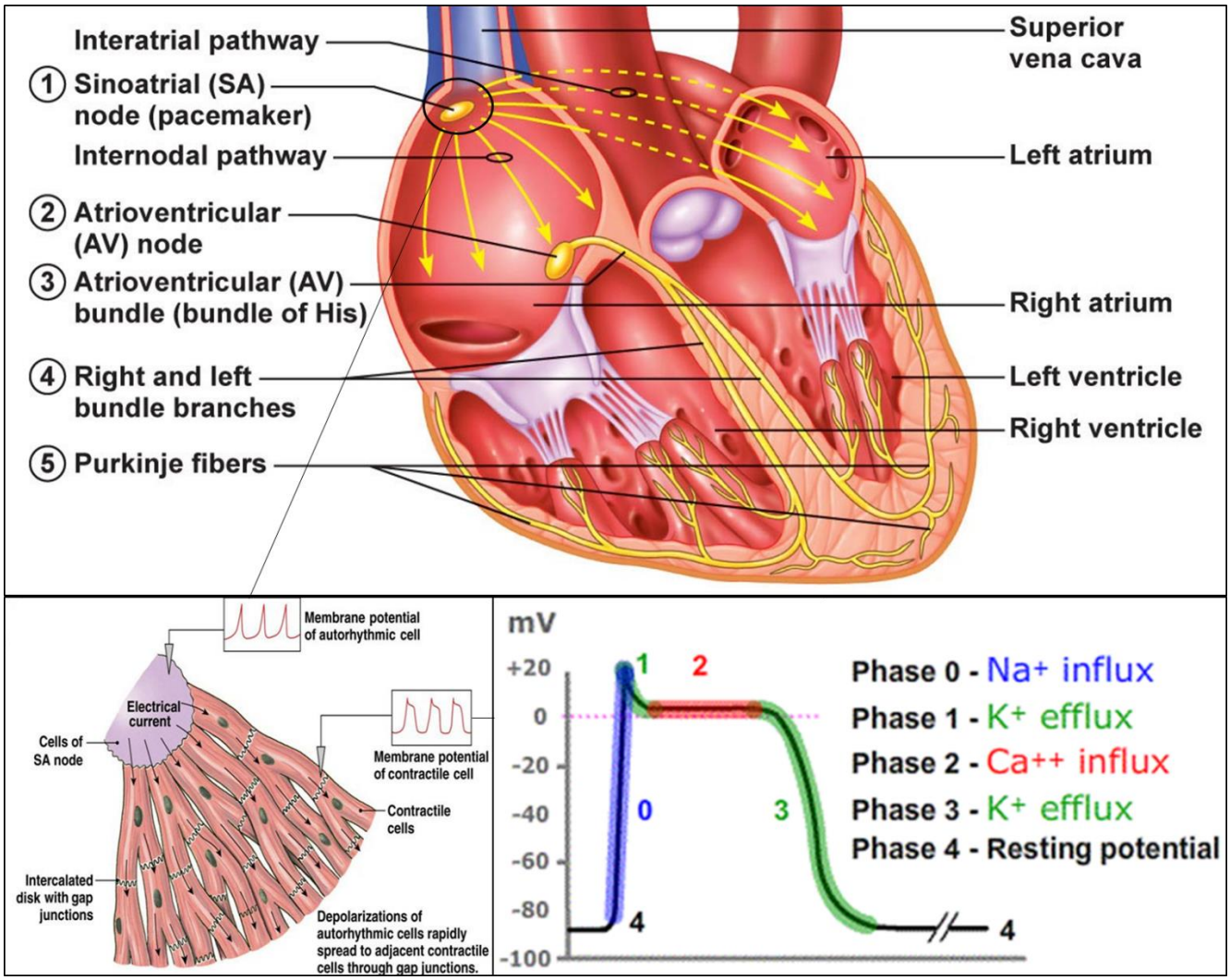


Figure 1.1. The conduction system and electrical transmission through the myocardium. The top figure illustrates the location of the different components of the conduction system. The bottom left shows the passage of electrical current from the SA node to the adjacent myocytes and then through the gap junctions between myocytes. The bottom right panel shows the phases of the action potential in a ventricular myocyte with the corresponding ion movement in or out of the myocyte (Marieb, 2004).

Mechanism of heart rate control

Under normal circumstances the heart rate is controlled by the sinoatrial node. The sinoatrial node has an intrinsic automaticity rate of 100-110 action potentials per minute. Unlike the ventricular myocardium, in the sinoatrial node the depolarising occurs primarily due to slow calcium currents instead of fast sodium currents. This means that depolarisation occurs at slower rate compared to the myocytes and that the action potential waveform appears different without a phase 1 or 2.

The initial slow spontaneous depolarisation phase is controlled by the pacemaker channels. As the potential increases the calcium channels open further increasing the potential until the threshold is reached causing depolarisation. The pacemaker channels then close. The repolarisation occurs as the potassium channels open and the calcium channels close returning the sinoatrial nodal cells to a state of slow spontaneous depolarisation.

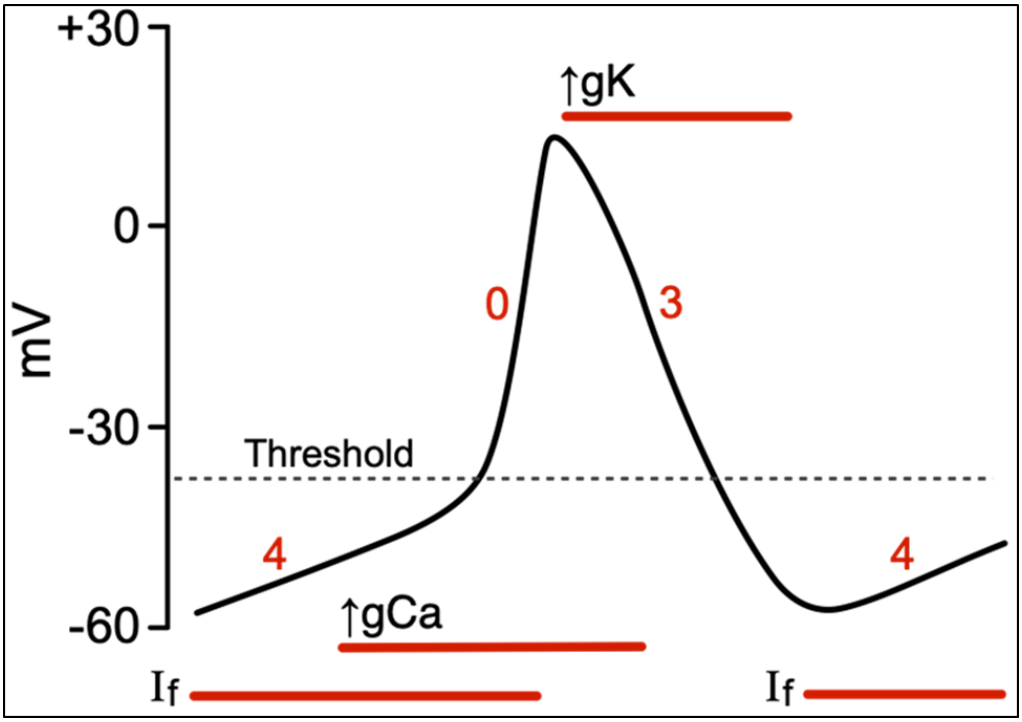


Figure 1.2. The sinoatrial node action potential is produced by the pacemaker current (I_f), calcium current (gCa) and potassium current (gK) and their respective ion channels (Klabunde, 2021).

Neural control of cardiac contraction

The sinoatrial is primarily modulated by the autonomic nerves. The vagal or parasympathetic input predominates over the sympathetic input at rest. The resting heart rate is reduced down to 60-80 beats per minute by the parasympathetic dominance.

During physical activity, the medullary centres controlling autonomic function reduce vagal inhibition and increase sympathetic stimulation of the SA node. This increases the heart rate.

The heart rate is determined by the rate of firing of the sinoatrial node. Sympathetic stimulation of the pacemaker cells of the sinus node raises the heart rate by either increasing the rate of diastolic depolarisation or by decreasing the threshold for

generation of an action potential. This is referred to as accelerated automaticity and is mediated through the ion channels of the sinoatrial node.

Noradrenaline secreted by the sympathetic nerves binds to the beta-adrenoceptors of the sinoatrial node. This increases the slope to reach threshold potential by acting on the pacemaker channels and the calcium channels to increase currents. This decreases the length of time to reach threshold therefore shortening diastole thus increasing heart rate (figure 1.3).

Acetylcholine released by the parasympathetic nerves binds the muscarinic receptors of the sinoatrial node. This decreases the slope to reach threshold potential by increasing current through the potassium channels and decreasing the current through the pacemaker channels and calcium channels. This increases the length of time to reach threshold therefore lengthening diastole thus slowing heart rate (figure 1.3).

Abnormalities in the electrical activity of the heart and its control mechanisms result in arrhythmia.

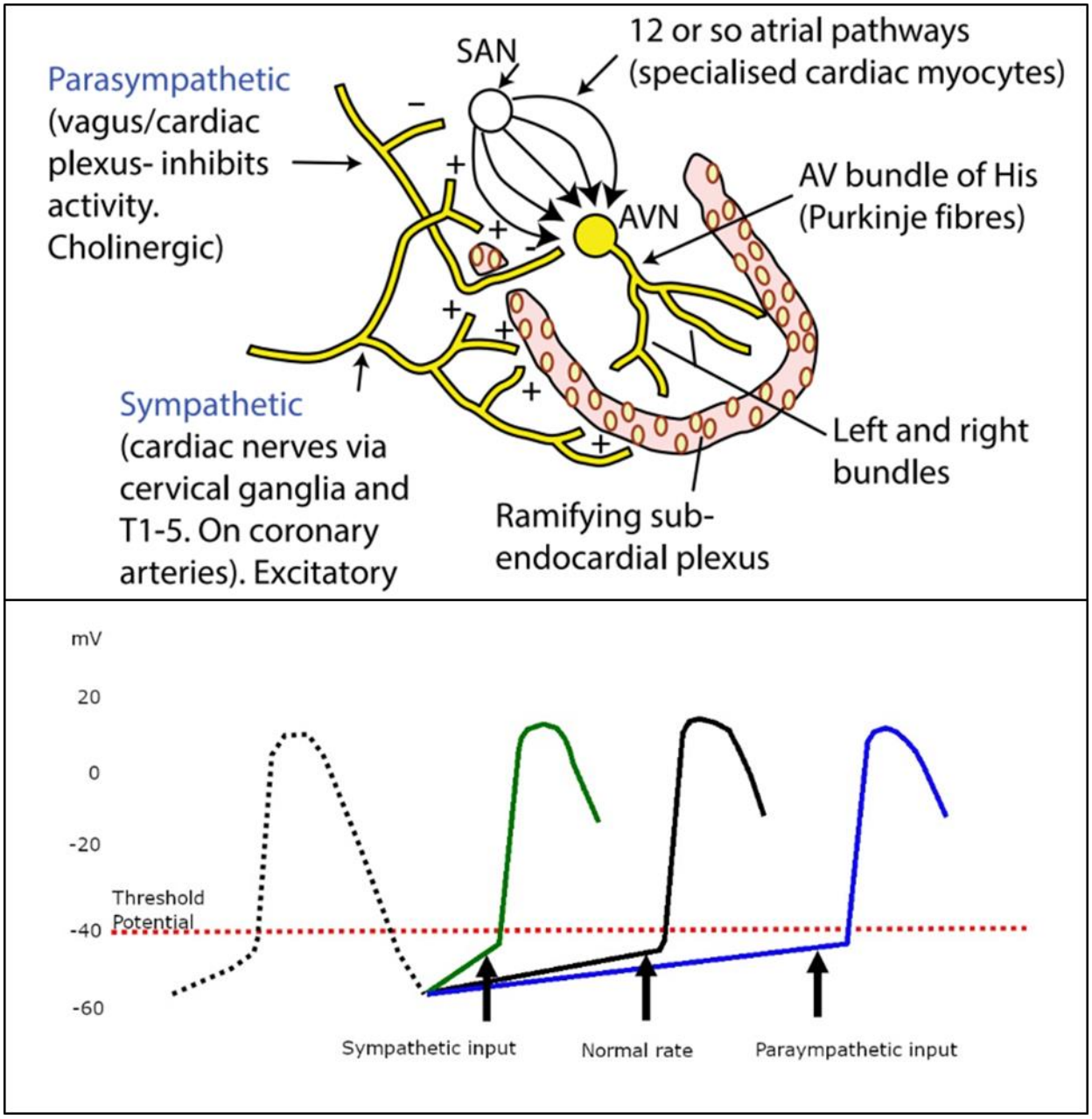


Figure 1.3. The effect of the autonomic nervous system on the heart. Sympathetic stimulation is excitatory whilst parasympathetic stimulation inhibits activity (Whitaker, 2020). *The lower panel shows the effect on the sinus node. Sympathetic input decreases the time to reach the threshold by increasing the slope and reduces the level at which threshold is reached. Parasympathetic input does the opposite increasing the time to reach threshold by decreasing the slope. These changes are mediated through the pacemaker current, the slow inward calcium current and potassium conductance.*

Mechanisms of arrhythmia

After Depolarisation

Damage to the myocardium can cause additional abnormal depolarisation at the end of the action potential. These are referred to as after-depolarisations and may trigger additional abnormal action potentials that result in arrhythmia. These are referred to as triggered activity and may be exacerbated by sympathetic stimulus, metabolic disturbance and drugs (see figure 1.4).

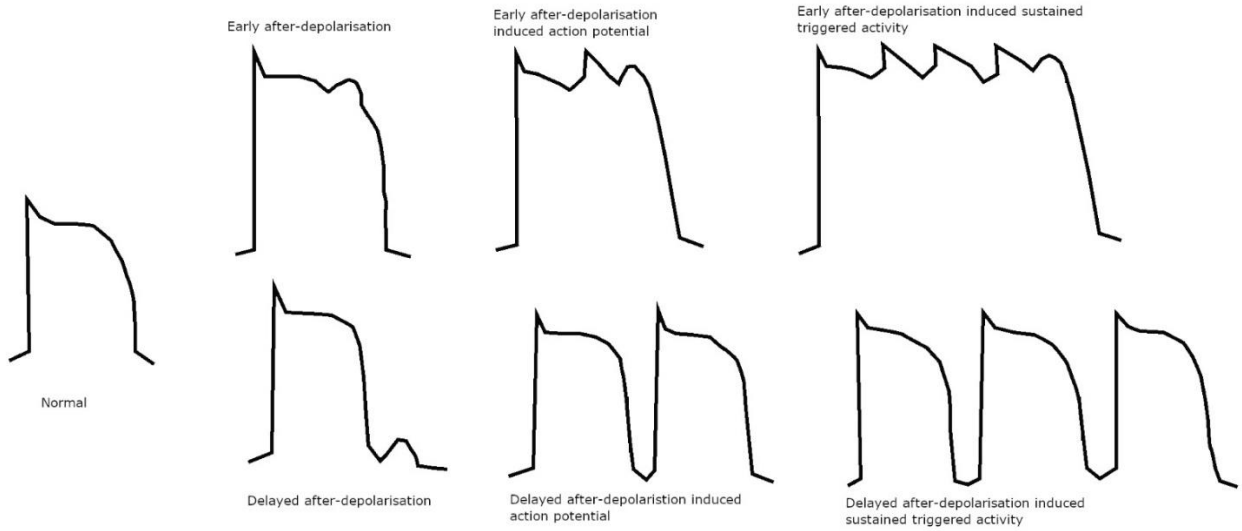


Figure 1.4. Early and late after-depolarisations. Both early and late after-depolarisations may induce further action potentials or sustained triggered activity leading to ventricular arrhythmia.

Re-entry

Re-entry may result in arrhythmia which occurs in areas of altered pathology such as ischaemia or scarring. Conduction is slowed through these areas when compared to the normal myocardium. The slowing occurs due to a change in electrophysiological properties resulting in functional heterogeneity. The initial wave of depolarisation

moves through the myocardium as usual, however as the depolarisation passes through the area of altered pathology it is slowed and re-enters the other side inducing an additional wave of depolarisation and a further beat. The impulse may travel in circles resulting in continuous abnormal beats leading to ventricular tachycardia (figure 1.5).

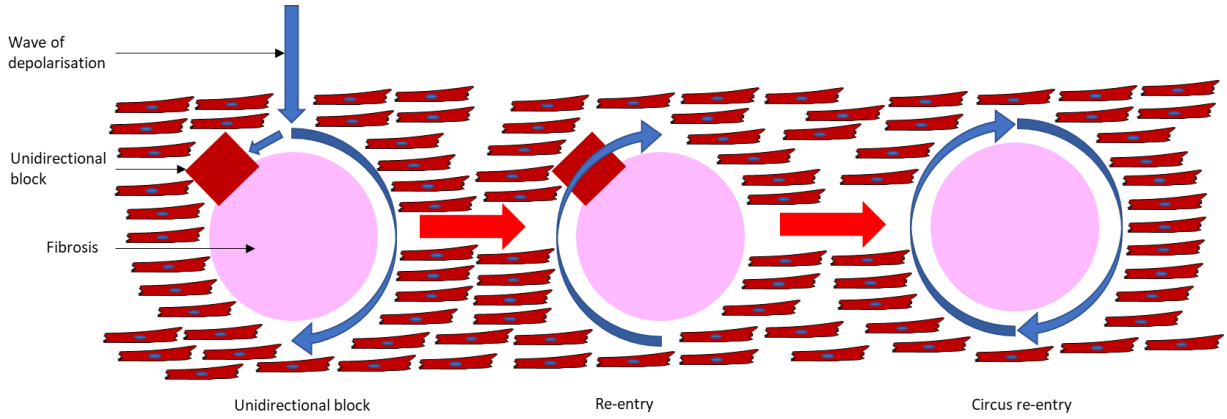


Figure 1.5. Theoretical model of re-entry. The conduction is blocked from moving in one direction around an area of anatomical substrate such as fibrosis. This leads to the wave of depolarisation moving around the other way and then moving through this blockage to trigger a further wave of depolarisation. This may cycle continuously resulting in sustained ventricular tachycardia.

Ischaemic heart disease is the most common cause of sustained VAs. Acute myocardial ischaemia related to occlusion of the coronary arteries causes polymorphic ventricular tachycardia and ventricular fibrillation. The ischaemic damage to the myocytes results in leakage of potassium into the extracellular space causing depolarisation of adjacent myocytes in the border zone of the infarction (Coronel *et al.*, 1989). This results in heterogeneity of conduction and refractoriness with conduction being slowed through this region and thereby acting as a pathway

for re-entry. Multiple foci and abnormal pathways may exist resulting in a polymorphic ventricular tachycardia.

Chronic damage with myocardial scar tissue causes monomorphic ventricular tachycardia through delayed conduction through scarred areas which results in re-entry and the triggering of additional waves of depolarisation. Ventricular scarring that may lead to re-entrant ventricular tachycardia also occurs in the cardiomyopathies (Sasaki *et al.*, 2013; Martin *et al.*, 2018).

The onset of ventricular fibrillation originates from Purkinje fibres as well as scar tissue. These substrates sustain ventricular fibrillation allowing it to spread though the ventricles. Purkinje fibres are implicated in ventricular fibrillation in 37% of cardiomyopathy patients (Haissaguerre *et al.*, 2022).

Changes in cardiac autonomic innervation may predispose to arrhythmia. The loss of innervation within infarcted tissue results in heterogeneity of innervation which has also been postulated to act as a substrate for VA. Previous work conducted within the atria of dogs with atrial fibrillation has suggested that parasympathetic heterogeneity may also play a role (Liu and Nattel, 1997; Chen *et al.*, 2014). See figure 1.6.

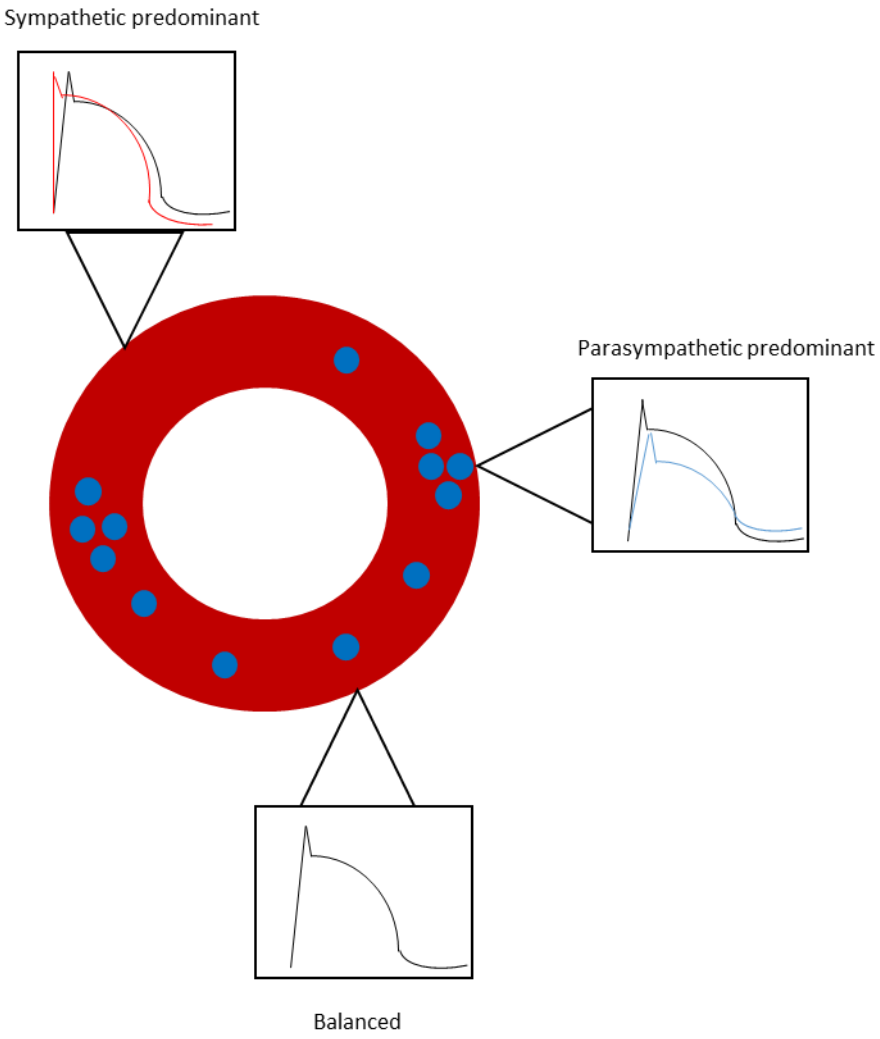


Figure 1.6. Heterogeneity of innervation causing regional electrophysiological alteration in the action potential length. In areas of dense parasympathetic innervation, the action potential is lengthened whereas in areas where the sympathetic predominates, the action potential is shortened. These spatial differences could provide a mechanism for re-entry as suggested by work performed in an a canine model of atrial fibrillation (Liu and Nattel, 1997; Chen et al., 2014).

Traditionally, there are two components that are thought to cause generation of a VA. An anatomic substrate, such as fibrosis isolating myocytes combines with transient triggers, such as a ventricular premature beat leading to electrical instability

[31]. There is now increasing evidence that abnormalities of the ANS have a central role to play as a trigger for these arrhythmias. It is emerging as a vital area for scientific research, and as a target for therapeutic intervention. Figure 1.7 shows a theoretical pathway for the development of VA (Vaseghi and Shivkumar, 2008; Shivkumar *et al.*, 2016).

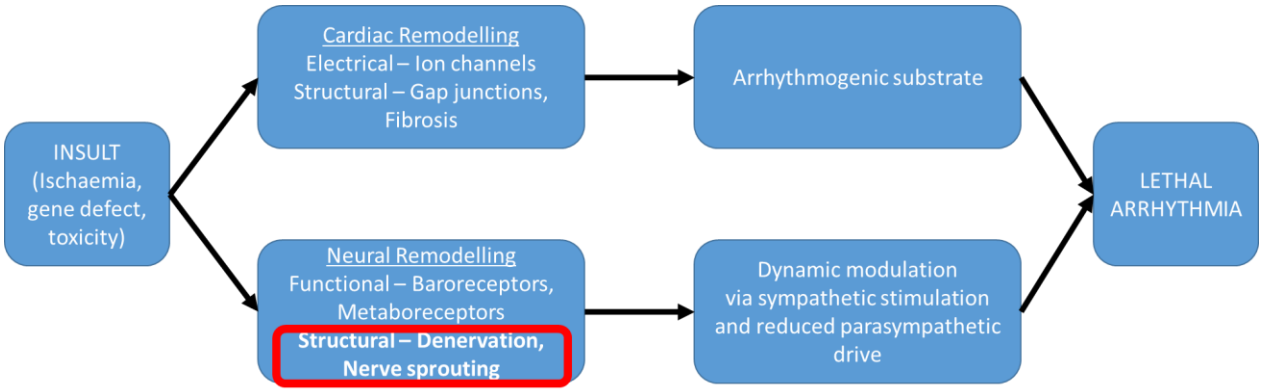


Figure 1.7. A theoretical pathway for the development of ventricular arrhythmia (Vaseghi and Shivkumar, 2008; Shivkumar et al., 2016). These structural changes are thought to occur within the ventricular myocardium.

The cardiac autonomic nervous system

The cardiac ANS is composed of the parasympathetic nervous system (PNS) and sympathetic nervous system (SNS). Traditionally, the PNS was thought of as being responsible for “rest and digest” and the SNS for “fight or flight”. The current thinking is that it is a more balanced, complimentary system where the SNS acts as a “quick response mobilizing system" and the PNS is a "more slowly activated dampening system". When referring to cardiac innervation, the ANS may be divided into the extrinsic system, lying outside the heart, and the intrinsic system which lies within the heart.

Sympathetic input

The pre-sympathetic nerves arise in the rostral ventrolateral medulla, the rostral ventromedial medulla and the dorsal area around the medial longitudinal fasciculus/lateral tegmental field. They exit the medulla and travel down the spinal cord where they synapse with relatively short preganglionic fibres. The cardiac sympathetic preganglionic cell bodies are located in the grey matter of the first six segments (T1–T6) in the intermediolateral nucleus of the thoracic spinal cord. Their fibres exit the spinal cord by the ventral roots where they pass into white rami to join the sympathetic chain. The preganglionic neurons synapse either on postganglionic neurons in ganglia at the segment of spinal origin or travel superiorly to the stellate ganglion and the adjoining inferior or middle cervical ganglions before synapsing with their target postganglionic neurons. The postganglionic fibres usually run in three nerves on the right side and four on the left. These fibres travel in close association with the subclavian veins running over both greater arteries. They enter the subepicardial fat around the origins of the greater vessels (Janes *et al.*, 1986). See figure 1.8 for an illustration of the cardiac sympathetic supply.

Parasympathetic input

The parasympathetic nerves arise in the dorsal vagal nucleus, nucleus ambiguous and nucleus tract solitarius of the medial medulla. These nerves exit the medulla as long preganglionic efferent fibres which run in the vagus nerves (cranial nerve 10). The fibres course down the vagus nerves with cardiac branches arising directly from the vagus nerve as well as from the recurrent laryngeal nerves. The cardiac branches arise in the mediastinum superior to the heart and interconnect with

sympathetic cardiopulmonary nerves anterior and posterior to the pulmonary artery (Janes *et al.*, 1986). They travel into the epicardial adipose tissue around the greater arteries where they synapse with postganglionic efferent fibres in ganglionic plexuses located in epicardial adipose tissue of the atria mainly (Armour *et al.*, 1997; Standring, 2021). Short postganglionic fibres travel to their target sites from the ganglionic plexuses. See figure 1.8 for an illustration of the cardiac parasympathetic supply.

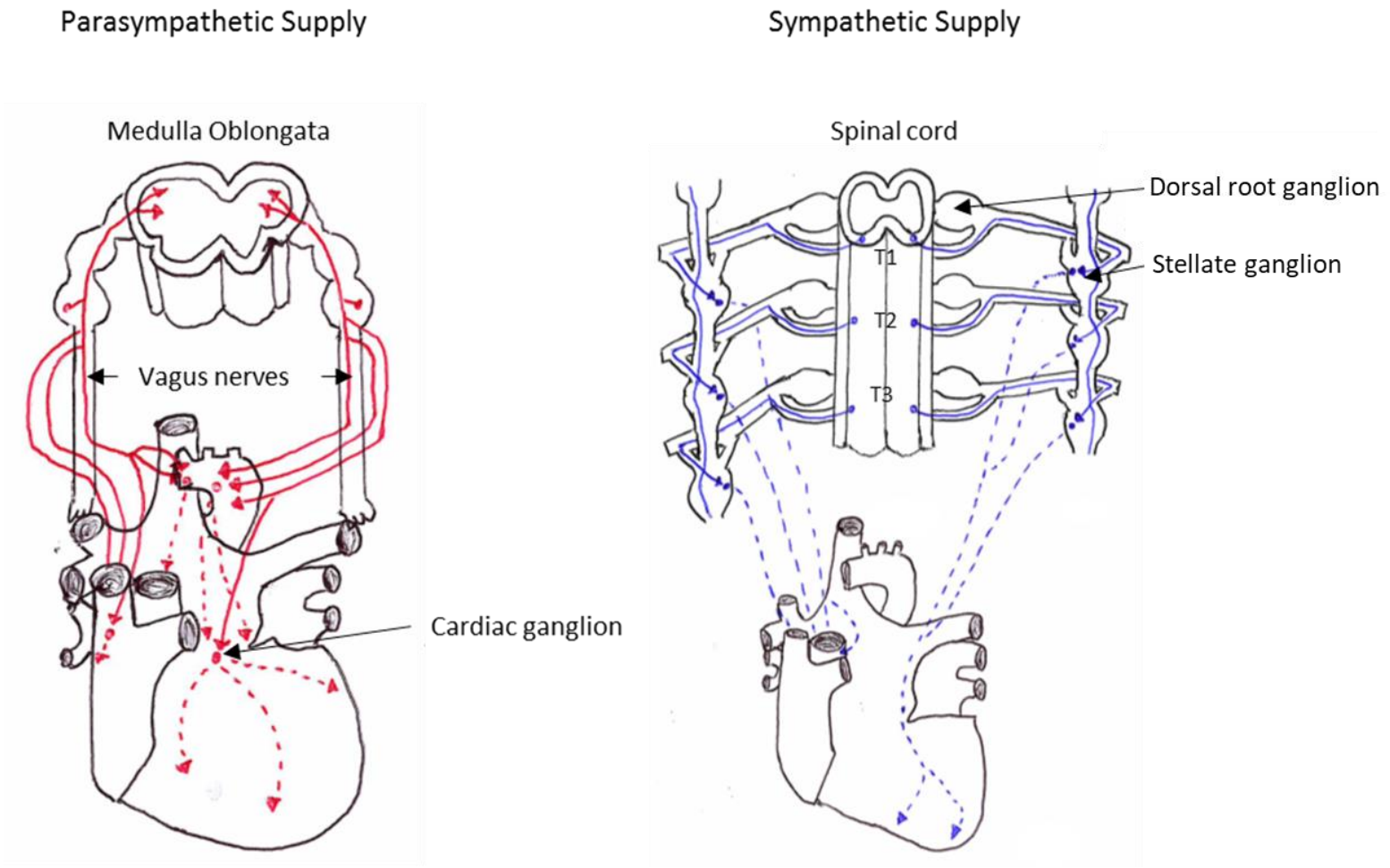


Figure 1.8. Autonomic neural input to the heart. The parasympathetic supply runs down the vagus nerve synapsing in the subepicardial fat with short postganglionic fibres running to target cells. The sympathetic supply synapses in the sympathetic chain with long postganglionic fibres running to target cells (Janes *et al.*, 1986; Netter, 2014).

The Human Intrinsic Cardiac Nervous System

Cardiac Ganglia in the Epicardial Fat

There are many studies in animals but few in humans. The intrinsic cardiac ganglia are located in the epicardial adipose tissue predominantly on the superior and posterior surfaces of the atria and around the aortic root and coronary arteries in the ventricles (Singh *et al.*, 1996; Armour *et al.*, 1997; Pauza *et al.*, 2000). This has been established in humans using a variety of techniques including haematoxylin and eosin staining (Singh *et al.*, 1996), methylene blue staining (Armour *et al.*, 1997) and acetylcholinesterase (Pauza *et al.*, 2000). The intrinsic cardiac ganglia have been reported to show local interconnecting circuit neurons as well as receiving input from mediastinal nerves and the myocardium and are postulated to act as a “mini brain” exerting localised control over the heart. It is estimated that there are over 14,000 neurons within the heart (Armour *et al.*, 1997).

The intrinsic cardiac ganglia in humans are well recognised to stain for parasympathetic markers (Wharton *et al.*, 1990; Gordon *et al.*, 1993; Singh *et al.*, 1999). There is still debate in the literature whether the ganglia stain for sympathetic markers in the normal adult heart (Wharton *et al.*, 1990; Gordon *et al.*, 1993; Singh *et al.*, 1999; Kawano, Okada and Yano, 2003; Hoover *et al.*, 2009; Petraitiene, Pauza and Benetis, 2014). Later studies using immunofluorescence, have suggested that the neurons of the ganglia contain a range of neurotransmitters in humans. Neuropeptides have been found including vasoactive intestinal polypeptide and substance P in a study of biopsies of the right atrium (Hoover *et al.*, 2009). In a study of 8 normal post mortem hearts using immunohistochemistry, the neurons of the cardiac ganglia were found to contain enzymes involved in the synthesis of monoamines and histamine and contain dopamine, serotonin, and histamine (Singh

et al., 1999). Nitrergic neurons are present within the ganglia with staining for nitric oxide synthetase (Hoover *et al.*, 2009). This suggests complex synaptology within the cardiac ganglia and a more substantial cardiac modulatory role than simple parasympathetic relay stations.

Innervation of the conduction system

As we have discussed, the cardiac rhythm is controlled through the passage of an electrical signal through the conduction system. The conduction system is composed of specialised myocytes and can be divided into the sinus node, the atrioventricular node, penetrating bundle and ventricular bundle branches.

Previous work has characterised the innervation within the conduction system in five normal hearts. They used immunofluorescence for protein gene product 9.5 (PGP 9.5) to examine general nerves and tyrosine hydroxylase (TH) for sympathetic nerves. A histochemical technique using acetylcholinesterase was used for parasympathetic nerves (Crick *et al.*, 1994). Their results aid in our understanding of the autonomic influences on cardiac rhythm.

The sinus node is a small mass of specialised tissue located at the junction between the superior vena cava and the ridge of the right atrial appendage is the cardiac pacemaker. The sinus node shows dense innervation by both sympathetic and parasympathetic fibres and bundles within the specialised myocytes (Crick *et al.*, 1994). There are more nerves in the middle of the node around the sinoatrial artery than at the periphery of the node. Numerous ganglia and nerve bundles are present around the node in the overlying epicardial fat.

The atrioventricular node is located at the base of the intra-atrial septum in the muscular atrioventricular septum, and in the triangle of Koch, an area defined by the

mouth of the coronary sinus, the tendon of Todaro and the septal leaflet of the tricuspid valve. The atrioventricular node is also densely innervated by both parasympathetic and sympathetic fibres and bundles allowing modulation of the junctional rate (Crick *et al.*, 1994; Hucker, Nikolski and Efimov, 2007). Ganglia were present in the atrioventricular groove below the coronary sinus but were fewer than around the sinus node.

The penetrating bundle divides into two bundle branches, the left and the right. The penetrating bundle is less densely innervated than the nodes but more densely innervated than the bundle branches (Crick *et al.*, 1994). The bundle branches are more densely innervated than the surrounding ventricular myocardium. Ganglia were not observed around the bundle branches.

The innervation of the conduction system is present from an early stage of life. In three normal neonatal hearts there was considerable innervation of the human cardiac conduction system at birth. In contrast, to the adult conduction there was a notable absence of innervation of the bundle branches (Chow *et al.*, 1993).

Normal human myocardial innervation

There are few studies of innervation within the adult ventricular myocardium from the 1990s. A study has examined the innervation within the endocardium and inner myocardium in five normal hearts. Computer assisted confocal image processing techniques were used on whole mount preparations. They used immunofluorescence for PGP 9.5 to examine general nerves and TH for sympathetic nerves. A histochemical technique using acetylcholinesterase was used for parasympathetic nerves. The endocardium contained an extensive neural plexus. There was a lower density of general innervation within the endocardium of the LV

than the RV and nerves lay in close proximity to endothelial cells.

Acetylcholinesterase activity displaying nerves were the most common subpopulation and showed a similar density between the RV and LV. TH immunoreactive nerves were denser in the RV than the LV (Marron et al., 1994). In 2003, Kawano et al, reported using point counting on ten fields from the atria and ventricles to quantify nerves on six hearts using TH immunohistochemistry and acetylcholinesterase. Nerve fibres were widely distributed through the heart with little difference between individuals. Large nerves and ganglion cells were observed in the epicardium and outer myocardium but it is not specified whether this is in the atria or ventricles. Thick nerves showed positivity for both acetylcholinesterase and TH and extended into the myocardium mainly accompanied by vessels. Larger nerves were noted in the outer myocardium with smaller nerves in the inner myocardium. The nerves were parallel to the myocytes and showed branching. Nerves surrounded the myocytes in the atrial myocardium. There was a greater number of parasympathetic nerves in the RV than the LV but no difference in sympathetic nerves. They found more sympathetic and parasympathetic nerves in the inner myocardium than the outer myocardium. The bases of the ventricles had more nerves than the apices (Kawano, Okada and Yano, 2003).

Another study examined the innervation of the epicardial and endocardial surfaces of 17 hearts from the atria and ventricles (age range 3 months to 37 years). PGP9.5 and TH immunohistochemistry and acetylcholinesterase histochemical staining was used to examine whole mount preparations with confocal and fluorescence microscopy.

Two types of nerves were described in the atria in the endocardium. Nerves show terminal varicose fibril arborisation covering a small area or terminal varicose fibril

arborisation covering a large area. The ventricular endocardium showed a distinct subtype of nerves where the fibrils were small and did not show arborisation.

In the LV, epicardial nerve fibrils arose from nerve bundles but were fewer than the atria. There were no nerve fibrils in the epicardium of the RV. The epicardial nerve fibrils were all sympathetic with no parasympathetic fibrils identified.

In the endocardium of the LV, a small non arborising ending nerve fibril, was present in the endocardial lining of the LV but not the RV. These endocardial nerve fibrils were mainly for sympathetic with less than 5% being parasympathetic (Marron *et al.*, 1995).

Using similar techniques, the leaflets of both the atrioventricular and arterial valves were examined (Marron *et al.*, 1996). The nerve bundles enter at the base of the leaflet and form an intricate network of both varicose and non-varicose bundles with extensive nerve fibrils. There was more parasympathetic innervation than sympathetic innervation.

Electron microscopy of the atrial myocardium of the human adult heart showed both unmyelinated and myelinated fibres present. Unmyelinated fibres made up over 70% of the large cardiac nerves. Larger unmyelinated nerve bundles show more fibres than smaller bundles. Myelinated fibres were present within unmyelinated nerve bundles (Pauziene, Pauza and Stropus, 2000). Several types of nerve terminals were differentiated by the presence of empty or dense cored vesicles including adrenergic and cholinergic innervation. Adrenergic nerve terminals showed small dense cored vesicles and small empty vesicles whereas cholinergic showed small empty vesicles and some large dense vesicles (Kyösola *et al.*, 1976). Nerve terminals lie within 100 nanometres of myocytes and terminal cells are present between nerve endings and muscle fibres. Whilst the nerve terminals are in close

proximity to myocytes there is no neuromuscular junction in the myocardium (Dastur, Vevaina and Manghani, 1989; Onicescu and Vidulescu, 1989).

Various other transmitter substances have been identified within nerve fibrils of the myocardium using immunohistochemistry including neuropeptide Y, vasoactive intestinal polypeptide and substance P (Rechardt *et al.*, 1986; Marron *et al.*, 1994, 1995; Tan *et al.*, 2018). Neuropeptide Y is a sympathetic co-transmitter which is present in the nerves around vessels, myocytes and the endocardium. It is involved in the vasoconstriction, cardiac remodelling and angiogenesis.

Vasoactive intestinal polypeptide functions as a nonadrenergic, noncholinergic neurotransmitter. It is present in nerve fibrils close to myocytes (Rechardt *et al.*, 1986). Vasoactive intestinal polypeptide is a potent vasodilator and is released in response to cholinergic agonists. It contributes to the regulation of normal coronary vasomotor tone. Vasoactive intestinal polypeptide increases coronary artery blood flow following parasympathetic stimulation. It also increases contractility of both the atria and ventricles and increases heart rate (Henning and Sawmiller, 2001).

Substance P is present in nerve fibrils in the cardiac ganglia and around vessels (Rechardt *et al.*, 1986). It increases the activity of cholinergic neurones resulting in decreased muscle contractility and heart rate. Substance P causes vasodilation of the vessels of the heart (Mistrova, Kruzliak and Chottova Dvorakova, 2016).

The extrinsic and intrinsic innervation of the heart plays a vital role in cardiac function. The conduction system is modulated by the ANS. The extrinsic innervation modulates sympathetic input to the heart through the stellate ganglion and parasympathetic input via the vagus nerve. The intrinsic cardiac ANS is made up of ganglia and interconnecting neurons and regulates cardiac electrical activity.

The intrinsic cardiac innervation has not been fully elucidated. Knowledge of how innervation affects function is important in treatment of cardiac disease. Better understanding of the intrinsic cardiac innervation will aid in the development of additional treatments for refractory arrhythmias in a range of conditions including the structurally normal heart and the cardiomyopathies (Julian *et al.*, 2022).

Overall Cardiac Autonomic Control – the brain heart axis

Animal models have been used to demonstrate the complex interactions within the brain heart axis. The ANS operates through the cardiovascular centres located within the medulla. These centres receive descending input and are regulated from the cerebral cortex, thalamus, and hypothalamus. In turn, further modulation occurs within the spinal cord and the sympathetic chain at the level of the stellate ganglion and the middle cervical ganglion. Finally, further regulation occurs at the level of the intrinsic cardiac nervous system (Cardinal *et al.*, 2009).

The neurons responsible for cardiac control can be classified as afferent, efferent or local circuit neurons. These neurones establish feedback loops involving the transmission of sensory information through afferent neurons to the intrinsic cardiac nervous system, the stellate ganglia, spinal cord and brainstem. These areas then feedback through efferent neurons to the heart (Fukuda *et al.*, 2015; Ardell and Armour, 2016). There is complex interaction and feedback between the different levels of control with the heart and the intrinsic cardiac nervous system lying at the centre (see figure 1.8).

Cardiac Autonomic Nervous Function and Assessment

To summarise, the cardiac ANS is composed of the SNS and PNS. The SNS acts as a “quick response mobilizing system" and the PNS is a "more slowly activated dampening system". The cardiac ANS regulates chronotropy (heart rate), iontropy (contractility), luisitropy (relaxation), dromotropy (conduction velocity) and bathmotropy (excitability) (Ajijola *et al.*, 2013; Fukuda *et al.*, 2015). Whilst the sympathetic input increases these effects via noradrenaline and the adrenergic receptors, the parasympathetic input does the opposite through acetylcholine and the muscarinic receptors. A fine balance exists between these two components to regulate the heart.

Autonomic tone may be assessed in a clinical setting through resting heart rate, exercise tolerance testing and heart rate variability. Poor prognostic indicators, found to be predictive of mortality or coronary disease, are increased resting heart rate, failure to achieve 85% of the age-predicted maximal heart rate on exercise tolerance testing, failure to decrease heart rate by more than 12 beats/min during the first minute after exercise and decreased heart rate variability (Ellestad, 1996; Lauer *et al.*, 1996). See table 1.1 for how alterations in the ANS effect different heart rate parameters.

Heart rate parameter	Parameter change indicative of poor prognosis	Parasympathetic input	Sympathetic input
Resting	↑	↓	↑
Maximal	↓	↔	↓
Recovery	↑	↓	↔
Low frequency variability	↓	↓	↓
High frequency variability	↓	↓	↔

Table 1.1. Different heart rate parameters, changes which are associated with poor prognosis and how they are influenced by the different arms of the autonomic nervous system.

Autonomic Dysregulation occurring at different levels

Autonomic dysregulation is defined as a chronic imbalance of the ANS and may be mediated through damage and loss of the nerves at various different levels within the ANS.

Epilepsy and ischemic stroke have been shown to influence heart function and may result in severe arrhythmia. Around 25% of patients experiencing stroke have significant cardiac arrhythmias. The risk of cardiac arrhythmia was found to be highest within the first 24 hours following stroke (Kallmünzer *et al.*, 2012). Around 24% of epileptics were found to have arrhythmia in a study of 1.4 million inpatients (Desai *et al.*, 2017). Furthermore, seizures frequently affect the heart rate and rhythm. Tachycardia occurs in 96% of seizures and the onset is usually within seconds of seizure onset persisting for several minutes after termination (Keilson,

Allen Hauser and Magrill, 1989). Thus, central nervous system damage and epilepsy can affect cardiac rhythm.

Cardiac autonomic dysfunction is reported within cancer survivors receiving various types of chemotherapy and receiving radiotherapy to the neck and thorax. Dysfunction was found in both the sympathetic and parasympathetic systems using heart rate deep breathing test, Valsalva manoeuvre, tilt-table test, and sudomotor testing. The dysfunction was most pronounced in the sympathetic branch (Noor *et al.*, 2020). This highlights that damage to the cardiac ANS may occur as a systemic process or be due to more localised damage.

In patients with acute myocardial infarction, the most powerful independent ECG predictor of 30-day mortality is resting heart rate (Hathaway et al, 1998). Impairment of the PNS and overactivity of SNS is predictive of mortality in humans in the setting of both heart failure and myocardial infarction (La Rovere et al., 1998, Nolan et al., 1998).

The right ventricular outflow tract is an important source of ventricular tachycardia in humans. A study of human RVOT preparations using optical mapping has found shorter action potential durations relative to the right ventricular apical region. Adrenergic stimulation of the RVOT using isoproterenol shortened the action potential and resulted in more increased premature ventricular contractions. Cholinergic stimulation using acetylcholine following adrenergic stimulation attenuated these arrhythmogenic effects (Aras *et al.*, 2022).

Myocardial innervation in disease

There is increasing recognition that cardiac innervation is altered within the myocardium of the ischaemic heart based on mouse studies and observation in

human hearts. Denervation occurs in areas of necrosis or dense fibrosis. Nerve sprouting occurs at the periphery of injured ventricular myocardium (Cao, Chen, *et al.*, 2000; Cao, Fishbein, *et al.*, 2000; Hasan *et al.*, 2006; Oh *et al.*, 2006; Zhu *et al.*, 2019). This process can lead to regional heterogeneity of sympathetic innervation. Radionucleotide studies using iodine-123 labelled metaiodobenzylguanidine, a chemical modified analogue of norepinephrine allows the evaluation of sympathetic innervation. Metaiodobenzylguanidine is stored in vesicles in the sympathetic nerve terminals and is not catabolized. Increased wash-out rates indicate cardiac sympathetic denervation and are associated with poor prognosis (Slart *et al.*, 2019). Regional heterogeneity of sympathetic innervation has been associated with SCD (Boogers *et al.*, 2010; Nishisato *et al.*, 2010; Fallavollita *et al.*, 2014). Animal studies and cell culture have demonstrated that the functional changes observed on radionucleotide studies are a result of a lack of norepinephrine uptake in sympathetic nerve terminals which results in higher interstitial norepinephrine, decreased myocardial adrenoceptor density and increased myocyte apoptosis (Liang, 2007). Parasympathetic nerves have shown damage in a report on hearts from 57 cases of SCD compared against aged matched controls. Acetylcholinesterase was used to study cholinergic nerves. The cholinergic nerves within the intracardiac nerve plexuses were oedematous and showed reduced staining. The nerve fibrils around the conduction system and blood vessels of the myocardium appeared normal (Shvalev, Zhuchkova and Vikhert, 1980).

A mouse study, has managed to restore innervation to scar tissue through the targeting of tyrosine phosphatase σ. This was observed to prevent dispersion of action potential duration, hypersensitivity to β-receptor stimulation and calcium mishandling on optical mapping rendering the heart resistant to induced arrhythmia

(Gardner *et al.*, 2015). These findings support the theory that abnormalities in innervation act as a substrate for arrhythmia independently of ischaemia or scar tissue.

The neurotransmitters identified in the cardiac nerve terminals have been implicated within the pathogenesis of cardiovascular disease. Neuropeptide Y has been implicated in pathological processes including ischaemia, arrhythmia and failure (Tan *et al.*, 2018). Substance P is implicated in cardiovascular response to stress as well as ischemia and reperfusion. Substance P is a potent inducer of neurogenic inflammation as it causes increased vascular permeability resulting in plasma protein extravasation (Mistrova, Kruzliak and Chottova Dvorakova, 2016).

Neuromodulation

Cardiac autonomic imbalance is characterized by chronic increased sympathetic stimulation and a reduction in parasympathetic input causes destabilisation of myocardial electrical activity promoting arrhythmia. Neuromodulation aimed at correcting the imbalance in the ANS has emerged as a promising treatment for arrhythmia. Interventions include pharmacological blockade of sympathetic neurotransmitters and neuropeptides, cardiac sympathetic denervation, thoracic epidural anaesthesia to reduce sympathetic activity. Vagal and Tragus nerve stimulation are used to increase parasympathetic input. The aims of these therapies to restore balance in the ANS thus preventing arrhythmia (van Weperen, Vos and Ajijola, 2021).

The SNS has long been a target for arrhythmia prevention (Coumel, Leclercq and Escoubet, 1987). Established strategies involve the use of beta blockers, or blockage of the renin-angiotensin-aldosterone pathway, to reduce sympathetic input.

Indeed, beta-blockers are well recognised to have a relative risk reduction of mortality of 34% in individuals with heart failure of any cause including cardiomyopathy (McMurray *et al.*, 2012).

Methods aimed at reducing sympathetic input include thoracic epidural anaesthetic, stellate ganglion block, cardiac sympathetic denervation or renal artery denervation (Vaseghi and Shivkumar, 2008; Chen *et al.*, 2014; Schwartz, 2014; Fukuda *et al.*, 2015; Franciosi *et al.*, 2017; Hanna, Shivkumar and Ardell, 2018; Assis *et al.*, 2019; Zhu *et al.*, 2019). Thoracic epidural anaesthesia has shown early promise in a small case series of individuals with refractory ventricular tachycardia (Bourke *et al.*, 2010; Do *et al.*, 2017). A systematic review on stellate ganglion block, although limited to mainly case reports, has suggested that it is an effective treatment for electrical storm (Meng *et al.*, 2017). Cardiac sympathetic denervation is a technique where the lower half of the stellate ganglion along with the ganglia at the T1 to T4 positions in the sympathetic chain are removed (Irie *et al.*, 2017). The technique has proven successful in the treatment of refractory VA in individuals with channelopathies (Schwartz *et al.*, 2004; Dusi *et al.*, 2019). Renal artery denervation has shown promise in small studies which demonstrate reduced arrhythmic burdens following the procedure (Armaganijan *et al.*, 2014, 2015; Evranos *et al.*, 2016).

Methods to increase parasympathetic tone include tragus nerve stimulation and vagal nerve stimulation (Chen *et al.*, 2014; Ng, 2014; Fukuda *et al.*, 2015; Franciosi *et al.*, 2017; Hanna, Shivkumar and Ardell, 2018; Zhu *et al.*, 2019). Tragus nerve stimulation involves the use of cutaneously applied stimulator to the ear to trigger the vagus nerve through its auricular branch. Early work on a group of individuals with paroxysmal atrial fibrillation presenting for ablation who were either randomised to low level tragus electrical stimulation or sham control has shown suppression of

atrial fibrillation in the study arm (Stavrakis *et al.*, 2015). Similarly, direct stimulation of the vagal nerve via the pre-ganglionic fibres running adjacent to the lateral aspect of the superior vena cava has been shown to suppress post-operative atrial fibrillation and attenuate intense inflammation following cardiac surgery when compared to sham control (Stavrakis *et al.*, 2017).

The structurally normal heart

The morphologically normal heart is found in a majority of non-ischaemic young sudden deaths and is labelled as sudden arrhythmic death syndrome (Fabre and Sheppard, 2006). A normal heart with the exclusion of other pathology at autopsy, in combination with the absence of toxicological findings, points to an underlying channelopathy in young individuals (Lahrouchi *et al.*, 2017). Whilst there are numerous publications on the structural findings at autopsy in diseased hearts (Finocchiaro *et al.*, 2019; Miles *et al.*, 2019; Westaby *et al.*, 2021), there is a paucity of literature on the morphologically normal heart. Past autopsy studies have focussed on organ weights and do not provide comprehensive measurements of atria, ventricles or subepicardial fat (De La Grandmaison, Clairand and Durigon, 2001; Wingren and Ottosson, 2015; Skurdal and Nordrum, 2016).

The Cardiomyopathies

The cardiomyopathies cause around 10-15% of all SCD (Hayashi, Shimizu and Albert, 2015). Cardiomyopathies are diseases of the heart muscle which affect size, shape and structure of the heart. The three main types are hypertrophic cardiomyopathy (HCM), arrhythmogenic cardiomyopathy (ACM), and dilated cardiomyopathy (DCM). See figure 1.9 for the appearances of the cardiomyopathies.

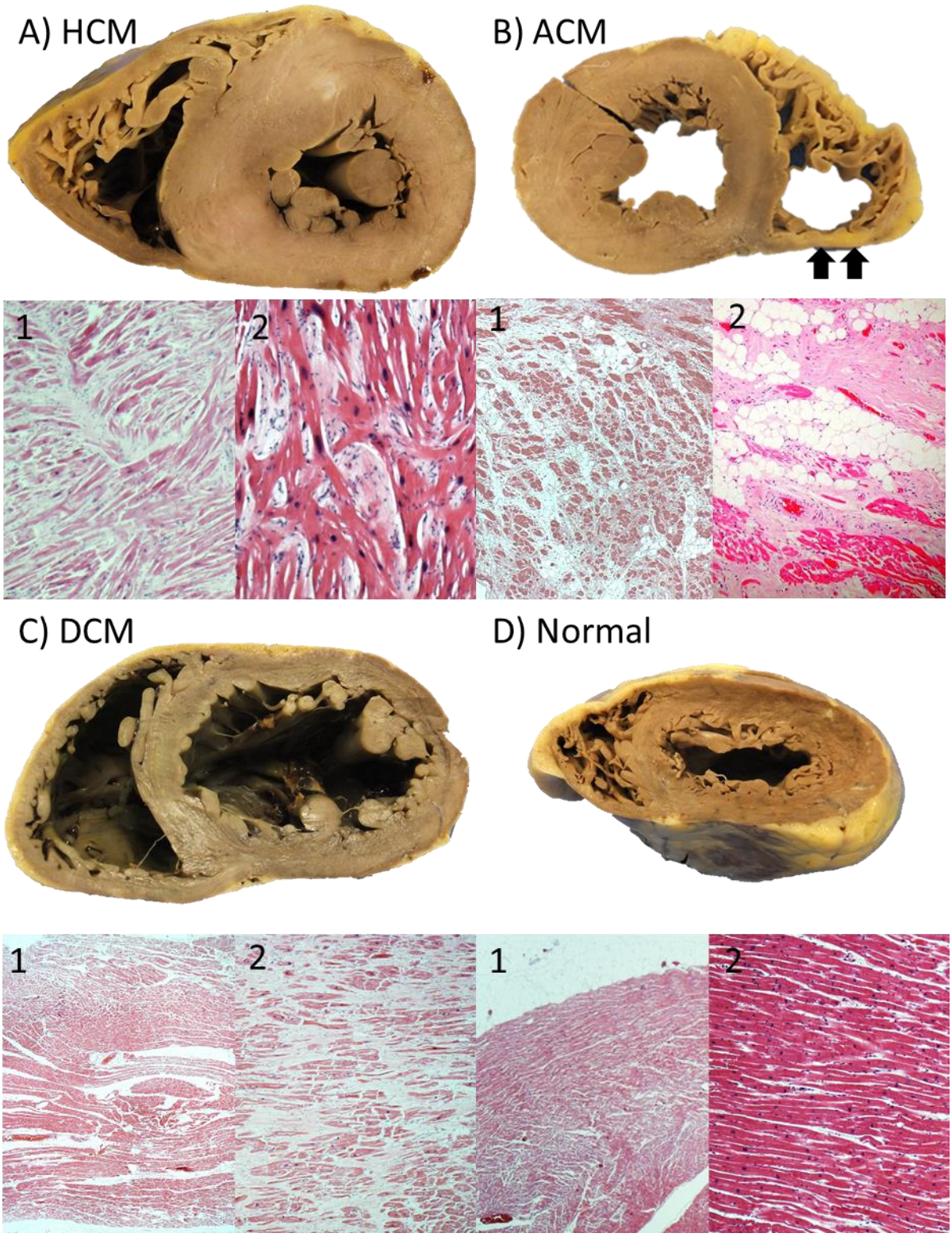


Figure 1.9 A) The macroscopic appearance of hypertrophic cardiomyopathy (HCM). Note the asymmetric septal left ventricular (LV) hypertrophy and the area of scarring. 1) Myocyte disarray in the right ventricle (RV) in HCM but also in the normal heart. 2)

Prominent LV myocyte disarray. B) The macroscopic appearance of arrhythmogenic cardiomyopathy (ACM). Note the fatty infiltration into the right ventricular wall, particularly in the posterior wall of RV (arrows) where it is particularly unusual to see this change in the normal heart. 1) RV (1) and LV (2) showing fat and fibrosis infiltrating into the wall in a subepicardial distribution. C) The macroscopic appearance of dilated cardiomyopathy (DCM). A dilated left ventricle with thinned walls. 1) The RV appears normal. 2) The LV shows diffuse interstitial and replacement fibrosis. D) The macroscopic appearance of the normal heart. Note the normal parallel arrangement of myocytes and the lack of fibrosis in both the right (1) and left (2) ventricle.

Hypertrophic Cardiomyopathy

HCM is clinically characterised by the presence of increased LV wall thickness not explained by abnormal loading conditions (Veselka, Anavekar and Charron, 2017). HCM is a genetic condition caused predominately by mutations in the sarcomeric proteins (Sabater-Molina *et al.*, 2018). HCM is the most common cardiomyopathy with a prevalence of 1 in 500 worldwide, although estimates range up to 1 in 200 (Maron *et al.*, 1995; Semsarian *et al.*, 2015; Veselka, Anavekar and Charron, 2017). Premature ventricular depolarisations are found in 80-90% with ventricular couplets and non-sustained ventricular tachycardia detected in 20-25% (Adabag *et al.*, 2010). Many individuals with HCM are asymptomatic and therefore it is frequently first diagnosed following SCD (Finocchiaro *et al.*, 2019; Maron *et al.*, 2020). The annual incidence of SCD in the general population of HCM patients is estimated to be 1% (Elliott *et al.*, 2006).

Arrhythmogenic cardiomyopathy

ACM is clinically defined by presentation related to arrhythmia and myocardial structural abnormalities. ACM is mainly caused by mutations in the genes encoding desmosomal proteins (Gandjbakhch *et al.*, 2018). ACM has an estimated prevalence of 1 in 1000 to 1 in 5000 (Corrado, Basso and Judge, 2017; McKenna, Maron and Thiene, 2017). Originally thought to be a right ventricular disease and denoted as arrhythmogenic right ventricular cardiomyopathy, it is now recognised to affect both ventricles with a recent study showing LV involvement in 87% of cases (Miles *et al.*, 2019). Many individuals with ACM remain asymptomatic in their early decades with a majority ultimately presenting with symptoms relating to arrhythmia (Corrado, Basso and Judge, 2017). A study of 439 index ACM patients found that 72% of the cohort experienced sustained VA over a median follow up of 7 years with an annual incidence of SCD of 0.5% emphasising that this is a highly malignant condition (Groeneweg *et al.*, 2015). This incidence is most likely an underestimate as it is frequently first diagnosed following sudden death (Miles *et al.*, 2019).

Dilated Cardiomyopathy

DCM is clinically characterised by dilation and impairment of one or both ventricles. DCM has a prevalence of 1 in 2500 (Merlo *et al.*, 2018). DCM is regarded as a morphological consequence of an extensive list of genetic and environmental insults (Bozkurt *et al.*, 2016; Japp *et al.*, 2016). In contrast to HCM and ACM, only 35% of cases are thought to be genetic with acquired causes including myocarditis, exposure to alcohol, drugs and toxins as well as metabolic and endocrine disturbances (Weintraub, Semsarian and Macdonald, 2017). VAs are found in

around 95% of individuals with DCM and the annual incidence of SCD is 2-4% (Neri *et al.*, 1986; Grimm and Maisch, 2002; Kadish *et al.*, 2004).

Innervation in Cardiomyopathy

Ajijola et al, examined human left stellate ganglia. They used thionine and an elastic van Geison trichrome stain to assess neuronal size. They found neuronal size was increased in the stellate ganglion of those with scarred hearts and non-ischaemic cardiomyopathy. They examined nerve density in the myocardium using S100 immunohistochemistry in an unspecified sub-cohort of scarred hearts and normal hearts but did not detect a difference (Ajijola *et al.*, 2012).

There are only two papers on innervation in cardiomyopathy. A study published in 1982, compared seven DCM hearts to five hearts from road traffic accident victims, only looking on haematoxylin and eosin staining of formalin fixed paraffin embedded tissue. A single tissue block from the posterolateral wall of the systemic venous sinus of the right atrium was used. The authors reported a significantly decreased number of neurons in DCM in the right atrium compared to normal (Amorim and Olsen, 1982). A previous study of individuals with end stage cardiac failure due to Chagas disease, hypertension, valvular disease and DCM used glyoxylic acid-induced fluorescence to identify catecholamines and counted neural structures. Tiocholine was used to identify cholinesterase activity with computer assisted calculation. Samples from 19 individuals of 12 atrial fragments and 18 ventricular fragments were examined for sympathetic innervation and 14 atrial fragments were examined for parasympathetic innervation quantifying 40 microscopic fields. Sympathetic innervation was “absent” in 9 of their samples. There were lower levels of both sympathetic innervation and parasympathetic in Chagas affected hearts compared to

failure due to other causes (Machado *et al.*, 2000). There are no reports on the histology of intrinsic innervation in HCM or ACM and none assessing regional ventricular innervation in cardiomyopathy. There are no reports of cardiac ventricular innervation in those experiencing SCD with cardiomyopathy.

Conclusion

Little is known about the normal cardiac innervation and the distribution of its individual components within the ventricular chambers. There is almost no information on the intrinsic innervation of the ventricles in cardiomyopathy. Cardiomyopathies cause alterations in the size, shape and structure of the heart. A common complication is VA, which arise locally in the ventricular myocardium and cause SCD. The cardiac ANS is intrinsic to VA generation and its dysfunction is strongly associated with mortality. At the centre of the ANS lies the intrinsic cardiac nervous system, a network of ganglionic plexuses and over 14,000 neurons. I will use immunohistochemical techniques to delineate ventricular innervation in detail. Clarification of the alterations which occur in the intrinsic cardiac nervous system within SCD victims with cardiomyopathy will help in selection of specific preventative and therapeutic strategies, and will accelerate their development. Specific innervation profiles in the cardiomyopathies may enable a better diagnostic characterisation, and may correlate with arrhythmic risk.

Hypotheses

1. There are quantifiable differences in cardiac anatomical measurements between ACM, DCM and HCM and non-cardiac death controls.

2. There are quantifiable differences in the proportion of ventricular collagen, fat and myocytes between ACM, DCM and HCM and non-cardiac death controls
3. There are quantifiable differences in the proportion of cardiac innervation in the ventricles between ACM, DCM and HCM and non-cardiac death controls.

Aims

1. To describe the causes of SCD from the CRY cardiac pathology database in detail.
2. To characterise the normal heart in terms of the weight, dimensions of the atria, ventricles, valves, epicardial fat, and fossa as well as coronary artery dominance.
3. To establish normal collagen, fat, myocytes within the RV and LV in normal hearts.
4. To establish normal general, sympathetic and parasympathetic innervation within the RV and LV in normal hearts.
5. To establish whether there are quantifiable differences in collagen, fat, myocytes in different regions of the RV and LV in normal hearts.
6. To establish whether there are quantifiable differences in general, sympathetic and parasympathetic innervation in different regions of the RV and LV.

7. To establish whether there are macroscopic differences in weight, dimensions of the atria, ventricles and subepicardial fat in ACM, DCM and HCM compared to the normal heart.
8. To establish if there are microscopic quantifiable differences in collagen, fat, myocytes in ACM, DCM and HCM compared to the normal heart.
9. To establish if there are microscopic quantifiable differences in general, sympathetic and parasympathetic innervation in ACM, DCM and HCM compared to the normal heart.

CHAPTER 2 METHODS

The Cardiac Risk in the Young Cardiovascular Pathology Laboratories

The Cardiac Risk in the Young Cardiovascular Pathology Laboratories (CRY-CPL) laboratories are located at St George's, University of London and are uniquely funded by the charity Cardiac Risk in the Young (CRY) as a national referral centre to establish the cause of SCD. The charity receives donations from the bereaved families of individuals experiencing SCD. The laboratories receive hearts from suspected SCD cases referred from across the United Kingdom. We have now established a unique national database with clinical details of all cases. The database has been built and originally customised for use as an SCD registry in collaboration with Dendrite Clinical Systems (Reading, United Kingdom). There is now an established pathway for referral with detailed documentation that is sent to referrers consisting of blank forms for the deceased details, referrer's detail's including coroner and pathologist, relative's tissue wishes (retention or return), and a family questionnaire (see figure 2.1 and supplementary material). There are also instructions on specimen preparation.

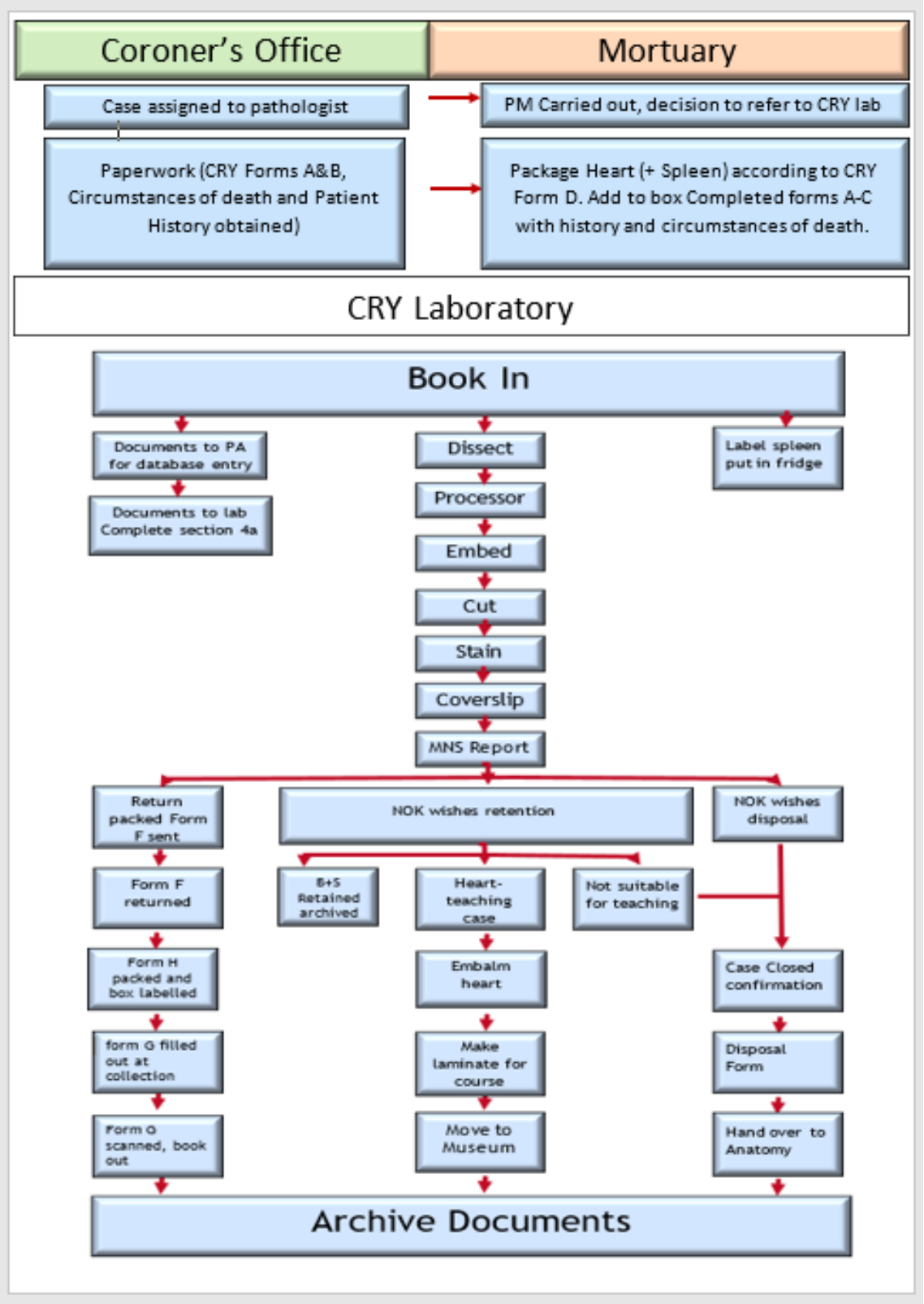


Figure 2.1. The pathway to and through the CRY laboratory. Cases are sent with filled CRY documents and then booked in and processed through the lab according to next of kin (NOK) wishes.

Clinical data collection

The heart referrals to the CRY-CPL Laboratory are accompanied by circumstances of death, primary care correspondence, clinical notes, coroner's history sheets, post mortem reports and family questionnaires. These are reviewed and all relevant information is entered onto the CRY national cardiovascular database.

The CRY national cardiovascular database

Data entry

A unique CRY number is generated for each incoming case; the accompanying patient related documents are scanned and saved as a PDF on the CRY drive. The database is on a secure St George's, University of London server and requires a username and password for access (figure 2.2).



Figure 2.2. Database entry point. Username and password are required for access.

A new patient is added to the system and the patient demographics are entered into section 1. The coroner's and referring pathologists' details are entered in section 2. The scanned documents are uploaded to section 2 of the database (figure 2.3).

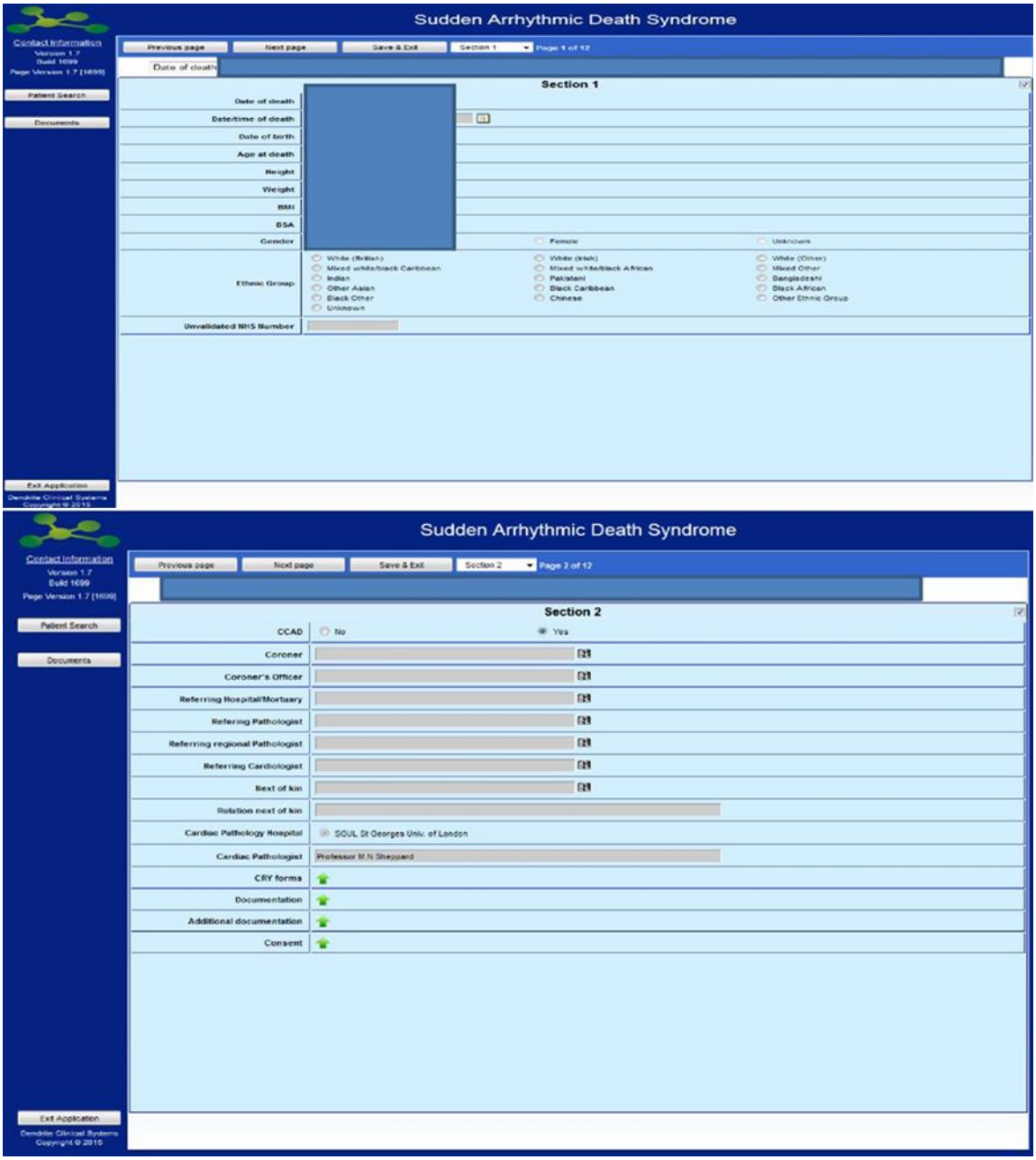


Figure 2.3. Sections 1 and 2 of the database. Demographics, details of coroners and referring pathologists are entered here. PDF documents are uploaded.

Clinical information and history as highlighted by the referring pathologist are entered in section 3. On section 4a, the details regarding return or retention of specimen are entered (figure 2.4).

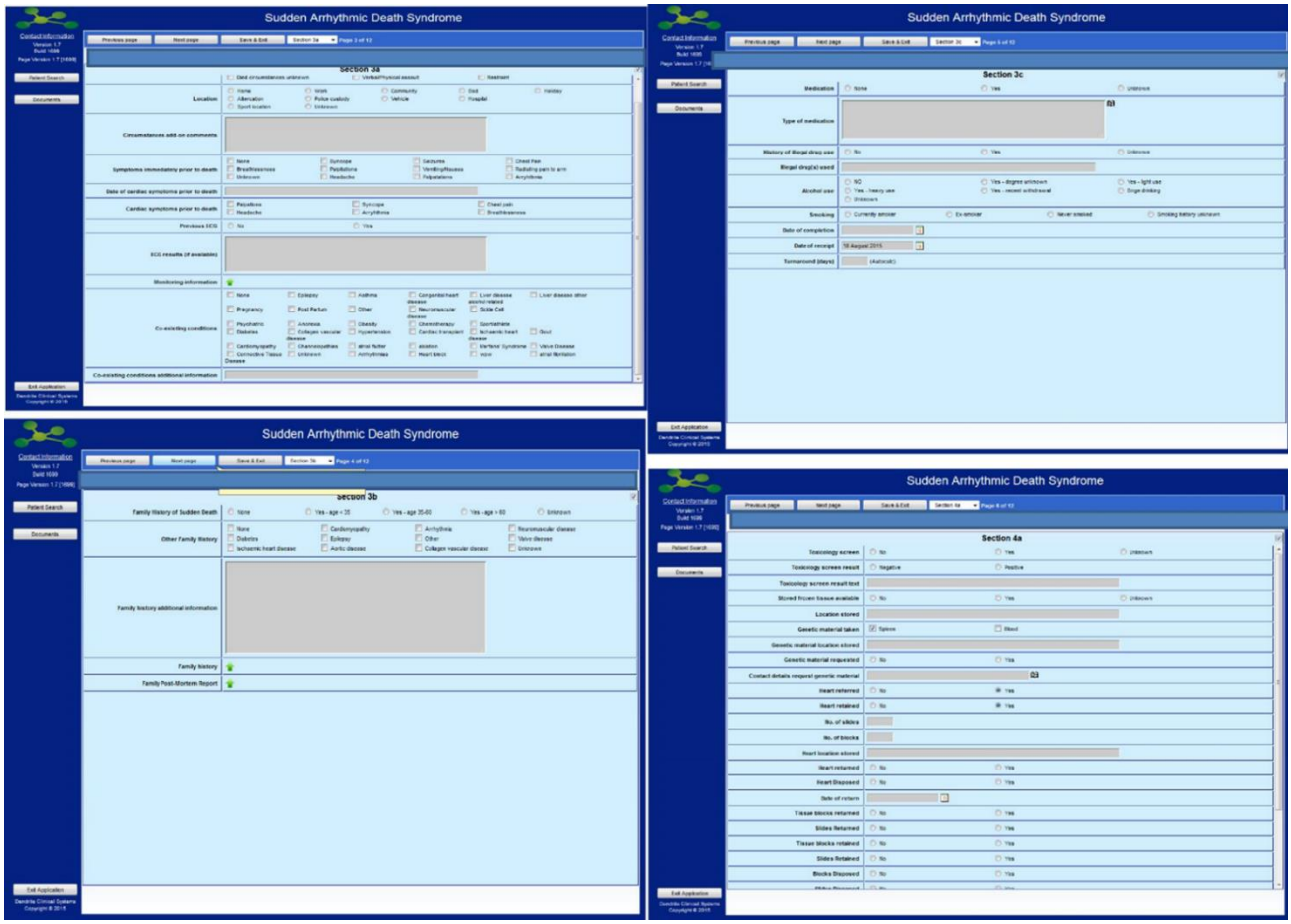


Figure 2.4. Sections 3a, b and c and section 4 contain past history and tissue retention details. Section 3 has details of symptoms, past medical history, medication, smoking, alcohol and drug use, as well as family history.

At cut-up, all macroscopic information about the coronary arteries, right and left side of the heart are entered in sections 4b-d. The pathologist will provide measurements and gross descriptions of the specimen. Macroscopic pictures taken at the cut-up are uploaded into the laboratory pictures folder in a new folder created for that unique CRY ID. The case is microscopically examined by the pathologist and a microscopic description, cause of death and final comment is entered in sections 4e and comments filled in. A letter or PDF report is sent to the referring coroner and pathologist.

Data extraction

To extract from the database, Cohort Manager is selected from the main menu, then export is selected. A new export based on sudden arrhythmic death syndrome registry is created (figure 2.5).

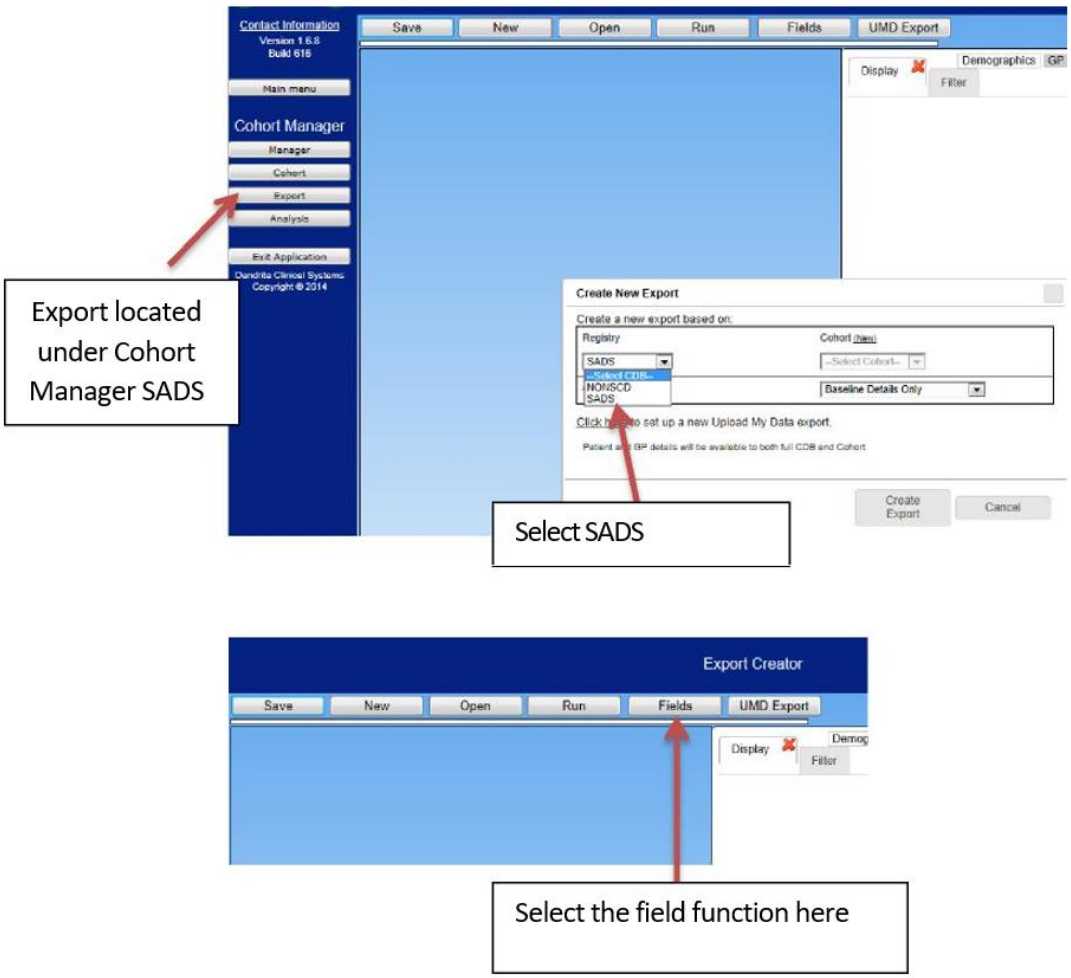


Figure 2.5. Cohort manager is used for extraction of the information on entered on the database. The different parameters can be selected for extraction once the baseline field has been selected.

All information required for the extraction is included by clicking on relevant boxes (for example: age at death, final diagnosis). If desired a filter may be applied to the

different parameters. When selecting coded entries, ensure to click the X and change the single choice format from code to description (figure 2.6).

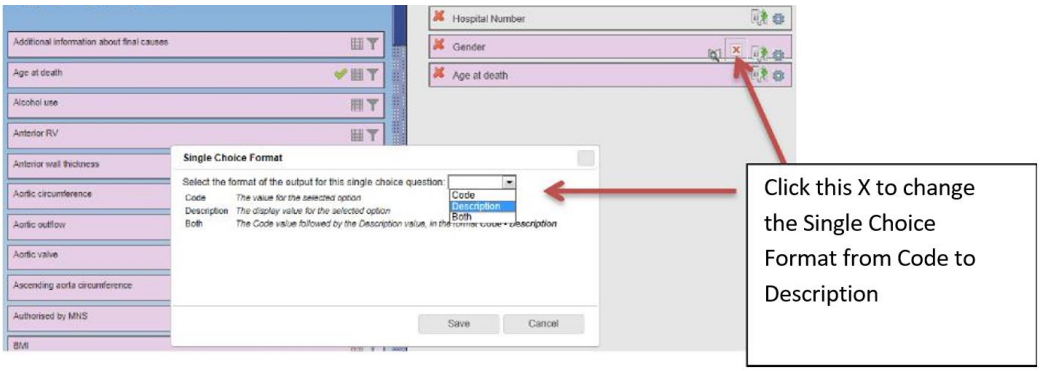


Figure 2.6. Selection of the parameters for extraction under the baseline field. For descriptive parameters the output must be changed to description.

The export is then saved under an appropriate name. The programme will then prompt you to run the export. Click the link to save the file by right clicking, save target as and adding .csv to the file name to save it as an excel file (figure 2.7).

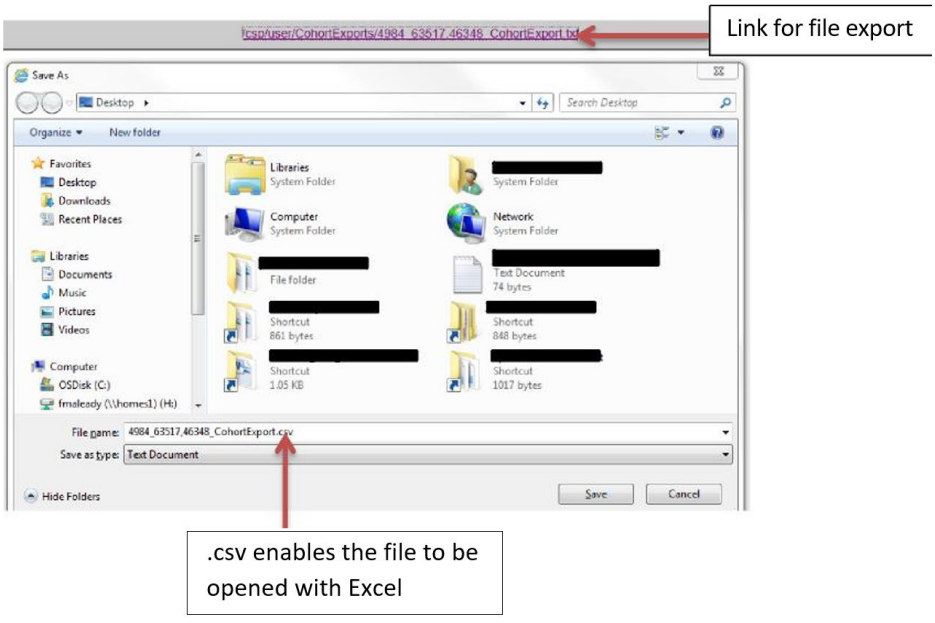


Figure 2.7. A comma separated values excel spreadsheet is created with the relevant data sorted into columns. The link is clicked to extract the file from the database.

Gross anatomical methods

Macroscopic pathological examination

This technique has been developed by Professor Sheppard to examine the hearts that come to the department. All hearts are looked at externally for pericardial thickening, adhesions, fibrinous pericarditis, rupture or infarction. The great vessels are examined to establish normal positioning and for evidence of aortic dissection. The coronary arteries are sliced at 2-3 mm intervals to look for evidence of disease such as significant atheroma, thrombosis or dissection in all branches. All branches should be examined down to the apex of the heart.

The atria are opened before looking at the ventricles. The atria are opened up into the appendages. We measure the right atrium between the entrance of the superior and inferior caval vein longitudinally and transversely from the entry of the inferior vena cava to the tip of the right atrial appendage. Then we look down to check the tricuspid valve morphology to look particularly for evidence of endocarditis, rupture or congenital abnormalities such as Ebstein. The interatrial septum and fossa ovalis are checked for patency and an atrial septal defect. The left atrium is measured transversely between the left and right superior pulmonary veins and longitudinally from the atrioventricular junction to the superior edge. Then the mitral valve is examined for evidence of prolapse up into the left atrium with ballooning or thickening or cordal rupture.

Once the atrioventricular valves are described, then we slice the ventricles transversely from the apex to mid ventricle at 5mm intervals. The slices are examined for pathology such as hypertrophy, fatty infiltration, fibrosis and infarction. Lesions can be focal so all levels should be examined carefully. Once the ventricles are described, then measurements can be made at the midventricular level halfway

between the atrioventricular junction and the apex of both ventricles. The cavity diameters are measured transversely excluding the trabeculae and papillary muscles. The muscle thickness and subepicardial fat of each ventricle is measured in the anterior, lateral and posterior walls along with the IVS. In addition, the right ventricular outflow tract (RVOT) is measured 10mm below the pulmonary valve. The subepicardial fat should exclude fat around the coronary arteries where it is always prominent. The presence or absence of fibrosis, infarction, or fat in the myocardium is commented on.

Once the atrioventricular valves are assessed as normal the atria are opened laterally extending through each valve down to the midventricular slice already made. Each atrium can then be looked at in detail and each appendage checked for thrombi. Both atrioventricular valves can be examined in detail and the annuli measured. The lateral LV cut usually separates the anterolateral and posteromedial papillary muscles on either side. In the RV, the trabeculae are prominent and the moderator band extends from the IVS to the free wall laterally. The papillary muscles are not as prominent as in the LV but usually there is anterior, septal and posterior muscle of variable size with attached cords.

The pulmonary valve is checked by inserting a finger up into the outflow tract. We then open anteriorly through the RVOT into the main pulmonary artery and examine for thrombi. The aortic valve is checked also by inserting a finger up into the outflow tract and seeing three leaflets before cutting through the middle of the anterior leaflet of the mitral valve out through the aorta. Both ventriculoarterial valves are measured at commissure insertion of all three leaflets to define the annulus of each. They are examined for calcification, fusion, thickening, thrombosis, perforations, ballooning and vegetations. The coronary artery ostia are examined in each sinus carefully for

anomalous origin. The ascending aorta is examined for evidence of dilatation, intimal atheroma thickening or dissection and the circumference is measured 20 mm above the valve.

Following removal of any clot and attached aorta, the heart is weighed. Blocks are taken for histology routinely from the midventricular slice to include anterior, lateral (including right atrium right coronary artery and atrioventricular junction) and posterior RV as well as the RVOT, 10mm below the pulmonary valve. Blocks are taken from the anterior, lateral (including left atrium, circumflex coronary artery and atrioventricular junction) and posterior LV as well as the anterior and posterior IVS. Normally, 7 -10 sections are examined. Sections of conduction tissue are also sampled routinely. Normally, 10-12 sections are examined. More blocks will be taken if specific pathology is found (figure 2.8).

Heart blocks protocol

Mary N Sheppard

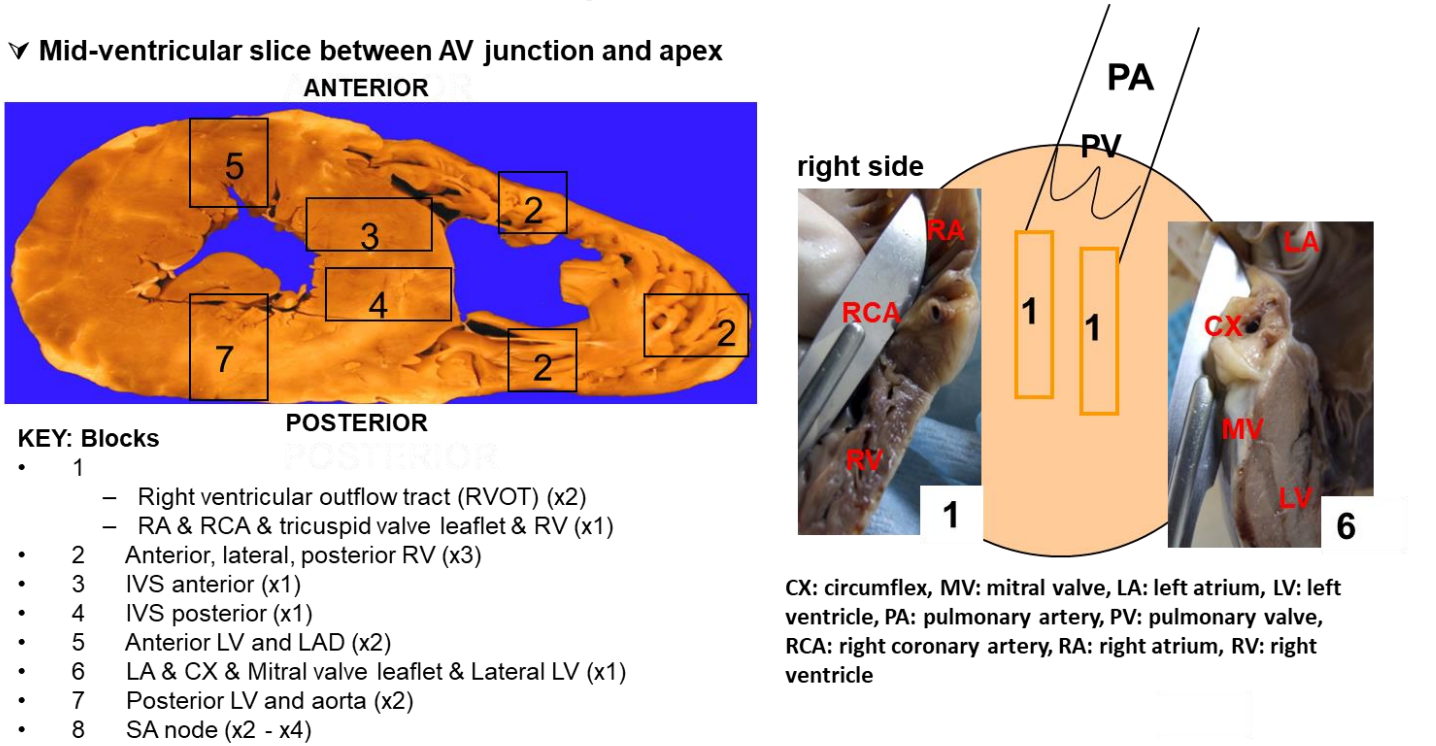


Figure 2.8. Blocking protocol from the CRY cardiovascular pathology laboratories. Ten blocks of tissue are taken as standard.

Methods for preparation of microscopic slides

Tissue Processing

Following dissection, the cassettes are placed in 10% formalin. They are then transferred into a chamber in a tissue processor which runs overnight. The tissue processor exchanges liquids within a temperature and pressure-controlled chamber. The chamber is filled with formalin until the process is ready to begin. Paraffin wax is hydrophobic therefore prior to its addition the water must be removed. A graded series of alcohols are used to remove the water from the specimen without distorting the tissue. Alcohol and wax are largely immiscible therefore the next step is the addition of an intermediate solvent called Xylene. Xylene replaces the alcohol in the specimen. Xylene also acts as a “clearing agent” providing optical clarity to the tissue and removing fat. The specimens can then be infiltrated with heated liquid paraffin wax. The wax is then cooled where it solidifies allowing highly accurate and reproducible sectioning utilising a microtome.

Steps:

Embedding

Following wax infiltration, the specimen must be formed into a block. The specimen is placed in a metallic mould which is subsequently filled with heated liquid paraffin wax. The specimen is pressed into the base of the moult in the orientation desired as the wax slowly solidifies. The wax is then topped up and a cassette is placed on top. The mould is then placed on a cold plate to solidify. The cassette and attached block are then removed from the mould ready for sectioning.

Sectioning

The blocks are then cooled on a cold plate. They are then placed in a microtome and trimmed at 10μm until the entire surface of the specimen can be visualised. The blocks are placed back on the cold plate prior to sectioning at 5μm using the microtome. The sections form ribbons which may then be floated out in a heated water bath. This is done by dragging the ribbon across the bath to eliminate folds. The sections are separated using forceps and the surplus sections are discarded. The remaining tissue section is then floated onto a glass slide. Selection of the type of glass slide is dependent on the planned application. Standard glass slides may be used for haematoxylin and eosin staining as well as tinctorial stains whereas adhesive poly-l-lysine slides are preferred for immunohistochemistry to prevent tissue loss.

Haematoxylin and Eosin Staining

The slides are placed on a hot plate for 10 minutes to melt the wax. The sections are then made aqueous by immersion through graded alcohols and finally water. They are then immersed in haematoxylin which stains the nuclei a purple colour. The slides are then washed in water and differentiated by repeatedly dipping in acid alcohol. This removes the haematoxylin from the cytoplasm leaving crisp nuclear staining. A further wash in water is performed before using Scott's tap water to blue the haematoxylin gently and minimise loss of tissue. The sections are then counterstained with using 1% eosin. Eosin stains the cytoplasm a pink colour. The slides are then washed with water and dehydrated using graded alcohols. This stain allows good appreciation of sampled organ structure and cellular morphology.

Picrosirius red stain

The slides are placed on a hot plate for 10 minutes to melt the wax. They are then made aqueous by immersion through graded alcohols and finally water. Slides are immersed in Weigert's haematoxylin and then washed with water. They are then placed in picro-sirius red for one hour. This stains collagen red and myocytes yellow. The haematoxylin stained nuclei appear grey/black following this step. The slides are then washed in acidified water and dehydrated using graded alcohols. This stain specifically highlights collagen content of myocardium and allows it quantitation as it is easily differentiated from the other myocardial components. The use of acidified water instead of water reduces the washout of dye (Kiernan, 2013, 2015). Picrosirius red marks more collagen than other methods such as Masson's trichrome (Rich and Whittaker, 2005; Huang *et al.*, 2013).

Immunohistochemistry

For immunohistochemistry, the sections are placed onto positively charged Superfrost glass slides which attract and adhere the tissue sections. Following drying or at a later date, these slides are placed on the hot plate to melt the wax. The sections are deparaffinised using xylene and then rehydrated using graded alcohols followed by distilled water. The aqueous slides are then washed in phosphate buffered saline.

For antigen retrieval, the slides are incubated in citrate buffer at a temperature of 92-94˚C for 20 minutes.

Following cooling, the slides are washed with distilled water and then phosphate buffered saline. Bovine serum albumin and then hydrogen peroxide are used to prevent background staining by blocking non-specific binding sites and endogenous

peroxidase activity respectively. The slides are then rinsed with phosphate buffered saline followed by bovine serum albumin. A hydrophobic Pap pen is then used to create a water barrier circle around the tissue section. The slides are placed in a humidity chamber and then covered with a further blocking buffer composed of normal serum from the species used for the secondary antibody (figure 2.9).

The slides are then incubated in a primary antibody solution diluted in the blocking buffer within the humidity chamber overnight.

The next day, the slides are washed with phosphate buffered saline and then with bovine serum albumin. A biotinylated secondary antibody is then diluted in the blocking buffer and used to bind to the primary antibody.

The slides are then washed with phosphate buffered saline and then bovine serum albumin. Avidin-biotin complex reagent is then added. This binds to the biotinylated secondary antibody providing more binding sites for the chromogen.

The slides are then rinsed with trisaminomethane buffer. A chromogen (ImmPACT VIP, Vector Laboratories) that produces an intense violet colour is then added to the slides. To halt colour development, the slides are then rinsed with distilled water.

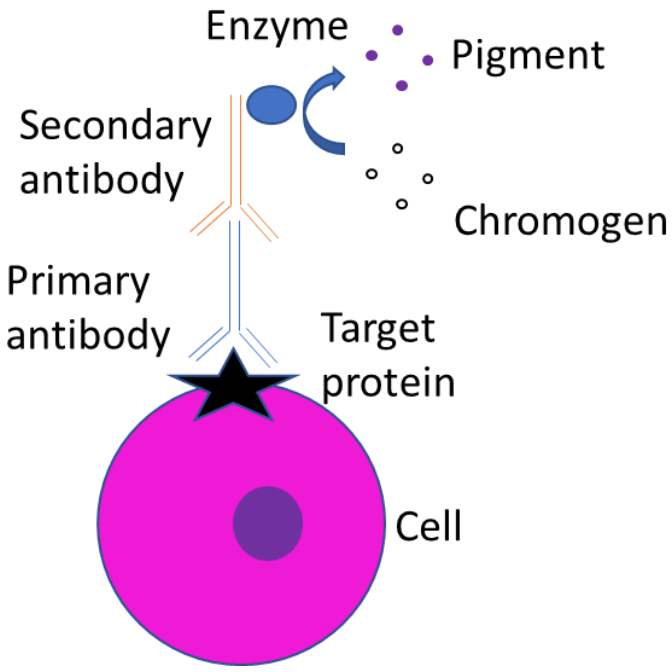


Figure 2.9. Immunohistochemistry method. A specific primary antibody is directed towards a cellular target protein. A secondary antibody with an enzyme attached binds the primary antibody. This enzyme then metabolises a chromogen or substrate to form a pigmented reaction product.

Sections are then counterstained with methyl green providing excellent contrast against violet. Slides are then rinsed with distilled water and then dehydrated using graded alcohols.

Antibodies

Details of the antibodies that have been used are in table 2.1.

Antibody	Company	Species	Ref	Optimal dilution
PGP9.5	Abcam	Rabbit monoclonal	ab108986	1:1500
Tyrosine hydroxylase	Abcam	Mouse monoclonal	ab129991	1:1500
Choline Transporter	EMD Millipore	Mouse monoclonal	MAB5514	1:2000

Table 2.1. Antibodies. The details of the antibodies used, including company producing the antibody, host species and reference number.

PGP9.5 is general neural marker (Marron *et al.*, 1994), TH marks sympathetic nerves (Marron *et al.*, 1994) and the choline transporter (CT) marks parasympathetic nerves (Misawa *et al.*, 2001; Kapur *et al.*, 2017). Whilst, PGP9.5 and TH stain in a uniform pattern along nerves, CT produces a granular pattern (Kapur *et al.*, 2017) which means that whilst the results can be compared between controls and cases, but comparisons between CT and the other stains are not possible.

Mounting

Following the different staining procedures described above, the sections are immersed in xylene and coverslipped utilising mounting medium. They mounted slides are left to dry in a fume hood and then cleaned using both xylene to remove additional mountant and alcohol as it dries fast and doesn't leave streaks.

Quality check

Following cleaning, the slides are quality checked for air bubbles and imperfections. Cases that do not meet the required standard are recleaned, re-coverslipped or restained with a new section as needed.

Staining optimisation

The staining protocol has been optimised. Antigen retrieval using a heated water bath has been used to minimise tissue loss which is a significant issue when using a microwave or a pressure cooker. Multiple blocking steps have been used to minimise background staining including the use of bovine serum albumin, hydrogen peroxide and species-specific serum. The avidin-biotin complex has been used to increase signal. A trisaminomethane buffer has been used to give a violet colour allowing differentiation from background erythrocytes, formalin pigment and lipofuscin. Individual antibodies have been optimised for time applied to tissue and concentration. This is achieved by running five serial dilutions from 1:100 to 1:1000 in the first instance and increasing or decreasing concentration as necessary. This is followed by five developing times varying from 10 seconds to 1 minute and adjusting up or down as necessary. This is done to ensure well developed staining with minimal background. A background methyl green stain has been used to provide the best contrast to the violet staining. The process has been run numerous times to identify and negate any potential issues with automated digital image analysis. The sinus node has been used as a positive control and omission of the primary antibody has been used as a negative control.

Microscopic examination

Microscopic analysis and diagnostic categorisation

The slides are then placed under the microscope to allow microscopic examination. Morphology is primarily assessed using haematoxylin and eosin stain. Fibrosis is assessed picro-sirius red stain. The following are a guide to the pathological features of different diseases resulting in SCD that have been developed by Professor Sheppard within the CRY cardiovascular pathology department and have been used to develop both national and international guidelines (Sheppard and Survana, 2015; Basso *et al.*, 2017; Sheppard, 2022) (table 2.2):

Pathology	Macroscopic Criteria	Microscopic Criteria
Hypertrophic cardiomyopathy	Left ventricular wall thickness >15 mm and/or increase in heart weight[ł].	Left ventricular myocyte disarray* (>20% of myocardial disarray in at least 2 cardiac sections) and myocyte hypertrophy with or without interstitial or replacement fibrosis and thick-walled blood vessels.
Arrhythmogenic cardiomyopathy	Right or left ventricular thinning, fatty replacement, fibrosis on the epicardial surface. Absence of coronary artery disease.	Fibrosis admixed with fatty infiltration of the myocardium originating from the epicardial surface (>20% in at least 2 cardiac sections).
Dilated cardiomyopathy	Increase in heart weight[ł] with dilated left ventricle (>40mm) and thin wall (<10mm). Absence of coronary artery disease.	Widespread diffuse interstitial or replacement fibrosis (>20% in at least 2 cardiac sections) in the left ventricle with atrophic myocytes.
Morphologically normal heart	Normal.	Normal.
*Myocyte disarray at the anteroseptal and posteroseptal junction is a normal finding. [ł] Increased heart weight is defined as >400g in females and >500g in males.		

Table 2.2. Pathological macroscopic and microscopic criteria used to assess for cardiac conditions leading to sudden cardiac death.

Terminology used to describe the layers of the heart on histology

The heart may be subdivided into a number of different layers when viewed histologically. There is a rim of mesothelium on the outside of the heart which is underlain by fibrous connective tissue which is referred to as the epicardium. Underlying the epicardium, there may be a layer of subepicardial fat or adipose tissue. The myocardium either lies inside of the subepicardial fat or directly abuts the epicardium. The myocardium may be broken down into the outer half and the inner half. The trabeculae and papillary muscles form part of the inner half. On the inner surface there is a rim of endothelium which is underlain by fibrous connective tissue which is referred to as the endocardium. A diagram of the layers of the heart is shown in figure 2.10.

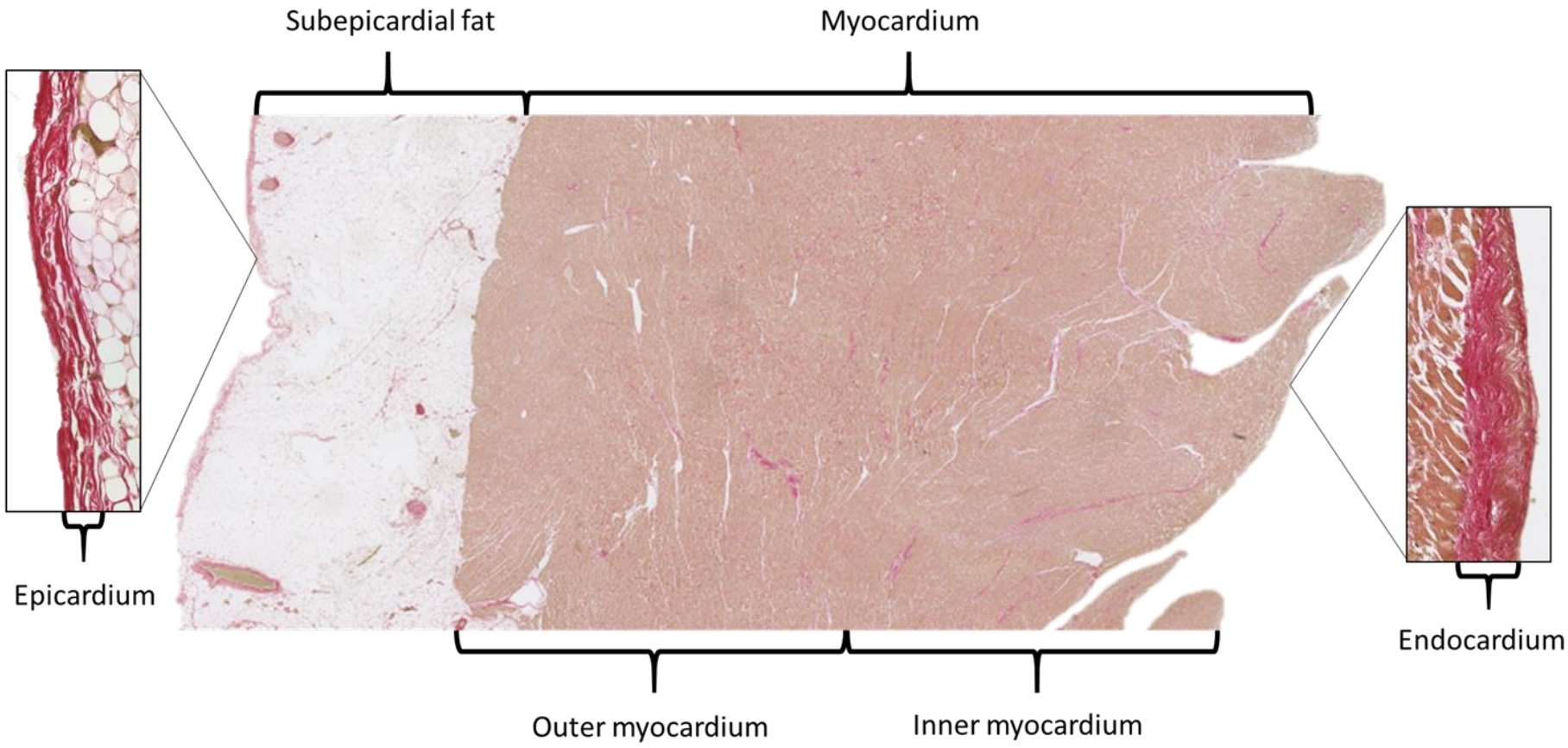


Figure 2.10. A picrosirius red stained section showing the different layers of the heart.

Slide Scanning

Digital imaging is performed using an automated Hamamatsu high resolution slide scanner (Hamamatsu Nanozoomer 2.0 RS, Hamamatsu, Japan). A colour threshold detection system has been optimised to specifically detect the tissue highlighted by the methyl green counterstain. The scanner then highlights this tissue and automatically assigns evenly distributed auto focus points within regions of interest. Slides are then scanned at 40X magnification. The system allows the generation of high-resolution images of the entire slide at high resolution (figure 2.11).



Figure 2.11. The Hamamatsu Nanozoomer 2.0 RS slide scanner. The slides are loaded into the tray and then autonomously scanned into digital images using the NDP.scan software.

Morphometric quantification

Automated and blinded quantification of histological staining is performed using Visiopharm (Visiopharm, Denmark). An imaging software application is utilised to enable automated selection of tissue area through colour thresholds along with size

and shape analysis. This tissue area is subsequently analysed using an application to identify specific regions of interest.

The collagen quantification application has been adapted from our previous method which was published (Miles *et al.*, 2020) (figure 2.12). The first step is based on colour threshold analysis using two filters which identifies the myocytes and collagen. Shape analysis is then performed to identify circular adipocytes from airspaces.

Interstitial fibrosis is defined as an accumulation of collagen around and encircling myocytes producing a mesh-like configuration. Replacement fibrosis is defined as a patch of continuous collagen in an area where myocytes would be expected.

The immunohistochemical staining protocol described above allows specific selection of violet stained neural structures allowing their differentiation from background confounders (figure 2.13). The application has been developed over time using numerous images and trial and error using multiple colour filters to select thresholds which ensure specific selection of violaceous staining whilst excluding other colours. Following the selection of the described regions of interest a stained area are obtained for each component.

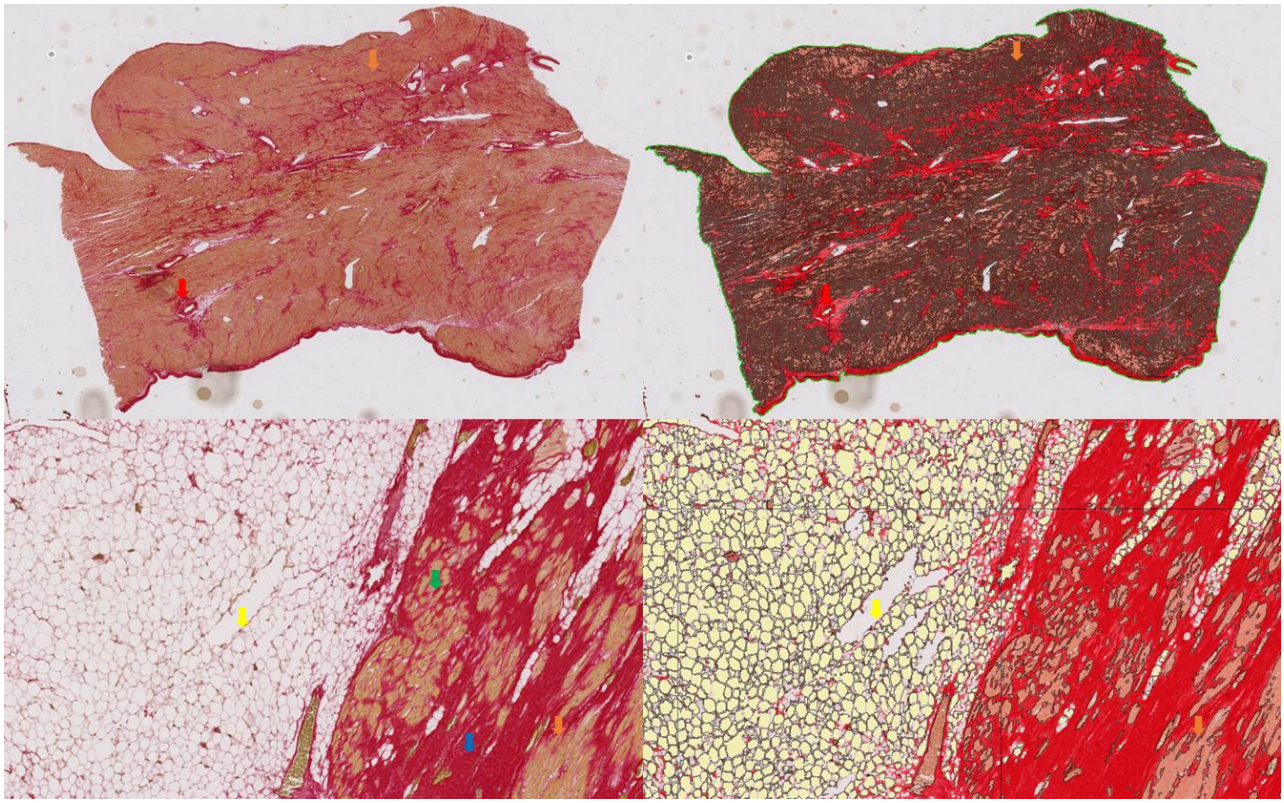


Figure 2.12. Picrosirius red stained section highlighted by the application in Visiopharm. The tissue is selected by an application and highlighted with a green line. The components of the tissue are then highlighted with darker red selecting the collagen (red arrow), lighter red selecting the myocytes (orange arrow) and yellow selecting the adipocytes (yellow arrow). Examples of interstitial fibrosis are shown by the green arrow and replacement fibrosis by the blue arrow.

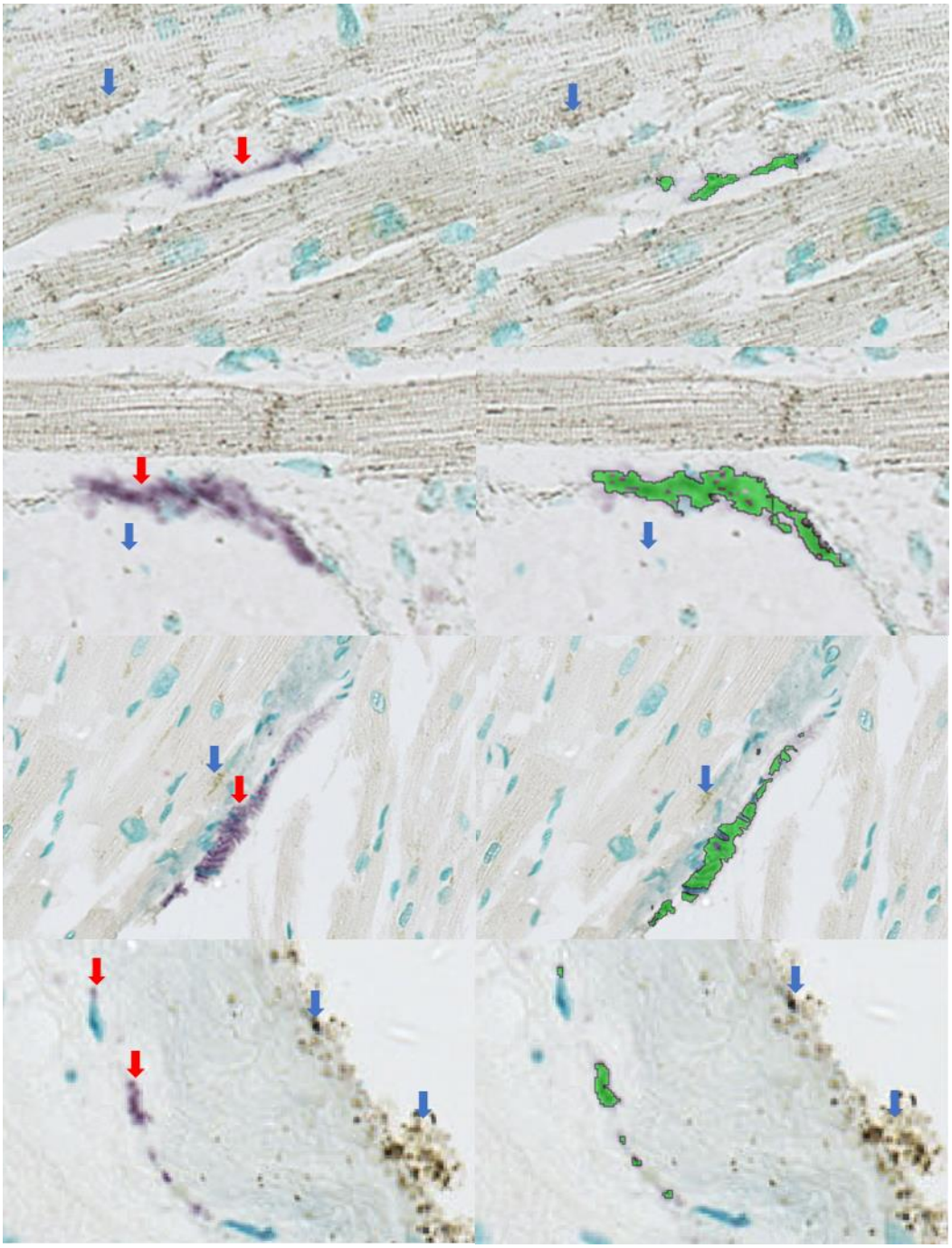


Figure 2.13. Visiopharm morphometric selection. The left panels show stained neural structures (red arrows) and background confounders (blue arrows). The right panels show Visiopharm selecting the PGP9.5 stained nerves (green) but not the background confounders (blue arrows). Excluded confounders are blood, lipofuscin, formalin pigment and contaminants.

Statistical analysis

All the variables have been explored and summarized according to their statistical type; categorical and binary data as frequencies and percentages, and continuous data as means, standard deviations, medians, first and third quartiles, and ranges. Two-sided T-test is used to compare normally distributed continuous variables. The Chi-square test is used to assess independency between two categorical variables with Fisher's exact test used when cross tabulations exhibited numbers smaller than 5. The Kruskal-Wallis test has been uses to assess non-normally distributed or ordinal variables.

Differences in myocardial composition between groups are assessed on actual proportional values for collagen and log transformed fat and myocyte proportions (as these values are skewed). A multilevel model is created to allow comparison of hierarchical dependent data based on myocardial location. Variables such as age, gender and ethnicity are incorporated into multivariable analysis. Predictions of collagen are expressed as arithmetic mean. Predictions of fat, myocytes, PGP9.5, TH and CT are expressed as geometric means. The structure of the hierarchical data within the multilevel model is shown in figure 2.14.

Statistical analyses used Stata version 16 (StataCorp, College Station, Texas, USA).

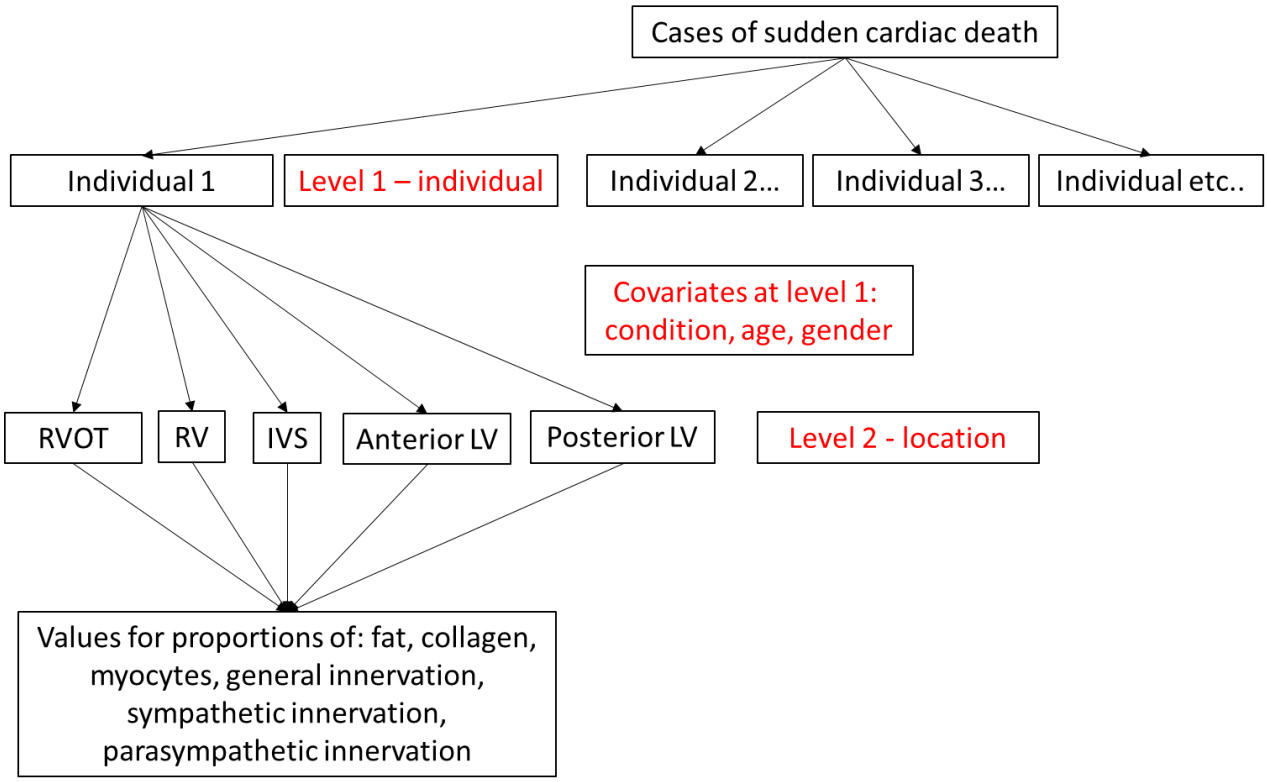


Figure 2.14. Structure of the data within the multilevel model. Locations included the right ventricular outflow tract (RVOT), the right ventricle (RV), the septum (IVS) and left ventricle (LV).

Bias

Multiple steps have been taken to eliminate bias within the study. Diagnoses have been reviewed by a panel including Professor Sheppard and Dr Westaby prior to inclusion in the study. Deidentification numbers are assigned to cases. Random number generation has been used to select both cases and slides to eliminate any selection bias. Scanning and image analysis has been performed blinded to diagnosis. Image analysis has been performed by a calibrated and optimised automated system.

Standards

Autopsies are performed according to the standards set out by the Royal College of Pathologists of the United Kingdom (https://www.rcpath.org/profession/guidelines/autopsy-guidelines-series.html) including the guideline for sudden death with likely cardiac pathology (Sheppard and Survana, 2015). Cardiac examination is carried out in line with the Association for European Cardiovascular Pathology guidelines for autopsy investigation of SCD (Basso *et al.*, 2017).

Case selection

From a total library of 931 cases, 11 cases of deaths with morphologically normal heart and a lethal level of drugs found on toxicity, 20 cases of ACM, 11 cases of DCM and 17 cases of HCM with retained tissue were selected (figure 2.15). Sections have been taken from the RVOT, RV, IVS, anterior and posterior LV for each case.

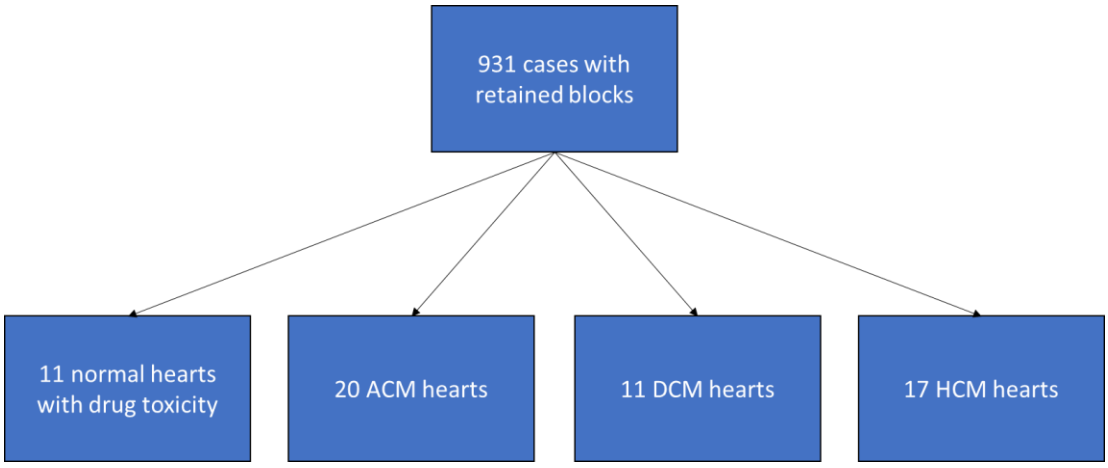


Figure 2.15. The selection of the retained tissue blocks from 931 retained cases of sudden cardiac death.

CHAPTER 3 OVERALL DATABASE

Introduction

SCD is a devasting and tragic event. SCD refers to an unexpected death of cardiovascular cause within one hour of the development of symptoms if witnessed or within 24 hours of last being seen well if unwitnessed ('Sudden cardiac death. Report of a WHO Scientific Group', 1985). Previous studies from around the globe have shown considerable variance in estimation of SCD rates with a range of 6-20% of all deaths and occurring with an incidence between 11-180 per 100,000 person years (Priori *et al.*, 2002; Kong *et al.*, 2011; Myerburg and Junttila, 2012; Stecker *et al.*, 2014; Wong *et al.*, 2019; Lynge *et al.*, 2021).

In the United Kingdom, SCD is estimated to cause 70,000 deaths per annum giving a rate of 113 per 100,000 person years (National Institute for Health and Care Excellence, 2014).

Professor Mary N Sheppard has been involved in the pathological investigations of SCD since the mid 1990's with her mentor, Professor Michael Davies, at St George's Hospital. Professor Davies assisted Donald Teare in his first description of hypertrophic cardiomyopathy (Teare, 1958) and elucidated the concept of plaque instability (Davies, 1996; Mills and Hall, 2003).

Previous studies from the United States and Denmark had identified thrombosis, ischaemia and infarction as the predominant causes of SCD (Schwartz and Gerrity, 1975; Voigt, 1976; Reichenbach, Moss and Meyer, 1977). Professor Davies was the first to investigate the causes of SCD in the United Kingdom (Davies and Popple, 1979). He built up an international reputation with an extensive practice providing second opinions on hearts with an internationally recognised and reputed slide collection (Mills and Hall, 2003).

In 2003, Professor Sheppard worked with him on a study of sudden, unexpected cardiac or unexplained death from coroners around England and found that, as other studies did, ischaemic heart disease made up 82.4% of cases. They identified a cohort comprising 4.1% with no clear cause of death. They suggested this was labelled as sudden arrhythmic death syndrome to highlight and increase awareness of this condition (Bowker *et al.*, 2003). As a result of this Professor Sheppard started to receive cases of SCD that were non-ischaemic as pathologists found they were a challenge, particularly the new concept of SADS. This resulted in a further report specifically looking at sudden adult death syndrome and non-ischaemic causes of sudden death. In 302 cases, morphologically normal hearts were found in 59.3% indicating that this entity was the most common cause of non-ischaemic sudden death in the UK (Fabre and Sheppard, 2006).

With the development of this referral practice, the charity, CRY, funded Professor Sheppard to establish a specialist referral centre for SCD. This was to facilitate fast-track expert cardiac pathology opinion for bereaved families.

The referral centre is based at St George's, University of London where this project has been undertaken.

<u>The Cardiac Risk in the Young Cardiovascular Pathology Laboratories</u>

The CRY-CPL laboratories, located at St George's, University of London, are uniquely funded as a national referral centre to establish the cause of death. The laboratories receive hearts from suspected SCD cases referred from throughout the United Kingdom. We have now established a unique national database with clinical and pathological details of all cases.

Aim

Using the established database, we aim to present the underlying causes of SCD from the CRY-CPL laboratories which receive referrals from throughout the United Kingdom. This is the largest SCD cohort ever published. The cases have all undergone post mortem examination and specialist cardiac evaluation.

Methods

Cardiac dissection and examination

The hearts are dissected and examined according to the method presented in chapter 2. The following is a brief summary. The heart is weighed following the removal of any blood clot. The coronary arteries are sliced at 2-3mm intervals to look for evidence of coronary artery disease. In cases with stenosis, a 2mm probe is used to assess the significance. Both atria are opened and the cavities and appendages are inspected for thrombi. The atrioventricular valves are inspected from the atrial aspect and assessed for patency. The heart is sliced transversely from the apex to the mid ventricle at 5mm intervals. The presence or absence of fibrosis, infarction, or fat in the myocardium is commented on. The atrioventricular chambers are opened laterally through the atrioventricular valves allowing visualisation of the four chambers and the atrioventricular valves. The semilunar valves are assessed for patency from the ventricles. The RVOT is opened through the pulmonary valve anteriorly. The LV outflow tract is opened through the anterior leaflet of the mitral valve. The ostia of the coronary arteries are inspected to examine for anomalous origin.

Cardiac sections

Blocks are taken for histology routinely from the anterior, lateral and posterior RV, the RVOT, the anterior, lateral and posterior LV as well as the IVS. Sections of coronary artery, atria and conduction tissue are also sampled routinely. Normally, 10 sections are examined though more blocks will be taken if specific pathology is found. Significant stenosis or thrombosis of the coronary arteries is serially sectioned for histological analysis if observed. Following processing of the blocks, the slides are stained with haematoxylin and eosin. A picrosirius red is used to highlight fibrosis, if required.

Diagnostic criteria

Table 3.1 shows the diagnostic criteria that we have developed and are used to assess for the major diseases that underlie SCD. Whilst these features are of great assistance in identifying pathology, their absence does not necessarily exclude the corresponding condition.

Pathology	Macroscopic Criteria	Microscopic Criteria
Hypertrophic cardiomyopathy	Left ventricular wall thickness >15 mm and/or increase in heart weight[†].	Left ventricular myocyte disarray* (>20% of myocardial disarray in at least 2 cardiac sections) and myocyte hypertrophy with or without interstitial or replacement fibrosis and thick walled blood vessels.
Arrhythmogenic cardiomyopathy	Right or left ventricular thinning, fatty replacement, fibrosis on the epicardial surface.	Fibrosis admixed with fatty infiltration of the myocardium originating from the epicardial surface (>20% in at least 2 cardiac sections).
Dilated cardiomyopathy	Increase in heart weight[†] with dilated left ventricle (>40mm) and thin wall (<10mm).	Widespread diffuse interstitial or replacement fibrosis (>20% in at least 2 cardiac sections) in the left ventricle with atrophic myocytes.
Idiopathic left ventricular hypertrophy	Left ventricular wall thickness >15 mm and increase in heart weight[†].	Myocyte hypertrophy with or without replacement or interstitial fibrosis. Absence of myocyte disarray.
Idiopathic left ventricular fibrosis	Normal heart weight and wall thickness with/without scarring macroscopically.	Replacement or interstitial fibrosis (>20% in at least 2 cardiac sections). Absence of myocyte disarray.
Hypertensive heart disease	Left ventricular wall thickness >15 mm and increase in heart weight[†].	Myocyte hypertrophy with fine interstitial fibrosis. Absence of myocyte disarray.
Obesity cardiomyopathy	Left ventricular wall thickness >15 mm and increase in heart weight[†].	Myocyte hypertrophy with or without replacement or interstitial fibrosis. Absence of myocyte disarray.
Myocarditis	Normal or dilated ventricles with variegated appearance.	Inflammation (>20% in at least 2 cardiac sections) with associated myocyte necrosis.
Coronary atherosclerosis	Atherosclerosis with luminal narrowing >75%. Inability to insert 2mm probe. Infarction or scarring.	Acute or chronic infarction.
Anomalous coronary artery	Anomalous origin of the coronary artery in the incorrect sinus, coronary artery atresia or congenital stenosis.	Acute or chronic infarction in the left ventricle.
Mitral valve prolapse	Prolapse of mitral valve above the atrioventricular junction with ballooning between chordae in one or both leaflets.	Myxoid degeneration with expansion in spongiosa of leaflets and destruction of fibrosa layer.

Aortic stenosis	Significant valve stenosis demonstrated by inability to insert a finger through the annulus, increase in heart weight[ł] and left ventricular wall thickness >15mm.	Myocyte hypertrophy and/or interstitial or replacement fibrosis.
Bicuspid aortic valve	Fusion of 2 aortic cusps, with or without presence of a raphe with significant valve stenosis and left ventricular wall thickness >15mm and increased heart weight[ł].	Calcification and degeneration of the valve leaflets. Myocyte hypertrophy with or without interstitial or replacement fibrosis.
Morphologically normal heart	Normal.	Normal.
*Myocyte disarray at the anteroseptal and posteroseptal junction is a normal finding. [ł] Increased heart weight is defined as >400g in females and >500g in males.		

Table 3.1. Pathological Macroscopic and Microscopic Criteria used to assess for the cardiac conditions leading to sudden cardiac death.

Causes of Sudden Cardiac Death from the CRY-CPL National Database

The CRY-CPL laboratories have received 6960 hearts between 1994 and 2020. Of these, 238 cases are excluded as they had a non-cardiac cause of death.

The most commonly referred age group is from 30-34 with age showing a normal distribution. Cases varied in aged from neonates to over 85 years old (figure 3.1).

SCD occurs almost twice as common in males compared to females (4398 vs 2285, 1.9:1). This male predominance is seen in most conditions underlying SCD especially in ACM (225 vs 46, 4.9:1) where males seem at a particularly elevated risk compared to females (figure 3.2 and 3.3).

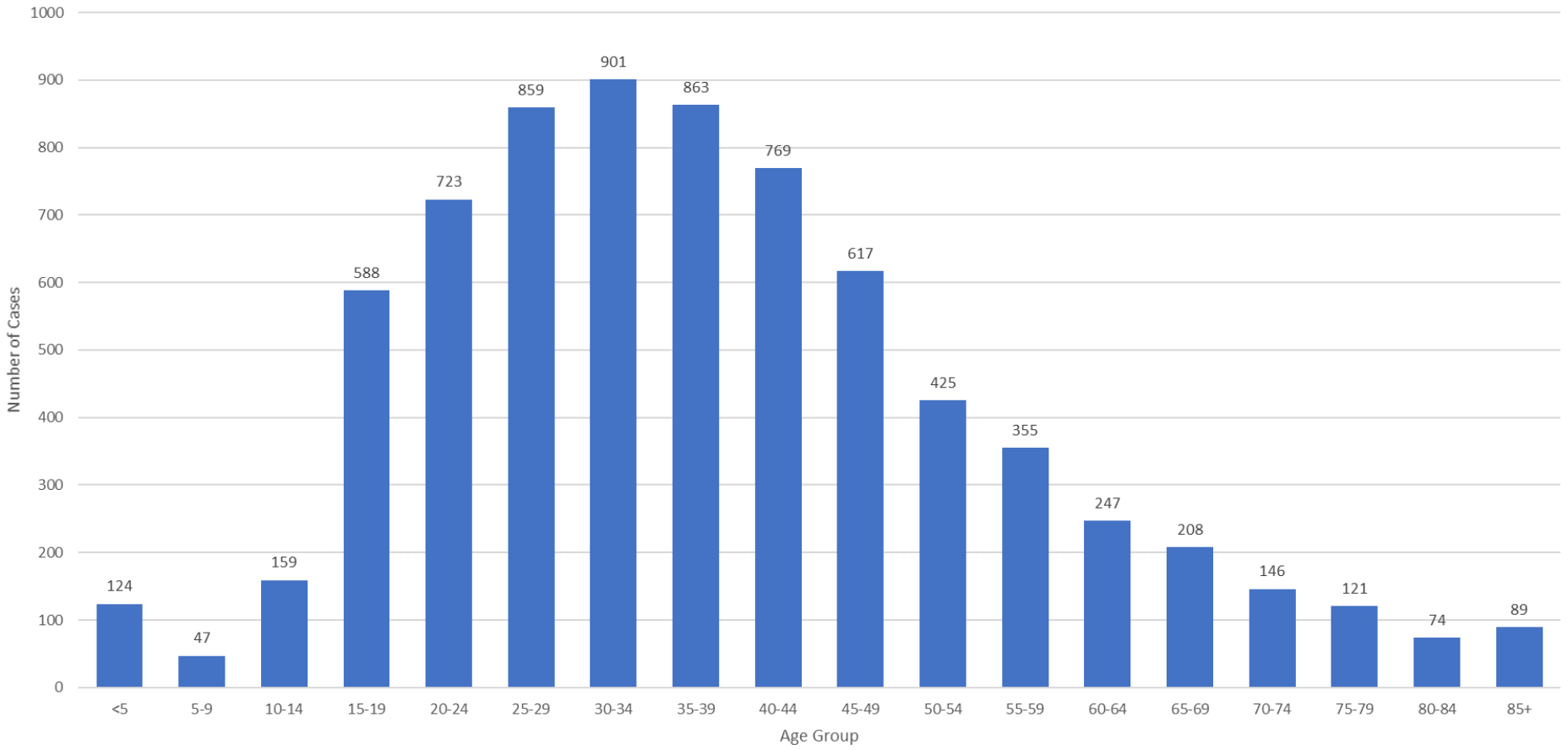


Figure 3.1. The age at death of the individuals who experienced sudden cardiac death and had their heart referred to the Cardiac Risk in the Young Cardiovascular Pathology Laboratories between 1994 and 2020. The most commonly referred age group is from 30-34.

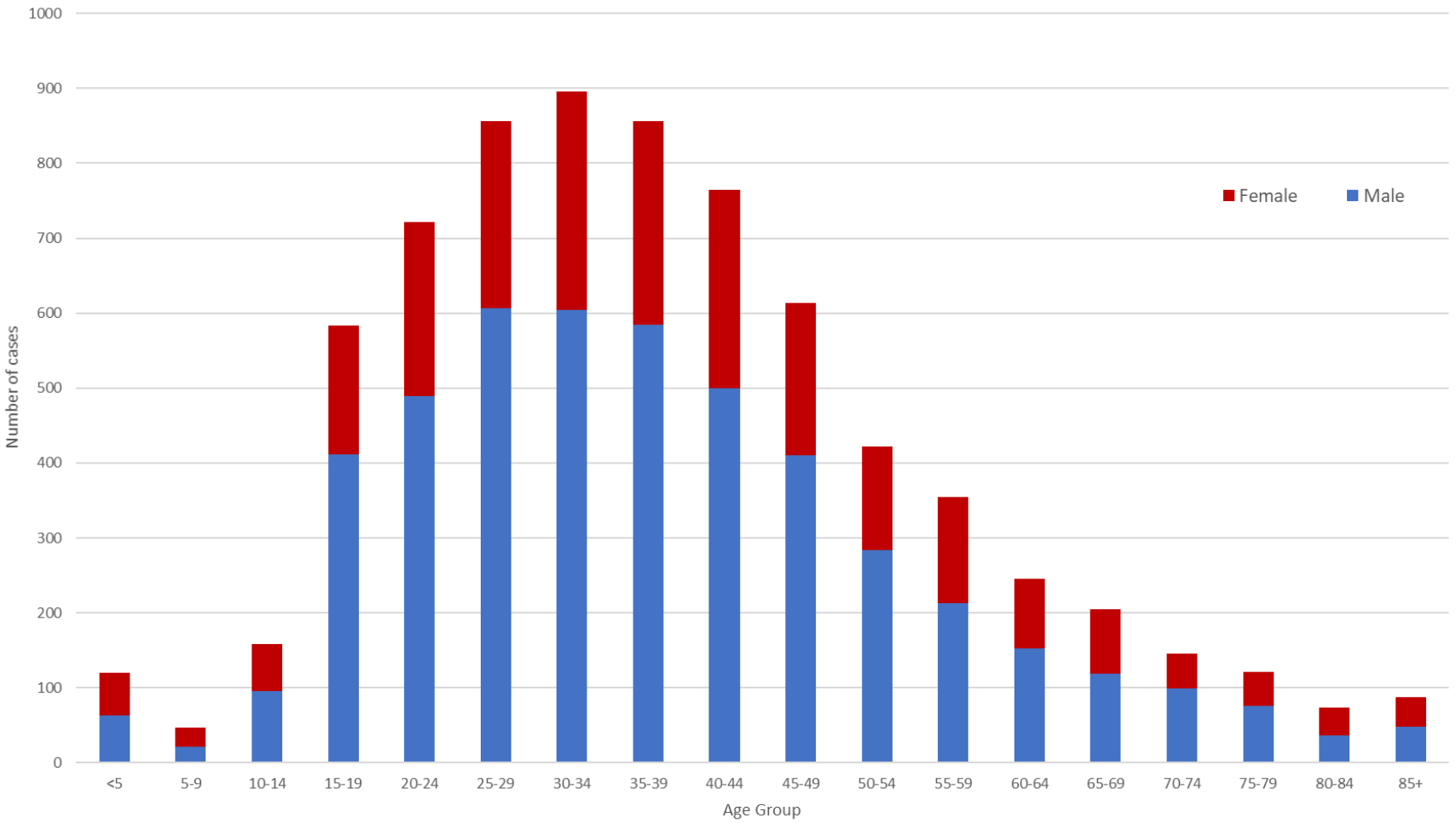


Figure 3.2. The age at death and sex of the individuals who experienced sudden cardiac death and had their heart referred to the Cardiac Risk in the Young Cardiovascular Pathology Laboratories between 1994 and 2020.

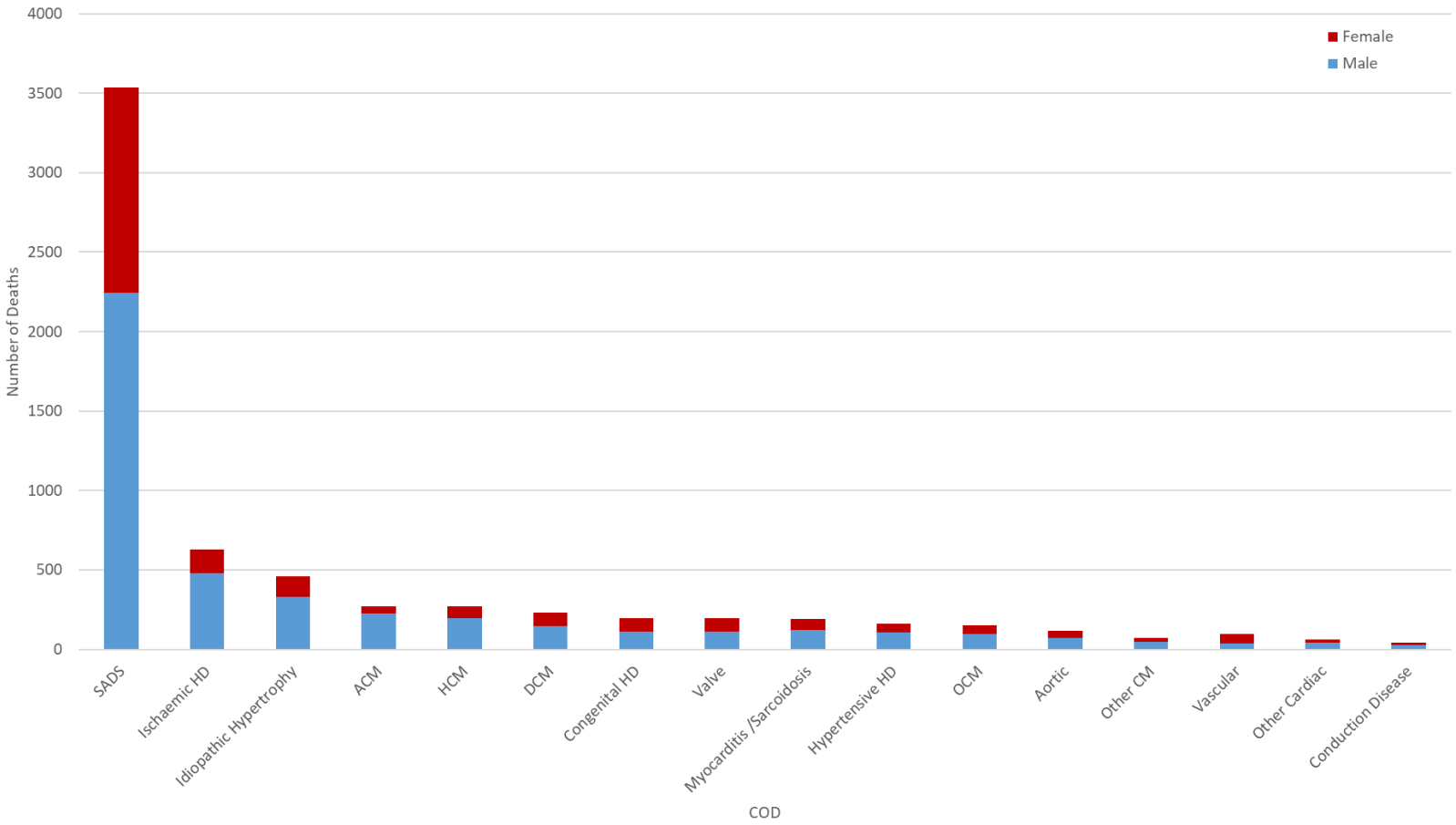


Figure 3.3. Causes of death (COD) broken down by gender. Sudden cardiac death occurs in males at an almost 2:1 ratio compared to females. ACM: arrhythmogenic cardiomyopathy, CM: cardiomyopathy, DCM: dilated cardiomyopathy, HCM: hypertrophic cardiomyopathy, HD: heart disease, OCM: obesity cardiomyopathy, SADS: sudden arrhythmic death syndrome.

Sudden arrhythmic death syndrome is the most common cause of death (3557, 53%) followed by the cardiomyopathies (1462, 22%) and then ischaemic heart disease (633, 9%). Valve disease (205, 3%), congenital heart disease (201, 3%) and myocarditis and sarcoidosis (199, 3%) are the next most common and made up similar proportions. Hypertensive heart disease (167, 2%), aortic disease (123, 2%) vascular disease (95, 1%) made up smaller proportions of the cohort. Other cardiac disease (63, 1%) included tumours, transplant and amyloidosis. Conduction disease (40, 1%) is reserved for cases of Wolff-Parkinson-White or total heart block diagnosed clinically where no pathological abnormality is detected. The causes of SCD are shown in figure 3.5.

The proportions of SADS was higher in younger individuals (65% vs 41%). The proportion of cardiomyopathy (27% vs 17%) and ischaemic heart disease (15% vs 4%), are higher in older individuals (figure 3.6).

Sudden arrhythmic death syndrome (2191 vs 1366, 1.6:1) and congenital heart disease (132 vs 66, 2:1) caused SCD more commonly in the younger population. Most other diseases caused SCD more commonly in the older population. Hypertensive heart disease is a much commoner cause in those over 35 (15 vs 147, 1:9.8). SCD in under 15-year olds are mainly due to sudden arrhythmic death syndrome (252, 61%), cardiomyopathy (66, 16%) and congenital heart disease (36, 9%) (figure 3.4).

When looking at just the cardiomyopathies, idiopathic hypertrophy (468, 32%) is most common followed by similar proportions of arrhythmogenic (278,19%), hypertrophic (263, 18%) and dilated (234, 16%) cardiomyopathies (figure 3.7).

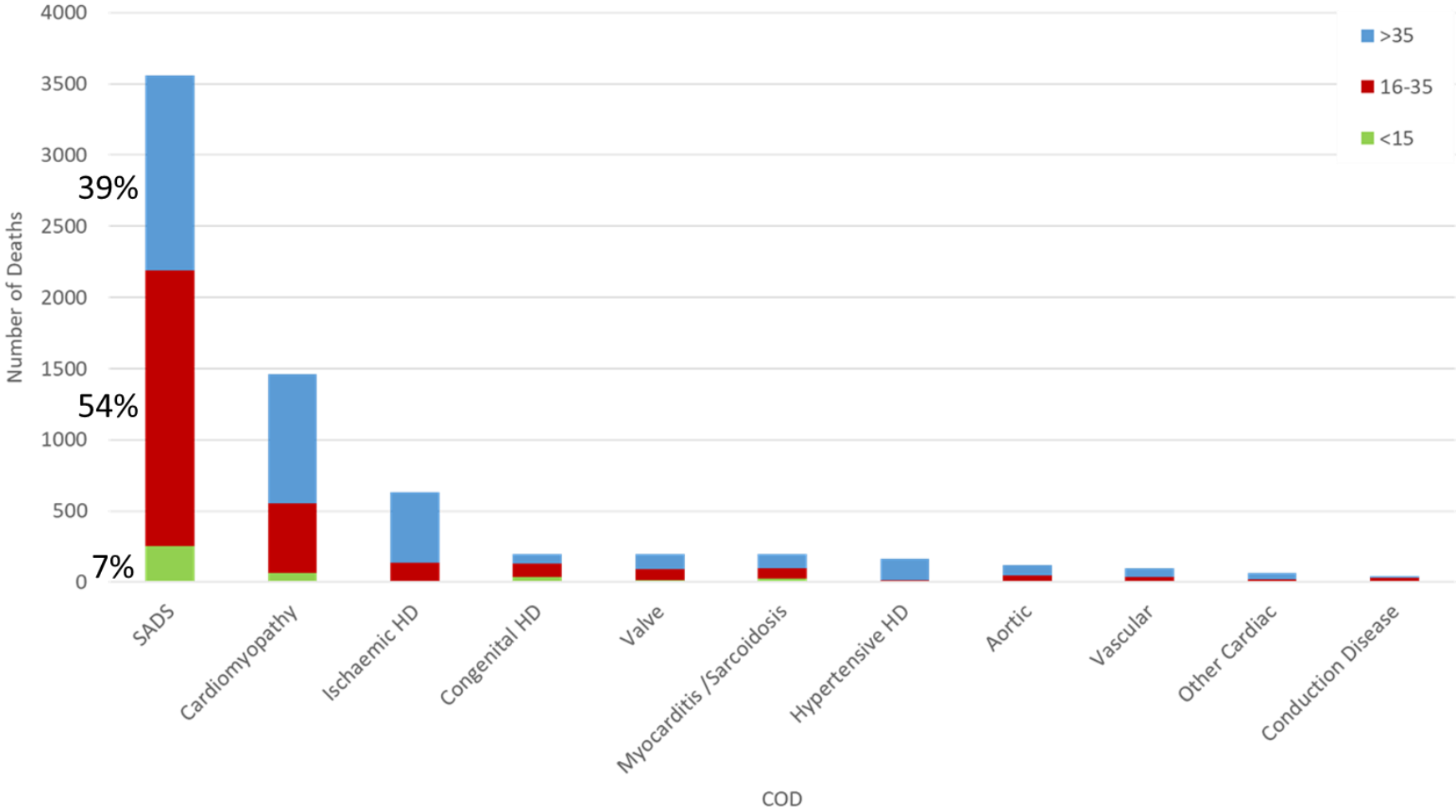


Figure 3.4. Sudden cardiac death generally occurs more commonly in most conditions in those over 35. Sudden arrhythmic death syndrome, our most common cause, and congenital heart disease are notable exceptions.

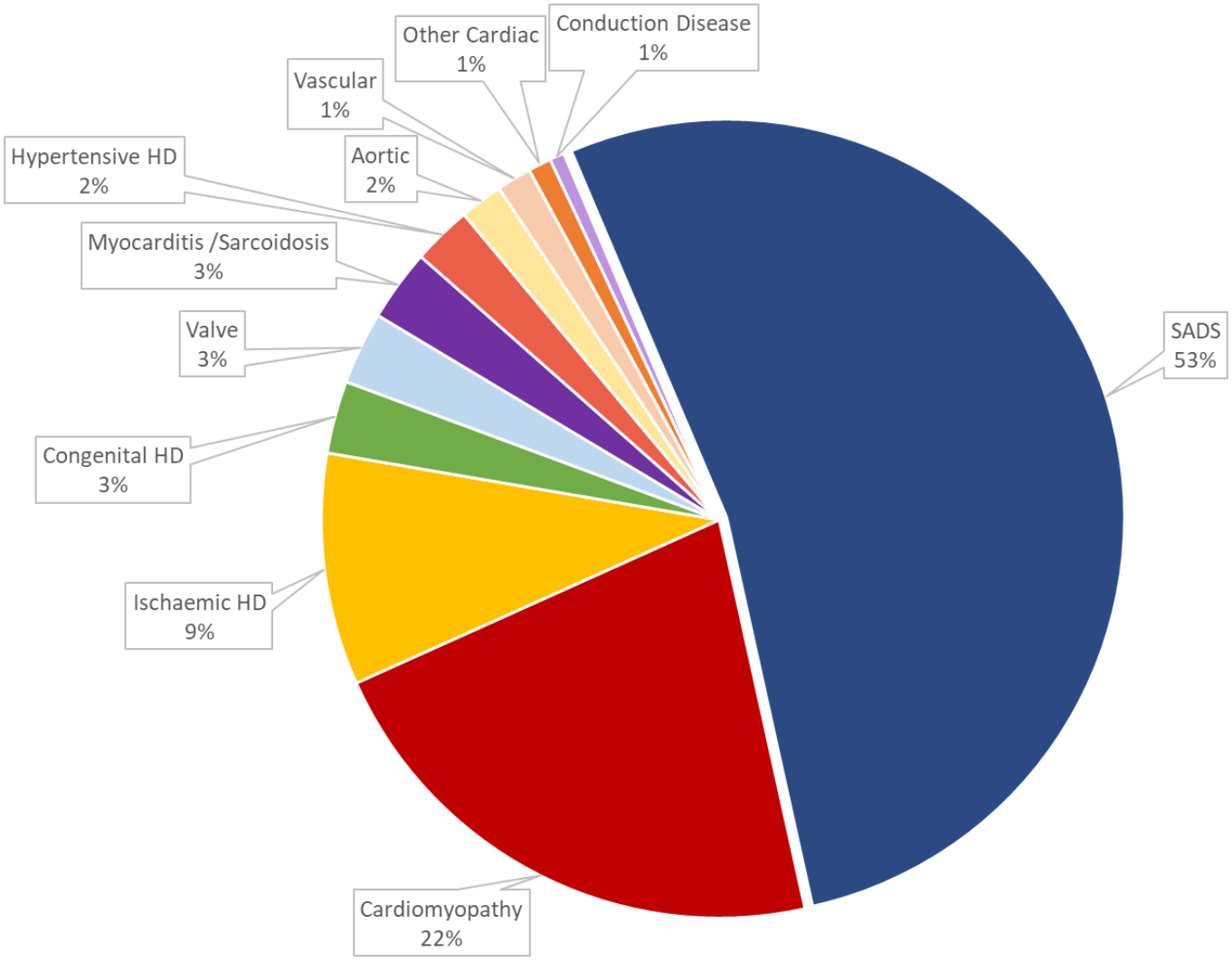


Figure 3.5. A pie chart illustrating the cardiovascular conditions underlying sudden cardiac death. Cardiomyopathies and sudden arrhythmic death syndrome (SADS), which are both heritable, make up 75% of cases.

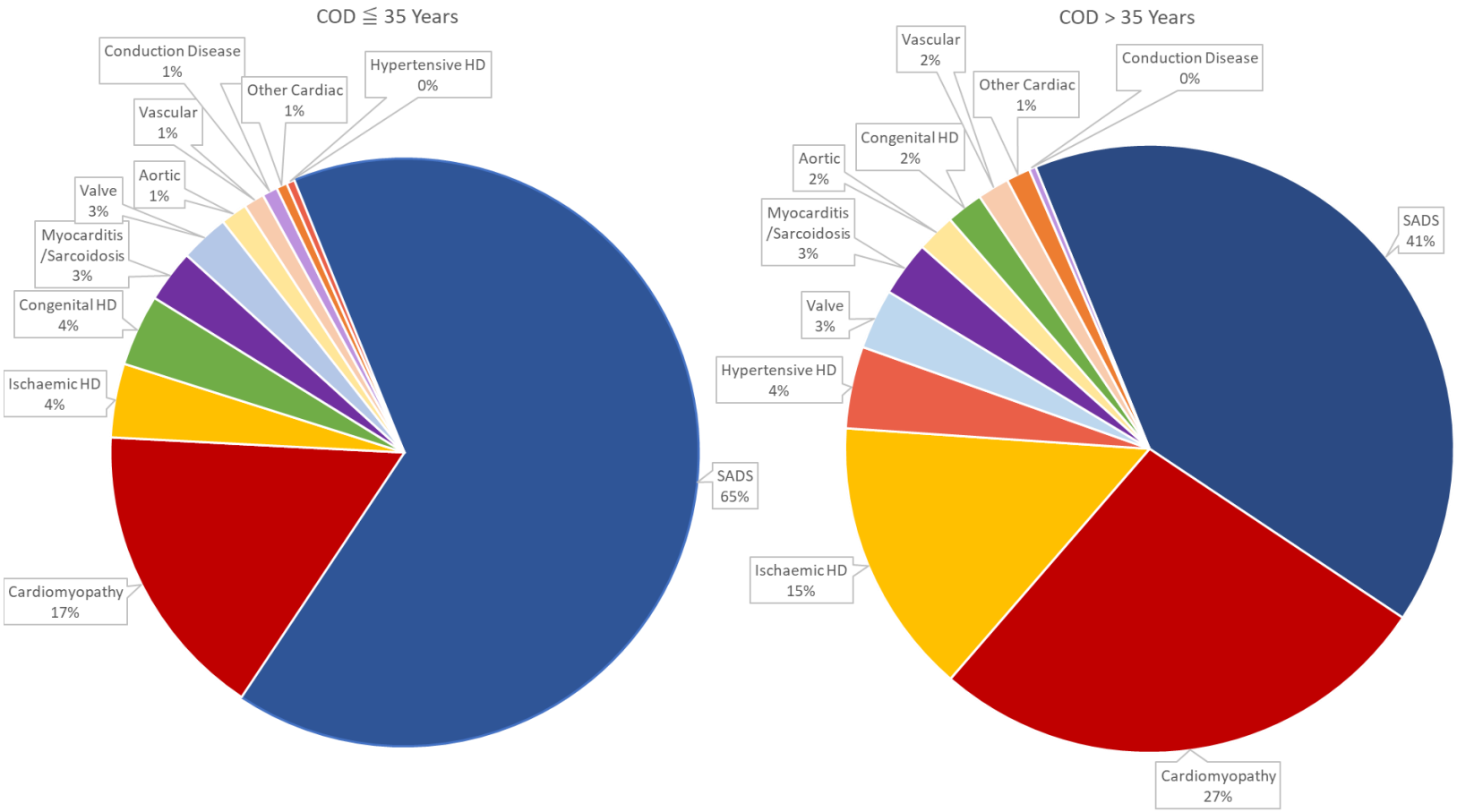


Figure 3.6. Pie charts illustrating the causes of death (COD) underlying sudden cardiac death in individuals 35 years old or less and in individuals older than 35 years. Sudden arrhythmic death syndrome (SADS) makes up a greater proportion in younger individuals. Genetic conditions including SADS and cardiomyopathy combined makes up over 80% cases in younger individuals.

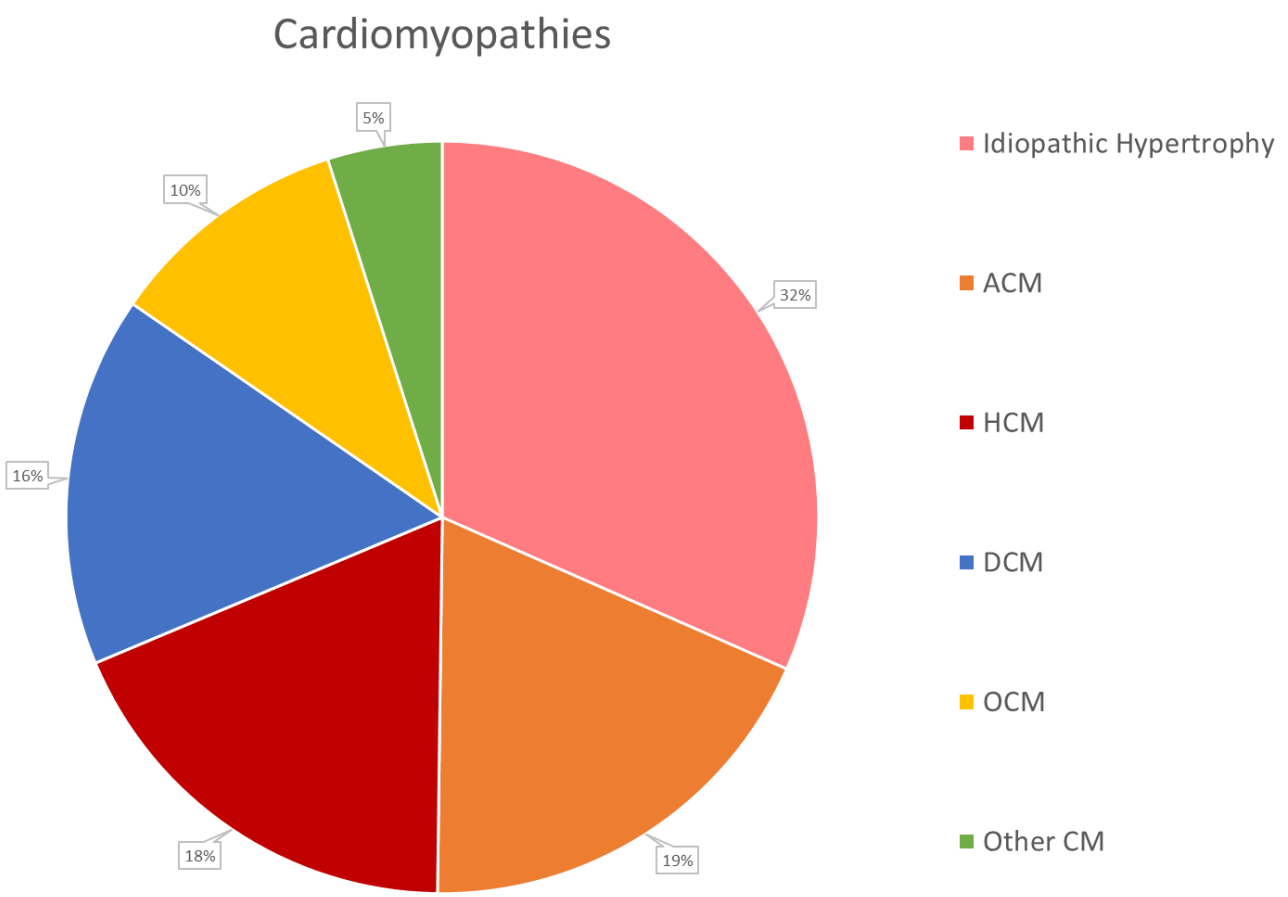


Figure 3.7. Pie chart illustrating the types of cardiomyopathy that lead to SCD and their respective proportions as a cause of SCD. Idiopathic hypertrophy is the most common followed by arrhythmogenic (ACM), hypertrophic (HCM), and dilated (DCM) cardiomyopathies. Obesity cardiomyopathy (OCM) made up a smaller proportion.

Discussion

This is the largest autopsy based SCD cohort ever reported. In this nationwide study from a large database developed in house, all cases have been autopsied and had specialist evaluation of the heart.

Previous autopsy based SCD studies have been limited by smaller numbers with the largest other study in Texas consisting of 902 cases (Eckart *et al.*, 2011). Most other studies cover only regional areas, exceptions to this are nationwide studies in Denmark, Australasia and Ireland (Margey *et al.*, 2011; Winkel *et al.*, 2011; Risgaard *et al.*, 2014; Bagnall *et al.*, 2016; Lynge *et al.*, 2021). Evaluation of all hearts solely in a specialist centre was only undertaken in one regional study (Corrado, Basso and Thiene, 2001). Select populations of athletes (Maron *et al.*, 2016) and military recruits (Eckart *et al.*, 2011) were used in two studies.

It is well recognised that ischaemic heart disease is the most common cause of SCD (Davies, 1981; Bowker *et al.*, 2003; Chappex *et al.*, 2015; Lynge *et al.*, 2021). Our series focusses on the non-ischaemic causes of SCD and we only receive a small proportion of ischaemic cases in our database.

Comparison to worldwide studies

The reported aetiology of SCD shows considerable variance in autopsy studies from around the world (Corrado, Basso and Thiene, 2001; Morentin, Suárez-Mier and Aguilera, 2003; Eckart *et al.*, 2011; Hookana *et al.*, 2011; Margey *et al.*, 2011; Bagnall *et al.*, 2016; Maron *et al.*, 2016; Lynge *et al.*, 2021) (figure 3.8).

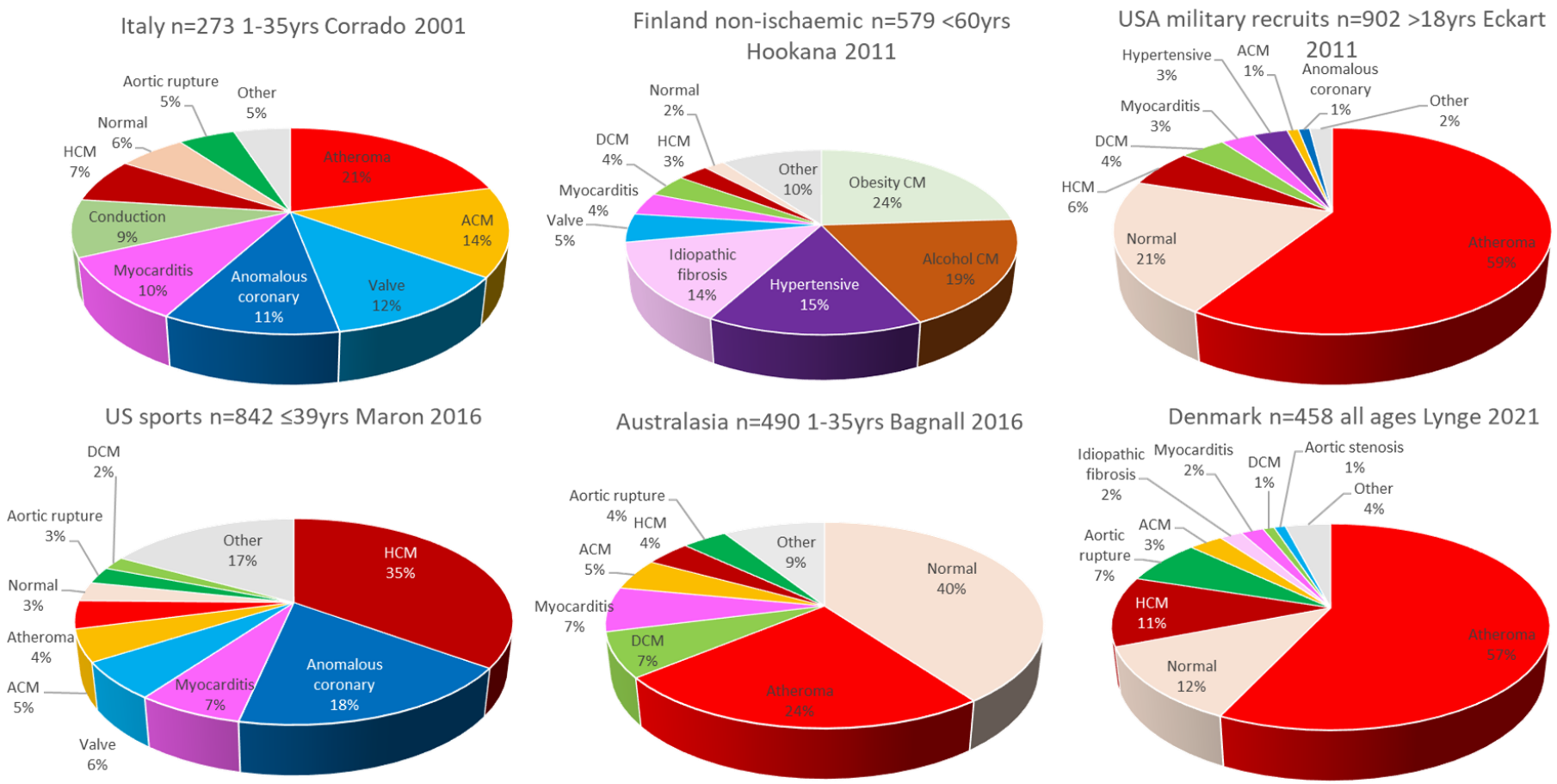


Figure 3.8. Pie charts showing the causes of death in autopsy based SCD studies from around the world. There is a large difference in cases of atheroma and normal hearts.

Sudden arrhythmic death syndrome and autopsy series

SADS as a cause of SCD shows great variance worldwide from 6-40% with other autopsy studies reporting lower proportions when examining both younger and older individuals. Studies of younger individuals show higher proportions than studies of older individuals.

An Italian study from the Veneto region examining 273 hearts from individuals aged 35 years or less found only 6% were unexplained (Corrado, Basso and Thiene, 2001). A regional Spanish study of 71 cases of SCD in 1-35 year olds found that the cause of death was unexplained in 38% (Morentin, Suárez-Mier and Aguilera, 2003). A US study of 842 competitive athletes aged less than 35 identified normal hearts in 3% of cases (Maron *et al.*, 2016). A nationwide Irish study of 116 cases in those aged 15 to 34 found sudden arrhythmic death syndrome in 27% (Margey *et al.*, 2011). A study from Texas in the United states of 902 subjects over the age of 18 years undergoing autopsy reported that the deaths were unexplained in 21% of cases (Eckart *et al.*, 2011). A study from Finland of non-ischaemic cases aged less than 60 years found normal hearts in 2%. A nationwide Danish study of 439 autopsied cases from individuals aged 1-49 reported SADS made up 48% in those younger than 35 years compared to 25% of those over 35 (Risgaard *et al.*, 2014). A Swiss study from Lausanne of 188 cases of SCD between 10-50 years found the cause was unexplained in 17% of cases (Chappex *et al.*, 2015). An Australian and New Zealand study of 490 SCDs in 1-35 year olds reported that cause of death was unexplained at autopsy in 40% cases (Bagnall *et al.*, 2016). A further Danish nationwide retrospective study by the same group which examined the reports from 458 autopsied cases of all ages found the cause of death to be unexplained in 29% (Lynge *et al.*, 2021). Figure 3.9 highlights the variability in the proportion of SADS.

The higher proportion of the normal heart or SADS within our cohort is explained by the cases that are selected to be referred to our centre. We receive less ischaemic cases as these are routinely diagnosed by the general autopsy practitioners resulting in higher proportions of other cardiac conditions. Additionally, normal hearts are more likely to be referred to our centre as we are nationally recognised centre for SADS.

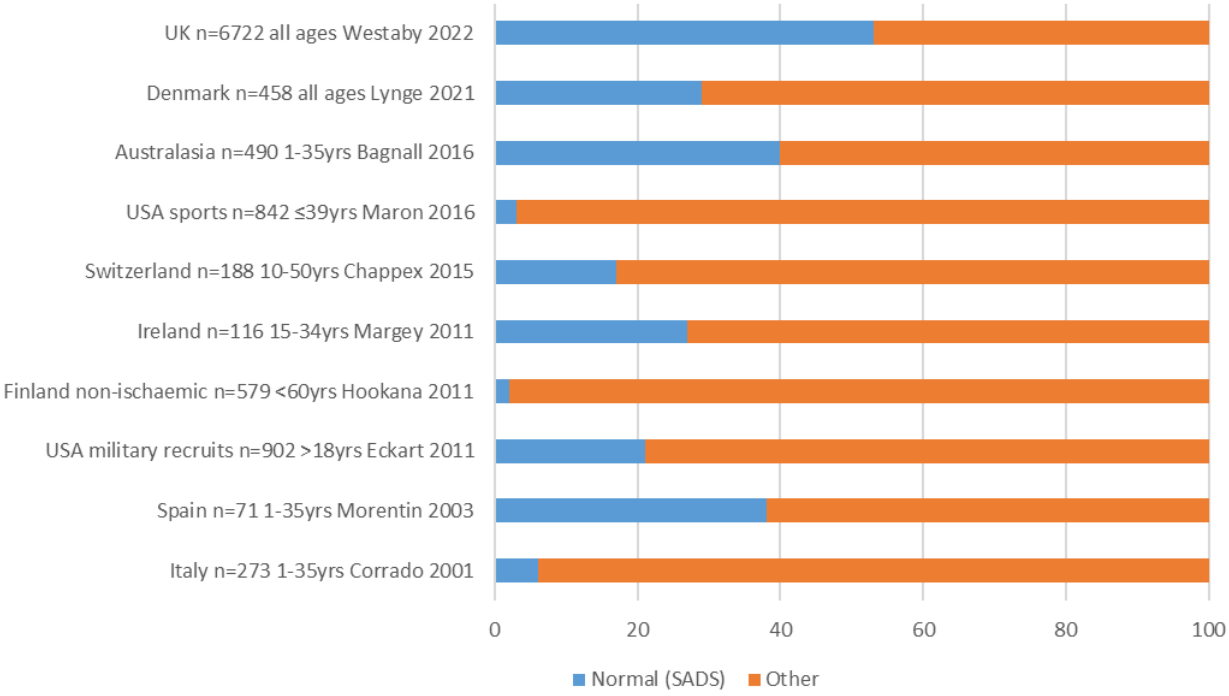


Figure 3.9. The percentage of SCD with normal hearts in other worldwide studies. There is marked variability in the proportion of SCD caused by SADS in other studies ranging from 2-40%.

Cardiomyopathies

Our study identified cardiomyopathies in 22% of SCD cases. Comparable to our findings, the nationwide Danish study report 17% (Lynge *et al.*, 2021), the Swiss

study report 23% (Chappex *et al.*, 2015), the Italian study report 26% (Corrado, Basso and Thiene, 2001) and the US military recruit study found cardiomyopathy in 15% (Eckart *et al.*, 2011). The non-ischaemic Finnish study reports 54% (Hookana *et al.*, 2011) and the US athlete study reports 43% (Maron *et al.*, 2016). These values are higher than what we observed. This is partially explained by the absence of ischaemic disease in the Finnish study and the low proportion of ischaemic disease and SADS in the US athlete study.

In younger individuals we report a lower burden of cardiomyopathy of 17% compared to 27% in older individuals. Similarly, the Australasian study of 1-35 year olds identified cardiomyopathy in 16% (Bagnall *et al.*, 2016) and the Spanish study of 1-25 year olds reported cardiomyopathies in 18% (Morentin, Suárez-Mier and Aguilera, 2003). The Irish study of 15-34 year olds reported cardiomyopathy in a higher proportion of their cases identifying it as a cause of SCD in 30% (Margey *et al.*, 2011). The Danish study did not identify a difference in the occurrence of SCD rates caused by cardiomyopathy in younger individuals compared to older individuals (Risgaard *et al.*, 2014).

When looking specifically at the proportion of cardiomyopathy there is wide variation between our study and others as well as between other studies (figure 3.10). We report idiopathic LV hypertrophy in 32%, with ACM in 19%, HCM in 18% and DCM in 16% of SCD caused by the cardiomyopathies.

In the studies reporting idiopathic LV hypertrophy it made up a similar proportion to our study. The Danish and Irish study reported 32-34% (Margey *et al.*, 2011; Winkel *et al.*, 2011) however it was not reported within the other studies. Idiopathic hypertrophy is now recognised to be distinct from HCM. A recent study from our centre screening the families of 46 decedents with idiopathic LV hypertrophy and

also performing molecular autopsy (Finocchiaro *et al.*, 2020). No family members were found to have HCM and no pathogenic or likely pathogenic mutations were found.

ACM as a proportion of cardiomyopathy causing SCD varied from 2-55%. The Italian study identified a much higher proportion of ACM at 55% (Corrado, Basso and Thiene, 2001). ACM was diagnosed in cases of fatty infiltration in the absence of fibrosis which would explain its higher proportion. The low proportion of 2% in the Finnish study is partially explained by the reporting of obesity cardiomyopathy and other cardiomyopathies (Hookana *et al.*, 2011).

HCM as a proportion of cardiomyopathy causing SCD varied from 3-83%. It was least frequent in the Scandinavian studies which is partially explained by the reporting of obesity cardiomyopathy, other cardiomyopathies and idiopathic LV hypertrophy (Hookana *et al.*, 2011; Winkel *et al.*, 2011). The highest proportion was found in the US athlete study and is partially explained by the select population (Maron *et al.*, 2016).

DCM as a proportion of cardiomyopathy causing SCD varied from 5-44% and generally showed a lower proportion that the other cardiomyopathies. The lowest proportion was in the US athlete study which is explained by the select population examined (Maron *et al.*, 2016).

Obesity cardiomyopathy is a newly recognised condition and was only reported in the Finnish study making up 44% (Hookana *et al.*, 2011). Obesity cardiomyopathy may have been labelled as idiopathic hypertrophy within other studies. The select population in the US athlete study would explain its absence (Maron *et al.*, 2016). The existence of obesity cardiomyopathy is still debated however obesity is a recognised clinical cause of LV hypertrophy in the absence of coronary disease

(Wang *et al.*, 2004; Obokata *et al.*, 2017; Robertson *et al.*, 2019, 2020; Litwin *et al.*, 2020). Raised heart weight is also observed in obesity at post mortem (De La Grandmaison, Clairand and Durigon, 2001; Wingren and Ottosson, 2015; Skurdal and Nordrum, 2016). We label this entity as obesity cardiomyopathy. Future follow up of individuals with this will elucidate whether there is underlying genetic cause or whether this is solely secondary to obesity.

Cardiomyopathy made up a greater proportion of SCD in those over 35 years in our study. This was also observed in the Danish registry and the Swiss study particularly with regard to idiopathic left ventricular hypertrophy (Risgaard *et al.*, 2014; Chappex *et al.*, 2015). One exception to this was ACM which presents with SCD more commonly in less than 35 year olds (Risgaard *et al.*, 2014; Chappex *et al.*, 2015) which is also present in our cohort.

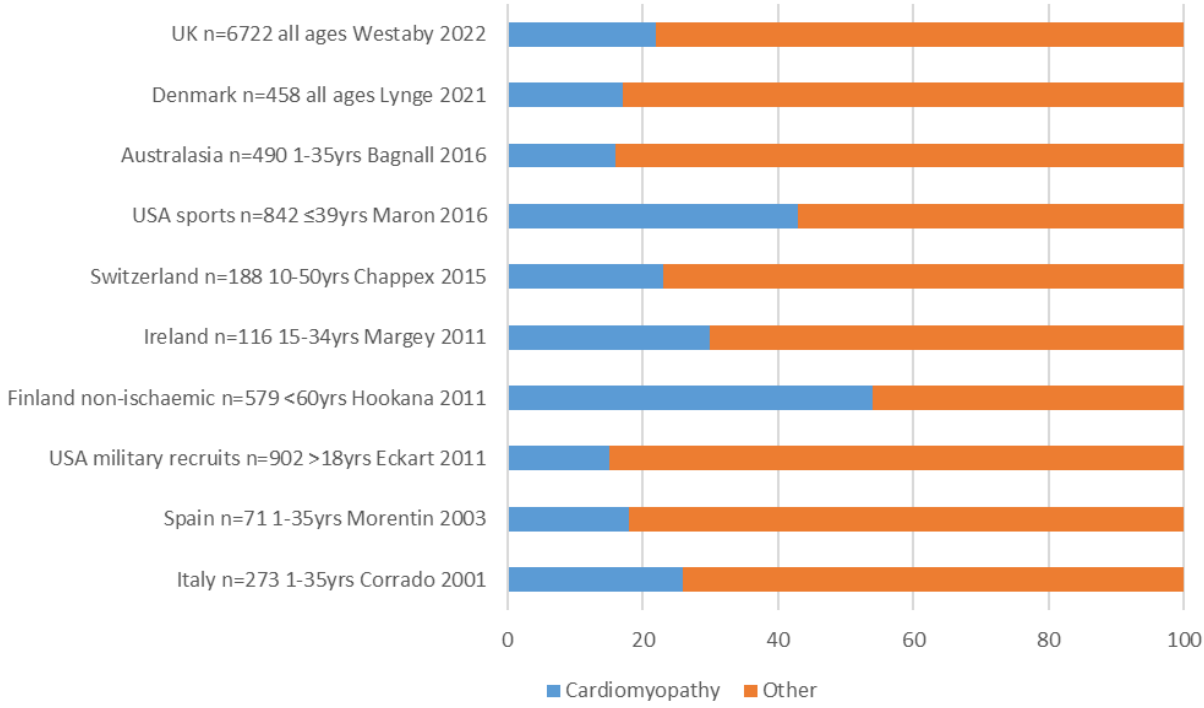


Figure 3.10. The percentage of SCD with cardiomyopathy in other worldwide studies. There is marked variability ranging from 15-54%.

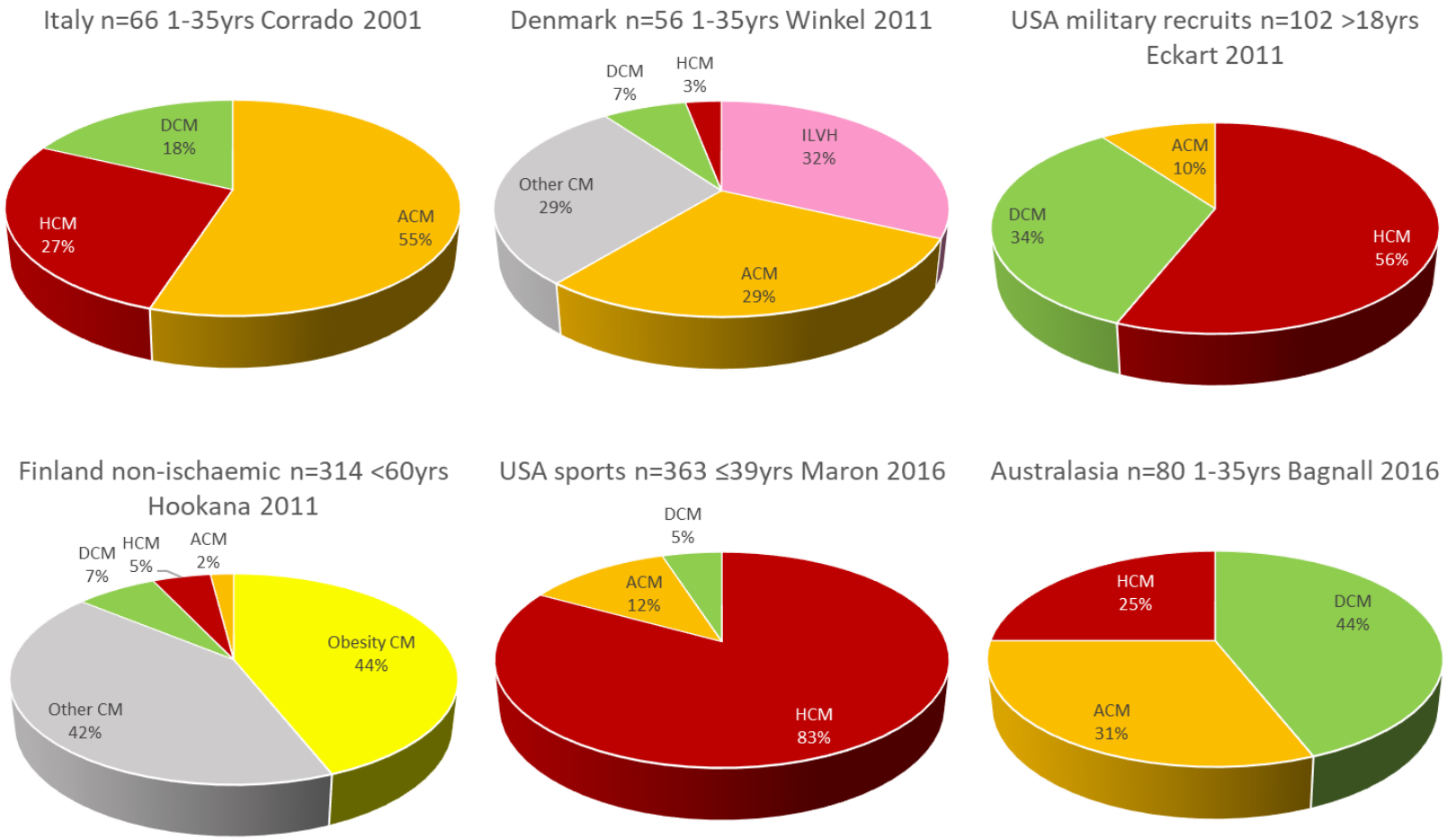


Figure 3.11. Pie charts illustrating the proportion of the different subtypes of cardiomyopathy accounting for SCD caused by cardiomyopathy in other worldwide studies.

Ischaemic heart disease

Ischaemic heart disease due to atheroma made up 9% of our cohort. Ischaemic heart disease is the most common cause of SCD (Bowker *et al.*, 2003). We receive a lower proportion of ischaemic heart disease. This is due to our status as a referral centre for non-ischaemic heart disease and that autopsy practitioners diagnose ischaemic heart disease and report to the coroner without referral. Other studies ranged from 4-59%. The US athlete study showed 4% which is explained by the select population (Maron *et al.*, 2016). As expected, most other studies showed higher proportions than our study.

Valve disease

Valve disease is a well-recognised cause of SCD incorporating entities such as mitral valve prolapse, aortic stenosis and endocarditis. In our study it made up 3% of cases. Other series have also highlighted it as a minor cause of SCD occurring at a range of less than 1% up to 16% (Corrado, Basso and Thiene, 2001; Eckart *et al.*, 2011; Hookana *et al.*, 2011; Chappex *et al.*, 2015; Maron *et al.*, 2016).

Mitral valve prolapse is important to identify as it can have genetic aetiology especially in younger individuals and therefore screening should be advised in blood relatives. We have published on this entity showing that the leaflets shows extensive multi-segment bileaflet prolapse with dilation of the annulus. There is LV fibrosis and hypertrophy in 81%. Fibrosis occurs most commonly in the posterior wall (Garbi, Lancellotti and Sheppard, 2018; Westaby and Sheppard, 2021).

Endocarditis is a rare cause of SCD. We published on this entity reporting 30 cases. Endocarditis occurs more commonly in males and can affect all four valves but occurred most commonly on the aortic valve. It occurs in those with normal valves,

valvular disease and following valve replacement surgery. Endocarditis is not diagnosed prior to autopsy in 70% of cases (Cooper *et al.*, 2021).

Congenital disease

We have published on sudden death in individuals with congenital disease highlighting the huge variation in the forms of congenital disease which can now be seen in the adult. SCD in individuals with congenital heart disease occurs in association with atrial septal defects, ventricular septal defects, tetralogy of Fallot, and transposition of the great arteries in both its regular and congenitally corrected variants (Westaby *et al.*, 2019). It has been observed to account for a similar proportion of SCD in other specialist cardiovascular pathology series (Corrado *et al.*, 2003). Frequently there is ventricular fibrosis in these individuals which is thought to account for their SCD however a small portion of individuals do not reveal a substrate for arrhythmia. Sequential segmental analysis and the "morphological method" are important for describing these complex cases which should be examined in a specialist centre (Westaby *et al.*, 2019).

Myocarditis and sarcoidosis

Myocarditis has been reported in 4-10% of autopsy cases in other series and has noted to be more common in males compared to females similar to our study (Corrado, Basso and Thiene, 2001; Margey *et al.*, 2011; Bagnall *et al.*, 2016; Lynge *et al.*, 2019). The cases can be divided by their inflammatory cell type into lymphocytic, eosinophilic, neutrophilic and giant cell (Sheppard, 2022). Most cases are lymphohistiocytic which can be associated with viral infection (Fabre and

Sheppard, 2006). Giant cell myocarditis has shown association with thymoma (Glennon, Petersen and Sheppard, 1996).

We have previously reported that cardiac sarcoidosis is rare occurring in 1% (Bagwan, Hooper and Sheppard, 2011). Cardiac sarcoidosis may exhibit a range of macroscopic findings including LV hypertrophy, dilation and fibrosis or may appear normal. Histology reveals fibrosis and lymphocytic infiltration that may mimic myocarditis. Non-necrotizing granulomas can be focal. It is important to sample conduction tissue in cases of sarcoidosis as it is frequently involved and can result in heart block (Bagwan, Hooper and Sheppard, 2011). It tends to occur in older individuals when compared to myocarditis.

Aorta

Aortic dissection and rupture are recognised causes of SCD within other studies which agree with our findings that it is a minor cause and generally found in less than 10% of cases. (Corrado, Basso and Thiene, 2001; Morentin, Suárez-Mier and Aguilera, 2003; Margey *et al.*, 2011; Bagnall *et al.*, 2016). It is important to advise screening in younger individuals deceased due to aortic dissection as it is frequently underlain by heritable connective tissue disease (Halushka *et al.*, 2016).

Vascular

Vascular causes included coronary artery dissection and vasculitis. Our previous study has highlighted that both these are rare with coronary artery dissection occurring in less than 1% of SCD. Coronary artery dissection occurred more commonly in females than males and in the left anterior descending more commonly

than elsewhere. The left anterior descending was most commonly affected in women whereas the right coronary was most affected in men (Hill and Sheppard, 2010). Coronary vasculitis has a varied macroscopic appearance including aneurysm, occlusive lesions or masses. Vasculitis was idiopathic or associated Churg-Strauss syndrome. Types of vasculitis included eosinophilic, lymphoplasmacytic and rarely giant cell arteritis (Hill and Sheppard, 2010; Norita, De Noronha and Sheppard, 2012).

Conduction disease

Conduction system abnormalities were seen in 1% which include Wolff-Parkinson-White or total heart block. They have been noted in 9% of cases in the Italian study (Corrado, Basso and Thiene, 2001) and 2% in one of the Danish studies (Risgaard *et al.*, 2014). These are slightly higher proportions than within our cohort. It is very rare to see any pathologic changes when examining these cases (Cohle, 2011).

Reasons for differences

Some of the observed differences will be due to small scale studies, regional variation and the absence of specialist examination. It has previously been reported that there is a disparity in diagnosis in 41% of cases examined by the general autopsy practitioner and a specialist (De Noronha *et al.*, 2014). There will also be observed differences due to variation in diagnostic criteria that have been used to identify cardiac disease underlying SCD. This highlights the importance of internationally agreed guidelines such as those produced by the Association of European Cardiovascular Pathologists on cardiac hypertrophy (Basso *et al.*, 2017). Globally agreed guidelines are needed.

Limitations

We receive mainly non-ischaemic cases from the UK as these are reported to the coroner by the pathologist and therefore these make up a lower proportion within our cohort.

Concluding remarks

In the UK, over 80% of non-ischaemic SCD is caused by sudden arrhythmic death syndrome and the cardiomyopathies. These conditions are important to identify given as they are heritable. Family screening by a cardiologist with an interest in inherited disease should be advised to identify affected blood relatives and allow for management and risk stratification. The importance of this database is that it gives us a research tool to further investigate the genetic causes of SCD as this thesis outlines.

Summary of findings

- SADS is the cause of death in 53%
- Cardiomyopathy is the cause of death in 22%
- ACM makes up 19% of cardiomyopathy cases
- HCM makes up 18% of cardiomyopathy cases
- DCM makes up 16% of cardiomyopathy cases
- There is marked variance in the causes of SCD worldwide particularly SADS and cardiomyopathy

CHAPTER 4 THE NORMAL HEART

Introduction

We have shown in chapter 3 that the morphologically normal heart is found in a majority of our young sudden deaths and is labelled as sudden arrhythmic death syndrome (SADS) which was coined by Michael Davies and expanded on the following years (Fabre and Sheppard, 2006). We have published on the clinical characteristics of this (Mellor *et al.*, 2014). A normal heart following an autopsy without other findings sufficient to account for death, in combination with the absence of a toxicological cause points to an underlying channelopathy in young individuals (Lahrouchi *et al.*, 2017).

Whilst there are numerous publications on pathological findings in structural heart disease (Finocchiaro *et al.*, 2019; Miles *et al.*, 2019; Westaby *et al.*, 2021), there is a paucity of literature on the morphologically normal heart. Given that the heart can be normal in the setting of SCD and this has been recognised for decades, this is surprising (Davies and Popple, 1979). Recent autopsy studies of the normal heart have focussed on just organ weight with little attention paid to cardiac dimensions (De La Grandmaison, Clairand and Durigon, 2001; Wingren and Ottosson, 2015; Skurdal and Nordrum, 2016). Studies of wall thickness and valve dimensions date back to the 1980s (Kitzman *et al.*, 1988).

We aimed to characterise the normal heart from those dying with SADS and provide insight from the large database at our specialist cardiovascular pathology laboratories. We have set out criteria to establish the dimensions of the atria, oval fossa, ventricle wall thickness and diameters, valve circumferences and subepicardial fat and report on patency of the oval fossa and coronary artery

dominance. This acts as a baseline for comparison for further future studies as well as imaging correlation.

Methods

Cases with morphologically normal hearts are identified from a cohort of 3602 referrals to the CRY-CPL laboratories between 2013 and 2020. A total of 1062 cases were considered normal.

Body mass index is calculated as weight (kg)/height^2 (m^2) (James, 2009). Body surface area is calculated by square root of (height (cm) x weight (kg)/3600) (Mosteller, 1987).

Morphologically normal hearts are identified on the basis of a heart weight of below 500 grams in males, and below 400 grams in females. Cases with significant coronary artery disease, valvular disease, or hypertensive disease are excluded. Histology is used to exclude cardiomyopathies, myocarditis and infiltrating diseases such as amyloid.

Hearts are examined both macroscopically and microscopically when the heart is considered normal. Macroscopic measurements are taken at the midventricular level included the thickness of the ventricular wall, the subepicardial fat and the chamber diameters (Figure 4.1). The RVOT is measured 10 millimetres (mm) below the pulmonary valve anteriorly (Figure 4.2). The left atrium is measured between the mouth of the left and right superior pulmonary veins, and from the atrioventricular junction to the superior surface. The right atrium is measured from the ostium of the inferior caval vein to the tip of the appendage and between the ostia of the inferior and superior caval veins (Figure 4.3).

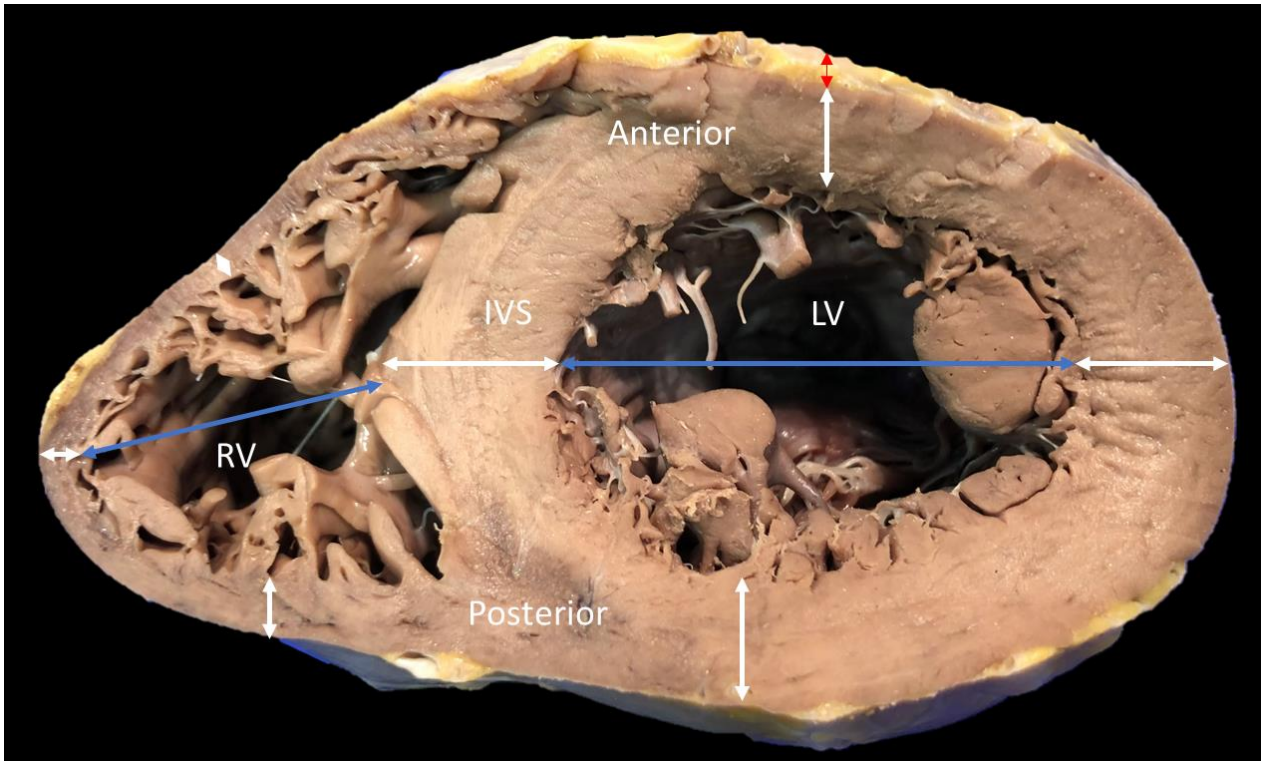


Figure 4.1. The ventricular measurements that are taken at a midventricular level shown on an image of a morphologically normal heart. Both the subepicardial fat (red) and mural thickness (white) are measured in the anterior, lateral and posterior positions on the right and left ventricles. The interventricular septum is measured. Mural thickness exclude the trabeculae and papillary muscles. Cavity diameters (blue) are measured from the mid septum to the lateral wall including the trabeculae and papillary muscles. IVS: interventricular septum; LV: left ventricle; RV: right ventricle.

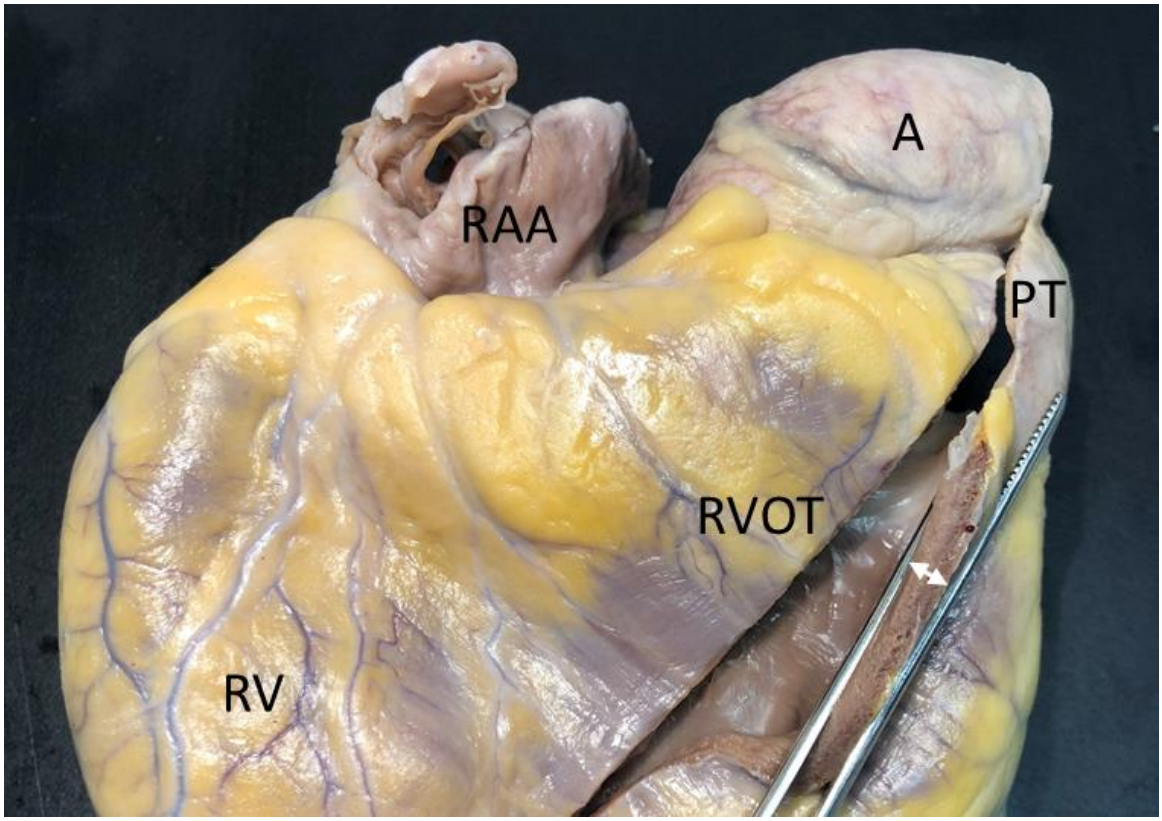


Figure 4.2. The right ventricular outflow tract. Subepicardial fat and mural thickness are taken 10 millimetres below the pulmonary valve. A: aorta; PT: pulmonary trunk; RAA: right atrial appendage; RV: right ventricle; RVOT: right ventricular outflow tract.

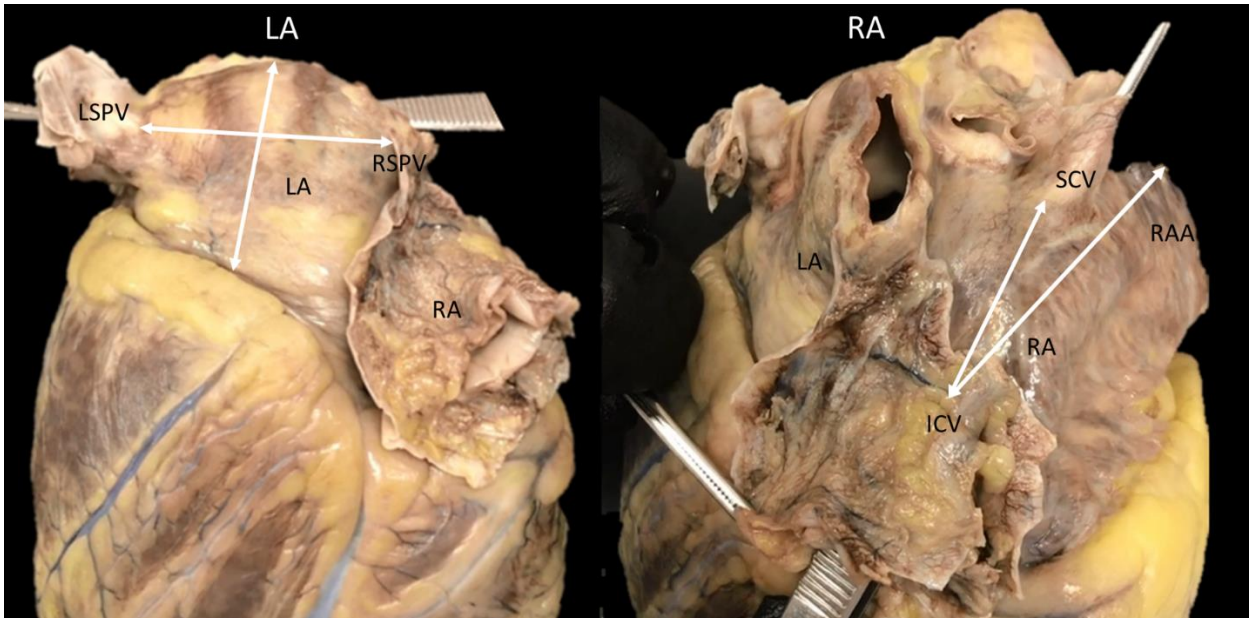


Figure 4.3. The atrial measurements that are taken at cardiovascular examination shown on an image of a morphologically normal heart. The left atrium is measured between the ostia of the left and right superior pulmonary veins, and from the atrioventricular junction to the superior surface. The right atrium is measured from the mouth of the inferior caval vein to the tip of the appendage and between the mouths of the inferior and superior caval veins. A: aorta; ICV: inferior caval vein; LIPV: left inferior pulmonary vein; RIPV: right inferior pulmonary vein; LA: left atrium; PT: pulmonary trunk; RA: right atrium; RAA: right atrial appendage; SCV: superior caval vein, LSVC: left superior pulmonary vein; RSPV: right superior pulmonary vein.

Statistics

All the variables have been explored and summarized according to their statistical type; categorical and binary data as frequencies and percentages, and continuous data as means, standard deviations, medians, first and third quartiles, and ranges. Two-sided T-test is used to compare normally distributed continuous variables. The

Chi-square test is used to assess independency between two categorical variables with Fisher's exact test used when cross tabulations exhibited numbers smaller than 5. The Kruskal-Wallis test is used to assess non-normally distributed or ordinal variables. Multiple linear regression has been used to estimate the relationship between multiple independent variables and a dependent variable. SPSS version 28 (IBM, New York, USA) is used for statistical analysis.

Results

Complete measurements are taken from 1062 morphologically normal hearts. The age at death is 34±12 years (33, 25-41, 18-100) and males predominated (n=701, 66%, 1.9:1). Age at death is similar in females and males (35±13, 33, 25-43, 18-100 vs 34±11, 32, 25-40, 18-82) (figure 4.4). Body mass index is 27±6 (26, 22-30, 10-58), which is comparable between females and males (27±7, 25, 21-31, 13-53 vs 27±6, 26, 23-29, 10-58). Body surface area is less in females (1.83±0.27, 1.80, 1.65-1.99, 1.17-2.80 vs 2.04±0.24, 2.03, 1.90-2.16, 1.16-3.02, $p<0.001$) (Figure 4.5 and Table 4.1).

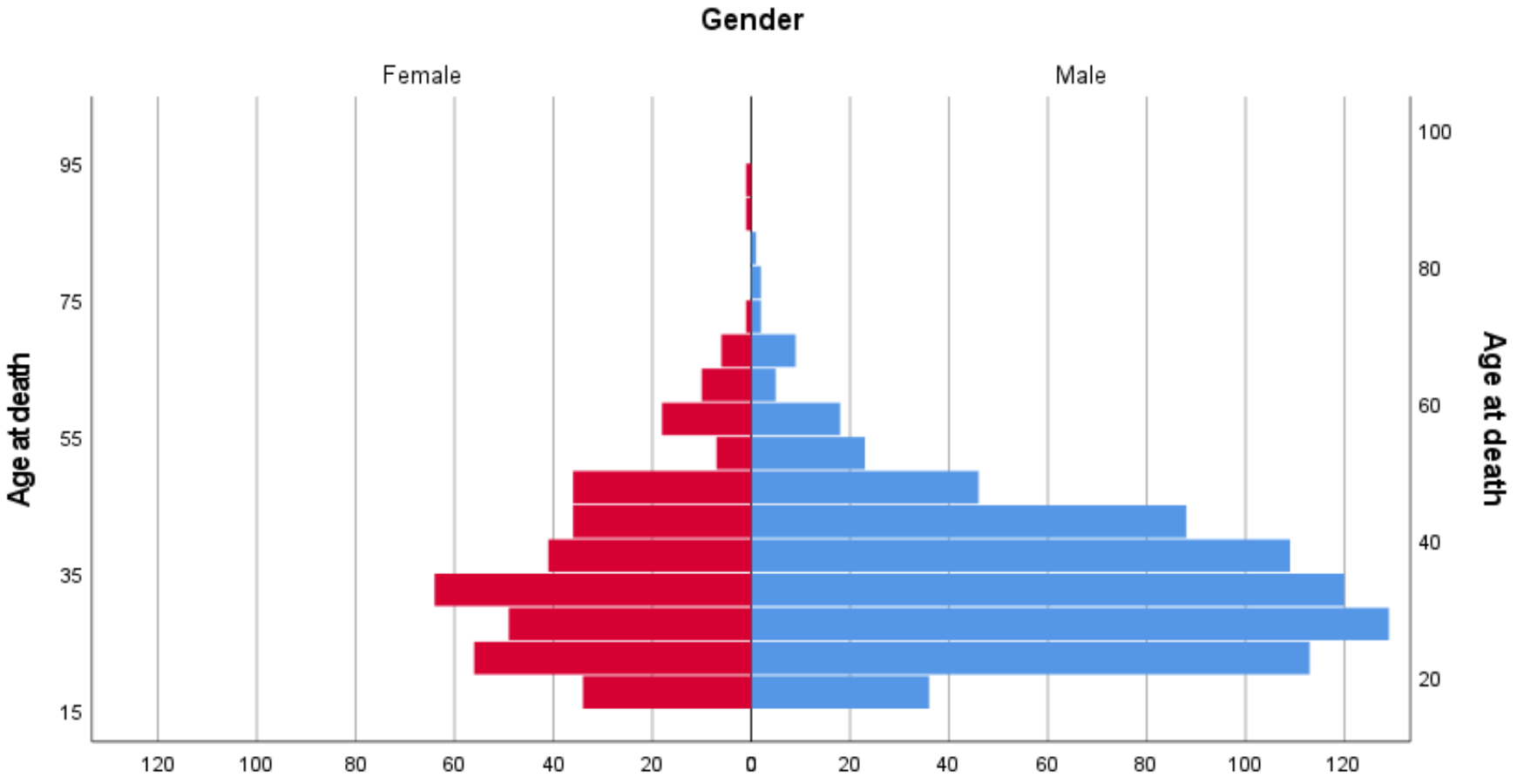


Figure 4.4. Population pyramid of number of deaths by age broken down into males and females for 1062 normal hearts.

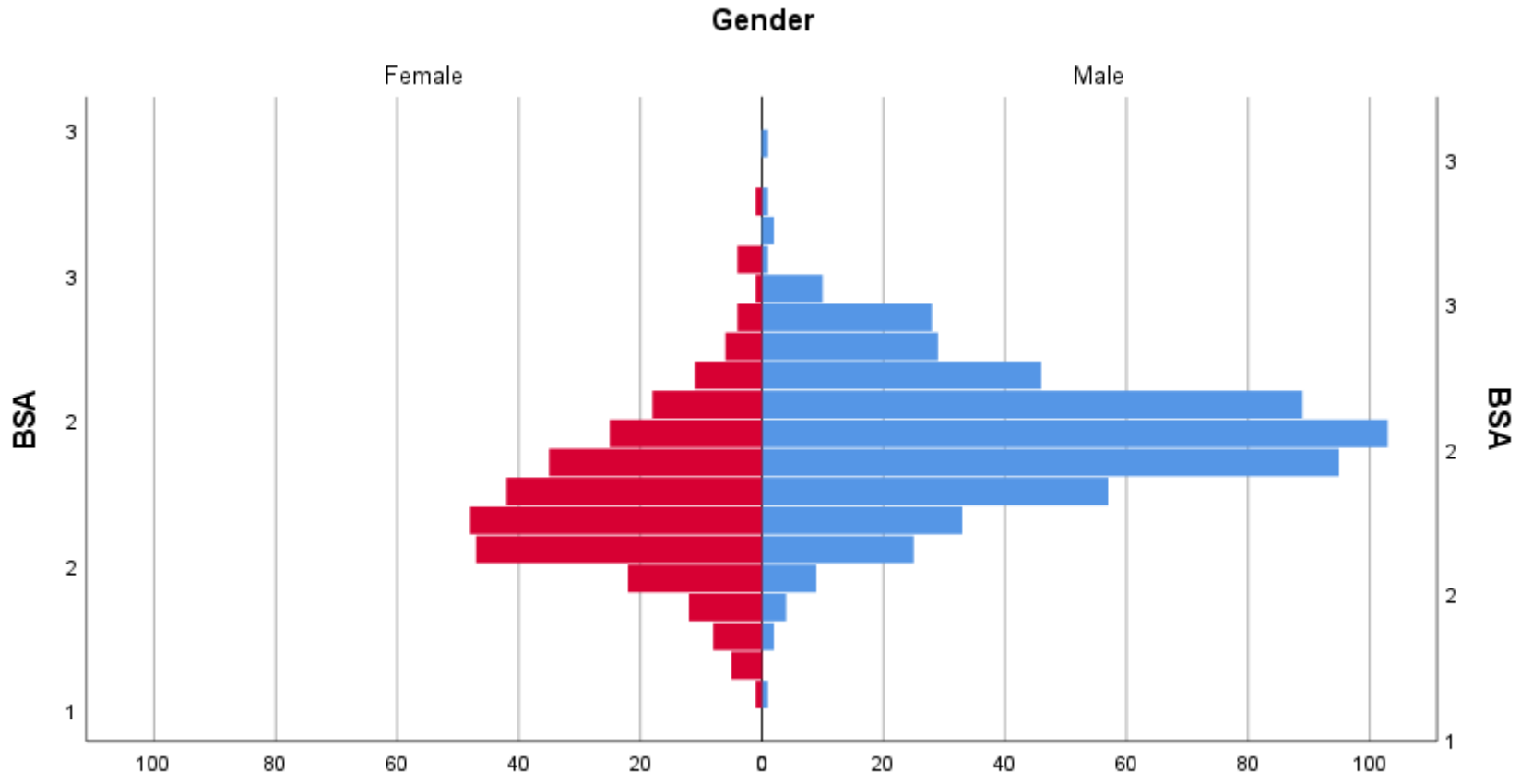


Figure 4.5. Population pyramid of body surface area broken down into males and females. Body surface area was higher in males than females.

Variable	Unit	Summary statistic	Normal hearts (n=1062)	Female (n=361)	Male (n=701)	p value
Age	Years	Mean±SD Median, Q1-Q3 Range	34±12 33, 25-41 18-100	35±13 33, 25-43 18-100	34±11 32, 25-40 18-82	0.119
Sex	Male: Female	Numbers Ratio	701:361 1.9:1	361 -	701 -	
Height	cm	Mean±SD Median, Q1-Q3 Range	174±10 175, 167-181 140-208	166±9 166, 161-172 140-193	179±8 178, 173-184 150-208	**<0.001**
Weight	kg	Mean±SD Median, Q1-Q3 Range	81±20 80, 67-91 29-176	74±21 70, 60-85 35-160	85±18 83, 73-93 29-176	**<0.001**
BMI	kg/m^2	Mean±SD Median, Q1-Q3 Range	27±6 26, 22-30 10-58	27±7 25, 21-31 13-53	27±6 26, 23-29 10-58	0.898
BSA	m^2	Mean±SD Median, Q1-Q3 Range	1.96±0.27 1.97, 1.78-2.13 1.16-3.02	1.83±0.27 1.80, 1.65-1.99 1.17-2.80	2.04±0.24 2.03, 1.90-2.16 1.16-3.02	**<0.001**

Table 4.1. Demographics for females and males. The table gives the age, sex, height, weight, body mass index (BMI) and body surface area (BSA) for the overall cohort and broken down into males and females.

Cardiac examination

The heart weight is 344±74grams (347, 291-396, 134-498) with females having a significantly lower mass than males (285±55, 282, 243-328, 134-399 vs 374±64, 375, 334-419, 191-498, p<0.001) (Table 4.2 and figure 4.6).

A multiple linear regression is calculated to predict heart weight based upon age, gender, height, weight, body mass index and body surface area. A significant regression equation is found ($F(3, 1058) = 392.280$, $p<.000$), with an R^2 of 0.525. Decedents predicted heart weight is equal to 56.682 – 68.276 (gender = female) + 133.053 (body surface area) + 1.442 (age). Heart weight increased 133.053 grams for each metre^2, 1.442 grams for each year of age and male hearts weigh 68.276 grams more than female hearts. Gender (importance 0.449), body surface area (importance 0.424) and age (importance 0.126) were significant independent predictors of heart weight. The model predicted 52.5% of heart weight according to R^2. Body mass index, body weight and height were not significant independent predictors of heart weight. Estimated means are shown in figure 4.7 and a reference table by body surface areas is provided in table 4.3.

Variable	Unit	Summary statistic	Normal heart (n=1062)	Female (n=361)	Male (n=701)	p value
Heart weight	g	Mean±SD Median, Q1-Q3 Range	344±74 347, 291-396 134-498	285±55 282, 243-328 134-399	374±64 375, 334-419 191-498	**<0.001**
Atria						
Right atrium 1	mm	Mean±SD Median, Q1-Q3 Range	57±12 60, 50-65 24-100	54±12 55, 45-60 25-80	58±13 60, 50-65 24-100	**<0.001**
Right atrium 2	mm	Mean±SD Median, Q1-Q3 Range	41±10 40, 35-50 20-80	40±10 40, 35-45 20-80	42±10 40, 35-50 20-80	**0.006**
Left atrium 1	mm	Mean±SD Median, Q1-Q3 Range	42±9 40, 35-50 16-85	41±9 40, 35-45 20-80	43±9 40, 35-50 16-85	**0.002**
Left atrium 2	mm	Mean±SD Median, Q1-Q3 Range	37±8 35, 30-40 14-70	36±8 35, 30-40 15-70	37±8 35, 30-40 14-70	**0.010**
Right ventricle						
Diameter	mm	Mean±SD Median, Q1-Q3 Range	29±6 30, 25-35 10-48	28±6 27, 25-30 10-45	30±6 30, 25-35 10-48	**<0.001**
Anterior wall	mm	Mean±SD Median, Q1-Q3 Range	2.7±1.0 3.0, 2.0-3.0 0.5-8.0	2.4±1.0 2.0, 2.0-3.0 0.5-6.0	2.8±1.1 3.0, 2.0-3.0 1.0-8.0	**<0.001**
Lateral wall	mm	Mean±SD Median, Q1-Q3 Range	2.8±1.0 3.0, 2.0-3.0 1.0-10.0	2.5±1.0 2.0, 2.0-3.0 1.0-7.0	2.9±1.1 3.0, 2.0-3.0 1.0-10.0	**<0.001**

Posterior wall	mm	Mean±SD Median, Q1-Q3 Range	3.6±1.0 4.0, 3.0-4.0 1.0-10.0	3.3±0.8 3.0, 3.0-4.0 1.0-6.0	3.7±1.0 4.0, 3.0-4.0 1.0-10.0	**<0.001**
RVOT wall	mm	Mean±SD Median, Q1-Q3 Range	3.2±1.0 3.0, 3.0-4.0 1.0-7.0	2.9±1.0 3.0, 2.0-3.0 1.0-7.0	3.4±1.0 3.0, 3.0-4.0 1.0-6.0	**<0.001**
Left ventricle						
Diameter	mm	Mean±SD Median, Q1-Q3 Range	31±7 30, 25-35 8-49	30±7 30, 25-35 8-49	31±7 30, 27-35 10-48	**0.007**
Septal wall	mm	Mean±SD Median, Q1-Q3 Range	13±3 12, 11-15 7-21	12±2 11, 10-13 7-20	13±3 13, 12-15 8-21	**<0.001**
Anterior wall	mm	Mean±SD Median, Q1-Q3 Range	12±2 12, 10-14 7-20	11±2 10, 10-12 7-20	12±2 12, 11-14 7-20	**<0.001**
Lateral wall	mm	Mean±SD Median, Q1-Q3 Range	12±2 12, 11-14 7-22	11±2 11, 10-12 7-20	13±2 12, 11-15 8-22	**<0.001**
Posterior wall	mm	Mean±SD Median, Q1-Q3 Range	12±2 11, 10-13 7-20	11±2 10, 10-12 7-20	12±2 12, 11-14 7-20	**<0.001**

Table 4.2. The heart weight and cardiac dimensions. The heart weight and dimensions of the atria and ventricles including the mural thickness of the anterior, lateral and posterior free walls of the left and right ventricles, the right ventricular outflow tract (RVOT) and the cavity sizes given for the entire cohort and broken down by gender.

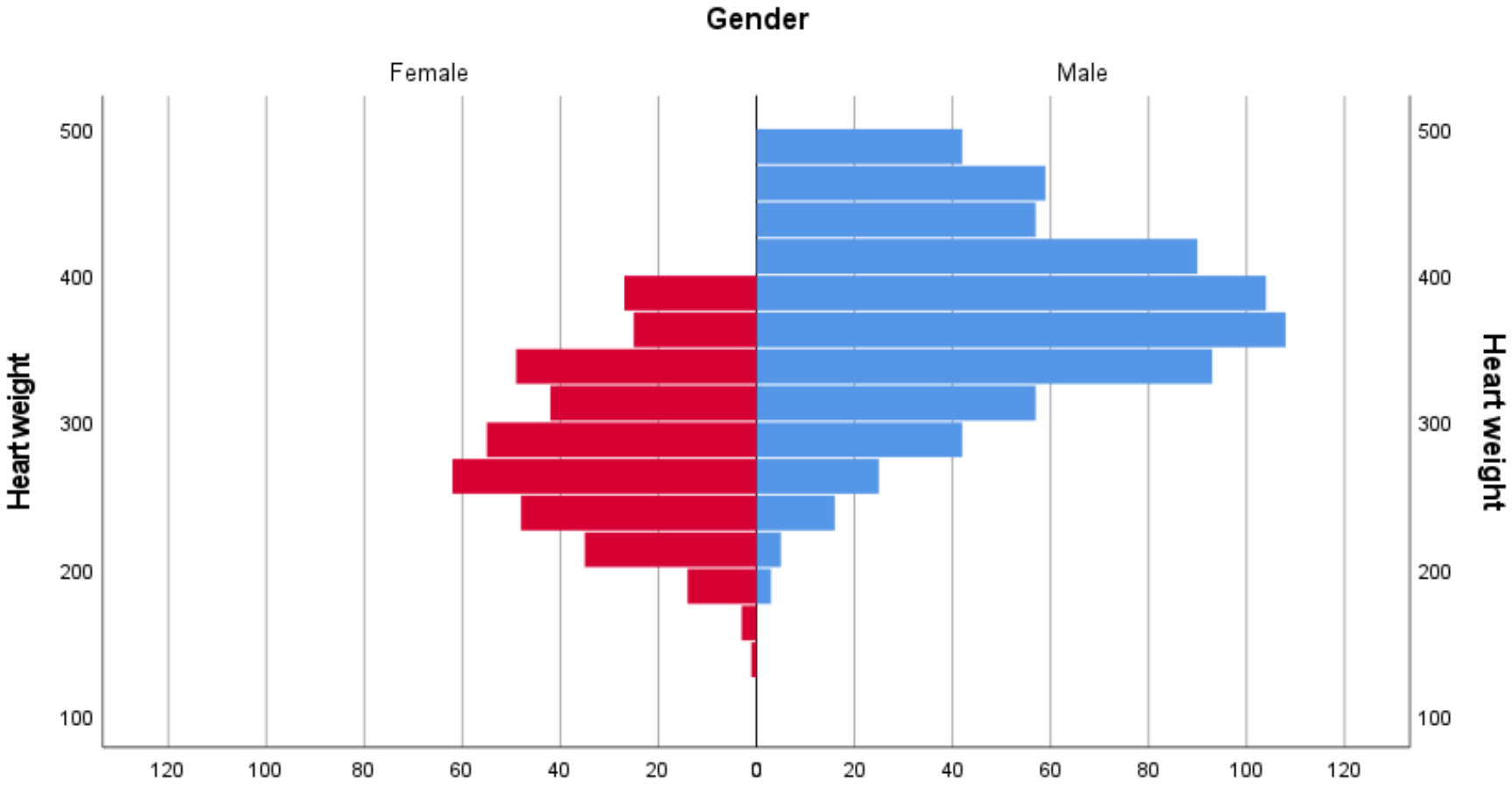


Figure 4.6. Population pyramid for heart weight in males and females.

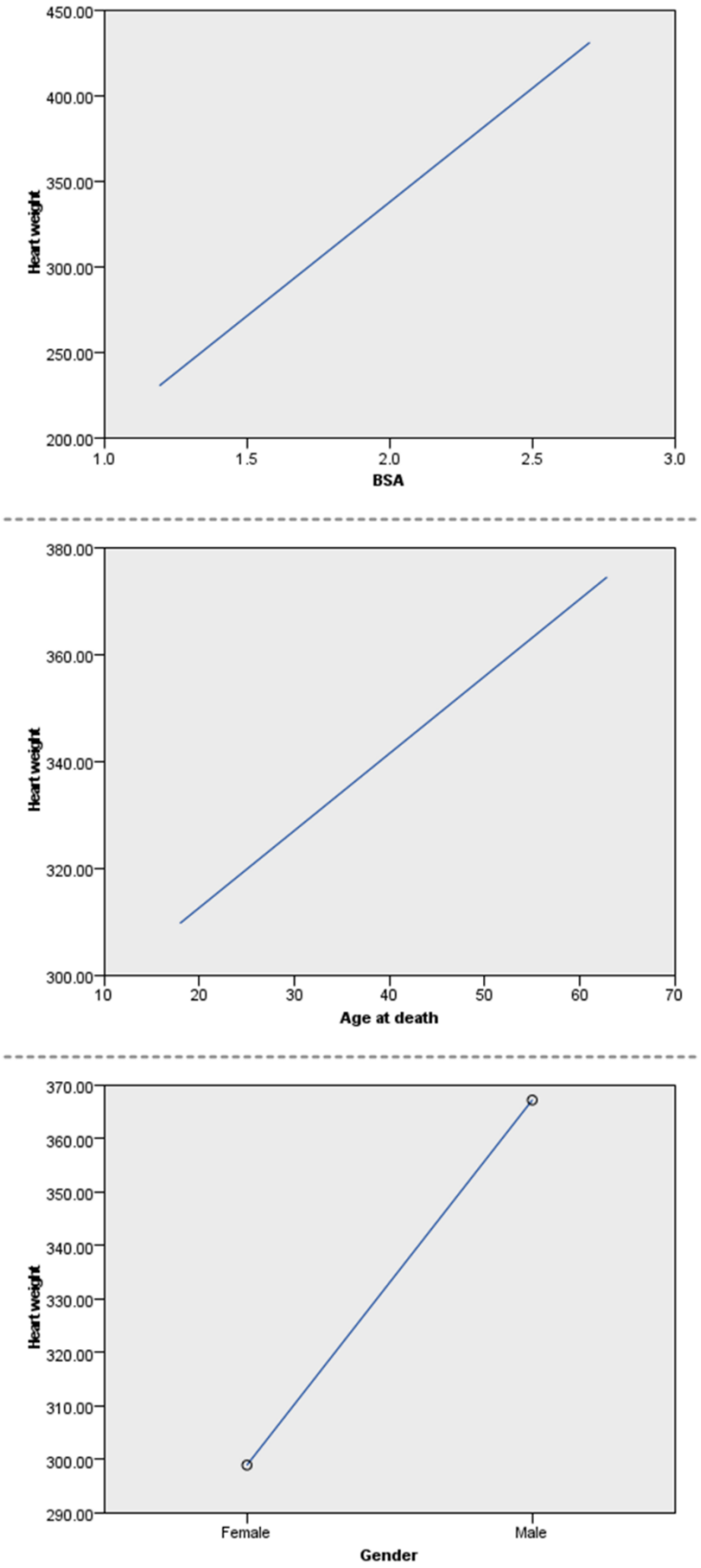


Figure 4.7. Estimated means based upon significant effects. Gender was the most important predictor of heart weight.

	Female		Male	
BSA	Predicted mean (g)	Predicted upper limit (g)	Predicted mean (g)	Predicted upper limit (g)
1.0	170	230	239	292
1.1	184	245	252	306
1.2	197	260	265	321
1.3	210	274	279	336
1.4	224	289	292	350
1.5	237	304	305	365
1.6	250	318	319	380
1.7	264	333	332	394
1.8	277	348	345	409
1.9	290	362	359	424
2.0	304	377	372	438
2.1	317	392	385	453
2.2	330	406	398	468
2.3	343	421	412	483
2.4	357	436	425	497
2.5	370	450	438	512
2.6	383	465	452	527
2.7	397	480	465	541
2.8	410	495	478	556
2.9	423	509	492	571
3.0	437	524	505	585

Table 4.3. Reference table for estimated normal heart weight and 95% confidence interval for increments of 0.1m^2 body surface area for males and females of 34 years of age. Predicted mean = 56.682 – 68.276 (gender = female) + 133.053 (body surface area) + 1.442 (age). Predicted upper limit = 86.392 – 61.382 (gender = female) + 146.876 (body surface area) + 1.717 (age).

Variable	Unit	Summary statistic	Normal hearts (n=1062)	Female (n=361)	Male (n=701)	p value
Coronary artery dominance						
Right	Count	Number/Total (percentage)	999/1062 (94%)	336/361 (93%)	663/701 (95%)	0.559
Left	Count	Number/Total (percentage)	52/1062 (5%)	20/361 (6%)	32/701 (5%)	
Codominance	Count	Number/Total (percentage)	11/1062 (1%)	5/361 (1%)	6/701 (1%)	
Oval fossa						
Width	mm	Mean±SD Median, Q1-Q3 Range	15±5 15, 12-18 4-40	15±5 15, 12-18 44-33	16±4 15, 12-18 5-40	0.337
Height	mm	Mean±SD Median, Q1-Q3 Range	14±4 14, 10-16 3-35	14±5 12, 10-16 3-33	14±4 14, 10-16 3-35	0.310
Probe patent	Count	Number/Total (percentage)	111/917 (12%)	45/312 (14%)	66/605 (11%)	0.122

Table 4.4. The oval fossa dimensions, presence of probe patency and coronary artery dominance. The coronary artery dominance, oval fossa dimensions and presence of probe patency for the entire cohort and broken down into females and males.

Coronary artery dominance

The arrangement of the coronary arteries, assessed by discerning the artery supplying the posterior descending artery, is right dominant in 999 (94%) cases, left dominant in 52 (5%) cases, and co-dominant in 11 (1%) cases. These proportions are similar in females and males (Table 4.4).

Atria

The right atrial measurement between the inferior caval vein ostium and the tip of the appendage is 57±12mm (60, 50-65, 24-100). The right atrial measurement between the ostia of the inferior and superior caval veins is 41±10mm (40, 35-50, 20-80). The left atrial measurement between the left and right superior pulmonary vein ostia is 42±9mm (40, 35-50, 16-85). The left atrial measurement between the atrioventricular junction and the superior surface of the left atrium is 37±8mm (35, 30-40, 14-70). These measurements are all significantly less in females compared to males (all $p<0.011$) (Table 4.2 and Figure 4.9).

Oval fossa

The oval fossa had a width of 15±5mm (15, 12-18, 4-40), and a height of 14±4 (14, 10-16, 3-35). The fossa is probe patent in 111 of 917 cases (12%) (Figure 4.8). These measurements are similar in females and males. There is probe patency in a slightly larger proportion of females than males (45, 14% vs 66, 11%) but this does not reach significance (Table 4.4).

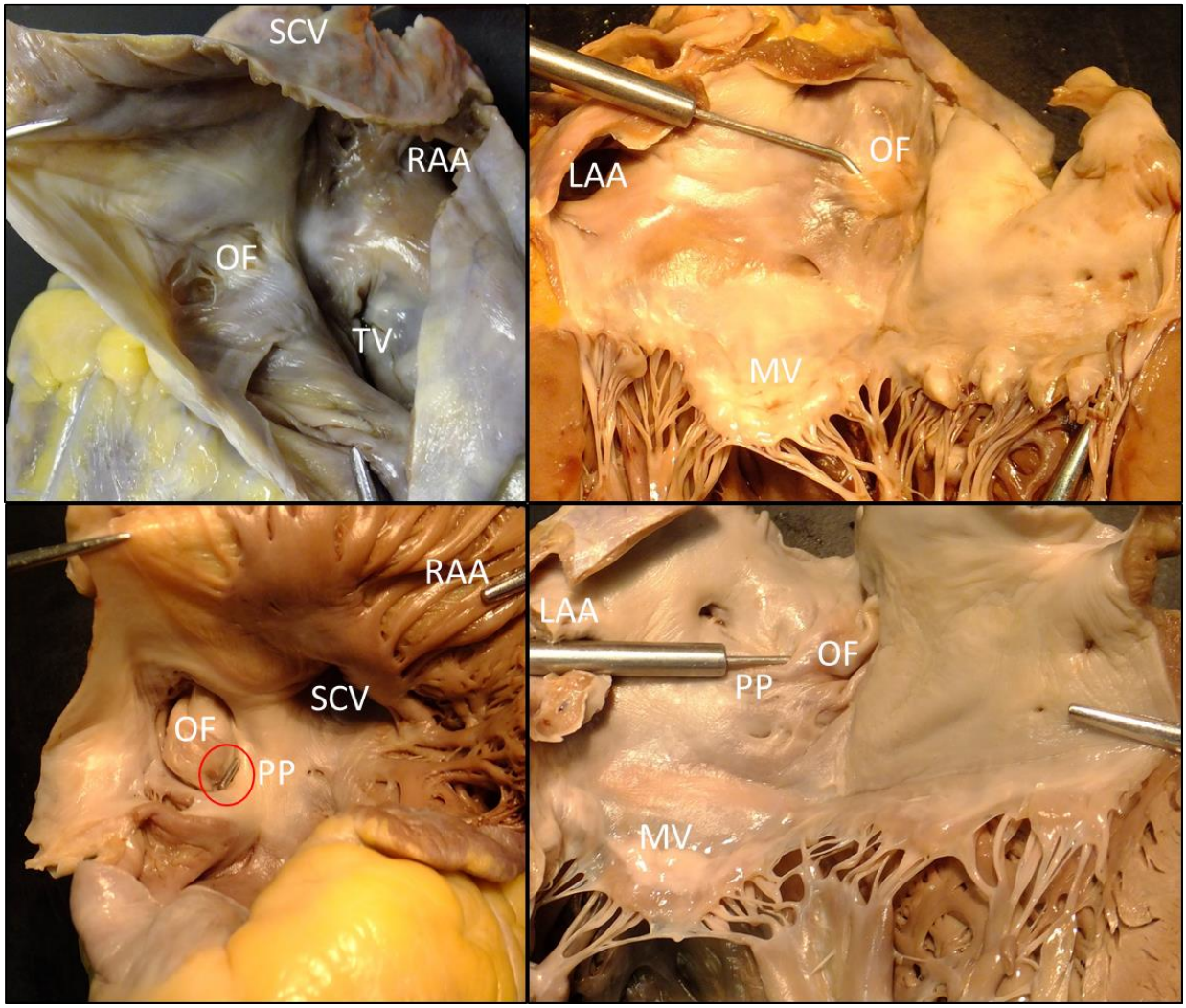


Figure 4.8. The normal oval fossa which may be probe patent. The left panels illustrate the oval fossa from the right atrium and the right panels illustrate the oval fossa from the left atrium. The top panels show an oval fossa which is not probe patent and the bottom panels shows an oval fossa where there is probe patency (circled in red). LAA: left atrial appendage; MV: mitral valve; OF: oval fossa; PP: probe patent; RAA: right atrial appendage; SCV: superior caval vein; TV: tricuspid valve.

Right ventricle

The average RV cavity diameter is 29±6mm (30, 25-35, 10-48). The RV mural thickness is 2.7±1.0mm (3.0, 2.0-3.0, 0.5-8.0) for the anterior wall, 2.8±1.0mm (3.0, 2.0-3.0, 1.0-10.0) for the lateral wall, 3.6±1.0mm (4.0, 3.0-4.0, 1.0-10.0) for the posterior wall, and 3.2±1.0mm (3.0, 3.0-4.0, 1.0-7.0) for the RVOT.

The cavity diameter and mural thickness measurements are all significantly smaller in females when compared to males (all $p<0.001$) (Table 4.2).

Left ventricle

The LV cavity diameter is 31±7mm (30, 25-35, 8-49). The septal wall thickness is 13±3mm (12, 11-15, 7-21). The LV mural thickness is 12±2mm (12, 10-14, 7-20) for the anterior wall, 12±2mm (12, 11-14, 7-22) for the lateral wall, and 12±2mm (11, 10-13, 7-20) for the posterior wall.

The thickness measurements, as well as the cavitary diameter, are all significantly smaller in females compared to males (all $p<0.007$).

Epicardial fat

The thickness of the RV epicardial fat is 1.2±1.3mm (1.0, 0-2.0, 0-8.0) for the anterior wall, 2.8±2.2mm (2.0, 1.0-4.0, 0-15.0) for the lateral wall, 0.2±0.6mm (0, 0-0, 0-6.0) for the posterior wall, and 0.9±1.2mm (1.0, 0-1.0, 0-9.0) for the RVOT.

These measurements are all significantly thicker in females when compared to males (all $p<0.045$) (Table 4.5 and figure 4.10).

Variable	Unit	Summary statistic	Normal heart (n=1062)	Female (n=361)	Male (n=701)	p value
Right ventricle						
Anterior fat	mm	Mean±SD Median, Q1-Q3 Range	1.2±1.3 1.0, 0-2.0 0-8.0	1.4±1.5 1.0, 0-2.0 0-8.0	1.1±1.2 1.0, 0-2.0 0-7.0	**0.002**
Lateral fat	mm	Mean±SD Median, Q1-Q3 Range	2.8±2.2 2.0, 1.0-4.0 0-15.0	3.1±2.5 2.0, 1.0-5.0 0-15.0	2.6±2.1 2.0, 1.0-3.0 0-15.0	**0.002**
Posterior fat	mm	Mean±SD Median, Q1-Q3 Range	0.2±0.6 0, 0-0 0-6.0	0.2±0.7 0, 0-0 0-6.0	0.1±0.5 0, 0-0 0-5.0	**0.045**
RVOT fat	mm	Mean±SD Median, Q1-Q3 Range	0.9±1.2 1.0, 0-1.0 0-9.0	1.0±1.3 1.0, 0-1.0 0-8.0	0.8±1.1 0, 0-1.0 0-9.0	**0.029**
Left ventricle						
Anterior fat	mm	Mean±SD Median, Q1-Q3 Range	0.7±1.3 0, 0-1.0 0-10.0	0.8±1.4 0, 0-1.0 0-10.0	0.6±1.2 0, 0-1.0 0-7.0	**0.011**
Lateral fat	mm	Mean±SD Median, Q1-Q3 Range	0.3±0.8 0, 0-0 0-9.0	0.4±0.9 0, 0-0 0-9.0	0.3±0.8 0, 0-0 0-6.0	0.082
Posterior fat	mm	Mean±SD Median, Q1-Q3 Range	0.1±0.6 0, 0-0 0-9.0	0.2±0.8 0, 0-0 0-9.0	0.1±0.4 0, 0-0 0-4.0	**0.027**

Table 4.5. Subepicardial fat thickness. The table shows the subepicardial fat thickness for the anterior, lateral and posterior walls of the right and left ventricular as well as the right ventricular outflow tract (RVOT).

The thickness of the LV adipose tissue is 0.7±1.3mm (0, 0-1.0, 0-10.0) for the anterior wall, 0.3±0.8mm (0, 0-0, 0-9.0) for the lateral wall, and 0.1±0.6mm (0, 0-0, 0-9.0) for the posterior wall.

These measurements are also significantly thicker in females when compared to males for the anterior and posterior walls (all $p<0.027$).

Valve circumference

The average tricuspid valvar circumference is 97±14mm (95, 90-105, 50-145). The pulmonary valvar circumference is 54±10mm (50, 50-60, 25-106).

The mitral valvar circumference is 77±13mm (75, 70-85, 45-125). The aortic valvar circumference is 52±8mm (50, 45-55, 33-90) and the ascending aortic circumference is 53±8mm (50, 50-60, 35-85).

All valvar circumferences, and the ascending aortic circumference, are significantly smaller in females when compared to males (all $p<0.001$) (Table 4.6). A summary of the main differences between males and females is given in figures 4.8-4.10.

Variable	Unit	Summary statistic	Normal heart (n=1062)	Female (n=361)	Male (n=701)	p value
Tricuspid valve circumference	mm	Mean±SD Median, Q1-Q3 Range	97±14 95, 90-105 50-145	92±13 90, 81-100 55-130	99±14 100, 90-110 50-145	**<0.001**
Pulmonary valve circumference	mm	Mean±SD Median, Q1-Q3 Range	54±10 50, 50-60 25-106	51±9 50, 45-55 25-80	56±10 55, 50-60 30-106	**<0.001**
Mitral valve circumference	mm	Mean±SD Median, Q1-Q3 Range	77±13 75, 70-85 45-125	74±11 70, 65-80 45-115	79±14 80, 70-90 45-125	**<0.001**
Aortic valve circumference	mm	Mean±SD Median, Q1-Q3 Range	52±8 50, 45-55 33-90	50±7 50, 45-55 35-75	53±8 50, 50-60 33-90	**<0.001**
Ascending aortic circumference	mm	Mean±SD Median, Q1-Q3 Range	53±8 50, 50-60 35-85	51±8 50, 45-55 35-80	54±8 55, 50-60 35-85	**<0.001**

Table 4.6. Valvular and aortic circumferences. The table gives the valvular circumferences for the atrioventricular valves, the semilunar valves and the ascending aorta for the entire cohort and broken into males and females.

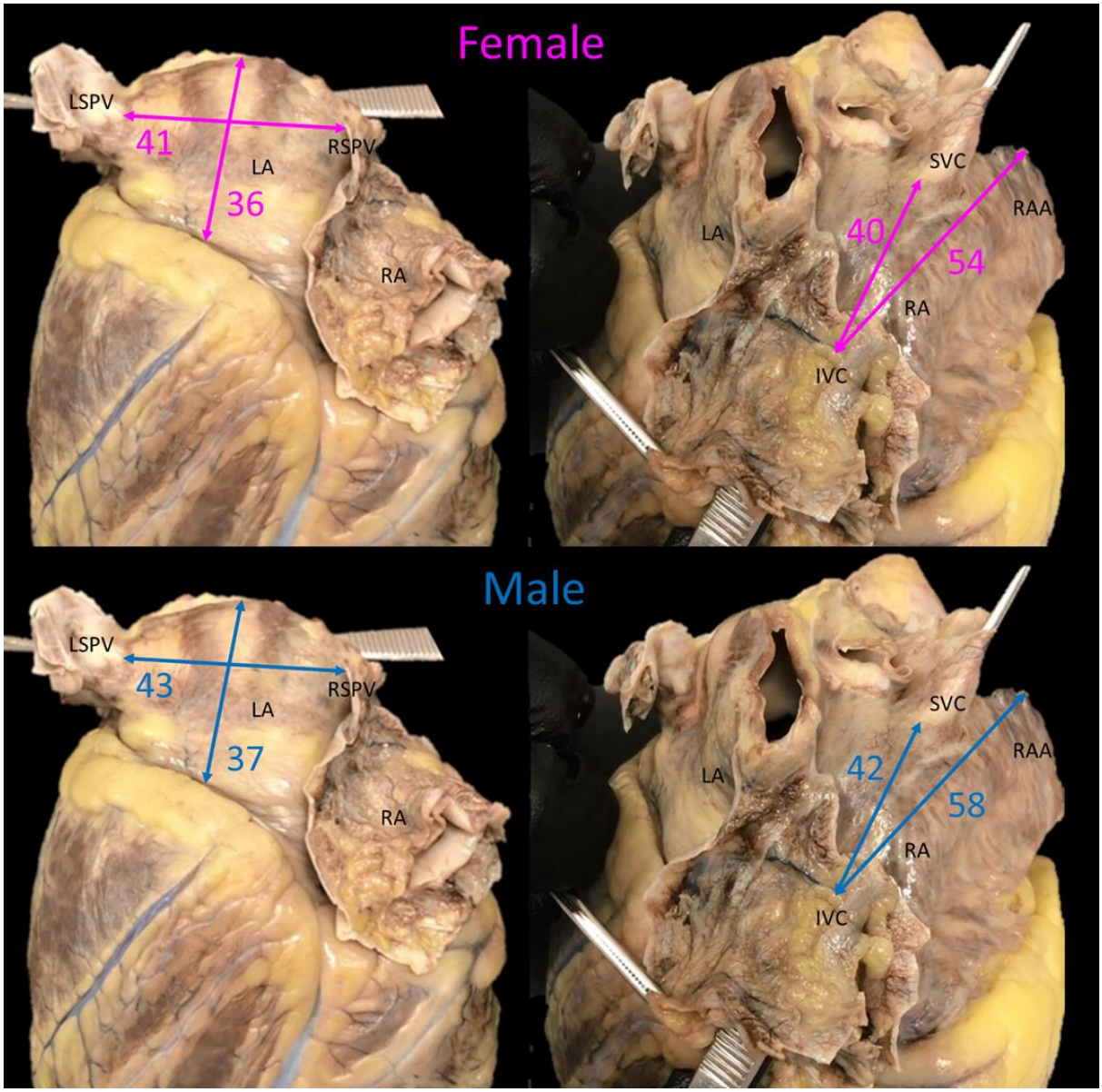


Figure 4.9. The average atrial measurements in females (pink) compared to males (blue). Females had smaller average measurements than males. ICV: inferior caval vein; LA: left atrium; LSPV: left superior pulmonary vein; RA: right atrium; RAA: right atrial appendage; RSPV: right superior pulmonary vein; SVC: superior caval vein.

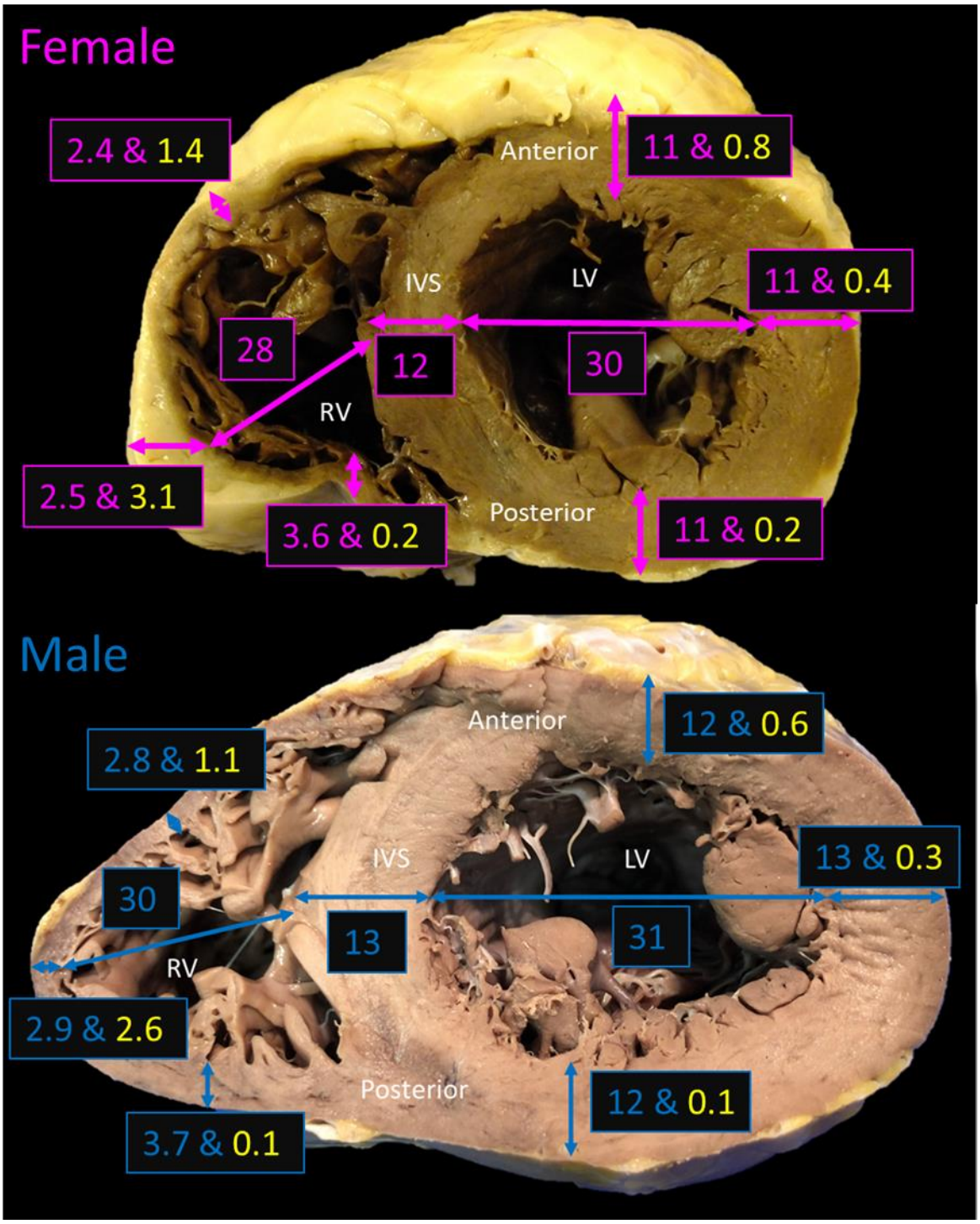


Figure 4.10. The average mural, subepicardial fat and cavity dimensions for females (pink) and males (blue). Subepicardial fat (yellow) is greater in females than males whilst muscular wall thickness and cavity diameters are greater in males. IVS: interventricular septum; LV: left ventricle; RV: right ventricle.

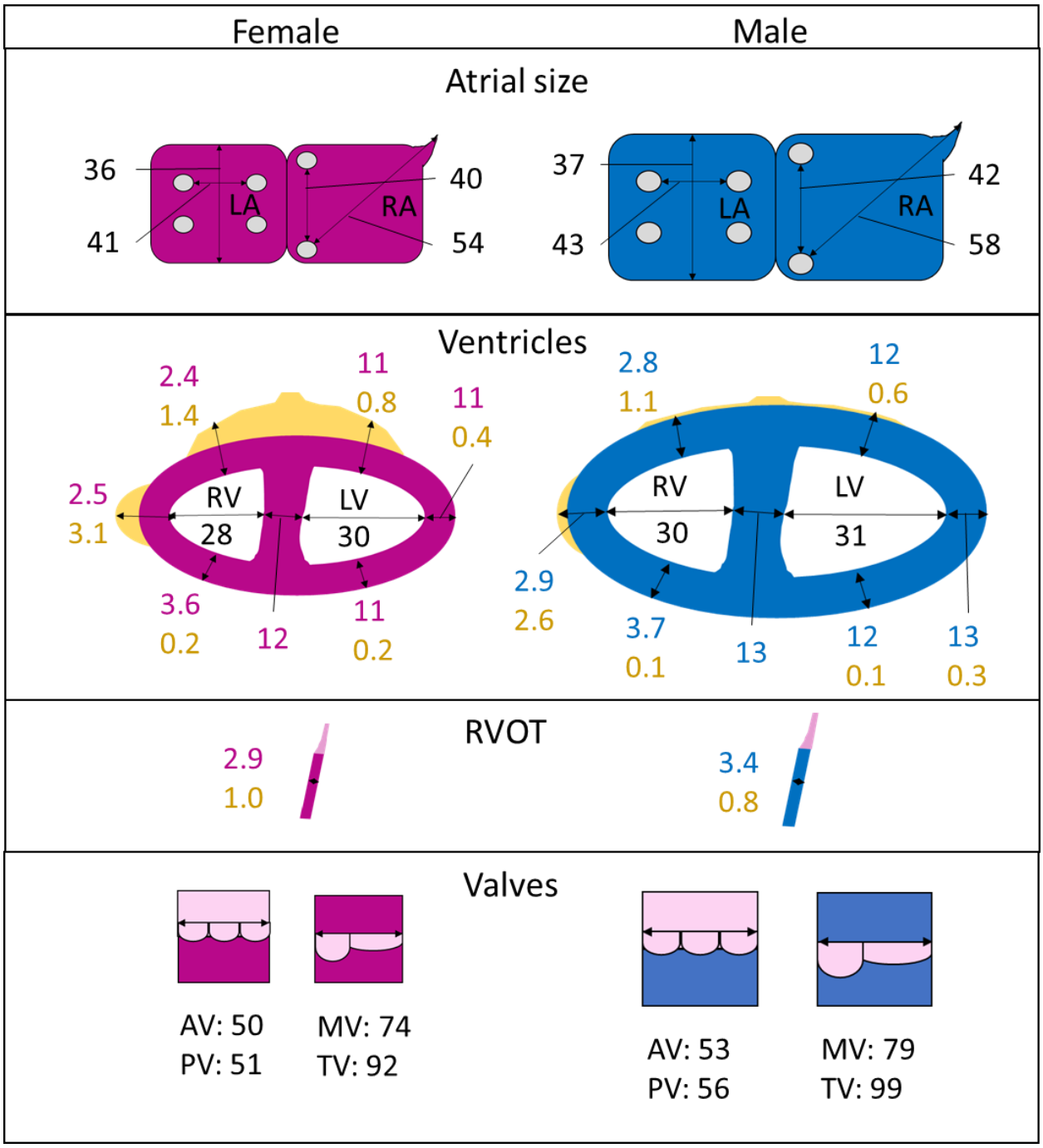


Figure 4.11. Graphic representation of the differences between female and male hearts. Subepicardial fat thickness are given in yellow and mural wall thickness in pink or blue. The dimensions of the right atrium (RA), left atrium (LA), mid-ventricular mural thickness, right ventricular outflow tract (RVOT) mural thickness and valvular circumferences are all smaller in females. Subepicardial fat thickness are greater in

females. AV: aortic valve; LV: left ventricle; MV: mitral valve; MVS: mid-ventricular slice; PV: Pulmonary valve; RV: right ventricle; TV: tricuspid valve.

Discussion

We provide the first comprehensive morphological analysis of the largest cohort of normal hearts over a range of ages on both genders. It is established that the male heart is heavier than the female heart (De La Grandmaison, Clairand and Durigon, 2001; Wingren and Ottosson, 2015; Skurdal and Nordrum, 2016). There have been descriptions of cardiac anatomy (Anderson and Becker, 1985; Anderson, Razavi and Taylor, 2004), but there are no comprehensive detailed measurements of the atria, ventricles, epicardial fat, fossa ovalis, valvar circumferences and ascending aorta described.

Heart weight

Previous studies have demonstrated heart weight is greater in males than females. In 1998, Kitzman et al reported on 765 autopsy specimens from those aged 20 to 99 years. In contrast to our findings they found body weight was a better predictor of normal heart weight than body surface area or height. Similar to our findings they report that males had a greater heart weight than females at all ages. They provide an average heart weight of 280g for a 70kg female and 349g for a 80kg male (Kitzman *et al.*, 1988).

In 2001, De La Grandmaison et al, reviewed the autopsy records from French Caucasian adults who died of external causes (De La Grandmaison, Clairand and Durigon, 2001). Organ weights were compared in 355 males and 329 females. They

found an average heart weight of 365g in males and 312g in females. In contrast to our findings age had the strongest correlation with heart weight. They also found body mass index correlated with heart weight. Despite this, males continued to possess considerably higher heart weights than females when stratified by body mass index. Heart weights ranged up to 630g in males and 590g in females which is considerably above what we consider normal.

Wingren and Ottoson, performed a nationwide analysis in Sweden of 27,645 adult autopsy cases with an external cause of death (Wingren and Ottosson, 2015). Histograms show heart weights to be considerably greater in males than females in underweight, normal/overweight and obese individuals but no average measurements broken down by gender are presented in the report. The most important explanatory variables for heart weight were body mass index, height and gender. Their graphs show heart weights ranging over 1000g which is markedly abnormal.

Skurdal and Nordrum, examined the autopsy reports from 692 Caucasian individuals above the age of 20 years old “without cardiac disease” (Skurdal and Nordrum, 2016). They found average heart weight to be 316g in females compared to 395g in males. Sex and body weight were the most important explanatory variables of heart weight. They include cases with heart weights close to 700g which is above what we consider normal and they acknowledge that these cases may represent cardiomyopathy.

Gaitskell et al, examined the reports from 384 adult autopsy cases from a single centre in the UK (Gaitskell, Perera and Soilleux, 2011). Average heart weight was 388g in males and 338g in females. The most important explanatory variables of

heart weight were gender and body surface area. Heart weight ranged up to 765g which we would consider markedly abnormal.

The average heart weights in these studies are comparable but higher in most than that found in the present study of 285g in females and 374g in males. This is most likely to be due to the inclusion of hearts which we would consider abnormal within their cohorts. In our cohort, cases with an unexplained heart weight above 400g in females and 500g in males are denoted as idiopathic LV hypertrophy and included in the cardiomyopathy group. Within this cohort with hypertrophy, we have found that 30% of decedents had relatives diagnosed with either cardiomyopathy or channelopathy upon cardiological screening. This was performed in 46 families of decedents (Finocchiaro *et al.*, 2020). HCM genes were not identified in this cohort suggesting this is a distinct entity.

Ventricular wall measurements

Kitzman et al, identified no difference between the mural measurements in males and females but this was based upon a single measurement of each ventricular free wall (Kitzman *et al.*, 1988). Their reported means for a combined group of females and males ranged from 3.4-4.0mm for the RV and 10.8-12.6mm for the LV throughout the decades. The mural measurements remained towards the upper end and relatively similar until after 70 years old where they began to decrease. Their measurements for the younger age group are comparable to ours.

Large cohort studies in living patients have used the modalities of echocardiography and magnetic resonance imaging to demonstrate that septal and posterior measurements of the LV wall are comparatively larger in males than females (Salton *et al.*, 2002; Kou *et al.*, 2014; Pelà *et al.*, 2016). A further large cohort study of over

4000 individuals, has observed RV mass, assessed by magnetic resonance imaging, to be comparatively greater in males (Kawut *et al.*, 2011). These reports support the established findings that males have greater myocardial mural muscle measurements.

Cavity size

The dimensions of the atria have not previously been studied in post mortem specimens and shown to exhibit differences between males and females. This is a novel method and these results will provide a reference for future studies as there is increasing emphasis on atrial disease and atrial fibrillation. Previous large cohort studies using imaging in individuals have similar findings between the genders to our study. Increased sizes of all four chambers in males compared to female has been observed previously on echocardiography and magnetic resonance imaging in three large studies (Salton *et al.*, 2002; Pfaffenberger *et al.*, 2013; Kou *et al.*, 2014).

Oval fossa

A large study of nearly 1000 hearts from the Mayo clinic found that up to one-third of individuals have fossas that remained patent subsequent to birth, particularly younger individuals (Hagen, Scholz and Edwards, 1984). An older study dating back to the 1920s, reports probe patency in 35% of 1000 consecutive hearts examined (Thompson and Evans, 1930). These were higher than the proportion in our study, but a study of 500 hearts from the United States found the incidence to be 17% (Seib, 1934) more in line with our findings. These differences may be explained by the force with which the probe is placed between the rim of the fossa and its floor during assessment. Patent oval fossa is recognised to serve as a conduit for

paradoxical embolization and ischaemic stroke and is therefore important to document in the normal population (Homma and Sacco, 2005).

Coronary arterial dominance

The literature shows considerable variation in coronary artery dominance in different studies and by method used.

The results of previous pathology studies of coronary artery dominance have shown marked variation. Estimates have ranged from 34-71% right dominance, 20-48% left dominance and 9-20% co-dominant in studies of 230-350 hearts (Schlesinger, 1940; Paulsen and Vetner, 1973; Von Lüdinghausen, 2003). We cannot explain this huge variation.

A study of 1453 cases using post mortem coronary angiogram reports 81% right dominance, 9.1% left dominance and 10% codominance (Knaapen *et al.*, 2013). Estimates of left dominance and co-dominance in living Caucasian populations using computed tomography angiography range from 5-10% and 3.8-20% percent respectively (Erol and Seker, 2012; Shriki *et al.*, 2012; Ihdayhid *et al.*, 2020).

Our study observed a lower proportion of co-dominance but is within the lower end of the estimate for left dominance examined by angiography. Left dominant circulation has been associated with poorer prognostic outcomes in individuals with and without coronary disease in a population of 1425 individuals referred for computed tomography coronary angiography. The presence of a left dominant circulation was identified as an independent risk factor for extensive myocardial infarction and death especially in individuals with coronary artery disease (Veltman *et al.*, 2012). This knowledge is important for cardiac interventionalists.

Valve circumference

Previous post mortem valvar studies have commented upon larger circumferences in males congruent with our study (Westaby *et al.*, 1984; Kitzman *et al.*, 1988). Kitzman states that the valve circumferences “were almost invariably greater in men than women for each of the decades” however they do not provide figures or numerical values broken down by gender (Kitzman *et al.*, 1988). Similar to our report, they found circumference of the tricuspid was largest followed by the mitral with the aortic and pulmonary valves being smallest and of a similar size. For their whole cohort, they show increases throughout the decades for the aortic and pulmonary valves whereas a decrease in the mitral and tricuspid after 70 years old. Their reported mean circumferences for the whole cohort ranged from 100-111mm for the mitral valve, 82-91mm for the tricuspid valve, 57-79mm for the aortic valve and 57-73mm for the pulmonary valve. The larger mean sizes observed in this report may be explained by an American population.

Westaby et al, report on 160 hearts from adults with and without congestive cardiac failure (Westaby *et al.*, 1984). Gender and failure were related to valve area but other variables such as body surface area were found to correlate poorly. They found larger circumferences in males compared to females in all valves. This study also observed the valves to have a greater circumference compared to ours, which may be explained by their older American population and the presence of cardiac disease such as ischaemic heart disease.

Subepicardial fat thickness

A previous study by professor Sheppard of 148 normal hearts, noted that RV subepicardial fat was increased with age and female sex. The greatest amount of

epicardial fat was seen in the lateral right ventricle wall, followed by the anterior wall with little or no fat present posteriorly. The lateral wall epicardial thickness ranged from 0-12mm. This is in line with these findings (Tansey, Aly and Sheppard, 2005). Gender differences in subepicardial fat thickness and volume assessed using echocardiography has shown varied results. Kim et al, reported on 628 patients with suspected angina and related epicardial adipose tissue thickness to coronary arterial disease, however they found no difference between the genders. They also observed that women had more subepicardial fat post-menopause (Kim *et al.*, 2018). A study of 371 patients with severe aortic stenosis showed that epicardial adipose tissue volume was greater in males than females in a study of 371 individuals with severe aortic stenosis (Mancio *et al.*, 2017). Epicardial adipose tissue was related to cardiac function in elderly females in another study by Kim et al of 152 individuals, but no difference was observed in between genders in individuals younger than 60 (Kim *et al.*, 2017). In contrast to these studies, we have found that the normal female heart has a greater subepicardial fat thickness. A post mortem study of “unselected” hearts from 172 males and 28 females published in German from 1989 noted that RV subepicardial fat was on average thicker in females (Schejbal, 1989). Whilst in keeping with our study, this included ischaemic and abnormal hearts.

Epicardial adipose tissue associations and role in disease

Increased epicardial adipose tissue has been related to myocardial mass (Corradi *et al.*, 2004). Corradi et al, studied 117 hearts comparing normal hearts to those with hypertrophy and/or ischaemia and found that there was a preserved ratio of fat to muscle in myocardial hypertrophy suggesting that fat increases with muscle thickness. Increased epicardial adipose tissue has also been related to smoking and

elevated heart rate (Miyazawa *et al.*, 2018). Miyazawa et al, used computed tomography to examine 623 Japanese men aged 40-79 years without a history of cardiovascular disease following them up for an average of 4.7 years finding that current smoker status and increased heart rate were independently associated with increases in subepicardial fat volume. The most established and promising relations, however, are to acute coronary events (Nakanishi *et al.*, 2014) and atrial fibrillation (Hatem and Sanders, 2014). Nakanishi et al, examined 517 non-obese patients with coronary disease using computed tomography following them up for 4 years and found that increases in subepicardial fat volume, despite risk management, were associated with increased high risk or obstructive plaques. The largest report demonstrating the relationship between atrial fibrillation and subepicardial fat derives from the Framingham Heart study. Computed tomography was used to examine 3217 participants, of which 54 developed atrial fibrillation. Pericardial fat volume was found to be associated with prevalent atrial fibrillation following adjustment for risk factors including body mass index (Thanassoulis *et al.*, 2010).

The extent of fat may also play a role in reducing the effects of catheter ablation (Nascimento Matos *et al.*, 2020; Zipse *et al.*, 2020). Nascimento Matos et al, followed up 575 patients undergoing pulmonary vein isolation for atrial fibrillation (Nascimento Matos *et al.*, 2020). Subepicardial fat was quantified using computed tomography. They found that pericardial fat was a strong independent predictor of atrial fibrillation relapse outperforming other recognised clinical risk factors. Zipse et al, used bovine myocardium with subepicardial fat to assess different radiofrequency ablation strategies (Zipse *et al.*, 2020). They found that increasingly thick subepicardial fat attenuated lesion size regardless of strategy.

There are various reports on the role of subepicardial fat in disease. It has been proposed to regulate granulopoiesis, and to serve as a source for inflammatory mediators leading to cardiovascular disease (Mazurek *et al.*, 2003; Horckmans *et al.*, 2018). It has also been linked to fibrosis and function following myocardial infarction as well as myocyte dysfunction in diabetes (Greulich *et al.*, 2012; Horckmans *et al.*, 2018). The differences in subepicardial fat between the genders should be adjusted for when assessing for disease.

Limitations

Our study will include cases where SCD is due to channelopathies. Due to the relatively lower numbers of old aged individuals in our sample population, it is uncertain how the heart weight calculator will perform in these individuals.

Concluding remarks

When evaluating the abnormal, it is of central importance to understand the normal. Gender is the most important predictor of heart weight. We provide an equation to calculate expected heart weight and reference table of expected heart weight according to body surface area for males and females. The fact that subepicardial fat is higher in females should be accounted for when examining this population. Similarly, it is important to account for the fact the female heart is smaller with regard to the measurements of mural thickness, cavity diameters and valvar circumferences so as not to under call pathologic alterations. This is further emphasised by the fact that gender is a modifier of cardiovascular health, disease, and medicine where discrepant outcomes occur for a variety of reasons (Mauvais-Jarvis *et al.*, 2020).

Summary of macroscopic findings in the normal heart

- Gender, body surface area and age predict heart weight
- Gender is the most important predictor of heart weight
- Heart weight is greater in males
- Both atria are larger in males
- There is no difference in the oval fossa dimensions for both genders
- 12% of oval fossas are probe patent with no difference between genders
- Both ventricular diameters are larger in males
- All muscle walls of both ventricles are thicker in males
- Epicardial fat is thicker in females in both ventricles
- All valve circumferences are larger in males
- Aortic vessel circumference is larger in males
- 94% are right coronary artery dominant, 5% are left coronary dominant and 1% are codominant with no difference between genders

CHAPTER 5 COMPOSITION OF THE NORMAL HEART: FAT, COLLAGEN, MUSCLE AND INNERVATION

Introduction

In chapter 3 we have shown that the morphologically normal heart underlies SCD in a majority of our cohort. This is followed by chapter 4 which established the normal dimensions of the heart. In this chapter we will examine the components of the normal ventricular tissue microscopically.

We will report on the muscle, fat and collagen composition of the ventricular myocardium. We also report on ventricular innervation in normal hearts. This will act as a baseline for comparison with cardiomyopathy cases.

The normal ventricular cardiac innervation has not previously been histologically characterised in detail and examined using objective automated reproducible quantitative analysis of the myocardium.

Cardiac innervation has been found to be altered within the ischaemic heart and it is postulated that this may contribute towards VA which may result in sudden death (Cao, Chen, *et al.*, 2000; Cao, Fishbein, *et al.*, 2000; Hasan *et al.*, 2006; Oh *et al.*, 2006; Zhu *et al.*, 2019).

Methods

11 hearts from individuals with lethal levels of toxic drugs are randomly selected for compositional and innervation analysis (see figure 2.15). These have been selected to represent truly normal hearts with a non-cardiac death. Sections from the RVOT, the RV free wall (including the anterior, lateral and posterior wall), the IVS, as well as the anterior and posterior LV free wall are stained with PSR, PGP9.5, TH and CT as already described in chapter 2. Positive controls of the sinus node and negative

controls with omission of primary antibody are utilised. Slides are scanned using a Hamamatsu Nanozoomer 2.0RS. Digital image analysis is performed using applications developed within the Visiopharm program (Visiopharm A/S, Agern Alle 24, 2970 Hørsholm, Denmark).

Statistics

Myocardial composition is assessed between areas using log transformed values for collagen, fat, myocyte, PGP9.5, TH and CT proportions (as these values are skewed). A multilevel model is created to allow comparison of hierarchical dependent data based on myocardial location. Variables such as age, sex and ethnicity are incorporated into multivariable analysis. Predictions of collagen, fat, myocytes, PGP9.5, TH and CT are expressed as geometric means and 95% confidence intervals.

Statistical analyses used Stata version 16 (StataCorp, College Station, Texas, USA).

Results

The age at death for 11 males with a morphologically normal heart is 34±11years. Heart weight is 364±63g. The dimensions of the atria, ventricle muscle wall thickness and diameters, valve circumferences and subepicardial fat measurements are provided in table 5.1 and compared with the normal heart from chapter 4.

	Controls	Normal	P value
Heart weight	364±63	344±74	.383
Right atrium 1	54±14	57±12	.435
Right atrium 2	41±9	41±10	.974
Left atrium 1	40±8	42±9	.429
Left atrium 2	36±8	37±8	.881
RV diameter	32±6	29±6	.186
Anterior RV Muscle	3±1	3±1	.901
Lateral RV Muscle	3±1	3±1	.666
Posterior RV Muscle	3±1	4±1	.053
RVOT Muscle	3±1	3±1	.322
LV diameter	33±6	31±7	.243
IVS	13±2	13±3	.953
Anterior LV Muscle	12±2	12±2	.968
Lateral LV Muscle	13±2	12±2	.702
Posterior LV Muscle	12±2	12±2	.968
Mitral valve	83±16	77±13	.124
Tricuspid valve	103±17	96±14	.117
Pulmonary valve	55±12	54±10	.718
Aortic valve	55±9	52±8	.144
Ascending aorta	57±8	53±8	.066
Anterior RV fat	1±1	1±1	.585
Lateral RV fat	2±1	3±2	.062
Posterior RV fat	0±0	0±1	.861
RVOT fat	1±1	1±1	.436
Anterior LV fat	1±1	1±1	.561
Lateral LV fat	0±0	0±1	.394
Posterior LV fat	0±1	0±1	.826

Table 5.1. Macroscopic heart measurements for the controls compared to the normal hearts. The means and standard deviations for heart weight (in grams), atrial dimensions, cavity diameters, muscular wall thickness, valvular and ascending aortic circumferences and epicardial fat thickness (in millimetres) are provided.

Compositional analysis

The microscopic description of the heart will move sequentially through from the epicardium to the endocardium using the terminology described in the methods.

Images of the RVOT, anterior, lateral and posterior RV, IVS, anterior and posterior LV stained with picrosirius red are shown in figures 5.1-5.7 respectively.

Collagen

Microscopically, collagen stains red with picrosirius red.

Epicardium and subepicardial fat

A dense thin line of collagen adjoins the epicardial surface representing the connective tissue of the epicardium which varies in thickness from 1-10 layers (figure 5.8). The epicardium frequently showed fibrous thickening within the RVOT (figure 5.8). Within the subepicardial fat, small wisps of collagen interweave between the adipocytes extending from the epicardium forming a web like structure (figure 5.9). Collagen is prominent and encasing both arteries and veins merging with the adventitia in the subepicardial fat (figure 5.10). This is most substantial around larger vessels where it forms multiple layers encircling the vessel merging with the adventitia. The large veins show 10-20 layers of collagen whilst the large arteries show from 7-10 layers of collagen (figure 5.10). The collagen is also present around medium and smaller vessels. The medium vessels show 5-6 layers and the small vessels show 2-3 layers (figure 5.10).

Large nerve bundles lie in the epicardial far especially around the blood vessels. On the outside of each epicardial nerve bundle there is a ring of collagen representing the epineurium. The largest nerves have 2-3 layers of collagen whilst most other nerves have a single dense ring of collagen. The individual nerve fibres within the bundles are embedded in collagen representing the endoneurium (figure 5.11).

In the subepicardial fat between the epicardium and the myocardial surface, there is a delicate framework of collagen between adipocytes as little whispy fibres

intersecting between individual adipocytes mainly surrounding capillaries (figure 5.9). Adjacent to the epicardium, collagen interweaves between adipocytes becoming more prominent approaching the myocardial surface compared to the middle of the subepicardial fat (figure 5.9). At the junction between the subepicardial fat and the myocardium there is often a whispy thin layer of collagen which lies on the surface of both ventricles and connects with the network of collagen lying between the adipocytes (figure 5.9).

Myocardium

There is a very delicate whispy network of collagen which interweaves between the individual myocytes representing the endomysium. Multiple fine delicate collagen wisps also connect myocytes together representing the perimysium (figure 5.12). This network of collagen is more prominent at the intersection between the subepicardial fat and myocardium. The network of collagen is also prominent in the RV particularly the posterior wall.

Similar to the subepicardial fat, collagen is concentrated on vessels encasing them and forming a complex network following the vessels through the myocardium to the endocardial surface (figures 5.13-5.15). The medium vessels continue to have 5-6 layers of adventitial collagen around them and the smaller vessels have 2-3 layers of collagen (figure 5.13-5.15). The collagen decreases moving towards the endocardial surface as the vessels become smaller (figure 5.15). In areas where the trabeculae and papillary muscles intersect with the ventricular wall, the collagen coalesces forming irregular patches (figure 5.16). These patches of collagen at the intersection between the myocardium and the trabeculae are more frequent in the RV because of the prominence of the trabeculae in RV compared to the LV. Within the trabeculae

and papillary muscles, the penetrating vessels are surrounded by more collagen than elsewhere in the myocardium (figure 5.17).

There is a dense layer of collagen underlying the endocardial surface representing connective tissue which ranges from 1-10 layers (figure 5.18). This is present along the inner surface of the myocardium throughout the heart, also enclosing trabeculae and papillary muscles. The endocardial collagen is frequently thicker in trabeculae and papillary muscles than elsewhere where it ranges from 4-12 layers (figure 5.18).

Fat

Fat appears clear on picrosirius red staining. The fat is predominantly distributed on the outer myocardial surface below the epicardium arranged as a continuous sheet (figure 5.19). The fat is always more prominent in the RV than the LV as shown macroscopically. This layer is present in the anterior and lateral RV free wall, the RVOT and the anterior LV and is much less in the posterior LV around arteries and veins. There is no well delineated layer of fat on either surface of the IVS just clusters of adipocytes. Microscopically, within the myocardium, fat is found around large vessels encasing both the perivascular collagen and the vessel itself (figure 5.13). This is most prominent in the free wall RV and RVOT. It present to a lesser extent in the LV and the IVS. The large vessels surrounded with fat extend into the inner third of myocardium of both ventricles (figure 5.13). Fatty infiltration of the myocardium in the absence of a large vessel is always present in the RV and can consist of single adipocytes up to a large layer (figure 5.20). The fat may extend extensively into the wall extending focally to the endocardium particularly in the anterior and lateral RV wall but not the posterior RV. This is not present in the IVS or

LV where the fat is only present with blood vessels and not alone like in the RV. Occasional adipocytes are present within the endocardium (figure 5.21).

Myocytes

Microscopically the myocytes appear yellow/orange on picrosirius red staining. Within the RV, the outermost myocytes are occasionally connected to the rest of the myocardium but are frequently isolated from the rest of the myocardium between strands of infiltrating fat (figure 5.22). Single and clusters of myocytes are embedded in the fat and can extend a considerable distance parallel to the rest of the myocardium (figure 5.22). The myocytes generally lie parallel and/or end to end to each other within these strands (figure 5.22). Frequently in the RV, there are alternating stretches of myocytes and adipocytes extending a considerable distance into the inner myocardium in most locations except for the posterior wall where there is little fat (figure 5.22).

Within the RV inner myocardium, the myocytes become predominant with less adipocytes except around blood vessels (figure 5.22). Within the RV inner wall, the myocytes exhibit a haphazard alignment with disarray being a prominent feature especially in trabeculae (figure 5.23).

Within the LV, there is a sharp delineation between the subepicardial fat and the myocytes with no infiltration of fat except around blood vessels (figure 5.19). This sharp delineation between subepicardial fat and myocardium contrasts with the RV where adipocytes infiltrate extensively into the myocardium. The vast majority of myocytes in the LV myocardium show a parallel arrangement lying side to side and end to end to one another. The myocytes of the trabeculae and around vessels show disarray (figure 5.23). The disarray of the trabeculae is less marked than in the RV

because the trabeculae are less prominent in the LV. The regular orientation of the myocytes in the LV is very different than in the RV where disorganisation is common.

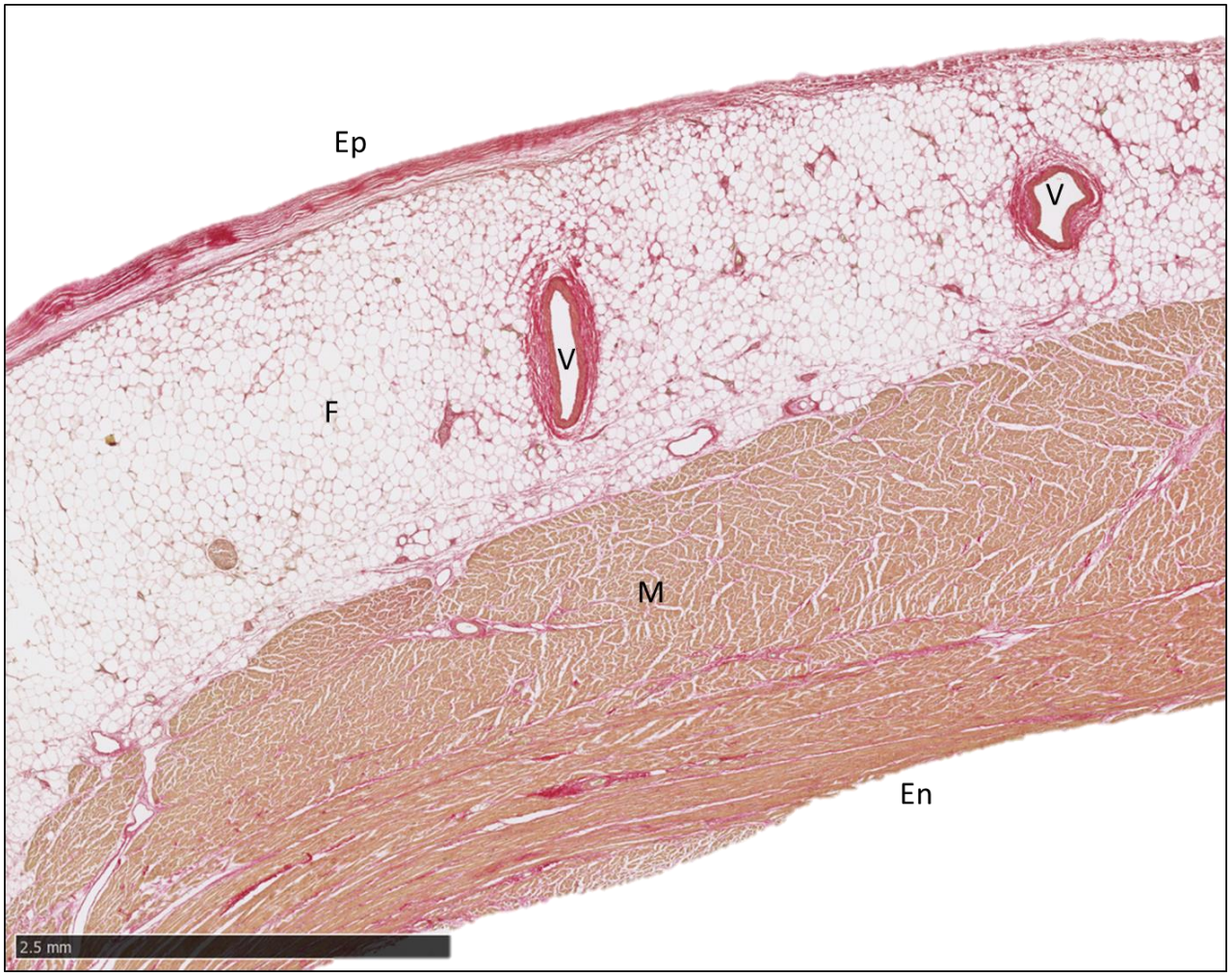


Figure 5.1. The right ventricular outflow tract. The epicardium (Ep) shows several layers of collagen. There is collagen around the vessels (V) in both the epicardial fat (F) and in the myocardium (M) (En – endocardium).

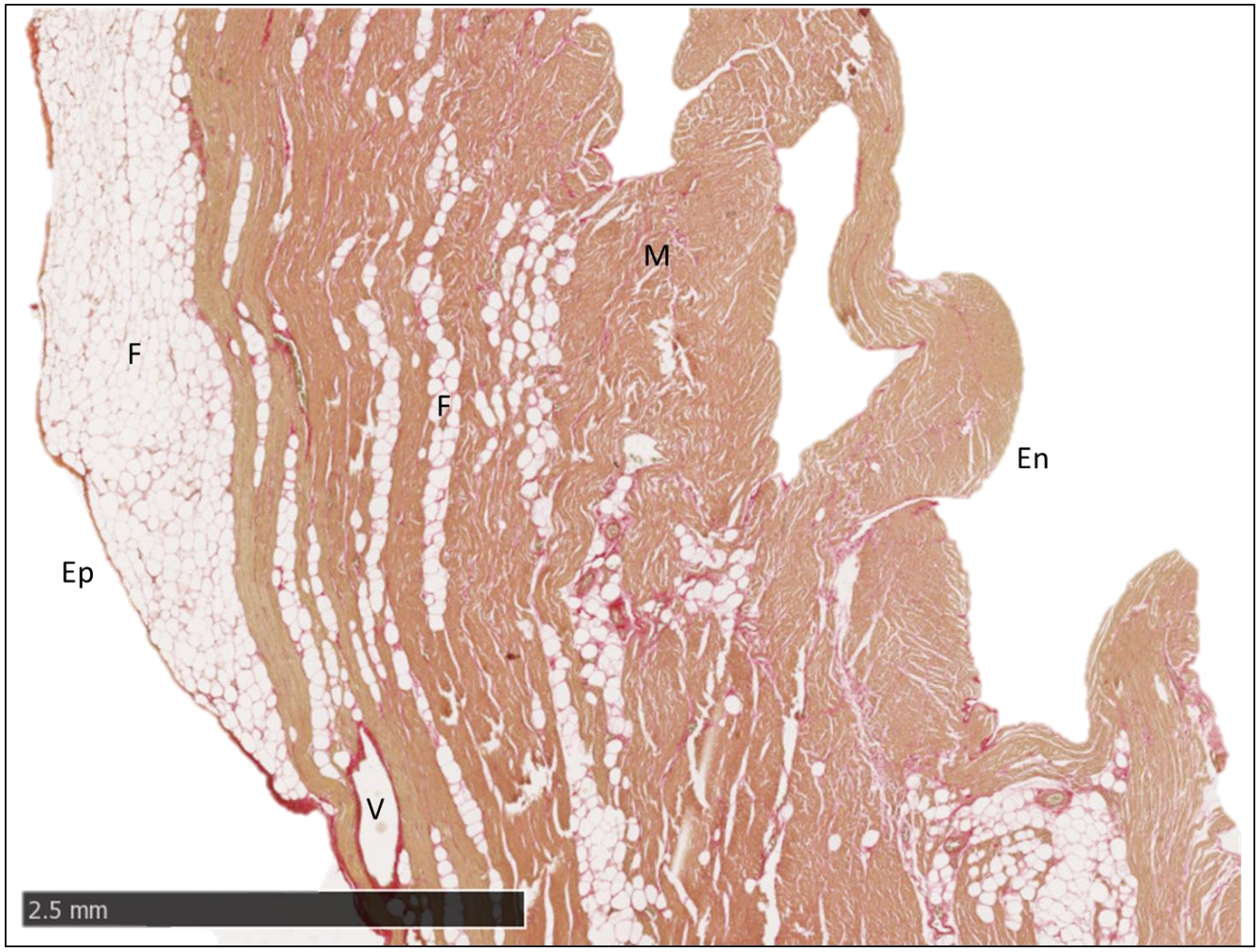


Figure 5.2. The anterior right ventricular wall. There is a layer of subepicardial fat (F) with fat infiltrating into the wall. (Ep – epicardium, En – endocardium)

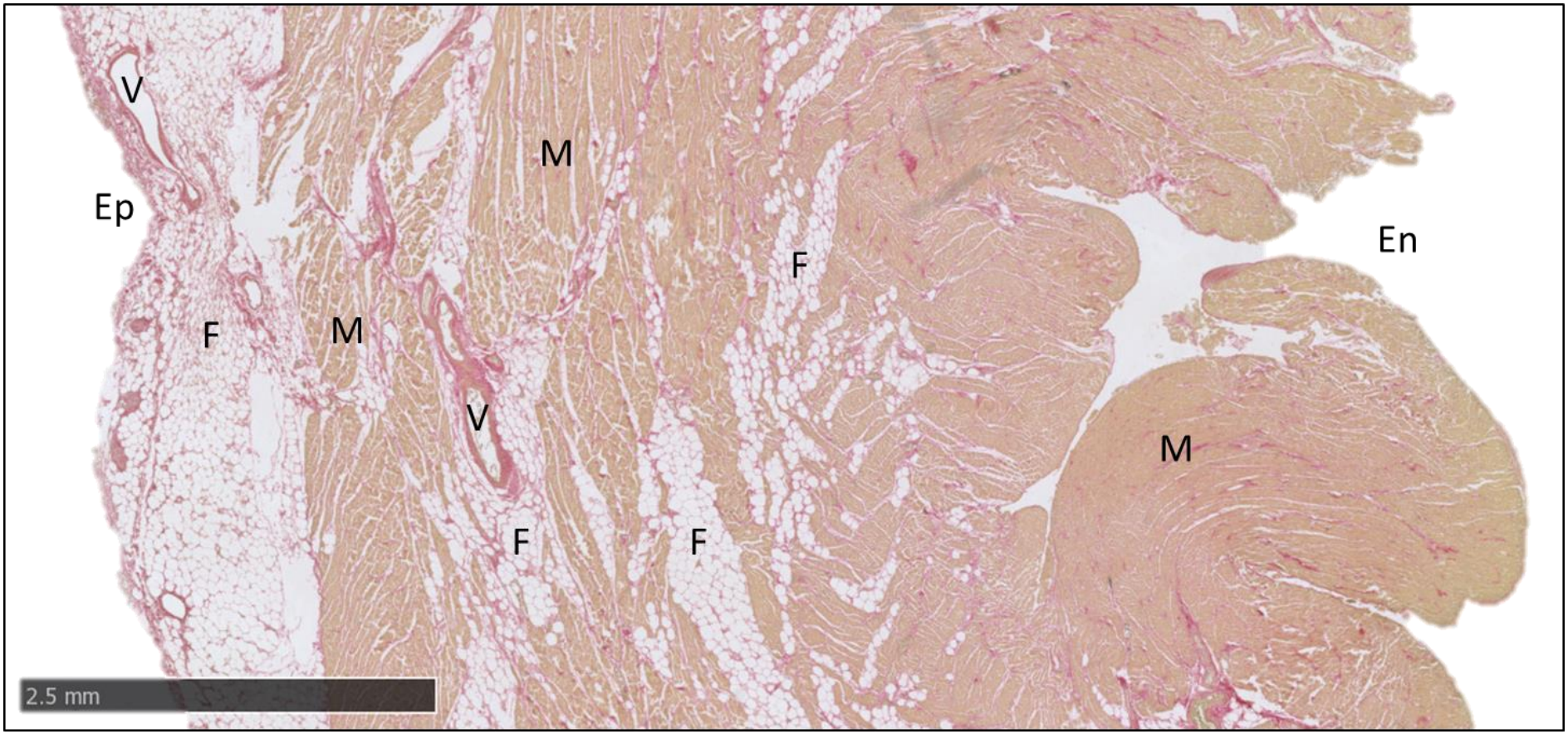


Figure 5.3. The lateral right ventricular free wall. Fat (F) infiltrates extensively into the myocardium. The epicardium (Ep), the vessels (V), myocytes (M) and endocardium (En) are marked.

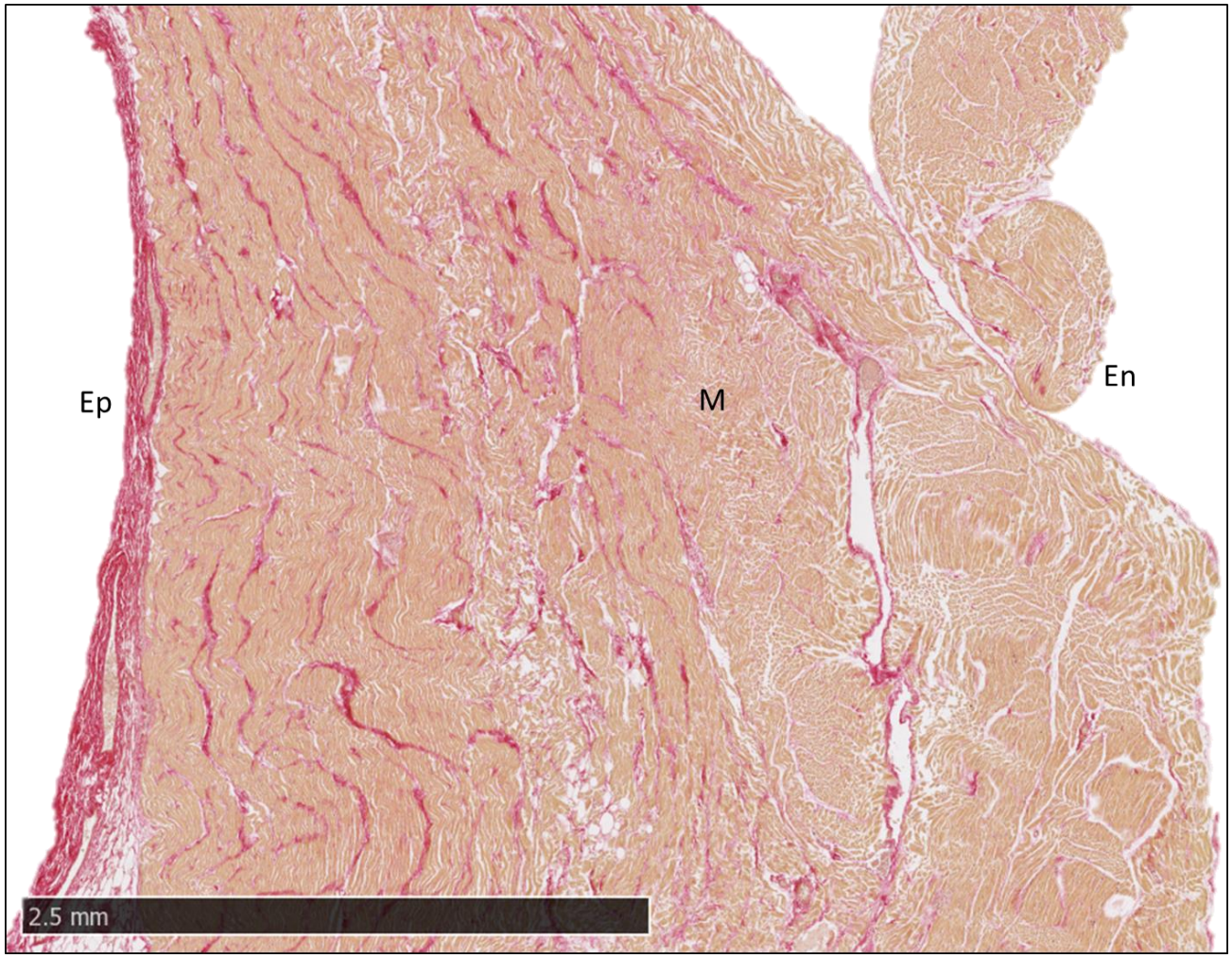


Figure 5.4. The posterior right ventricular wall. Note the absence of fat and more collagen than elsewhere. (Ep – epicardium, En – endocardium, M – myocardium).

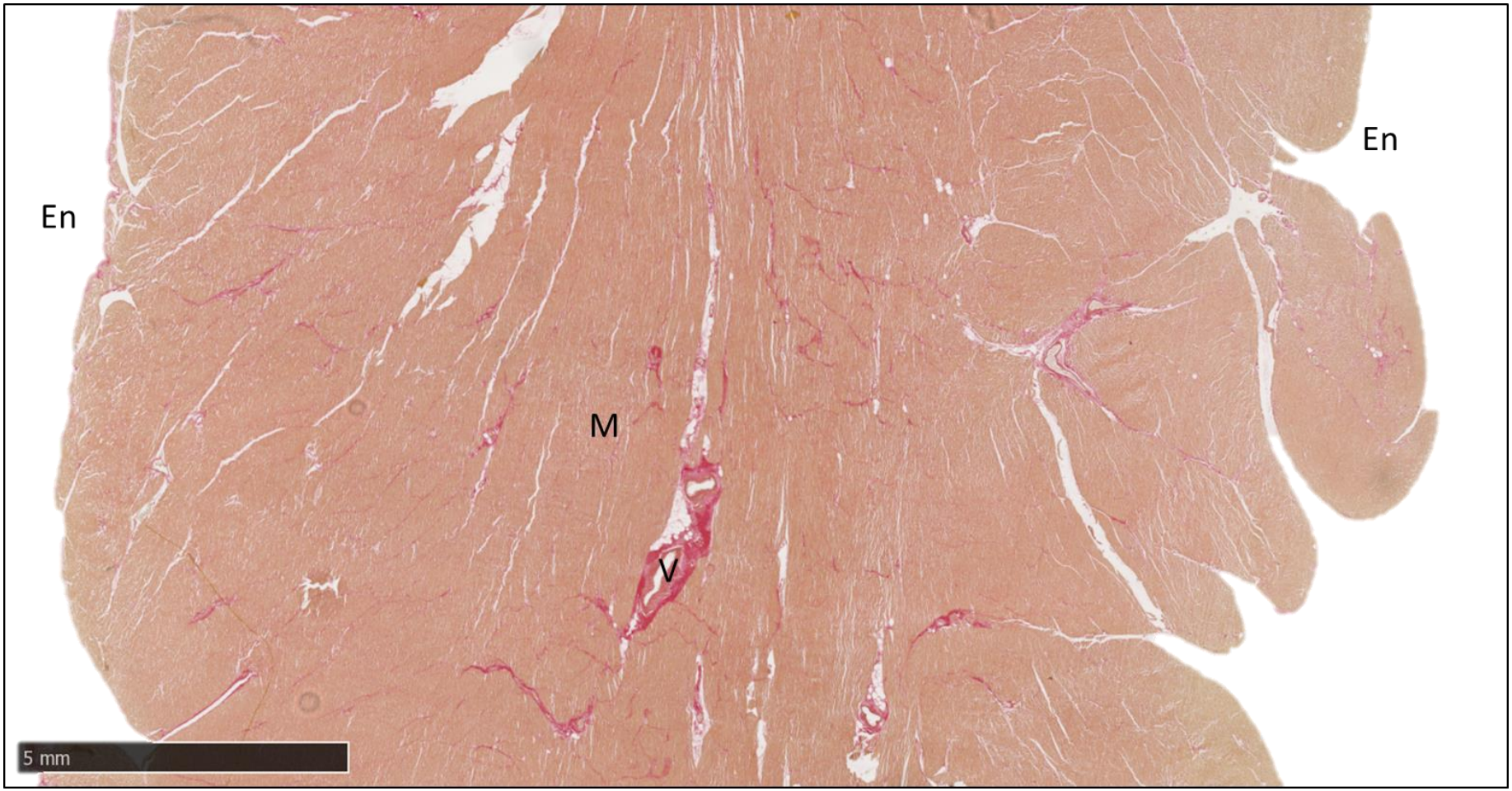


Figure 5.5. The interventricular septum. The endocardium (En) is seen on both sides of the myocardium in the septum. Collagen and fat are highlighted around the vessels (V). Myocardium (M) is marked.

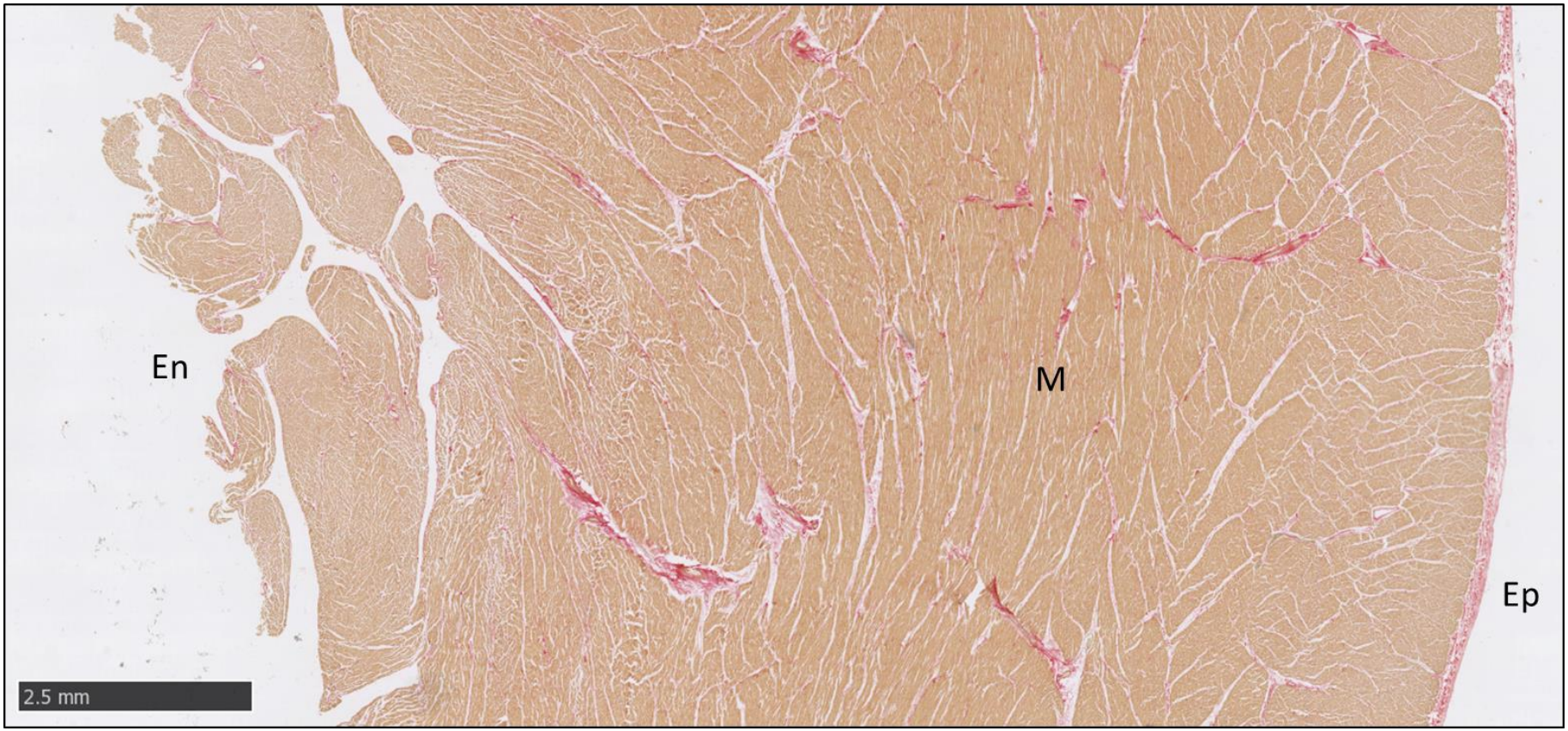


Figure 5.6. The anterior left ventricle. Collagen is highlighted around vessels in the myocardium (M). Note there is no subepicardial fat. The trabecular endocardium (En) and epicardium (Ep) are marked.

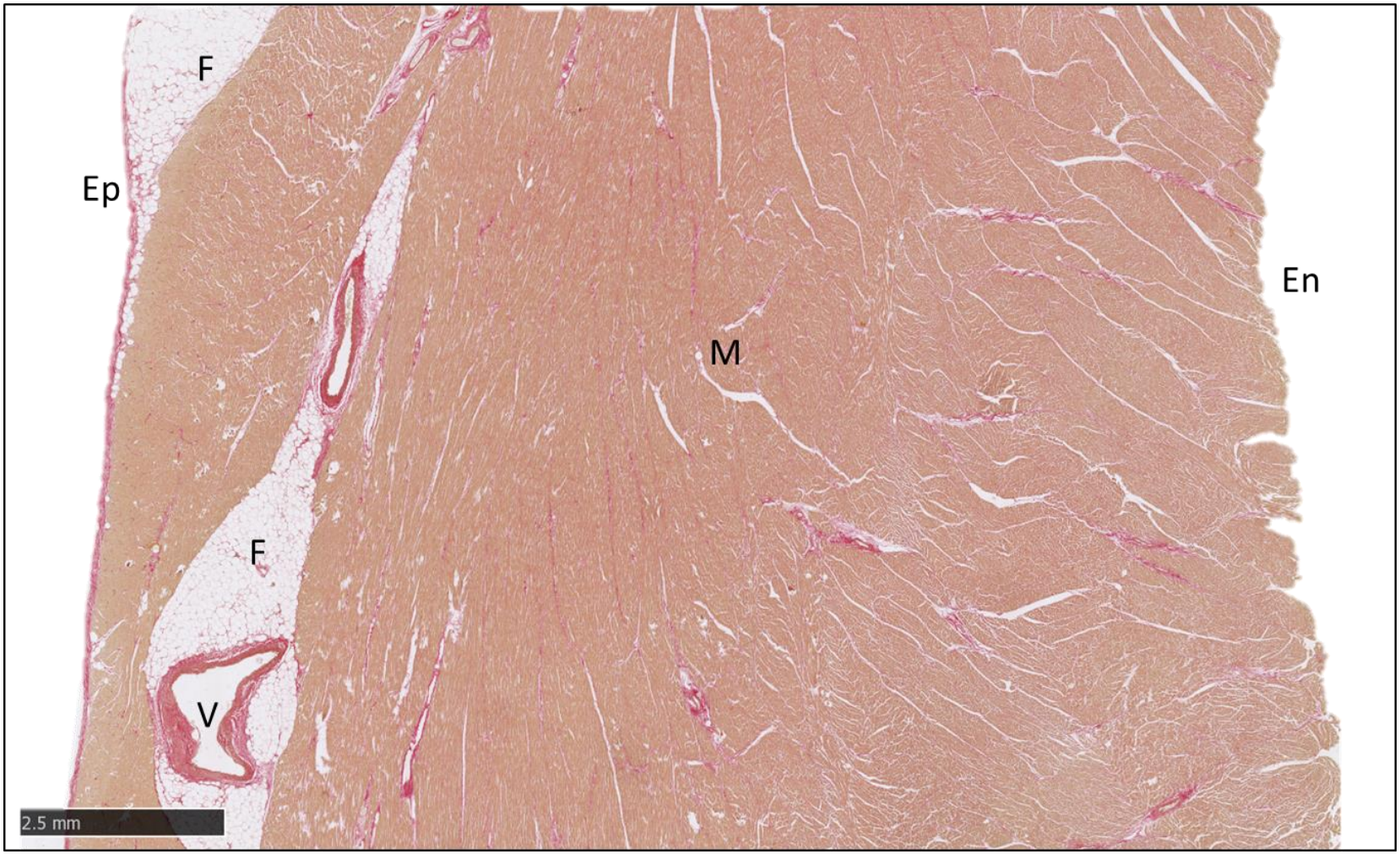


Figure 5.7. The posterior left ventricle. There is fat (F) seen around a vessel (V). The epicardium (Ep), myocardium (M) and endocardium (En) are marked.

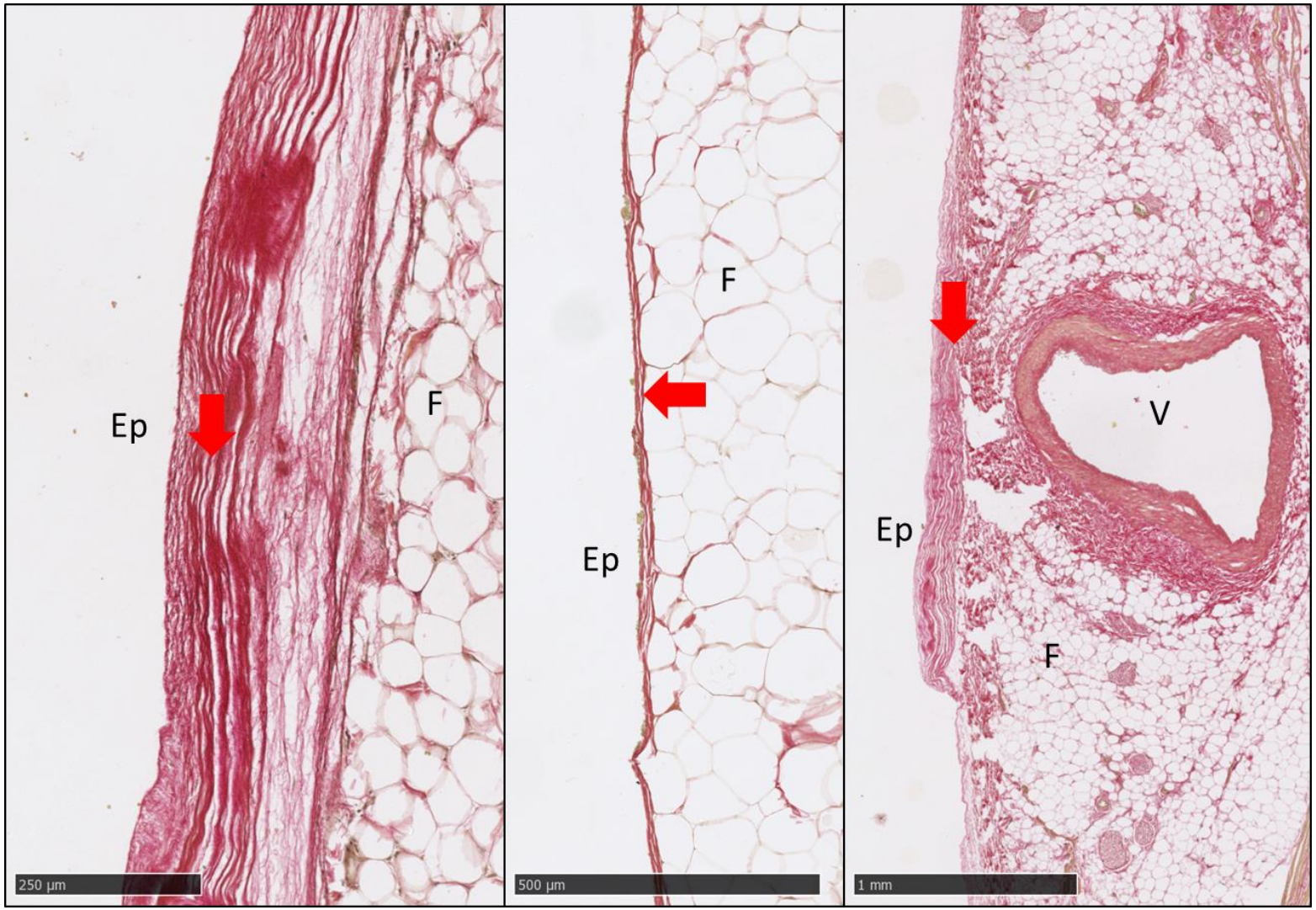


Figure 5.8. The epicardial (Ep) collagen (arrows) varies in thickness. It is frequently thicker overlying vessels (V) (Fat - F).

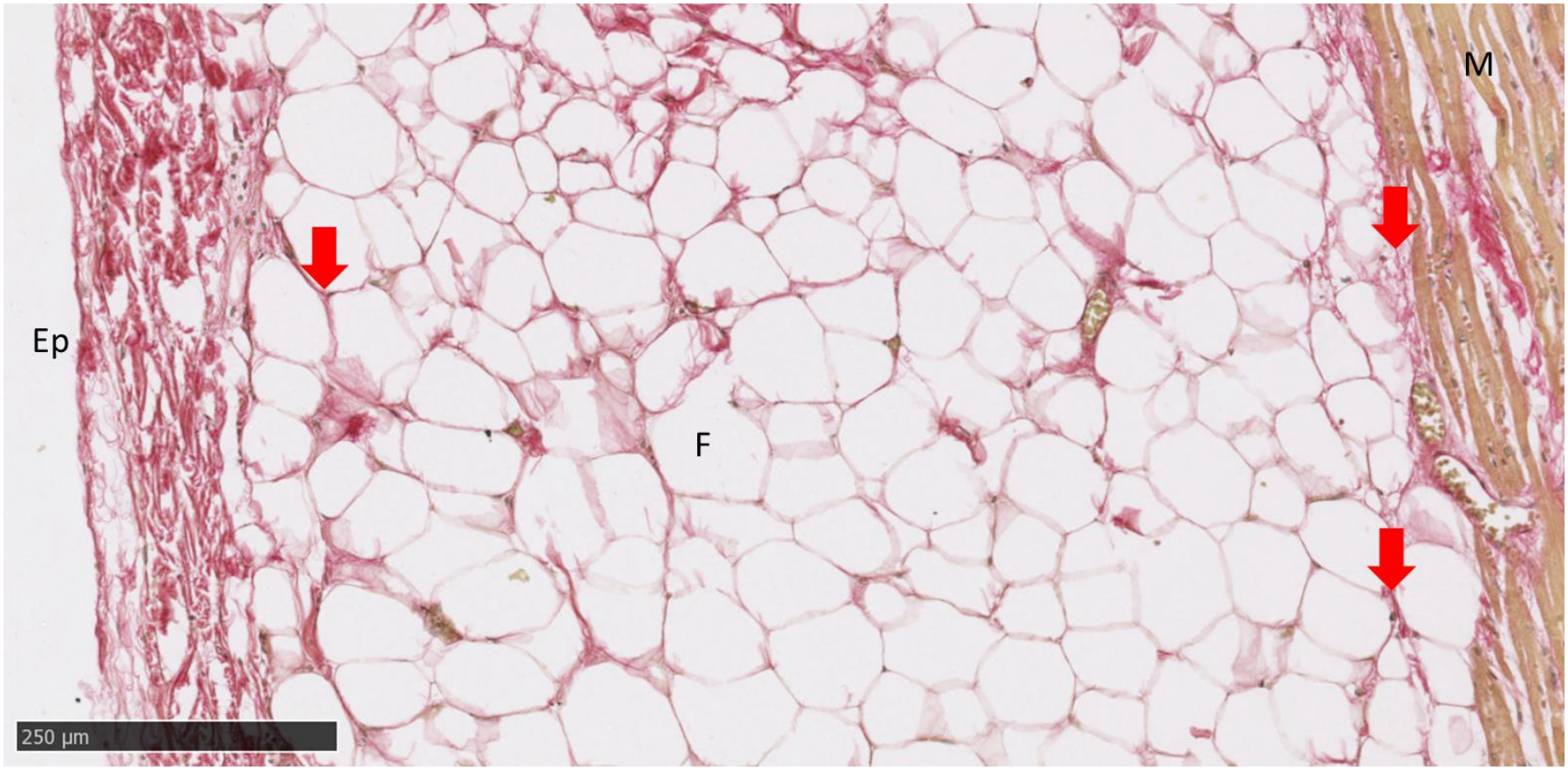


Figure 5.9. Collagen between adipocytes (F) and around capillaries. There are layers of collagen in the epicardium (Ep). The collagen coalesces as a whispy layer on the myocardial (M) surface.

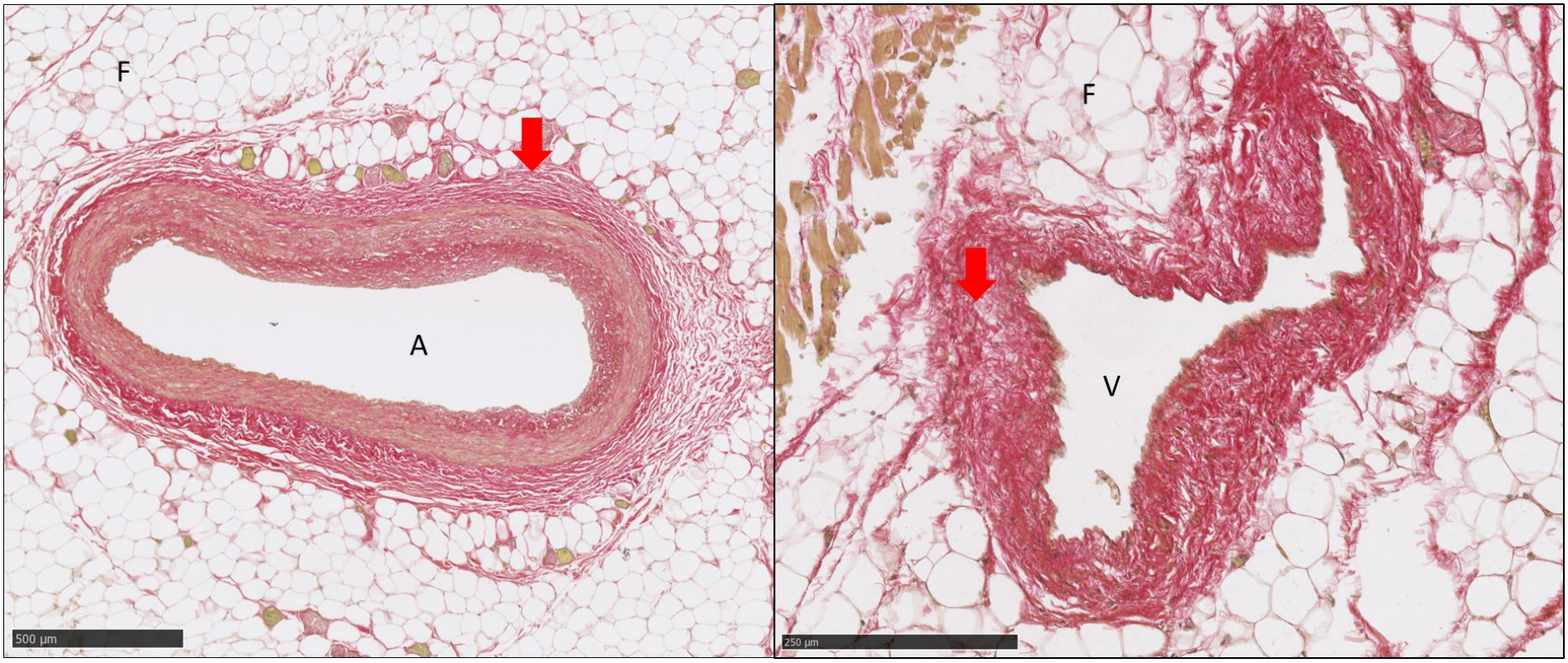


Figure 5.10. Collagen (arrows) around an artery (A) and a vein (V) in the epicardial fat representing the adventitia. There are several layers of collagen seen around the vessels in the epicardial fat which varies depending on the size of the vessel. The left side shows a large artery and the right side shows a vein. Note there are more collagen layers around the vein. Note the intima of the coronary arteries often have layers of collagen.

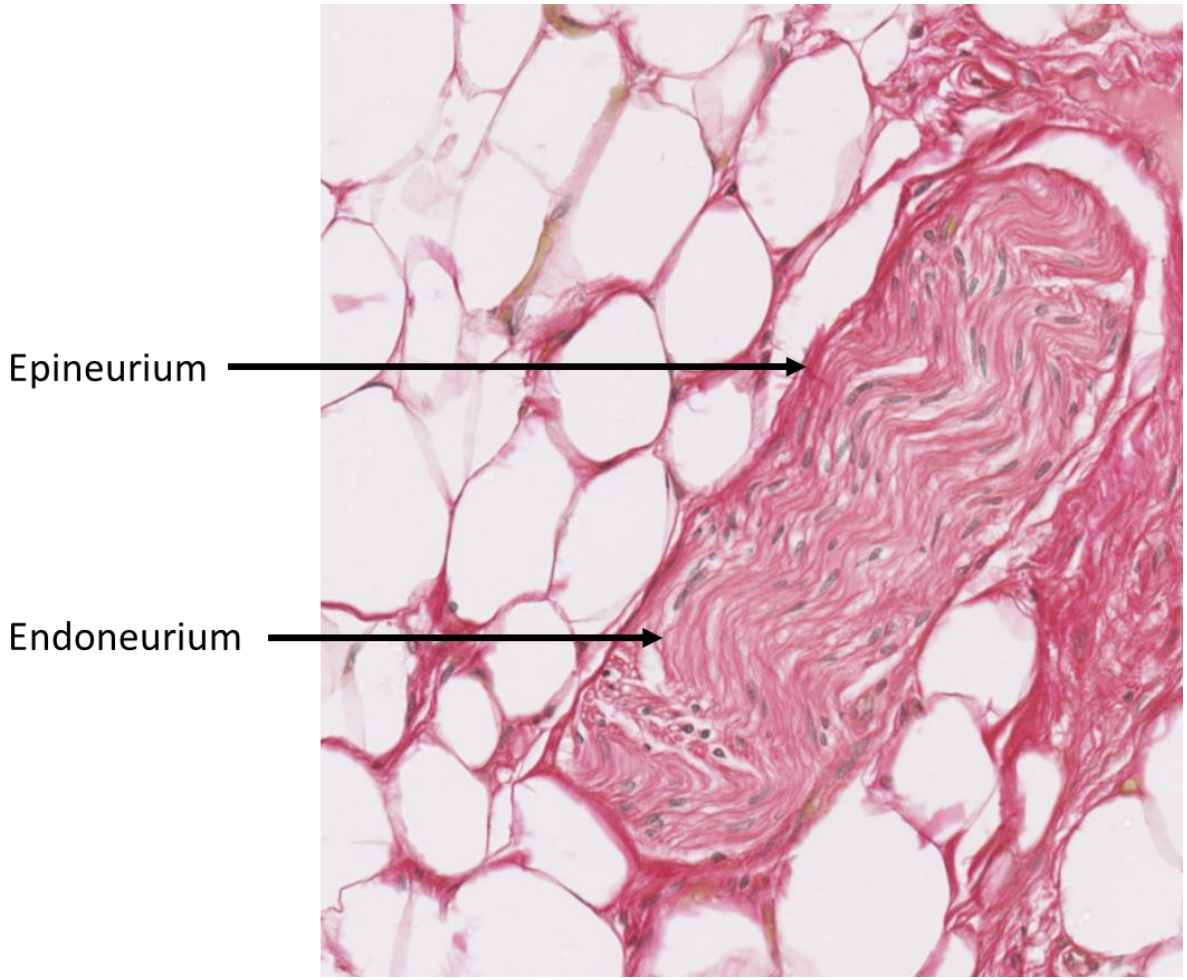


Figure 5.11. The different layers of collagen in the nerves of the subepicardial fat. The nerve is surrounded by epineurium and the individual fibres are surrounded by endoneurium.

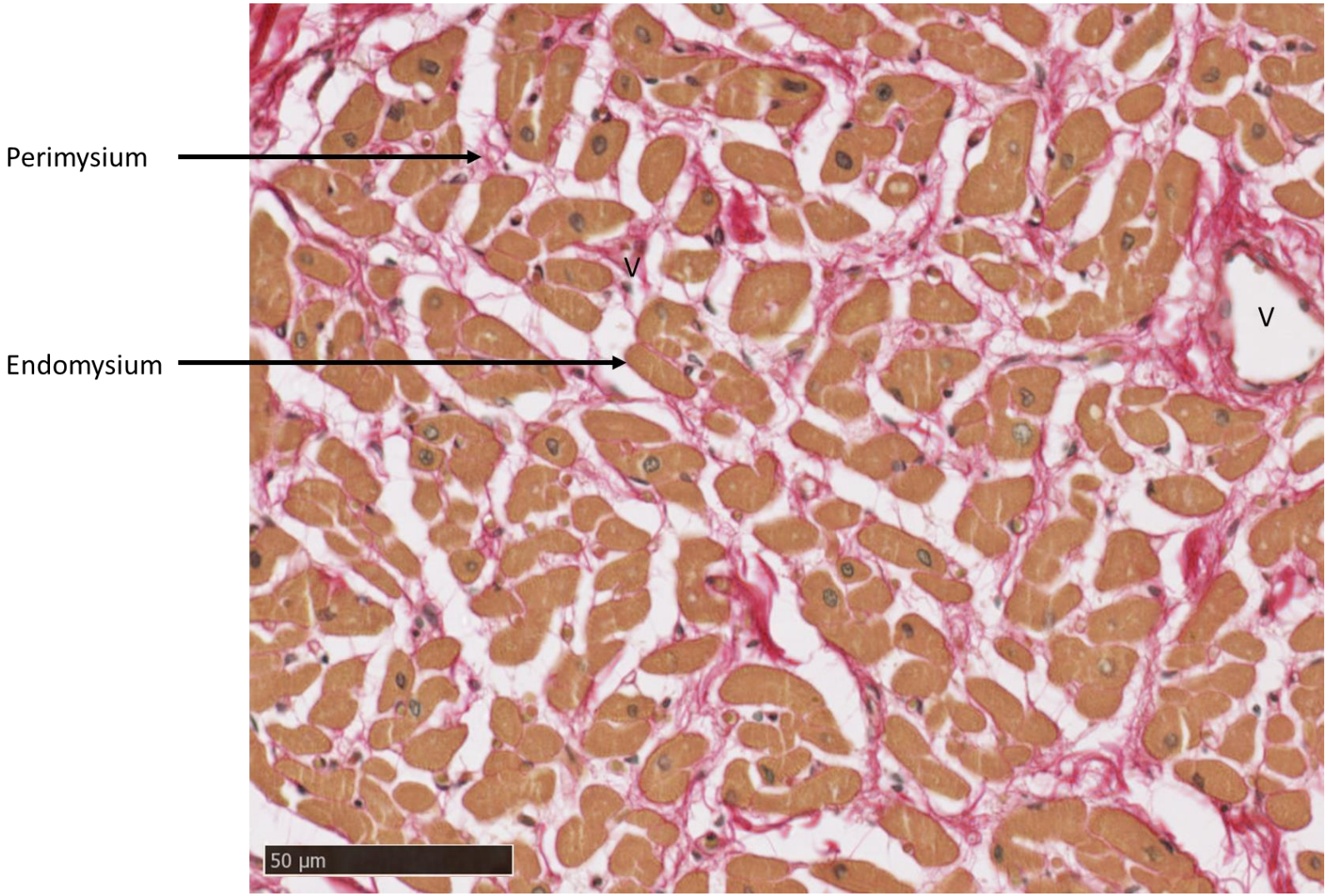


Figure 5.12. Collagen around myocytes. Endomysium lies on the surface and perimysium between myocytes. (V – blood vessels).

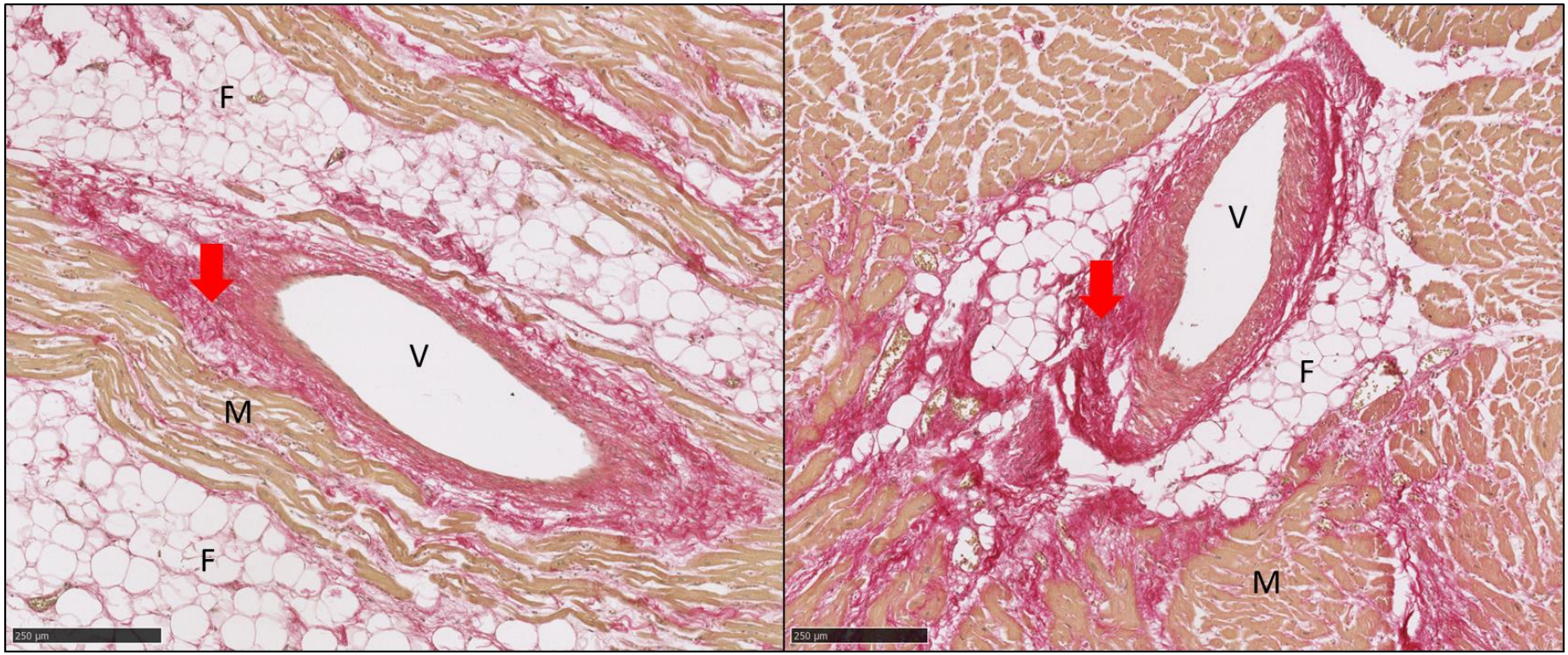


Figure 5.13. Collagen (arrows) and fat (F) around large vessels (V) in the myocardium (M). Layers of collagen are observed around the vessels representing the adventitia.

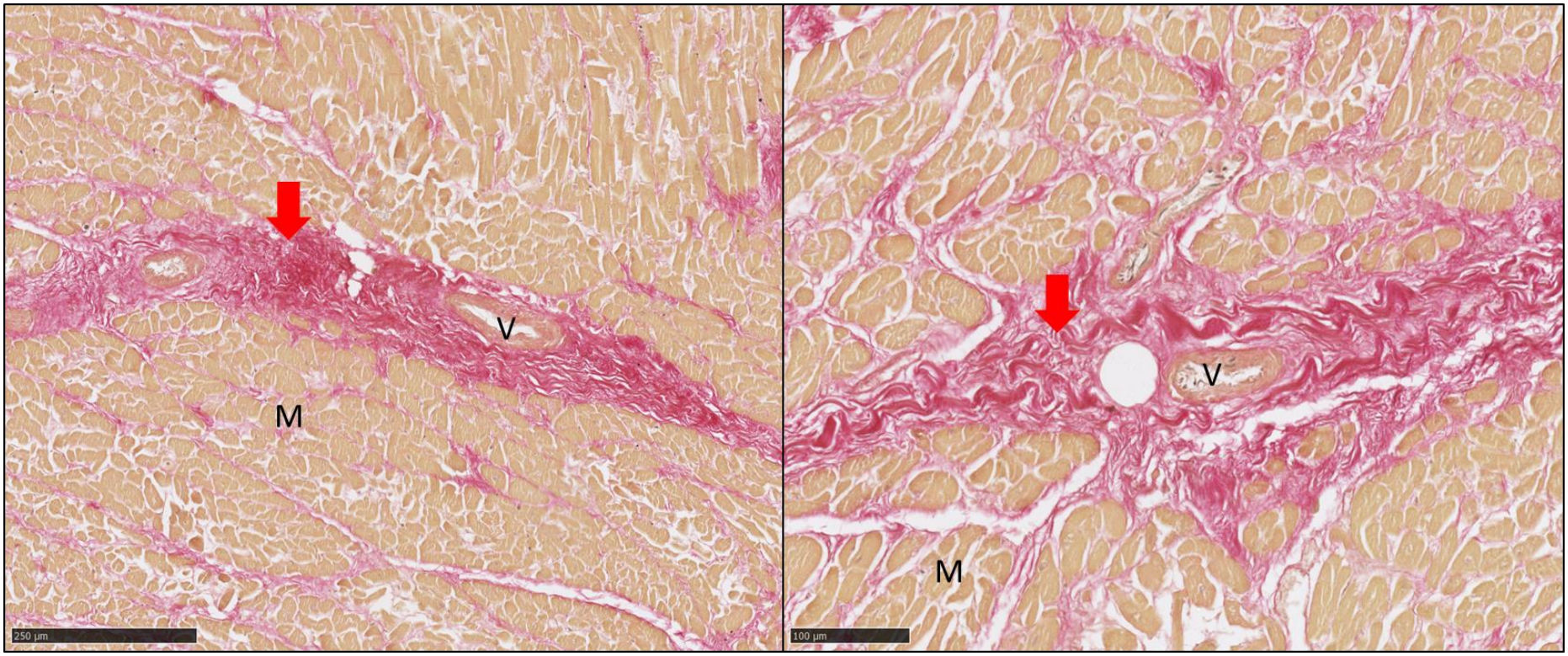


Figure 5.14. Collagen (arrow) around small vessels (V). Multiple layers of collagen are seen around smaller vessels within the myocardium (M).

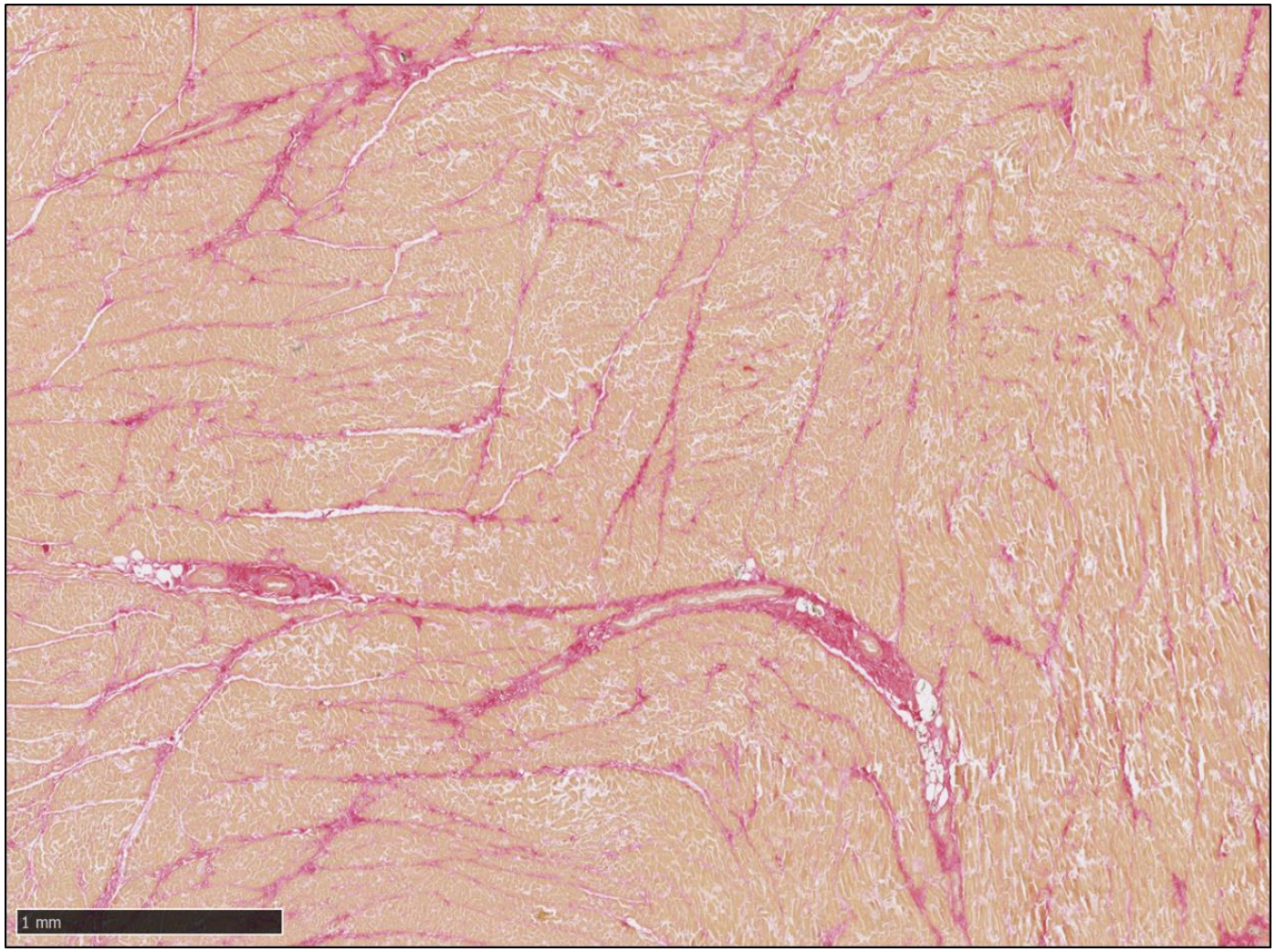


Figure 5.15. Complex networks of small vessels in the myocardium which are highlighted by their surrounding collagen.

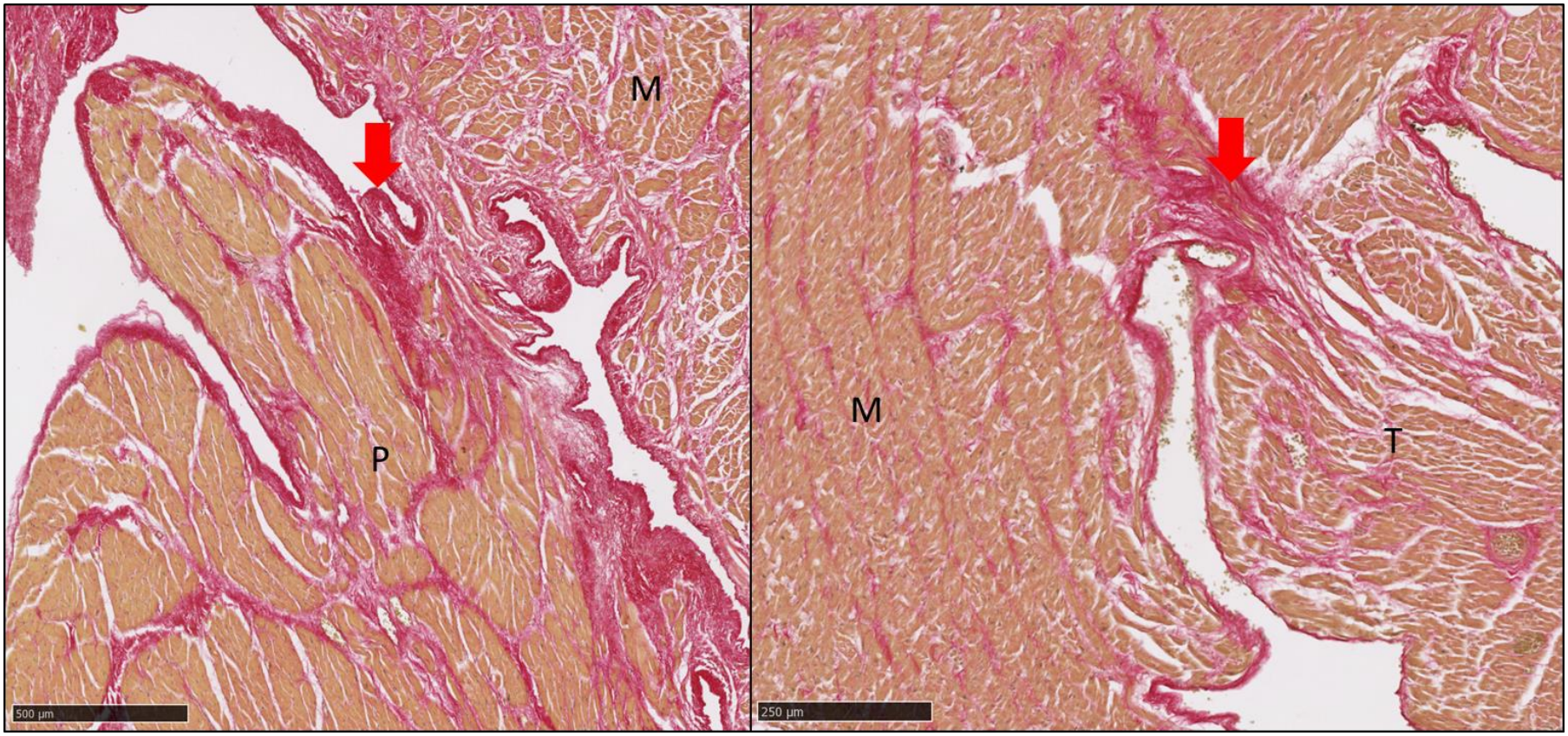


Figure 5.16. Patches of collagen (arrows) where the papillary muscles (P) and trabeculae (T) arise from the myocardium (M).

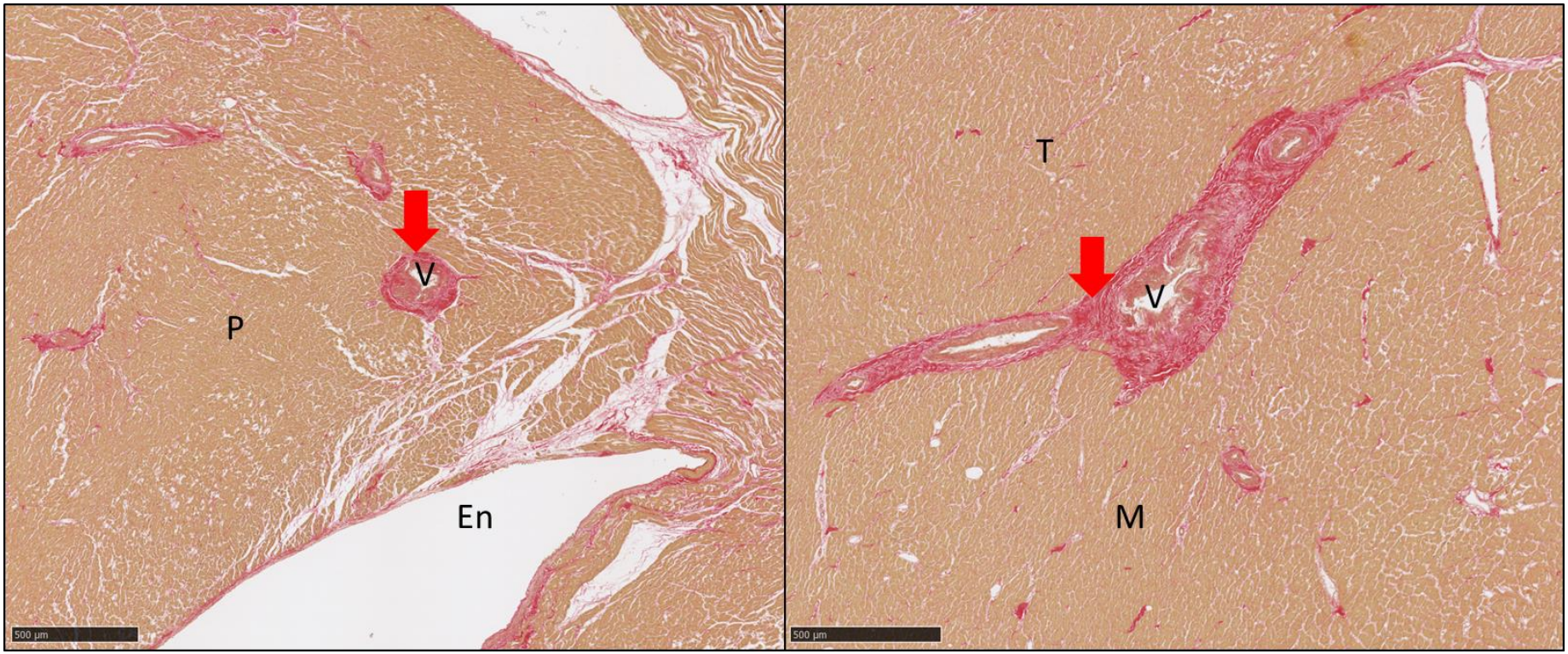


Figure 5.17. Thick collagen (arrows) around the vessels (V) in the papillary muscles (P) and trabeculae (T) (myocytes – M).

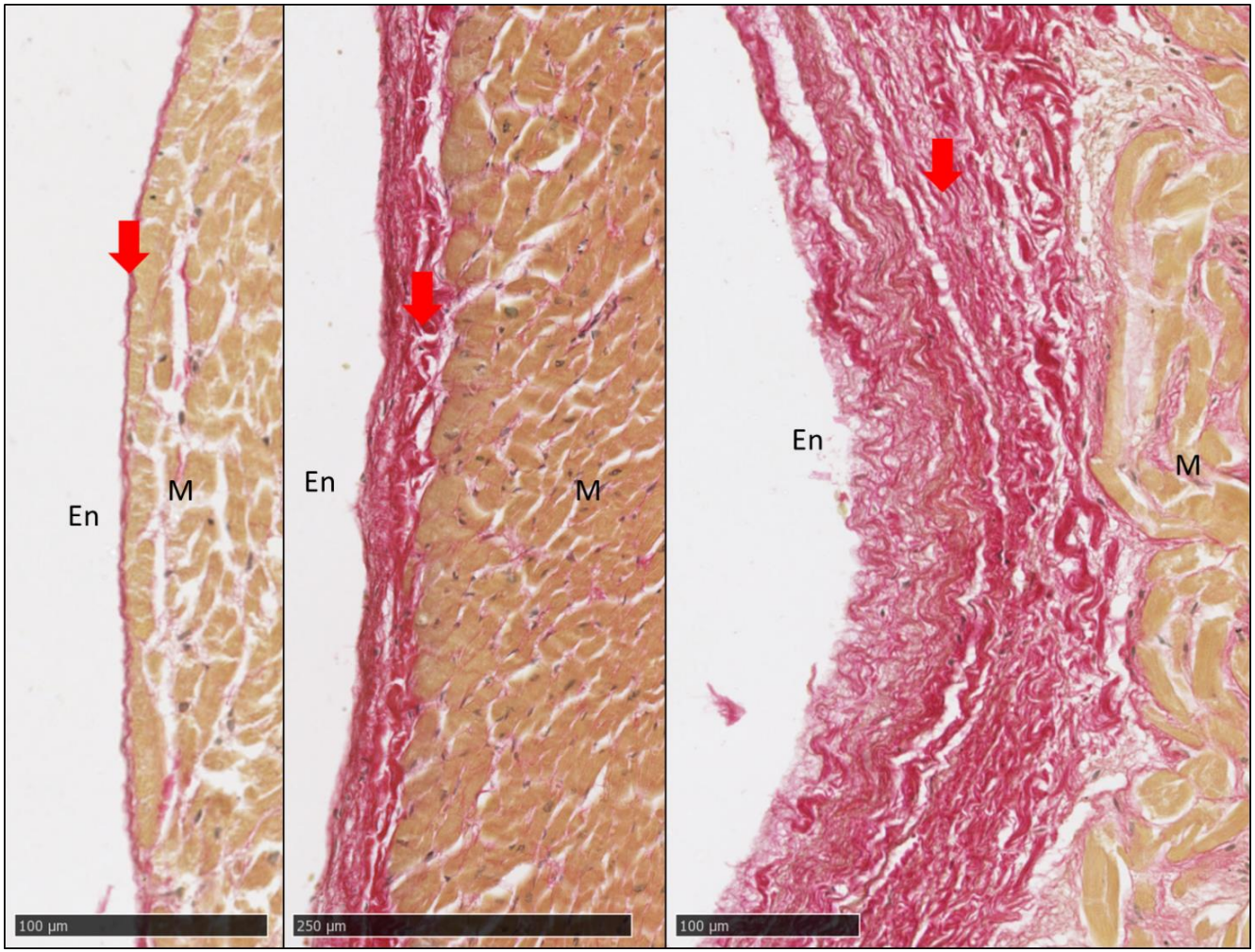


Figure 5.18. Endocardial (En) collagen (arrows). There is variation in thickness of the endocardial collagen from a single layer to over 10 layers (myocytes – M).



Figure 5.19. There is a well-defined divide between the fat (F) and myocytes (M) in the left ventricle. Occasionally fat is seen entering the myocardium around vessels.

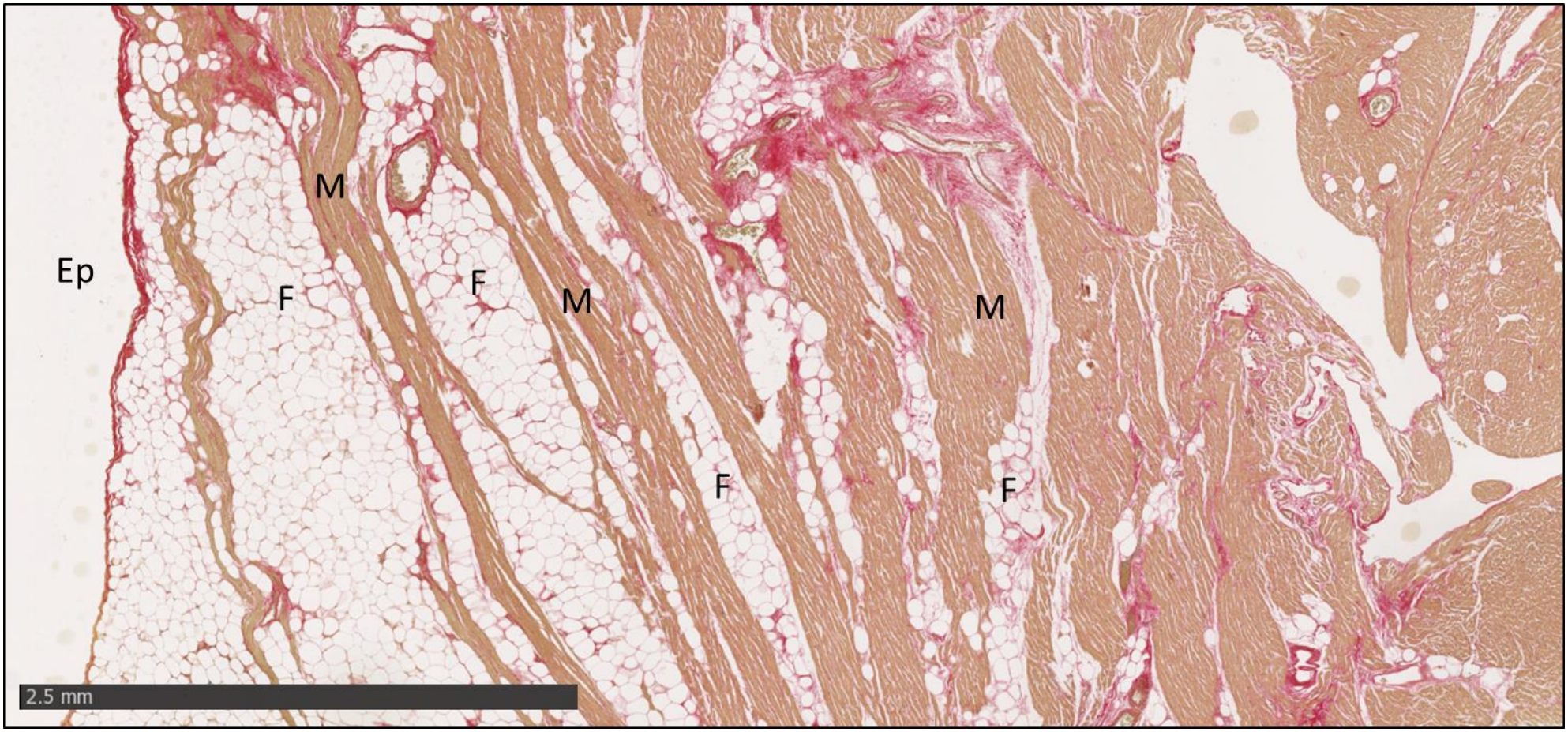


Figure 5.20. Myocytes encased by adipocytes in the right ventricle. Strands of fat (F) alternating with strands of myocytes (M).

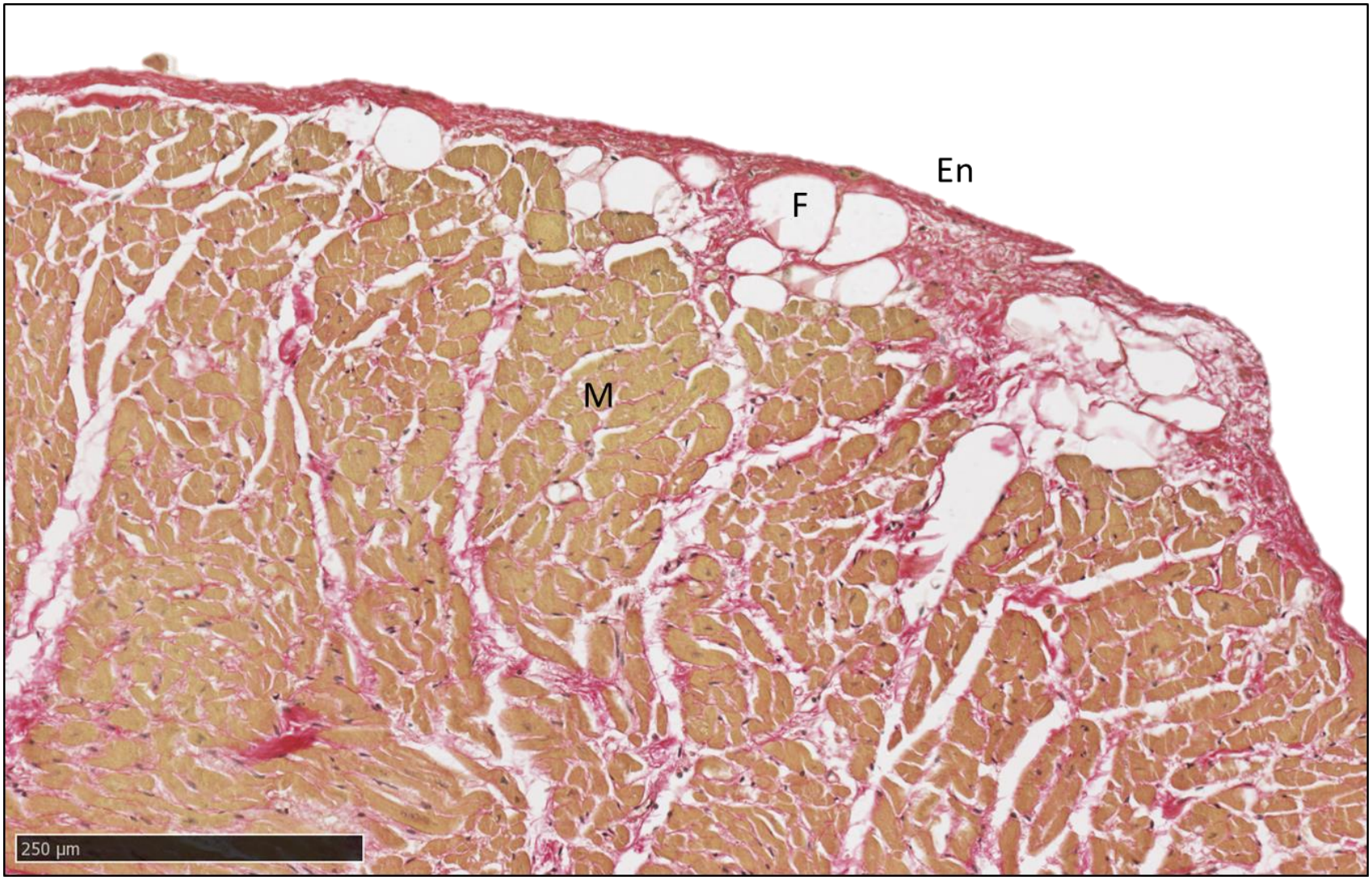


Figure 5.21. Fat (F) in the endocardium (En). Adipocytes are occasionally observed within the endocardium (myocardium – M).

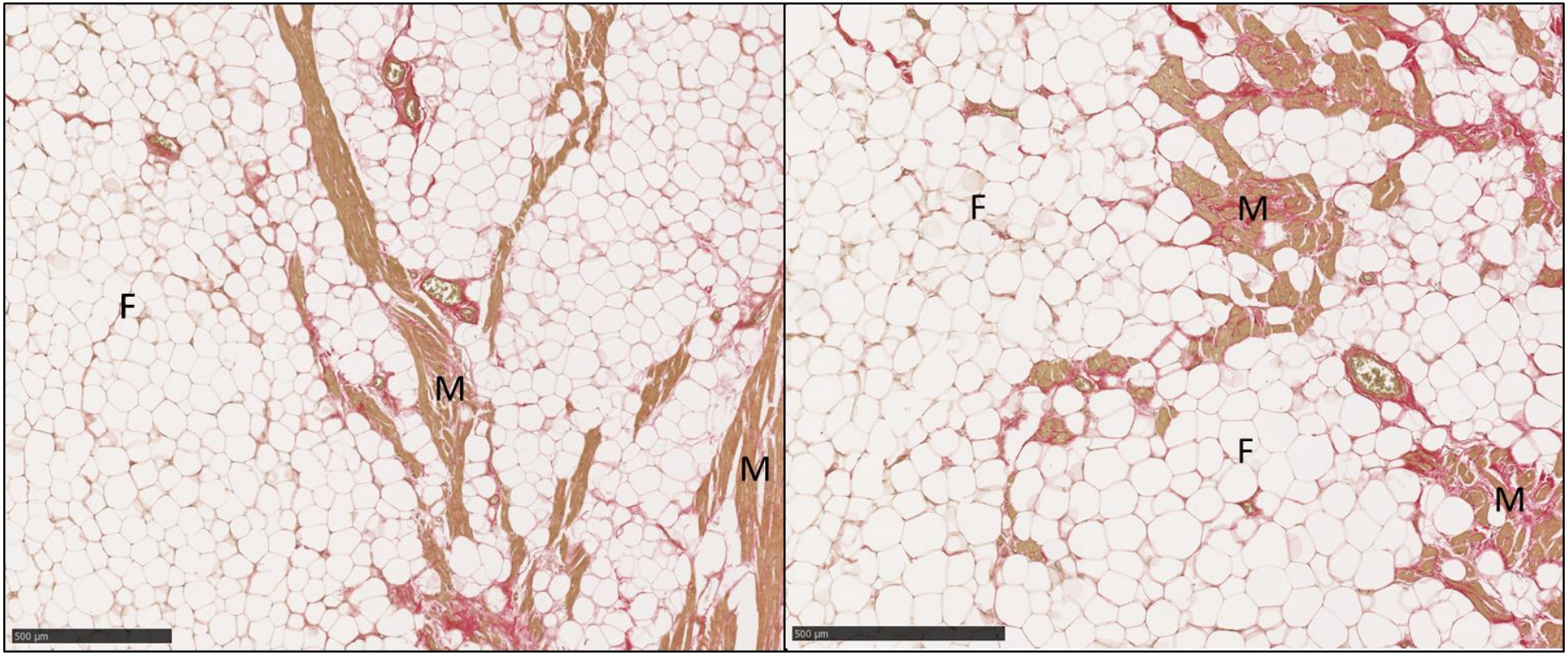


Figure 5.22. The myocytes (M) of the outer myocardium in the right ventricle are isolated in strands or small clusters embedded within fat (F). The myocytes within the strands are normally orientated to each other in parallel or end to end but may also appear haphazardly arranged.

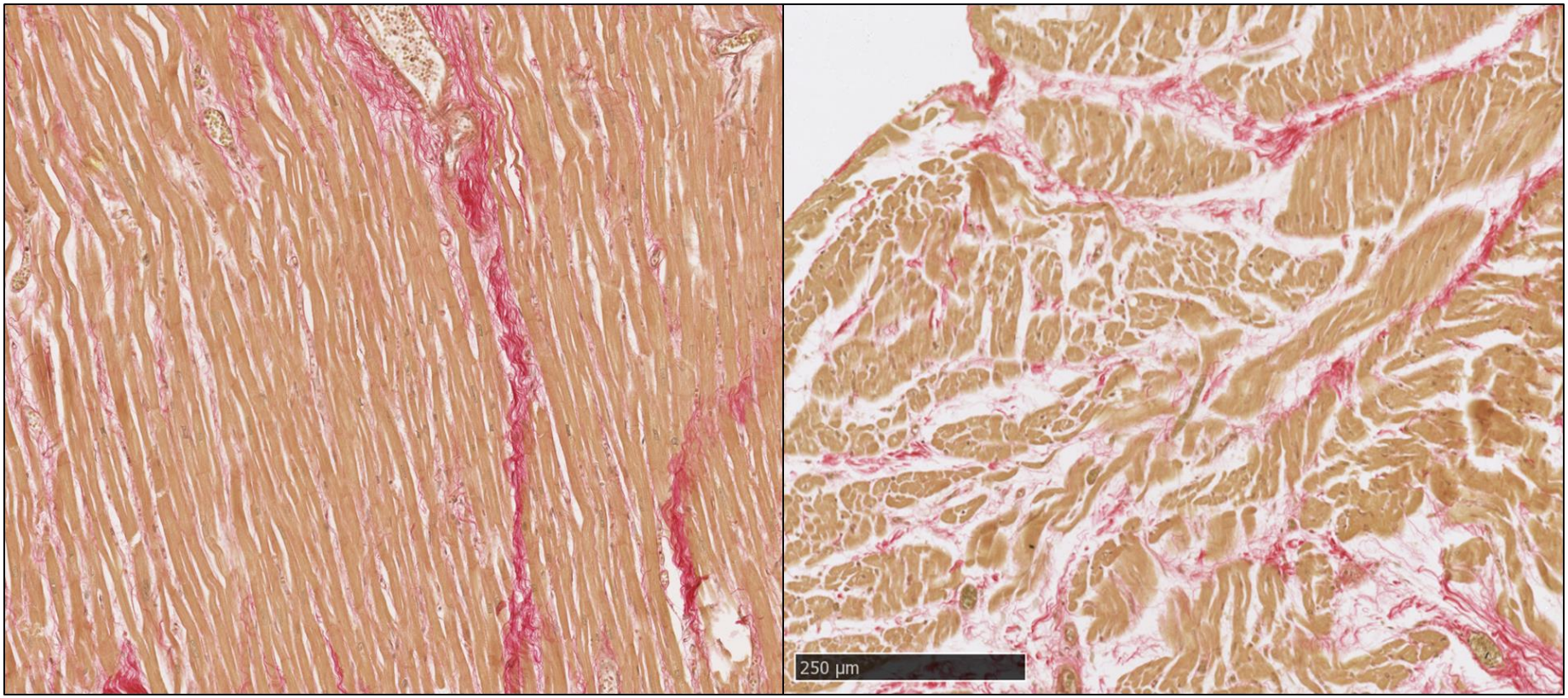


Figure 5.23. Myocyte arrangement. Left: the myocytes are generally arranged in parallel. Right: disorganised myocytes are commonly present close to the endocardial surface, in trabeculae and papillary muscles as well as at the junction with the subepicardial fat and around vessels.

Quantitative analysis

Collagen

Collagen proportions does not show a significant difference by location examined. The ventricular myocardium has an overall average of 11% and ranges from 8-15% between locations (table 5.2).

Fat

Fat proportion showed differences depending on location sampled with more fat in the RV than the LV. Fat has an overall average of 6% ranging from 2-10% between locations. There is 10% in the RVOT and RV free wall with 4-8% in the LV and 2% in the IVS. There is more fat in the RVOT than the IVS (ratio 4.0, 95%CI 1.7-9.4, $p<0.01$) and the posterior LV (ratio 2.6, 95%CI 1.1-6.15, $p=0.02$). There is more fat in the RV than the IVS (ratio 4.2, 95%CI 1.8-9.8, $p<0.01$) and the posterior LV (ratio 2.8, 95%CI 1.2-6.4, $p<0.02$). There is more fat in the anterior LV than the IVS (ratio 3.2, 95%CI 1.4-7.5) (table 5.2 and figure 5.24).

Myocytes

There is no significant difference in the proportion of myocytes between locations. Myocytes made up an average proportion of 77% with a range between 71-86%.

Component	Collagen % of tissue area		Fat % of tissue area		Myocytes % of tissue area	
Location	Collagen	95% CI	Fat	95% CI	Myocytes	95% CI
All	10.70	7.22-15.86	5.89	4.37-7.92	76.97	68.26-86.77
RVOT	11.15	7.24-17.15	**9.83**	**6.44-14.99**	71.76	61.69-83.45
RV	14.60	9.49-22.46	**10.23**	**6.70-15.60**	71.31	61.31-82.94
IVS	8.39	5.45-12.90	**2.43**	**1.59-3.70**	85.72	73.69-99.69
ALV	9.45	6.14-14.53	**7.78**	**5.10-11.87**	76.65	65.90-89.15
PLV	10.87	7.06-16.71	**3.72**	**2.43-5.67**	80.33	69.06-93.42

Table 5.2. Predicted proportions (geometric mean and confidence interval) of the ventricular myocardium made up by collagen, fat and myocytes in the normal heart. The results are broken down for the right ventricular outflow tract (RVOT), the right ventricle (RV), the interventricular septum (IVS), the anterior left ventricle (ALV) and the posterior left ventricle (PLV).

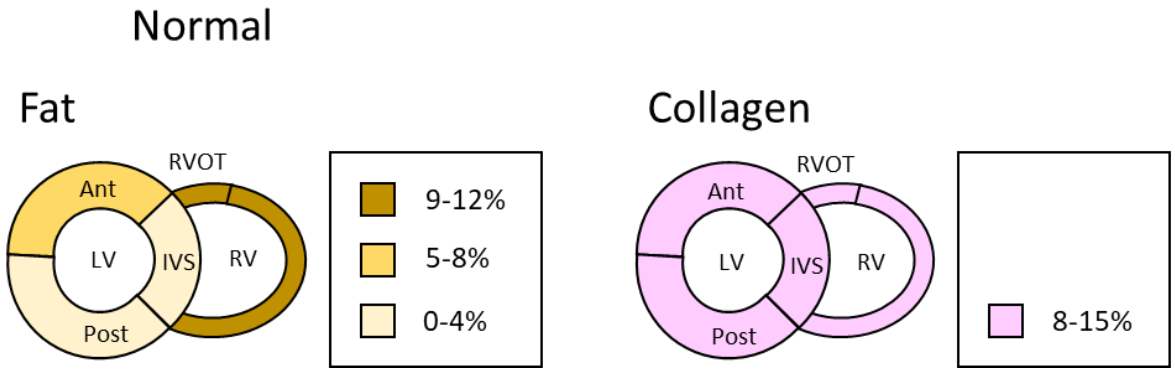


Figure 5.24. Proportional composition of the normal ventricular myocardium by fat and collagen. The percentages are illustrated for the right ventricular outflow tract (RVOT), right ventricle (RV), the interventricular septum (IVS) and the anterior and posterior left ventricle (LV).

Innervation of the normal ventricular myocardium and overlying subepicardial fat

The nerves are either described as nerve bundles or individual nerve fibrils (figure 5.25). Nerve bundles are a collection of fibres lying together. Individual nerve fibrils are single thin threadlike fibres.

General innervation

Within the subepicardial fat, large nerve bundles are present beneath the epicardial surface. These are most prominent around the coronary arteries where they lie close to the adventitia and in the surrounding adipose tissue (figure 5.26). They are not present within the media of any vessels. Large and smaller nerve bundles are also frequent between adipocytes within the subepicardial fat in the absence of vessels. Individual nerve fibrils are not present within the subepicardial fat of the ventricles. No ganglia are observed in the epicardial fat at the midlevel of the ventricles. The nerve bundles when entering the myocardium always follow the blood vessels (figure 5.27). The nerve bundles lie alongside vessels within the closely associated adipose tissue and adventitia. Individual nerve fibrils are present within the adventitia adjacent to the media.

Within the myocardium, there is an extensive network of both nerve bundles and individual nerve fibrils in both the outer myocardium and inner myocardium (figure 5.28). The nerve bundles lie within the adventitia of blood vessels (figure 5.28). The large nerve bundles of the outer myocardium become gradually smaller, dividing and become smaller nerve bundles in the inner myocardium. Large nerve bundles are most common in the outer myocardium and are only occasionally seen in the inner myocardium. Medium sized nerve bundles are seen throughout the myocardium and are most concentrated in the middle myocardium. Small nerve bundles are present

in a more even distribution throughout the myocardium. Small individual nerve fibrils are present throughout the myocardium from the outer myocardial surface to the endocardial surface however they are more prominent in the inner myocardium. Individual fibrils extend between, lying parallel and touching individual myocytes (figure 5.28). The individual nerve fibrils are not present adjacent to all myocytes. These individual nerve fibrils also lie adjacent to small vessels and are present within the endocardium (figure 5.29).

The RV and RVOT are much more densely innervated than the LV with many more large nerves in the subepicardial fat and myocardium (figure 5.30). Similarly, the small individual nerve fibrils are far more frequently present within the myocardium of the RV and RVOT (figure 5.30).

Sympathetic innervation

TH stained many of the larger nerve bundles in the subepicardial fat. It frequently stained only a percentage of the fibres within the nerve bundles. Within the subepicardial fat, the TH stained nerve bundles lie alongside vessels in the surrounding adipose tissue and also between adipocytes otherwise unassociated. The TH stained nerve bundles intersect the junction between the subepicardial fat and the surface of the myocardium where they are always associated with blood vessels. In the myocardium, the medium and smaller nerve bundles frequently stain uniformly for TH. The TH stained nerve bundles form a complex network throughout the myocardium. These nerve bundles remain associated with vessels lying in the surrounding fat around larger vessels and directly adjacent to smaller vessels within the myocardium (figure 5.31). Analogous to the vessels, they are smaller approaching the endocardial surface with more larger nerve bundles in outer

myocardium and more smaller nerve bundles in the inner myocardium. The individual nerve fibrils lie parallel alongside adjoining small vessels. To a lesser degree, they are also intricately associated with myocytes lying parallel to them touching the myocyte border. The fibrils are also present within the endocardium. They are more common in the inner myocardium than the outer myocardium.

Parasympathetic innervation

CT staining is much less compared sympathetic in the nerve bundles in the subepicardial fat where it stained only focally within fibres (figure 5.32). Smaller nerve bundles stain darkly within the myocardium and are present from the epicardial surface to the endocardial surface but are far less numerous than those stained by TH (figure 5.32). These nerve bundles associate with vessels but also between myocytes within the myocardium as opposed to those stained with TH. Small individual nerve fibrils have a granular staining pattern. The fibrils are present throughout the myocardium but most prominently in the inner myocardium. The individual nerve fibrils are far more numerous than those stained by TH. The individual nerve fibrils are intricately associated with, adjoining and lying on the surface of myocytes (figure 5.32). To a lesser degree, they are closely associated with small vessels. The fibrils are also present on the endocardium. A graphical summary of the nerve distribution is given in figure 5.33.

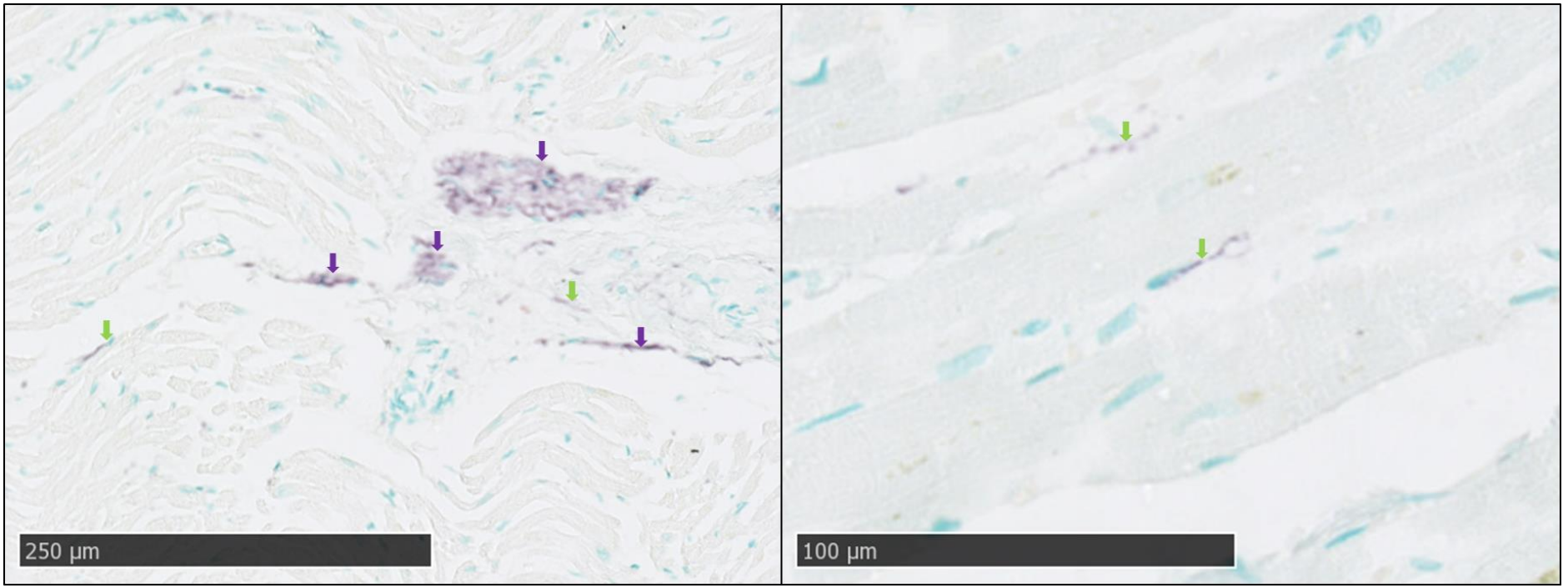


Figure 5.25. Variably sized nerve bundles (purple arrows) and individual nerve fibrils (green arrows) in the myocardium. The nerve bundles appear as a series of ill-defined lines parallel to one another. The fibrils appear as a linear streak or granular.

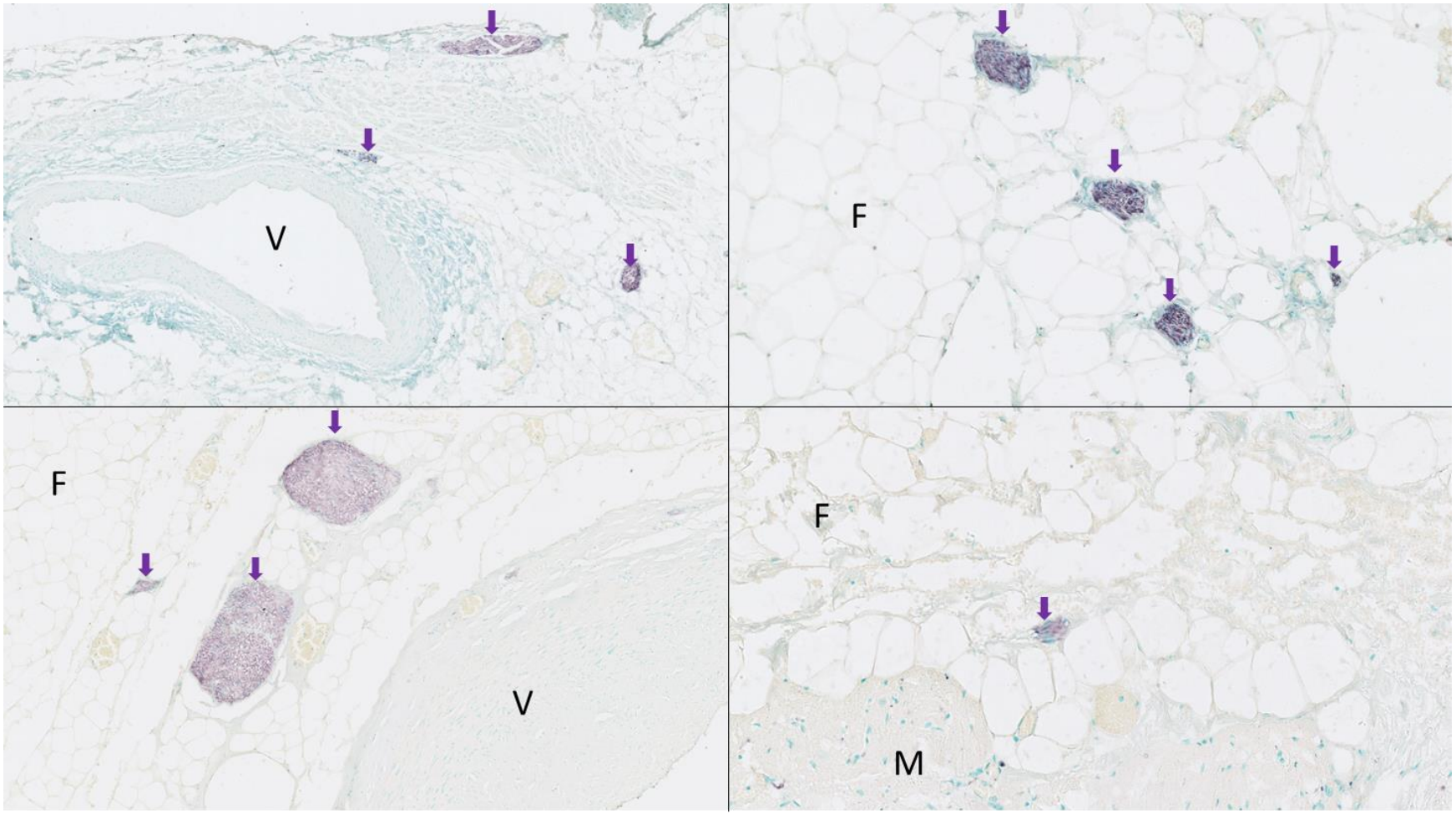


Figure 5.26. PGP9.5 immunostaining (purple arrows) in the subepicardial fat (F). Large and small nerve bundles in the subepicardial fat most prominently around large vessels (V) and also unassociated (myocytes – M).

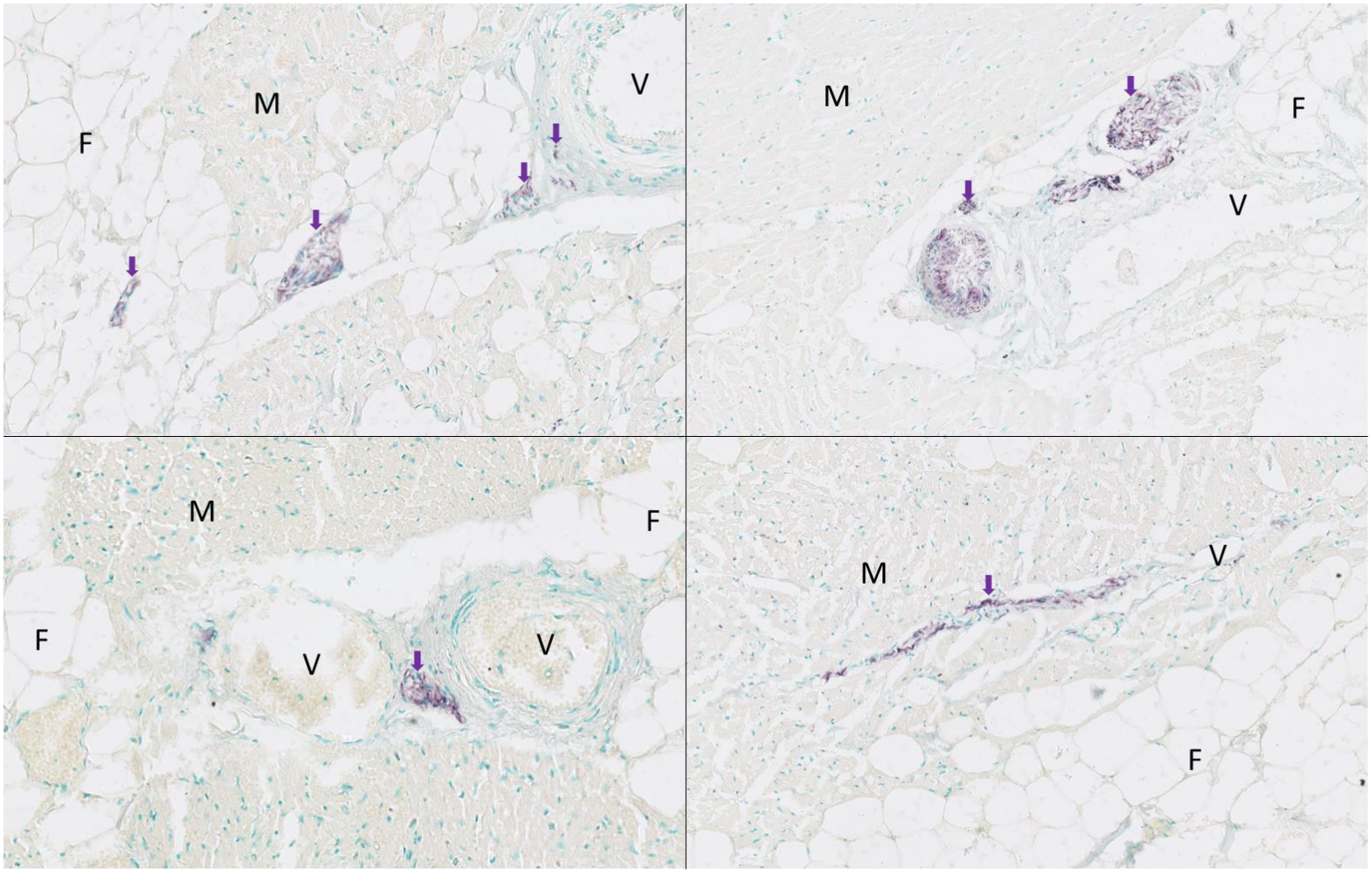


Figure 5.27. PGP9.5 immunostaining of nerve bundles (purple arrows), entering the myocardium (M) from the subepicardial fat (F). The large nerve bundles enter the myocardium predominantly associated with large vessels (V).

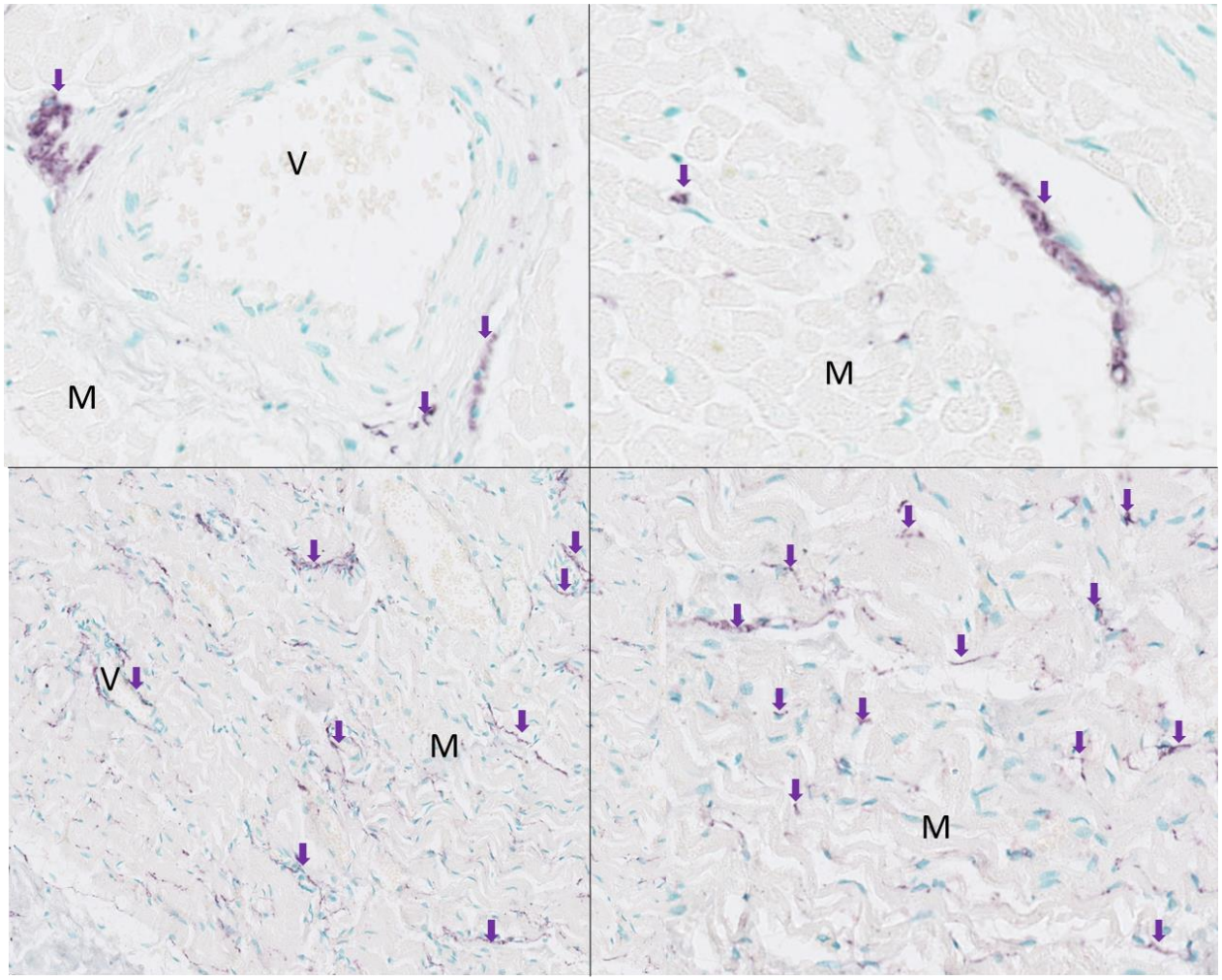


Figure 5.28. Upper panels - Smaller PGP9.5 immunostained nerve bundles and nerve fibrils (purple arrows) alongside vessels (V).

Lower panels - Individual nerve fibrils are throughout the myocardium (M) intricately associated with myocytes and vessels.

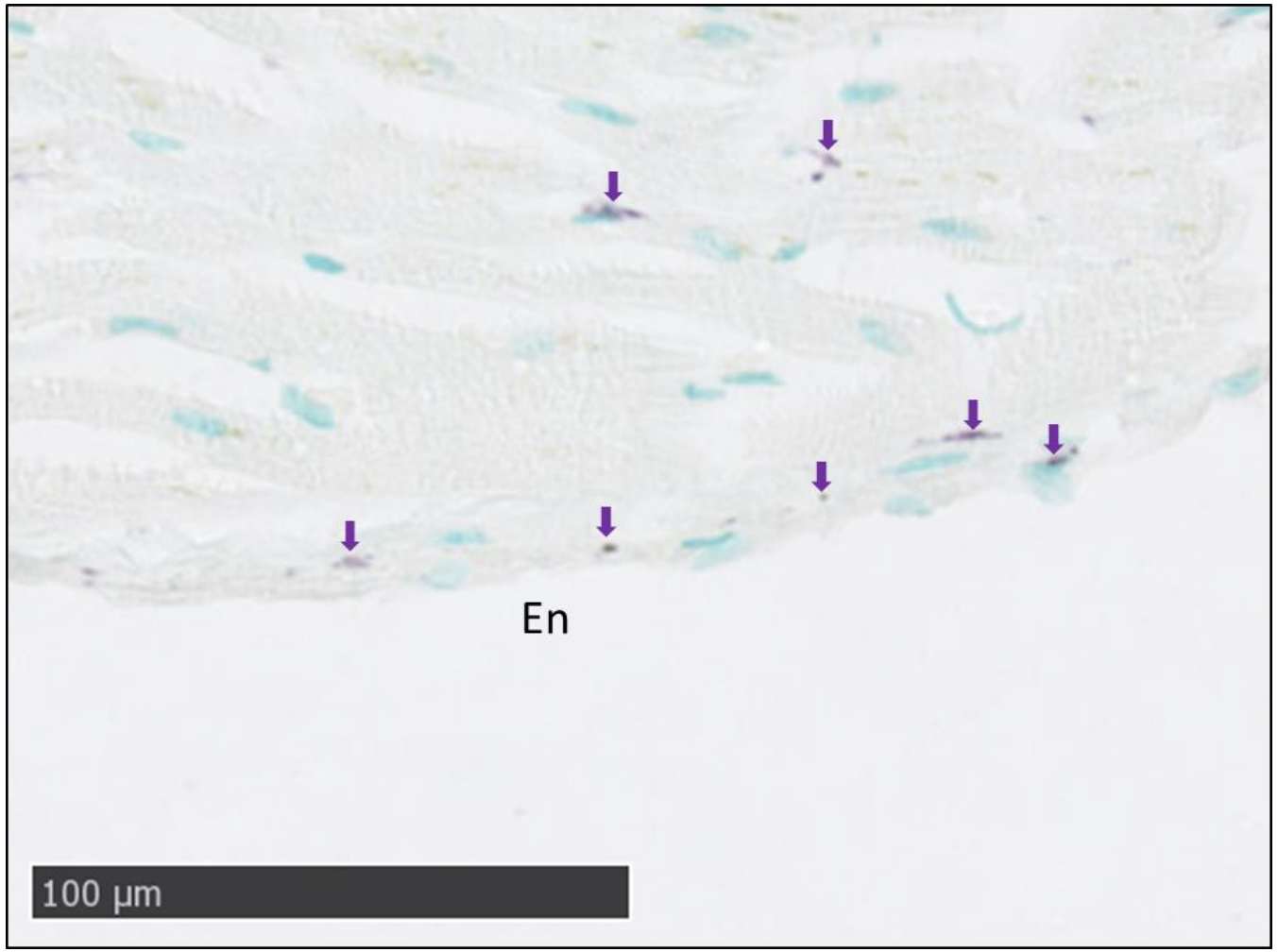


Figure 5.29. Individual nerve fibrils (purple arrows) present in the endocardium and underlying myocardium in intricate association with myocytes.

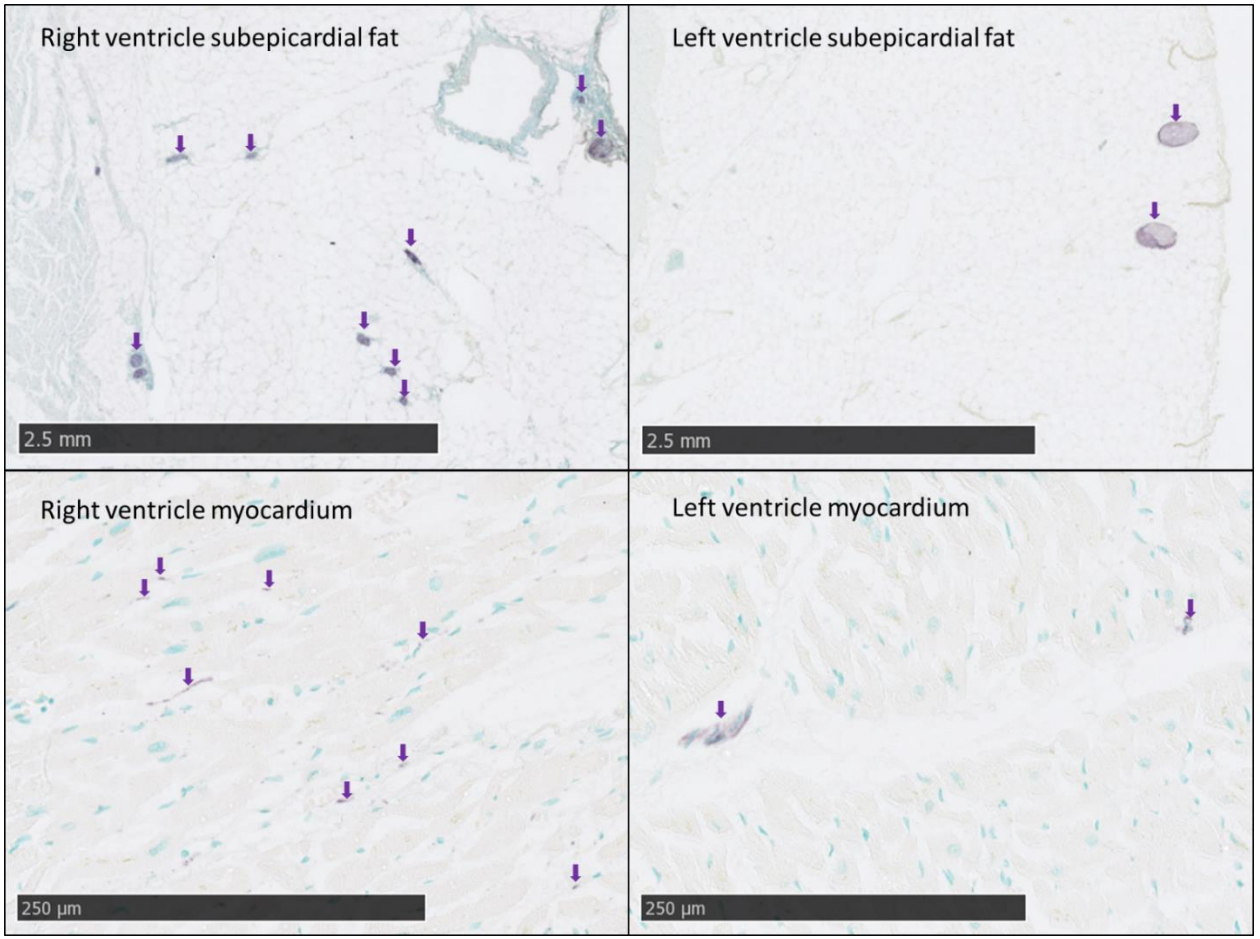


Figure 5.30. There are more PGP9.5 stained nerve bundles in the subepicardial fat of the RV than the LV and more individual nerve fibrils in the myocardium of the RV compared to the LV.

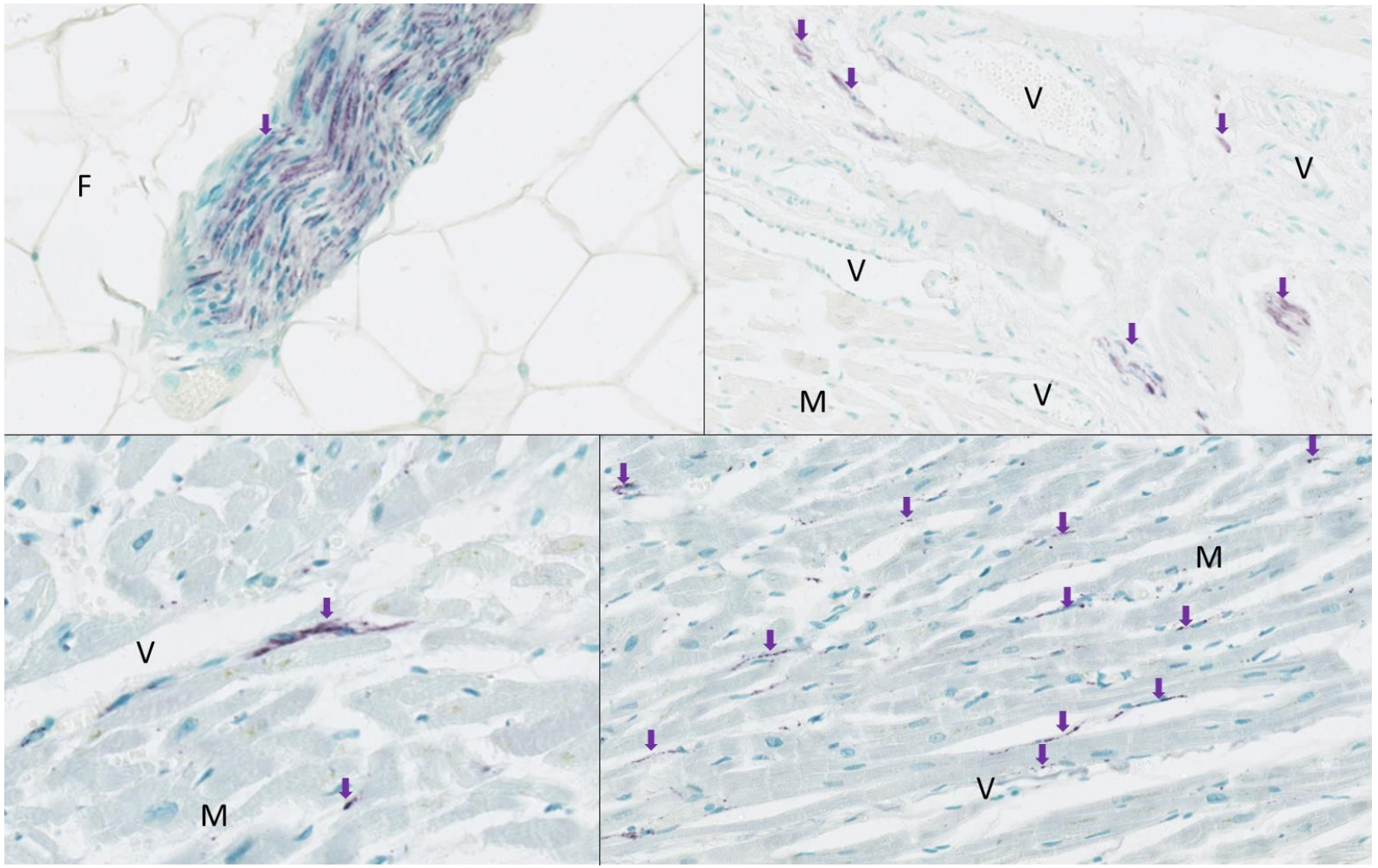


Figure 5.31. TH stained sympathetic innervation (purple arrows). A sub-cohort of fibres within large nerve bundles in subepicardial fat (F) stain for TH. TH nerve bundles extend with vessels (V). Individual nerve fibrils adjoin myocytes (M).

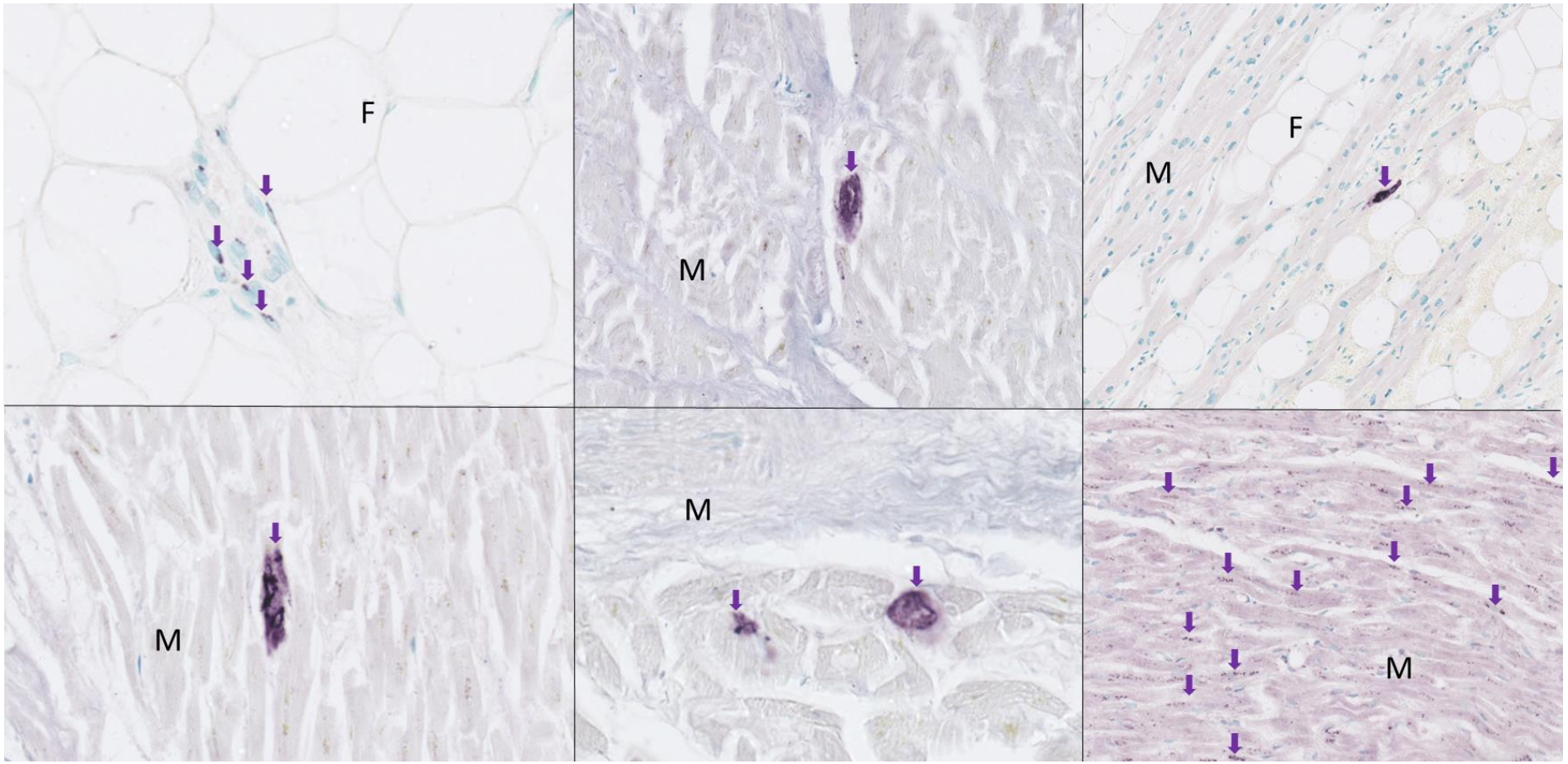


Figure 5.32. CT stained parasympathetic innervation (purple arrows). There is little focal staining within large nerve bundles in the subepicardial fat (F). There is strong staining of nerve bundles within the myocardium (M). The majority are small individual nerve fibrils which showed a granular staining pattern within the myocardium closely associated with myocytes.

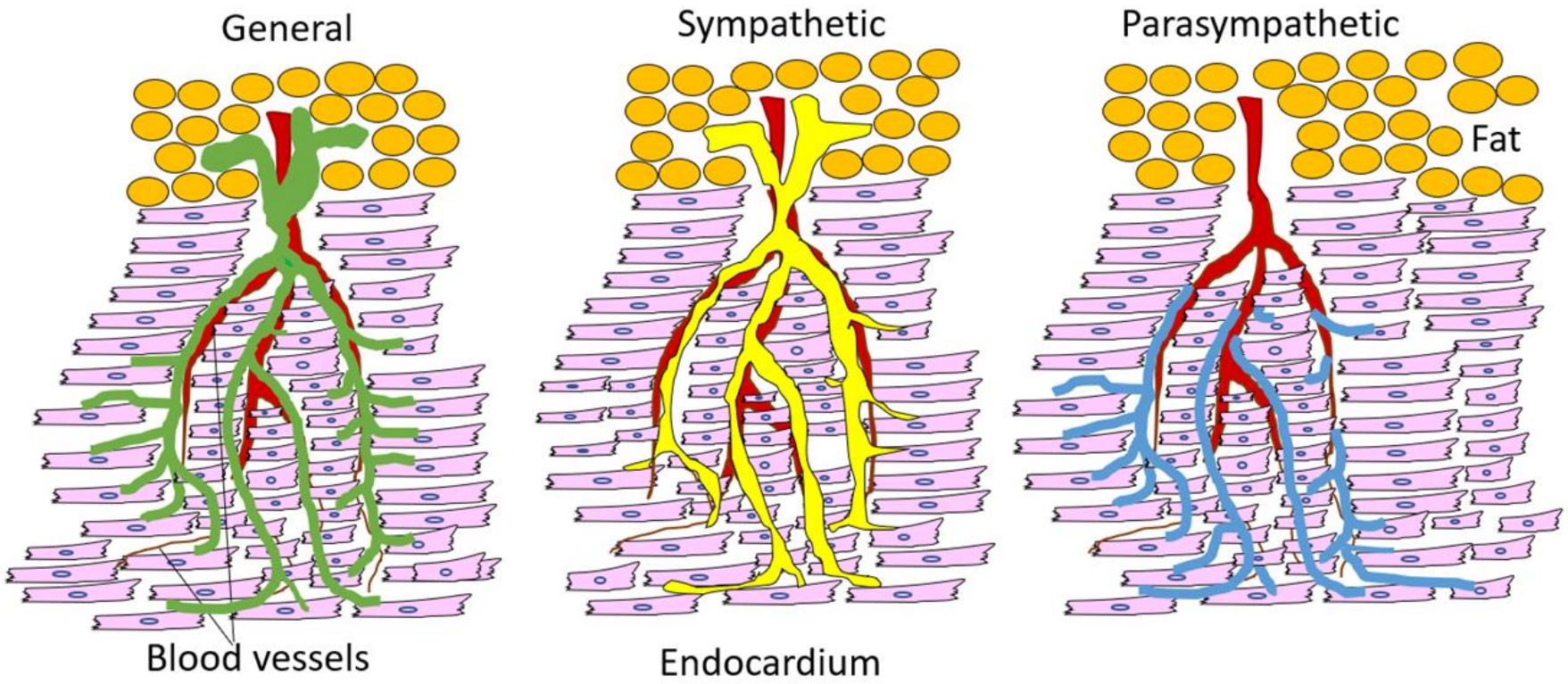


Figure 5.33. Graphical representation of the innervation of the ventricular myocardium. Large nerve bundles enter from the subepicardial fat and arborise around myocytes as they approach the endocardial surface. The sympathetic innervation is more associated with vessels. Parasympathetic innervation is more associated with myocytes.

Quantitative analysis of the normal heart

The primary cohort analysis is performed solely on the normal heart cohort using multilevel modelling to assess innervation by location. The different staining patterns for the immunohistochemistry means that the results are not directly comparable between stains.

General innervation

The variance in PGP9.5 staining proportion in the examined locations do not reach statistical significance. There is an overall average of 0.04% of the tissue staining for PGP9.5 with the RVOT and RV having a proportion of 0.06%, the IVS and anterior LV having 0.03% and the posterior LV having 0.02%.

Sympathetic innervation

There are no significant differences in TH staining by location. TH stains an overall average of 0.04% of the tissue with the IVS, the anterior and posterior LV having 0.03%, the RVOT 0.04% and the RV free wall having 0.06%.

Parasympathetic innervation

There is no evidence for a difference in CT staining between locations. There is an overall average of 0.02% of tissue stained by CT with the highest proportion in the RV of 0.03% and the lowest of 0.01% in the RVOT.

The expected values for percentage of tissue staining for the different markers of innervation in the normal heart are given in table 5.3 and figure 5.34. There is no evidence of an effect of proportion of collagen (p=0.434) or fat (p=0.287) on PGP9.5, TH or CT staining.

Stain	PGP9.5 % of tissue area		TH % of tissue area		CT % of tissue area	
Location	Mean	95% CI	Mean	95% CI	Mean	95% CI
All	0.036	0.018-0.069	0.035	0.017-0.069	0.022	0.008-0.057
RVOT	0.061	0.027-0.134	0.037	0.015-0.090	0.014	0.004-0.043
RV	0.057	0.026-0.126	0.062	0.025-0.151	0.027	0.008-0.083
IVS	0.027	0.012-0.058	0.031	0.012-0.075	0.024	0.007-0.072
ALV	0.032	0.014-0.069	0.031	0.012-0.074	0.020	0.006-0.060
PLV	0.020	0.008-0.043	0.025	0.010-0.060	0.026	0.008-0.078

Table 5.3. The predicted proportions (geometric mean and confidence interval) of the tissue which stained with the respective neural markers. PGP9.5 stains general innervation, TH stains sympathetic nerves and the CT stains parasympathetic nerves. The regions are the right ventricular outflow tract (RVOT), right ventricle (RV), interventricular septum (IVS), anterior left ventricle (ALV) and posterior left ventricle (PLV). The staining is not directly comparable between the different stains.

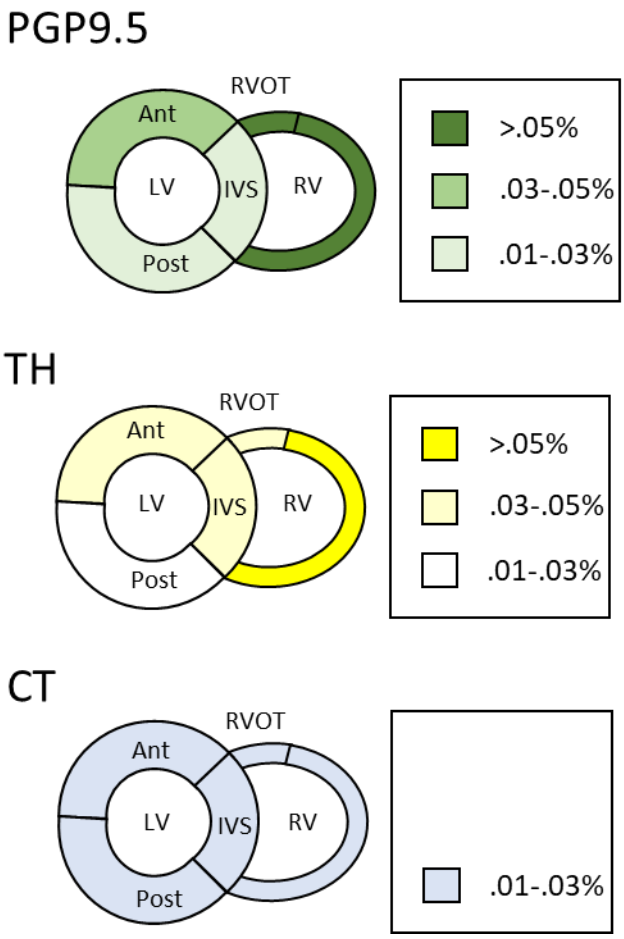


Figure 5.34. Innervation in the normal heart. General innervation marked by PGP9.5 is proportionally greater in the right ventricle (RV) and the right ventricular outflow tract (RVOT). Sympathetic innervation marked by TH is greatest in the RV with the least in the posterior left ventricle (LV). Parasympathetic innervation marked by the CT showed a more even distribution throughout the ventricles.

Quantitative analysis of entire cohort

A secondary total cohort analysis using multilevel modelling is performed which incorporated both the normal heart and the cardiomyopathies to assess innervation by location. There are differences in the proportion of tissue staining for PGP9.5 between locations.

General innervation

PGP9.5 staining is proportionally less in the posterior LV than the RVOT (ratio 0.41, 95%CI 0.20-0.85, p=0.02). PGP9.5 staining is proportionally less in the posterior LV (ratio 0.40, 95%CI 0.19-0.81, p=0.01) and IVS (ratio 0.48, 95%CI 0.23-0.98, p=0.04) than the RV.

Sympathetic and parasympathetic innervation

TH and CT staining do not show differences by location.

The overall cohort results by location are shown in table 5.4.

Stain	PGP9.5 % of tissue area		TH % of tissue area		CT % of tissue area	
Location	Mean	95% CI	Mean	95% CI	Mean	95% CI
All	0.017	0.013-0.023	0.027	0.020-0.036	0.034	0.022-0.053
RVOT	**0.026**	**0.017-0.036**	0.027	0.017-0.039	0.028	0.017-0.046
RV	**0.027**	**0.018-0.038**	0.041	0.027-0.060	0.040	0.024-0.064
IVS	**0.013**	**0.008-0.018**	0.024	0.015-0.035	0.031	0.019-0.050
ALV	0.017	0.011-0.024	0.027	0.017-0.039	0.040	0.024-0.064
PLV	**0.011**	**0.007-0.015**	0.019	0.012-0.028	0.035	0.021-0.057

Table 5.4. The predicted proportions (geometric mean and confidence interval) of the tissue which stained with the respective neural markers for the overall cohort including normal and cardiomyopathy hearts. PGP9.5 stains general innervation, TH stains sympathetic nerves and CT stains parasympathetic nerves. The regions are the right ventricular outflow tract (RVOT), right ventricle (RV), interventricular septum (IVS), anterior left ventricle (ALV) and posterior left ventricle (PLV). The staining is not directly comparable between the different stains.

Discussion

This is the first study to provide a detailed description of the collagen, fat and myocytes present in the normal human ventricular myocardium using picrosirius red and to autonomously quantify innervation in the epicardial fat and ventricular myocardium using digital image analysis.

Composition of the ventricular myocardium

It is important for the pathologist to recognise the distribution of collagen, fat and myocytes in the normal heart. The overinterpretation of non-pathological normal collagen may lead to incorrect diagnoses being made. A previous study was undertaken by Professor Sheppard of 158 hearts which had also been examined by the referring pathologist (De Noronha *et al.*, 2014). Professor Sheppard's and the referring pathologist's diagnoses were compared. Out of 80 normal hearts included in the study, 50 were described correctly with the remaining 30 cases being called pathological. Therefore, it is important for pathologists to be aware of the normal heart structure. Our study demonstrates the normal collagen that is seen within the heart which can be overinterpreted.

Our previous morphometric study of the normal ventricular myocardium which utilised the same method and showed collagen proportions of 15% in the RV, 10% in the LV and 9% in the IVS in 29 control hearts (Miles *et al.*, 2020). This is similar to the present study where we show collagen proportions of 11% in the RV, 9-11% in the LV and 8% in the IVS although we do not find significant differences between the RV and LV.

Previous studies utilising a variety of methods have shown more varied results (Oken and Boucek, 1957; Lenkiewicz, Davies and Rosen, 1972; Van Suylen *et al.*, 1996).

A previous study by Michael J Davies examined 40 human hearts from individuals aged 14-92 years using Lendrum's picromallory stain on the IVS alone reporting 25%. They report measurements from the RV to be 20-30% and the LV to be 15-25% in three cases. The collagen was relatively evenly distributed in agreement with our study (Lenkiewicz, Davies and Rosen, 1972). The higher values in this study are most likely due to the assessment of collagen gel rather than just solid staining collagen and the use of a different stain.

A study using digital image analysis on Sirius red stained myocardial sections from 16 hearts found proportions more in line with our studies (Van Suylen *et al.*, 1996). They report values of 5-6% in the RV and 3% in the IVS and LV which were lower than our proportions. These lesser values may be explained by technique variation as the use of acidified water in our protocol has been proposed to reduce the washout of dye when used rather than water (Kiernan, 2013, 2015).

Previous biochemical studies have shown much lower proportions of collagen within the ventricles. Oken et al, used colourimetry to assess hydroxyproline concentrations and weight in hydrolysed human myocardial samples from 43 normal hearts. They report concentrations of 0.99% in the RV and 0.74% of the LV. The differences are most likely due to the assessment of collagen by weight as opposed to area.

The present study reports similar proportions of fat compared to our previous study (Miles *et al.*, 2020). This previous study reported adipose tissue to make up 12% of the RV, 5% of the LV and 2% of IVS. This is similar to the findings in this study of 10% of the RV, 4-8% in the LV and 2% of the IVS. The slightly lower proportion of fat

may be due to the inclusion of females within our previous study as females have more fat in the RV (Tansey, Aly and Sheppard, 2005).

Fat can make up a considerable proportion of the lateral RV wall. Tansey et al, examined the hearts of 148 individuals with non-cardiac causes of death (Tansey, Aly and Sheppard, 2005). They found an average of 6-15% of fat in the lateral RV in individuals 20-39 years of age. They also observed that the lateral wall had the largest amount of fat with some fat in the anterior RV and little or no fat in the posterior RV. This is broadly in line with the findings in this study. The report highlights that prominent fatty infiltration of the RV is a normal finding.

The myocyte proportions within this study are similar to our previous study using the same technique (Miles *et al.*, 2020). Our previous study reported 66% in the RV, 81% in the LV and 88% in the IVS. This compares to 71-72% in the RV, 77-80% in the LV and 86% in the IVS within the present study.

Previous studies on the volume of cells within the heart also have estimates that are similar to our myocytes proportion. Vliegen et al, studied 16 normal human hearts calculating cell area using a point grid on microscopic slides (Vliegen *et al.*, 1991). They found 81% myocytes to 18% non-myocytes. Within the literature other estimations from mammalian hearts range from 67%-80% myocytes with 20-33% non-myocytes (Vliegen *et al.*, 1991; Jugdutt *et al.*, 2003). These findings are similar to ours however with regard to cell numbers, rather than volume, these estimates reverse. Dissociation of hearts into a single cell suspension or counting cell types on histology have been used to assess cell numbers. These studies report that only 25-35% of the myocardium is myocytes and 65-75% are non-myocytes (Nag, 1980; Vliegen *et al.*, 1991).

Innervation of the ventricular myocardium

Morphological studies of human ventricular innervation are few. Pianca et al, used TH immunofluorescence on a single clarified whole-mount block from a neonate heart (Pianca *et al.*, 2019). They took six non-consecutive sections of the midlevel of the ventricular myocardium. They show the complex arborising nature of the sympathetic innervation.

There are two three previous immunohistochemical studies on adult human ventricular myocardial innervation which both agree with our findings that there is a greater nerve density in the RV as compared to the LV (Marron *et al.*, 1994; Kawano, Okada and Yano, 2003). A previous study used computer assisted confocal image processing techniques on whole mount preparations of the endocardium from 5 adults. PGP9.5 and TH immunohistochemistry along with acetylcholinesterase, a histochemical marker of parasympathetic nerves in fresh tissue, was used to examine nerve area. There was a higher percentage stained area of general innervation in the RV than the LV within the endocardium reflecting our findings of increased innervation in the RV compared to the LV (Marron *et al.*, 1994). Also, in keeping with our findings within the myocardium, there was a higher percentage area of sympathetic nerves in the RV endocardium in comparison to the LV and a relatively similar percentage area of parasympathetic nerves in the endocardium of the LV and RV. Kawano et al, used point counting on six hearts from men aged 50–68 years without cardiovascular disease. They used TH immunohistochemistry and a histochemical technique for acetylcholinesterase to examine 26 sections. They found that there was more sympathetic and parasympathetic staining nerves in the atria than the ventricles and that the ventricular base had more innervation than the apex. Similar to our study, they found a greater nerve density of both sympathetic and to a

lesser extent parasympathetic in the RV than the LV (Kawano, Okada and Yano, 2003). They found more sympathetic nerves in the anterior wall than the posterior wall which contrasts with our findings. They agree our observation that the inner myocardium has a greater number of parasympathetic nerves than the outer myocardium. Their pictures of sympathetic nerves show a nerve bundle in the subepicardial fat and an arborising fibre in the myocardium. Their pictures of the parasympathetic innervation show granular staining intricately associated myocytes particularly within the endocardium which agrees with our images also.

A further study reported the innervation of the epicardial and endocardial surfaces of 17 hearts from mainly children (age range 3 months to 37 years). PGP9.5 and TH immunohistochemistry and acetylcholinesterase histochemical staining was used to examine whole mount preparations of both atria and ventricles with confocal and fluorescence microscopy. In keeping with our findings within the ventricular myocardium, the general nerve fibrils they observed in the ventricular endocardium were single thin threadlike fibres. Similar to our findings this study found there were no nerve fibrils in the epicardium of the RV. In contrast to our findings, they found nerve fibrils in the epicardium of the LV which were frequently marked frequently by TH but not acetylcholinesterase.

Nerve fibrils were only described in the endocardium of the LV and not in the RV. Also in contrast to our findings the nerve terminals of the endocardium stained mainly for TH with less than 5% staining for acetylcholinesterase (Marron *et al.*, 1995). These differences may be explained by the predominantly paediatric population that was studied. In keeping with our study, their photographs demonstrate complex arborisation of innervation.

Our findings that the nerve bundles are associated with large vessels which lie in the epicardial fat and in the myocardium where the nerve bundles are surrounded by fat as observed microscopically in anatomical studies (Standring, 2021).
No previous morphological studies has examined the innervation of the RVOT in the human heart.

Innervation and functional consequences

The higher innervation present within the RVOT that we have demonstrated may help to explain why it is considered more “arrhythmogenic” than other areas, particularly in structurally normal hearts. The RVOT is considered to be the most common place of origin for benign ventricular premature beats and idiopathic ventricular tachycardia as well as commonly in conditions underlying sudden arrhythmic death syndrome such as Brugada, long QT and catecholaminergic polymorphic ventricular tachycardia (Belhassen and Viskin, 1993; Haïssaguerre *et al.*, 2003; Maury, 2011; Nademanee *et al.*, 2015; Boukens, Coronel and Christoffels, 2016). Furthermore the relatively higher sympathetic input of the RV may explain some of the functional differences observed between the ventricles (Zandstra *et al.*, 2021). Adrenergic stimulation shows different responses in the RV and LV. During exercise, athletes have been shown to have a relatively greater wall stress in the RV compared to the LV (La Gerche *et al.*, 2011). Further supporting this assertion, sympathetic nerve stimulation in dogs has shown greater increases in contractility and systolic pressure in the RV compared with the LV (Abe *et al.*, 1987; Molina *et al.*, 2014).

Limitations

The study is limited by its small number of cases and male dominance.

Concluding remarks

When evaluating the abnormal, it is of central importance to understand the normal. We present the distribution and proportions of collagen, fat and myocytes in the ventricles.

Collagen coalesces in the inner trabeculae of the normal heart. This collagen can be mislabelled as fibrosis if pathologists are not familiar with the normal distribution.

There is more fat in the RV than the LV and IVS. Fat lies is predominantly located between the epicardium and the outer myocardium. Fat infiltrates into the RV but not the LV wall in the normal heart.

There is a complex network of general, sympathetic and parasympathetic nerves in the heart. Large nerve bundles are present in the epicardial fat which enter the myocardium with vessels. Within the myocardium, there is a complex network of small nerve bundles and fibrils. Both sympathetic and parasympathetic nerve fibrils are intricately associated with vessels and myocytes.

Innervation is proportionally greatest in the RVOT and the RV. This may aid in our understanding as to why the RVOT is a focus point for generation of a number of arrhythmias.

Summary of microscopic findings in the normal heart ventricular subepicardial fat and myocardium

- There is no difference in the proportion of collagen between ventricles
- There is more fat in the RV than the LV

- There is no difference in the proportion of myocytes between ventricles
- Large nerve bundles in the epicardial fat enter the myocardium with vessels
- Nerve fibrils intricately associate with both myocytes and vessels
- Sympathetic fibrils associate more with vessels
- Parasympathetic fibrils associate more with myocytes
- There is more general innervation in the RVOT and RV free wall than the LV
- There is a trend toward more sympathetic innervation in the RV than the LV
- There is no difference in parasympathetic innervation between the ventricles

CHAPTER 6 ARRHYTHMOGENIC CARDIOMYOPATHY

Introduction

In chapter 5, we established the composition of the normal ventricular myocardium and its innervation. In this chapter, we establish whether there are differences in tissue composition and innervation in ACM compared to the normal heart.

ACM is an inherited condition affecting the myocardium and causing young SCD particularly in athletes (Miles *et al.*, 2019). Underlying genetic alterations are found within the cardiac desmosomal proteins (Awad, Calkins and Judge, 2008). Clinical diagnosis currently relies on a complex scoring system known as the task force criteria (Marcus *et al.*, 2010). Arrhythmia and SCD are well recognised to occur during or immediately after exercise suggesting that adrenergic stimulation and autonomic imbalance are contributing factors (Corrado *et al.*, 2003; Miles *et al.*, 2019). Furthermore, sympathectomy for intractable ventricular tachycardia in ACM has shown some promise (Assis *et al.*, 2019).

Methods

ACM decedents with suitable retained tissue were studied from a library of 931 cases (see figure 2.15). As stated in the methods, ACM is diagnosed on the basis of the presence of fibrosis with or without fat in an epicardial distribution in either or both ventricles in the absence of coronary artery disease. Cases with a history of heart failure, coexisting conditions which may have contributed to death, valvular disease and hypertensive disease are excluded. Exactly as with the normal hearts, sections from the RVOT, the RV free wall (including the anterior, lateral and posterior wall), the IVS, as well as the anterior and posterior LV free wall are stained with PSR, PGP9.5, TH and CT. Positive controls of the sinus node and negative controls

with the primary antibody omitted are utilised. Slides are scanned using a Hamamatsu Nanozoomer 2.0RS. Digital image analysis is performed using applications developed within the Visiopharm program (Visiopharm A/S, Agern Alle 24, 2970 Hørsholm, Denmark).

Statistics

Differences between groups are assessed using log transformed values for collagen, fat, myocyte, PGP9.5, TH and CT proportions (as these values are skewed). A multilevel model is created to allow comparison of hierarchical dependent data based on myocardial location. Variables such as age, sex and ethnicity are incorporated into multivariable analysis. Predictions of collagen, fat, myocytes, PGP9.5, TH and CT are expressed as geometric means and 95% confidence intervals.

Statistical analyses used Stata version 16 (StataCorp, College Station, Texas, USA).

Results

Twenty cases of ACM with suitable retained tissue are identified. The age at death is 36±13 years comprising 18 males and 2 females. The heart weight is 429±75g. Macroscopically, the heart showed fibrosis in both ventricles in 7 cases. In one case there is solely RV fibrosis and in 6 cases there is solely LV fibrosis identified macroscopically. Five cases appear normal macroscopically (figure 6.1).

The ACM macroscopic measurements are compared to 10 male controls. The dimensions of the atria, ventricle muscle wall thickness and diameters, valve circumferences and subepicardial fat measurements are provided in table 6.1 and compared to controls.

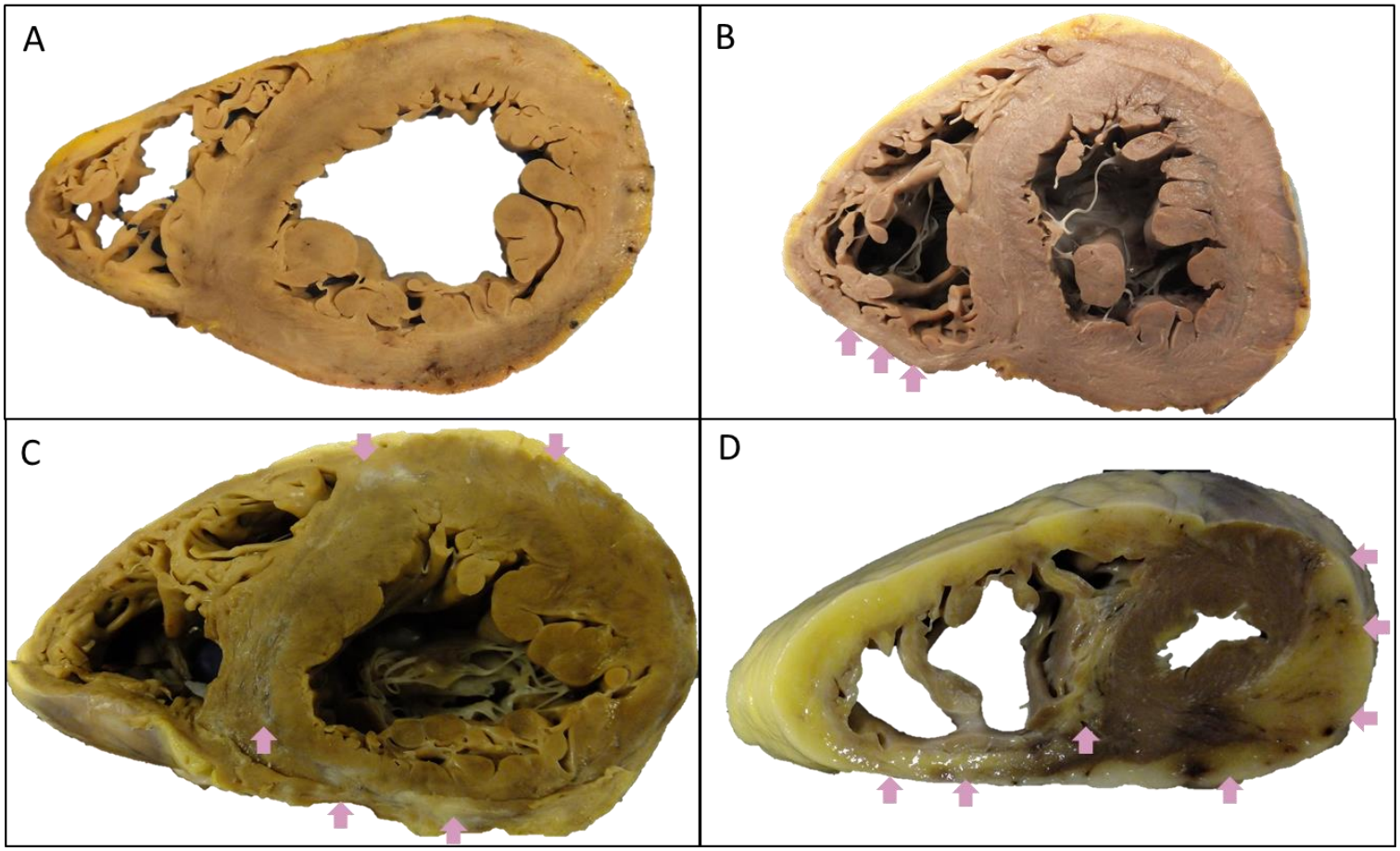


Figure 6.1. The variability in the macroscopic appearance of ACM. A) A normal appearing case. B) Solely posterior right wall fibrosis. C) Solely left ventricular fibrosis. D) Biventricular macroscopic fibrosis and fatty infiltration. The arrows mark fibrosis.

	ACM	Control	P value	Validation of significant findings in wider ACM cohort (n=319)
Heart weight	**429±75**	**364±63**	**.020**	**443±100, p<0.01**
Right atrium 1	56±9	54±14	.532	
Right atrium 2	49±14	41±9	.128	
Left atrium 1	43±7	40±8	.245	
Left atrium 2	38±8	36±8	.538	
RV diameter	36±10	32±6	.177	
Anterior RV Muscle	2±1	3±1	.462	
Lateral RV Muscle	**2±1**	**3±1**	**.017**	3±1, p=1
Posterior RV Muscle	**4±1**	**3±1**	**.049**	**4±1, p<0.01**
RVOT Muscle	3±1	3±1	.569	
LV diameter	38±9	33±6	.129	
IVS	13±4	13±3	.804	
Anterior LV Muscle	12±2	12±2	.652	
Lateral LV Muscle	12±4	13±2	.597	
Posterior LV Muscle	11±3	12±2	.744	
Mitral valve	83±18	83±16	.891	
Tricuspid valve	101±20	103±17	.791	
Pulmonary valve	56±11	55±12	.828	
Aortic valve	49±14	55±9	.204	
Ascending aorta	53±9	57±8	.188	
Anterior RV fat	2±1	1±1	.084	
Lateral RV fat	**4±3**	**2±1**	**.020**	2±2, p=1
Posterior RV fat	0±1	0±0	.791	
RVOT fat	1±2	1±1	.197	
Anterior LV fat	1±1	1±1	.600	
Lateral LV fat	1±1	0±0	.221	
Posterior LV fat	0±1	0±1	.618	

Table 6.1. Macroscopic heart measurements for arrhythmogenic cardiomyopathy compared to the normal hearts. The means and standard deviations for heart weight (in grams), atrial dimensions, cavity diameters, muscular wall thickness, valvular and ascending aortic circumferences and epicardial fat thickness (in millimetres) are provided. Significant structural changes have been examined in the overall ACM cohort to allow it to serve as a validation cohort.

There is an increase in heart weight (429±75g vs 364±63g, p=0.02).

The lateral RV muscle thickness is reduced (2±1 vs 3±1, p=0.02) and the lateral RV fat is increased (4±3 vs 2±1, p=0.02). There is an increase in the posterior RV muscle thickness (4±1 vs 2±1, p=0.49). The remaining macroscopic measurements for the RV and LV do not show significant differences to controls. The increase in heart weight and thickening of the posterior RV wall were further validated in the wider ACM cohort (table 6.1).

Correlations between measurements

The correlations between measurements are shown in table 6.2. From the variables that were significantly different than the normal heart there is a significant moderate negative correlation between lateral RV muscle wall thickness and lateral RV subepicardial fat thickness (figure 6.2). This is in keeping with fat replacing the lateral muscle wall with disease progression. There were no other significant correlations between measurements that were significantly different from the normal heart.

		1	2	3	4	5	6	7	8	9	10	11	12	13	14	15	16	17	18	19	20	21	22	23	24	25	26
1	Heart weight																										
2	Anterior RV muscle wall	.13																									
3	Lateral RV muscle wall	.12	.48*																								
4	Posterior RV muscle wall	.25	.62**	.27																							
5	RVOT muscle wall	.64**	.04	-.01																							
6	Interventricular septum	.16	.65**	.14	.24	.21																					
7	Anterior LV muscle wall	.23	.32	.22	.45	.18	.69**																				
8	Lateral LV muscle wall	.05	.45	.11	.45	.1	.76**	.85**																			
9	Posterior LV muscle wall	.1	.44	.19	.53*	-.06	.51*	.83**	.91**																		
10	RV anterior epicardial fat	.36	.04	-.22	.36	.3	.35	.19	.22	.1																	
11	RV lateral epicardial fat	-.14	-.17	-.50*	.05	-.29	.28	.17	.15	0	.52*																
12	RV posterior epicardial fat	.15	-.35	-.47*	0	-.14	-.15	-.21	-.26	-.3	.52*	.54*															
13	RVOT epicardial fat	-.41	.26	-.04	.36	-.79**	-.1	.04	.11	.21	-.16	.51*	.12														
14	LV anterior epicardial fat	-.17	.08	.04	-.26	.02	-.01	-.3	-.4	-.34	-.37	-.21	.04	-.16													
15	LV lateral epicardial fat	.33	-.16	.26	.16	-.13	-.45	-.23	-.59**	-.37	-.04	-.14	.21	.15	.01												
16	LV posterior epicardial fat	-.29	-.11	.03	-.35	-.01	-.04	-.03	-.09	-.07	-.26	.01	-.15	.15	.34	-.14											
17	Right atrium 1	.11	-.26	.15	-.34	.12	-.27	-.19	-.17	-.24	.04	-.23	.35	-.29	.16	.09	.1										
18	Right atrium 2	.3	.35	.04	.43	.02	.23	.14	.31	.47*	.01	-.3	-.3	.18	-.03	-.09	.04	-.19									
19	Left atrium 1	-.29	.16	.17	-.17	.16	.31	-.03	0	-.02	-.33	-.27	-.44	-.22	.61**	-.3	.3	-.14	.23								
20	Left Atrium 2	.4	-.03	.01	.08	.18	-.09	.02	-.02	.05	-.1	-.25	-.26	-.18	-.02	.09	-.36	-.23	.47*	.23							
21	Diameter of RV chamber	-.13	-.26	-.52*	-.22	.19	-.25	-.21	-.19	-.29	.01	.37	.41	.11	-.08	-.04	.44	-.01	-.3	-.38	-.50*						
22	Diameter of LV chamber	.2	-.03	-.01	-.05	-.03	-.3	-.43	-.60**	-.49*	-.2	-.2	.38	.05	.44	.66**	-.07	.33	-.04	-.02	-.02	.13					
23	Mitral valve circumference	-.21	.2	-.02	.02	.06	-.24	-.12	-.12	-.16	-.23	-.27	-.12	.13	.03	.05	.33	-.01	0	.15	-.36	.34	.31				
24	Tricuspid annulus circumference	-.35	.19	-.13	-.18	-.07	-.03	.23	.24	.09	-.24	-.04	-.21	.19	-.04	-.26	.15	.02	-.24	.13	-.32	.15	-.04	.69**			
25	Pulmonary valve circumference	-.16	.52*	.1	.24	0	.22	.31	.33	.17	.01	.06	-.03	.14	-.04	-.21	-.23	-.12	-.21	.06	-.34	-.03	0	.56*	.72**		
26	Aortic circumference	-.24	.2	.12	-.23	-.04	.63**	.15	.11	0	.09	.18	-.08	-.11	.28	-.14	.29	-.08	-.11	.49*	-.3	-.01	.11	.01	.14	.18	
27	Ascending aorta circumference	-.67**	.24	.04	.05	-.41	.42	.23	.22	.16	-.18	.27	-.15	.45	.24	-.23	.3	-.2	-.14	.44	-.41	.02	.01	.46*	.54*	.53*	.93**

*Table 6.2. Correlations between variables. Significant strong correlations are highlighted in red and significant moderate correlations are highlighted in yellow. There is a significant negative correlation between lateral RV muscle and lateral RV fat (*p<.05, **p<.01).*

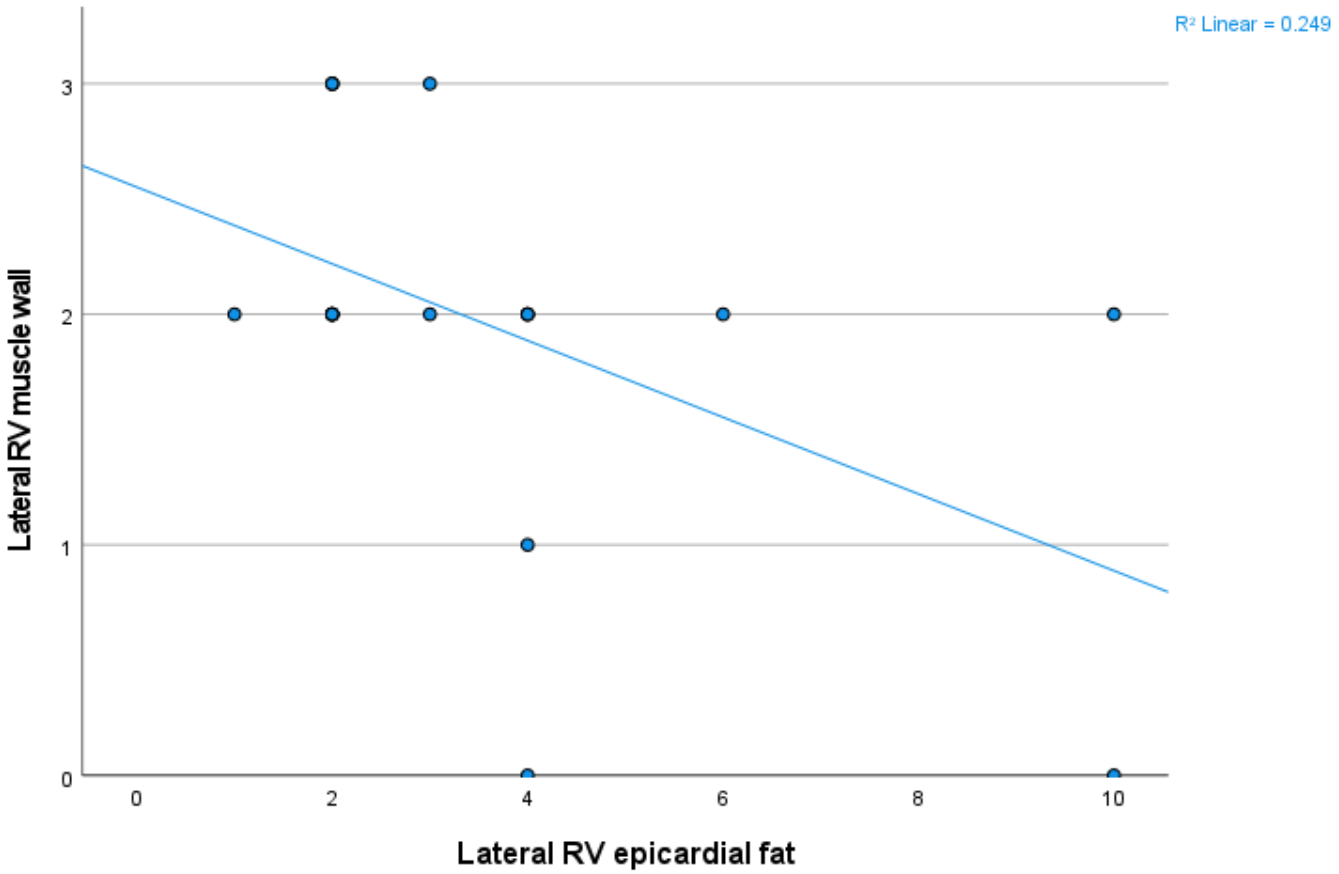


Figure 6.2. Plot of lateral RV muscle wall against lateral RV epicardial fat. There is a significant moderate negative correlation between lateral RV epicardial fat and lateral RV muscle wall. As fat increases in the lateral RV wall, the muscle thickness decreases. This represents fatty replacement of the lateral RV wall.

Ventricular myocardium compositional analysis

Collagen

There is considerable variation in the areas that are involved between the hearts with ACM (figures 6.3-6.7). There is biventricular ACM in 7 cases in which both ventricles show fibrosis. There is LV dominant ACM in 7 decedents where fibrosis predominates in the LV. There is RV dominant ACM in 6 decedents where fibrosis predominates in the RV.

The layer of collagen underlying the epicardium is thickened overlying areas of disease (figure 6.8).

Within the myocardium, two patterns of fibrosis are observed. The first is interstitial fibrosis which forms a meshwork of collagen encasing myocytes and the second is replacement fibrosis which forms patches of collagen replacing myocytes. Fibrosis is most pronounced around myocytes at the intersection between the subepicardial fat and outer myocardium.

Within the RV and RVOT, the patterns of interstitial and replacement fibrosis show dramatic variation. Interstitial fibrosis is present at the intersection between the subepicardial fat and the outer myocardium and can be present transmurally from the outer myocardium all the way into the trabeculae (figure 6.4). In other cases, the interstitial fibrosis is more localised lying at just the intersection between the subepicardial fat and the outer myocardium (figure 6.9). There can be an abrupt transition to normal myocardium or fibrosis can merge into normal areas (figure 6.9). Small areas of replacement fibrosis merge with the network of interstitial fibrosis.

Within the LV, replacement fibrosis is present at the intersection between the subepicardial fat and the myocardium. The replacement fibrosis is admixed with infiltrating fat and extends into the myocardium (figure 6.10). The extent of fibrosis

varied within and between cases. The involvement ranges from focal changes adjacent to the subepicardial fat to full thickness patchy replacement fibrosis present adjacent to the endocardium. There are frequently long continuous stretches of replacement fibrosis within just the outer edge of the myocardium (figure 6.11). Similar to the RV, fibrosis in the outer myocardium lies next to normal areas and can show an abrupt transition (figure 6.12). Interstitial fibrosis is present at the edges of replacement fibrosis (figure 6.13) and frequently links areas of replacement fibrosis together (figure 6.14). The interstitial fibrosis extends considerably further into the myocardium towards the endocardial surface than the replacement fibrosis (figure 6.14). The posterior LV wall shows the most extensive amount of collagen replacement (figure 6.7).

The RV and RVOT are mainly affected by interstitial fibrosis with small patches of replacement fibrosis whereas the LV and IVS show more prominent replacement fibrosis with interstitial fibrosis at the edges.

The admixture of fat and fibrosis is present in the RVOT, RV free wall as well as the anterior and posterior LV (figure 6.3, 6.4, 6.6 and 6.7). This contrast with the IVS which shows a streak of fibrosis through the central midwall without admixed fat (figure 6.5). This streak shows empty spaces (figure 6.15). Fibrosis is present in the right side of the IVS in one case of right dominant ACM and one biventricular ACM. Fibrosis is present in the left side of the IVS in one case of left dominant ACM.

The collagen that lies around vessels frequently connects and merges with both replacement and interstitial fibrosis but the fibrosis is not centred on the vessels (figure 6.16).

Fat

Fat is present in the locations described as in the normal heart lying between the epicardium and myocardium in the LV and RV and showing infiltration into the RV myocardium (figures 6.3, 6.9, 6.14). Fat in the myocardium is extremely variable in both extent and location in ACM.

Within areas of fibrosis in the RV myocardium there is frequently admixed fat (figures 6.3, 6.4). This is present in the forms of single or clusters of adipocytes up to fat completely replacing the myocardium into the trabeculae with just occasional residuals stands and myocytes or fibrosis (figures 6.3, 6.4, 6.16).

The LV also shows marked variation in the amount of fat present with fibrosis which ranges from solely fibrosis (figure 6.6) to large amounts of admixed fat (figure 6.7). The fat is present in the form of single adipocytes up to large clusters of fat replacing much of the outer myocardium with stands and patches of myocytes or collagen on the outer myocardial surface dissociated from the residual myocardium (figures 6.7, 6.10, 6.11). Fat never completely replaces the full thickness of the LV wall. Adipocytes are frequently present within patches of replacement fibrosis or between islands of myocytes showing interstitial fibrosis (figures 6.10, 6.11, 6.18). Admixture of fat with fibrosis is rarely present in the IVS (figure 6.5).

The RV (figure 6.3, 6.4) showed more extensive fatty infiltration than the LV (figure 6.6, 6.7).

Myocytes

There is loss of myocytes in the areas of replacement fibrosis and fatty infiltration (figures 6.3, 6.4, 6.6, 6.7-6.11). Residual islands of myocytes are present within areas of fibrosis and fat (figures 6.4, 6.6, 6.7, 6.18). The RV shows more extensive loss of myocytes than the LV (figures 6.3, 6.4, 6.6, 6.7). The loss of myocytes is

transmural in the RV whereas in the LV it rarely extends into the inner myocardium. Within the IVS, myocyte loss is most prominent in the middle of the wall. There is always myocyte hypertrophy in ACM cases particularly within and around areas of fibrosis where there are also degenerative features including vacuolation and myofibrillar loss (figure 6.19). Occasional myocytes display variation in nuclear size, shape and staining (figure 6.19). Myocyte disarray is not seen in arrhythmogenic cardiomyopathy.

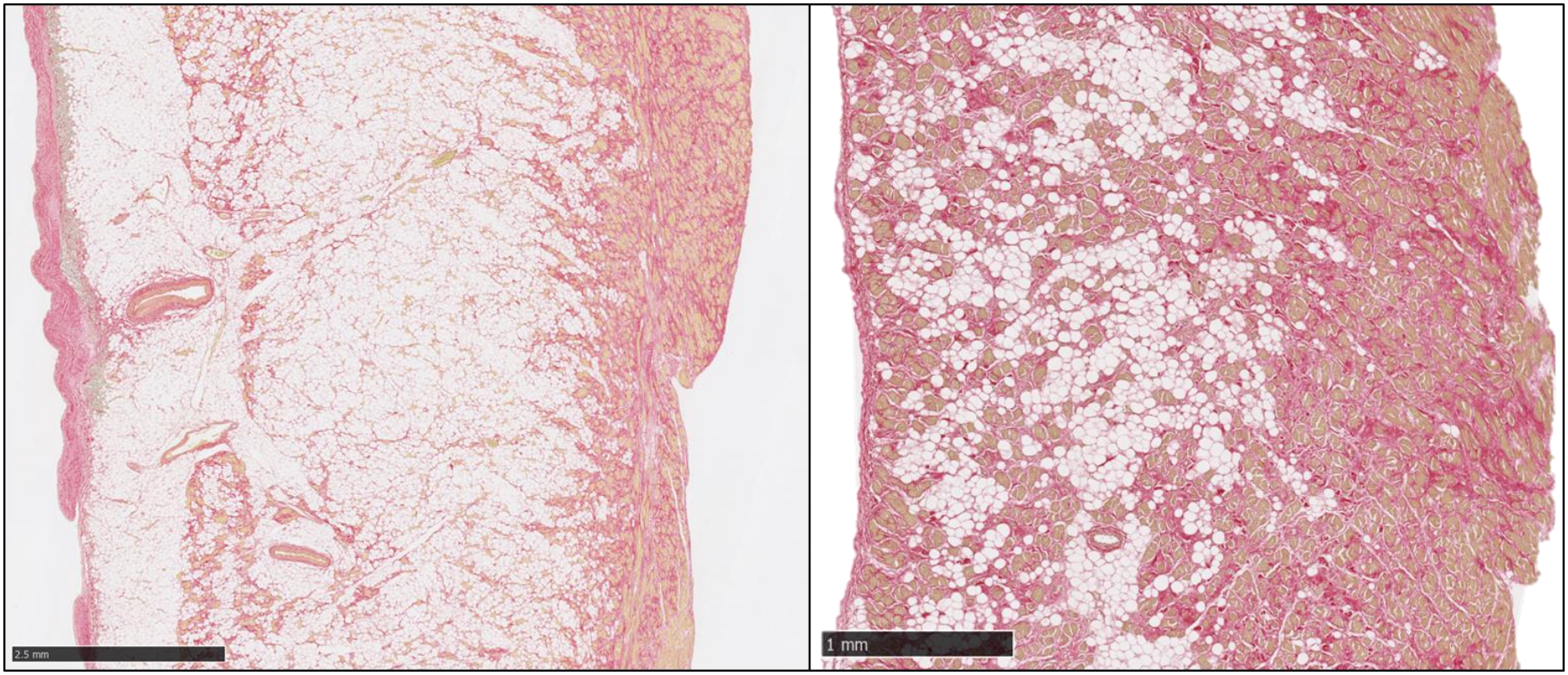


Figure 6.3. The right ventricular outflow tract shows variability in its involvement by collagen and fat within the myocardium. It may show extensive fatty infiltration with collagen. This highlights the variability of fat and collagen replacement.

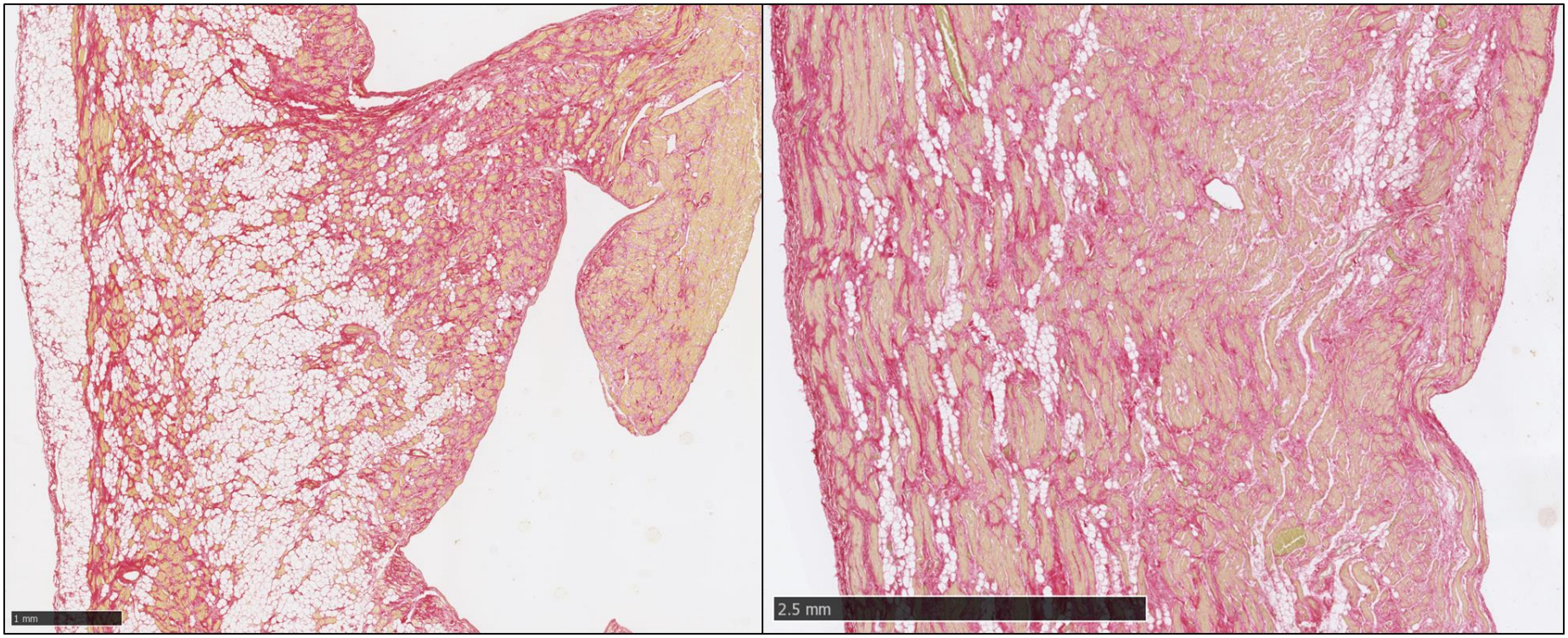


Figure 6.4. The right ventricle shows variation of involvement by fat and collagen. It shows extensive fatty infiltration with collagen or predominantly collagen with smaller amounts of admixed fat.

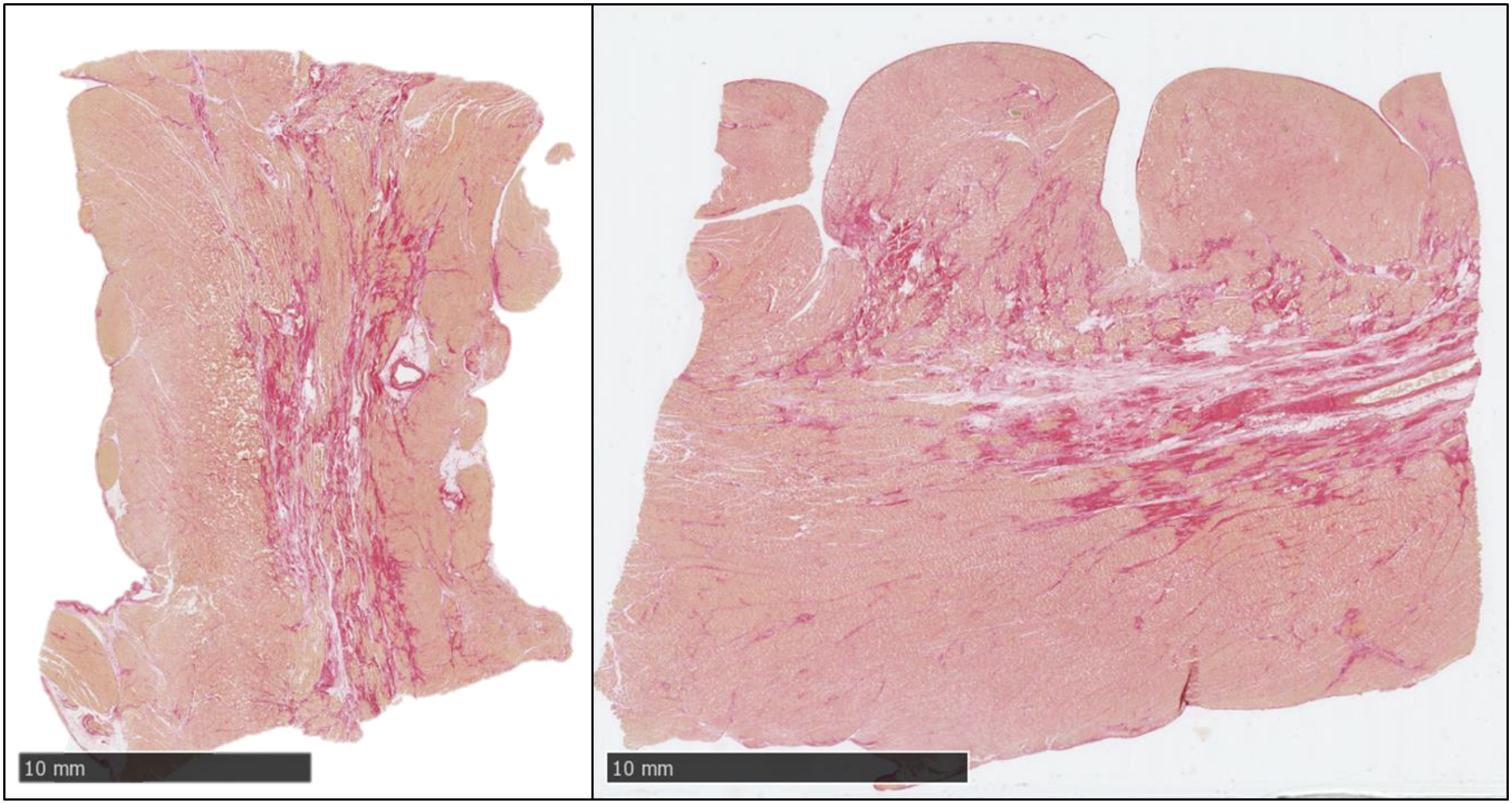


Figure 6.5. The septum shows involvement by fibrosis without fat. There is a streak of replacement collagen through the midwall which may extend to either the right of left side.

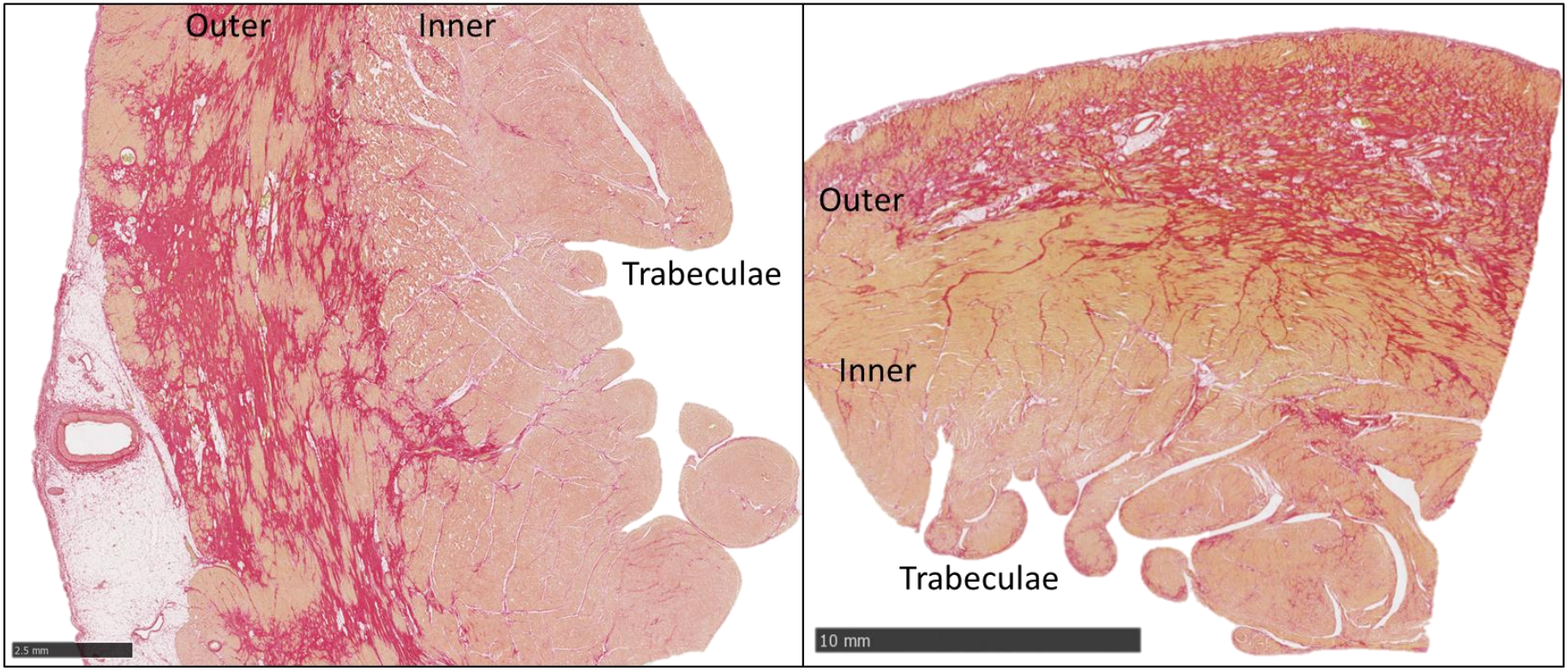


Figure 6.6. The anterior left ventricular wall shows variation in involvement by both replacement and interstitial fibrosis in the outer half of the myocardium. There is less admixed fat in the left ventricle (picrosirius red stain).

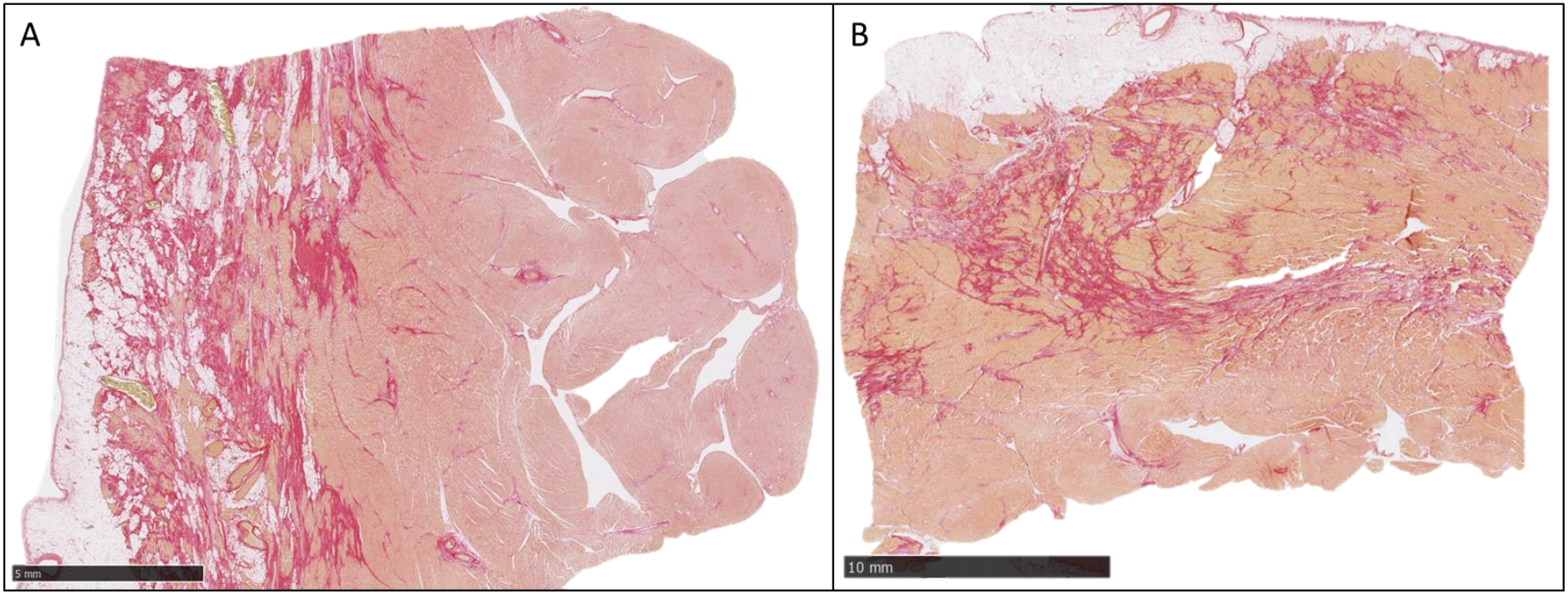


Figure 6.7. The posterior left ventricular wall shows varied involvement by collagen and fat. A) Replacement fibrosis admixed with fatty infiltration in the outer myocardium. B) Mainly fibrosis in the outer myocardium.

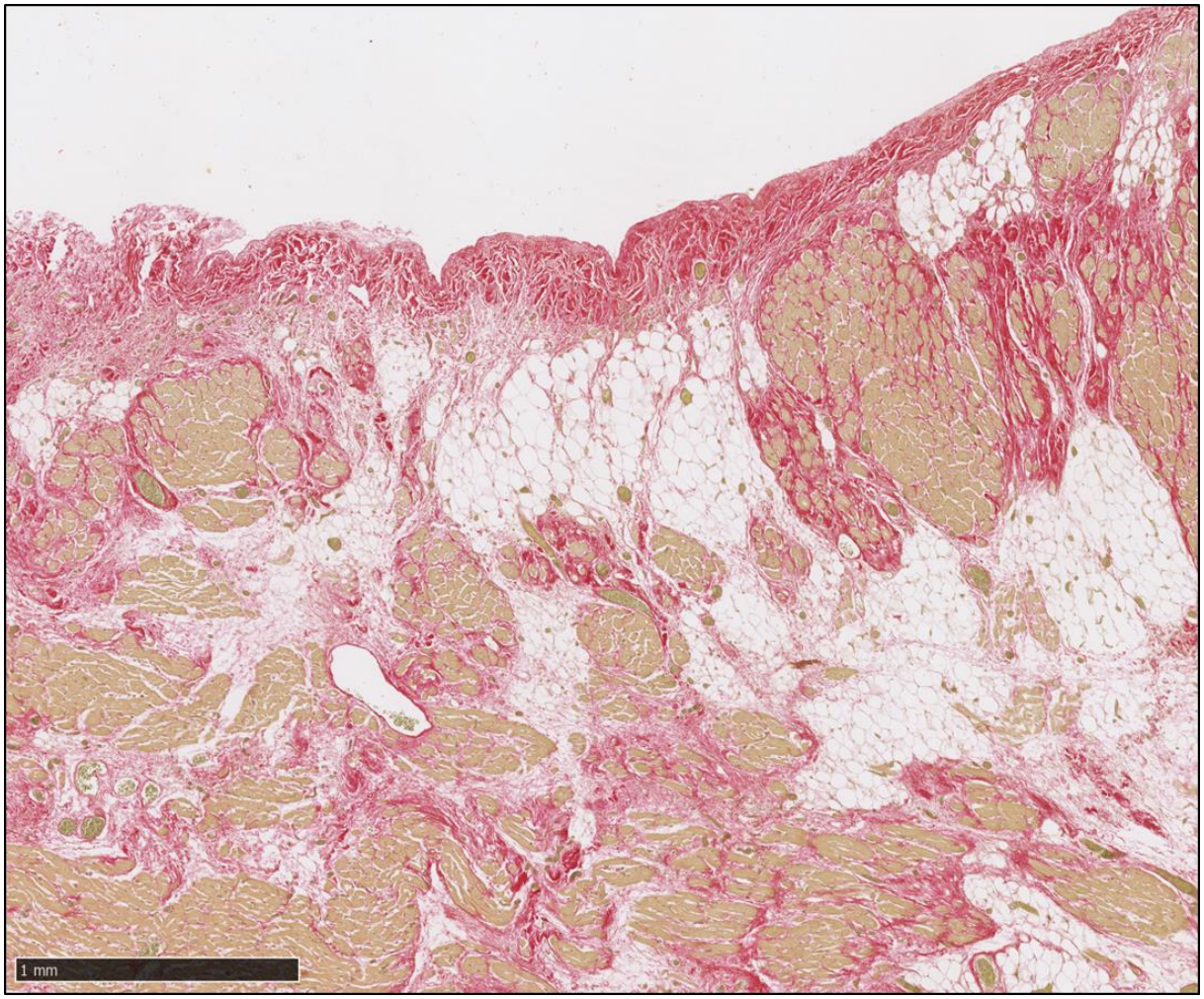


Figure 6.8. The epicardial collagen layer is thickened in diseased areas in arrhythmogenic cardiomyopathy. Note the collagen at the intersection with isolated bundles of myocytes.

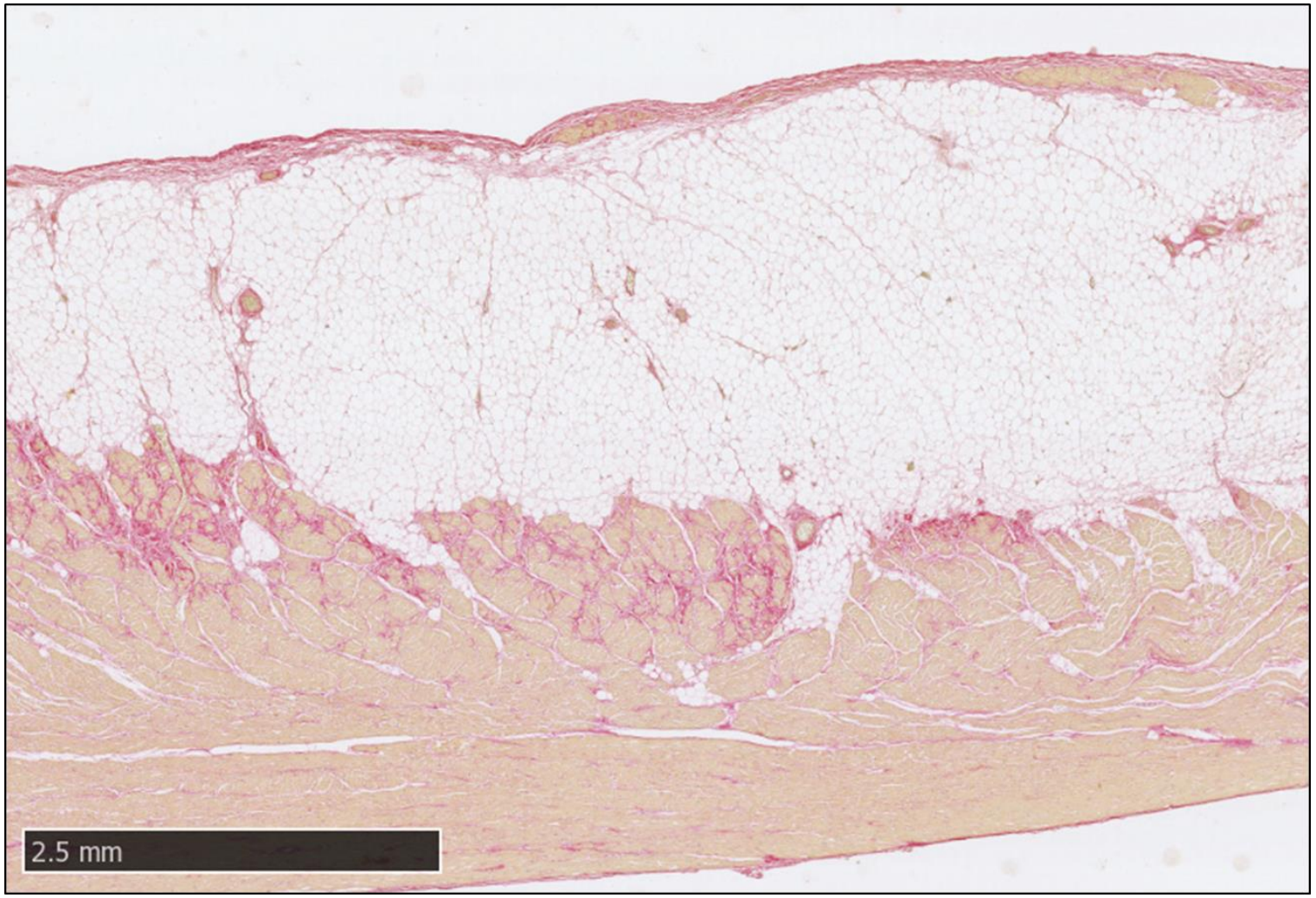


Figure 6.9. Area of transition between normal and fibrosis at intersection of the subepicardial fat and outer myocardium of the RV.

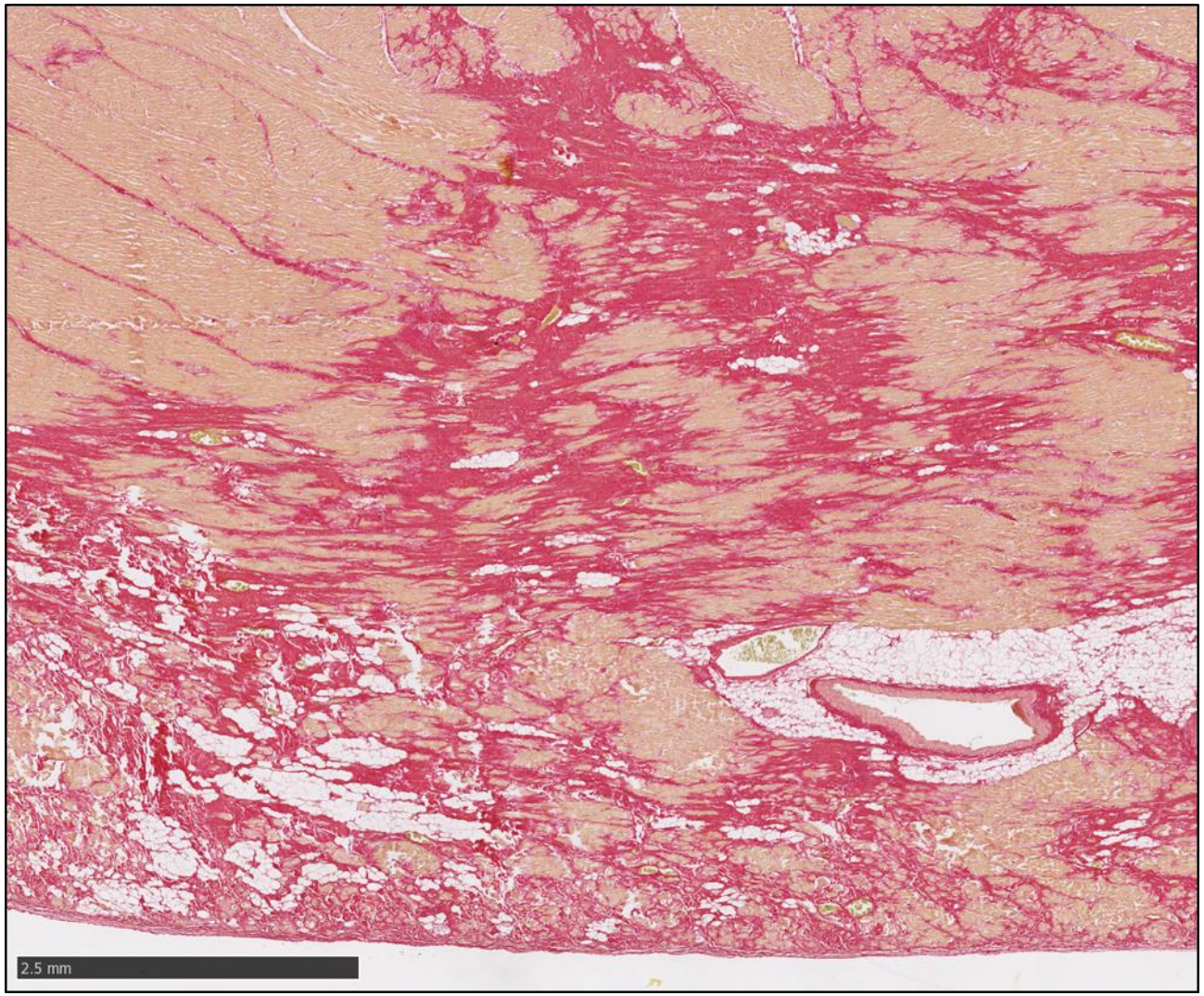


Figure 6.10. Fat and fibrosis in the outer myocardium in arrhythmogenic cardiomyopathy.

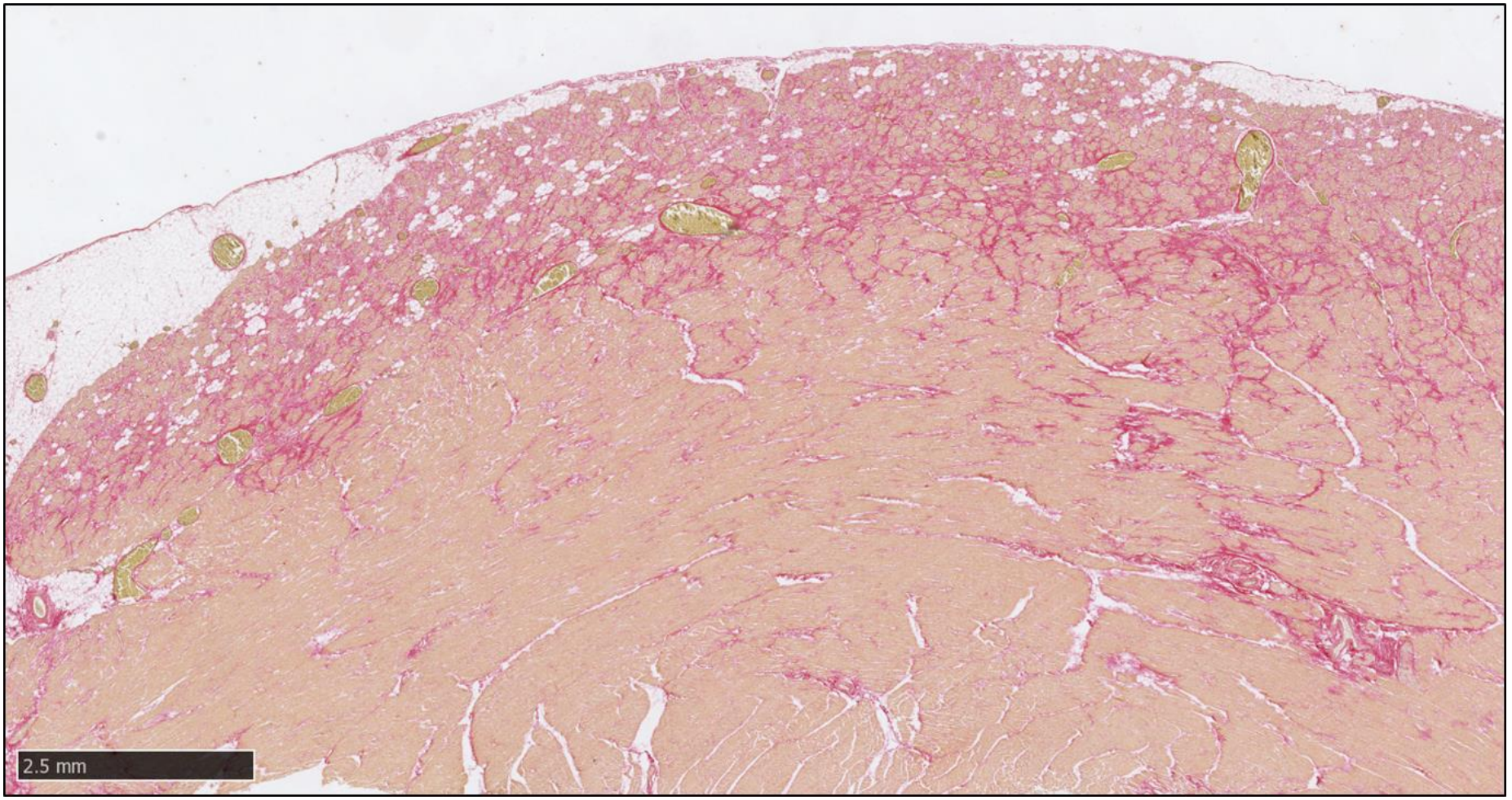


Figure 6.11. Fat and fibrosis are present in long continuous stretches in the outer myocardium in arrhythmogenic cardiomyopathy.

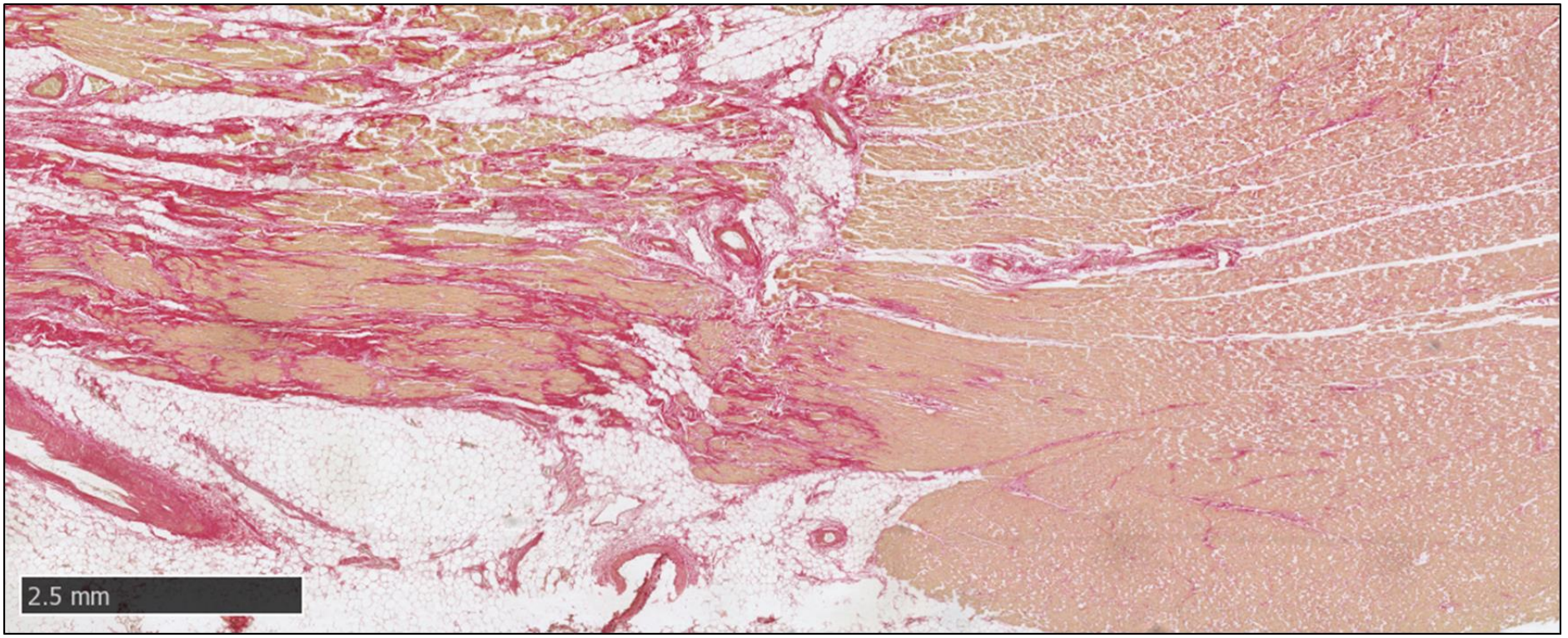


Figure 6.12. An abrupt transition between normal myocardium and fat and fibrosis present in the outer left ventricular myocardium.

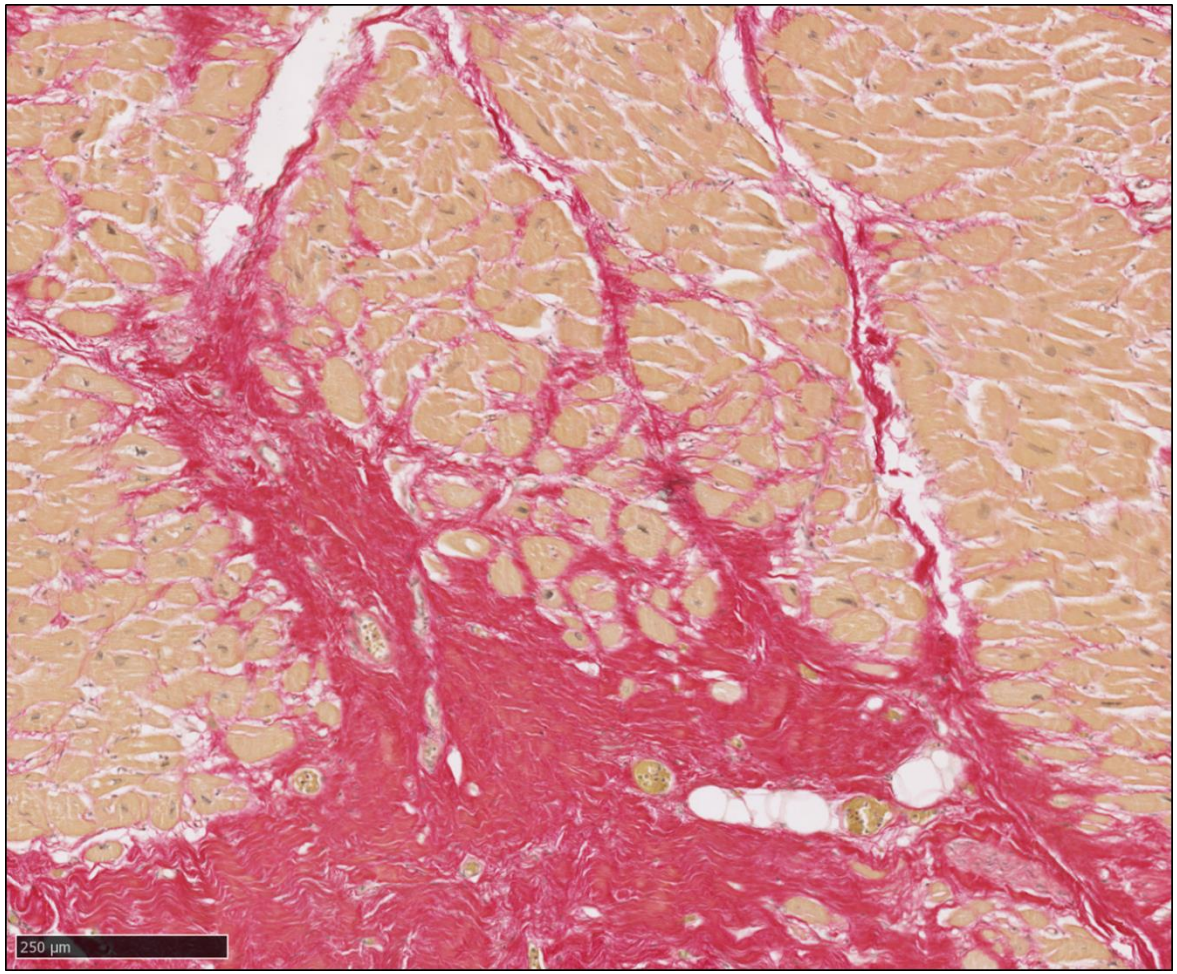


Figure 6.13. Interstitial fibrosis extends and interweaves between myocytes at the edge of patches of replacement fibrosis in arrhythmogenic cardiomyopathy.

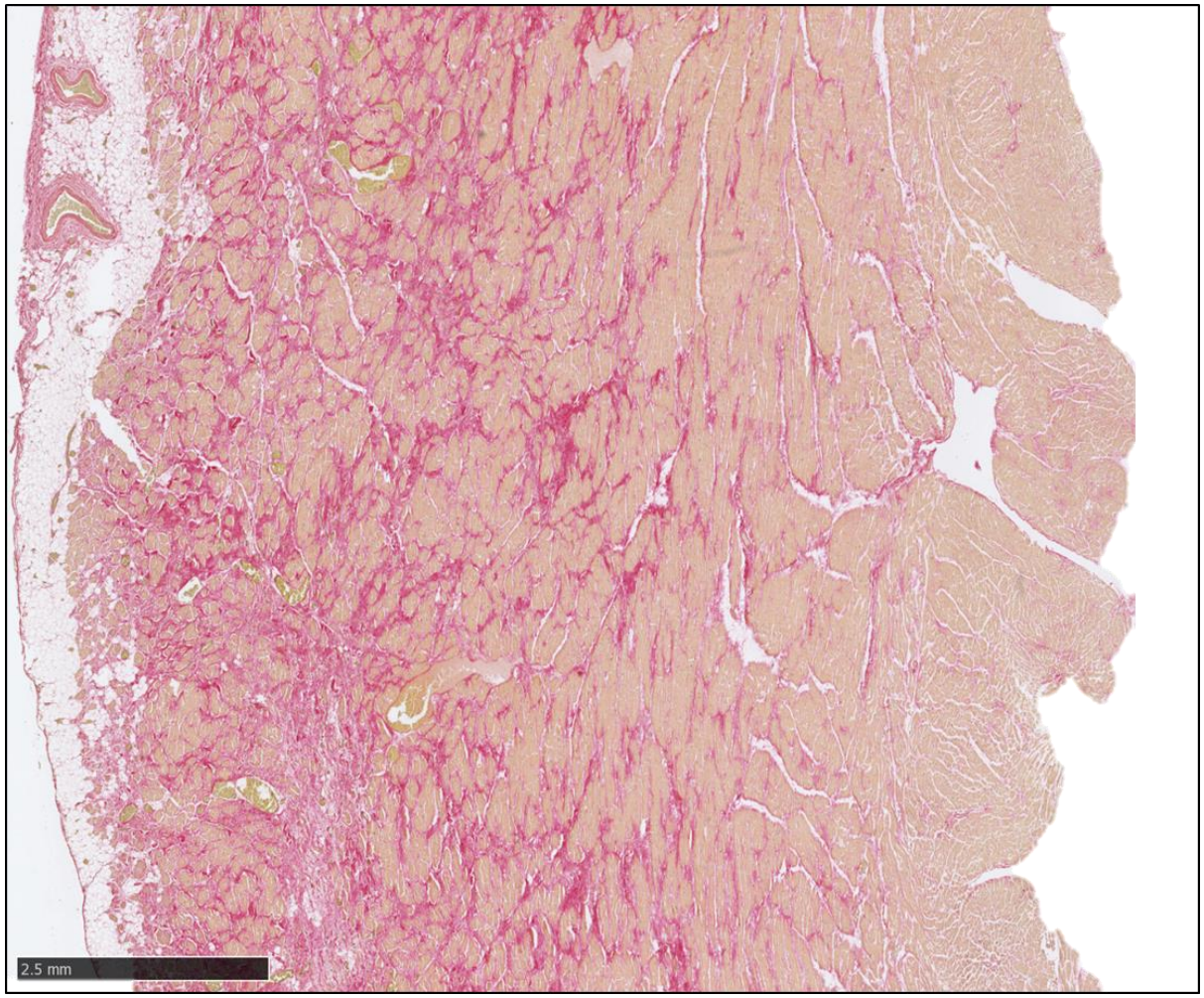


Figure 6.14. Interstitial fibrosis extends in networks through from the outer myocardium into the inner myocardium considerably further than the patchy replacement fibrosis.

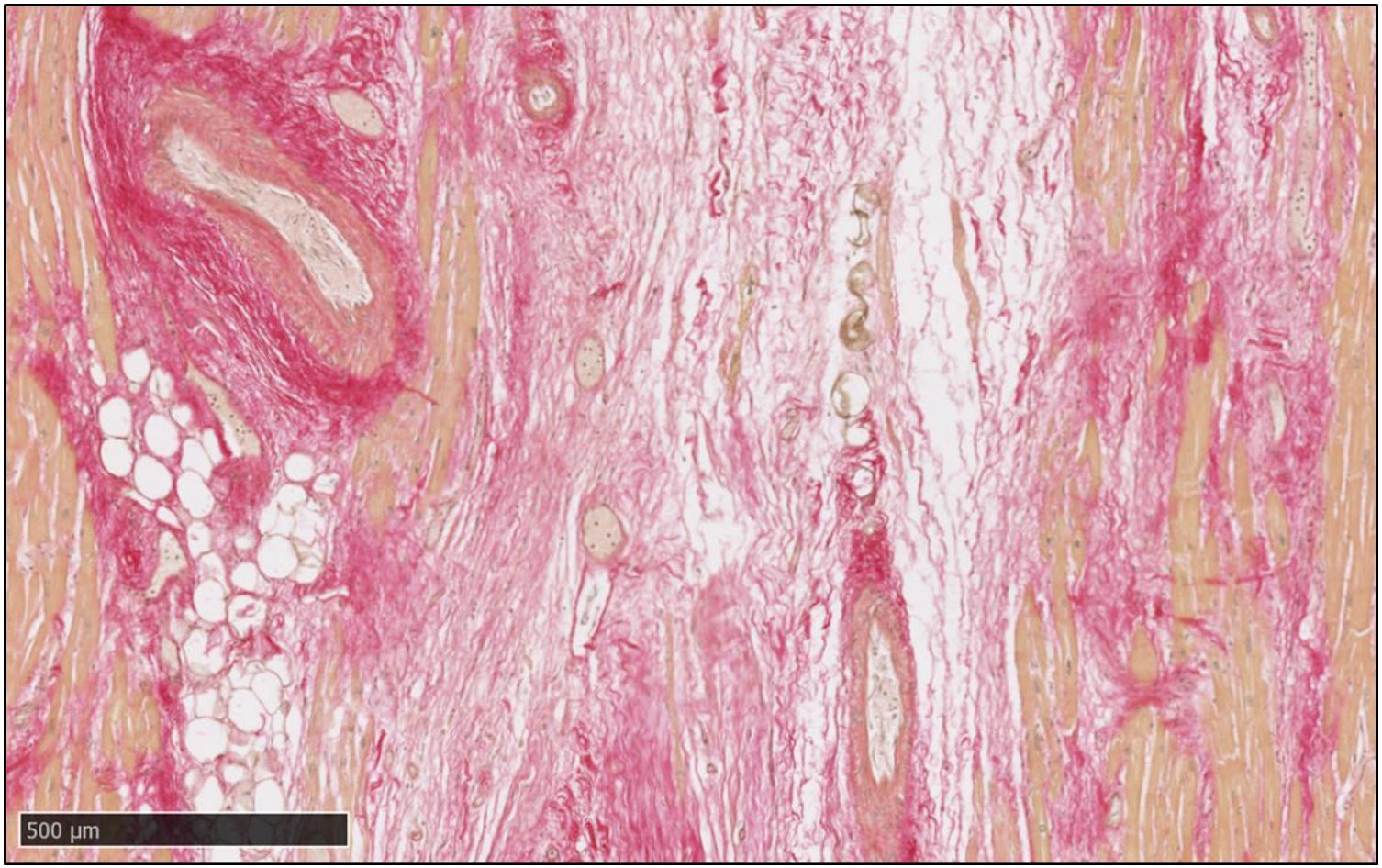


Figure 6.15. Empty spaces in a streak of fibrosis running through the midwall of the septum in arrhythmogenic cardiomyopathy.

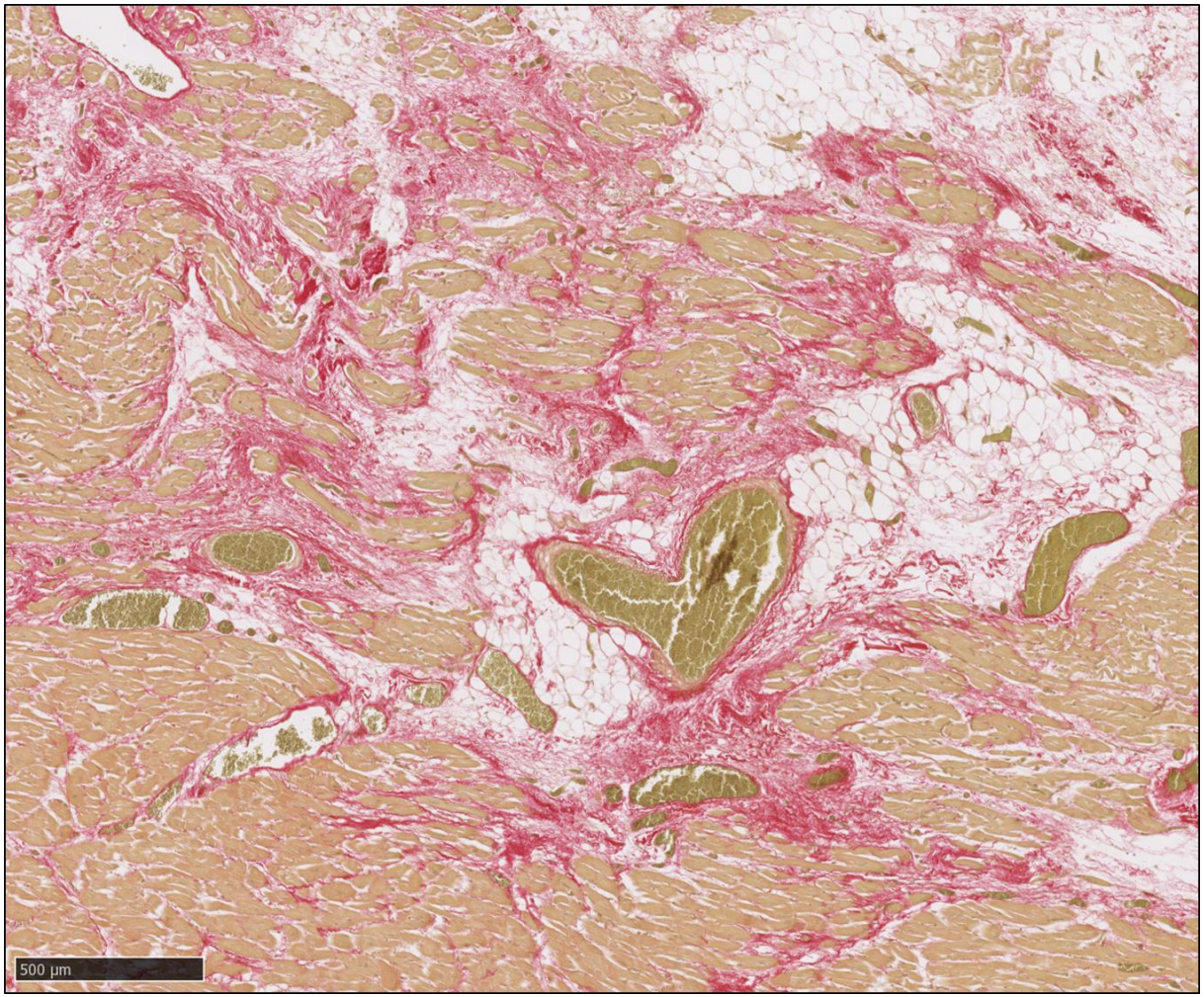


Figure 6.16. Fat and fibrosis around vessels in arrhythmogenic cardiomyopathy but it is not centred on vessels.

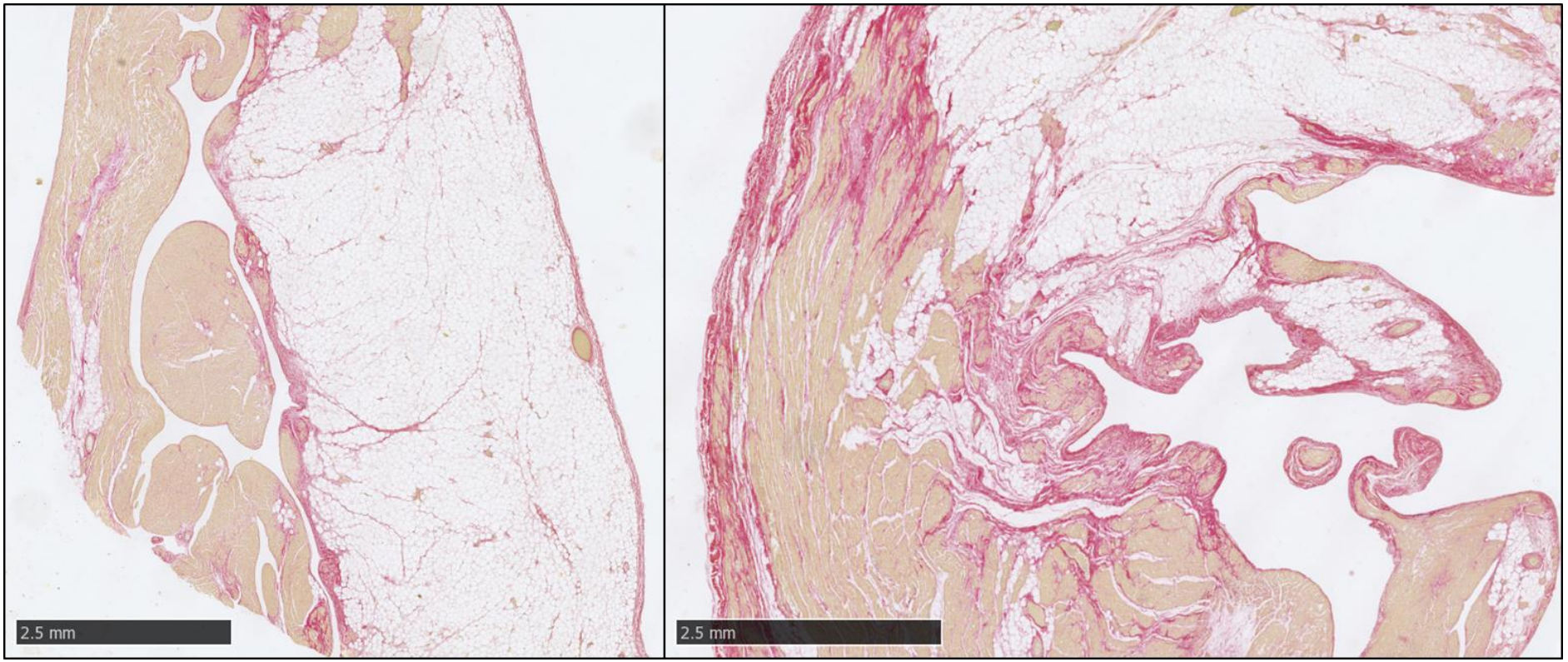


Figure 6.17. The right ventricle shows almost complete transmural fat replacement which can extend prominently into the trabeculae. There is great variation in fat and fibrosis in the RV.

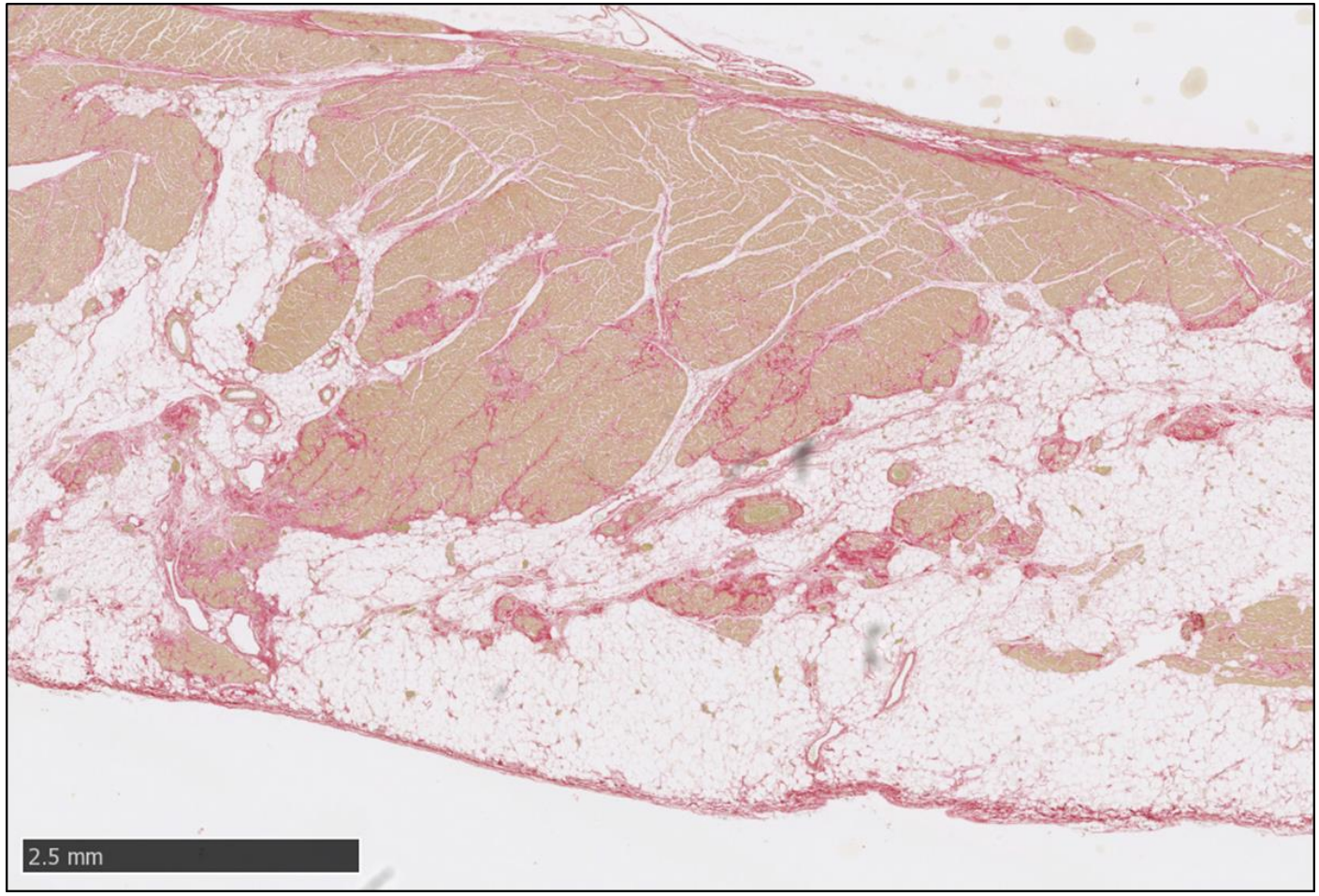


Figure 6.18. Residual islands of myocytes lie within adipose tissue surrounded by collagen.

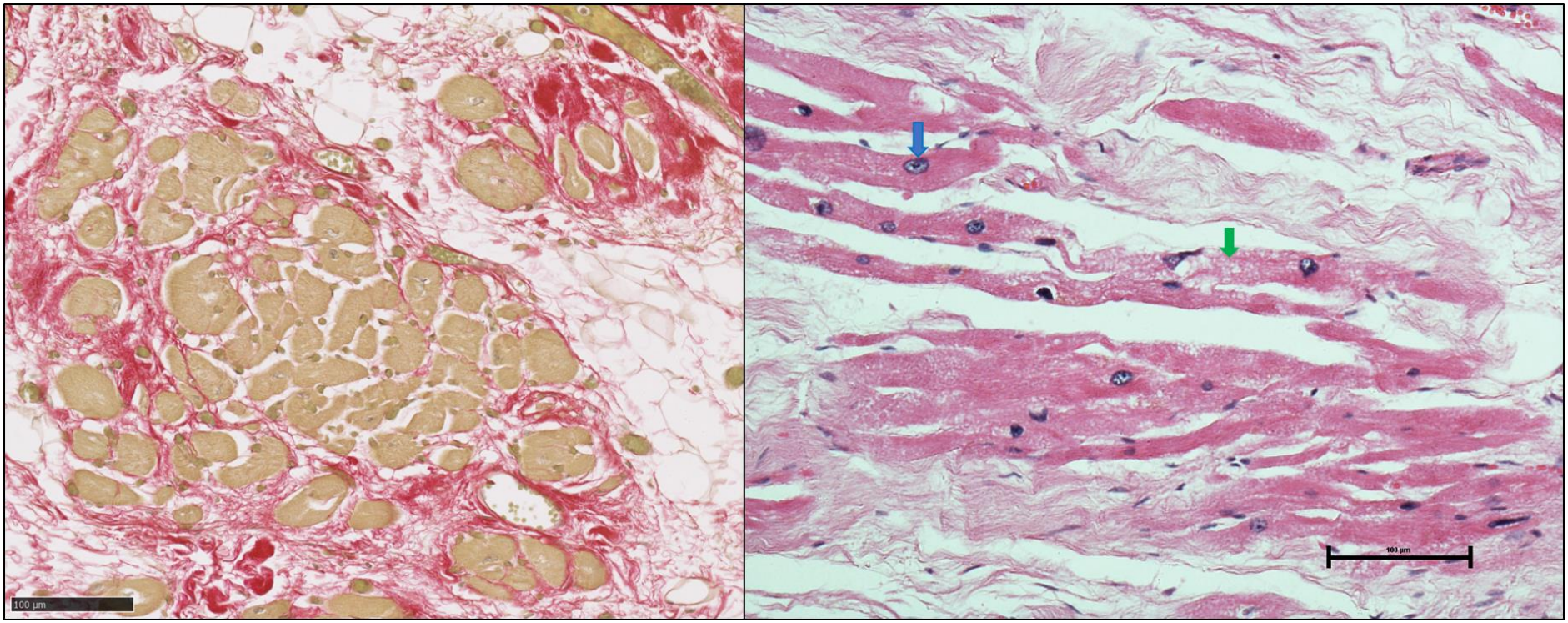


Figure 6.19. The myocytes in arrhythmogenic cardiomyopathy. The myocytes show hypertrophy particularly in areas of fibrosis and show variation in nuclear size, shape and staining (blue arrow). Degenerative features such as vacuolation (green arrow) and myofibrillar loss are present. (left – picrosirius red, right – haematoxylin and eosin).

Quantitative analysis

Collagen

ACM hearts show increased collagen with an overall average of 28% collagen compared to 11% in controls (ratio 2.7, 95%CI 1.3-5.3, p<0.01). The RVOT (ratio 2.8, 95%CI 1.3-5.8, p=0.01), RV (ratio 2.3, 95%CI 1.1-4.9, p= 0.03), IVS (ratio 2.6, 95%CI 1.2-5.6, p= 0.01), anterior LV (ratio 2.5, 95%CI 1.2-5.4, p= 0.01) and posterior LV (ratio 3.1, 95%CI 1.47-6.6, p<0.01) show increased collagen compared to controls (table 6.2).

Fat

There are no statistically significant increases in fat compared to controls when fat is assessed in proportion against collagen and myocytes. As with the normal heart, there are differences in the proportion of fat between regions with 14-15% in the RV, 7-8% in the LV and 3% in the IVS. When collagen is excluded from the proportional analysis and fat is assessed as a proportion compared to myocytes, the fat is increased in the posterior LV wall compared to controls (12% vs 4% ratio 2.6, 95%CI 1.3-5.6, p=0.01).

Myocytes

The proportion of myocytes is reduced in ACM compared to controls with 55% compared to 77% in controls (ratio 0.71, 95%CI 0.58-0.87, p<0.01). The RVOT (ratio 0.62, 95%CI 0.48-0.81, p=0.01), RV (ratio 0.65, 95%CI 0.50-0.85, p<0.01) and posterior LV (ratio 0.68, 95%CI 0.52-0.88, p<0.01) show a significant reduction in the proportion of myocytes compared to the normal heart.

The proportions for collagen, fat and myocytes in ACM and controls are shown in table 6.2 and figure 6.20.

Component	Condition	ACM		Control	
	Location	Expected	95% CI	Expected	95% CI
Collagen	All	**28.44**	**21.23-38.08**	**10.70**	**7.22-15.86**
	RVOT	**30.72**	**22.31-42.27**	**11.15**	**7.25-17.15**
	RV	**33.97**	**24.68-46.75**	**14.60**	**9.49-22.46**
	IVS	**22.01**	**15.99-30.29**	**8.39**	**5.45-12.90**
	ALV	**23.96**	**17.41-32.98**	**9.45**	**6.14-14.53**
	PLV	**33.81**	**24.56-46.53**	**10.87**	**7.06-16.71**
Fat	All	8.34	6.69-10.38	5.89	4.37-7.92
	RVOT	14.13	10.33-19.33	9.83	6.44-14.99
	RV	15.06	11.01-20.60	10.23	6.70-15.60
	IVS	3.13	2.29-4.28	2.43	1.59-3.70
	ALV	8.44	6.17-11.54	7.78	5.10-11.87
	PLV	7.16	5.23-9.79	3.72	2.43-5.67
Myocytes	All	**54.59**	**49.94-59.67**	**76.97**	**68.26-86.77**
	RVOT	**44.59**	**39.86-49.87**	**71.76**	**61.69-83.45**
	RV	**46.38**	**41.46-51.87**	**71.31**	**61.31-82.94**
	IVS	69.14	61.81-77.33	85.72	73.69-99.69
	ALV	62.32	55.71-69.70	76.65	65.90-89.15
	PLV	**54.41**	**48.64-60.86**	**80.33**	**69.06-93.42**

Table 6.3. Predicted proportions (geometric mean and confidence interval) of the ventricular myocardium made up by collagen, fat and myocytes for arrhythmogenic cardiomyopathy (ACM) compared to control cases. The proportions for collagen, fat and myocytes are given for the right ventricular outflow tract (RVOT), right ventricular free wall (RV), interventricular septum (IVS), anterior and posterior left ventricle (ALV and PLV).

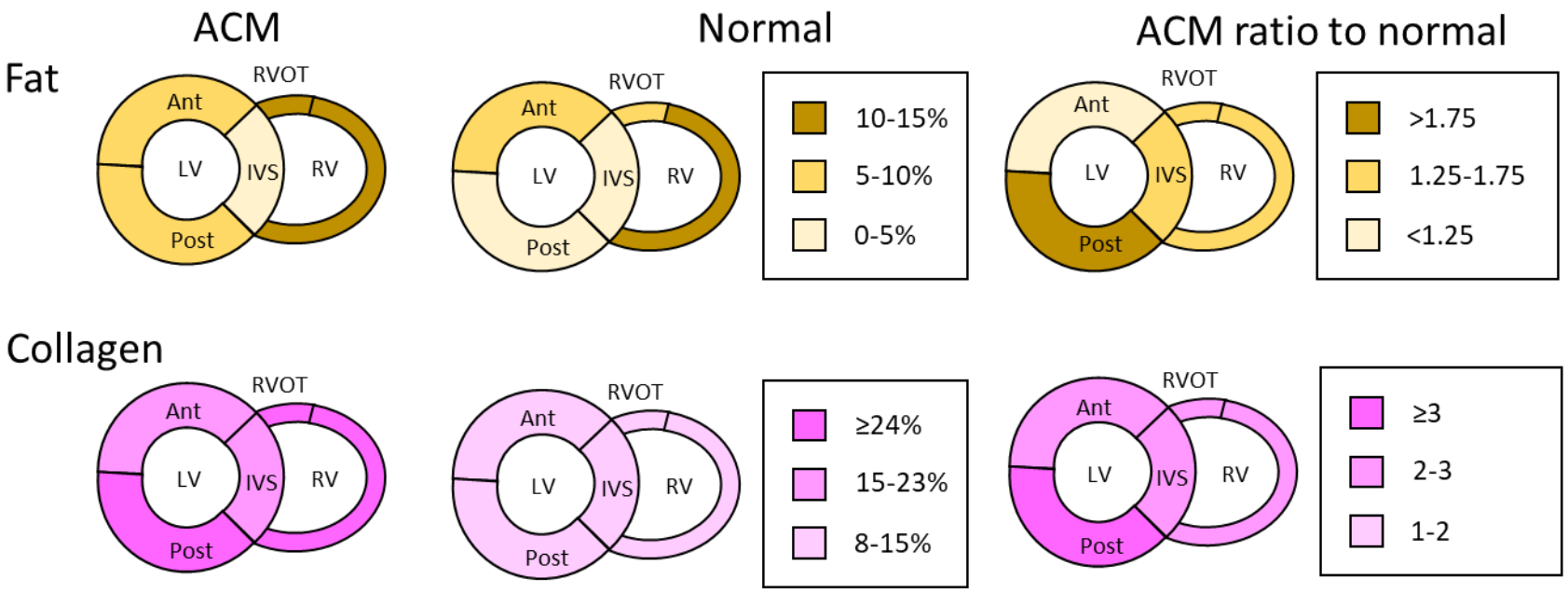


Figure 6.20. Percentage and ratio of fat and collagen in the arrhythmogenic cardiomyopathy (ACM) heart ventricular myocardium compared to normal. The values are given for the right ventricle (RV), right ventricular outflow tract (RVOT), interventricular septum (IVS), the anterior left ventricle (LV) and the posterior left ventricle. There are increases in collagen throughout the heart in arrhythmogenic cardiomyopathy with the posterior LV wall affected to the greatest degree. There was an increase in fat in the posterior LV wall.

Innervation of the ventricular myocardium and overlying subepicardial fat

General innervation

Within ACM, there is a similar distribution of nerves as within the normal heart (see figure 5.33). Within normal areas in the subepicardial fat, there are few large nerve bundles (figure 6.21 and 6.22). The large nerve bundles are associated with the coronary arteries and large vessels in the fat lying in and around the adventitia. They are also independent of the vessels between adipocytes within the subepicardial fat. There are few small nerve bundles within the epicardial fat. The large and small nerve bundles extend from the subepicardial fat into the myocardium and remain associated with blood vessels in the perivascular adipose tissue. Within the myocardium, nerve bundles are present transmurally. There are only occasional large nerve bundles and few small nerve bundles present in the myocardium (figure 6.21). Small nerve bundles are present throughout the myocardium but are most prominent in the inner myocardium. Individual fibrils extend between, parallel and adjoin with individual myocytes throughout the myocardium. There are few individual nerve fibrils in the myocardium. The individual nerve fibrils are most prominent in the inner myocardium. The fibrils are also present alongside and adjoining small vessels. They are also present on the endocardial surface.

Within areas of fibrosis in the outer myocardium, there are few large nerve bundles. Large nerve bundles are seen in the fat admixed with fibrosis. Small nerve bundles are occasionally present embedded in fibrosis but are more prominent within the fat. They are seen alongside residual myocytes. Within areas of fibrosis and fatty infiltration, the nerves still frequently lie adjacent to vessels. There are numerous granular staining individual nerve fibrils present within areas of collagen within the

myocardium (see figures 6.22 and 6.23). Individual nerve fibrils are not present within areas of fat infiltration.

Sympathetic innervation

TH showed a similar distribution to the normal heart away from areas of altered pathology, staining a percentage of fibres within the nerve bundles located within the epicardial fat. They are also always associated with vessels moving in from the epicardium to the myocardium (figure 6.25). There are few large nerve bundles in the myocardium. Large nerve bundles are more prominent in the outer myocardium. There are few small nerve bundles which are more prominent in the inner myocardium. Smaller individual nerve fibrils are most frequently present alongside and adjoining small vessels but also in association with myocytes. There are few individual nerve fibrils throughout the unaffected myocardium (figure 6.26). Fibrils are also present on the endocardial surface. Within areas of fibrosis and fat, TH stained many of the small individual nerve fibrils entering and within areas of replacement fibrosis. The fibrils are present in the replacement fibrosis without myocytes or vessels. In areas of fibrosis and fat infiltration, the outer myocardium had more individual nerve fibrils than the inner myocardium.

Parasympathetic innervation

CT showed a similar distribution to the normal heart away from areas of altered pathology. There is only occasional focal staining within fibres in the subepicardial fat. Smaller nerve bundles extend across the entire myocardium in association with vessels but also freely within the myocardium. Small individual nerve fibrils are more numerous than within the normal heart and showed a similar granular staining

pattern (figure 6.26 and 6.27). The fibrils are present throughout the myocardium but most prominently in the inner myocardium. The individual nerve fibrils are intricately associated with and adjoin and lie on the surface of myocytes. To a lesser degree, they are also closely associated with and adjoin small vessels. The fibrils are also present in the endocardium.

Within areas of fat and fibrosis, small nerve bundles are seen at a similar frequency to the normal myocardium. They are present in the fat alongside vessels and in areas of fibrosis. The individual nerve fibrils are present at similar frequency to within the normal myocardium lying within areas of replacement fibrosis. Within areas of replacement fibrosis, there are similar numbers of TH and CT staining individual nerve fibrils. The individual nerve fibrils also lie alongside residual myocytes within replacement fibrosis.

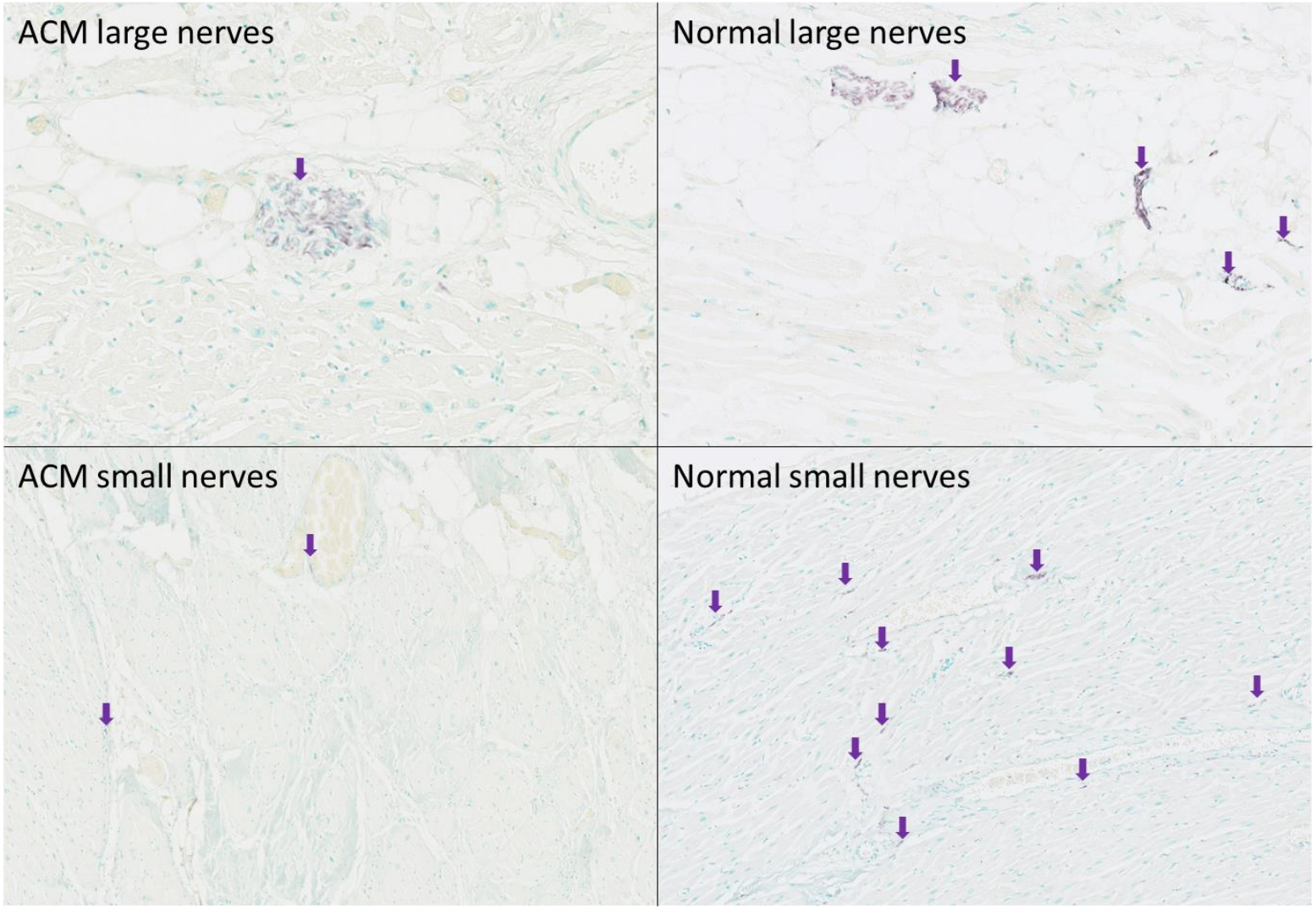


Figure 6.21. Few PGP9.5 stained (purple arrows) large and small nerve bundles in arrhythmogenic cardiomyopathy cases.

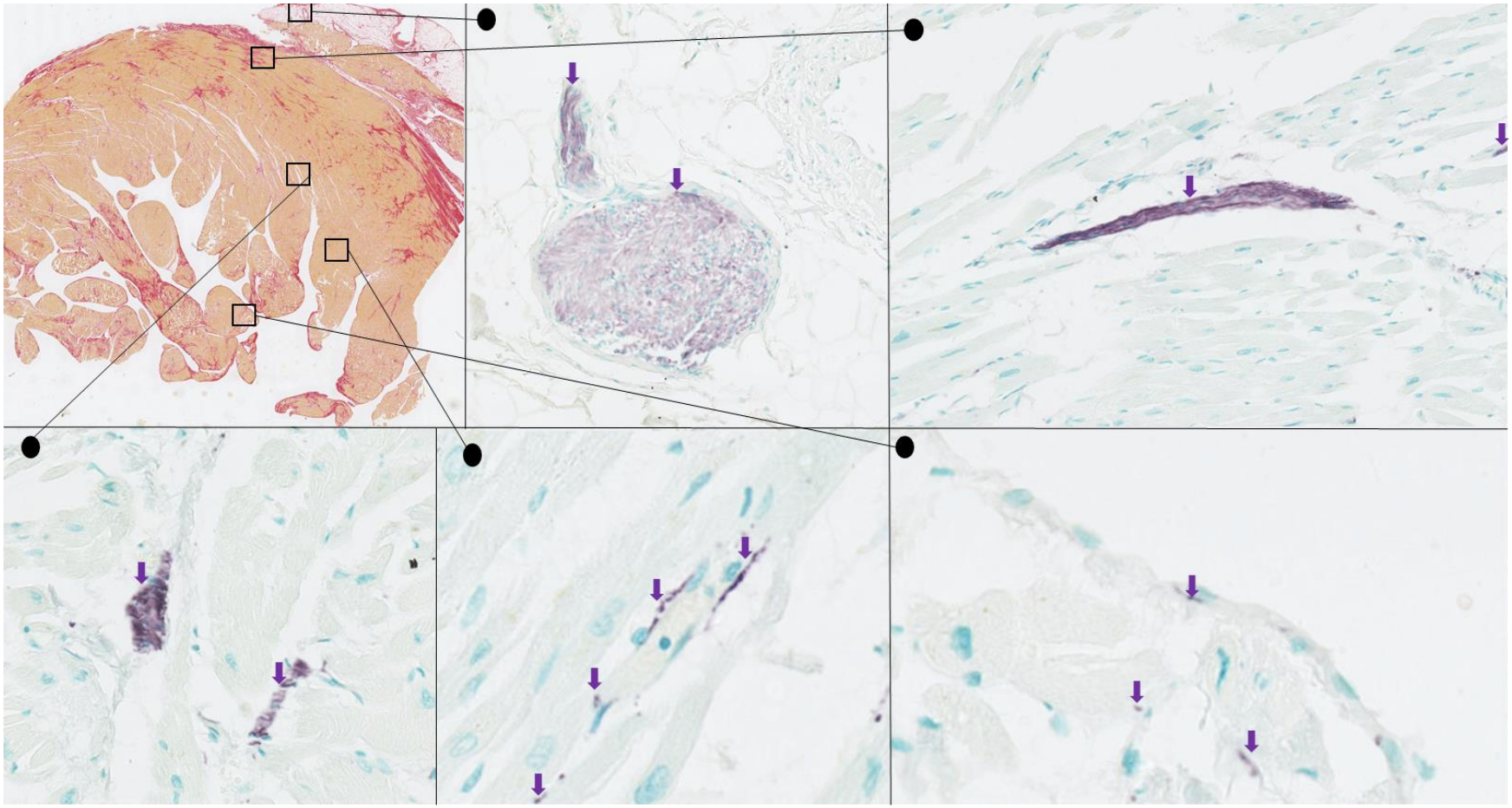


Figure 6.22. Nerve distribution (arrows) in an anterior left ventricle of an individual with arrhythmogenic cardiomyopathy showing epicardial fibrous infiltration. PGP9.5 stained nerve large and small nerve bundles as well as individual nerve fibrils are in a similar distribution to control hearts (left top - picrosirius red stain, other images – PGP9.5 stain).

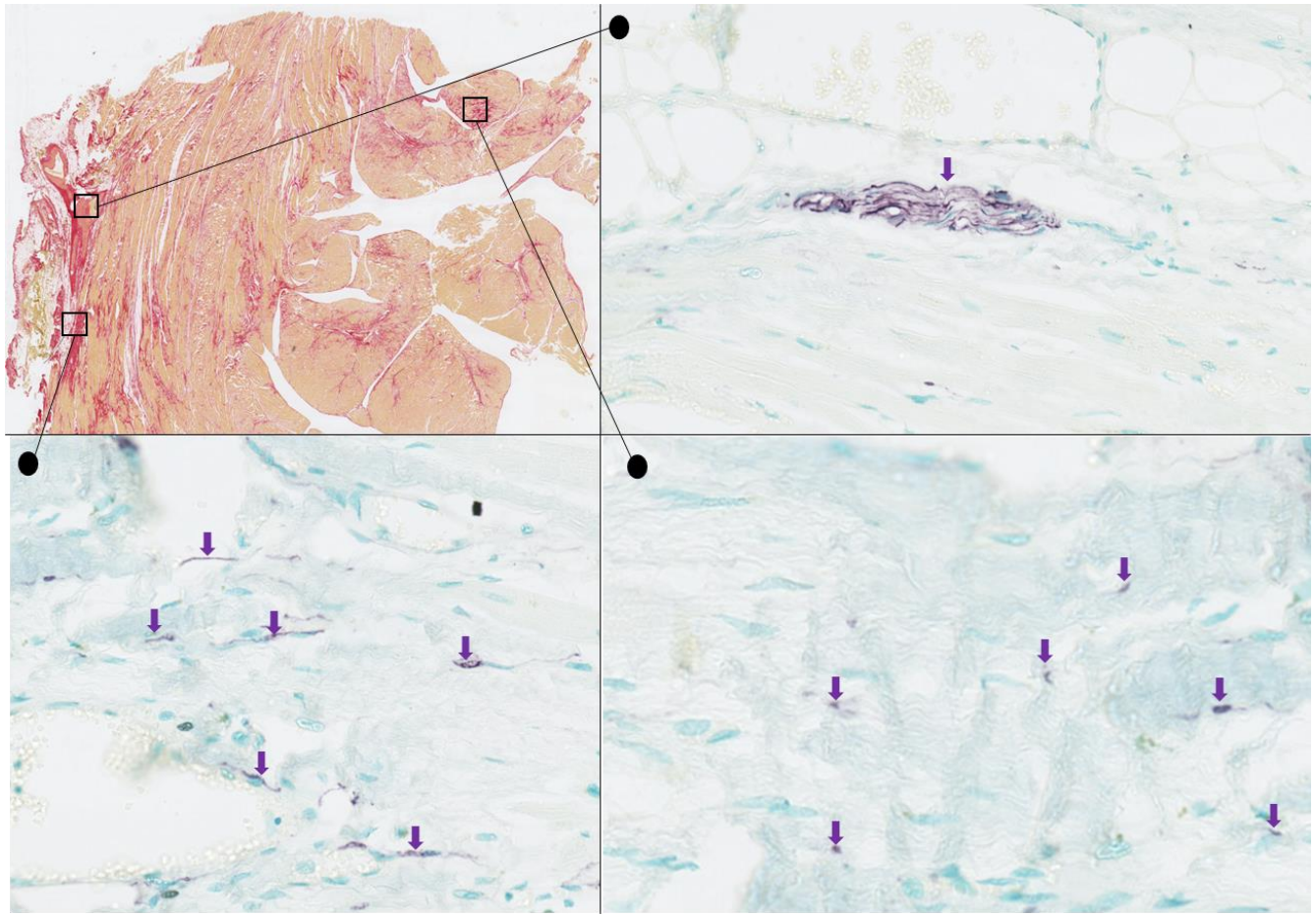


Figure 6.23. Nerve distribution (arrows) in a posterior left ventricle of an individual with arrhythmogenic cardiomyopathy showing epicardial fibrofatty infiltration. PGP9.5 stained large bundles are present in fatty infiltration with few in areas of fibrosis. Individual nerve fibrils are seen within areas of replacement fibrosis (top left - picrosirius red stain, others – PGP9.5 stain).

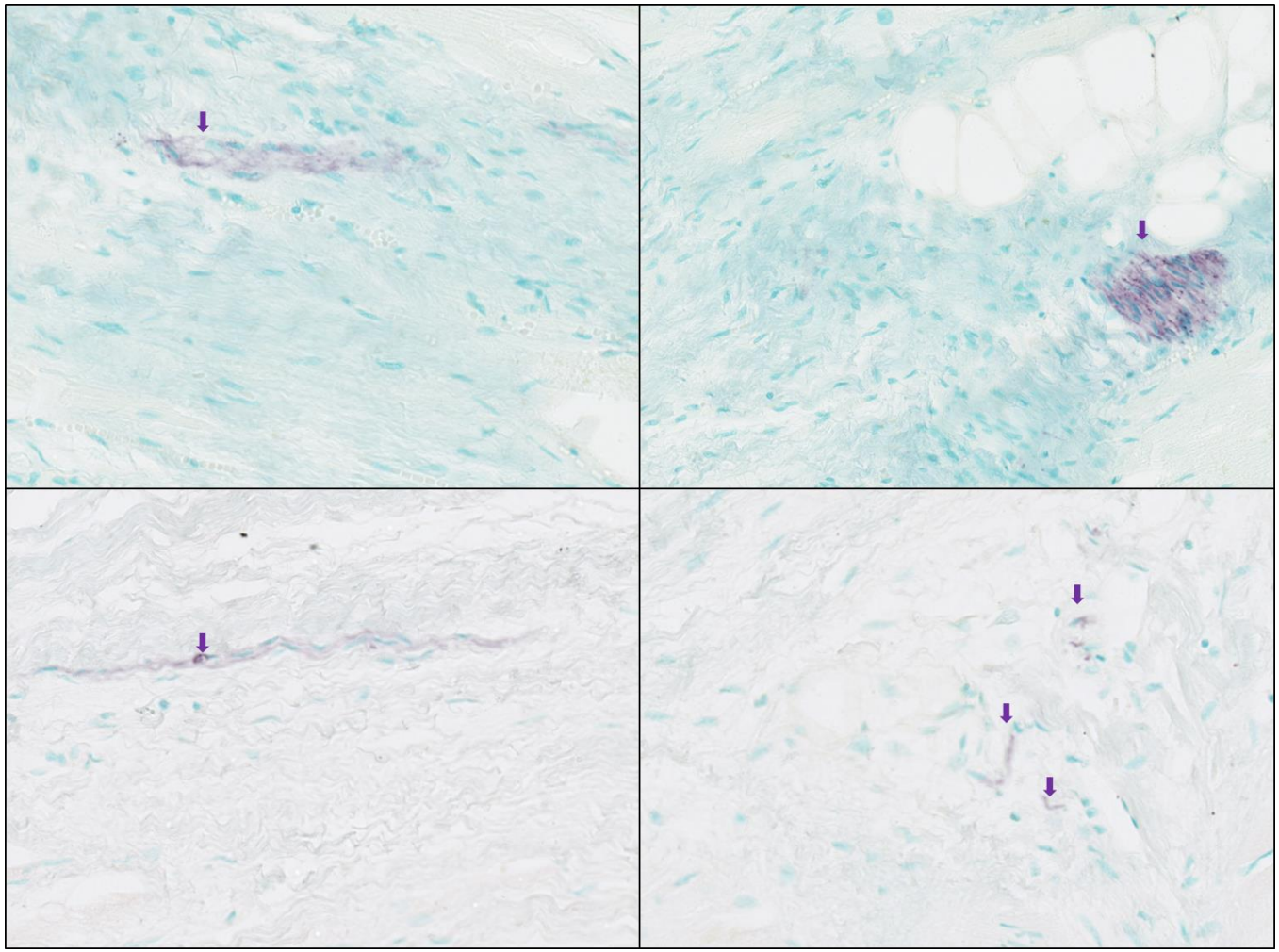


Figure 6.24. PGP9.5 stained (purple arrows) few large and small nerve bundles in replacement fibrosis. Fibrils were present in replacement fibrosis.

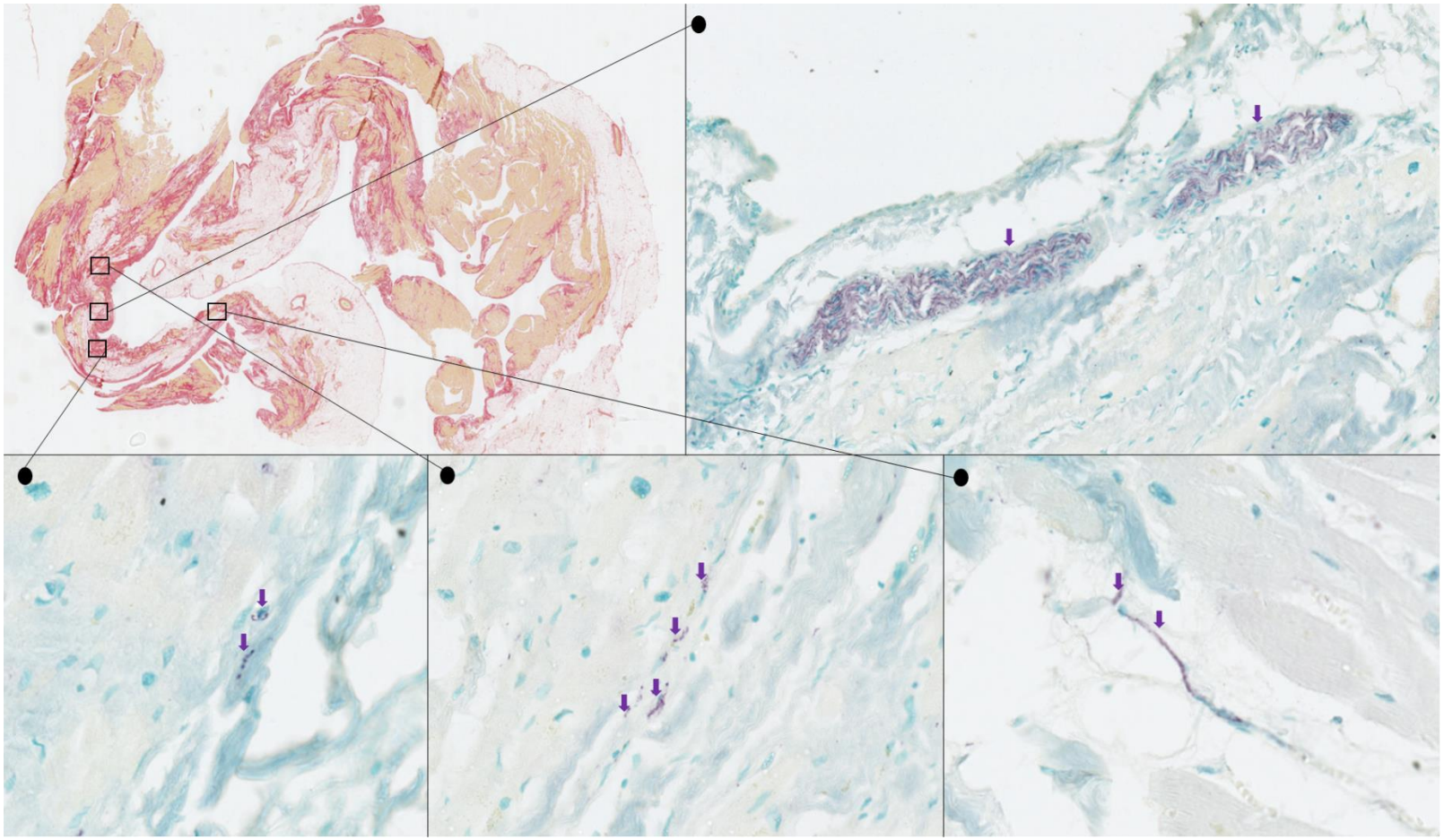


Figure 6.25. Sympathetic innervation (arrows) is decreased in arrhythmogenic cardiomyopathy. Tyrosine hydroxylase stained nerves showed a similar distribution to normal and PGP9.5 but are less frequent. Large and small nerve bundles as well as fibrils are seen in areas of fibrofatty infiltration (left top - picrosirius red stain, others – tyrosine hydroxylase stain).

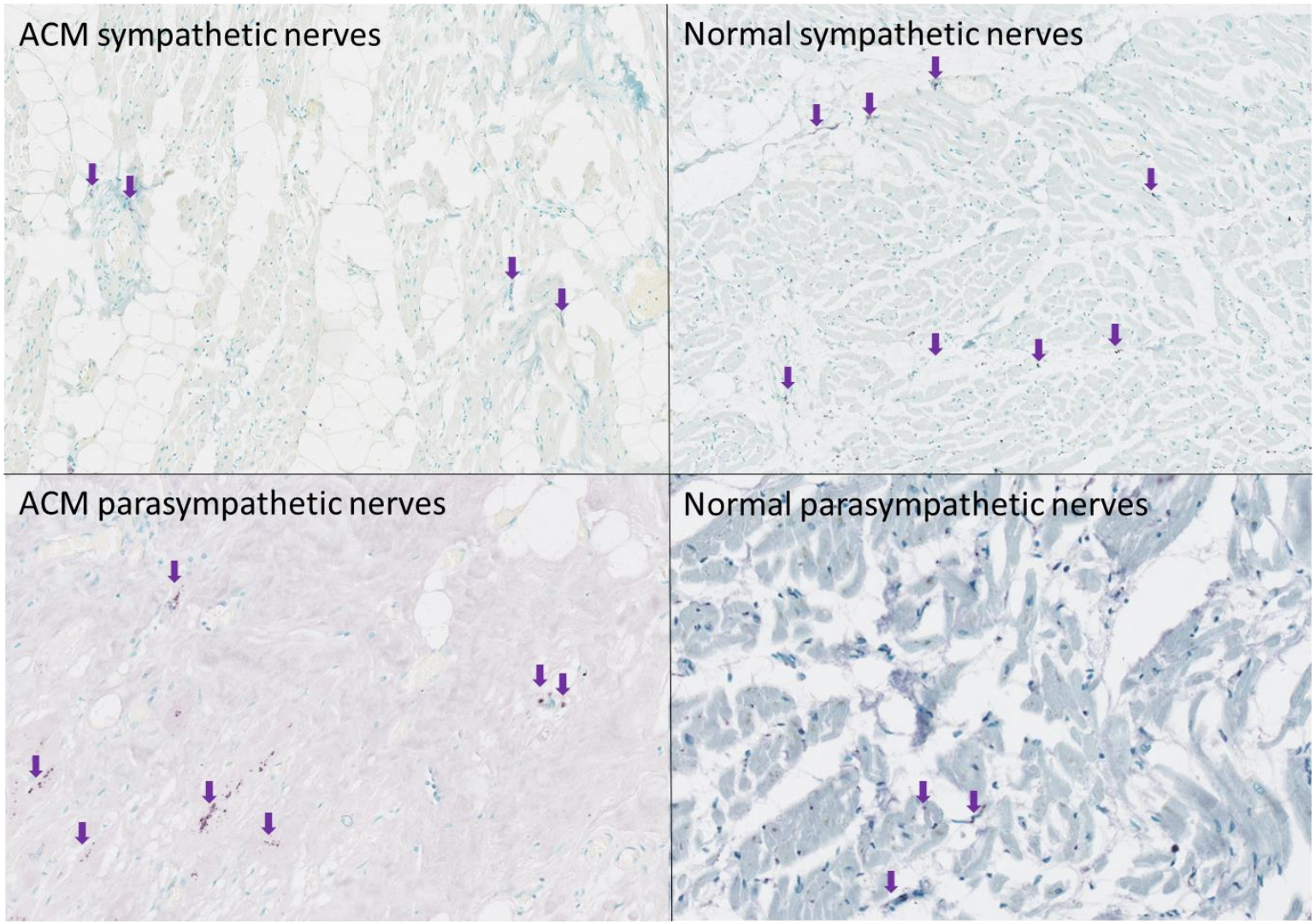


Figure 6.26. Few TH stained small bundles and fibrils in ACM. Frequent CT stained nerve fibrils in fibrosis in ACM.

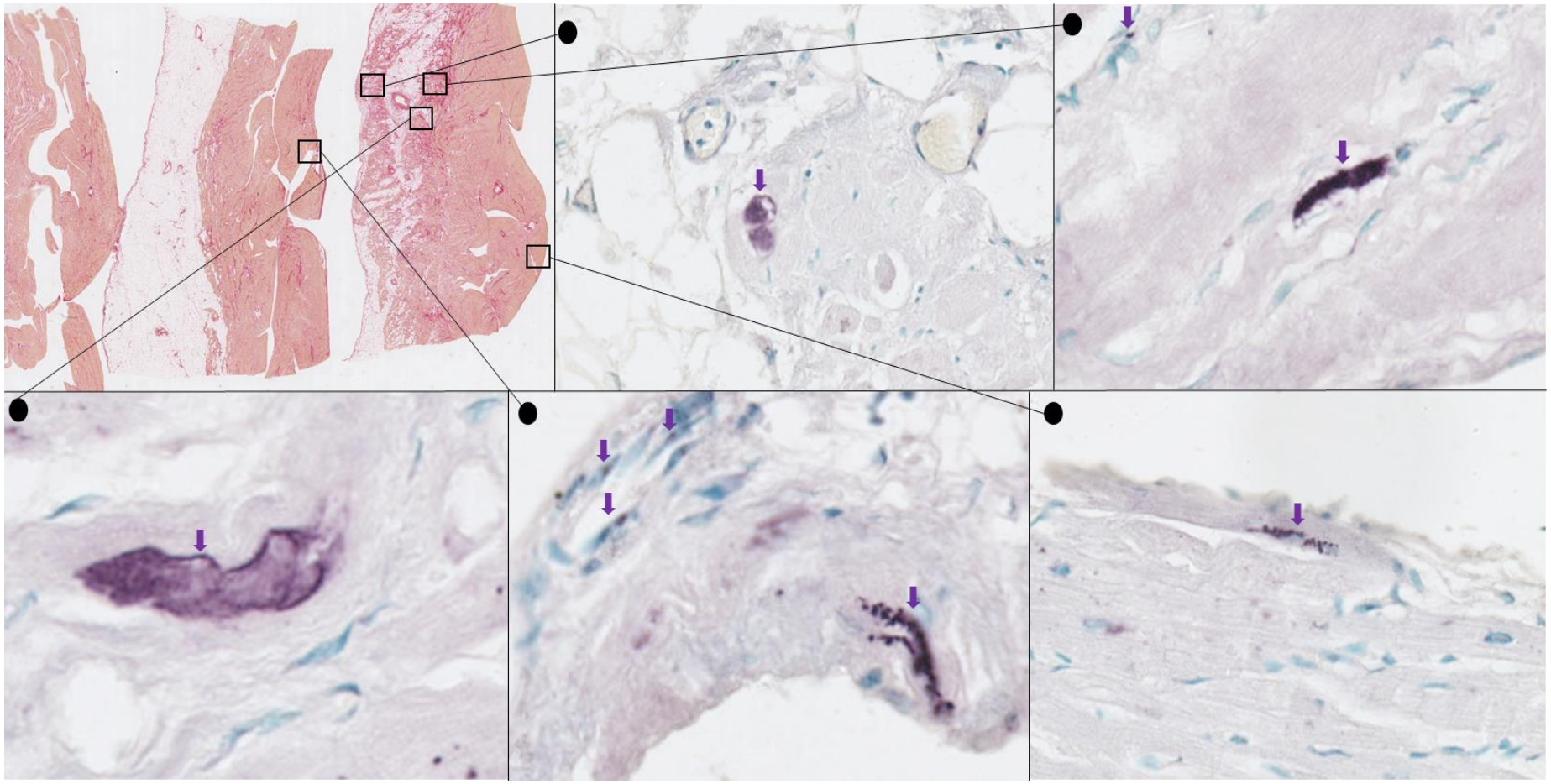


Figure 6.27. Parasympathetic innervation (arrows) in arrhythmogenic cardiomyopathy. CT staining nerves are frequent in arrhythmogenic cardiomyopathy. Nerve bundles are seen in areas of replacement fibrosis. Fibrils are most prominent in the inner myocardium and are present in areas of replacement fibrosis (top left - picrosirius red stain, others – CT stain).

Quantitative analysis of all sections

There are no statistically significant differences between ACM and control hearts when the whole heart is examined.

General innervation

The average PGP9.5 staining is 0.01% in ACM compared to 0.04% in normal hearts. The RVOT, RV and anterior LV show 0.02%, and the IVS and posterior LV show 0.01%.

Sympathetic innervation

TH staining does not show statistically significant changes overall or by region. The RV showed 0.04%, the IVS and anterior LV showed 0.03%, and the RVOT and posterior LV showed 0.02%.

Parasympathetic innervation

CT staining does not show statistically significant changes overall or by region. The CT stained 0.05% of the RV and anterior LV, 0.4% of the RVOT and posterior LV and 0.3% of the IVS.

The proportions of staining by the general nerve marker PGP9.5, the sympathetic nerve marker TH and the parasympathetic nerve marker CT are shown in table 6.3 and figure 6.28.

Stain	Condition	ACM		Control	
	Region	Mean	95% CI	Mean	95% CI
PGP9.5 % of tissue area	All	0.013	0.008-0.021	0.036	0.018-0.069
	RVOT	0.018	0.010-0.032	0.061	0.027-0.134
	RV	0.015	0.008-0.026	0.057	0.026-0.126
	IVS	0.012	0.006-0.021	0.027	0.012-0.058
	ALV	0.016	0.008-0.028	0.032	0.014-0.069
	PLV	0.008	0.004-0.014	0.020	0.008-0.043
TH % of tissue area	All	0.027	0.016-0.045	0.035	0.017-0.069
	RVOT	0.022	0.011-0.042	0.037	0.015-0.090
	RV	0.037	0.019-0.071	0.062	0.025-0.151
	IVS	0.030	0.015-0.059	0.031	0.012-0.075
	ALV	0.032	0.016-0.062	0.031	0.012-0.074
	PLV	0.019	0.009-0.036	0.025	0.010-0.060
CT % of tissue area	All	0.041	0.019-0.085	0.022	0.008-0.057
	RVOT	0.037	0.016-0.084	0.014	0.004-0.043
	RV	0.049	0.021-0.113	0.027	0.008-0.083
	IVS	0.033	0.014-0.075	0.024	0.007-0.072
	ALV	0.050	0.021-0.115	0.020	0.006-0.060
	PLV	0.038	0.016-0.088	0.026	0.008-0.078

Table 6.4. Predicted proportions (geometric mean and confidence interval) of the ventricular myocardium stained by PGP9.5, TH and CT for arrhythmogenic cardiomyopathy (ACM) and normal control hearts. The proportions are given for the right ventricular outflow tract (RVOT), right ventricular free wall (RV), interventricular septum (IVS), anterior and posterior left ventricle (ALV and PLV).

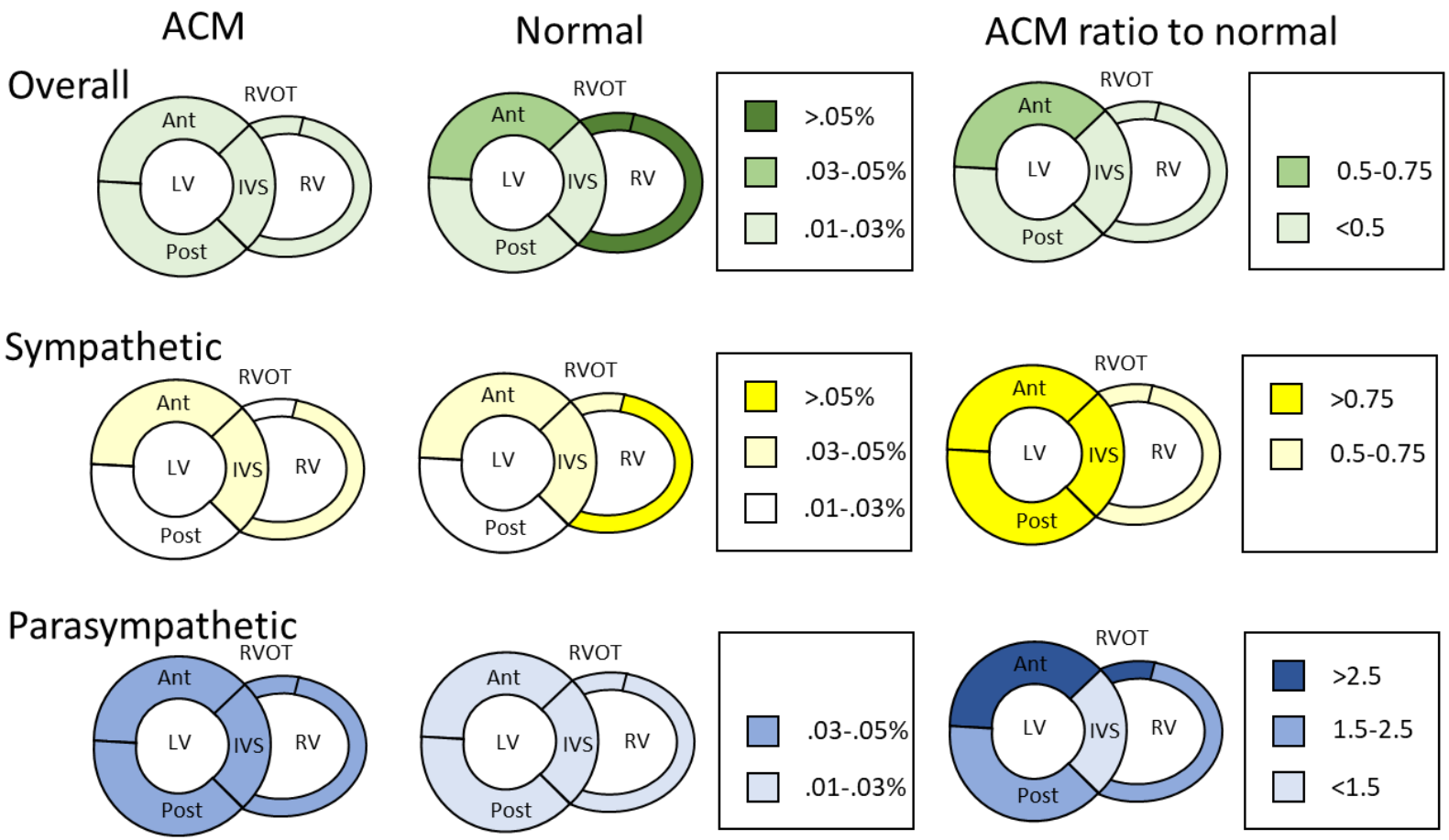


Figure 6.28. Percentage and ratio of overall, sympathetic and parasympathetic innervation in ACM heart ventricular myocardium compared to normal. There was a trend towards a reduction in general innervation.

Diseased area quantification

A subcohort of sections showing a proportion of collagen greater than two standard deviations from the mean of the normal heart (≥28%) are selected and compared to normal hearts. This is present in the RVOT in 12 cases, the RV in 13 cases, the IVS in 6 cases, the anterior LV in 10 cases and the posterior LV in 14 cases.

General innervation

When comparing diseased ACM sections to normal hearts there is a significant decrease in PGP9.5 in the RV (ratio 0.23, 95%CI 0.06-0.97, p=0.04).

Sympathetic and parasympathetic innervation

When comparing diseased ACM sections to normal hearts there are no significant differences in TH or CT staining.

The proportions of the different innervation in diseased sections for ACM are shown in table 6.4.

Stain	Condition	ACM		Control	
	Region	Expected	95% CI	Expected	95% CI
PGP9.5	All	0.012	0.006-0.020	0.036	0.018-0.069
	RVOT	0.020	0.010-0.038	0.061	0.027-0.134
	RV	**0.013**	**0.006-0.025**	**0.057**	**0.026-0.126**
	IVS	0.009	0.004-0.021	0.027	0.012-0.058
	ALV	0.017	0.008-0.034	0.032	0.014-0.069
	PLV	0.006	0.003-0.011	0.020	0.008-0.043
TH	All	0.012	0.006-0.020	0.035	0.017-0.069
	RVOT	0.039	0.017-0.086	0.037	0.015-0.090
	RV	0.053	0.024-0.115	0.062	0.025-0.151
	IVS	0.027	0.009-0.074	0.031	0.012-0.075
	ALV	0.028	0.012-0.065	0.031	0.012-0.074
	PLV	0.016	0.007-0.033	0.025	0.010-0.060
CT	All	0.040	0.018-0.084	0.022	0.008-0.057
	RVOT	0.041	0.015-0.103	0.014	0.004-0.043
	RV	0.048	0.019-0.120	0.027	0.008-0.083
	IVS	0.041	0.013-0.129	0.024	0.007-0.072
	ALV	0.038	0.014-0.100	0.020	0.006-0.060
	PLV	0.033	0.013-0.082	0.026	0.008-0.078

Table 6.5. Predicted proportions (geometric mean and confidence interval) of the ventricular myocardium stained by PGP9.5, TH and CT for arrhythmogenic cardiomyopathy (ACM) diseased sections and normal control hearts. The proportions are given for the right ventricular outflow tract (RVOT), right ventricular free wall (RV), interventricular septum (IVS), anterior and posterior left ventricle (ALV and PLV).

Power calculation

Based on an alpha of 0.05 and a power of 0.8, we predict a sample size of 47 ACM and 47 normal hearts should be sufficient to detect a significant difference in overall innervation stained by PGP9.5 in ACM.

Discussion

This is the first pathological study to delineate innervation in ACM and the first to objectively autonomously quantify fat and fibrosis using picrosirius red in pathologically diagnosed ACM hearts.

Macroscopic findings in ACM

The ACM hearts weighed 429g and showed an increase of 65g in heart weight compared to controls. Heart weight has also been noted to be increased in previous pathology studies including one recently published (Basso *et al.*, 1996; Miles *et al.*, 2019). Basso et al, examined 30 ACM hearts finding heart weights ranging up to 600g however they included cases with solely fatty infiltration in the absence of fibrosis (Basso *et al.*, 1996). Our previous study of 202 ACM hearts, reported 27% of men and 23% of women had elevated heart weight (Miles *et al.*, 2019).

The macroscopic findings in the lateral RV of thicker fat and thinner muscle as well as isolated thickening of the posterior RV has also not been previously specifically identified. Localised muscular hypertrophy of the posterior RV starkly contrasts with the original theory of a “triangle of dysplasia” with fat and fibrosis causing dilation or aneurysm of the RVOT, RV apex and RV posterior wall most frequently in ACM (Marcus *et al.*, 1982). This localised hypertrophy may occur as a response to damage elsewhere in the RV akin to the regional compensatory hypertrophy that occurs following myocardial infarction elsewhere in the ventricle (Henderson, 1996). Compensatory hypertrophy of the myocytes around scarred areas in ACM has also been previously described and is commented upon within a European consensus paper on cardiac hypertrophy, further supporting this assertion (Basso *et al.*, 1996, 2021).

Our macroscopic findings emphasise that macroscopic changes in ACM are subtle and this highlights the importance of taking histology in cases of sudden death where the heart appears normal.

Fibrosis and fat in ACM

Fibrosis and fat are now recognised to occur in both ventricles in individuals with ACM (Miles *et al.*, 2019). There is fibrosis throughout the regions examined with fat only significantly increased in the posterior LV. The RV and RVOT show more involvement by fat than the LV but there is not a significant increase in fat compared to the normal heart. This is explained by the extent of fat that is present within the RV of the normal heart as well as the variation in the presence of admixed fat with the fibrosis. Originally labelled as right ventricular dysplasia, the RV is considered a site of predilection for ACM particularly for fatty infiltration (Marcus *et al.*, 1982) however it is now recognised that fatty infiltration alone is not diagnostic of ACM as it is also present in the normal heart (Tansey, Aly and Sheppard, 2005).

The greatest amount of fibrosis is present in the RVOT, RV and posterior LV. This partially agrees with a previous histological fibrosis quantification study. Masson's trichrome was used for analysis which marks less collagen than picrosirius red (Rich and Whittaker, 2005; Huang *et al.*, 2013). Colour deconvolution was used to assess 8 clinically diagnosed ACM hearts of which 7 were from individuals with desmosomal or phospholambin mutations. They demonstrated that the RV and the posterolateral LV wall were most affected in cases with these mutations (Sepehrkhouy *et al.*, 2017). Damage most marked in the posterior LV wall has also previously been observed in hypertensive heart disease. As opposed to ACM, the fibrosis is found in an inner myocardial distribution in hypertensive heart disease (Westaby *et al.*, 2021).

This may suggest a vulnerability of the posterior LV wall to damage. Furthermore, a rat model of pressure overload-induced hypertrophy has associated depressed angiogenesis and reduced capillary density with fibrogenesis within the posterior wall. They found collagen deposition and myocyte hypertrophy most pronounced in the posterolateral wall. Capillary density was reduced in the same regions (Xiao *et al.*, 2018).

In keeping with our findings of fibrosis located in an epicardial distribution, electrophysiological studies have found arrhythmia originates from the epicardium. Electrogram abnormalities are found in the epicardial area of individuals with ACM and ventricular tachycardia. Ventricular tachycardia can be controlled using mapping of epicardial substrate and ablation (Garcia *et al.*, 2009). Ablation aimed at the epicardium helps prevent future arrhythmia. Strategies including both the epicardium and the endocardium achieve higher levels of long-term freedom from arrhythmia than endocardial ablation alone in ACM patients (Bai *et al.*, 2011). Furthermore, VA is recognised to originate from the RV, RVOT and posterior LV wall in keeping with our findings of fibrosis within these regions (Corrado *et al.*, 1997).

The dramatic phenotypic variability in ACM serves to highlight the importance of adequate sampling of both the RV including the RVOT and the LV. In our laboratories, we have the ability to re-review the heart following microscopic examination and take further blocks if the diagnosis is in question.

<u>Comparison to histology study on innervation in ischaemic heart disease</u>

A previous study on ischaemic heart disease has described that nerves are present around areas of fibrosis. Vracko et al, used S100 immunohistochemistry to stain sections from 17 ischaemic hearts from individuals aged 36-89 (Vracko, Thorning

and Frederickson, 1991). They describe greater densities of nerves in areas of fibrosis than in adjacent myocardium. Nerves were seen to aggregate on the periphery of fibrosis with few or absent nerves in the centre of fibrosis. This contrasts with our findings in ACM where nerve fibrils were seen throughout areas of fibrosis and aggregation at the periphery of patches was not noted as a feature.

Correlation to imaging studies

In agreement with our findings of a reduction of innervation in diseased areas, sympathetic function has been observed to be reduced using imaging. Witcher et al, compared 8 ACM patients with 29 controls using positron emission tomography to identify the maximum binding capacity of a beta-receptor antagonist to examine post synaptic beta-adrenergic receptor density in the LV. They found a reduction in the density in ACM patients compared to controls (Wichter *et al.*, 2000). A further study, by the same group of 42 ACM patients compared to 10 controls used metaiodobenzylguanidine single photon emission computed tomography. They found abnormal tracer uptake in 25 of their ACM patients. Over a follow up of nearly 12 years, 22 of these went on to experience life threatening VA compared to only 6 with a normal tracer uptake. They associated impairment of sympathetic function with future recurrence of ventricular tachyarrhythmia independent of RV dysfunction (Paul *et al.*, 2011).

This correlates well with our trend towards reduced overall and sympathetic innervation in a sudden death cohort.

No imaging studies are found of the parasympathetic innervation.

Correlation to clinical and animal findings

The innervation changes may contribute to autonomic dysregulation. A study of the heart rate variability of 46 individuals with ACM using Holter monitoring compared them to 30 healthy subjects (Folino *et al.*, 2002). ACM patients showed reduced heart rate variability compared to controls. Eight of their ACM patients suffered sustained ventricular tachycardia but there was no difference in heart rate variability in these individuals compared to the rest of the ACM cohort. They interpreted this autonomic dysfunction as reflecting sympathetic dominance with a reduction in vagal activity. The overall loss in innervation in diseased areas may lead to a reduction in autonomic influence and this would be supported by the finding that heart rate variability is decreased in ACM. Contrastingly to these findings however, we found a trend towards a reduction in the sympathetic nerve area with a corresponding weak trend towards an increase in parasympathetic nerve area. This may suggest that ventricular structural innervation does not correlate with electrical activity assessed through Holter monitoring.

An animal study has linked arrhythmia with uneven sympathetic function in the myocardium. Han and Moe studied 30 dogs utilising electrodes attached to the heart at varying distances from a primary point of stimulation and stimulated the stellate ganglion. They found the degree of dispersion of the refractory period was increased by stimulation of the cardiac sympathetic nerves and decreased by administration of sympathomimetic amines. This dispersion was strongly correlated with a lower threshold to produce of ventricular fibrillation. They suggested this was a consequence of non-uniform distribution of adrenergic function in the myocardium (Han and Moe, 1964). This correlates well with our findings of reduced innervation most marked in the diseased RV suggesting that this patchy disease may cause uneven denervation.

Sympathetic neurotransmitters have found to be decreased with ACM. Biochemical analysis has been performed of 15 biopsies from ACM patients and compared to 5 control biopsies as well 10 from individuals with RVOT tachycardia. The only protein to show a decrease in ACM compared to controls was norepinephrine concentrations. This was also present at a higher level compared to individuals with RVOT tachycardia (Paul *et al.*, 2014). This further supports the occurrence of adrenergic dysfunction in ACM and would support our trend towards reduced sympathetic innervation.

Concluding remarks

This is the first pathological study to delineate innervation in ACM and the first to objectively autonomously quantify fat and fibrosis using picrosirius red in pathologically diagnosed ACM hearts.

Macroscopically, the heart weight is slightly increased with thicker fat and thinner muscle in the lateral RV wall and thicker muscle in the RV posterior wall. Microscopically, there are increases in collagen throughout the regions examined representing fibrosis. There are corresponding loses of the proportion of myocytes in the RVOT, RV and posterior LV. Fat is increased in posterior LV sections. Subtle macroscopic findings and dramatic phenotypic variability in microscopic findings highlight the importance of adequate cardiac histological sampling at autopsy. There is a trend towards a decrease in general innervation in ACM. There is a decrease in general innervation in RV sections exhibiting fibrosis in ACM. The innervation findings require further investigation to establish a potential role in arrhythmogenesis in ACM.

Summary of findings in ACM

Macroscopic

- Heart weight is greater
- Atria and ventricles are not dilated
- Lateral RV muscle wall is thinned
- Posterior RV muscle wall is thicker
- No differences in other RV muscle walls or LV muscle walls
- Lateral RV wall epicardial fat is thicker
- No differences in epicardial fat elsewhere

Microscopic findings in ACM ventricular subepicardial fat and myocardium

- Collagen is increased overall
- Myocytes are decreased overall
- Fat is increased in the posterior LV wall but not elsewhere
- There is a non-significant trend of reduction in general innervation
- There is a reduction in general innervation in the RV in sections with fibrosis
- There is no difference in sympathetic or parasympathetic innervation

CHAPTER 7 DILATED CARDIOMYOPATHY

Introduction

In chapter 5, we established the composition of the normal ventricular myocardium and its innervation. In this chapter, we examine whether there are differences in tissue composition and innervation in DCM compared to the normal heart.

DCM is a heart muscle disorder in which one or both the ventricular cavities enlarge, stretching and thinning the chamber walls, which is not explained by abnormal loading conditions or ischaemic damage (Pinto *et al.*, 2016). DCM has a prevalence of 1 in 2500 (Merlo *et al.*, 2018) and is regarded as a morphological consequence of an extensive list of causes (Bozkurt *et al.*, 2016; Japp *et al.*, 2016). Around 35% of cases are thought to be genetic with acquired causes including myocarditis, exposure to alcohol, drugs and toxins as well as metabolic and endocrine disturbances (Weintraub, Semsarian and Macdonald, 2017). As we have shown in chapter 3, it causes 4% SCD in our cohort but makes up a smaller proportion of cases when compared to HCM and ACM particularly within younger individuals (Kadish *et al.*, 2004; Fabre and Sheppard, 2006).

Methods

DCM decedents with suitable retained tissue are identified from our library of 931 retained cases (see figure 2.15). As stated in the methods, DCM is pathologically diagnosed on the basis of a dilated and/or thin walled LV and supported by an increase in heart weight, premortem diagnosis and histological evidence of fibrosis. Cases with coexisting conditions which may have contributed to death, valvular disease, hypertensive disease and significant coronary disease are excluded. Exactly as with the normal hearts, sections from the RVOT, the RV free wall

(including the anterior, lateral and posterior wall), the IVS, as well as the anterior and posterior LV free wall are stained with PSR, PGP9.5, TH and CT. Positive and negative controls are utilised. Slides are scanned using a Hamamatsu Nanozoomer 2.0RS. Digital image analysis is performed using applications developed within the Visiopharm program (Visiopharm A/S, Agern Alle 24, 2970 Hørsholm, Denmark).

Statistics

Differences between groups are assessed using log transformed values for collagen, fat, myocyte, PGP9.5, TH and CT proportions (as these values are skewed). A multilevel model is created to allow comparison of hierarchical dependent data based on myocardial location. Variables such as age, sex and ethnicity are incorporated into multivariable analysis. Predictions of collagen, fat, myocytes, PGP9.5, TH and CT are expressed as geometric means and 95% confidence intervals.

Statistical analyses used Stata version 16 (StataCorp, College Station, Texas, USA).

Results

Eleven cases of DCM meeting inclusion criteria with suitable retained tissue are identified. The age at death is 44±14years comprising 8 males and 3 females. The heart weight is 488±111g. The LV is dilated in 9 cases, the other two cases show wall thinning. Of the 9 cases with dilated LV, 5 also showing thin walls (figure 7.1). Of the 9 cases with dilated LV, 3 show RV dilation. Average diameter of the RV is 34±20mm and average diameter of the LV is 43±10mm. The minimal wall thickness for the LV is 9.6±0.9mm.

The DCM macroscopic measurements are compared to controls.

The dimensions of the atria, ventricle muscle wall thickness and diameters, valve circumferences and subepicardial fat measurements are provided in table 7.1 and compared to controls.

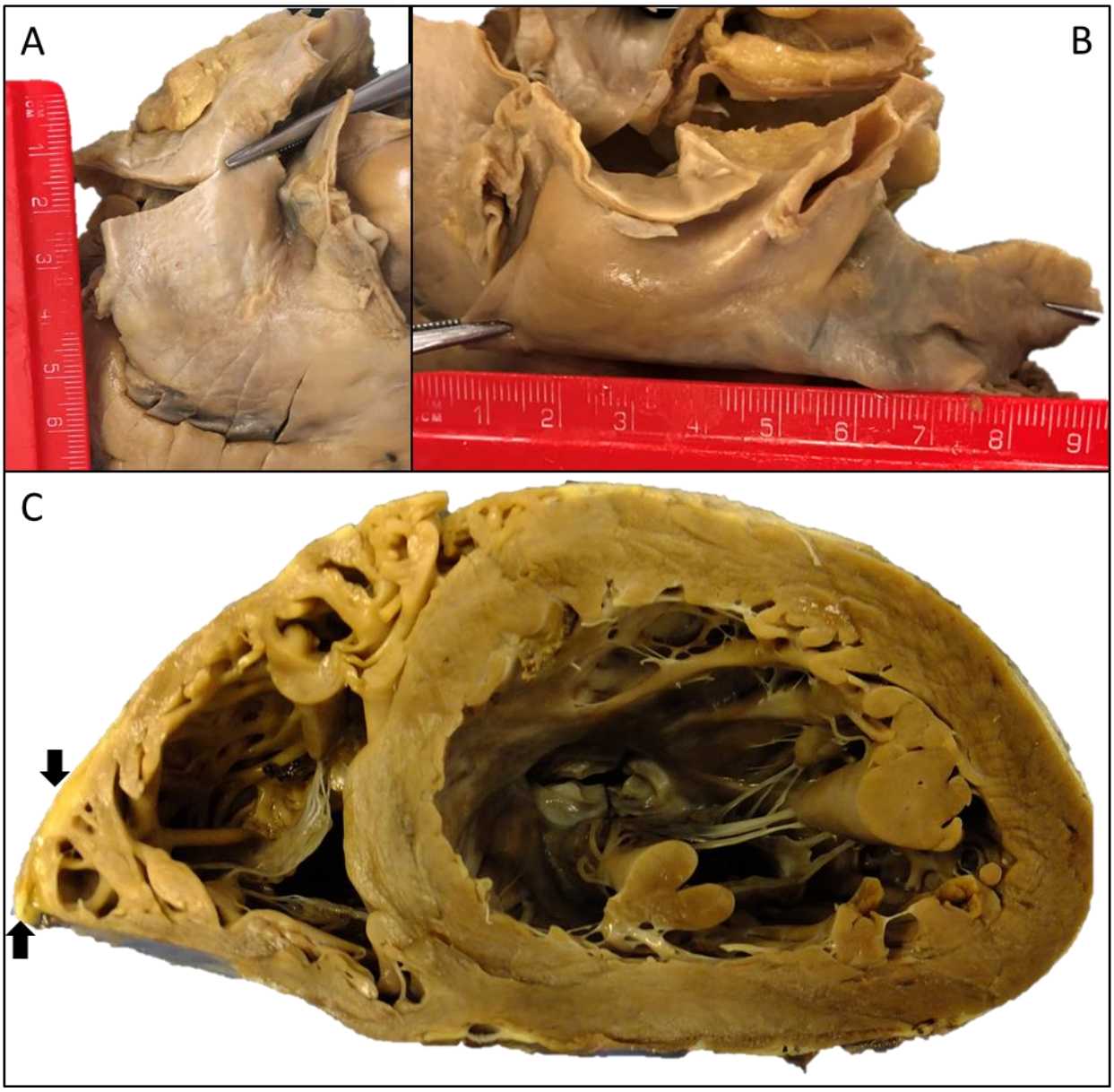


Figure 7.1. Typical findings in DCM. A) A dilated left atrium. B) A dilated left atrium. C) Dilated and thinned left ventricle. Note the epicardial fat on the lateral wall of the right ventricle (black arrows).

	DCM	Control	P value	Validation of significant findings in wider DCM cohort (n=243)
Heart weight	**488±111**	**364±63**	**.004**	**504±169, p<0.01**
Right atrium 1	66±18	54±14	.103	
Right atrium 2	**54±15**	**41±9**	**.028**	**49±12, p=0.03**
Left atrium 1	**55±19**	**40±8**	**.028**	**48±10, p<0.01**
Left atrium 2	**50±15**	**36±8**	**.018**	42±10, p=0.05
RV diameter	34±10	32±6	.476	
Anterior RV Muscle	**4±1**	**3±1**	**.038**	3±1, p=1
Lateral RV Muscle	4±1	3±1	.189	
Posterior RV Muscle	**4±1**	**3±1**	**.007**	**4±1, p<0.01**
RVOT Muscle	**4±1**	**3±1**	**.039**	**4±1, p<0.01**
LV diameter	**43±10**	**33±6**	**.016**	**47±12, p<0.01**
IVS	12±3	13±3	.098	
Anterior LV Muscle	11±1	12±2	.079	
Lateral LV Muscle	**11±1**	**13±2**	**.019**	12±3, p=0.27
Posterior LV Muscle	11±2	12±2	.352	
Mitral valve	85±18	83±16	.783	
Tricuspid valve	105±17	103±17	.825	
Pulmonary valve	56±19	55±12	.863	
Aortic valve	54±8	55±9	.703	
Ascending aorta	58±9	57±8	.804	
Anterior RV fat	1±1	1±1	.807	
Lateral RV fat	**3±2**	**2±1**	**.009**	2±2, p=1
Posterior RV fat	0±2	0±0	.569	
RVOT fat	1±1	1±1	.201	
Anterior LV fat	1±1	1±1	.422	
Lateral LV fat	1±1	0±0	.078	
Posterior LV fat	0±0	0±1	.863	

Table 7.1. Macroscopic heart measurements for the dilated cardiomyopathy compared to normal hearts. The means and standard deviations for heart weight (in grams), atrial dimensions, cavity diameters, muscular wall thickness, valvular and ascending aortic circumferences and epicardial fat thickness (in millimetres) are provided. Significant structural changes have been examined in the overall DCM cohort to allow it to serve as a validation cohort.

There is an increase in heart weight (488±111g vs 364±63g, p=0.04).

The distance between the ostia of the inferior and superior caval veins is increased (54±15mm vs 41±9mm, p=0.03).

Both left atrial measurements are increased (55±19mm vs 40±8mm, p=0.03 & 50±15mm vs 36±8mm).

Right ventricle measurements

The anterior (4±1mm vs 3±1mm, p=0.04) and posterior (4±1mm vs 3±1mm, p<0.01) RV muscle walls are thickened along with the RVOT muscle (4±1mm vs 3±1mm, p=0.04). The RV cavity diameter and lateral RV muscle wall thickness are not significantly increased.

Left ventricle measurements

The LV cavity diameter is increased 43±10mm vs 33±6mm, p=0.02). The lateral LV muscle is thinned (11±1mm vs 13±2mm, p=0.02). The IVS, anterior and posterior LV walls are not significantly thinned compared to controls.

The subepicardial fat is increased in thickness on the lateral RV (3±2mm vs 2±1mm, p<0.01). There are no significant increases in subepicardial fat elsewhere.

Validation in wider cohort

The increase in heart weight, increase in atrial measurements, increase in right ventricular muscle wall thickness and increase in LV diameter have been further validated in the wider cohort (table 7.1).

Correlations between measurements

The correlations between measurements are shown in table 7.2. From the variables that were significantly different than the normal heart there is a significant strongly positive correlation between the right and left atrial measurements (figure 7.2). There

were no other significant correlations between measurements that were significantly different from the normal heart.

		1	2	3	4	5	6	7	8	9	10	11	12	13	14	15	16	17	18	19	20	21	22	23	24	25	26
1	Heart weight																										
2	Anterior RV muscle wall	.19																									
3	Lateral RV muscle wall	.58	.68*																								
4	Posterior RV muscle wall	.54	.32	.39																							
5	RVOT muscle wall	-.05	.6	.59	.51																						
6	Interventricular septum	-.22	-.09	-.2	-.15	-.56																					
7	Anterior LV muscle wall	.22	.06	.01	.35	.16	.08																				
8	Lateral LV muscle wall	.5	.15	.4	.43	.05	.37	.71*																			
9	Posterior LV muscle wall	.24	.06	-.24	.03	-.43	.21	.64*	.34																		
10	RV anterior epicardial fat	.61*	-.36	-.04	.17	-.51	.04	-.06	.06	.22																	
11	RV lateral epicardial fat	.27	-.05	-.23	.55	-.26	.26	.08	.21	.13	.4																
12	RV posterior epicardial fat	-.34	-.63*	-.42	C	C	-.22	-.16	-.42	-.34	.04	-.24															
13	RVOT epicardial fat	.43	-.48	-.46	.42	-.47	.2	-.11	-.01	.31	.79*	.97**	C														
14	LV anterior epicardial fat	-.1	.36	.21	.1	.27	.35	.4	.27	.44	-.08	-.27	-.22	-.29													
15	LV lateral epicardial fat	.45	.23	.38	.07	-.07	.07	.5	.37	.44	.41	-.2	-.23	-.16	.55												
16	LV posterior epicardial fat	.26	.42	.72*	.15	.31	.17	.2	.39	-.13	.06	-.35	-.15	-.48	.58	.73*											
17	Right atrium 1	.23	.23	.41	.46	.02	.35	-.46	.01	-.57	.27	.4	C	.27	-.01	.05	.43										
18	Right atrium 2	.46	.43	.74*	.5	.42	.01	-.02	.28	-.25	.37	-.04	C	-.05	.51	.56	.82**	.6									
19	Left atrium 1	-.26	-.36	-.26	.32	-.15	-.06	-.26	-.47	-.37	.14	-.11	.89**	.11	-.15	-.07	.08	.68	.63								
20	Left Atrium 2	.37	-.04	.41	.59	.31	-.22	0	.22	-.48	.29	-.02	.49	-.05	-.14	.17	.47	.48	.81*	.64							
21	Diameter of RV chamber	.65*	.42	.65*	.17	.27	-.55	.1	.05	.19	.21	-.41	-.14	-.32	.13	.57	.43	-.07	.41	-.08	.31						
22	Diameter of LV chamber	.43	-.12	.43	-.13	.05	-.45	-.12	.12	-.37	.18	-.39	.23	-.3	-.44	.1	.22	-.1	.19	.19	.65	.48					
23	Mitral valve circumference	.32	.73*	.80**	.42	.80*	-.49	.06	.17	-.2	-.36	-.32	-.2	-.51	.19	.07	.41	.04	.46	-.12	.38	.6	.35				
24	Tricuspid annulus circumference	.65*	.34	.73*	.38	.38	-.56	-.04	.12	-.24	.22	-.23	.1	-.2	-.13	.3	.45	.19	.57	.25	.78*	.78**	.75**	.72*			
25	Pulmonary valve circumference	.62*	.72*	.71*	.38	.19	.04	.19	.53	.25	.01	.11	.89**	-.26	.14	.37	.35	.25	.45	-.73*	-.16	.48	.1	.46	.31		
26	Aortic circumference	.66*	.24	.45	.07	-.18	-.22	.01	.36	.1	.07	.02	-.38	.02	-.45	-.05	-.1	-.15	-.18	-.36	.12	.47	.6	.37	.52	.63*	
27	Ascending aorta circumference	.65*	.18	.5	.39	.21	-.5	.25	.37	0	.05	-.1	.07	-.12	-.33	.09	.1	-.15	.12	.09	.6	.61*	.74**	.6	.81**	.32	.77**

*Table 7.2. Correlations between variables. Significant strong correlations are highlighted in red. There is a significant positive correlation between the second measurements of the right and left atria (*p<.05, **p<.01).*

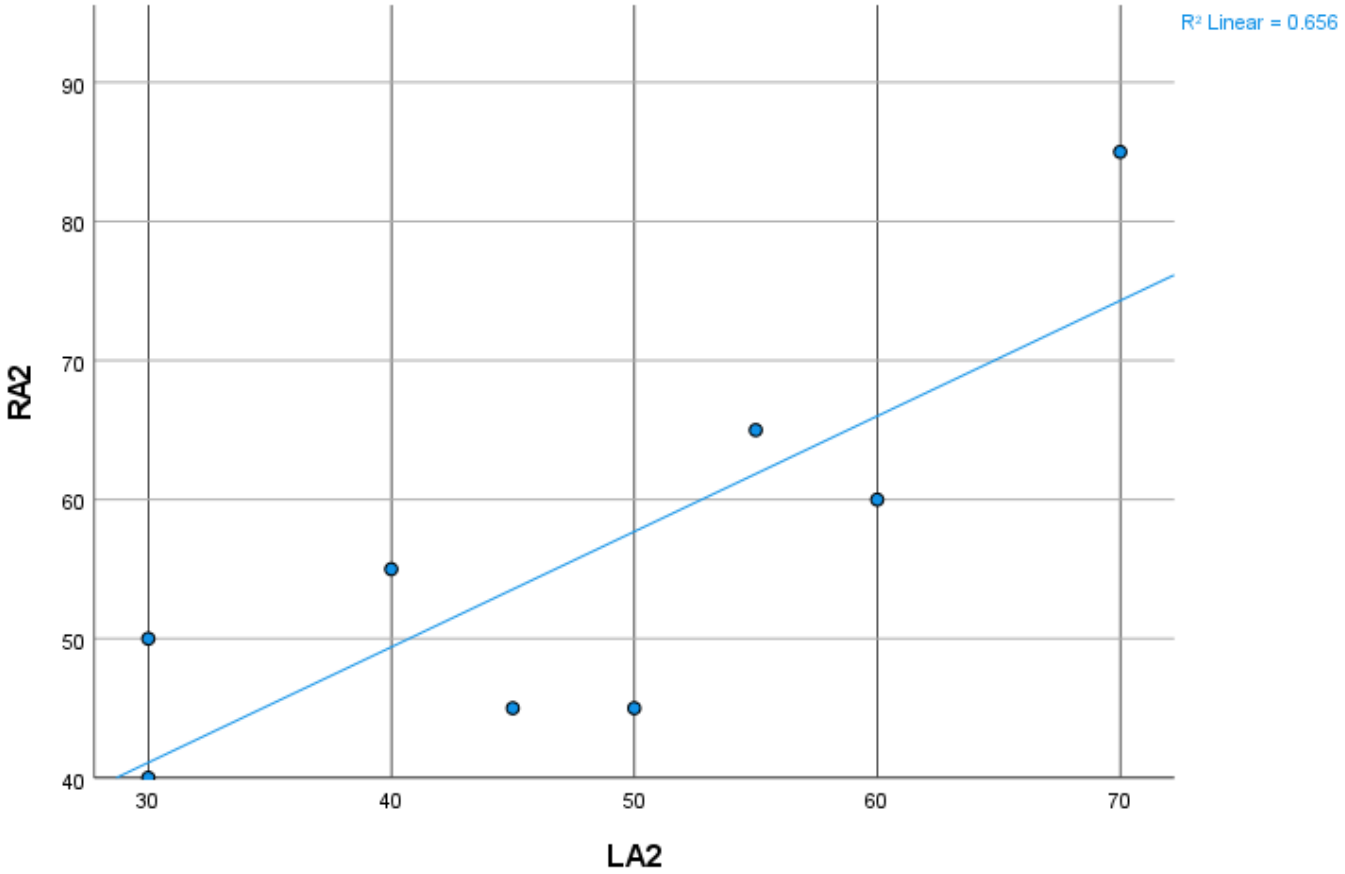


Figure 7.2. Plot of left atrial measurement 2 against left atrial measurement 2. There is a significant positive correlation between the measurements of the left and right atria. This suggests that the atria enlarge in tandem in DCM.

Ventricular myocardium compositional analysis

Collagen

There is considerable variation in the amount and location of fibrosis in DCM hearts. DCM hearts show networks of interstitial fibrosis stretching through the inner myocardium predominantly in the LV with more subtle transmural interstitial fibrosis in the RV (figure 7.3-7.7).

Within the LV myocardium, areas of fibrosis frequently coalesce around vessels (figure 7.8). The LV myocardium shows an extensive interweaving network of interstitial fibrosis which is present in the inner myocardium and variably extends towards the outer myocardial surface where it becomes subtler (figure 7.9). This ranges from fibrosis heavily concentrated adjacent to the endocardium in the inner myocardium to transmural diffuse involvement of the entire myocardium (figure 7.7). Patches of replacement fibrosis are present in the inner myocardium which connect with the network of interstitial fibrosis (figure 7.9). Long continuous stretches of interstitial fibrosis interconnecting with small patches of replacement fibrosis extend through the LV free wall inner myocardium (figure 7.10). These continuous stretches of fibrosis are also present in the IVS where it is present distributed transmurally (figure 7.5, 7.10). The posterior LV wall shows the most extensive replacement fibrosis. Epicardial fibrosis is not seen in isolation.

The endocardial collagen shows marked thickening which extends around the trabeculae and papillary muscles (figure 7.11). Endocardial collagen thickening is present throughout the LV and IVS but not in the RV or RVOT.

Within the RVOT and RV free wall, there is a subtle network of interstitial fibrosis with occasional patches of replacement fibrosis admixed (figure 7.3, 7.4). The

interstitial fibrosis is present transmurally and merges with the perivascular collagen. The RVOT and RV are affected to a much lesser degree than the IVS and LV.

Fat

The fat is present in the same locations and in similar amounts as in the normal heart. The fat is predominantly distributed as subepicardial fat infiltrating into underlying myocardium in the RV free wall and RVOT (figure 7.3, 7.4) as thinner layer of subepicardial fat in the anterior LV free wall (figure 7.6). A very thin layer of subepicardial fat is present on the posterior LV (figure 7.7). Within the myocardium, fat is present around large vessels in both ventricles. Fatty infiltration of the myocardium in the absence of a large vessel is frequent in the RV and RVOT consisting of single adipocytes up to a whole sheet with several layers of adipocytes. Fatty infiltration into the LV is not present in DCM.

Myocytes

There is loss of myocytes in areas of replacement fibrosis which are scattered throughout the inner myocardium of the LV. Myocytes are frequently isolated from one another encircled by a thick layer of collagen in areas of interstitial fibrosis (figure 7.12). The myocytes show a decrease in width with occasional nuclear enlargement (figure 7.12). Other myocytes are enlarged especially surrounding areas of replacement fibrosis. In the inner myocardium, particularly adjacent to the endocardium, the myocytes show vacuolation and myofibrillary loss (figure 7.12). This is most prominent when the myocytes are embedded in fibrosis. Myocyte disarray is not present in DCM.

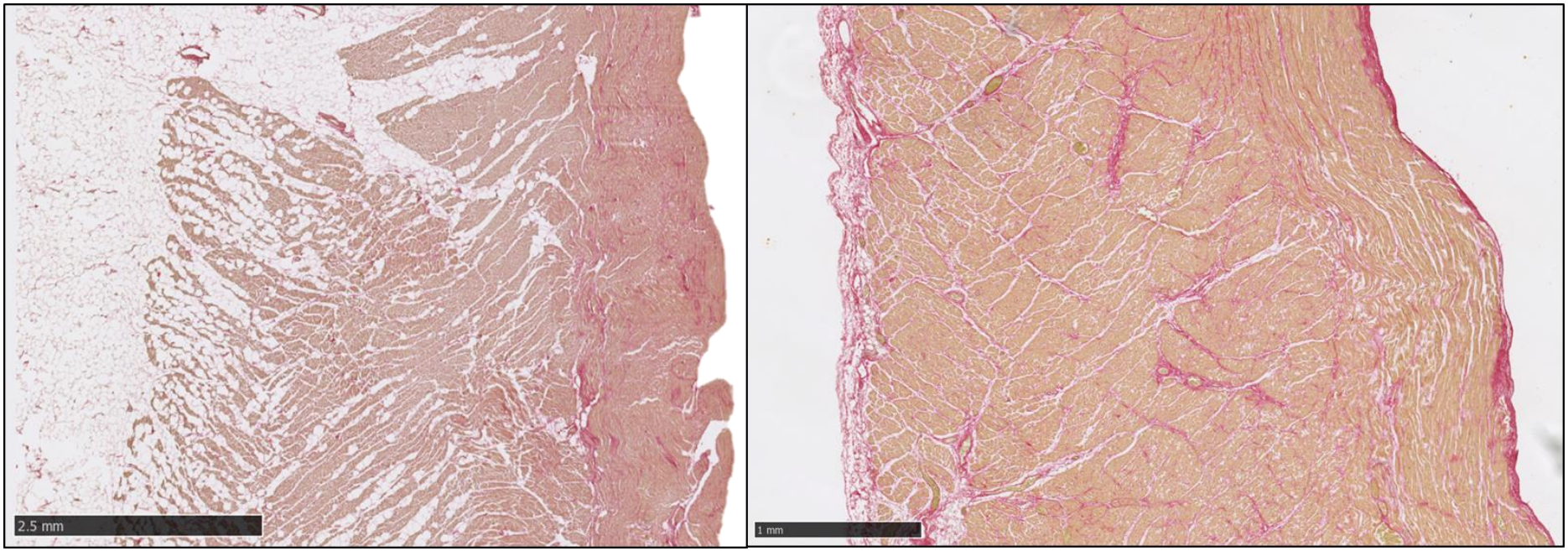


Figure 7.3. Networks of subtle interstitial and perivascular fibrosis are present in the right ventricular outflow tract in dilated cardiomyopathy. Note the variation in fat content as well.

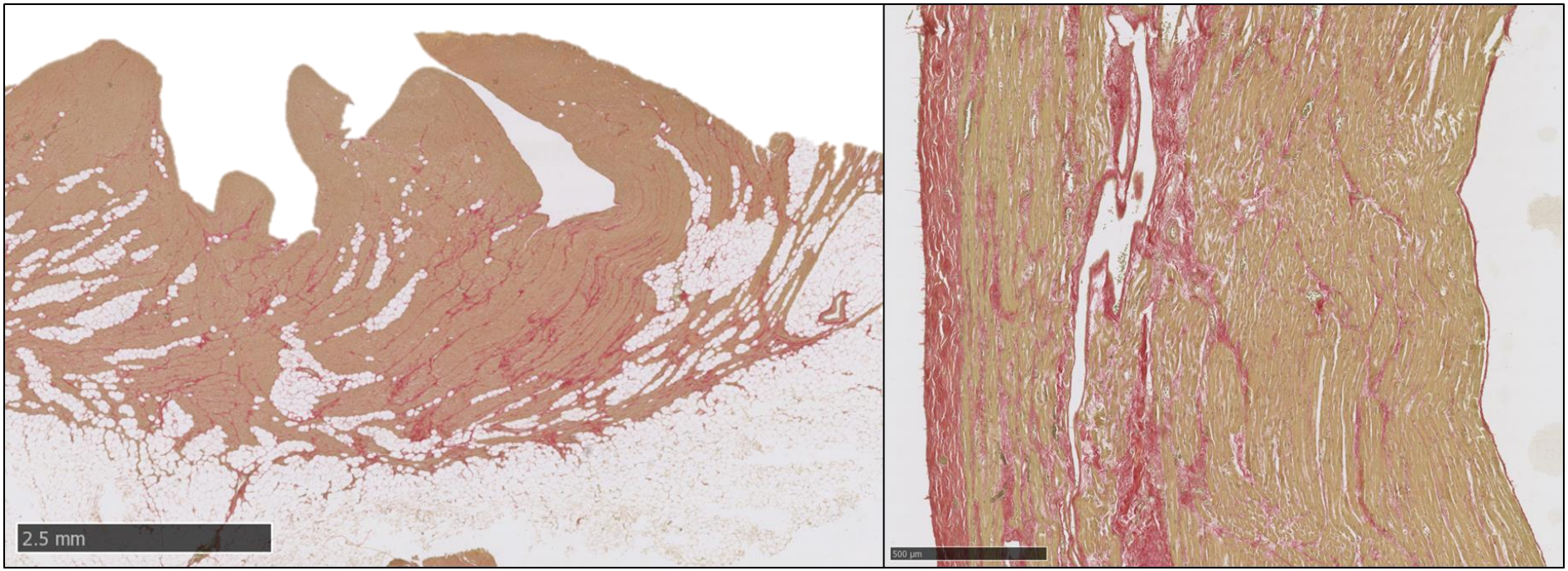


Figure 7.4. Networks of subtle interstitial and perivascular fibrosis are present in the right ventricle.

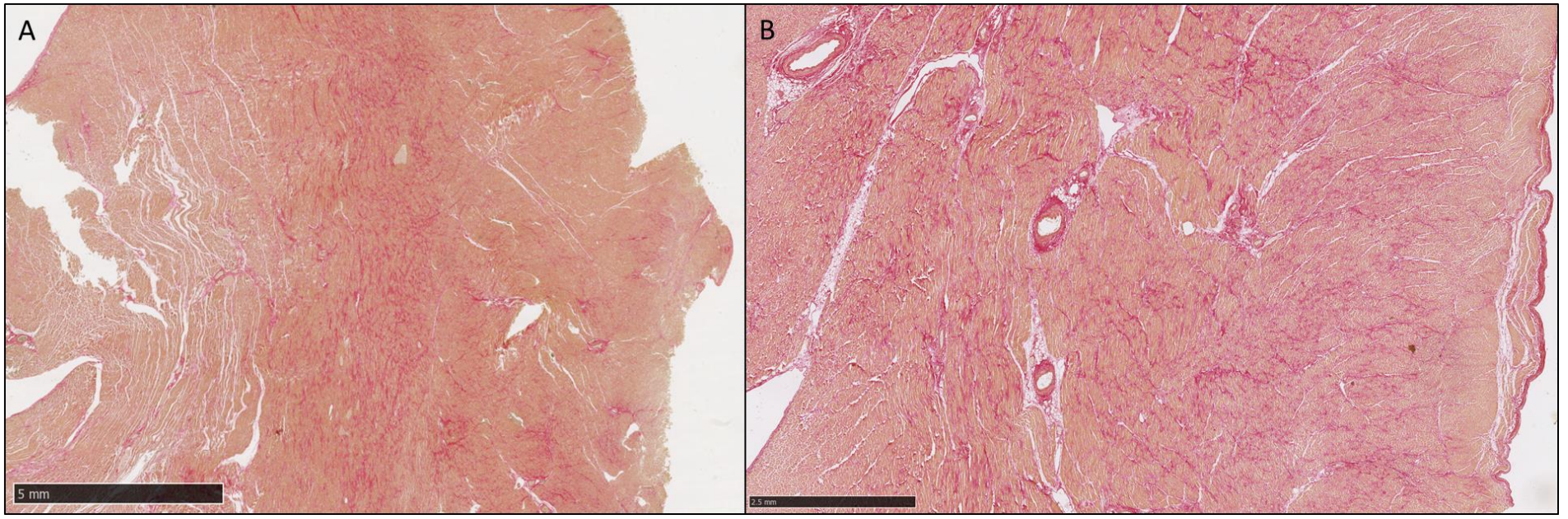


Figure 7.5. The septum shows large networks of interstitial fibrosis interlinking with replacement fibrosis present in the midwall (A) and transmurally (B).

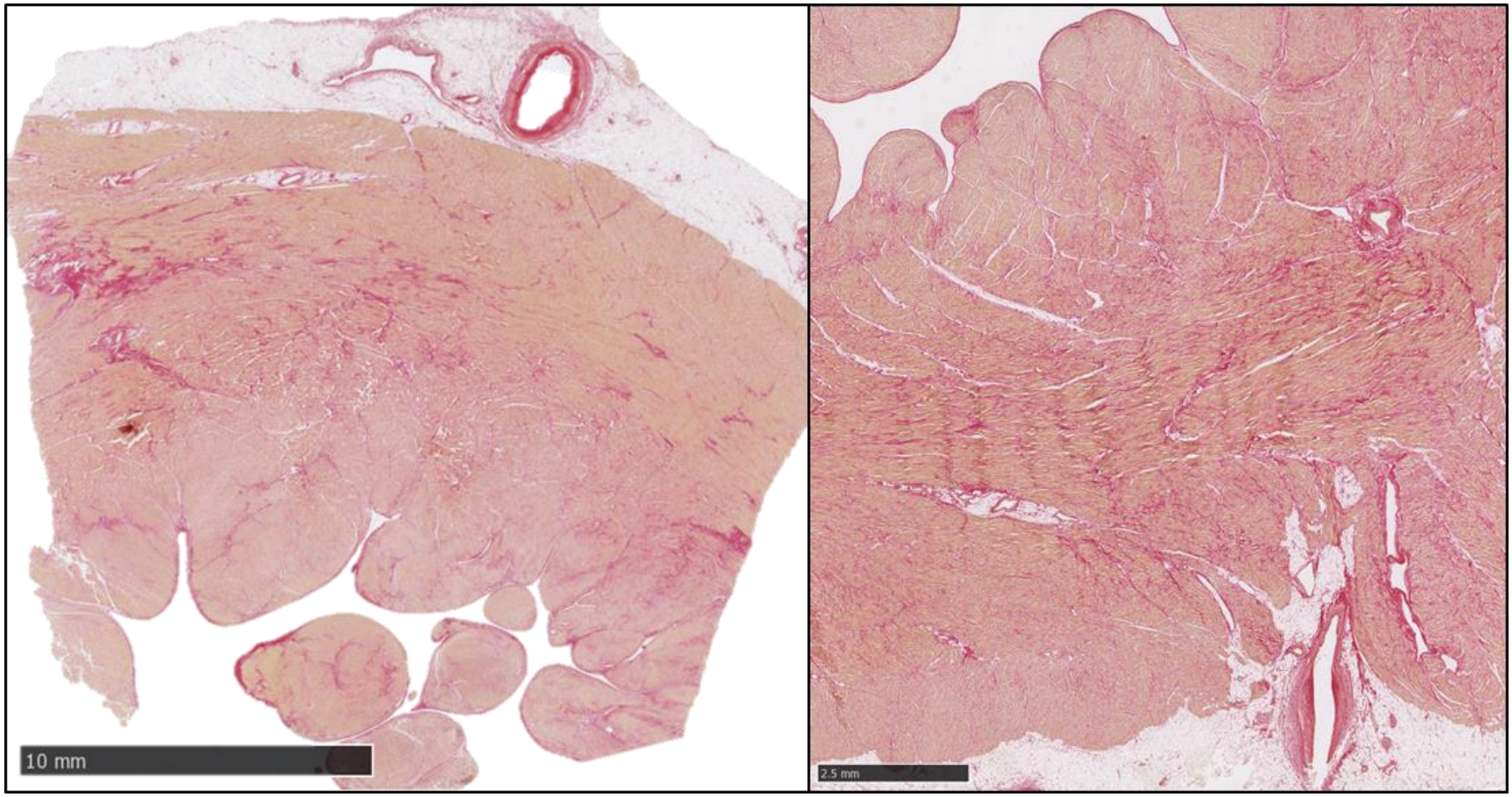


Figure 7.6. The anterior left ventricle shows diffuse interstitial fibrosis interlinking with replacement fibrosis. The fibrosis is concentrated on the mid to inner myocardium.

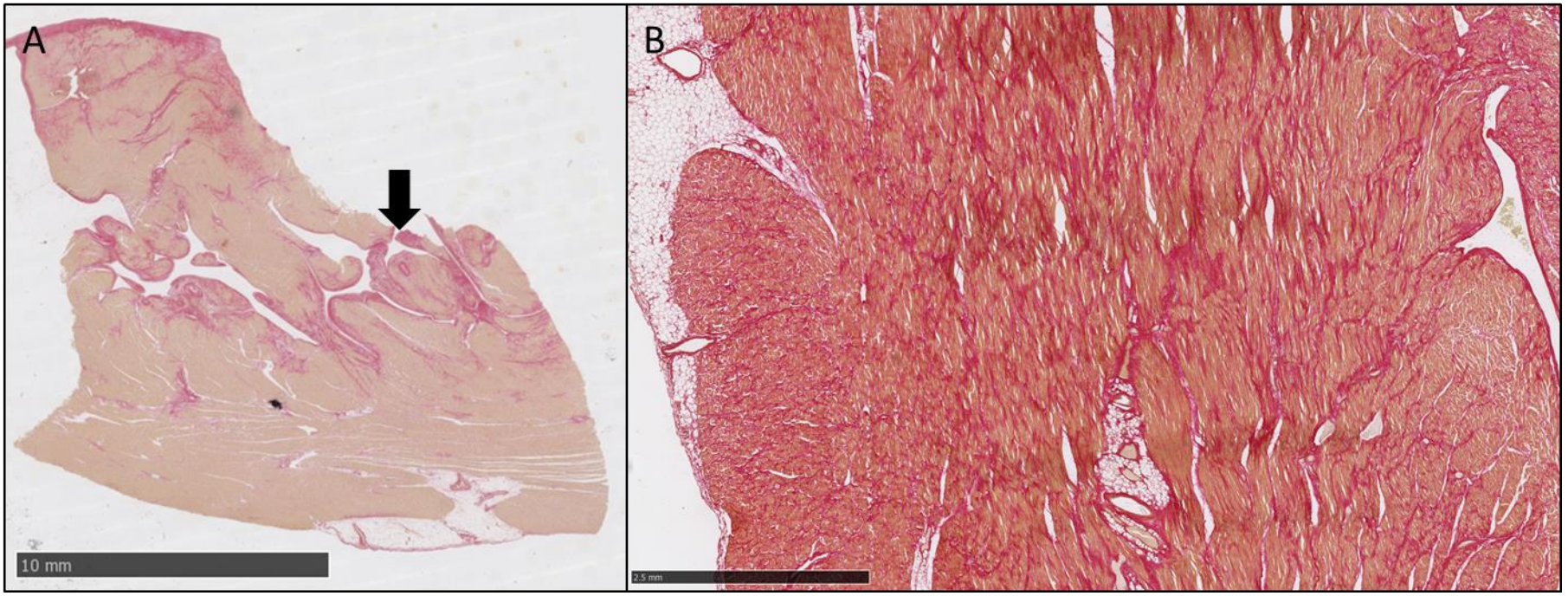


Figure 7.7. The posterior left ventricle shows variable interstitial fibrosis and replacement fibrosis. (A) Interstitial and replacement fibrosis adjacent to the endocardium (arrow) in the inner wall. (B) Transmural diffusely distributed interstitial and replacement fibrosis.

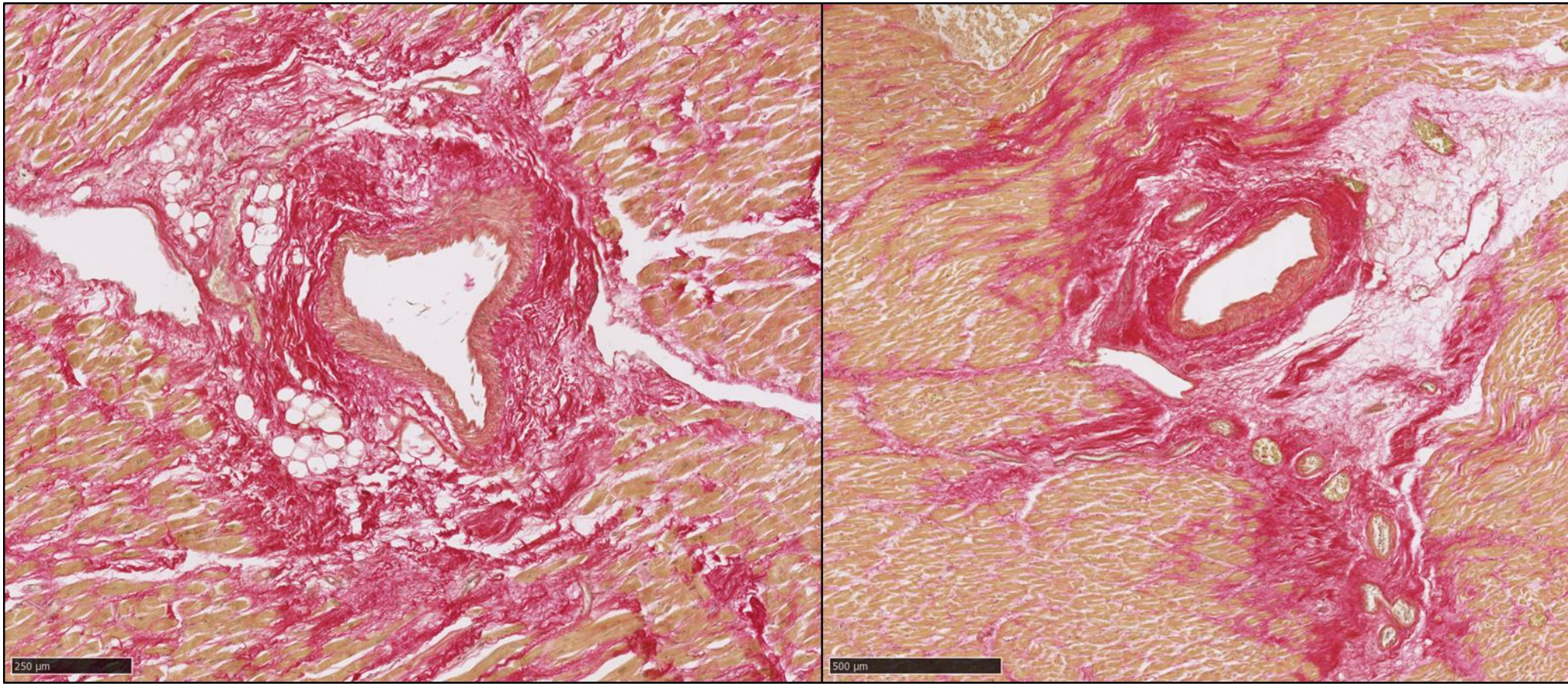


Figure 7.8. Fibrosis merges into the perivascular collagen which appears more prominent in dilated cardiomyopathy.

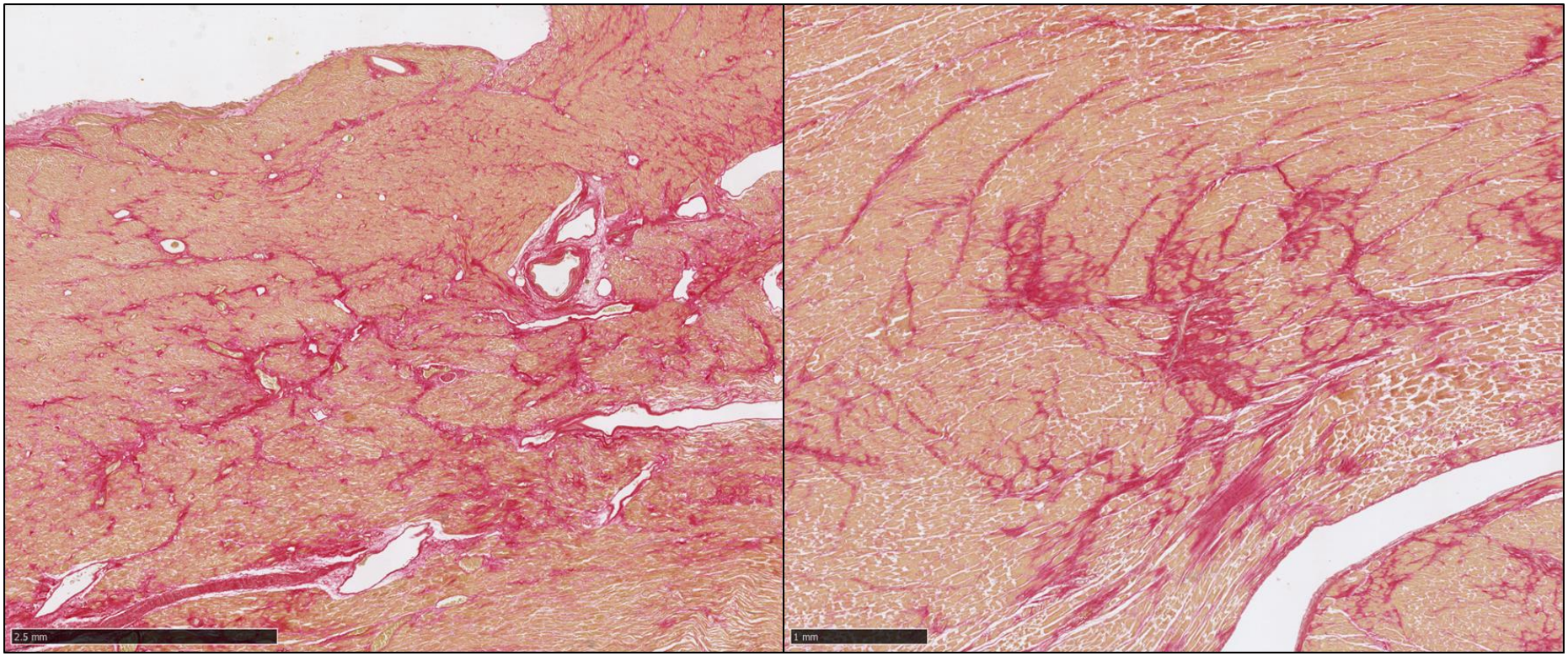


Figure 7.9. Networks of interstitial and replacement fibrosis in the inner myocardium adjacent to the endocardium.

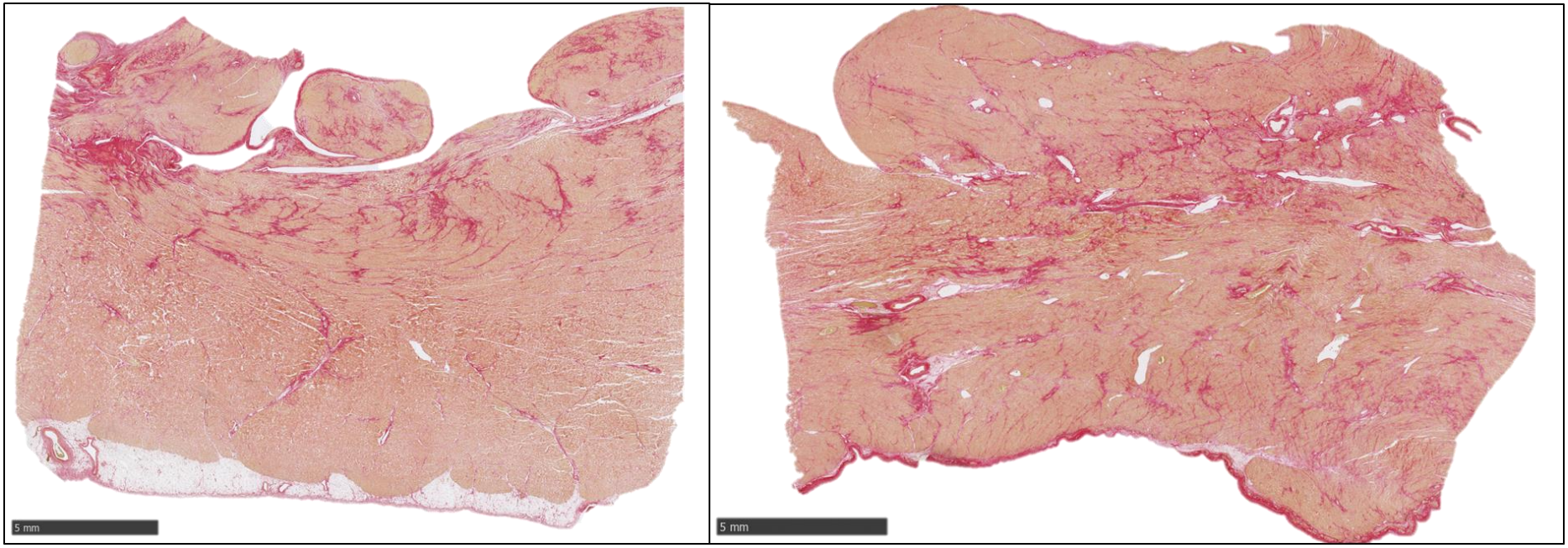


Figure 7.10. The inner myocardium of the free wall and the midwall of the septum show continuous stretches of involvement.

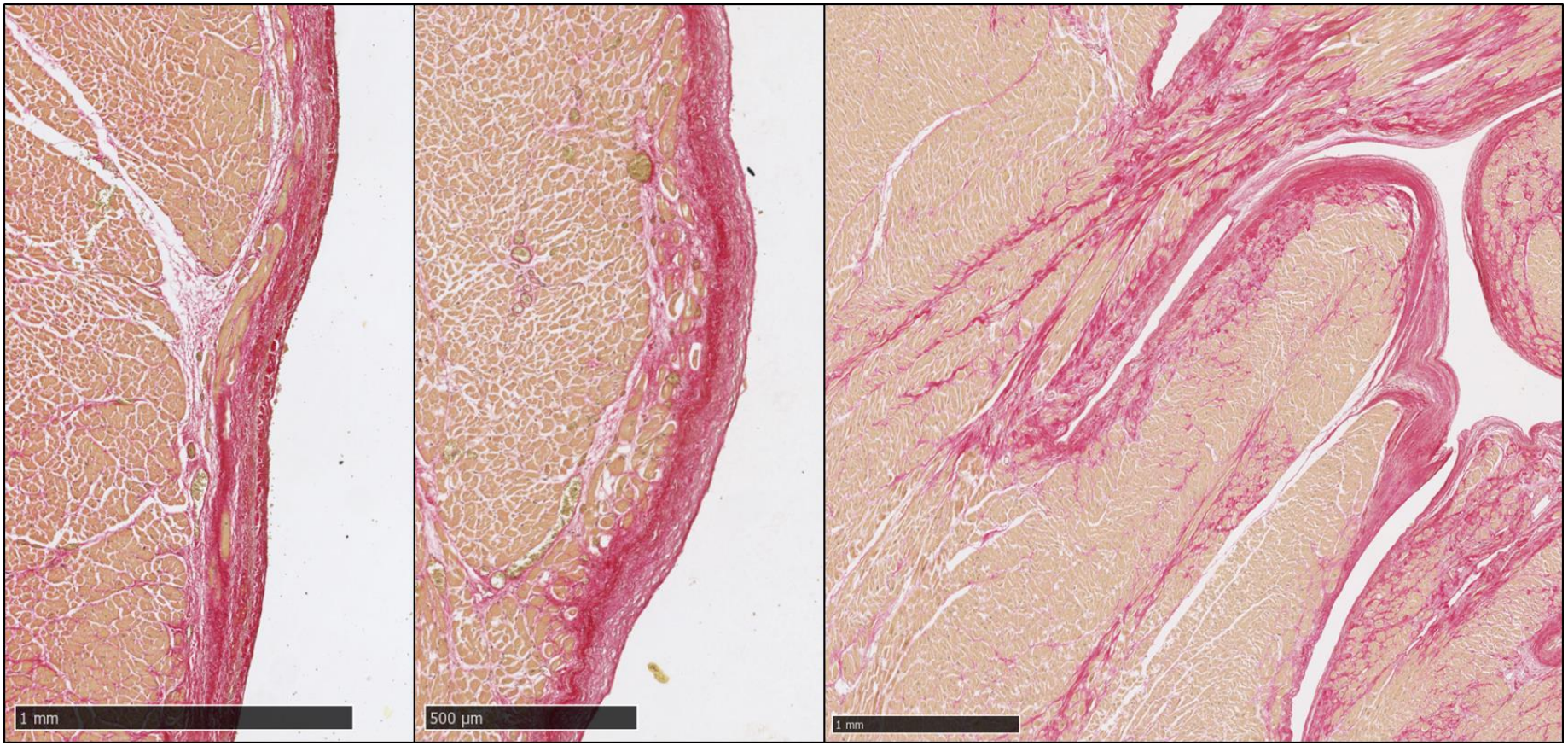


Figure 7.11. The endocardial collagen is thickened. This is also seen surrounding trabeculae and papillary muscles.

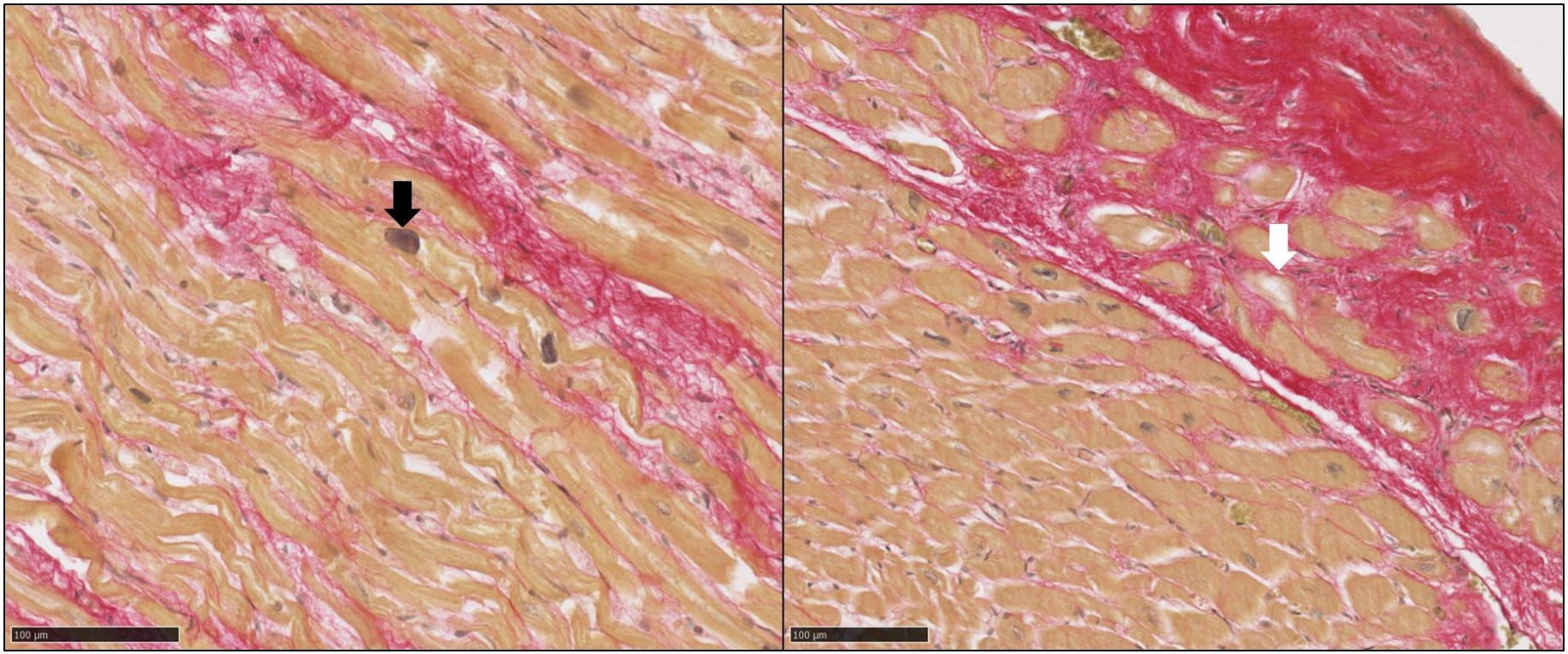


Figure 7.12. Myocytes in dilated cardiomyopathy. The myocytes show changes including a reduced width with nuclear enlargement (black arrow) and show vacuolation and myofibrillary loss (white arrow) particularly in the inner myocardium. Other myocytes show hypertrophy particularly in areas around replacement fibrosis.

Quantitative analysis

Collagen

In DCM, overall there is an overall average collagen proportion of 20% compared to 11% in the normal heart but this does not reach significance.

There is a significant increase in collagen in the IVS (ratio 2.5, 95%CI 1.0-5.9, p=0.04), compared to the normal heart. The anterior and posterior LV showed 18% and 24% collagen respectively compared to 9% and 11% in the normal heart but this does not reach significance.

Fat

In DCM, the fat proportion is 6% which is similar to the normal heart.

As with the normal heart, there are differences in the proportion of fat between regions. There is 10-12% fat in the RV and RVOT, 9% in the anterior LV and 2-3% in the IVS and posterior LV. There are no significant differences between the fat proportion in DCM and the normal heart.

Myocytes

There is an overall loss of myocytes compared to normal hearts (ratio 0.8, 95%CI 0.6-1.0, p=0.04).

The RVOT showed a reduction in myocytes compared to normal hearts (ratio 0.72, 95%CI 0.53-0.98, p=0.03). The RV shows a 58% proportion of myocytes compared to 71% in the normal heart but this does not reach significance. The IVS shows 68% myocytes compared to 86% but this does not reach significance. The anterior LV shows 60% myocytes compared to 77% but this does not reach significance. The posterior LV shows 65% compared to 80% but this does not reach significance.

The proportions for collagen, fat and myocytes in DCM and controls are shown in table 7.3 and figure 7.13.

Component	Condition	DCM		Control	
	Location	Expected	95% CI	Expected	95% CI
Collagen	All	20.08	13.54-29.76	10.70	7.22-15.86
	RVOT	17.08	11.03-26.43	11.15	7.25-17.15
	RV	21.53	13.91-33.32	14.60	9.49-22.46
	IVS	**20.60**	**13.31-31.88**	**8.39**	**5.45-12.90**
	ALV	17.89	11.56-27.69	9.45	6.14-14.53
	PLV	24.06	15.54-37.23	10.87	7.06-16.71
Fat	All	5.78	4.30-7.78	5.89	4.37-7.92
	RVOT	12.52	8.21-19.09	9.83	6.44-14.99
	RV	10.80	7.08-16.47	10.23	6.70-15.60
	IVS	1.88	1.23-2.87	2.43	1.59-3.70
	ALV	9.16	6.01-13.97	7.78	5.10-11.87
	PLV	2.78	1.82-4.24	3.72	2.43-5.67
Myocytes	**All**	**60.23**	**53.42-67.90**	**76.97**	**68.26-86.77**
	RVOT	**51.87**	**44.59-60.32**	**71.76**	**61.69-83.45**
	RV	57.88	49.76-67.31	71.31	61.31-82.94
	IVS	67.83	58.31-78.88	85.72	73.69-99.69
	ALV	60.27	51.81-70.09	76.65	65.90-89.15
	PLV	64.60	55.54-75.13	80.33	69.06-93.42

Table 7.3. Predicted proportions (geometric mean and confidence interval) of the ventricular myocardium made up by collagen, fat and myocytes for dilated cardiomyopathy (DCM) compared to control cases. The proportions for collagen, fat and myocytes are given for the right ventricular outflow tract (RVOT), right ventricular free wall (RV), interventricular septum (IVS), anterior and posterior left ventricle (ALV and PLV).

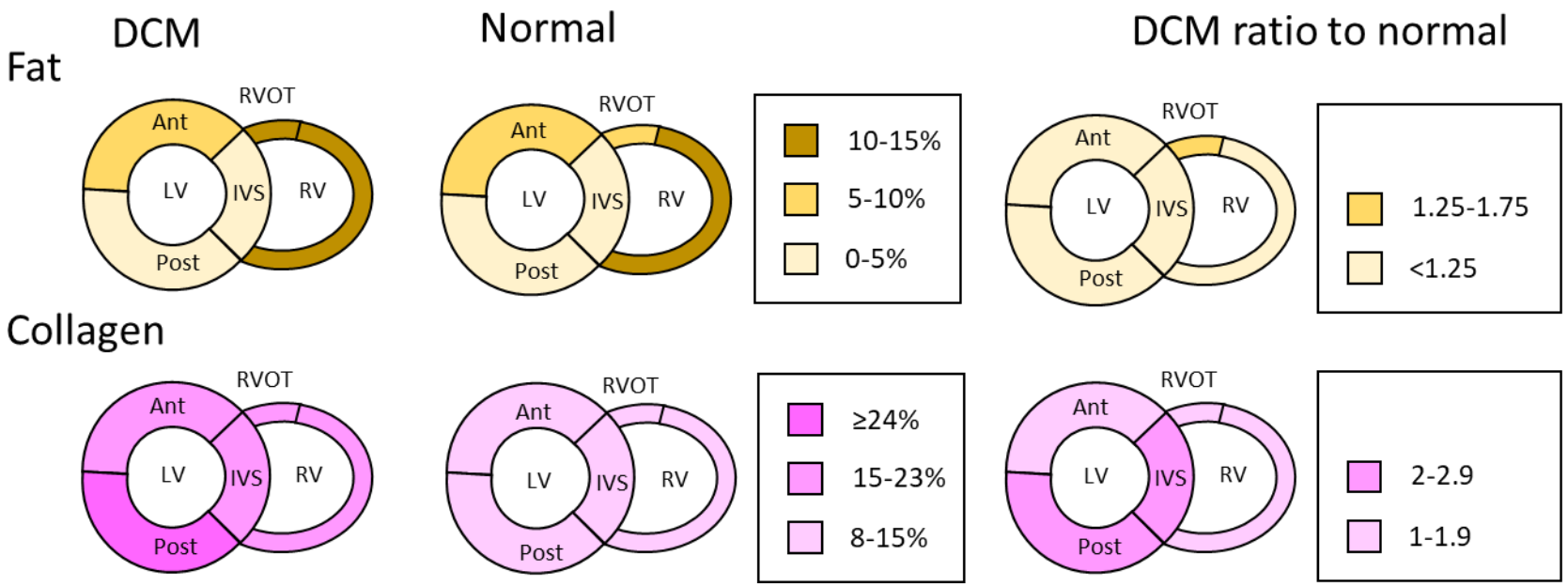


Figure 7.13. Percentage and ratio of fat and collagen in the dilated cardiomyopathy (DCM) heart ventricular myocardium compared to normal. The values are given for the right ventricle (RV), right ventricular outflow tract (RVOT), interventricular septum (IVS), the anterior left ventricle (LV) and the posterior left ventricle. There is an increase in collagen in the septum of dilated cardiomyopathy.

Innervation of the ventricular myocardium

General innervation

Within DCM, the distribution of nerves is similar to the normal heart (figure 5.33) but with a reduction in areas of fibrosis.

Within the subepicardial fat, there are few large nerve bundles (figure 7.14 and 7.15). They are associated with the coronary arteries and large vessels in the fat lying in and around the adventitia. Small nerve bundles are present independent of the vessels between adipocytes within the subepicardial fat. The nerve bundles extend from the subepicardial fat into the myocardium and remain associated with blood vessels lying in the perivascular adipose tissue. Within the myocardium, there are few large and small nerve bundles. Only occasional large nerve bundles are present in the outer myocardium. There are few small nerve bundles present throughout the myocardium which are most prominent in the inner myocardium. The large and small nerve bundles remain in close association with blood vessels situated in the periadventitial fat and then extending down alongside smaller vessels of the inner myocardium. Individual fibrils extend between, parallel and adjoin with individual myocytes throughout the myocardium in areas where the architecture is normal throughout the full thickness myocardium. The nerve fibrils are present alongside small vessels. There are few individual nerve fibrils throughout the myocardium but these are more prominent in the inner half of the myocardium. Nerve fibrils are present on the endocardial surface. No ganglia are present in the ventricular myocardium.

In the patches of replacement fibrosis, there are no large nerve bundles. Granular staining nerve fibrils are present within areas of fibrosis (figure 7.16). The individual

nerve fibrils lie in the dense fibrosis without clear cellular association (figures 7.15-7.17).

Sympathetic innervation

TH showed a similar distribution to the normal heart away from areas of altered pathology, staining a percentage of fibres within the nerve bundles within the epicardial fat. The nerve bundles are always associated with vessels moving in from the subepicardial fat to the myocardium (figure 7.17). Smaller individual nerve fibrils are most frequently present alongside and adjoining small vessels but also in association with myocytes. The individual nerve fibrils are evenly spread through both the inner and outer myocardium. Individual nerve fibrils are frequently seen alongside small vessels. Fibrils are present in the endocardium. There were few small nerve bundles within areas of replacement fibrosis. Within areas of both interstitial and replacement fibrosis, TH sparsely stained small individual nerve fibrils (figure 7.18).

Parasympathetic innervation

CT showed a similar distribution to the normal heart away from areas of altered pathology. There is only occasional focal staining within fibres in the subepicardial fat. Small nerve bundles are present transmurally in association with vessels but between myocytes within the myocardium. Small individual nerve fibrils are frequently present showing a granular staining pattern (figure 7.19). The individual nerve fibrils are present throughout the myocardium but most prominently in the inner myocardium. The individual nerve fibrils are intricately associated with and adjoin and lie on the surface of myocytes. To a lesser degree, they are also closely

associated with and adjoining small vessels. The fibrils are also present in the endocardium. There are few small nerve bundles in areas of replacement fibrosis. The individual nerves fibrils are frequently present within interstitial fibrosis (figure 7.18). They lie within the mesh-like collagen network adjoining and intricately associated with the myocytes. The individual nerve fibrils are only occasionally present within areas of replacement fibrosis.

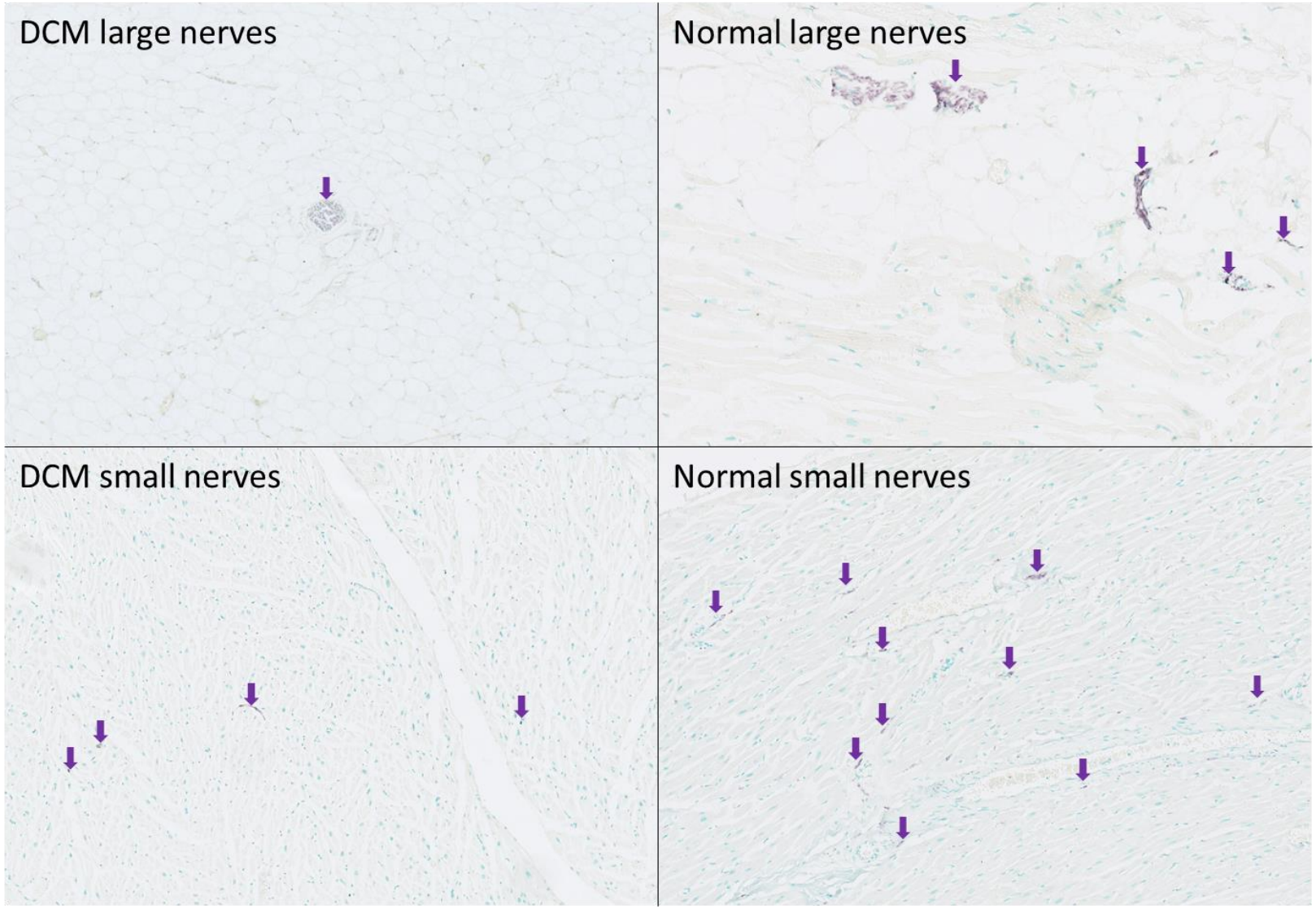


Figure 7.14. Few PGP9.5 stained (purple arrows) large bundles (top) and small bundles (bottom) in dilated cardiomyopathy.

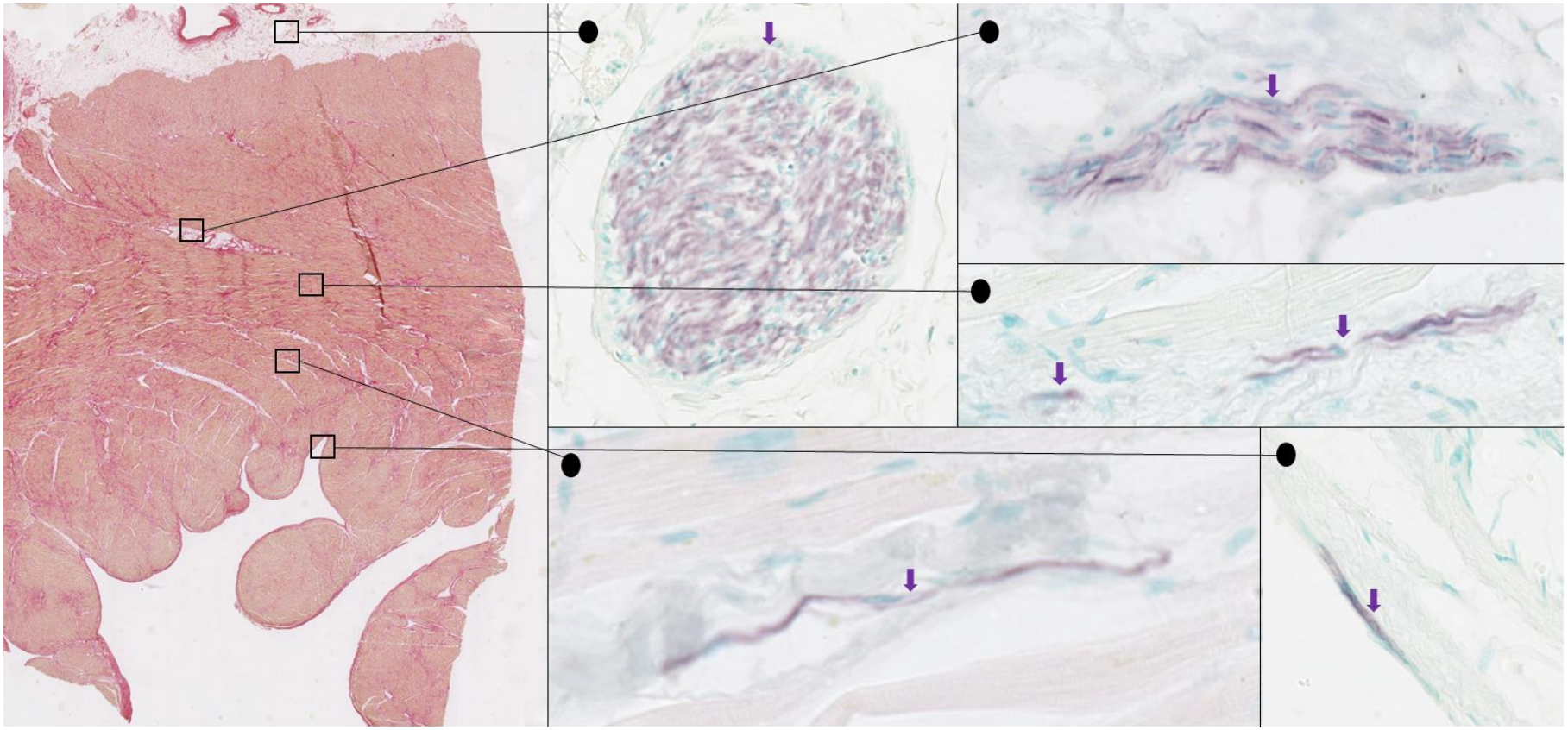


Figure 7.15. Nerve distribution (arrows) in the anterior left ventricle of an individual with dilated cardiomyopathy showing diffuse interstitial fibrosis. PGP9.5 stained large and small bundles as well as fibrils are in a similar distribution to control hearts (left - picrosirius red stain, others – PGP9.5 stain).

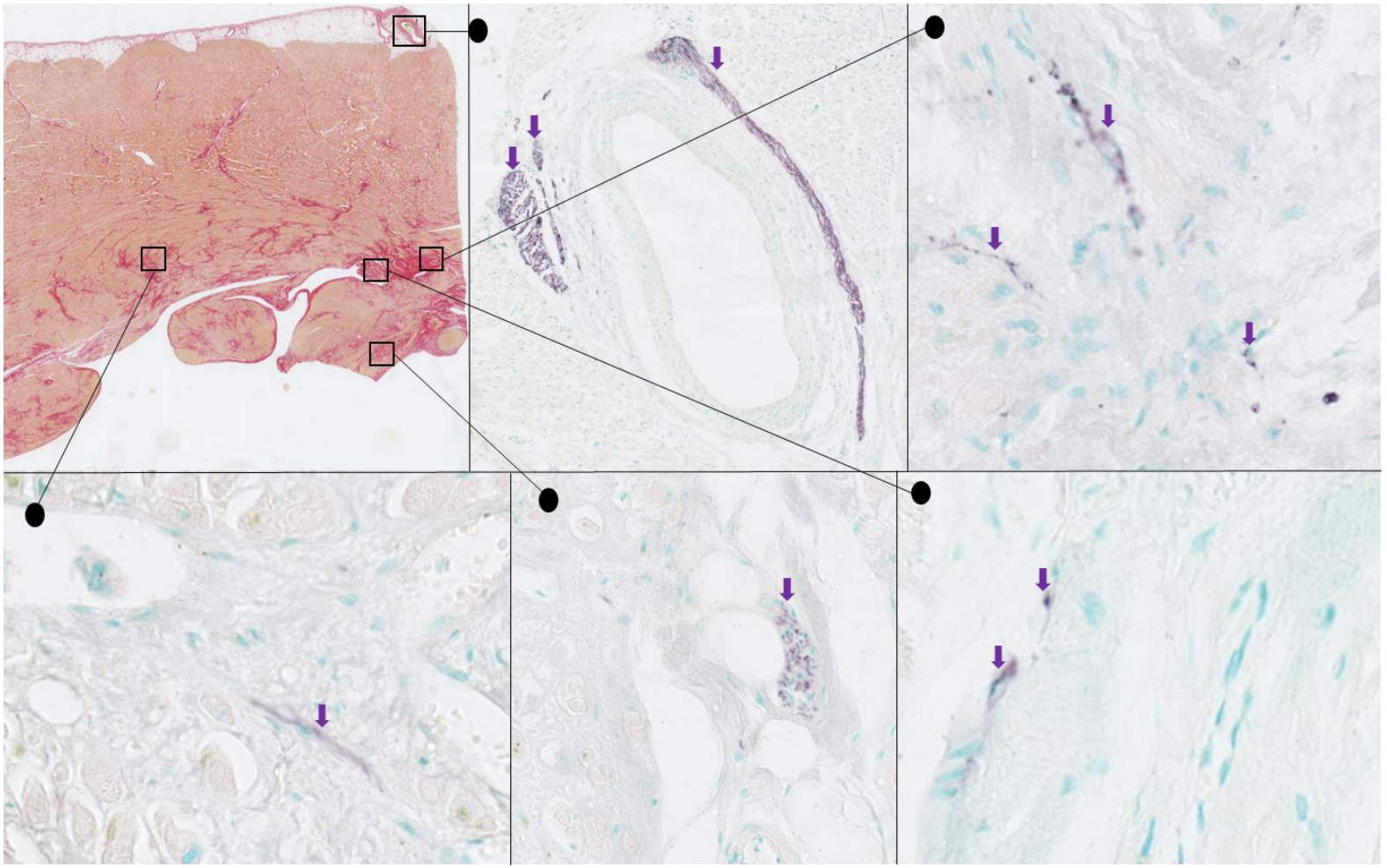


Figure 7.16. Nerve distribution (arrows) in the anterior left ventricle of an individual with dilated cardiomyopathy showing interstitial and replacement fibrosis predominantly in the inner myocardium. PGP9.5 staining shows few bundles. Individual nerve fibrils are present in areas of replacement fibrosis (top left - picrosirius red stain, others – PGP9.5 stain).

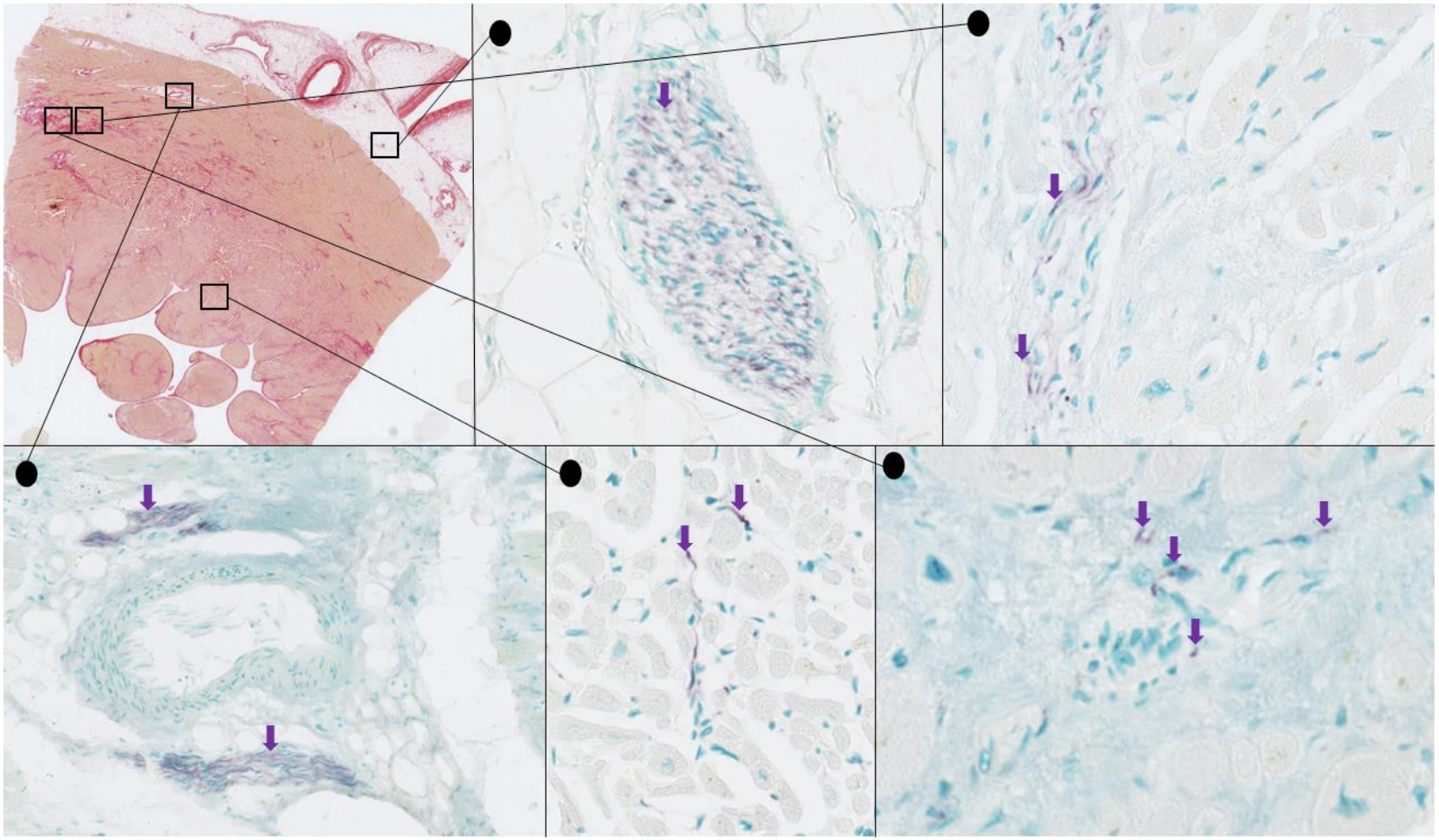


Figure 7.17. Sympathetic innervation (arrows) is decreased in dilated cardiomyopathy. Tyrosine hydroxylase stained large and small bundles are around blood vessels showing a similar distribution to control hearts. There are few nerve bundles in areas of fibrosis. Nerve fibrils are present in replacement fibrosis (top left - picrosirius red stain, others – tyrosine hydroxylase stain).

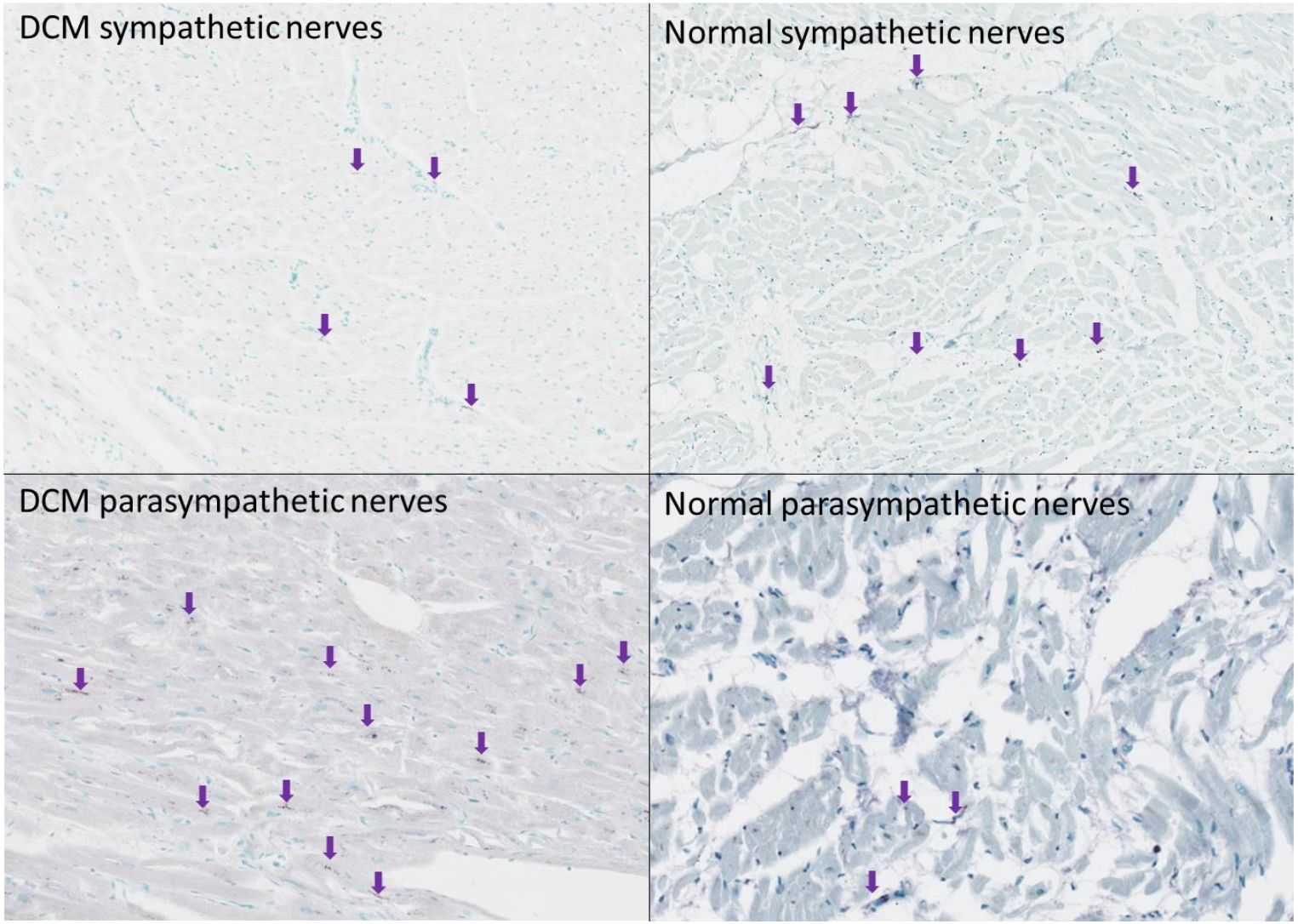


Figure 7.18. TH stains few small nerve bundles and fibrils in DCM. CT stains frequent individual nerve fibrils in DCM.

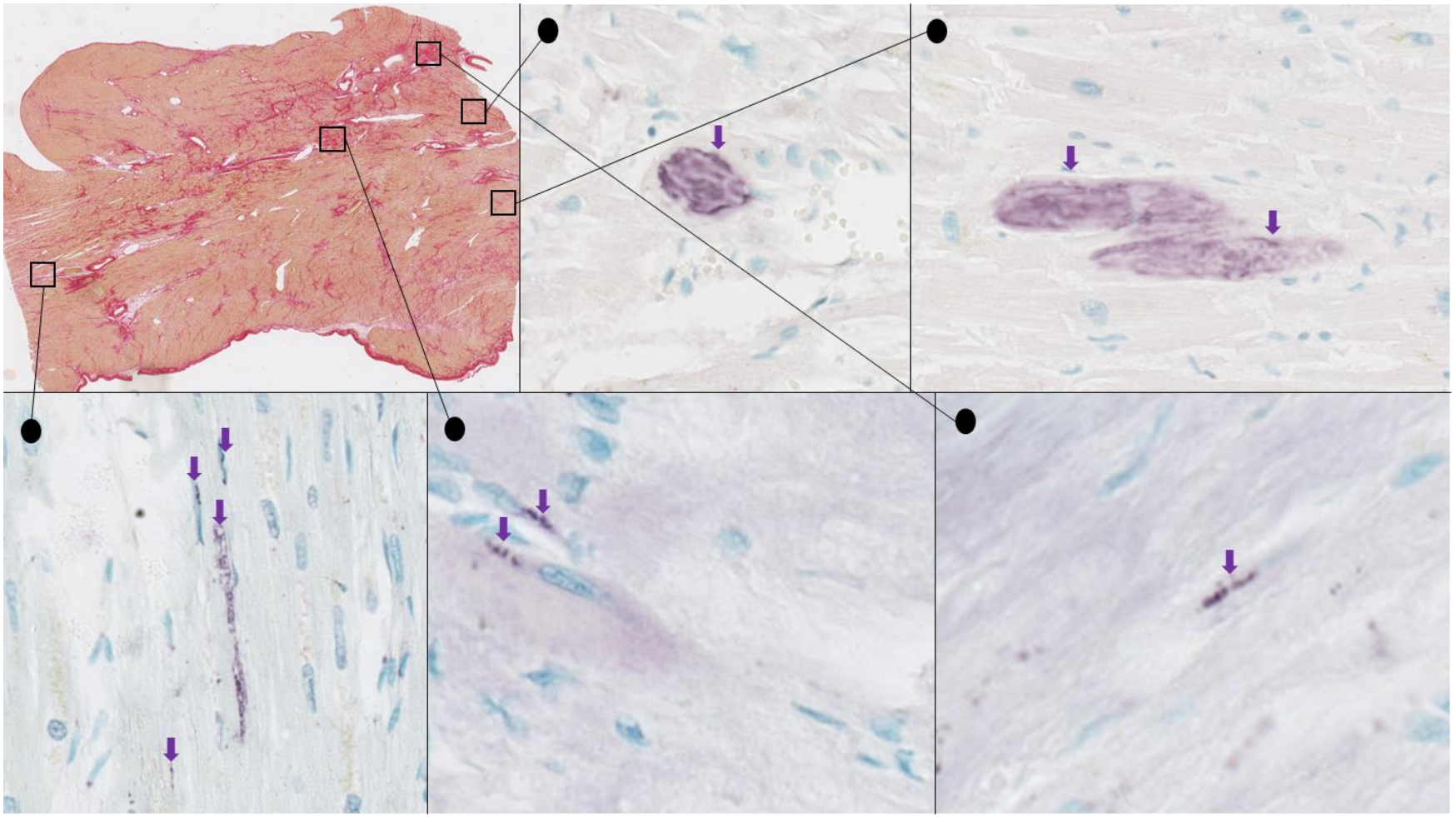


Figure 7.19. Parasympathetic innervation (arrows). Small bundles are present between myocytes. Individual nerve fibrils are present around myocytes and in areas of replacement fibrosis (top left - picrosirius red stain, others – CT stain).

Quantitative analysis

General innervation

There is no significant difference between PGP9.5 staining in the normal heart and DCM hearts. There is 0.01% overall of the myocardium examined staining for PGP9.5 in DCM compared to 0.04% in the normal heart. The RV and anterior LV show 0.02% and the RVOT, IVS and posterior LV show 0.01%.

Sympathetic innervation

There is no significant difference between TH staining in the normal heart and DCM hearts. The RV showed 0.04%, the anterior and posterior LV showed 0.02% and the IVS and RVOT showed 0.01%.

Parasympathetic innervation

CT staining does not show statistically significant changes overall or by region.

The proportions of staining by the general nerve marker PGP9.5, the sympathetic nerve marker TH and the parasympathetic nerve marker CT are shown in table 7.4 and figure 7.20.

Stain	Condition	DCM		Control	
	Region	Mean	95% CI	Mean	95% CI
PGP9.5 % of tissue area	All	0.014	0.007-0.027	0.036	0.018-0.069
	RVOT	0.014	0.006-0.030	0.061	0.027-0.134
	RV	0.023	0.010-0.050	0.057	0.026-0.126
	IVS	0.012	0.005-0.026	0.027	0.012-0.058
	ALV	0.020	0.008-0.042	0.032	0.014-0.069
	PLV	0.008	0.003-0.017	0.020	0.008-0.043
TH % of tissue area	All	0.017	0.008-0.033	0.035	0.017-0.069
	RVOT	0.012	0.004-0.028	0.037	0.015-0.090
	RV	0.039	0.015-0.094	0.062	0.025-0.151
	IVS	0.014	0.005-0.034	0.031	0.012-0.075
	ALV	0.015	0.006-0.037	0.031	0.012-0.074
	PLV	0.015	0.006-0.036	0.025	0.010-0.060
CT % of tissue area	All	0.037	0.013-0.098	0.022	0.008-0.057
	RVOT	0.022	0.007-0.067	0.014	0.004-0.043
	RV	0.046	0.014-0.139	0.027	0.008-0.083
	IVS	0.039	0.012-0.118	0.024	0.007-0.072
	ALV	0.037	0.012-0.112	0.020	0.006-0.060
	PLV	0.048	0.015-0.145	0.026	0.008-0.078

Table 7.4. Predicted proportions (geometric mean and confidence interval) of the ventricular myocardium stained by PGP9.5, TH and the CT for dilated cardiomyopathy (DCM) and normal control hearts. The proportions are given for the right ventricular outflow tract (RVOT), right ventricular free wall (RV), interventricular septum (IVS), anterior and posterior left ventricle (ALV and PLV).

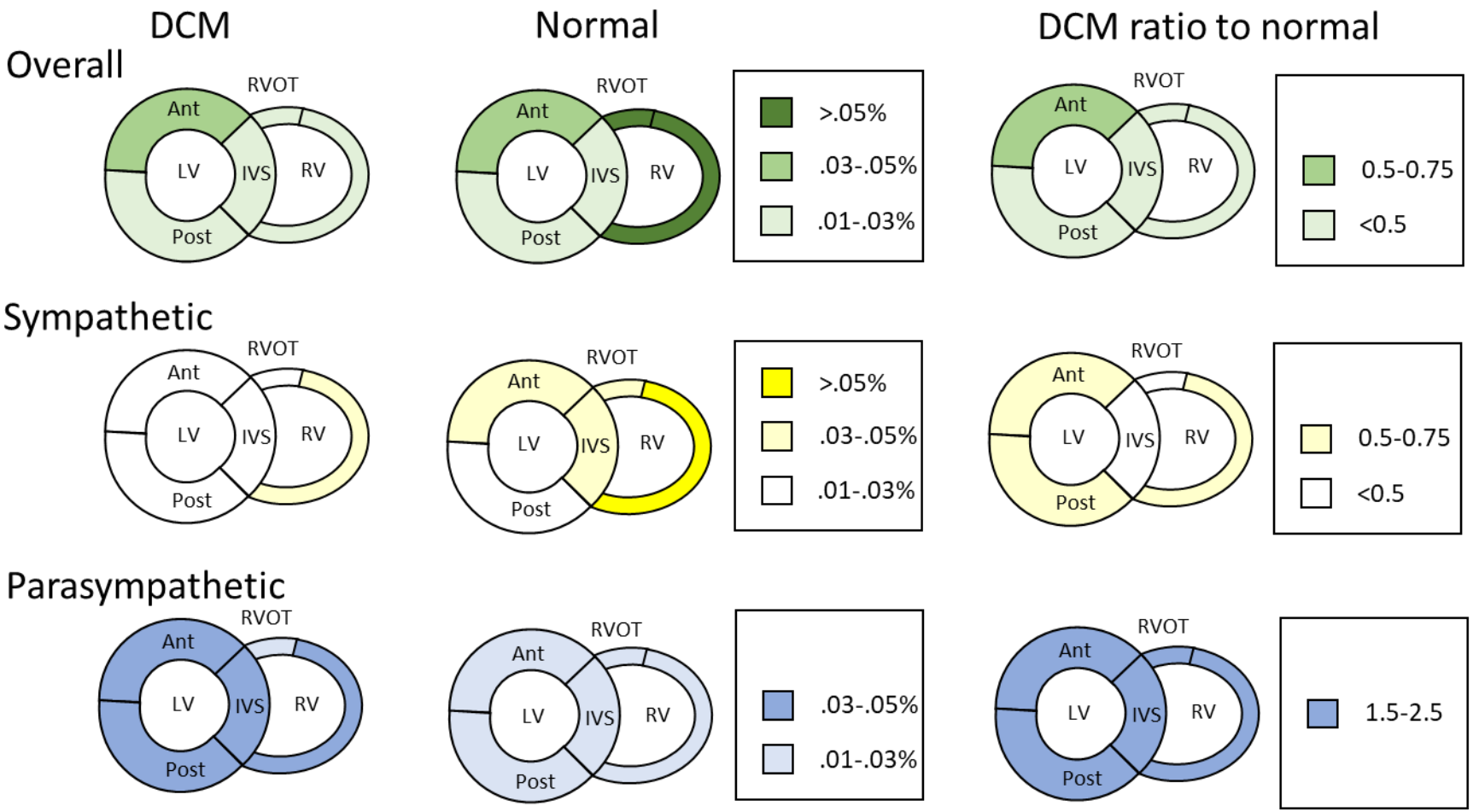


Figure 7.20. Percentage and ratio of overall, sympathetic and parasympathetic innervation in DCM ventricular myocardium compared to normal. The values are given for the RV, RVOT, IVS, anterior and posterior LV. There is a trend towards a reduction in general and sympathetic innervation.

Sections showing fibrosis quantification

A subcohort of sections showing a proportion of collagen two standard deviations from the mean of the normal heart (≥28%) are selected and compared to normal hearts. This is present in the RVOT in 5 cases, the RV in 4 cases, the IVS in 5 cases, the anterior LV in 4 cases and the posterior LV in 5 cases.

General innervation

The RVOT shows a significant reduction of PGP9.5 staining compared to normal hearts (ratio 0.14, 95%CI 0.02-0.93, p=0.04). There are no significant differences for PGP9.5 between DCM hearts and normal hearts overall or in the RV, IVS, anterior or posterior LV.

Sympathetic and parasympathetic innervation

When comparing diseased DCM sections to normal hearts there are no significant differences in TH or CT staining.

The proportions of the different innervation in diseased sections for DCM are shown in table 7.5.

Stain	Condition	DCM		Control	
	Region	Expected	95% CI	Expected	95% CI
PGP9.5	All	0.014	0.005-0.036	0.036	0.018-0.069
	RVOT	**0.009**	**0.002-0.026**	**0.061**	**0.027-0.134**
	RV	0.019	0.006-0.062	0.057	0.026-0.126
	IVS	0.021	0.006-0.062	0.027	0.012-0.058
	ALV	0.019	0.005-0.060	0.032	0.014-0.069
	PLV	0.009	0.003-0.027	0.020	0.008-0.043
TH	All	0.014	0.005-0.036	0.035	0.017-0.069
	RVOT	0.010	0.002-0.037	0.037	0.015-0.090
	RV	0.028	0.007-0.112	0.062	0.025-0.151
	IVS	0.016	0.004-0.059	0.031	0.012-0.075
	ALV	0.011	0.002-0.043	0.031	0.012-0.074
	PLV	0.011	0.003-0.041	0.025	0.010-0.060
CT	All	0.056	0.014-0.207	0.022	0.008-0.057
	RVOT	0.032	0.006-0.149	0.014	0.004-0.043
	RV	0.047	0.009-0.239	0.027	0.008-0.083
	IVS	0.066	0.014-0.312	0.024	0.007-0.072
	ALV	0.082	0.016-0.422	0.020	0.006-0.060
	PLV	0.067	0.014-0.311	0.026	0.008-0.078

Table 7.5. Predicted proportions (geometric mean and confidence interval) of the ventricular myocardium stained by PGP9.5, TH and the CT for dilated cardiomyopathy (DCM) diseased sections and normal control hearts. The proportions are given for the right ventricular outflow tract (RVOT), right ventricular free wall (RV), interventricular septum (IVS), anterior and posterior left ventricle (ALV and PLV).

Power calculation

Based on an alpha of 0.05 and a power of 0.8, we predict a sample size of 52 DCM and 52 normal hearts should be sufficient to detect a significant difference in overall innervation stained by PGP9.5 in unselected sections in DCM.

Discussion

This is the first study to provide detailed macroscopic findings, describe and autonomously quantify ventricular innervation in DCM and the first to objectively autonomously quantify fat, fibrosis and myocytes using picrosirius red in pathologically diagnosed DCM hearts.

Macroscopic findings in DCM

The DCM hearts have an increased weight of 488g with an increased LV diameter of 43mm and a thinner lateral LV muscle wall of 11mm. An increased heart weight and dilated LV with/without LV wall thinning are well recognised macroscopic findings in DCM (Basso *et al.*, 2021).

We found three of the four atrial measurements are increased indicating that the atria are dilated in DCM. Bi-atrial enlargement has not been recognised in previous pathology studies. A previous clinical study has identified left atrial enlargement and found it to be a major predictor of SCD. Modena et al, examined a prospective cohort of 123 patients with DCM using clinical evaluation, echocardiography, exercise test and Holter monitoring (Modena *et al.*, 1997). They found that a left atrial size of more than 45mm was the principal independent predictor of prognosis and was associated with a mortality of 54% compared to 29% in those without left atrial dilation. This supports the finding of left atrial dilation in a SCD cohort. Atrial enlargement is a recognised risk factor for the development of atrial fibrillation. Atrial fibrillation is found in 9% of patients with DCM. Untreated permanent AF is an independent predictor of mortality in DCM patients (Nuzzi *et al.*, no date).

We found that most muscle measurements in the RV are increased in thickness. Right ventricular wall thickness increases have not been identified in previous

pathology studies. It has been identified as a feature of DCM in a cardiac resonance imaging study (Vormbrock *et al.*, 2014). They found ventricular remodelling of both ventricles in DCM patients. RV muscle mass was found to be predicted by LV muscle mass and pulmonary artery pressure.

We also found that lateral RV epicardial fat is thicker in DCM. This contrasts with a previous imaging study. Cardiac resonance imaging was used to calculate an epicardial fat mass in DCM patients compared to those with healthy hearts (Doesch *et al.*, 2013). This found a lower amount of epicardial fat mass in DCM patients compared to those with healthy hearts but this was measuring from the base to the apex of the ventricle rather than at the midventricular level.

Fibrosis distribution in DCM

We found a considerable variability in the amount of fibrosis present in our sudden death cohort with only significantly increased fibrosis in the IVS. It has previously been recognised that histological abnormality may appear minimal when compared to functional abnormality in DCM (Davies, 1984). De Leeuw et al, examined 37 end stage failure explant hearts without coronary artery disease and compared them to 35 controls with known cardiac disease (Leeuw *et al.*, 2001). They used Masson's trichrome and scored fibrosis by eye. There was replacement fibrosis in 57% of cases and interstitial fibrosis in 76% of cases also suggesting that a proportion of cases do not show fibrosis.

A previous pathology study of 9 end stage failure DCM hearts has similar results with regard to collagen proportion. Unverferth et al, examined 1 section from the RV, IVS and LV each using Masson's trichrome and point counting (Unverferth *et al.*, 1986). They found an average of 20% fibrosis compared to 4% in controls. There was more

fibrosis in the inner half of the myocardium than the outer half in the LV which is similar to our study. There were higher amounts of fibrosis in the RV in DCM than controls.

A histological study using digital image analysis on end stage explant or autopsy hearts using Masson's trichrome for analysis (Sepehrkhouy *et al.*, 2017). They show collagen levels of 14-20% in DCM cases which is similar to the proportion of collagen that we observed in our cohort. They also showed inner myocardial fibrosis of the LV in broad agreement with our study.

Further supporting our findings of septal collagen increase with a trend towards an increase in the LV free wall in our sudden death cohort, previous imaging studies have shown prognostic implications for fibrosis in this distribution in DCM. Resonance imaging detected septal late gadolinium uptake in large cohort studies of DCM patients, has been associated with the occurrence of SCD particularly when the uptake is present in the midwall and even when the extent is small (Assomull *et al.*, 2006; Halliday *et al.*, 2019). The risk is observed to be further elevated with coexisting free wall involvement.

Similar to our results a biopsy study has shown a decrease in myocyte proportion in DCM. Angelini et al, examined biopsies from 29 clinically diagnosed DCM patients and 30 transplanted hearts seven days post operation (Angelini *et al.*, 1996). They found 20% fibrosis with myocytes making up a proportion of 63% which is similar to the 60% that we observed. We postulate that myocyte proportion is reduced due to the presence of fibrosis but also due to muscle wall thinning in our cohort.

Thrombi are frequently found in DCM particularly within the LV. It is thought that this fibrous endocardial thickening occurs in DCM due to the organisation and

incorporation of old thrombi into the endocardium (Still, 1961; Waller *et al.*, 1995; Gallo, P, D'Amati, 2001).

Comparison to previous histological studies of cardiac innervation

Other histological studies looking at components of the SNS support the loss of innervation. A previous study of individuals with cardiac failure due to Chagas disease, hypertension, valvular disease and DCM used glyoxylic acid-induced fluorescence to identify catecholamines and counted neural structures. Tiocholine was used to identify cholinesterase activity with computer assisted calculation. Rat atria were used as controls. They predominantly studied the atria however 18 ventricular samples were examined for just sympathetic innervation. They quantified 40 microscopic fields. The regions examined are not provided for any of the samples and which ventricle is examined is not specified for 10 specimens. Sympathetic innervation was found to be "absent" in many of their samples. They observed lower levels of both sympathetic and parasympathetic innervation in Chagas affected hearts compared to failure due to other causes (Machado *et al.*, 2000). They also state that denervation was severe in the other failure hearts including non-Chagas related DCM.

Apoptotic pathways are enhanced in cardiac failure which results in myocyte apoptosis (Olivetti *et al.*, 1997). Loss of nerves may occur alongside myocytes as dysfunction progresses which would explain the changes seen in this cardiac failure population. These findings agree with our trend towards denervation discerned in areas of fibrosis in DCM.

A previous study of ganglion cells within DCM primarily looking at cases caused by Chagas disease and specifically looking the posterolateral wall of the right atrium has shown a reduction in these cells compared to normal control hearts (Amorim and Olsen, 1982). A loss of ganglion cells is likely to occur in combination with the loss of nerve bundles and fibrils within the myocardium.

Oki et al, reported on biopsies from 13 older DCM patients with a mean age of 55 from both the LV and RV. The sympathetic innervation was compared to 9 control patients with angina using TH immunohistochemistry. In keeping with our trend, they observed a decrease in sympathetic fibres in the subendocardial myocardium in both the RV and LV compared to individuals with angina (Oki *et al.*, 1994).

Correlation to previous imaging studies

Further supporting the histological findings, sympathetic function assessed by nuclear studies has been shown to correlate with adverse outcomes. Radionucleotide studies have been used to examine the heart utilising 123I-metaiodobenzylguanidine scintigraphy which allows assessment of sympathetic terminal activity. Washout rates, which is the time to loss of contrast enhancement of the heart, are higher when there is lower sympathetic activity. These studies have observed the incidence of SCD is higher in individuals with lower sympathetic activity (Kasama *et al.*, 2012; Chimura *et al.*, 2019). Kasama et al, studied 56 DCM patients with an ejection fraction of greater than 45% for an average of 4.5 years. They found that individuals with late potentials, a predictor of VA, had a higher washout rate (representing a lower sympathetic activity) and furthermore that the incidence of SCD was increased when a higher washout rate was seen in combination with late potentials (Kasama *et al.*, 2012). Chimura et al, reported on 42 DCM patients

following them up for an average of 9 years. They found that higher washout rate in combination with late gadolinium enhancement were an independent predictor of heart failure, VA and cardiac death in DCM patients (Chimura *et al.*, 2019). These findings of lower sympathetic activity support the trend of sympathetic denervation in our sudden death cohort.

Imaging for parasympathetic nerves has not been performed in DCM. A new technique involving the use of 11C-donepezil and photon emission tomography using 11C-donepezil has been proposed to allow the visualisation of parasympathetic denervation (Gjerløff *et al.*, 2014). However, positron emission tomography using methylquinuclidinyl benzilate has been used to calculate muscarinic receptors. DCM was found to be associated with an upregulation of myocardial muscarinic receptors compared to controls (Le Guludec *et al.*, 1997). This is in keeping with our possible trend of increased parasympathetic nerve fibrils.

Correlation to clinical and animal findings

Mildly symptomatic DCM patients have previously been shown to have an attenuated response to exercise using 24-hour Holter monitoring and exercise radionuclide ventriculography indicating an altered autonomic input (Nagaoka *et al.*, 1996). This would support our trend of reduced overall and sympathetic innervation. Sympathetic denervation in DCM may contribute towards decreased contractility and hence failure. Kasama et al, studied the effect of the twelve months of Carvedilol using metaiodobenzylguanidine scintigraphy and echocardiography on 30 DCM patients. They showed improvement in both cardiac sympathetic nerve activity and echocardiographic parameters demonstrating the benefit of beta blockade. This

raises the possibility that sympathetic reactivation/reinnervation could be beneficial in the restoration of function (Kasama *et al.*, 2007).

Increased parasympathetic innervation may play a role in both dysfunction and sudden death. The vagal nerve has previously been targeted as a potential therapy in heart failure. Vagal nerve stimulation was used on a cohort of 87 heart failure patients. There were no improvements in remodelling or function assessed by echocardiography and blood testing in individuals with therapy compared to sham controls however it did show an improvement in quality of life (Zannad *et al.*, 2015). This may be explained by the fact that vagal nerve stimulation appears to be effective as a treatment for depression (Aaronson *et al.*, 2017).

Heart rate, blood pressure and plasma noradrenaline has been monitored in DCM patients at baseline and at peak response during physiological and pharmacological interventions. Prior to cardiac failure DCM patients were found to have impairment of parasympathetic function with no increase in sympathetic activity (Amorim *et al.*, 1981). This suggests that parasympathetic withdrawal precedes sympathetic activation during the development of DCM.

Limitations

The study is limited by its small numbers.

Concluding remarks

This is the first study to delineate, describe and autonomously quantify ventricular innervation in DCM and the first to objectively autonomously quantify fat and fibrosis using picrosirius red in pathologically diagnosed DCM hearts.

There are a number of macroscopic changes including an increase in heart weight, bi-atrial dilation, thickening of the RVOT, anterior and posterior RV muscle walls, dilation of the LV and thinning of the lateral LV muscle wall. Lateral RV subepicardial fat is thicker.

There is increased collagen in the IVS of DCM hearts representing fibrosis. There is an overall loss of myocyte proportion in DCM hearts.

General and sympathetic innervation are lower than within the normal heart in all areas examined but this does not reach significance. There is a significant reduction in general innervation in the RVOT when it shows fibrosis.

Loss of myocytes and innervation may both contribute to the reduction of ventricular function that is observed clinically in DCM.

Summary of findings in DCM

Macroscopic

- Heart weight is increased
- Both atria are dilated
- The RV is not dilated
- The RV muscle walls are thickened
- The LV is dilated
- Lateral LV muscle wall is thinned
- No differences in LV muscle wall elsewhere
- Lateral RV epicardial fat is thicker
- No differences in epicardial fat measurements elsewhere

Microscopic findings in DCM ventricular subepicardial fat and myocardium

- Collagen is increased in the septum but not elsewhere

- Myocytes are reduced overall
- There is a non-significant trend towards a reduction in general innervation
- The RVOT has reduced general innervation in sections showing fibrosis
- There is a non-significant trend towards a reduction in sympathetic innervation
- No difference in parasympathetic innervation

CHAPTER 8 HYPERTROPHIC CARDIOMYOPATHY

Introduction

In chapter 5, we established the composition of the normal ventricular myocardium and its innervation. In this chapter, we examine whether there are differences in tissue composition and innervation in HCM compared to the normal heart.

HCM is present in 1 in 500 people (Maron *et al.*, 1995; Semsarian *et al.*, 2015). It is a common cause of SCD in the young (Finocchiaro *et al.*, 2019). The condition is clinically characterised by increased LV wall thickness which is not explained by abnormal loading conditions (Veselka, Anavekar and Charron, 2017). HCM is a heritable condition caused predominately by mutations in the sarcomeric proteins (Sabater-Molina *et al.*, 2018). Many individuals with HCM are asymptomatic and therefore it is frequently first diagnosed following sudden death (Finocchiaro *et al.*, 2019).

Methods

HCM decedents with suitable retained tissue are identified from a library of 931 cases (see figure 2.15). As stated in the methods, HCM is diagnosed on the basis of myocyte disarray present in over 20% of two sections of the midwall of the LV away from the septal-free wall junctions. Supporting features are an increase in heart weight, asymmetric LV hypertrophy and a subaortic impact lesion. Cases with a history of heart failure, coexisting conditions which may have contributed to death, valvular disease, significant coronary disease and hypertensive disease are excluded. Exactly as with the normal hearts, sections from the RVOT, the RV free wall (including the anterior, lateral and posterior wall), the IVS, as well as the anterior and posterior left ventricular free wall are stained with PSR, PGP9.5, TH and CT.

Positive and negative controls are utilised. Slides are scanned using a Hamamatsu Nanozoomer 2.0RS. Digital image analysis is performed using applications developed within the Visiopharm program (Visiopharm A/S, Agern Alle 24, 2970 Hørsholm, Denmark).

Statistics

Differences between groups are assessed using log transformed values for collagen, fat, myocyte, PGP9.5, TH and CT proportions (as these values are skewed). A multilevel model is created to allow comparison of hierarchical dependent data based on myocardial location. Variables such as age, sex and ethnicity are incorporated into multivariable analysis. Predictions of collagen, fat, myocytes, PGP9.5, TH and CT are expressed as geometric means and 95% confidence intervals.

Statistical analyses used Stata version 16 (StataCorp, College Station, Texas, USA).

Results

Seventeen cases of HCM with retained tissue are identified. The age at death is 37±17years comprising 13 males and 4 females. The heart weight is 522±151g. At cardiac examination, 16 cases show LV wall thickening. One case does not show LV wall thickening but shows macroscopic fibrosis. There is RV wall thickening in 4 cases.

Ten cases show asymmetric LV wall thickening with two of these also showing RV wall thickening. Of ten cases with asymmetric LV wall thickening macroscopic fibrosis is present in 2 cases.

Symmetrical LV wall thickening is present in 6 cases with 2 of these also showing RV wall thickening. Of 6 cases with symmetrical LV wall thickening there is macroscopically identified fibrosis in 4 cases.

An impact lesion with corresponding thickening of the anterior leaflet of the mitral valve is noted in 7 (figure 8.1).

The dimensions of the atria, ventricle muscle wall thickness and diameters, valve circumferences and subepicardial fat measurements are provided in table 8.1 and compared to controls.

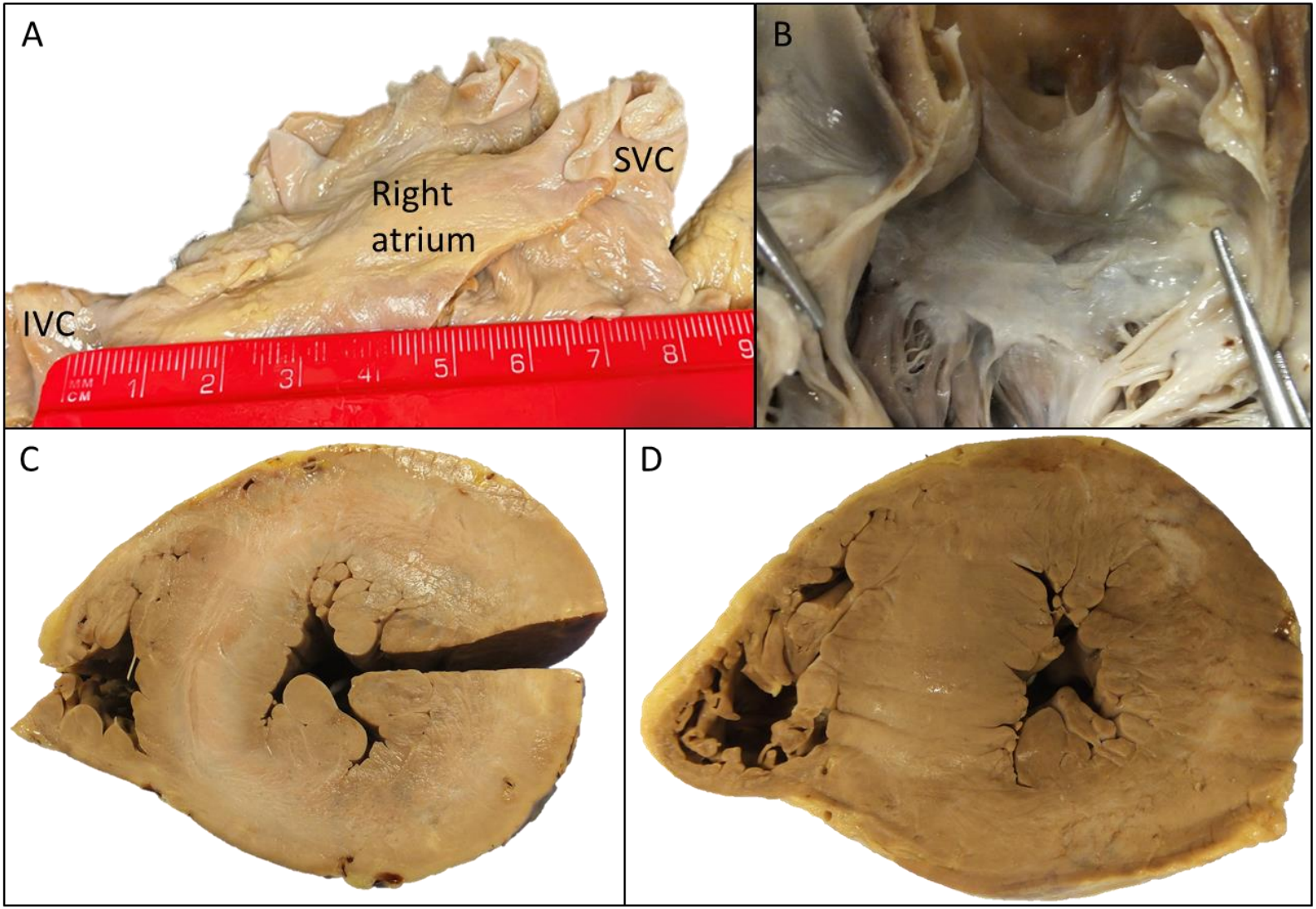


Figure 8.1. Gross findings. A) Right atrial enlargement. B) Impact lesion. Symmetrical (C) and asymmetrical septal hypertrophy (D).

	HCM	Control	P value	Validation of significant findings in wider HCM cohort (n=304)
Heart weight	**522±151**	**364±63**	**.003**	**553±182, P<0.01**
Right atrium 1	**71±26**	**54±14**	**.045**	**65±17, p=0.04**
Right atrium 2	53±18	41±9	.063	
Left atrium 1	48±14	40±8	.112	
Left atrium 2	45±15	36±8	.090	
RV diameter	27±8	32±6	.115	
Anterior RV Muscle	4±1	3±1	.099	
Lateral RV Muscle	4±1	3±1	.153	
Posterior RV Muscle	**4±1**	**3±1**	**.002**	4±2, p=0.1
RVOT Muscle	**4±1**	**3±1**	**.002**	**4±1, p<0.01**
LV diameter	29±8	33±6	.145	
IVS	**19±6**	**13±3**	**.004**	**20±6, p<0.01**
Anterior LV Muscle	**16±4**	**12±2**	**.009**	**17±4, p<0.01**
Lateral LV Muscle	**15±4**	**13±2**	**.041**	**16±4, p=0.01**
Posterior LV Muscle	**14±3**	**12±2**	**.027**	**16±4, p<0.01**
Mitral valve	73±17	83±16	.100	
Tricuspid valve	99±21	103±17	.560	
Pulmonary valve	54±7	55±12	.700	
Aortic valve	50±7	55±9	.101	
Ascending aorta	52±9	57±8	.156	
Anterior RV fat	1±1	1±1	.890	
Lateral RV fat	2±3	2±1	.380	
Posterior RV fat	0±1	0±0	.977	
RVOT fat	1±1	1±1	.441	
Anterior LV fat	1±3	1±1	.696	
Lateral LV fat	0±1	0±0	.415	
Posterior LV fat	0±1	0±1	.376	

Table 8.1. Macroscopic heart measurements for hypertrophic cardiomyopathy compared to normal hearts. The means and standard deviations for heart weight (in grams), atrial dimensions, cavity diameters, muscular wall thickness, valvular and ascending aortic circumferences and epicardial fat thickness (in millimetres) are provided. Significant structural changes have been examined in the overall HCM cohort to allow it to serve as a validation cohort.

The HCM macroscopic measurements are compared to controls. There is an increase in heart weight (522±151g vs 364±63g, $p<0.01$).

The distance between the inferior caval vein ostium and the tip of the right atrial appendage is increased (71±26g vs 54±14g, $p<0.05$). The remaining atrial measurement do not show significant increases.

The posterior RV (4±1g vs 3±1g, $p<0.01$) and RVOT (4±1g vs 3±1g, $p<0.01$) muscular walls are thickened. The remaining RV measurements do not show significant thickening.

The IVS muscular wall is thickened (19±6 vs 13±3, $p<0.01$). The anterior (16±4g vs 12±2g, $p<0.01$), lateral (15±4g vs 13±2g, $p=0.04$) and posterior (4±1g vs 3±1g, $p=0.03$) LV muscular walls are thickened.

There are no significant changes in epicardial fat thickness.

The increase in heart weight, increase in right atrial size, increase in right ventricular muscle wall thickness and increase in left ventricular muscle wall thickness have been further validated in the wider HCM cohort (table 8.1).

Correlation between measurements

The correlations between measurements are shown in table 8.2. From the variables that were significantly different than the normal heart there are significant strongly positive correlations between heart weight and LV free wall muscle thickness measurements. This means that as LV free wall thickness increases heart weight also increases (figure 8.2). There is a significant moderate positive correlation between RVOT and posterior RV muscle wall thickness meaning that as the RVOT muscle increases, the posterior RV muscle wall also increases (figure 8.2). There are also significant strongly positive correlations between anterior and lateral LV

muscle wall thickness and lateral and posterior LV wall thickness suggesting that the LV free wall enlarges together (figure 8.3). There is a significant moderate positive correlation between RVOT muscle wall thickness and interventricular septal wall thickness meaning that these measurements increase in tandem (figure 8.3). There is a significant positive moderate correlation between posterior RV and LV muscle wall thickness meaning that the two measurements enlarge in tandem (figure 8.3). There were no other significant correlations between measurements that were significantly different from the normal heart.

		1	2	3	4	5	6	7	8	9	10	11	12	13	14	15	16	17	18	19	20	21	22	23	24	25	26
1	Heart weight																										
2	Anterior RV muscle wall	-.19																									
3	Lateral RV muscle wall	.07	.48																								
4	Posterior RV muscle wall	.39	.35	.55*																							
5	RVOT muscle wall	.47	.06	.34	.56*																						
6	Interventricular septum	.42	.12	-.03	.26	.50*																					
7	Anterior LV muscle wall	.71**	-.17	-.09	.4	.39	.48																				
8	Lateral LV muscle wall	.67**	.16	.01	.45	.46	.26	.68**																			
9	Posterior LV muscle wall	.66**	.21	.27	.50*	.36	.23	.44	.77**																		
10	RV anterior epicardial fat	.31	-.24	.07	-.23	.07	-.2	-.05	.07	.14																	
11	RV lateral epicardial fat	.16	.49*	.46	.01	.09	-.06	-.29	.25	.50*	.36																
12	RV posterior epicardial fat	-.21	-.07	.33	-.13	.	-.17	-.41	-.4	-.28	-.22	.09															
13	RVOT epicardial fat	.51*	.14	.47	.05	.15	.16	.08	.31	.58*	.42	.61*	.27														
14	LV anterior epicardial fat	.54*	.25	.26	.50*	.13	.39	.47	.47	.60*	-.16	.17	.11	.53*													
15	LV lateral epicardial fat	-.01	.15	.28	.1	.1	-.05	.05	-.07	.3	-.02	.08	-.14	.13	-.07												
16	LV posterior epicardial fat	.12	.04	.41	.22	.17	.14	.22	-.08	.21	-.26	-.08	.32	.32	.32	.74**											
17	Right atrium 1	.12	-.05	.27	.02	-.24	-.34	-.22	-.1	.17	.19	.47	-.02	.15	-.2	.09	-.1										
18	Right atrium 2	.09	0	.28	.	-.04	-.41	-.43	0	.33	.31	.70**	.15	.28	-.06	.05	-.17	.73**									
19	Left atrium 1	-.07	-.41	-.21	.15	-.09	.12	.06	-.31	-.4	-.4	-.62*	.23	-.41	.19	-.4	-.04	-.2	-.16								
20	Left atrium 2	.23	.23	.37	.09	-.08	-.28	-.38	.11	.46	.25	.79**	.18	.5	.19	.06	-.07	.69**	.91**	-.22							
21	Diameter of RV chamber	.16	.51*	.14	-.04	-.26	.03	-.06	.15	.35	.28	.48	-.02	.59*	.51*	.05	.03	-.1	.02	-.44	.28						
22	Diameter of LV chamber	.29	-.50*	-.18	.17	.06	-.06	.4	.16	-.2	-.14	-.56*	.13	-.16	0	-.44	-.08	.01	-.33	.41	-.32	-.4					
23	Mitral valve circumference	.2	-.09	-.18	.1	-.26	-.02	.05	.3	.37	.11	.25	-.23	.14	.44	-.33	-.26	.21	.38	.35	.5	.15	-.05				
24	Tricuspid annulus circumference	.38	-.44	-.04	.05	-.27	.05	.27	.04	.25	-.04	.04	.08	.17	.38	-.09	.18	.52*	.3	.38	.32	-.11	.29	.57*			
25	Pulmonary valve circumference	.38	-.25	.08	.17	0	.08	.02	.12	.21	-.18	.16	.4	.27	.42	-.44	-.09	.38	.48	.52*	.55*	-.16	.32	.61*	.70**		
26	Aortic circumference	.19	-.3	-.02	-.18	-.21	-.37	-.32	-.08	.12	.29	.34	.47	.37	.08	-.29	-.2	.46	.60*	-.03	.64**	.16	.18	.22	.39	.59*	
27	Ascending aorta circumference	.37	-.2	.05	.01	-.04	-.32	-.2	.16	.36	.31	.49	.3	.39	.15	-.23	-.24	.57*	.74**	-.11	.78**	.15	.12	.31	.39	.64*	.93**

*Table 8.2. Correlations between variables in HCM. Significant strong correlations are highlighted in red and significant moderate correlations are highlighted in yellow. There were correlations between heart weight and LV wall thicknesses, between RV wall thicknesses, between the RVOT thickness and intraventricular septum thickness, between LV wall thicknesses and between posterior RV and posterior LV wall thicknesses (*p<.05, **p<.01).*

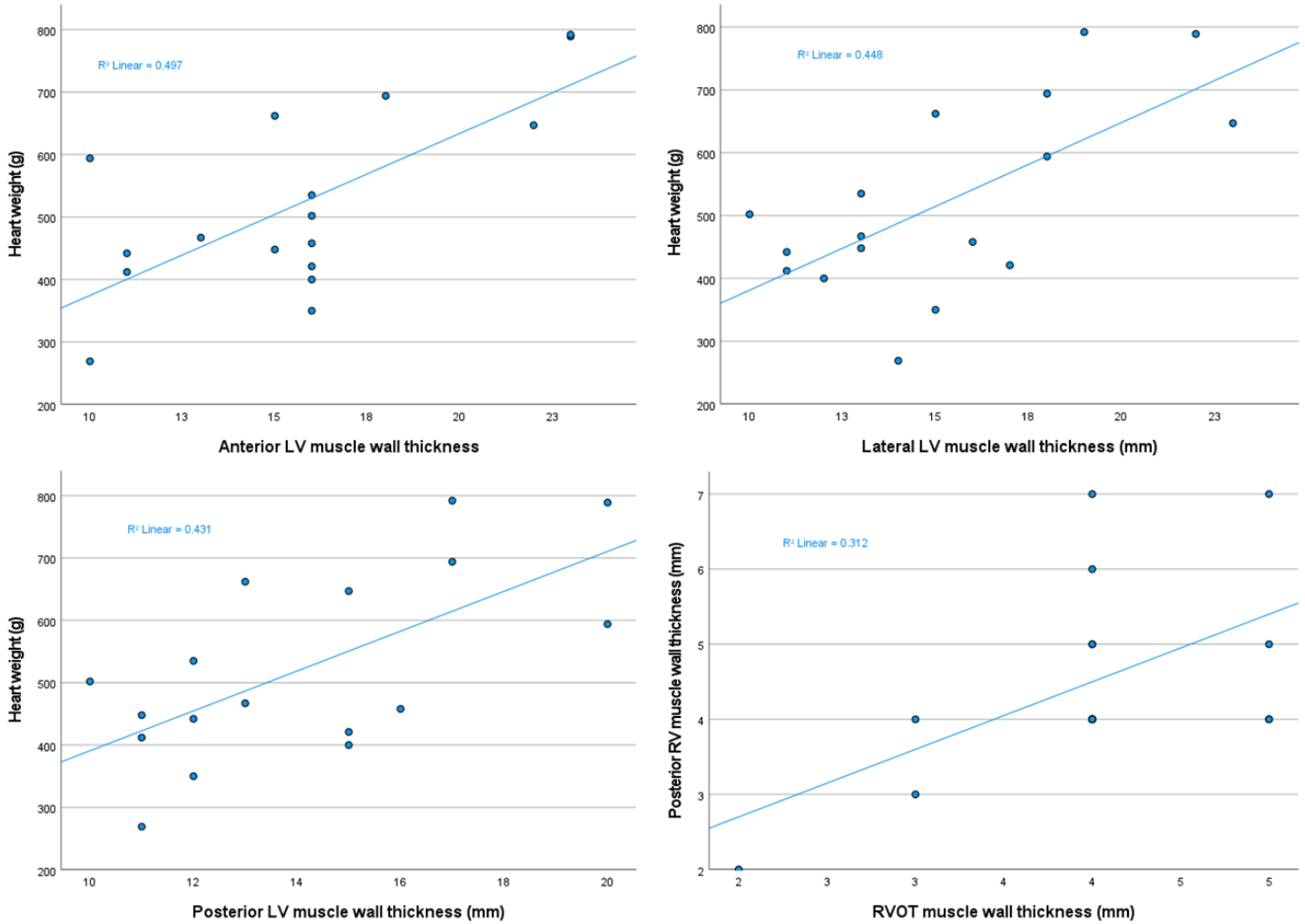


Figure 8.2. Plots of heart weight against LV free wall thicknesses and of posterior RV wall and RVOT wall thicknesses. LV free wall increases in thickness with increases in heart weight. Posterior RV and RVOT wall thicknesses increase together.

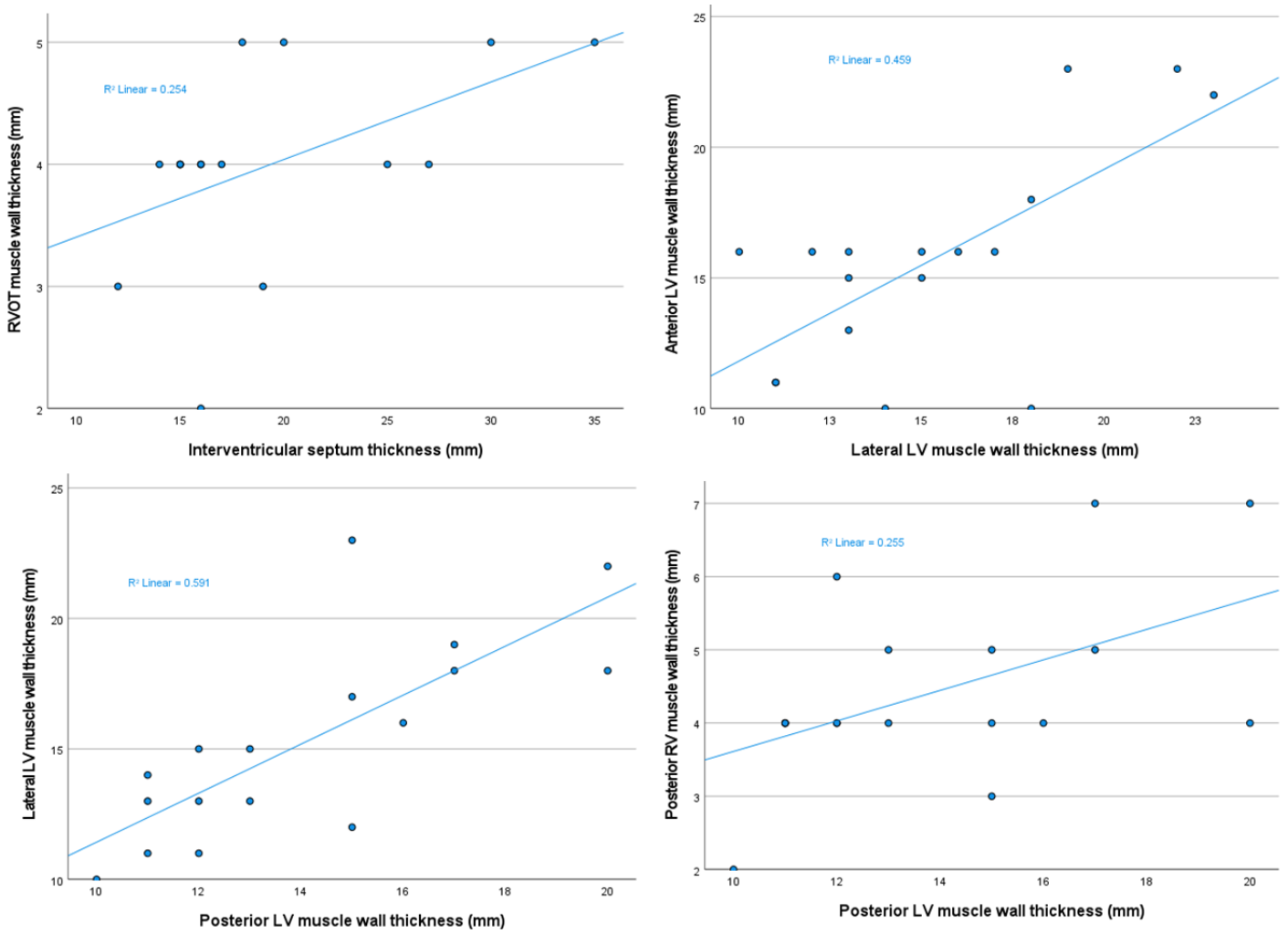


Figure 8.3 Plots of RVOT against intraventricular septum and LV free wall thicknesses against each other. The RVOT an intraventricular septum increase in thickness together. The LV free muscle wall measurements increase together.

Ventricular myocardium compositional analysis

Collagen

There is considerable variation in the amount and location of fibrosis in HCM hearts (figure 8.4-8.8).

The ventricular myocardium shows extensive interweaving networks of interstitial fibrosis in the LV (figure 8.7 and 8.8). Within the LV, the meshwork of interstitial fibrosis connects with patchy replacement fibrosis (figure 8.7). Within the anterior and posterior LV, the fibrosis is either distributed transmurally or within the inner and midwall of the LV (figure 8.7). The fibrosis ranges from focal interstitial fibrosis to extensive replacement fibrosis occupying much of the myocardium. The fibrosis is never present in solely at the junction between the subepicardial fat and outer myocardium. Similarly, in the IVS the myocardium shows an extensive interweaving network of interstitial fibrosis with large areas of replacement fibrosis which are distributed transmurally (figure 8.6). The fibrosis in the IVS is most prominent in the midwall and ranges from focal areas to extensive replacement fibrosis occupying much of the myocardium (figure 8.6). Both interstitial and replacement fibrosis are present away from areas of disarray.

Interstitial fibrosis is always present in areas of myocyte disarray. Interstitial fibrosis fills the spaces produced by the disarrayed myocytes (figure 8.9). This produces a deranged interstitial pattern with an irregular web-like pattern which is readily detected on picrosirius red stain (figure 8.7-8.9). Myocyte disarray is also present around patches of replacement fibrosis (figure 8.10). The sections with lots of myocyte disarray show more extensive interstitial and replacement fibrosis than those with some or no disarray.

Within the LV free wall inner myocardium, there are long continuous stretches of extensive interstitial fibrosis interconnecting with small patches of replacement fibrosis and extending into the trabeculae and papillary muscles (figure 8.11). The trabeculae and papillary muscles show large areas of replacement fibrosis (figure 8.12).

The RV and RVOT show variation in the presence and extent of fibrosis. The RV ranges from appearing normal to transmural interstitial fibrosis with large areas of replacement fibrosis (figure 8.5). The trabeculae of the RV show large patches of replacement fibrosis (figure 8.5). The RVOT ranges from appearing normal to transmural interstitial and small areas of replacement fibrosis (figure 8.4). The sections with lots of myocyte disarray show more extensive interstitial and replacement fibrosis than those with some or no disarray.

Collagen coalesces around vessels within the myocardium of both ventricles and is particularly prominent in areas of fibrosis (figure 8.13).

The endothelial collagen layer showed an increase in thickness on one side of the IVS in 3 cases (figure 8.14).

Fat

The fat is present in the same locations and in similar amounts described in the normal heart. The fat is predominantly distributed between the epicardium and myocardium of the RV free wall, RVOT and the anterior LV free wall. A thin layer of subepicardial fat is sometimes present on the posterior LV. Within the myocardium, fat is present around large vessels. Fatty infiltration of the myocardium in the absence of a large vessel is frequent in the RV and RVOT consisting of single adipocytes up to a whole sheet. Frequently, the fat appears proportionally less

compared to the normal heart due an increase in myocardial area. Admixed fat is seen in large areas of dense replacement fibrosis in the IVS and anterior LV in two cases, and in the posterior LV in one case. The fat within the fibrosis is never present at the intersection between the subepicardial fat and the myocardium.

Myocytes

Both the RV and LV myocardium are thickened in HCM. Wall thickening is more marked in the LV.

The myocytes in HCM frequently show florid disorganisation and are orientated in a haphazard fashion representing myocyte disarray. Areas of myocyte disarray can be patchy and lie next to normally arranged myocytes. There is both disarray of the bundles of myocytes and of the individual myocytes themselves (figure 8.9). Myocyte disarray is present throughout the heart in HCM. This is most frequent and florid in the IVS. The IVS and LV show lots of disarray whereas the RV and RVOT show a more variable appearance. The RV and RVOT range from no disarray to extensive transmural disarray.

Areas of disarray are embedded within interstitial fibrosis plugging the gaps between the myocytes. Replacement fibrosis is seen within and around areas of myocyte disarray.

Myocytes show frequent hypertrophied forms throughout the myocardium, most prominent around areas of replacement fibrosis (figure 8.15). There is nuclear enlargement of the myocytes (figure 8.15). Within the individual myocytes, particularly within areas of disarray there is splaying and disorganisation of the myofibrils (figure 8.15).

Loss of myocytes is patchy throughout the myocardium and present in both the outer and inner wall in a randomly distributed fashion. There is considerable variation in the size of the areas of myocyte loss ranging from small areas within a network of interstitial fibrosis to large areas occupying most of the myocardium (figures 8.4, 8.6). There is loss of myocytes within the trabeculae and papillary muscles.

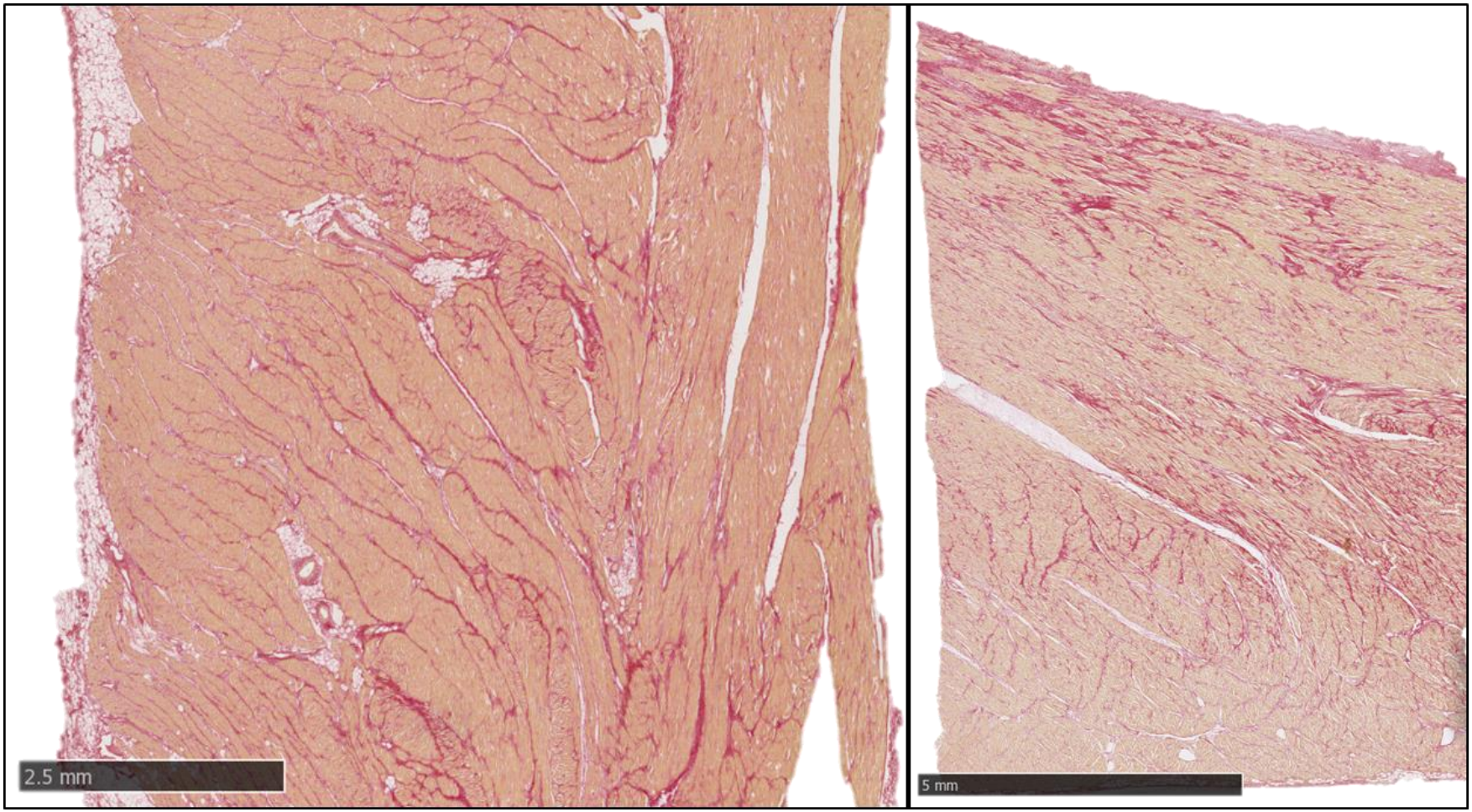


Figure 8.4. The right ventricular outflow tract shows interstitial fibrosis and small patches of replacement fibrosis which appears more prominent around vessels and is present transmurally.

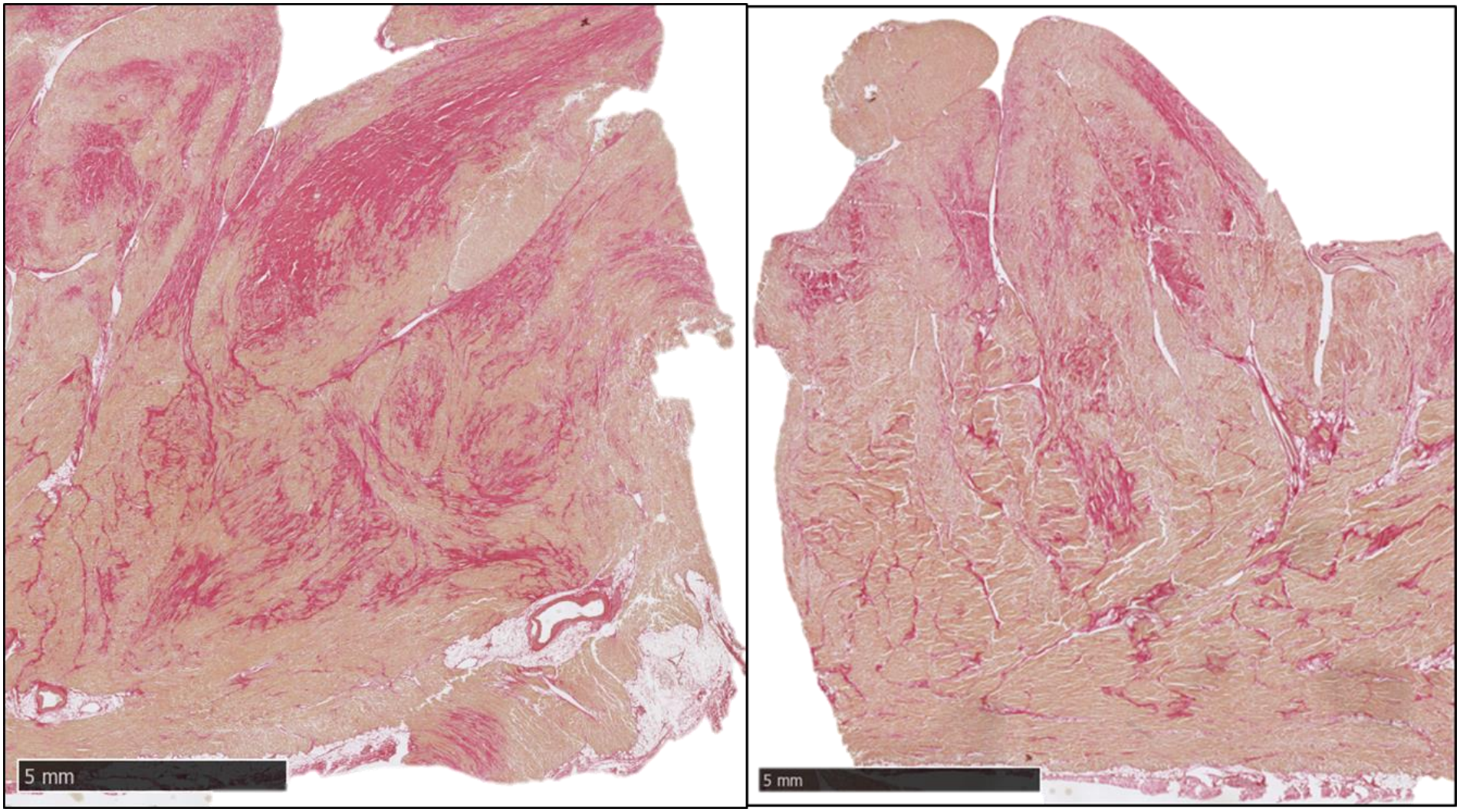


Figure 8.5. The right ventricle shows patchy replacement and interstitial fibrosis which affects the wall and trabeculae.

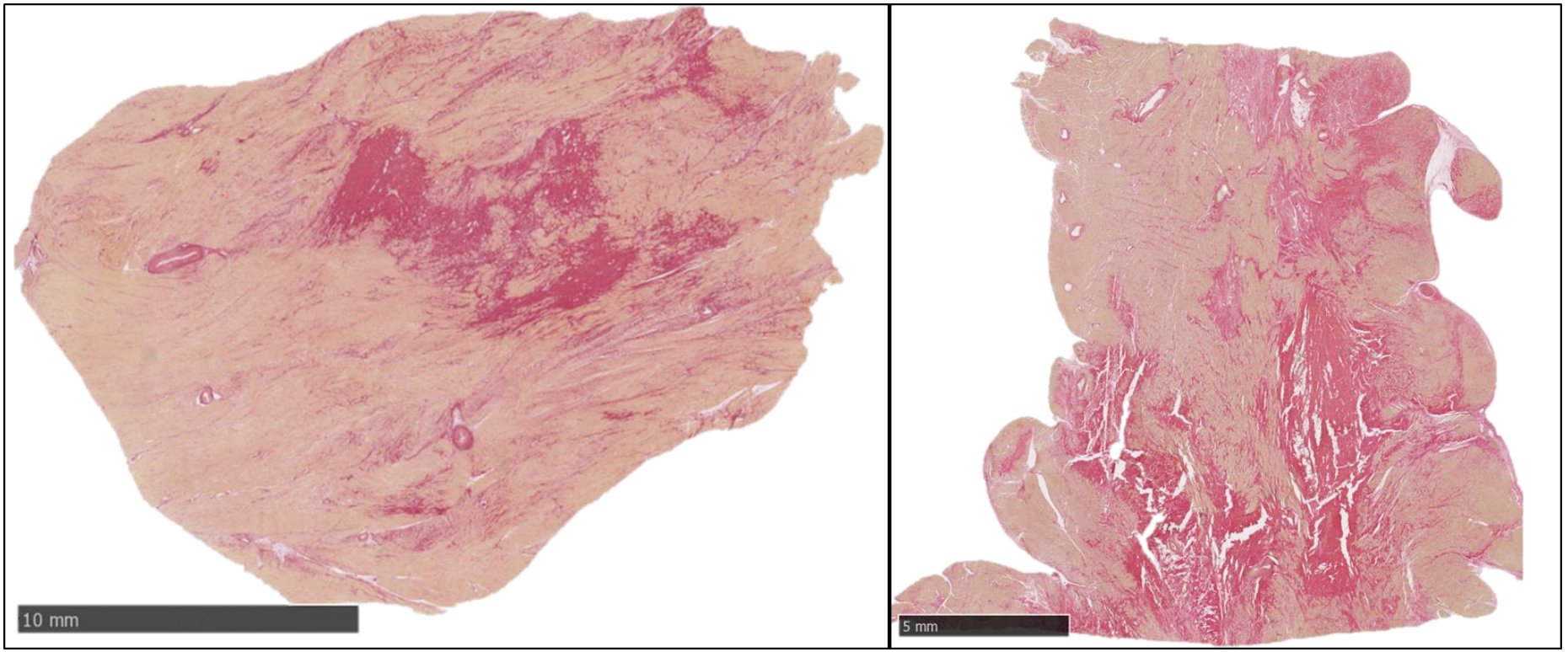


Figure 8.6. The septum shows patches of replacement fibrosis which are randomly distributed throughout the wall and interlinked by interstitial fibrosis.

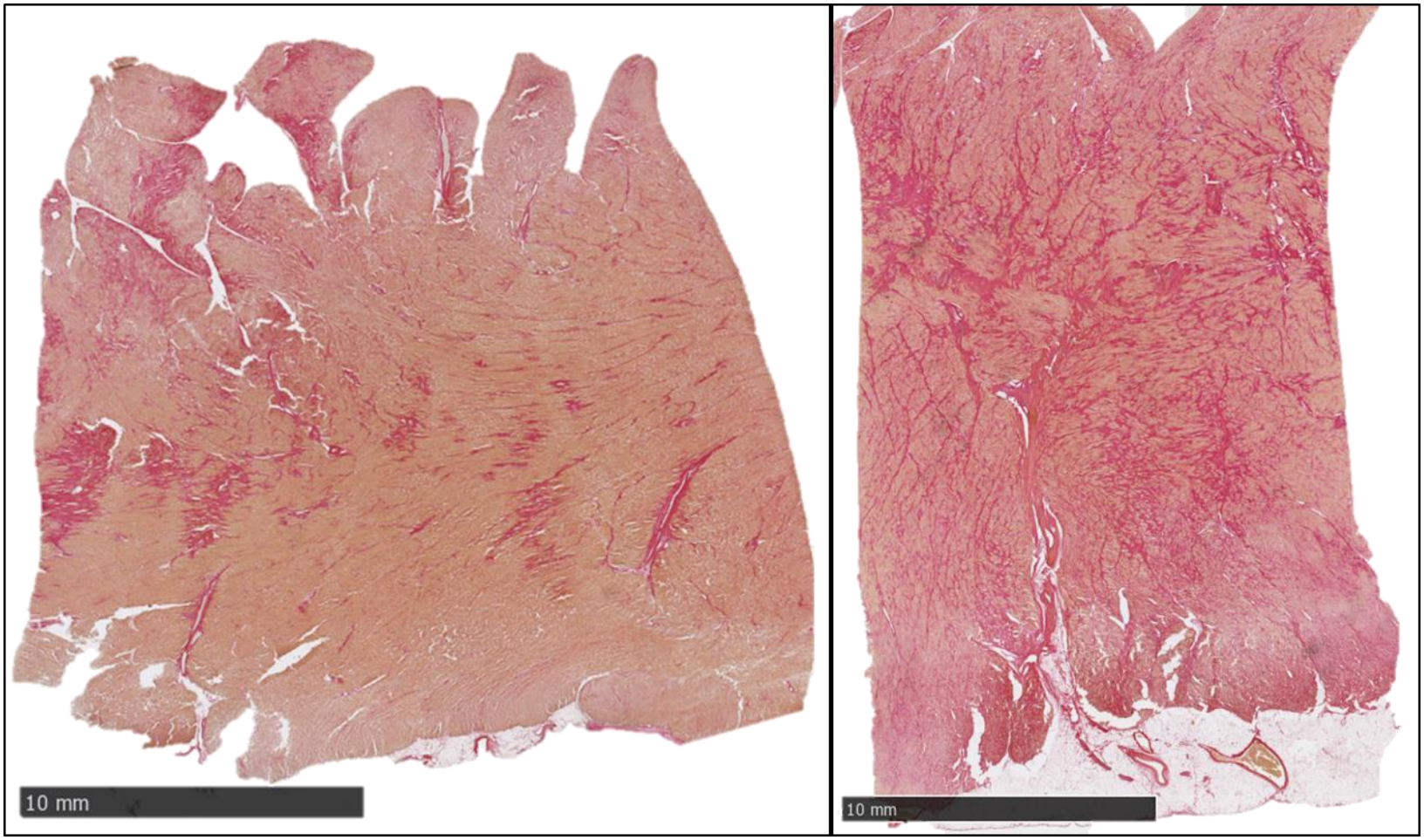


Figure 8.7. The anterior left ventricle shows variable involvement ranging from randomly distributed patchy replacement fibrosis with interstitial fibrosis to full thickness interstitial and replacement fibrosis.

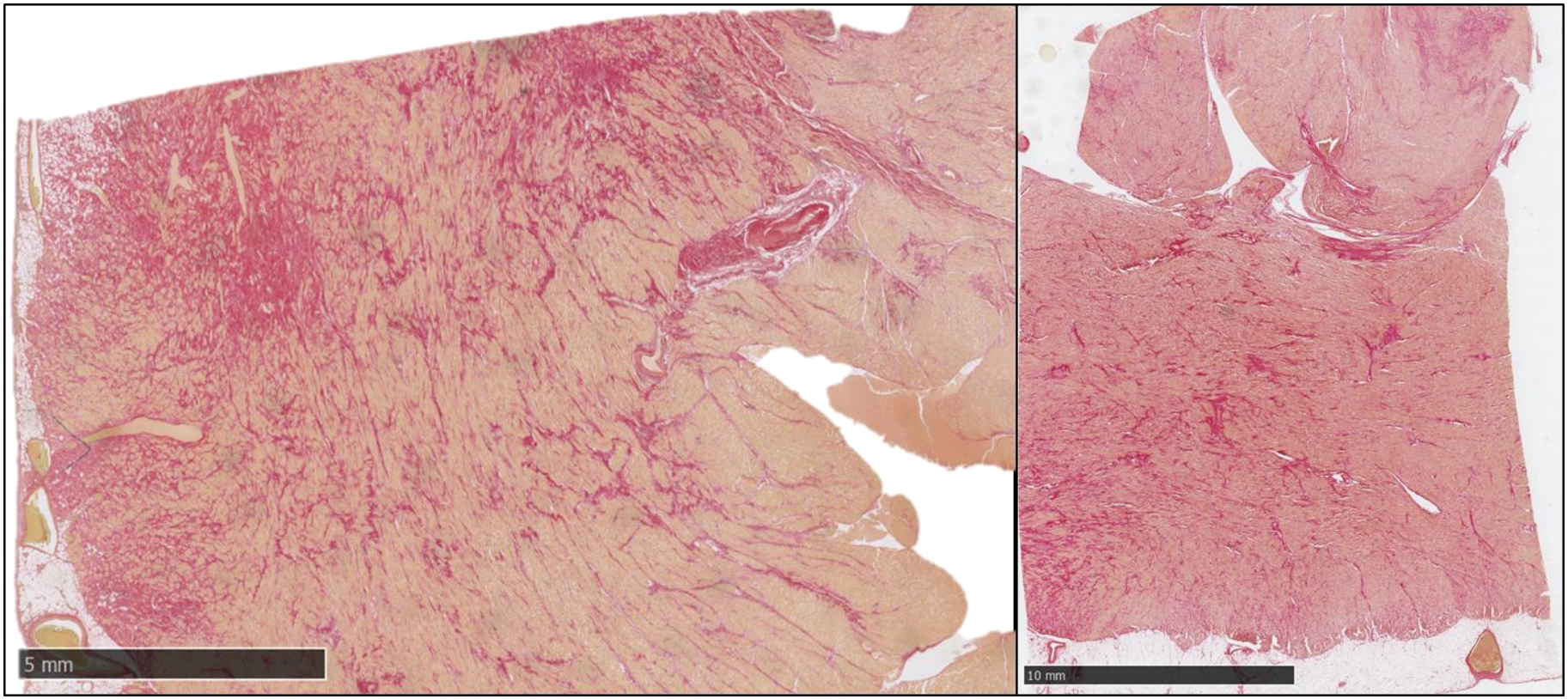


Figure 8.8. The posterior left ventricle showed full thickness interstitial fibrosis which interconnected with randomly distributed patchy replacement fibrosis.

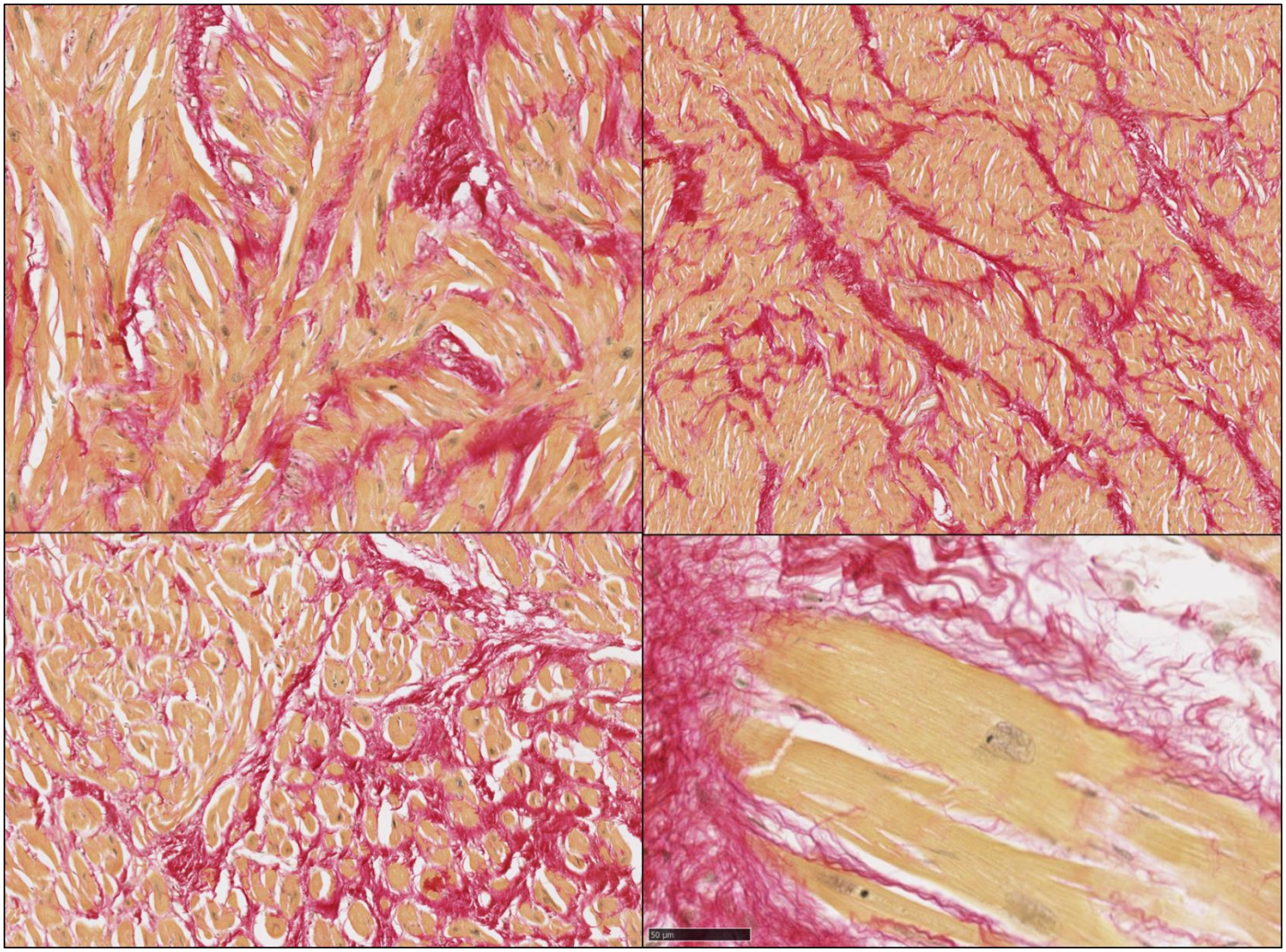


Figure 8.9. Myocyte disarray and hypertrophy. The myocytes show individual and bundle disarray with hypertrophy. Not increased collagen in areas of disarray.

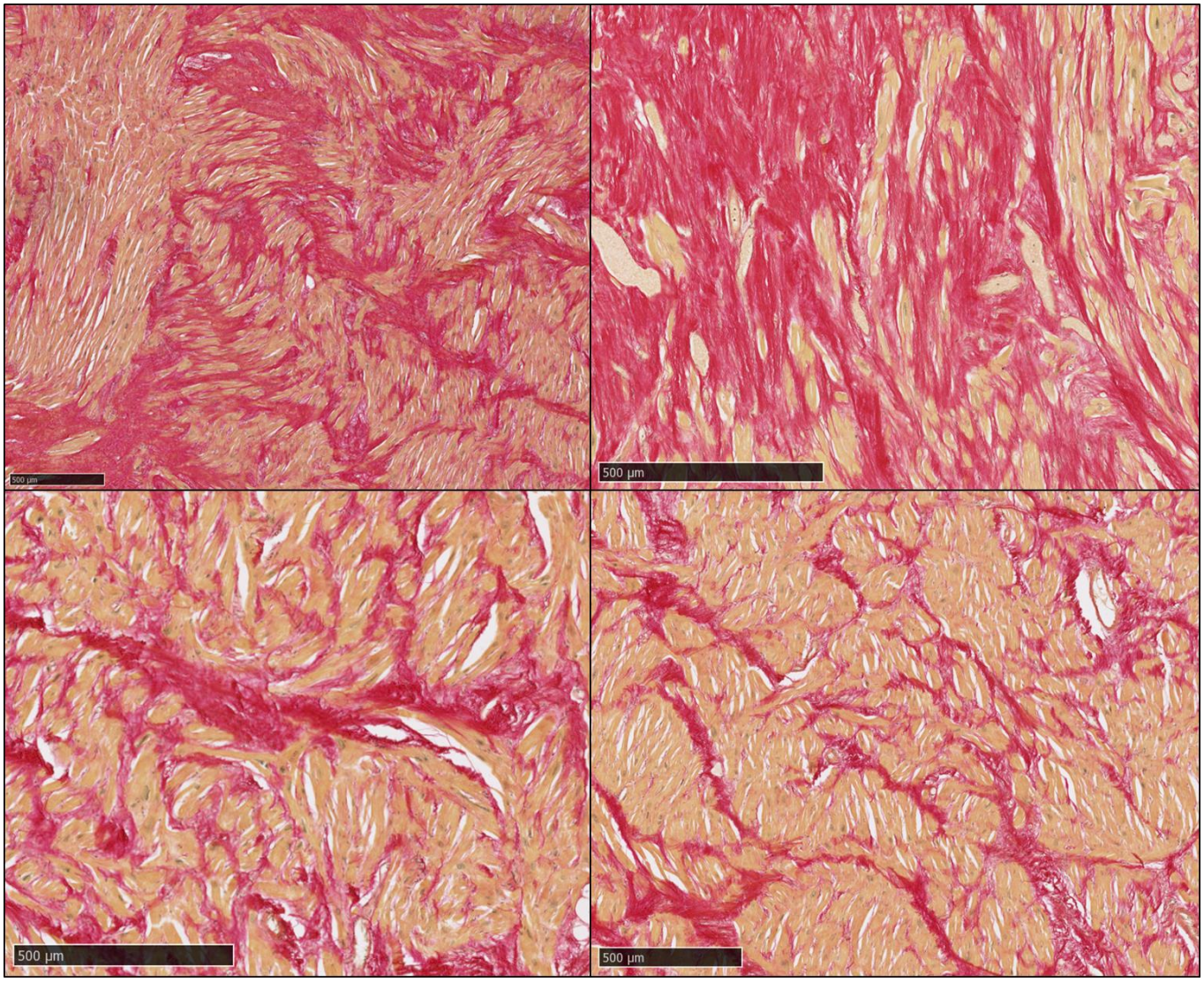


Figure 8.10. Myocyte disarray and fibrosis. Myocyte disarray with interstitial and replacement fibrosis.

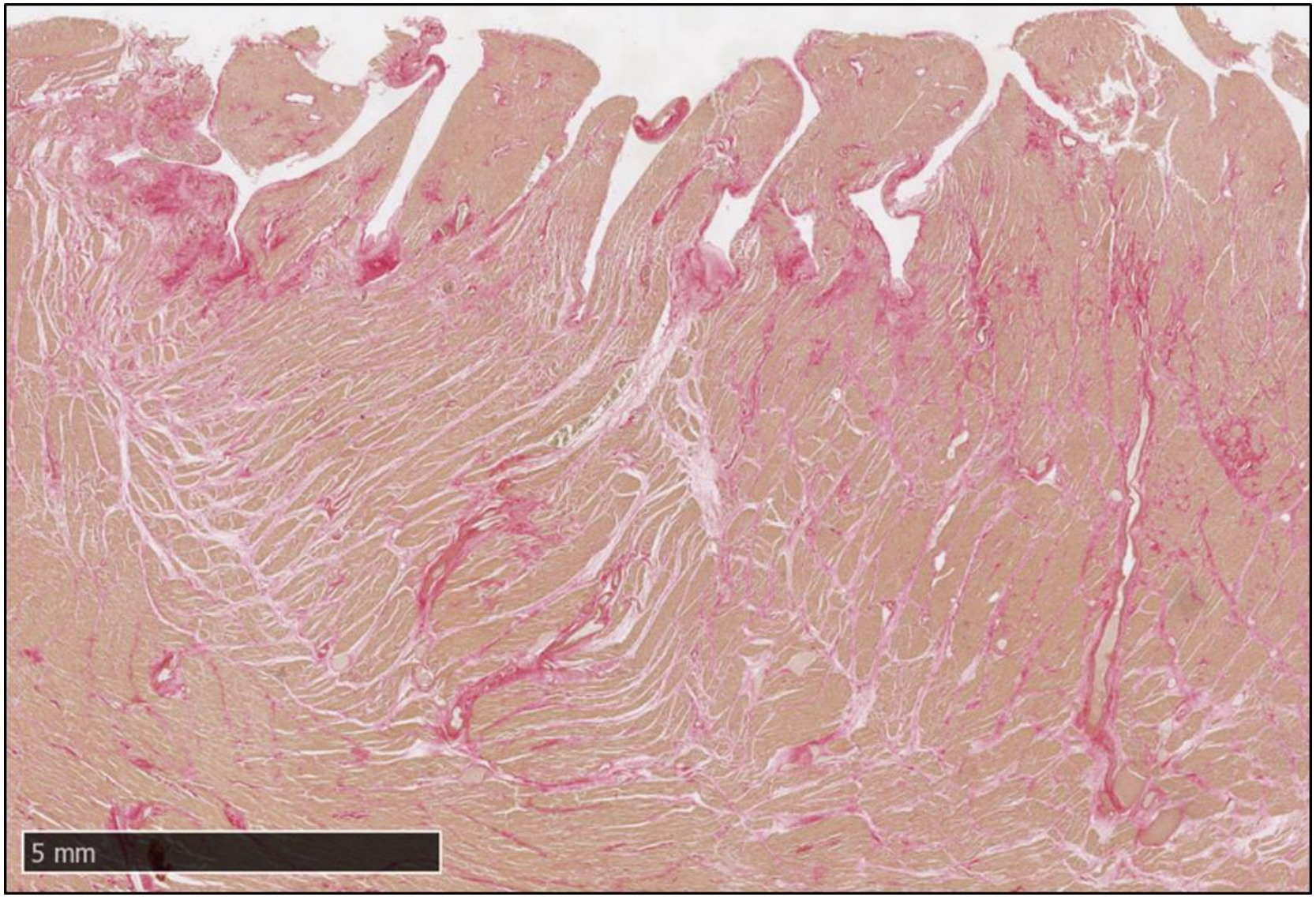


Figure 8.11. Interstitial fibrosis extends around in continuous stretches in the inner myocardium.

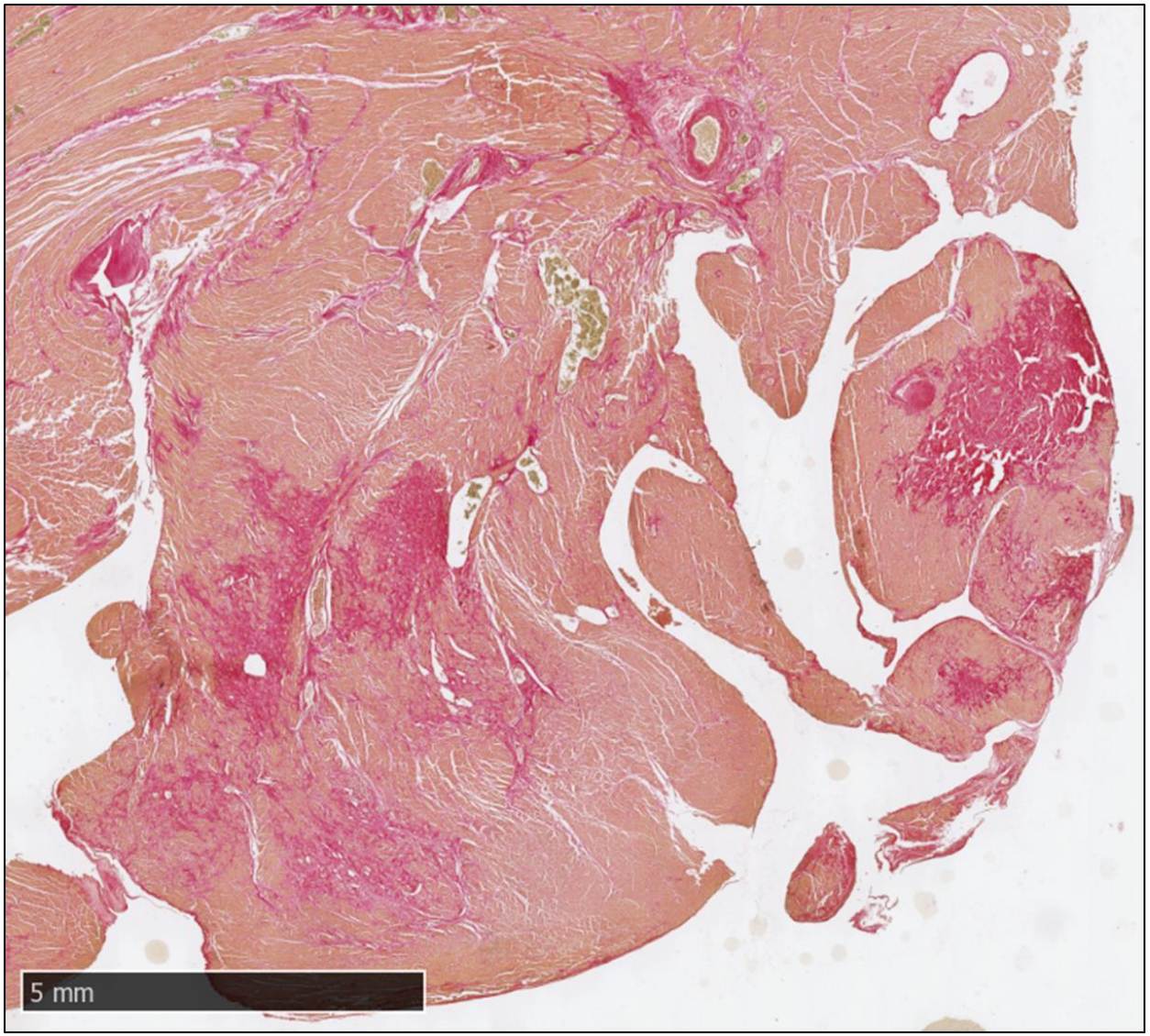


Figure 8.12. There is replacement fibrosis within the trabeculae and papillary muscles in HCM.

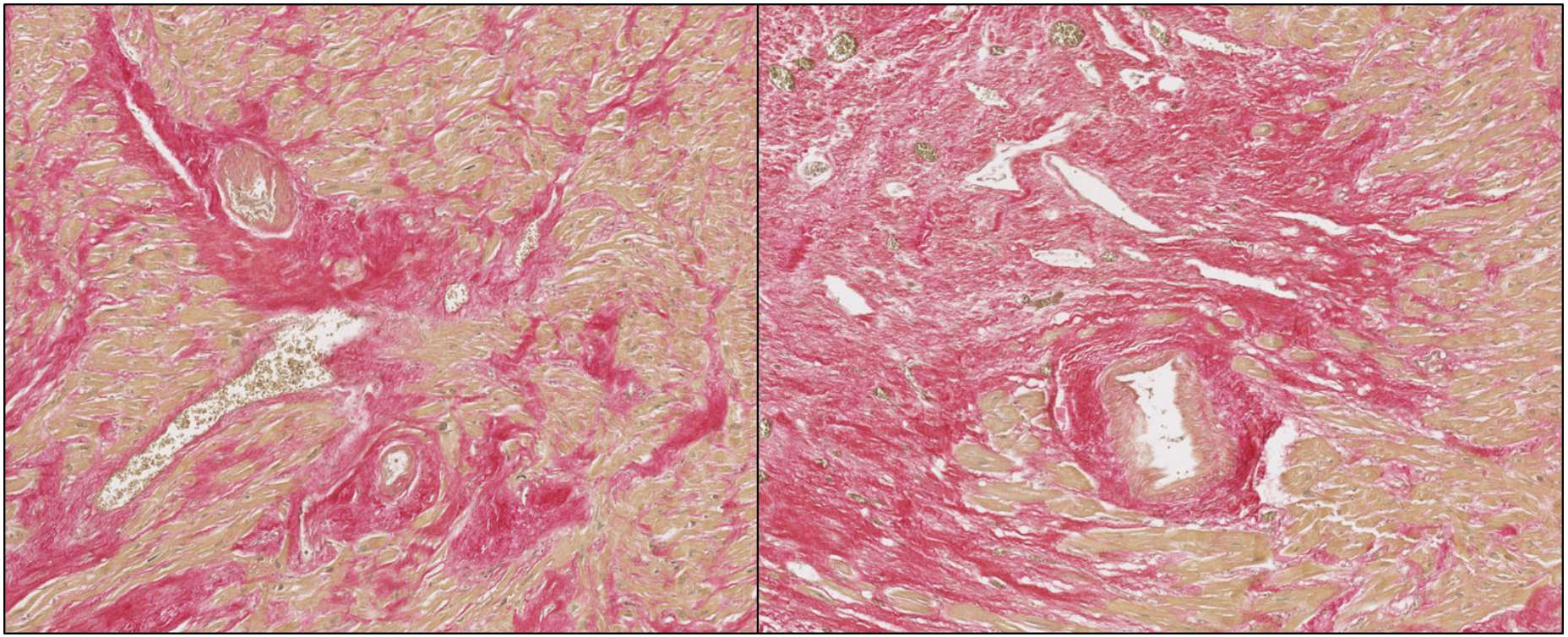


Figure 8.13. Collagen around vessels in hypertrophic cardiomyopathy.

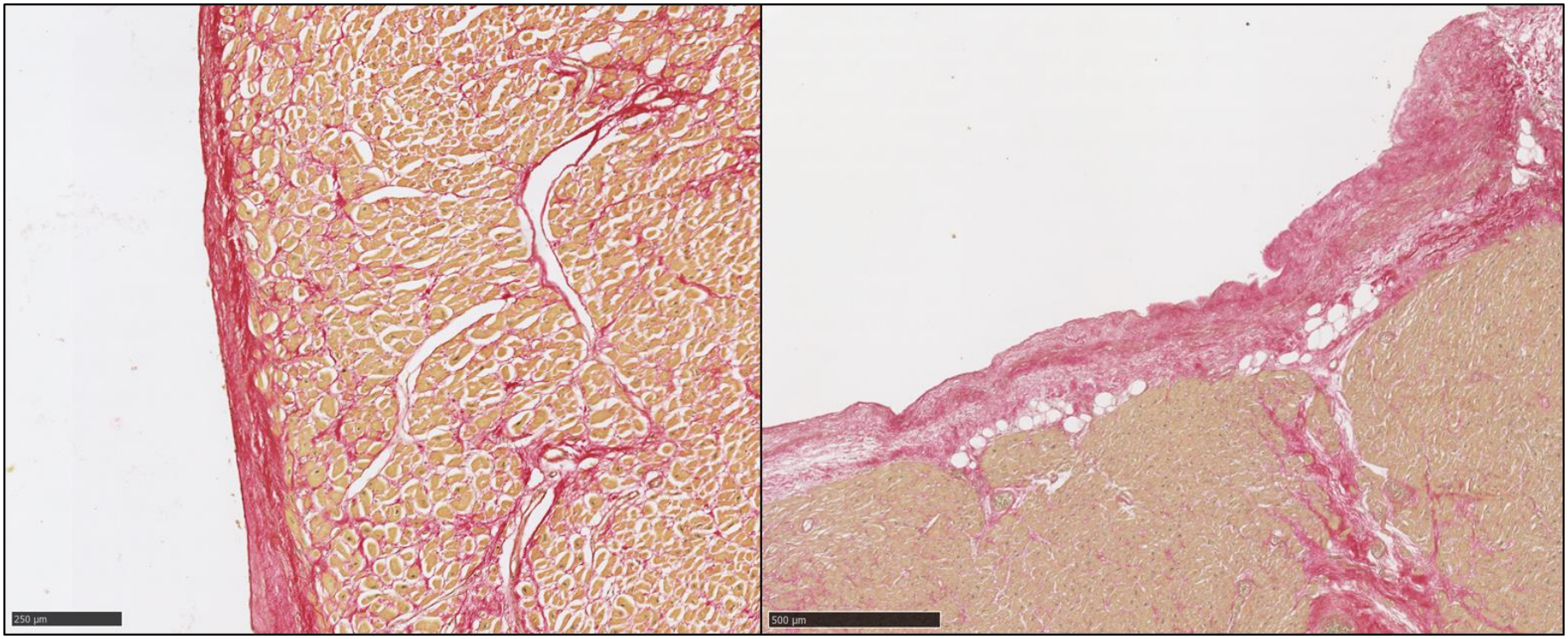


Figure 8.14. The endocardial collagen shows thickening in hypertrophic cardiomyopathy. Fat is seen within the endocardial collagen.

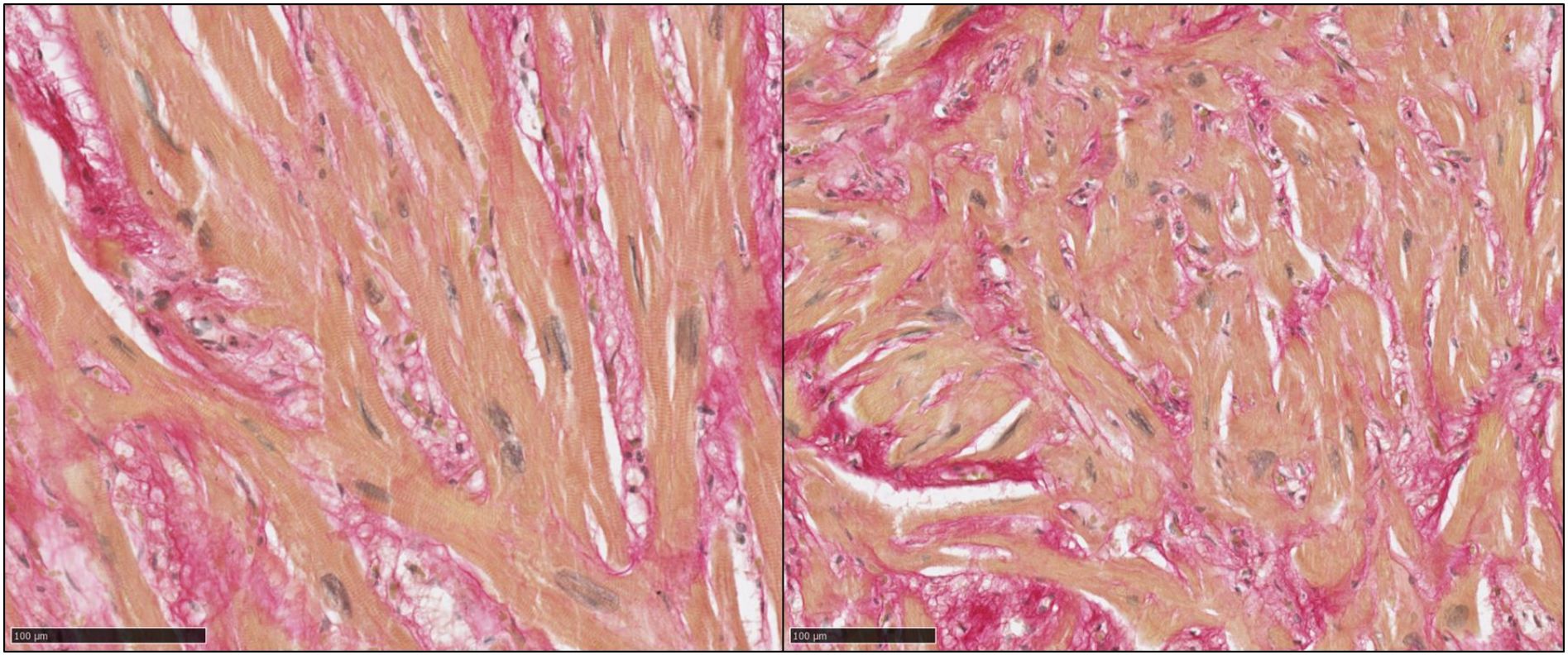


Figure 8.15. Nuclear enlargement and splaying with disorganisation of the myofibrils within myocytes is frequently present in areas of disarray in hypertrophic cardiomyopathy.

Quantitative analysis

Collagen

There is an overall increase in collagen in HCM compared to the normal heart (ratio 2.48, 95%CI 1.22-5.04, p=0.01). There are increases in collagen in the IVS (ratio 3.4, 95%CI 1.6-7.5, p<0.01), anterior LV (ratio 3.3, 95%CI 1.5-7.1, p<0.01) and posterior LV (ratio 2.5, 95%CI 1.1-5.4, p=0.02) in HCM compared to controls. The RVOT and RV show 23-24% collagen compared to controls which show 11% and 15% respectively but this is not significant.

Fat

As with the normal heart, there are differences in the proportion of fat between regions. The RV shows 10%, the RVOT shows 7% and the anterior and posterior LV and the IVS shows 2-4%. There is no significant difference between the proportion of fat in the HCM hearts and controls.

Myocytes

There is a significant reduction in the proportion of myocytes overall in the HCM heart (ratio 0.7, 95%CI 0.6-0.9, p<0.01). There is a significant reduction in the proportion of myocytes in the IVS (ratio 0.7, 95%CI 0.5-0.9, p<0.01), the anterior LV (ratio 0.7, 95%CI 0.5-1.0, p=0.03) and the posterior LV (ratio 0.8, 95%CI 0.6-1.0, p<0.05). The RVOT and RV show 54-56% myocytes compared to 71-72% in the normal heart but this does not reach significance.

The proportions for collagen, fat and myocytes in HCM and controls are shown in table 8.3 and figure 8.16.

Component	Condition	HCM		Control	
	Region	Expected	95% CI	Expected	95% CI
Collagen	All	**26.50**	**19.30-36.37**	**10.70**	**7.217-15.86**
	RVOT	23.16	16.29-32.90	11.15	7.24-17.15
	RV	23.93	16.84-34.00	14.60	9.49-22.46
	IVS	**28.61**	**20.13-40.65**	**8.39**	**5.45-12.90**
	ALV	**30.90**	**21.74-43.91**	**9.45**	**6.14-14.53**
	PLV	**26.66**	**18.76-37.87**	**10.87**	**7.06-16.71**
Fat	All	4.50	3.54-5.71	5.89	4.37-7.92
	RVOT	7.24	5.15-10.16	9.83	6.44-14.99
	RV	10.09	7.19-14.17	10.23	6.70-15.60
	IVS	1.77	1.26-2.49	2.43	1.59-3.70
	ALV	4.30	3.06-6.04	7.78	5.10-11.87
	PLV	3.31	2.35-4.64	3.72	2.43-5.67
Myocytes	All	**57.29**	**52.02-63.09**	**76.97**	**68.26-86.77**
	RVOT	55.90	49.50-63.12	71.76	61.69-83.45
	RV	54.34	48.12-61.36	71.31	61.31-82.94
	IVS	**58.95**	**52.20-66.56**	**85.72**	**73.69-99.69**
	ALV	**56.57**	**50.09-63.88**	**76.65**	**65.90-89.15**
	PLV	**60.92**	**53.95-68.79**	**80.33**	**69.06-93.42**

Table 8.3. Predicted proportions (geometric mean and confidence interval) of the ventricular myocardium made up by collagen, fat and myocytes for hypertrophic cardiomyopathy (HCM) and controls. The proportions are given for the right ventricular outflow tract (RVOT), right ventricular free wall (RV), interventricular septum (IVS), anterior and posterior left ventricle (ALV and PLV).

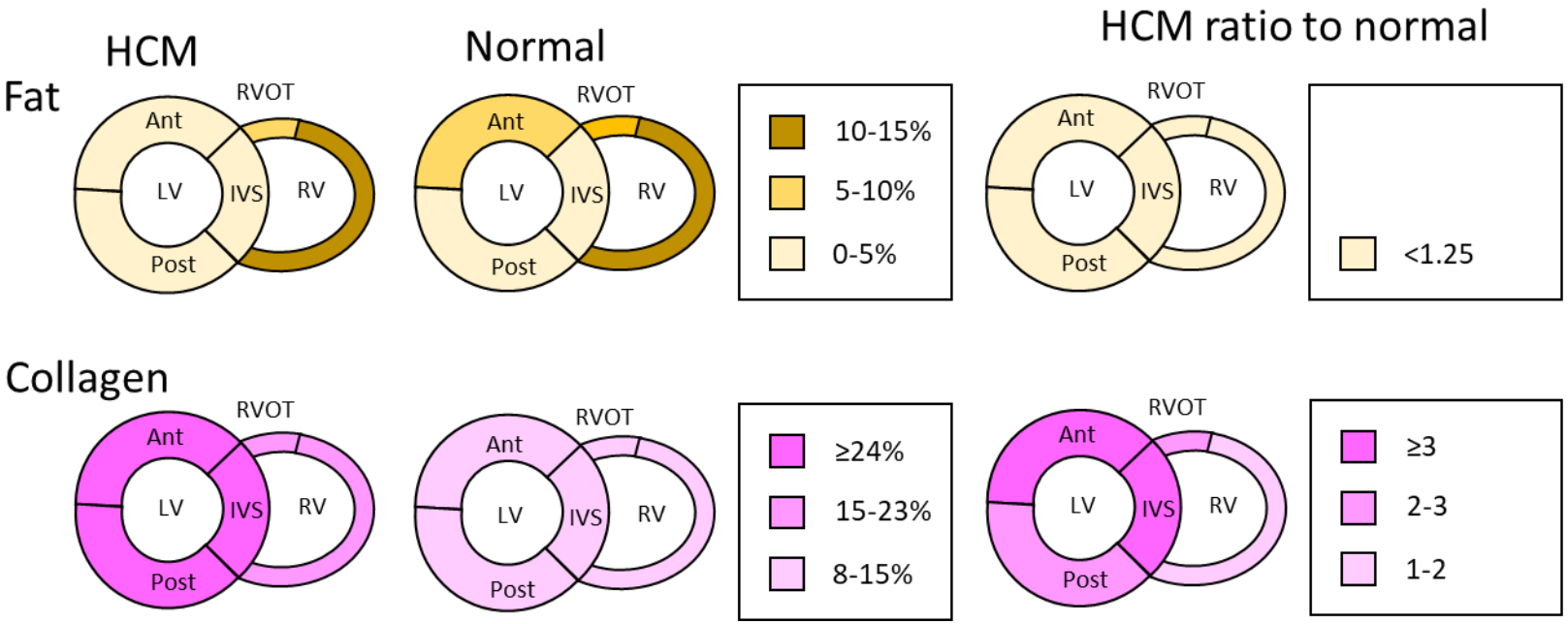


Figure 8.16. Percentage and ratio of fat and collagen in the hypertrophic cardiomyopathy (HCM) heart ventricular myocardium compared to normal. The values are given for the right ventricle (RV), right ventricular outflow tract (RVOT), interventricular septum (IVS), the anterior left ventricle (LV) and the posterior left ventricle. There is more collagen in the left ventricle in HCM.

Innervation of the ventricular myocardium

General innervation

Within HCM, the distribution of nerves is similar to the normal heart (figure 5.33). Within the subepicardial fat, there are few large nerve bundles (figure 8.17 and 8.18). They are associated with the coronary arteries and large vessels in the fat lying in and around the adventitia. They are also independent of the vessels between adipocytes within the subepicardial fat. The nerve bundles extend from the subepicardial fat into the myocardium and remain associated with blood vessels lying in the perivascular adipose tissue. Within the myocardium, there are few large nerve bundles in the myocardium which are most prominent in the outer myocardium. The nerve bundles become gradually smaller and divide. The small nerve bundles are located transmurally but most prominently in the inner myocardium. There are few small nerve bundles in the epicardial half of the myocardium. The nerve bundles remain in close association with blood vessels initially coursing in the adipose tissue and then adjacent to the smaller vessels. Individual fibrils extend between, lie parallel to and adjoin individual myocytes throughout the myocardium. The fibrils are more common in the inner myocardium. The fibrils are also alongside and adjoining small vessels. They are present in the endocardium. No ganglia are present in the ventricular myocardium.

Within areas of interstitial fibrosis, fewer large and smaller nerve bundles are present. Small individual nerve fibrils are frequent and are embedded in the network of interstitial collagen adjacent to myocytes (figure 8.19). In the patches of replacement fibrosis, there are few large and small nerve bundles. Frequent granular staining individual nerve fibrils are present within replacement fibrosis (figures 8.18-8.19). In areas of disarray within the interstitial fibrosis there are few large or small

large nerve bundles. There are frequent individual nerve fibrils present within areas of myocyte disarray present within the interstitial fibrosis(figure 8.20).

Sympathetic innervation

TH showed a similar distribution to the normal heart, away from areas of altered pathology, staining a percentage of fibres within the nerve bundles located in the epicardial fat. There are few large and small nerve bundles in the epicardial fat. They are also always associated with vessels moving in from the epicardium to the myocardium (figure 8.21). Within the myocardium, there are few large and small nerve bundles. The large nerve bundles are mainly present in the outer half of the myocardium. The small nerve bundles are present transmurally and most prominent in the inner half of the myocardium. Small individual nerve fibrils are most frequently present alongside and adjoining small vessels but also in association with myocytes. There are few individual nerve fibrils in the inner myocardium (figure 8.22). Fibrils are also present in the endocardium. Within areas of fibrosis, TH stained many small individual nerve fibrils within areas of both interstitial and replacement fibrosis. As interstitial fibrosis is frequently admixed with myocyte disarray, the fibrils are frequent in areas of disarray. There are few large and small nerve bundles in areas of disarray. The fibrils are frequently present within interstitial fibrosis adjacent to myocytes and small vessels. Individual nerve fibrils are present within areas of replacement fibrosis. Individual nerve fibrils are frequent within the midwall with few seen in the inner wall.

Parasympathetic innervation

CT showed a similar distribution to the normal heart away from areas of altered pathology. There is only occasional focal staining within fibres in the subepicardial fat. There are few small nerve bundles in the outer myocardium. The small nerve bundles are present transmurally in association with vessels but also independently within the myocardium. Small individual nerve fibrils are frequent and show a granular staining pattern (figure 8.22). The fibrils are present throughout the myocardium. There are many individual nerve fibrils in the midwall. The individual nerve fibrils are intricately associated with, adjoin and lie on the surface of myocytes. To a lesser degree, they are also closely associated with and adjoining small vessels. The fibrils are also present in the endocardium. The fibrils are frequent within areas of interstitial fibrosis (figure 8.23). They lie within the mesh-like collagen network adjoining and intricately associated with the myocytes. Individual nerve fibrils are frequently present in areas of myocyte disarray within the interstitial fibrosis. There are frequent individual nerve fibrils present in areas of replacement fibrosis.

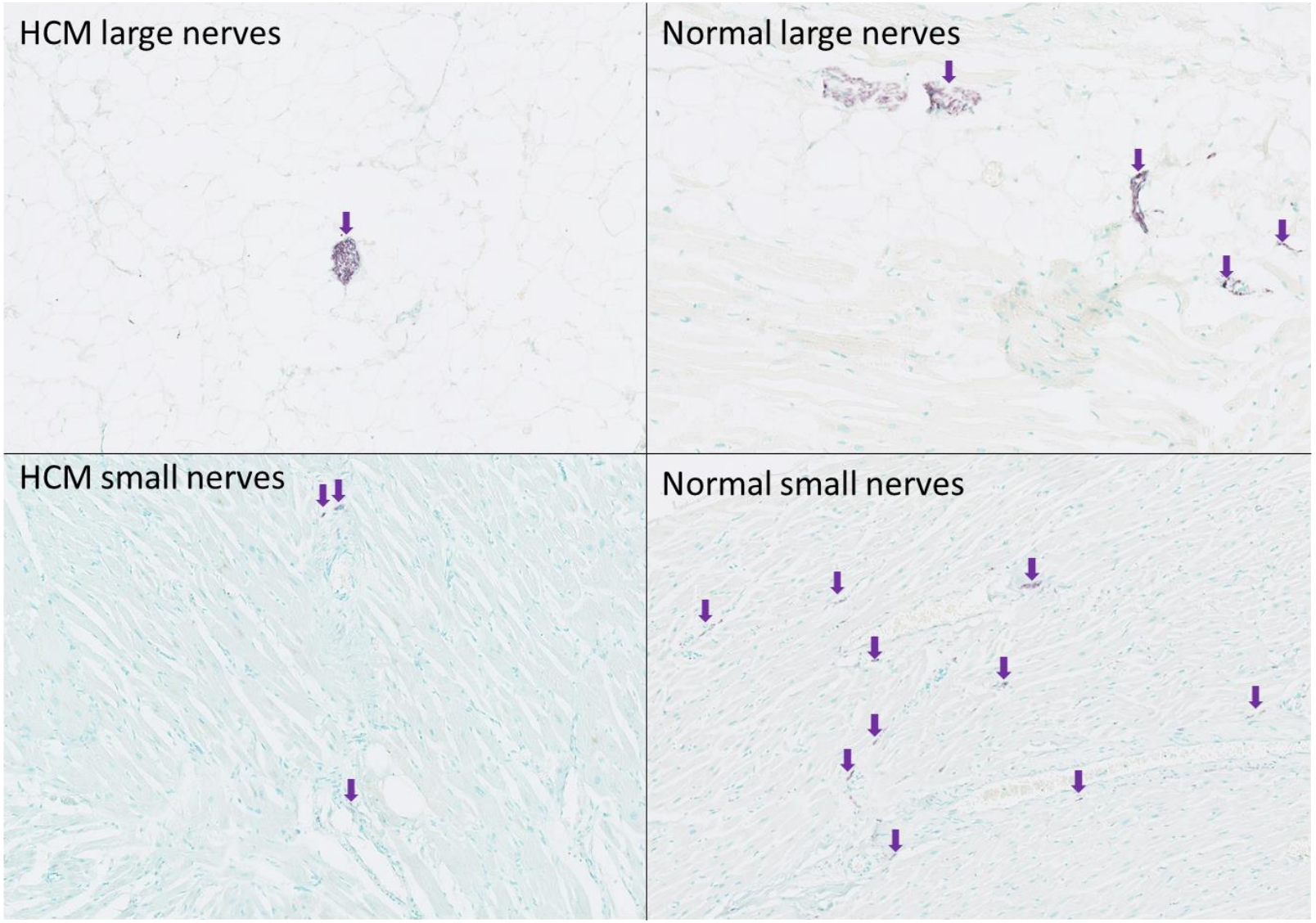


Figure 8.17. Few PGP9.5 staining (purple arrows) large and small nerve bundles in hypertrophic cardiomyopathy.

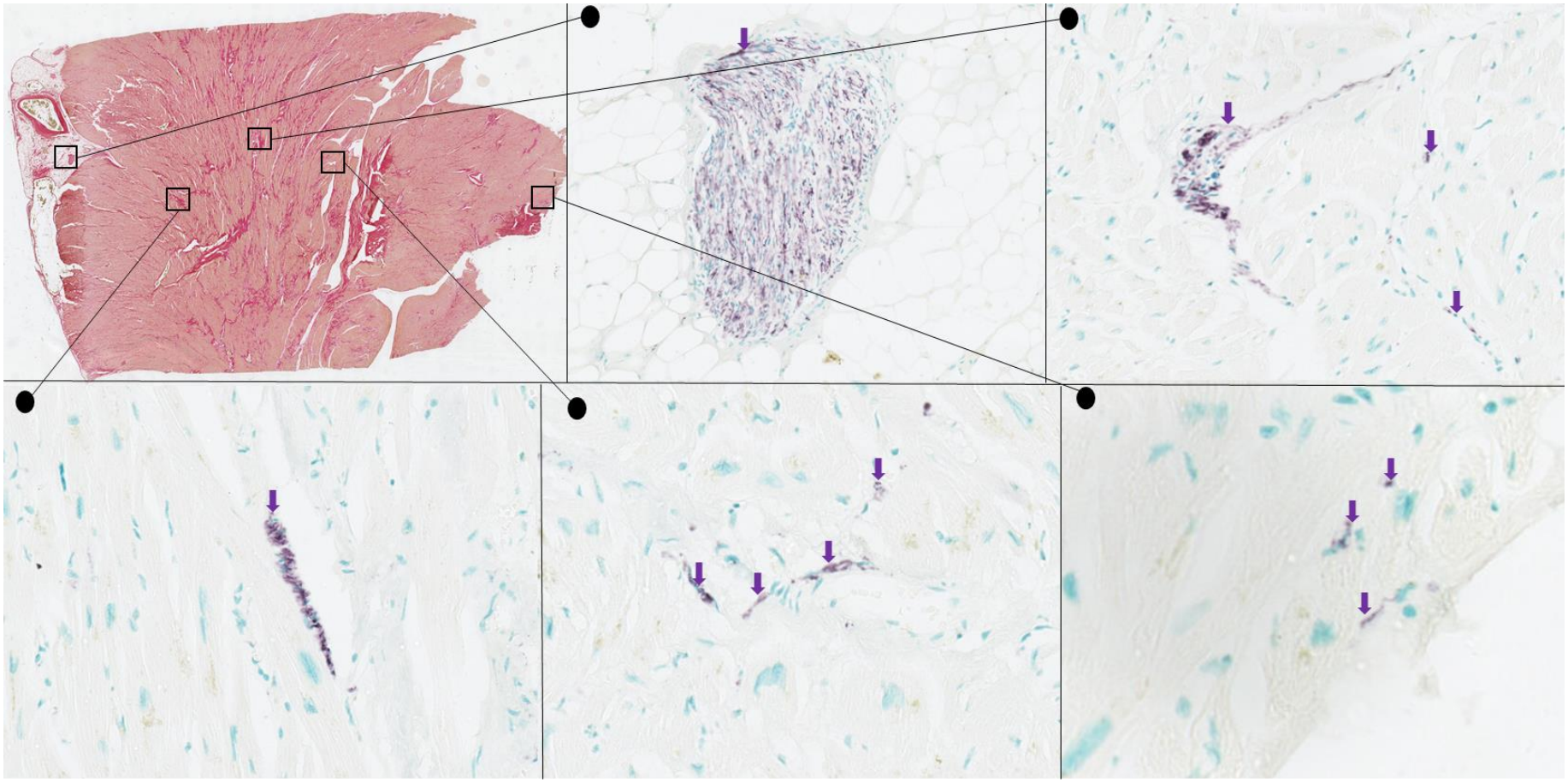


Figure 8.18. Nerve distribution (arrows) in the septum of an individual with hypertrophic cardiomyopathy showing interstitial and replacement fibrosis. PGP9.5 staining large bundles are present in epicardial fat. Small nerve bundles are present in the myocardium. Nerve fibrils are seen in fibrosis between disarrayed myocytes (top left – picrosirius red stain, others – PGP9.5 stain).

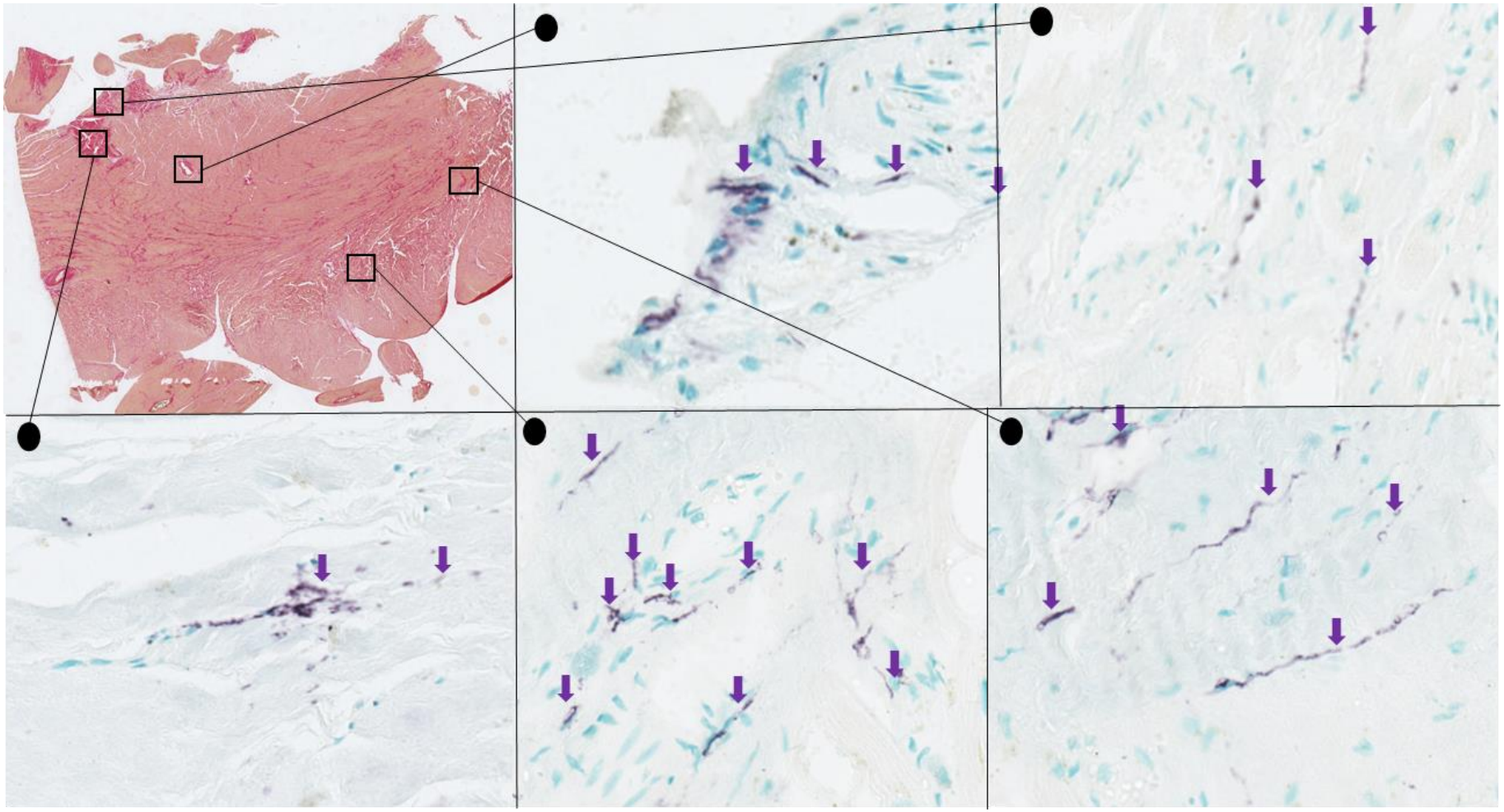


Figure 8.19. Nerve distribution (arrows) in septum of an individual with hypertrophic cardiomyopathy showing interstitial and replacement fibrosis. PGP9.5 stained small nerve bundles are present around vessels. Fibrils are seen within areas of replacement fibrosis (top left – picrosirius red stain, others – PGP9.5 stain).

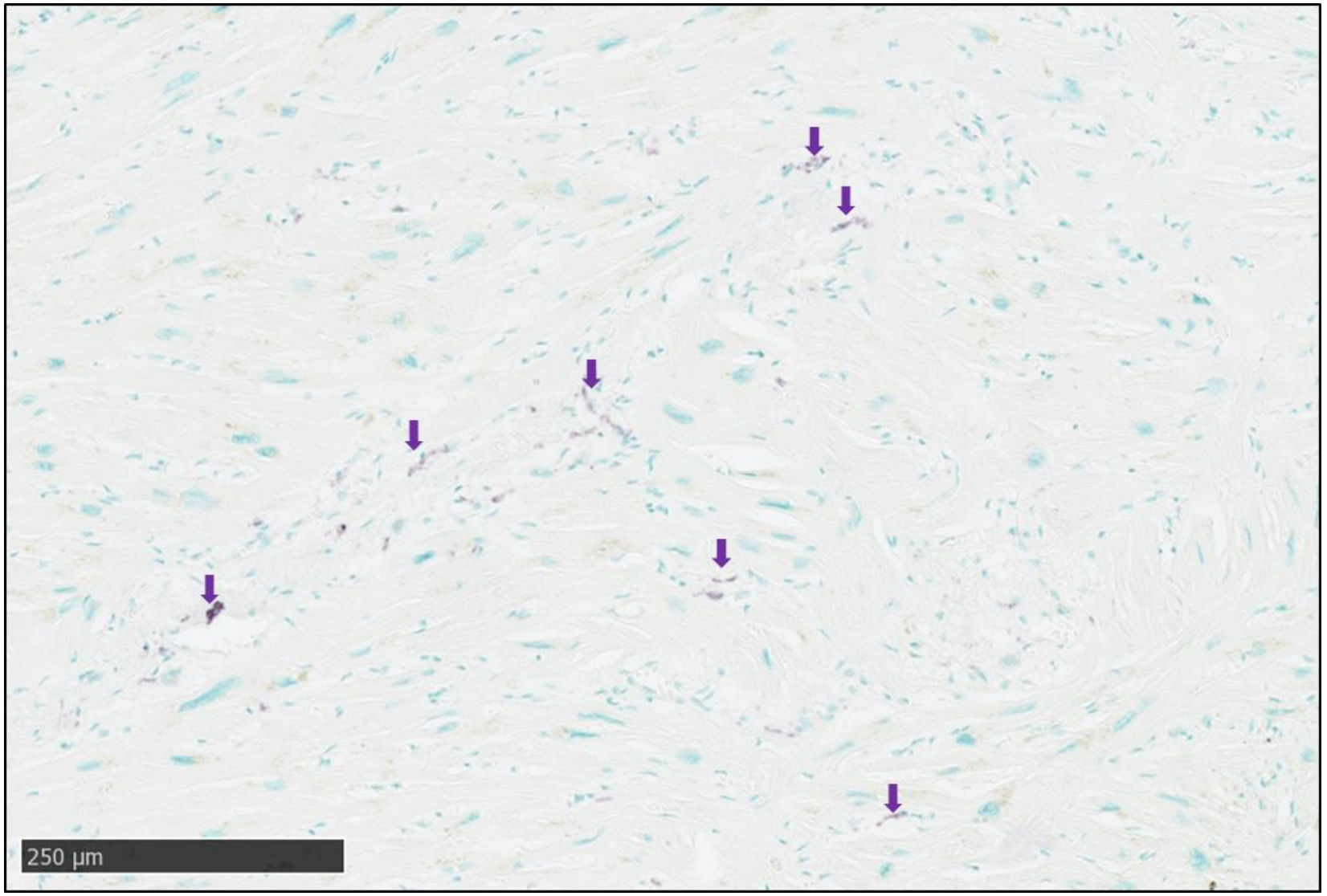


Figure 8.20. Nerve fibres and fibrils (arrows) within an area of myocyte disarray.

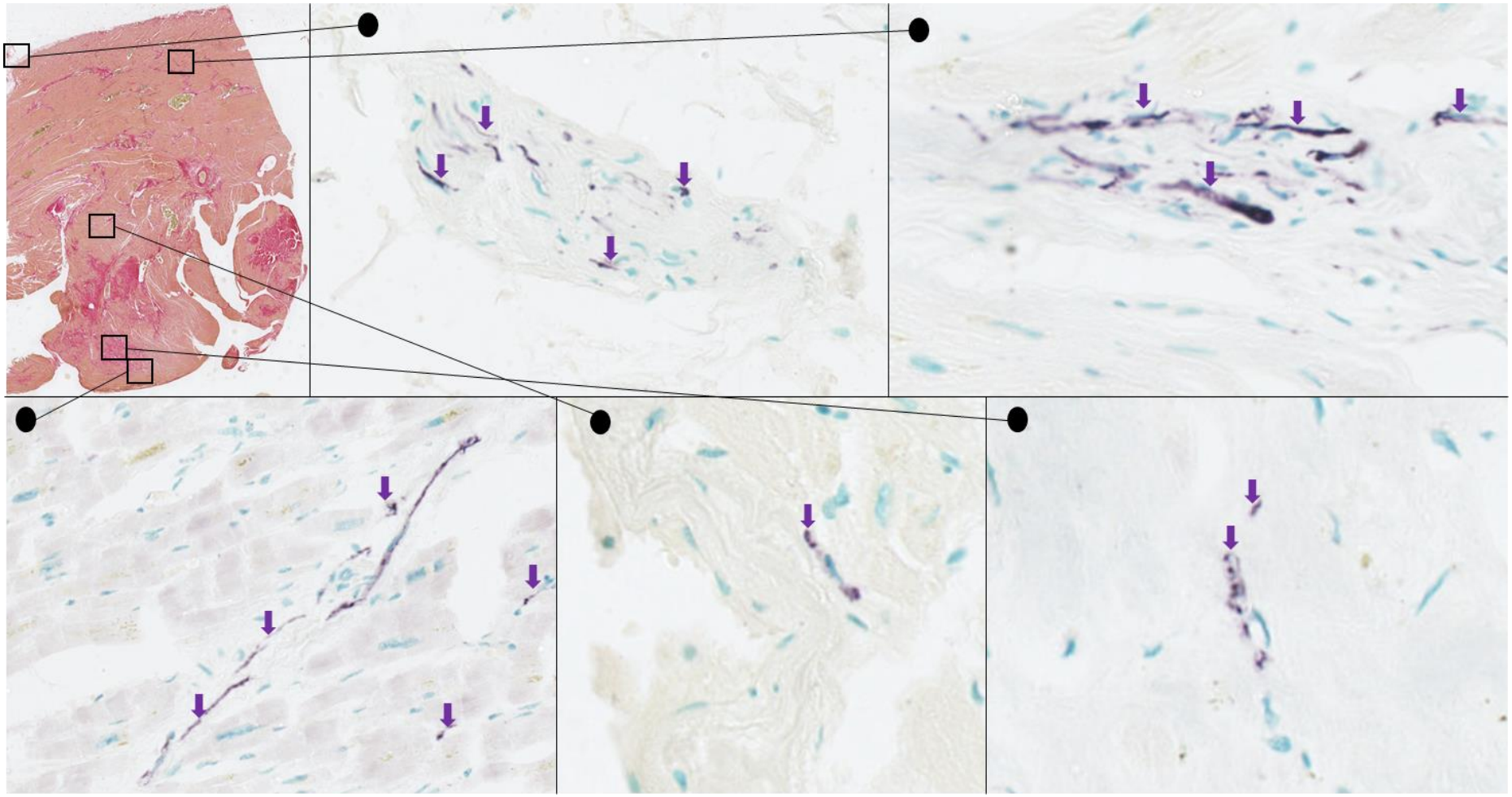


Figure 8.21. Sympathetic innervation (arrows) is decreased in hypertrophic cardiomyopathy. TH stained nerve bundles are frequently around blood vessels showing staining of a percentage of fibres. Small bundles and individual nerve fibrils are present in replacement fibrosis (top left – picrosirius red stain, others - tyrosine hydroxylase stain).

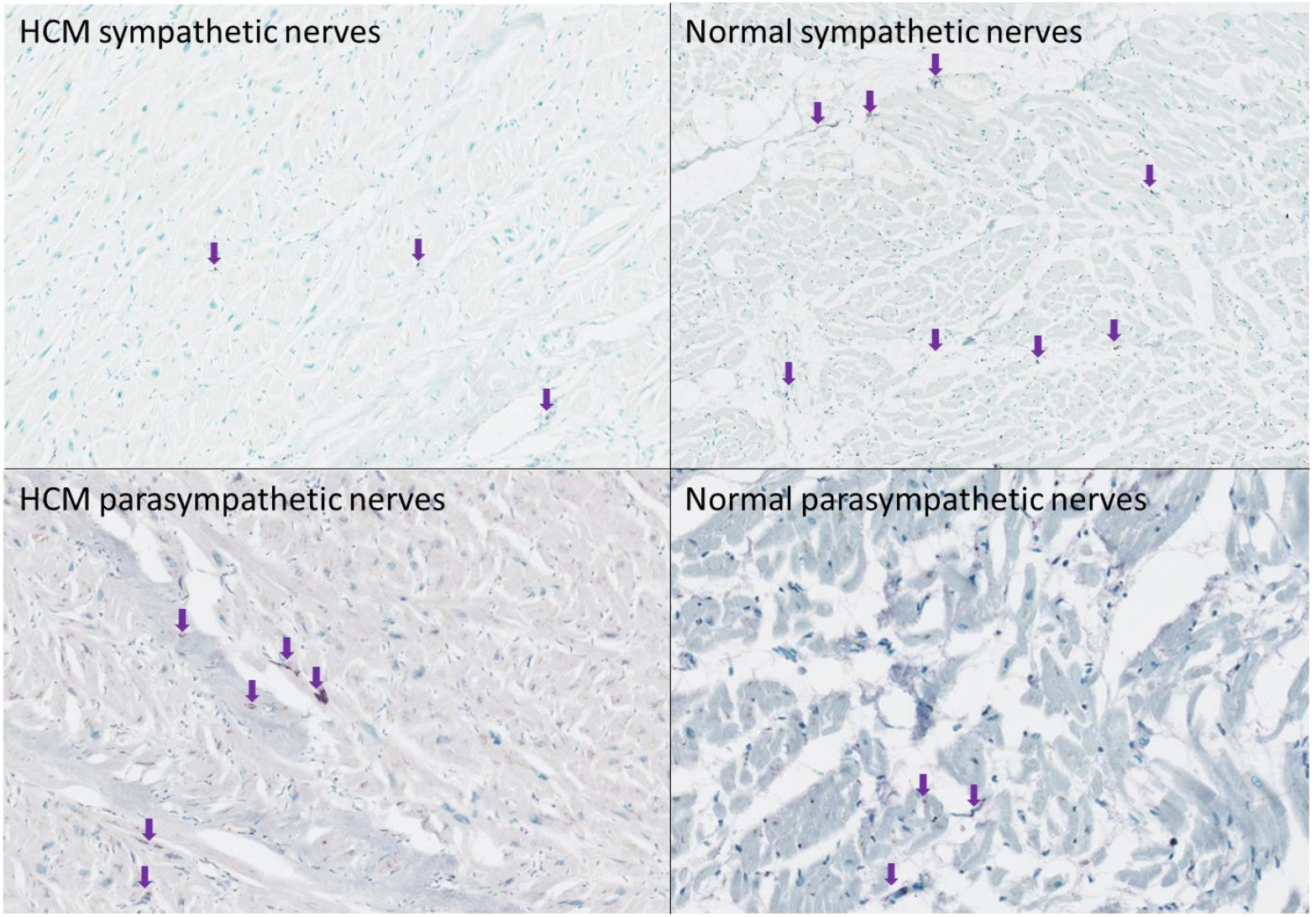


Figure 8.22. Few TH stained small nerve fibres and fibrils and frequent CT stained fibrils in hypertrophic cardiomyopathy.

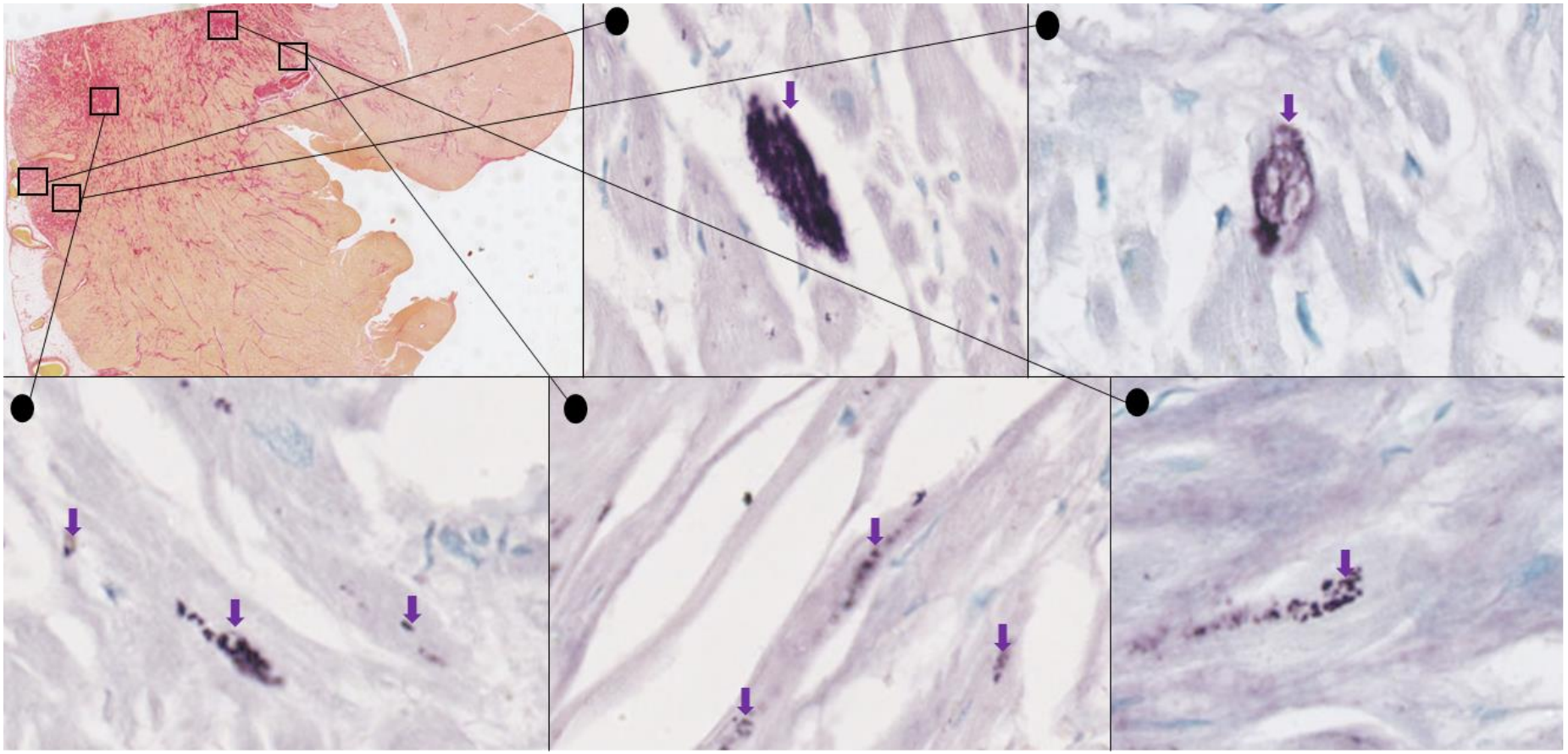


Figure 8.23. Parasympathetic innervation (arrows) in hypertrophic cardiomyopathy. CT staining bundles are present in the myocardium and in areas of replacement fibrosis. CT stained individual nerve fibrils are present in areas of replacement fibrosis and the inner myocardium. (top left – picrosirius red stain, others - CT stain).

Quantitative analysis

General innervation

There are no significant differences in PGP9.5 staining between HCM hearts and controls. Overall PGP9.5 staining is 0.02% in HCM hearts compared to 0.04% in the normal heart. The RV is 0.04%, the RVOT is 0.03% and the IVS, anterior and posterior LV is 0.01%.

Sympathetic innervation

There are no significant differences between PGP9.5 staining in HCM hearts and controls. There is 0.05% in the RVOT, 0.04% in the RV, 0.03% in the anterior LV and 0.02% in the IVS and posterior LV.

Parasympathetic innervation

CT staining does not show statistically significant changes. CT staining is 0.04% compared to 0.02% in the normal heart. There is 0.05% in the anterior LV, 0.04% in the RVOT and RV, and 0.03% in the IVS and posterior LV.

The proportions of staining by the general nerve marker PGP9.5, the sympathetic nerve marker TH and the parasympathetic nerve marker CT are shown in table 8.4 and figure 8.24.

Stain	Condition	HCM		Control	
	Region	Mean	95% CI	Mean	95% CI
PGP9.5 % of tissue area	All	0.017	0.009-0.028	0.036	0.018-0.069
	RVOT	0.033	0.017-0.062	0.061	0.027-0.134
	RV	0.036	0.019-0.067	0.057	0.026-0.126
	IVS	0.009	0.004-0.016	0.027	0.012-0.058
	ALV	0.011	0.005-0.020	0.032	0.014-0.069
	PLV	0.012	0.006-0.022	0.020	0.008-0.043
TH % of tissue area	All	0.029	0.016-0.049	0.035	0.017-0.069
	RVOT	0.047	0.022-0.095	0.037	0.015-0.090
	RV	0.037	0.018-0.076	0.062	0.025-0.151
	IVS	0.021	0.010-0.042	0.031	0.012-0.075
	ALV	0.028	0.013-0.057	0.031	0.012-0.074
	PLV	0.019	0.009-0.039	0.025	0.010-0.060
CT % of tissue area	All	0.037	0.016-0.080	0.022	0.008-0.057
	RVOT	0.039	0.015-0.095	0.014	0.004-0.043
	RV	0.036	0.014-0.087	0.027	0.008-0.083
	IVS	0.030	0.012-0.073	0.024	0.007-0.072
	ALV	0.050	0.020-0.123	0.020	0.006-0.060
	PLV	0.031	0.012-0.076	0.026	0.008-0.078

Table 8.4. Predicted proportions (geometric mean and confidence interval) of the ventricular myocardium stained by PGP9.5, TH and CT for hypertrophic cardiomyopathy (HCM) and normal control hearts. The proportions are given for the right ventricular outflow tract (RVOT), right ventricular free wall (RV), interventricular septum (IVS), anterior and posterior left ventricle (ALV and PLV).

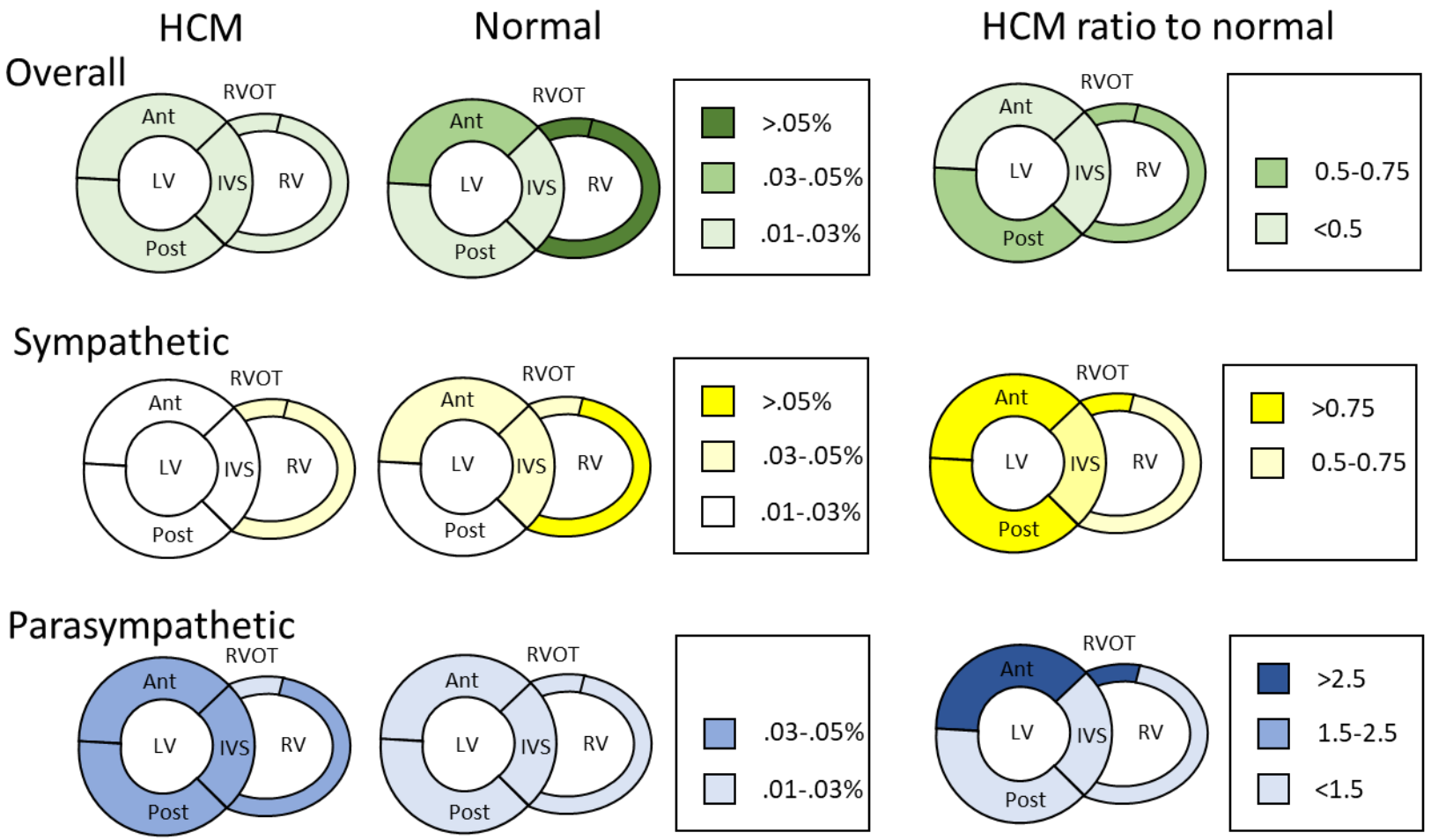


Figure 8.24. Percentage and ratio of overall, sympathetic and parasympathetic innervation in the HCM ventricular myocardium compared to normal. The values are given for the RV, RVOT, IVS, the anterior and posterior LV. There is a trend towards a reduction in general innervation.

Diseased area quantification

A subcohort of sections showing a proportion of collagen two standard deviations from the mean of the normal heart (≥28%) are selected and compared to normal hearts. This is present in the RVOT in 9 cases, the RV in 8 cases, the IVS in 12 cases, the anterior LV in 11 cases and the posterior LV in 13 cases.

General, sympathetic and parasympathetic innervation

When comparing diseased HCM sections to normal hearts there are no significant differences in PGP9.5, TH or CT staining.

The proportions of the different innervation in diseased sections for HCM are shown in table 8.5.

Stain	Condition	HCM		Control	
	Region	Expected	95% CI	Expected	95% CI
PGP9.5	All	0.015	0.007-0.027	0.036	0.018-0.069
	RVOT	0.033	0.015-0.070	0.061	0.027-0.134
	RV	0.036	0.016-0.078	0.057	0.026-0.126
	IVS	0.009	0.004-0.017	0.027	0.012-0.058
	ALV	0.014	0.006-0.028	0.032	0.014-0.069
	PLV	0.011	0.005-0.021	0.020	0.008-0.043
TH	All	0.015	0.007-0.027	0.035	0.017-0.069
	RVOT	0.044	0.017-0.110	0.037	0.015-0.090
	RV	0.026	0.010-0.067	0.062	0.025-0.151
	IVS	0.024	0.010-0.056	0.031	0.012-0.075
	ALV	0.033	0.014-0.078	0.031	0.012-0.074
	PLV	0.027	0.012-0.060	0.025	0.010-0.060
CT	All	0.032	0.013-0.076	0.022	0.008-0.057
	RVOT	0.026	0.008-0.075	0.014	0.004-0.043
	RV	0.030	0.009-0.091	0.027	0.008-0.083
	IVS	0.025	0.009-0.068	0.024	0.007-0.072
	ALV	0.055	0.019-0.153	0.020	0.006-0.060
	PLV	0.031	0.011-0.082	0.026	0.008-0.078

Table 8.5. Predicted proportions (geometric mean and confidence interval) of the ventricular myocardium stained by PGP9.5, TH and CT for hypertrophic cardiomyopathy (HCM) and normal control hearts. The proportions are given for the interventricular septum (IVS), anterior and posterior left ventricle (ALV and PLV).

Power calculation

Based on an alpha of 0.05 and a power of 0.8, we predict a sample size of 70 HCM and 70 normal hearts should be sufficient to detect a significant difference in overall innervation stained by PGP9.5 in unselected section in HCM.

Discussion

This is the first study to pathologically delineate, describe and autonomously quantify innervation in HCM and the first to objectively autonomously quantify fat and fibrosis using picrosirius red.

Macroscopic findings in HCM

An increased heart weight and LV hypertrophy are expected findings in HCM and the LV may show marked heterogeneity with either a symmetric or asymmetric pattern of hypertrophy (Varnava *et al.*, 2000; Basso *et al.*, 2021). A previous pathology study has found similar findings to our study (Varnava *et al.*, 2000). Asymmetrical hypertrophy in 65% with a maximal wall thickness was 23mm and an impact lesion in 45%. We have recently characterised our HCM cohort giving wall thickness of 197 hearts as 21mm in the IVS, 19mm in the anterior wall and 17mm in the posterior LV (Finocchiaro *et al.*, 2019). This is similar to the cohort reported here.

Thickening of the RV muscular wall has been previously reported (Varnava *et al.*, 2000). An RV wall thickness of over 4mm was found in 41 hearts and a thickness of over 8mm was found in 18 cases. The present study did not identify RV hypertrophy to the same degree.

Right atrial enlargement has not been previously described on pathological examination but it has been described in a previous study looking at sudden death in HCM by Barry Maron back in 1981 (Maron, Roberts and Epstein, 1982). In a cohort of 106 individuals echocardiography identified right atrial enlargement in 8 individuals.

An echocardiographic imaging study has identified left atrial enlargement in HCM (Debonnaire *et al.*, 2017). Increases in linked left atrial volume were linked to the

development of atrial fibrillation. Furthermore, left atrial diameter is an independent predictor of SCD and forms part of the used risk stratification model for SCD in HCM (O'Mahony *et al.*, 2014). Left atrial size was not significantly increased in our cohort. This may be due to the relatively younger cohort studied.

Left ventricular fibrosis

With regard to the increase in collagen in the LV, other histological studies have shown increases throughout the LV. A previous study of 10 HCM hearts using trichrome, showed increases in the anterior, lateral and posterior left ventricular walls as well as the IVS compared to controls (Tanaka *et al.*, 1986). A study of 30 explanted end stage cardiac failure HCM hearts has used trichrome staining. (Leone *et al.*, 2012; Galati *et al.*, 2016). More than 33% of the LV myocardium was replaced by fibrosis however there were no controls used in this study. This proportion of collagen is higher than 27% which we report despite the use of trichrome and would be explained by the population being composed of end stage failure patients rather than those experiencing SCD. In a further study utilising the same technique and specimens, Foa et al, compared 27 myectomy specimens to 30 antero-basal septal samples from end stage HCM explants hearts (Foà *et al.*, 2019). They found 10.3% fibrosis in the myectomy specimens and 34.6% in the septum from end stage failure HCM hearts. The lower value in the myectomy specimens compared to our study may be explained by a variety of factors including the use of trichrome as opposed to picrosirius red. A further plausible explanation is that fibrosis is most prominent in the midwall of the IVS in our cohort which would not have been included in myectomy specimens. Finally, it may suggest that there is more fibrosis in those experiencing SCD than those undergoing myectomy.

Our study of HCM contrasts with findings in hypertensive heart disease. Our previous study has highlighted that there is a clinical overlap between hypertensive heart disease and HCM (Westaby *et al.*, 2021). Fibrosis in these hearts was in a predominantly inner myocardial distribution and composed of mainly interstitial fibrosis. This contrasts with HCM where the fibrosis shows a mix of both replacement and interstitial fibrosis and is distributed transmurally.

Right ventricular fibrosis

RV fibrosis has been previously noted in end stage cardiac failure explanted HCM hearts (Galati *et al.*, 2016) in the study described above but to our knowledge this has not been reported in a sudden death cohort previously. A previous report observed 1% of fibrosis in the RV using elastic van Geison staining in 72 HCM hearts however the cohort included cardiac failure patients as well as SCD (Varnava *et al.*, 2000). The lower proportion of collagen may be due to the removal of the papillary muscles and trabeculations from the samples, the use of elastic van Gieson and calibration to just detect fibrosis rather than all collagen. Sugihara et al, examined biopsies from the RV of 19 HCM patients. This revealed 25% fibrosis in the RV inner myocardium (Sugihara *et al.*, 1988). This is similar to our findings of 24% proportion of collagen in the RV. RV fibrosis is seen along with LV fibrosis in the HCM population experiencing SCD.

Comparison to histology study on innervation in ischaemic heart disease

A previous study on ischaemic heart disease has described that nerves are present around areas of fibrosis. Vracko et al, used S100 immunohistochemistry to stain sections from 17 ischaemic hearts from individuals aged 36-89 (Vracko, Thorning

and Frederickson, 1991). They sampled fibrosis and adjacent normal appearing myocardium from the anterior, lateral and posterior LV. They describe greater densities of nerves in areas of fibrosis than in adjacent myocardium. Nerves were seen to aggregate on the periphery of fibrosis with few or absent nerves in the centre of fibrosis. This contrasts with our findings in HCM where nerve fibrils were seen throughout areas of fibrosis and aggregation at the periphery of patches was not seen.

Correlation to imaging studies

Previous imaging studies have used positron emission tomographic scanning using 6-[18F]-fluorodopamine (Li *et al.*, 2000) and metaiodobenzylguanidine myocardial scintigraphy on HCM patients (Terai *et al.*, 2003). These studies demonstrate decreased neuronal uptake of catecholamines in the hypertrophied myocardium of individuals with HCM. This is indicative of reduced sympathetic function. Reduced sympathetic function progresses with the development of failure and is predictive of VA (Li *et al.*, 2000; Terai *et al.*, 2003). Alterations in sympathetic activity were global but most marked in the IVS in end stage heart failure HCM patients similar to the findings of our sudden death cohort (Terai *et al.*, 2003). The most powerful predictor of ventricular tachyarrhythmia was found to be higher washout rate which is representative of attenuated sympathetic activity rather than regional heterogeneity (Terai *et al.*, 2003). We did not identify a reduction in sympathetic activity which may suggest that sympathetic function does not correlate with structural neural loss. Imaging for parasympathetic nerves has not been performed in HCM. A new technique involving the use of 11C-donepezil and photon emission tomography

using 11C-donepezil has been proposed to allow the visualisation of parasympathetic denervation (Gjerløff *et al.*, 2014).

Correlation to clinical findings

Losses in general innervation may lead to a reduction in autonomic control in HCM. This assertion is supported by previous studies of heart rate variability. Multiple studies have shown a reduction in global and parasympathetic influences on heart rate variability in HCM (Counihan *et al.*, 1993; Gilligan *et al.*, 1993; Mörner *et al.*, 2005). Counihan et al, found this to be more pronounced in those with symptoms and arrhythmias, confoundingly however, they also noted that heart rate variability was increased in HCM individuals with an adverse family history (Counihan *et al.*, 1993).

A study in individuals with HCM has examined the relationship between a marker of electrical instability and regional variation in sympathetic function. Metaiodobenzylguanidine scintigraphy findings were assessed alongside QT dispersion, a marker of regional variation of ventricular repolarisation, in a study of 25 patients with HCM. Surprisingly, in this study, QT dispersion was observed to correlate negatively with regional variability of sympathetic activity. They suggested that the QT dispersion observed in HCM is therefore not a reflection of increased heterogeneity of sympathetic activity (Shimizu *et al.*, 2001). Taken with the variability in sympathetic innervation seen in our study, this may suggest that the relationship between structural changes and autonomic dysregulation is more complex than solely sympathetic denervation.

The relationship between heart rate variability and hypertrophy has been previously examined in HCM. Limbruno et al, analysed heart rate variability in 28 HCM patients

with left ventricular outflow tract obstruction, 22 non-obstructive HCM patients and 28 controls using passive tilting. Impaired heart rate variability was identified only in HCM individuals with obstruction. Furthermore, the impairment observed within this group was found to correlate with myocardial hypertrophy rather than obstruction gradient (Limbruno *et al.*, 1998). This would support our observation that the greatest decreases of innervation are observed in the IVS and anterior wall where hypertrophy is most frequently observed in HCM.

Our findings raise the possibility the anterior of the heart may have parasympathetic hyperinnervation compared to elsewhere in HCM. This contrasts to previous clinical studies described above which suggest decreased parasympathetic influence (Counihan *et al.*, 1993; Gilligan *et al.*, 1993; Mörner *et al.*, 2005). This may suggest, as with sympathetic findings, that structural neural changes in the ventricular myocardium do not necessarily correlate with the functional changes seen in HCM.

Concluding remarks

This is the first study to pathologically delineate, describe and autonomously quantify innervation in HCM and the first to objectively autonomously quantify fat and fibrosis using picrosirius red.

Macroscopic findings in HCM include an increased heart weight, right atrial dilation, thickening of the RV muscular wall and thickening of the IVS and LV free wall. Collagen is increased in HCM heart in the LV, IVS and RV representing fibrosis. Fibrosis is distributed transmurally and is composed of both replacement and interstitial fibrosis which contrasts with hypertensive heart disease where fibrosis is interstitial and present in the inner wall.

There is a trend towards a reduction in general innervation overall and within sections showing fibrosis.

Summary of findings in HCM

Macroscopic

- Heart weight is increased
- The right atrium is dilated
- The left atrium is not dilated
- RV muscle wall is thickened
- The LV muscle walls are all thickened
- No differences in epicardial fat

Microscopic findings in HCM ventricular subepicardial fat and myocardium

- There is an increase in collagen overall
- There is no difference in fat
- There is a reduction in myocytes overall
- There is a non-significant trend towards a reduction in general innervation
- There is no difference in sympathetic and parasympathetic innervation

CHAPTER 9 GRAPHICAL SUMMARY AND CONCLUSIONS

Hypotheses

4. There are quantifiable differences in cardiac anatomical measurements between ACM, DCM and HCM and non-cardiac death controls.
5. There are quantifiable differences in the proportion of ventricular collagen, fat and myocytes between ACM, DCM and HCM and non-cardiac death controls
6. There are quantifiable differences in the proportion of cardiac innervation in the ventricles between ACM, DCM and HCM and non-cardiac death controls.

Aims

The aims of this thesis are:

1. To describe the causes of SCD from the CRY cardiac pathology database in detail.
2. To characterise the normal heart in terms of the weight, dimensions of the atria, ventricles, valves, epicardial fat, and fossa as well as coronary artery dominance.
3. To establish normal collagen, fat, myocytes within the RV and LV in normal hearts.
4. To establish normal general, sympathetic and parasympathetic innervation within the RV and LV in normal hearts.
5. To establish whether there are quantifiable differences in collagen, fat, myocytes in different regions of the RV and LV in normal hearts.

6. To establish whether there are quantifiable differences in general, sympathetic and parasympathetic innervation in different regions of the RV and LV.
7. To establish whether there are macroscopic differences in weight, dimensions of the atria, ventricles and subepicardial fat in ACM, DCM and HCM compared to the normal heart.
8. To establish if there are microscopic quantifiable differences in collagen, fat, myocytes in ACM, DCM and HCM compared to the normal heart.
9. To establish if there are microscopic quantifiable differences in general, sympathetic and parasympathetic innervation in ACM, DCM and HCM compared to the normal heart.

This thesis is based upon human hearts referred to a national cardiac pathology centre. A combination of techniques including direct anatomical examination, detailed measurements, histochemical staining for collagen, immunohistochemistry for nerves and digital image analysis have been used to provide comprehensive characterisation. This chapter will summarise the major findings of the thesis, discuss clinical implications and suggest future work.

Summary

In chapter 3, we present the causes of death in the largest autopsy based SCD cohort ever examined. We show the structurally normal heart or SADS and cardiomyopathy cause a majority of SCD, particularly in young individuals (figure 9.1). SADS is the cause of death in 53% and cardiomyopathy in 22%. ACM made up 19% of cardiomyopathy case with HCM making up 18% and DCM making up 16%.

These conditions are important to identify at autopsy as they are heritable therefore screening is vital for surviving blood relatives. We highlight the dramatic variation in the causes of SCD around the world and compare to our own study.

In chapter 4, as SADS is the most common cause of SCD, we provide comprehensive morphological analysis with detailed measurements from a large cohort of normal male and female hearts over a range of ages. Heart weight was predicted by gender, body surface area and age. Gender was the most important predictor of heart weight. We provide an equation to calculate expected heart weight with a reference table.

This is the first morphological study to provide comprehensive detailed measurements of the heart. Females have smaller atrial dimensions, muscular ventricular wall thickness, cavity diameters, valvular and aorta circumferences but thicker subepicardial fat. There is no difference between coronary artery dominance, oval fossa dimensions and patency between males and females

The thicker subepicardial fat in females should be accounted for when examining this population. Increased epicardial fat is a risk factor for atrial fibrillation, coronary artery disease and SCD which are less common in females (Hatem and Sanders, 2014; Nakanishi *et al.*, 2014; Fuller *et al.*, 2017).

It is important to account for the fact the female heart is smaller with regard to the atria, ventricular cavity and muscle thickness as well as valves so as not to under call pathologic alterations. These differences are sumarised in figure 9.2.

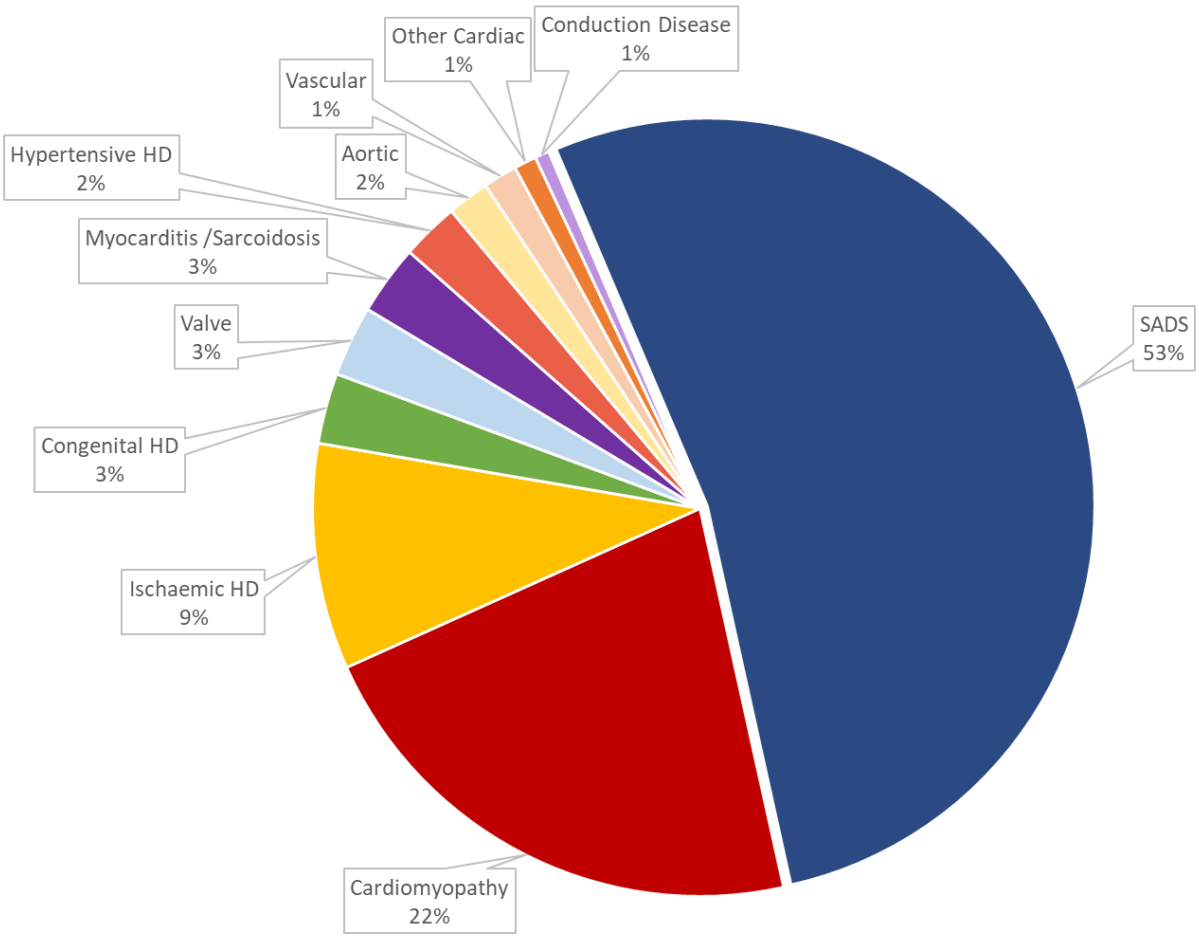


Figure 9.1. *The conditions underlying sudden cardiac death in our cohort.*

Cardiomyopathy and sudden arrhythmic death syndrome (SADS) are most common.

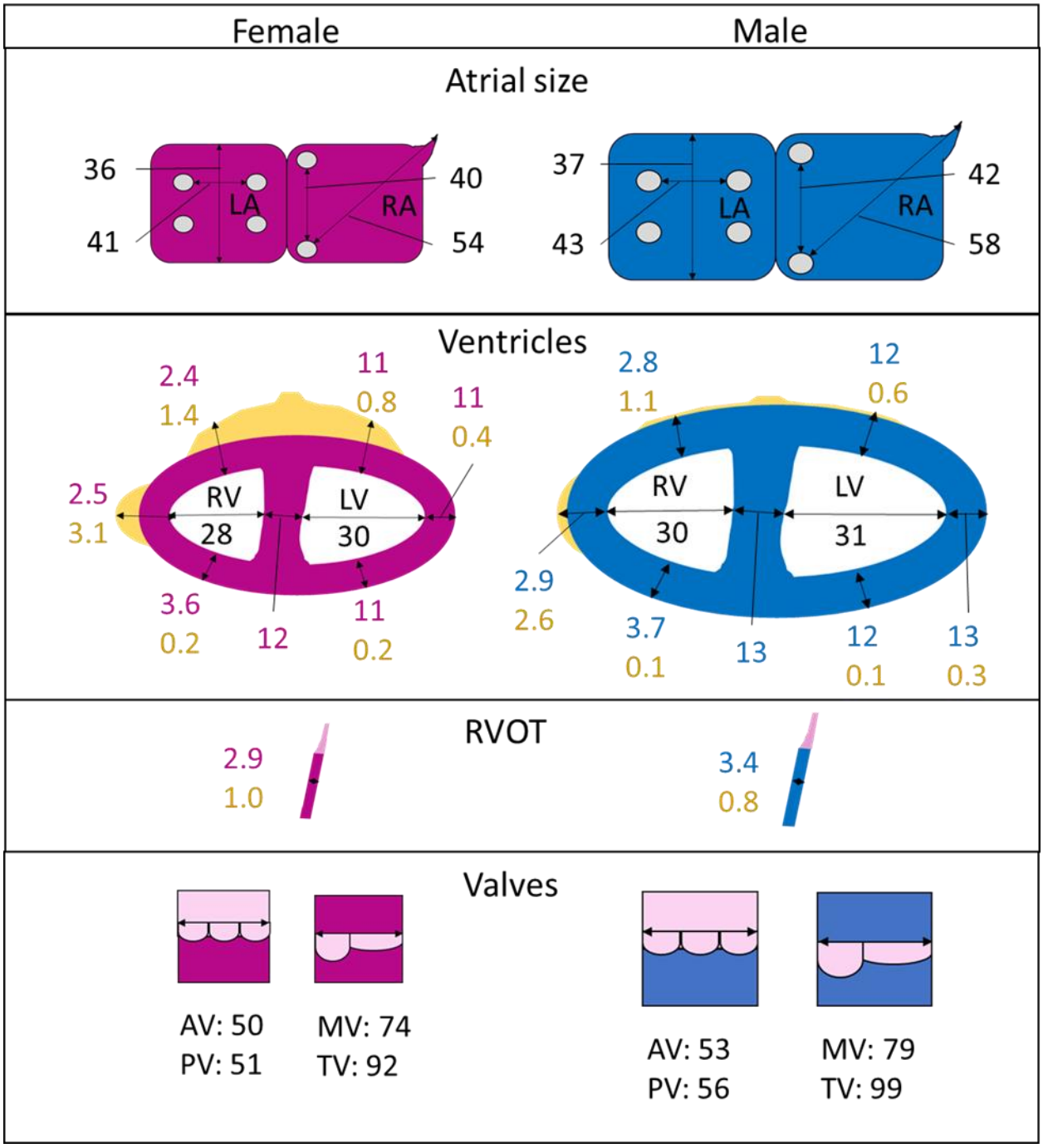


Figure 9.2. The major differences between male and female hearts. Subepicardial fat thickness are given in yellow and mural wall thickness in pink and blue. AV: aortic valve; LA: left atrium; LV: left ventricle; MV: mitral valve; MVS: mid-ventricular slice; PV: Pulmonary valve; RA: right atrium; RV: right ventricle; TV: tricuspid valve.

In chapter 5, we describe the fat, collagen and myocytes in the normal heart and use automated compositional analysis to quantify their proportions. When evaluating the abnormal, it is of central importance to understand the normal.

In the normal heart, there is no evidence of a difference in the proportion of collagen between the RV and LV. Collagen is present as connective tissue joining the epicardium to the subepicardial fat and joining the endocardium to the inner myocardium. There is an extensive fine network of collagen present between both the adipocytes of the subepicardial fat and the myocytes of the myocardium. Layers of collagen encircle both vessels and nerve bundles. Collagen coalesces in the inner trabeculae of the normal heart where it may be mislabelled as fibrosis.

There is more fat in the RV than the LV and particularly the IVS. Fat is predominantly located between the epicardium and the outer myocardium. Fat infiltrates into the RV wall but not the LV wall in the normal heart. The presence of fat within the RV myocardium is a normal finding.

In the normal heart, there is no evidence of a difference in the proportion of myocytes between the RV and LV. Myocytes are occupy most of the space between the epicardium or subepicardial fat and the endocardium.

We have established that there is a complex network of nerves in the heart. Large nerve bundles are present in the epicardial fat which enter the ventricular myocardium with vessels. Within the ventricular myocardium, there are small nerve bundles and individual nerve fibrils. Both sympathetic and parasympathetic nerve fibrils are intricately associated with vessels and myocytes. Sympathetic associate more with vessels and parasympathetic associate more with myocytes.

Nerve fibrils in close proximity to ventricular vessels may modulate vasoconstriction and vasodilation (Henning and Sawmiller, 2001; Mistrova, Kruzliak and Chottova

Dvorakova, 2016). Nerve fibrils in close proximity to ventricular myocytes may play a role in modulating muscle contractility, conduction velocity and cellular excitability (Ajijola *et al.*, 2013; Fukuda *et al.*, 2015).

Automated analysis is used to quantify general, sympathetic and parasympathetic innervation. When regional variation is examined in all hearts, general innervation is proportionally greatest in the RVOT and the RV. This may aid in our understanding as to why the RVOT is a focus point for generation of a number of arrhythmias. The higher levels of innervation may result in higher concentrations of neurotransmitters potentiating greater effects within this region compared to the LV (Kienzle *et al.*, 1992).

Sympathetic innervation shows a similar trend to overall innervation with higher proportions in the RV than the LV but this is not significant. Parasympathetic innervation is more evenly distributed. The proportions of each component are summarised in figure 9.3.

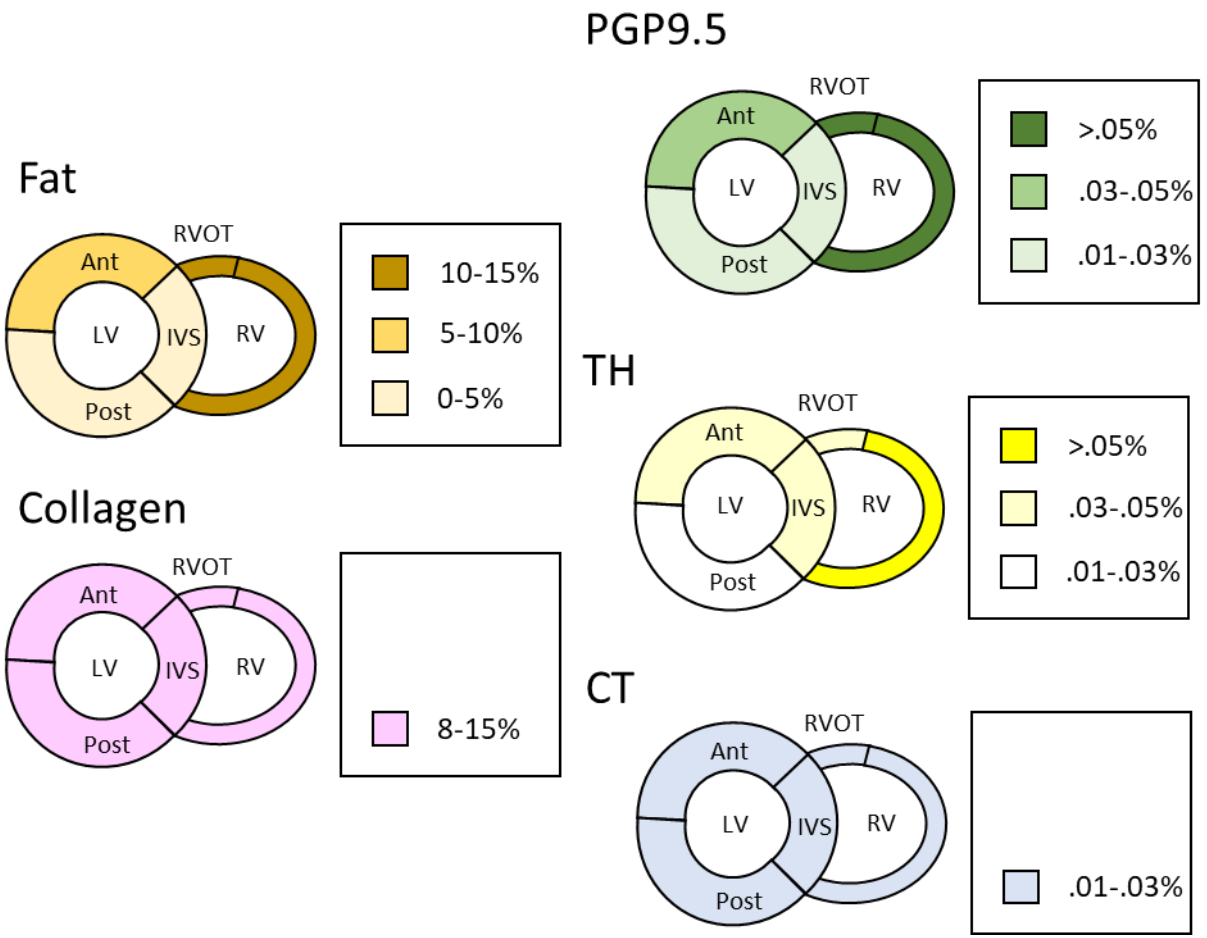


Figure 9.3. Proportional compositional analysis of the normal heart for fat, collagen and innervation by right ventricular outflow tract (RVOT), right ventricle (RV), septum (IVS), anterior and posterior left ventricle (LV).

Within chapters 6, 7 and 8, we compared ACM, DCM and HCM to normal hearts using macroscopic measurements, microscopic examination, regional analysis of fat, collagen, myocytes and innervation.

Macroscopic changes in cardiomyopathy

Macroscopically the cardiomyopathies show distinct features. All cardiomyopathies show an increase in heart weight. Heart weight is most increased in HCM. The increase in heart weight is smallest in ACM where the heart weight is frequently normal. Increase in cardiac mass has been strongly associated with SCD (Haider *et al.*, 1998; Stevens, Reinier and Chugh, 2013).

The presence of atrial dilation varied by type of cardiomyopathy. DCM shows bi-atrial dilation whereas HCM shows just right atrial dilation. Contrastingly, the atria are not dilated in ACM. There is an elevated risk of SCD associated with atrial enlargement and fibrillation (Reinier *et al.*, 2014).

The RV was not dilated in any of the cardiomyopathies. RV muscle wall changes are present in all three cardiomyopathies. ACM shows thinning of the lateral RV muscle wall with thickening of the posterior RV muscle wall. This contrasts with both DCM and HCM where the RV muscular wall shows more generalised thickening. RV dysfunction independently increases the risk of SCD and has an additive effect when combined with LV dysfunction when assessed by echocardiography (Pandat *et al.*, 2020).

The LV shows changes in both diameter and muscular wall thickness depending on cardiomyopathy. The LV cavity diameter is increased in dilated cardiomyopathy but not in ACM or HCM. The LV and IVS muscle walls are all thickened in HCM which is distinct from DCM where there is thinning of the lateral LV wall. ACM does not show

changes in the thickness of the LV muscle wall. LV muscle mass has been strongly associated with SCD (Haider *et al.*, 1998; Stevens, Reinier and Chugh, 2013). Epicardial fat is thicker in just the lateral RV for both ACM and DCM. No changes are present in the epicardial fat for HCM. Thicker epicardial fat has been associated with arrhythmia in heart failure patients when assessed by echocardiography (Parisi *et al.*, 2020).

Overall, macroscopic changes are subtle in ACM which contrasts with DCM which shows changes in all four ventricles and HCM which shows biventricular muscular wall thickening. In HCM, the marked LV wall thickening contrasts with wall thinning in DCM.

Microscopic collagen, fat and myocytes in the Cardiomyopathies

Compositional regional tissue analysis of the cardiomyopathies shows distinct differences to normal and between the different conditions. These differences are predominantly regional changes in collagen because of fibrosis (figure 9.4). Each cardiomyopathy demonstrated considerable phenotypic variation with regard to the distribution of fibrosis.

ACM shows dramatic variation in the distribution and amount of fibrosis. ACM could show a biventricular pattern of fibrosis, predominantly RV fibrosis or predominantly LV fibrosis. The fibrosis is always present in the outer myocardium and frequently admixed with fat. There is fibrosis throughout the heart with corresponding regional losses of myocytes in the RVOT, RV and posterior LV. Fat is increased in the posterior LV but not elsewhere.

There is considerable variability in the distribution and amount of fibrosis in DCM which is always more prominent in the LV than the RV. The IVS showed fibrosis

however the LV free wall does not reach significance. When present, the fibrosis is centred on the midwall of the IVS and within the inner and middle wall of the LV free wall. DCM shows the least fibrosis of the cardiomyopathies however there is an overall loss of myocytes in DCM. There is no difference in fat.

HCM showed varied distribution and amount of fibrosis. HCM shows fibrosis throughout the IVS and LV. Patchy fibrosis is present transmurally in both the IVS and LV. The RV could also show fibrosis in HCM. There is a reduction in myocytes overall in HCM. There is no difference in fat in HCM.

Overall, the cardiomyopathies show marked variability with regard to the distribution and amount of fibrosis. ACM affects both ventricles and is combined with fat in an outer myocardial distribution whereas both DCM and HCM predominantly show fibrosis with no fat in the LV. DCM shows fibrosis mainly within the inner and middle myocardium of the LV whereas the fibrosis in HCM is patchy and distributed throughout the wall.

Innervation in the Cardiomyopathies

This is the first histological study to examine innervation in ACM and HCM and the first to use automated analysis to quantify innervation. Automated analysis is used to quantify general, sympathetic and parasympathetic innervation within each cardiomyopathy and compared to normal.

Whilst there are very few large and small nerve bundles present in areas of fibrosis, individual nerve fibrils are present in areas of fibrosis in the cardiomyopathies. This contrasts with areas of fibrosis in ischaemic heart disease where nerves are concentrated at the edge of fibrosis with few within fibrosis (Cao, Fishbein, *et al.*, 2000).

There is a non-significant trend towards a decrease in general innervation in ACM. There is a decrease in general innervation in RV sections exhibiting fibrosis in ACM. There is no difference in sympathetic or parasympathetic innervation in ACM.

Within DCM, general and sympathetic innervation are decreased compared to the normal heart in all areas examined but this does not reach significance. There is a significant reduction in general innervation in the RVOT in sections showing fibrosis in DCM. There is no difference in parasympathetic innervation in DCM.

Within HCM, there is a trend towards a decrease in general innervation overall and within sections showing fibrosis. There is no difference in sympathetic or parasympathetic innervation in HCM.

All the cardiomyopathies demonstrate a trend towards a decrease in general innervation throughout the myocardium and in sections exhibiting fibrosis however these changes are mostly not significant. This may suggest that denervation occurs in a more localised distribution rather than throughout sections and as a patchy process akin to fibrosis in the cardiomyopathies.

General, sympathetic and parasympathetic innervation are shown as a ratio to normal for the regions examined in the different cardiomyopathies in figure 9.5.

Figure 9.6 shows the relationship between collagen and innervation. There is no clear correlation between the percentage of fibrosis and innervation.

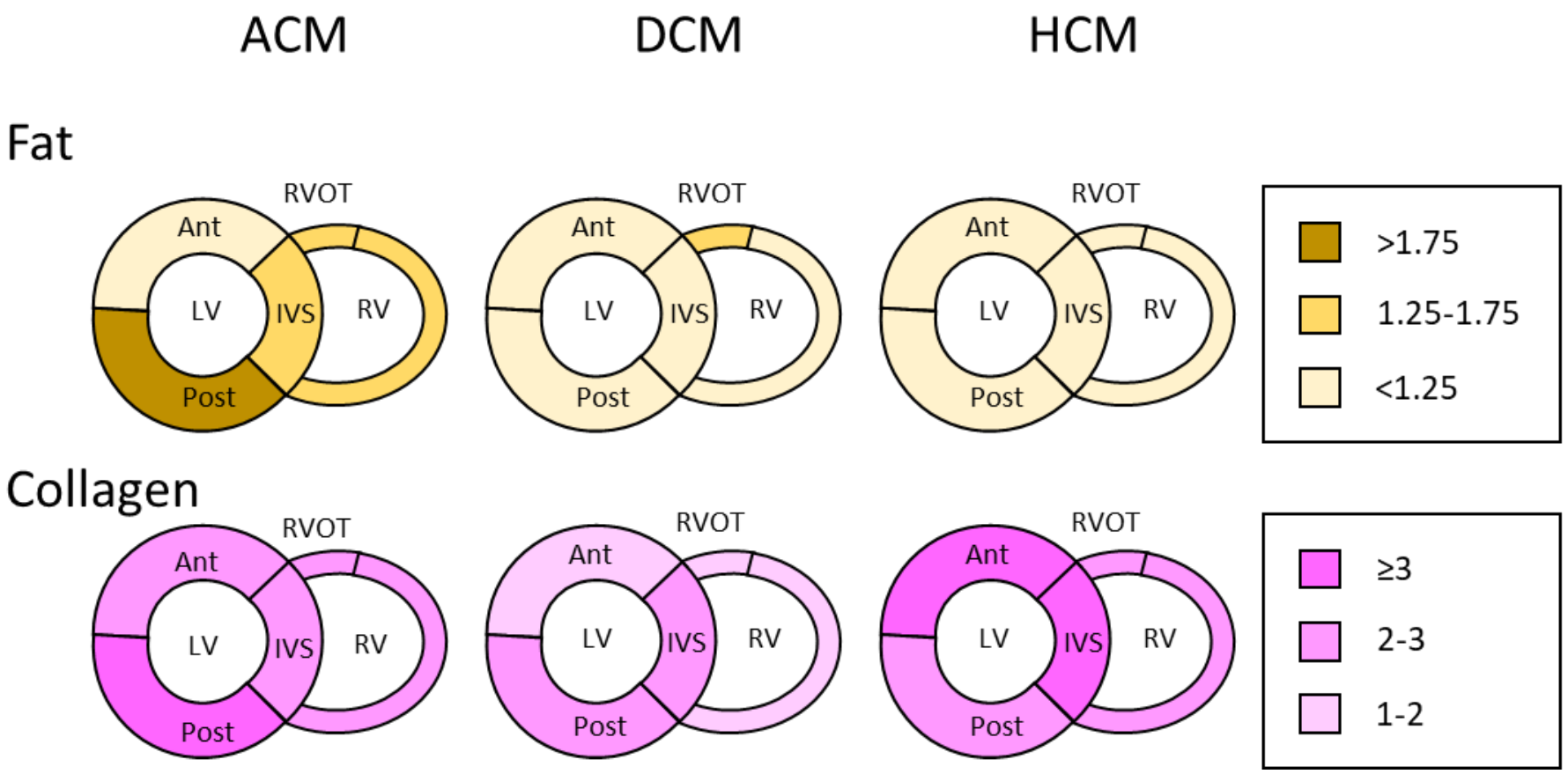


Figure 9.4. Ratio of fat and collagen in the cardiomyopathies to normal non-cardiac death hearts by right ventricular outflow tract (RVOT), right ventricle (RV), septum (IVS), anterior and posterior left ventricle (LV). ACM: arrhythmogenic cardiomyopathy; DCM: dilated cardiomyopathy; HCM: hypertrophic cardiomyopathy.

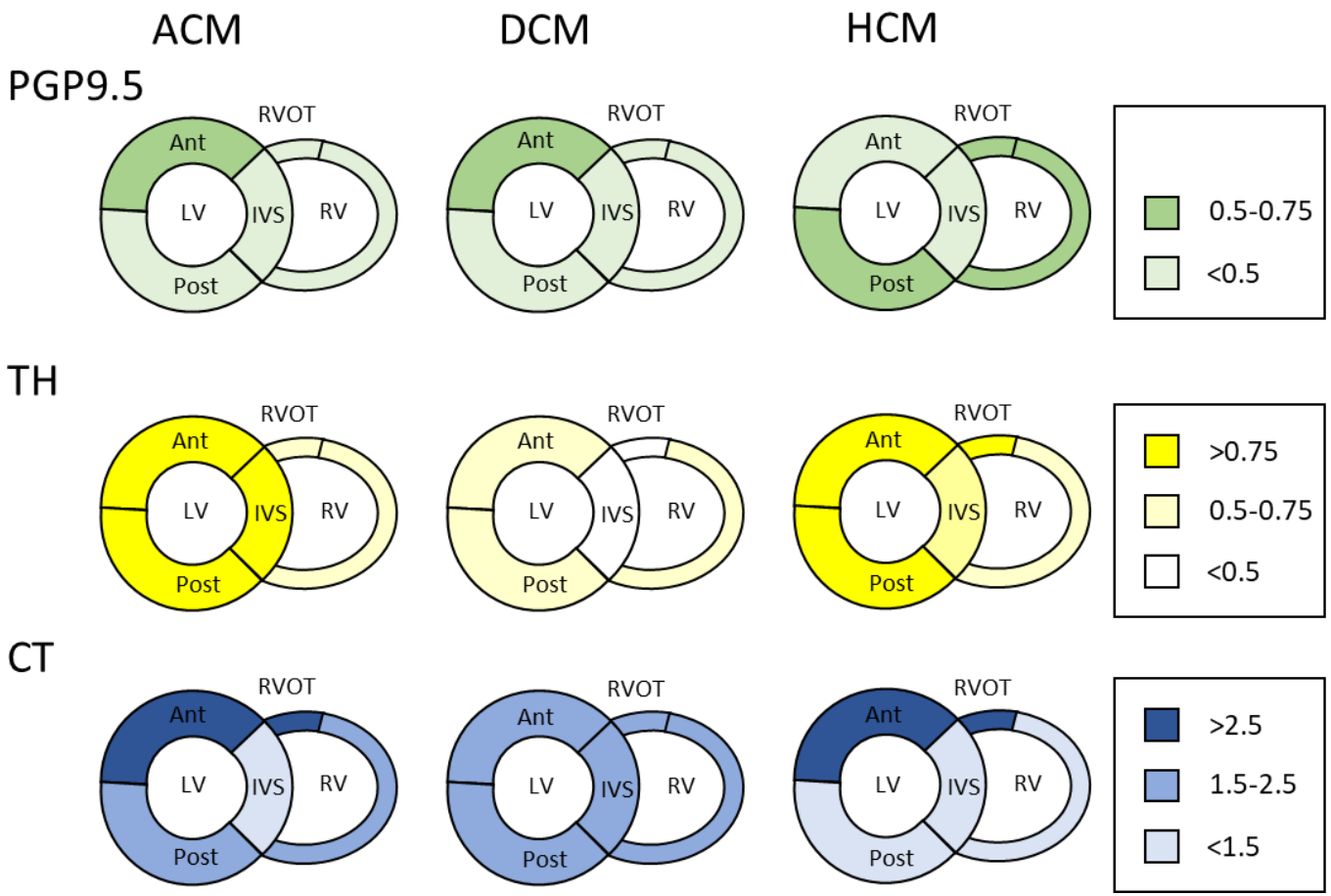
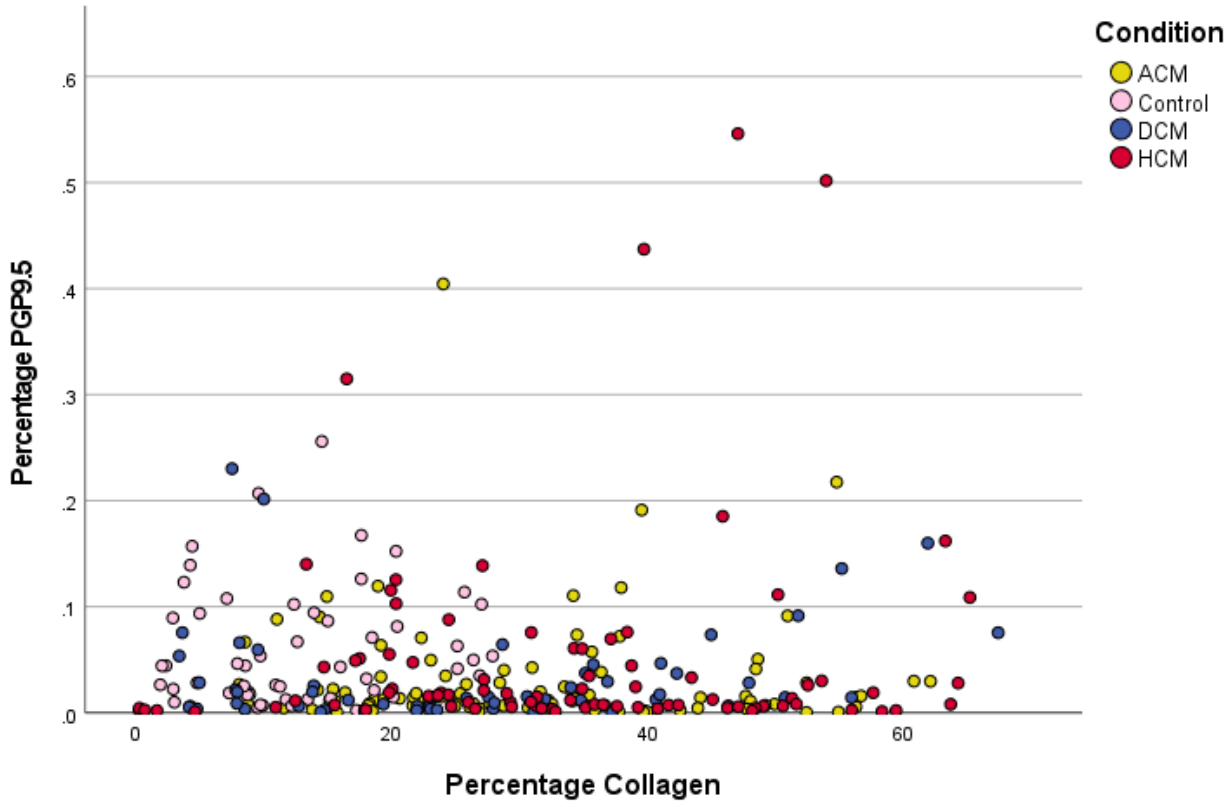
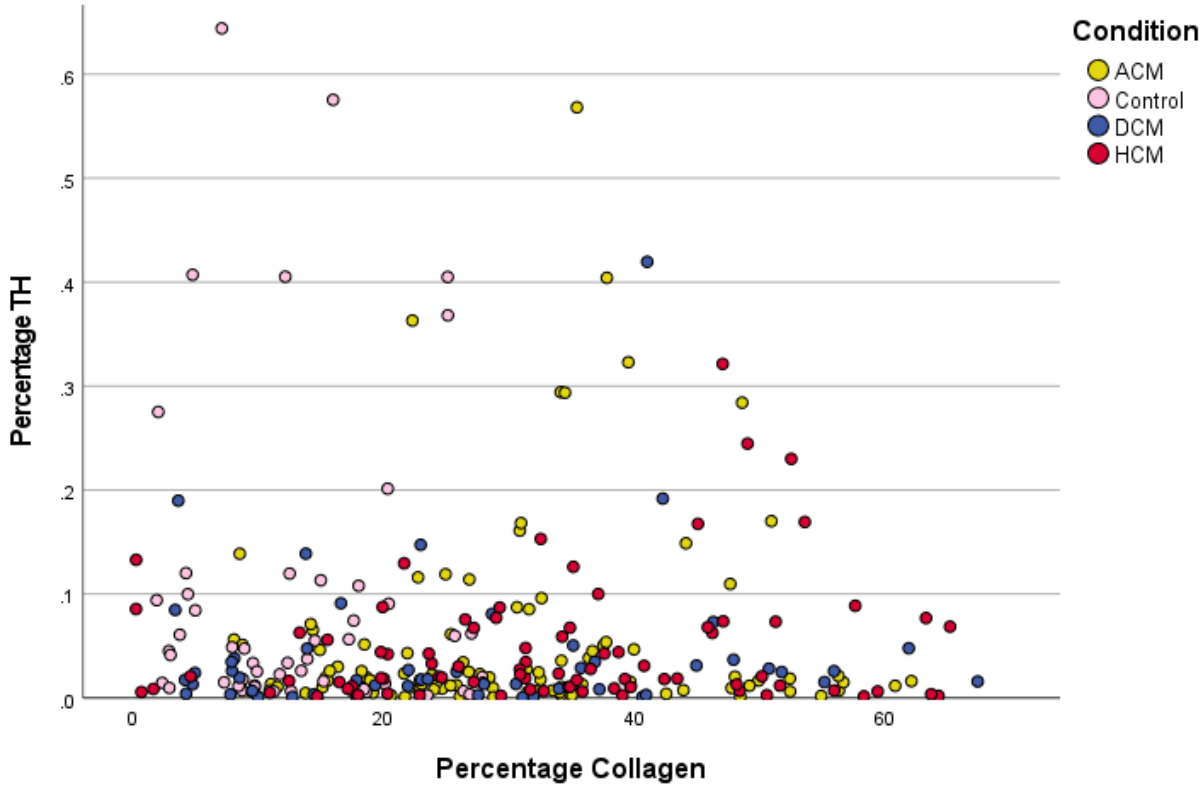


Figure 9.5. Ratio of general (PGP9.5), sympathetic (TH) and parasympathetic (CT) innervation in the cardiomyopathies to normal non-cardiac death hearts by right ventricular outflow tract (RVOT), right ventricle (RV), septum (IVS), anterior and posterior left ventricle (LV). ACM: arrhythmogenic cardiomyopathy; DCM: dilated cardiomyopathy; HCM: hypertrophic cardiomyopathy.


Condition
ACM
Control
DCM
HCM
Percentage PGP9.5
.0
.1
.2
.3
.4
.5
.6
0
20
40
60
Percentage Collagen


Condition
ACM
Control
DCM
HCM
Percentage TH
.0
.1
.2
.3
.4
.5
.6
0
20
40
60
Percentage Collagen

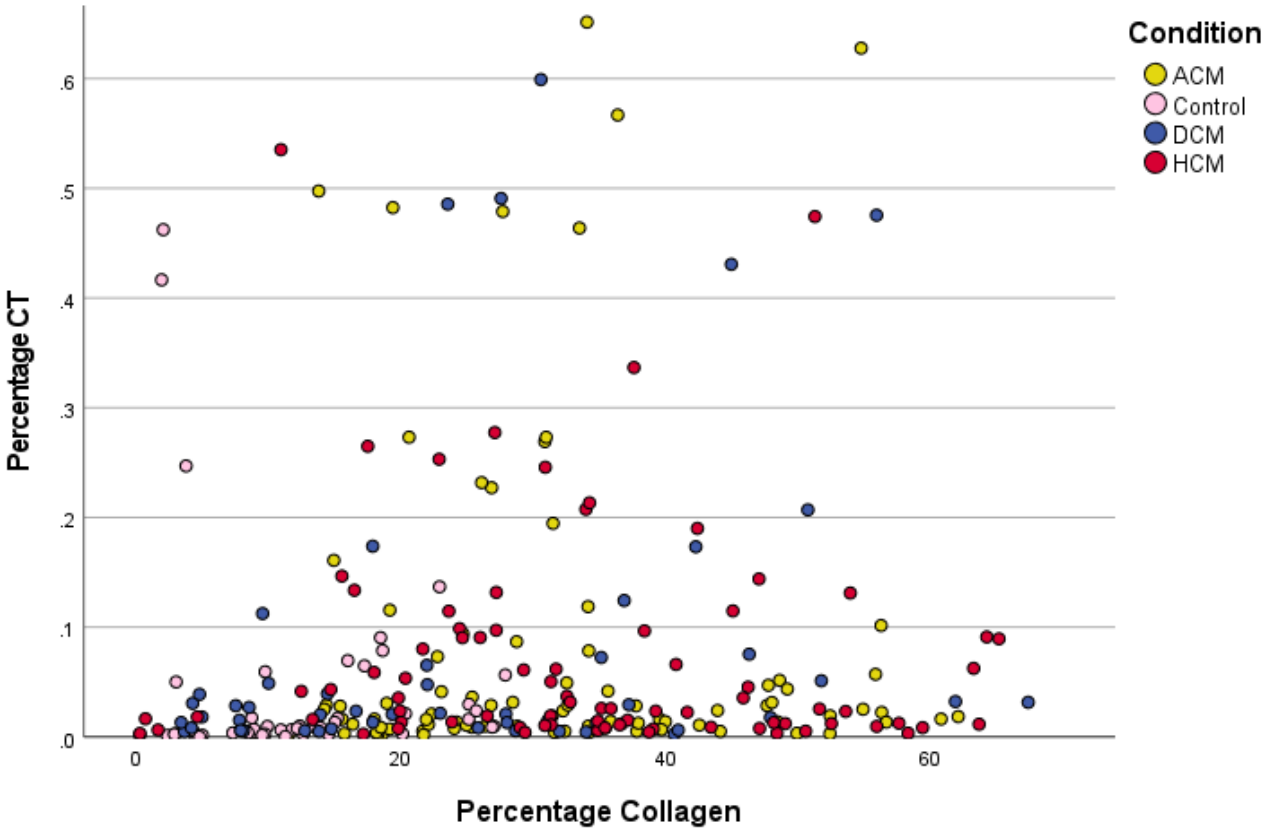


Figure 9.6. Pairwise correlation scatterplot showing relationship of collagen to general innervation (PGP9.5), sympathetic innervation (TH) and parasympathetic innervation (PGP9.5).

Clinical Implications

The thicker subepicardial fat in females should be accounted for when examining, risk stratifying and treating this population. Similarly, it is important to account for the fact the female heart is smaller with regard to the atria, ventricular cavity and muscle thickness as well as valves so as not to under call or under treat pathological abnormalities. Gender is an important modifier of cardiovascular health, disease, and medicine with discrepant outcomes occurring for a variety of reasons (Mauvais-Jarvis *et al.*, 2020).

The macroscopic and microscopic features described in ACM and DCM should help their differentiation using late gadolinium uptake and T1-mapping on resonance imaging (Moon *et al.*, 2013). The main distinguishing feature is the presence of replacement fibrosis in an epicardial distribution throughout the LV in ACM compared to interstitial fibrosis most prominent in the IVS with subtle interstitial fibrosis of the inner LV free wall.

The microscopic features of transmural interstitial and replacement fibrosis throughout the IVS and LV free wall in HCM should help in its differentiation from hypertensive heart disease using late gadolinium uptake and T1-mapping on resonance imaging (Moon *et al.*, 2013). Hypertensive heart disease contrastingly shows interstitial fibrosis in an inner myocardial distribution.

Innervation is proportionally higher in the RVOT. This may aid in our understanding as to why the RVOT is a focus point for generation of a number of arrhythmias.

The cardiomyopathies demonstrate regional structural losses in general innervation in sections showing fibrosis. Denervation may occur as a patchy process with loss of nerve bundles in combination with fibrosis. These changes require further investigation to establish a role in arrhythmogenesis.

Within DCM, the loss of myocytes and innervation may explain the reduction of ventricular function observed clinically in DCM. Reinnervation could prove beneficial in the restoration of function (Kasama *et al.*, 2007).

Limitations

Although localization of antigens using immunohistochemistry is a widely accepted and used technique, there is the possibility that other "non-specific" epitopes may be

recognised. The neural markers used in this study are highly specific and a specialised protocol has been developed to minimise background staining.

A further drawback of immunohistochemistry is that the presence of staining does not imply that the nerve is functionally active or even viable. It is therefore possible that the staining has marked damaged and non-functional nerves.

Quantitative techniques are frequently limited by subjective discrimination of structures, operator error and variation in tissue processing and staining. Automated image analysis using an app specifically developed to analyse the staining pattern has been used to overcome subjectivity and operator error. Tissue processing has been performed according to a standard protocol within our lab to minimise variation. A consistent staining protocol with optimal antibody dilutions and random sample selection has been used to minimise variation and eliminate bias.

Another limitation is time and resources. More time would have enabled the study of a greater number of cases. Greater numbers of normal hearts comprising of both genders and as wide an age range as possible would have allowed further interpretation of the effect of age and sex and helped to increase the power of the study.

Factors such as duration of disease and therapy prior to death were not controlled and it uncertain whether these variables would have affected the demonstration of cardiac innervation. The observations in cardiomyopathy are from a sudden death cohort and therefore may not extend to the wider cardiomyopathy population.

Information on genetic or family follow up results was not available for the cohort studied. This information would have enabled correlation with pathological findings.

Blinding and bias reduction

Multiple steps have been taken to eliminate bias within the study. Diagnoses have been reviewed by a panel including Professor Sheppard and Dr Westaby prior to inclusion in the study. Deidentification numbers are assigned to cases. Random number generation has been used to select both cases and slides to eliminate any selection bias. Scanning and image analysis has been performed blinded to diagnosis. Image analysis has been performed by a calibrated and optimised automated system. The automated system removes the possibility of operator bias in the image analysis.

Future work

Future work will aim to develop autonomous tools to identify areas of interest on immunostained sections. Selection of areas composed of solely fat and myocytes in normal hearts would allow quantification of innervation within both subepicardial fat and the myocardium. Selection of areas of pathology such as replacement fibrosis and myocyte disarray would allow quantification of innervation within these regions. This would reveal whether the process of denervation is centred on these areas compared to the background myocardium. The trends observed in sympathetic and parasympathetic innervation require further investigation and confirmation in a larger cohort.

Future mechanistic work will assess neuroregulatory molecules to allow identification of altered expression within disease states. Neurotrophins and semaphorins should be examined to establish whether there is altered regulation within cardiomyopathy tissue compared to controls. Quantitative polymerase chain reaction will be used to assess the level of messenger RNA expression for molecules implicated in neural

growth, survival and repulsion such as nerve growth factor, semaphorin 3A, growth associated protein 43, synaptophysin and tropomyosin receptor kinase A (Ieda *et al.*, 2007; Caporali and Emanueli, 2009; Houlton *et al.*, 2019).

Additionally, in vitro studies utilising cell culture of fibroblasts, myocytes and endothelial cells would be performed to assess the effect of these molecules. Collagen production, hypertrophy, proliferation and survival within the different cell lines will be assessed.

Murine models of cardiomyopathy will be used to test the effects of the administration of molecules targeted at neurotrophin signalling pathways with the aim of promoting neuronal survival and regeneration.

We will continue to prospectively collect splenic material which will enable us to determine whether there are correlations between genotype and alterations in cardiac innervation. For instance, in those cardiomyopathies with high risk of SCD such as the laminopathies (Van Rijsingen *et al.*, 2012).

Cardiac innervation will now be assessed in other conditions, such as ischaemic heart disease, atrial fibrillation and sudden arrhythmic death syndrome. This would leverage the substantial population of sudden arrhythmic death syndrome cases collected at St George's with linked molecular autopsy data. We would therefore be able to examine differential innervation in disorders such as catecholaminergic polymorphic ventricular tachycardia and long QT syndrome. Both disorders have shown clinical benefit from cardiac sympathectomy and whether a myocardial abnormality of innervation is in part responsible for the therapeutic response is unknown (Bos *et al.*, 2013; De Ferrari *et al.*, 2015).

We would also leverage digital Holter monitors from cardiomyopathy patients under follow-up and compare to digital Holter results from healthy controls collected as part

of our other research. Heart rate variability and turbulence, markers of autonomic function, could then be studied for associations with imaging phenotype and outcomes and therefore development of biomarkers for therapeutic targeting of patients.

References

Aaronson, S. T. *et al.* (2017) 'A 5-year observational study of patients with treatment-resistant depression treated with vagus nerve stimulation or treatment as usual: Comparison of response, remission, and suicidality', *American Journal of Psychiatry*, 174(7), pp. 640–648. doi: 10.1176/appi.ajp.2017.16010034.

Abe, Y. *et al.* (1987) 'The effect of cardiac sympathetic nerve stimulation on the right ventricle in canine heart', *Japanese Circulation Journal*, 51(5), pp. 535–542. doi: 10.1253/jcj.51.535.

Ackerman, M., Atkins, D. L. and Triedman, J. K. (2016) 'Sudden cardiac death in the young', *Circulation*. doi: 10.1161/CIRCULATIONAHA.115.020254.

Adabag, A. S. *et al.* (2010) 'Sudden cardiac death: Epidemiology and risk factors', *Nature Reviews Cardiology*. doi: 10.1038/nrcardio.2010.3.

Ajijola, O. A. *et al.* (2012) 'Extracardiac neural remodeling in humans with cardiomyopathy', *Circulation: Arrhythmia and Electrophysiology*, 5(5), pp. 1010–1016. doi: 10.1161/CIRCEP.112.972836.

Ajijola, O. A. *et al.* (2013) 'Functional differences between junctional and extrajunctional adrenergic receptor activation in mammalian ventricle', *https://doi.org/10.1152/ajpheart.00754.2012*, 304(4), pp. 579–588. doi: 10.1152/AJPHEART.00754.2012.

Al-Khatib, S. M. *et al.* (2018) '2017 AHA/ACC/HRS Guideline for Management of Patients With Ventricular Arrhythmias and the Prevention of Sudden Cardiac Death', *Circulation*. doi: 10.1161/CIR.0000000000000549.

Aliot, E. M. *et al.* (2009) 'EHRA/HRS expert consensus on catheter ablation of ventricular arrhythmias', *Europace*. doi: 10.1093/europace/eup098.

Amorim, D. S. *et al.* (1981) 'Is there autonomic impairment in congestive (dilated)

cardiomyopathy?', *The Lancet*, 317(8219), pp. 525–527. doi: 10.1016/S0140-6736(81)92863-4.

Amorim, D. S. and Olsen, E. G. J. (1982) 'Assessment of heart neurons in dilated (congestive) cardiomyopathy', *British Heart Journal*. doi: 10.1136/hrt.47.1.11.

Anderson, R. H. and Becker, A. E. (1985) 'Cardiac pathology — an integrated text and colour atlas', *International Journal of Cardiology*, 8(2), pp. 220–221. doi: 10.1016/0167-5273(85)90295-5.

Anderson, R. H., Razavi, R. and Taylor, A. M. (2004) 'Cardiac anatomy revisited', *Journal of Anatomy*. Wiley-Blackwell, pp. 159–177. doi: 10.1111/j.0021-8782.2004.00330.x.

Angelini, A. *et al.* (1996) 'Endomyocardial biopsy in arrhythmogenic right ventricular cardiomyopathy', *American Heart Journal*, pp. 203–206. doi: 10.1016/S0002-8703(96)90416-0.

Aras, K. *et al.* (2022) 'Electrophysiology and Arrhythmogenesis in the Human Right Ventricular Outflow Tract.', *Circulation. Arrhythmia and electrophysiology*, p. CIRCEP121010630. doi: 10.1161/CIRCEP.121.010630.

Ardell, J. L. and Armour, J. A. (2016) 'Neurocardiology: Structure-Based Function', *Comprehensive Physiology*, 6(4), pp. 1635–1653. doi: 10.1002/CPHY.C150046.

Armaganijan, L. *et al.* (2014) 'Renal Denervation Using an Irrigated Catheter in Patients with Resistant Hypertension: A Promising Strategy?', *Arquivos Brasileiros de Cardiologia*. doi: 10.5935/abc.20140034.

Armaganijan, L. V. *et al.* (2015) '6-Month Outcomes in Patients With Implantable Cardioverter-Defibrillators Undergoing Renal Sympathetic Denervation for the Treatment of Refractory Ventricular Arrhythmias', *JACC: Cardiovascular Interventions*. doi: 10.1016/j.jcin.2015.03.012.

Armour, J. A. *et al.* (1997) ‘Gross and microscopic anatomy of the human intrinsic cardiac nervous system’, *Anatomical Record*, 247(2), pp. 289–298. doi: 10.1002/(SICI)1097-0185(199702)247:2<289::AID-AR15>3.0.CO;2-L.

Assis, F. R. *et al.* (2019) ‘Cardiac sympathectomy for refractory ventricular tachycardia in arrhythmogenic right ventricular cardiomyopathy’, *Heart Rhythm*. doi: 10.1016/j.hrthm.2019.01.019.

Assomull, R. G. *et al.* (2006) ‘Cardiovascular magnetic resonance, fibrosis, and prognosis in dilated cardiomyopathy’, *Journal of the American College of Cardiology*, 48(10), pp. 1977–1985. doi: 10.1016/J.JACC.2006.07.049.

Awad, M. M., Calkins, H. and Judge, D. P. (2008) ‘Mechanisms of disease: Molecular genetics of arrhythmogenic right ventricular dysplasia/cardiomyopathy’, *Nature Clinical Practice Cardiovascular Medicine*. Nat Clin Pract Cardiovasc Med, pp. 258–267. doi: 10.1038/ncpcardio1182.

Bagnall, R. D. *et al.* (2016) ‘A Prospective Study of Sudden Cardiac Death among Children and Young Adults’, *New England Journal of Medicine*, 374(25), pp. 2441–2452. doi: 10.1056/nejmoa1510687.

Bagwan, I. N., Hooper, L. V. B. and Sheppard, M. N. (2011) ‘Cardiac sarcoidosis and sudden death. The heart may look normal or mimic other cardiomyopathies’, *Virchows Archiv : an international journal of pathology*, 458(6), pp. 671–678. doi: 10.1007/S00428-010-1003-8.

Bai, R. *et al.* (2011) ‘Ablation of ventricular arrhythmias in arrhythmogenic right ventricular dysplasia/cardiomyopathy: Arrhythmia-free survival after endo-epicardial substrate based mapping and ablationablation of ventricular arrhythmias in arrhythmogenic right ventricular dysplasia/cardiomyopathy arrhythmia-free survival after endo-epicardial substrate based mapping and ablation’, *Circulation: Arrhythmia*

and Electrophysiology, 4(4), pp. 478–485. doi: 10.1161/CIRCEP.111.963066.

Basso, C. *et al.* (1996) 'Arrhythmogenic Right Ventricular Cardiomyopathy', *Circulation*, 94(5), pp. 983–991. doi: 10.1161/01.CIR.94.5.983.

Basso, C. *et al.* (2017) 'Guidelines for autopsy investigation of sudden cardiac death: 2017 update from the Association for European Cardiovascular Pathology', *Virchows Archiv*, 471(6), pp. 691–705. doi: 10.1007/S00428-017-2221-0/TABLES/4.

Basso, C. *et al.* (2021) 'Cardiac hypertrophy at autopsy', *Virchows Archiv*, 479(1), pp. 79–94. doi: 10.1007/S00428-021-03038-0/FIGURES/13.

Belhassen, B. and Viskin, S. (1993) 'Idiopathic Ventricular Tachycardia and Fibrillation', *Journal of Cardiovascular Electrophysiology*. John Wiley & Sons, Ltd, pp. 356–368. doi: 10.1111/j.1540-8167.1993.tb01236.x.

Boogers, M. J. *et al.* (2010) 'Cardiac Sympathetic Denervation Assessed With 123-Iodine Metaiodobenzylguanidine Imaging Predicts Ventricular Arrhythmias in Implantable Cardioverter-Defibrillator Patients', *Journal of the American College of Cardiology*. doi: 10.1016/j.jacc.2009.12.066.

Bos, J. M. *et al.* (2013) 'Left cardiac sympathetic denervation in long QT syndrome: analysis of therapeutic nonresponders', *Circulation. Arrhythmia and electrophysiology*, 6(4), pp. 705–711. doi: 10.1161/CIRCEP.113.000102.

Boukens, B. J., Coronel, R. and Christoffels, V. M. (2016) 'Embryonic development of the right ventricular outflow tract and arrhythmias'. doi: 10.1016/j.hrthm.2015.11.014.

Bourke, T. *et al.* (2010) 'Neuraxial modulation for refractory ventricular arrhythmias: Value of thoracic epidural anesthesia and surgical left cardiac sympathetic denervation', *Circulation*. doi: 10.1161/CIRCULATIONAHA.109.929703.

Bowker, T. J. *et al.* (2003) 'Sudden, unexpected cardiac or unexplained death in

England: A national survey', *QJM - Monthly Journal of the Association of Physicians*, 96(4), pp. 269–279. doi: 10.1093/qjmed/hcg038.

Bozkurt, B. *et al.* (2016) 'Current Diagnostic and Treatment Strategies for Specific Dilated Cardiomyopathies: A Scientific Statement from the American Heart Association', *Circulation*. doi: 10.1161/CIR.0000000000000455.

Cao, J. M., Chen, L. S., *et al.* (2000) 'Nerve sprouting and sudden cardiac death', *Circulation Research*. doi: 10.1161/01.RES.86.7.816.

Cao, J. M., Fishbein, M. C., *et al.* (2000) 'Relationship between regional cardiac hyperinnervation and ventricular arrhythmia', *Circulation*. doi: 10.1161/01.CIR.101.16.1960.

Caporali, A. and Emanueli, C. (2009) 'Cardiovascular Actions of Neurotrophins', *Physiological reviews*, 89(1), p. 279. doi: 10.1152/PHYSREV.00007.2008.

Cardinal, R. *et al.* (2009) 'Spatially divergent cardiac responses to nicotinic stimulation of ganglionated plexus neurons in the canine heart', *Autonomic neuroscience : basic & clinical*, 145(1–2), pp. 55–62. doi: 10.1016/J.AUTNEU.2008.11.007.

Chappex, N. *et al.* (2015) 'Sudden cardiac death among general population and sport related population in forensic experience', *Journal of Forensic and Legal Medicine*, 35, pp. 62–68. doi: 10.1016/J.JFLM.2015.07.004.

Chen, P. S. *et al.* (2014) 'Role of the autonomic nervous system in atrial fibrillation: Pathophysiology and therapy', *Circulation Research*. doi: 10.1161/CIRCRESAHA.114.303772.

Chimura, M. *et al.* (2019) 'Late gadolinium enhancement on cardiac magnetic resonance combined with 123I- metaiodobenzylguanidine scintigraphy strongly predicts long-term clinical outcome in patients with dilated cardiomyopathy', *PLoS*

ONE, 14(6). doi: 10.1371/JOURNAL.PONE.0217865.

Chow, L. T. *et al.* (1993) 'Innervation of the human cardiac conduction system at birth.', *Heart*, 69(5), pp. 430–435. doi: 10.1136/HRT.69.5.430.

Cohle, S. D. (2011) 'Histopathology of the Cardiac Conduction System in the Investigation of Sudden Unexpected Death':, *https://doi.org/10.23907/2011.027*, 1(2), pp. 206–215. doi: 10.23907/2011.027.

Cooper, S. T. E. *et al.* (2021) 'The role of endocarditis in sudden cardiac death: highlighting the value of the autopsy, pathological features and cardiac complications', *Cardiovascular Pathology*. doi: 10.1016/j.carpath.2020.107292.

Coronel, R. *et al.* (1989) 'Distribution of extracellular potassium and electrophysiologic changes during two-stage coronary ligation in the isolated, perfused canine heart', *Circulation*. doi: 10.1161/01.CIR.80.1.165.

Corradi, D. *et al.* (2004) 'The ventricular epicardial fat is related to the myocardial mass in normal, ischemic and hypertrophic hearts', *Cardiovascular Pathology*, 13(6), pp. 313–316. doi: 10.1016/j.carpath.2004.08.005.

Corrado, D. *et al.* (1997) 'Spectrum of Clinicopathologic Manifestations of Arrhythmogenic Right Ventricular Cardiomyopathy/Dysplasia: A Multicenter Study', *Journal of the American College of Cardiology*, 30(6), pp. 1512–1520. doi: 10.1016/S0735-1097(97)00332-X.

Corrado, D. *et al.* (2003) 'Does Sports Activity Enhance the Risk of Sudden Death in Adolescents and Young Adults?', *Journal of the American College of Cardiology*, 42(11), pp. 1959–1963. doi: 10.1016/j.jacc.2003.03.002.

Corrado, D., Basso, C. and Judge, D. P. (2017) 'Arrhythmogenic cardiomyopathy', *Circulation Research*. doi: 10.1161/CIRCRESAHA.117.309345.

Corrado, D., Basso, C. and Thiene, G. (2001) 'Sudden cardiac death in young

people with apparently normal heart', *Cardiovascular Research*, 50(2), pp. 399–408. doi: 10.1016/S0008-6363(01)00254-1.

Coumel, P., Leclercq, J. F. and Escoubet, B. (1987) 'Beta-blockers: Use for arrhythmias', *European Heart Journal*. doi: 10.1093/eurheartj/8.suppl_a.41.

Counihan, P. J. *et al.* (1993) 'Assessment of heart rate variability in hypertrophic cardiomyopathy. Association with clinical and prognostic features', *Circulation*, 88(4 Pt 1), pp. 1682–1690. doi: 10.1161/01.CIR.88.4.1682.

Crick, S. J. *et al.* (1994) 'Innervation of the human cardiac conduction system: A quantitative immunohistochemical and histochemical study', *Circulation*. doi: 10.1161/01.CIR.89.4.1697.

Dastur, D. K., Vevaina, S. C. and Manghani, D. K. (1989) 'Fine structure of A: autonomic nerve fibers and terminals in human myocardium; and B: myocardial changes in congenital heart disease.', *Ultrastructural pathology*, 13(4), pp. 413–431. doi: 10.3109/01913128909048492.

Davies, M. J. (1981) 'Pathological view of sudden cardiac death', *British heart journal*, 45(1), pp. 88–96. doi: 10.1136/HRT.45.1.88.

Davies, M. J. (1984) 'The cardiomyopathies: a review of terminology, pathology and pathogenesis', *Histopathology*, 8(3), pp. 363–393. doi: 10.1111/J.1365-2559.1984.TB02351.X.

Davies, M. J. (1996) 'Stability and Instability: Two Faces of Coronary Atherosclerosis', *Circulation*, 94(8), pp. 2013–2020. doi: 10.1161/01.CIR.94.8.2013.

Davies, M. J. and Popple, A. (1979) 'Sudden unexpected cardiac death—a practical approach to the forensic problem', *Histopathology*, 3(4), pp. 255–277. doi: 10.1111/j.1365-2559.1979.tb03008.x.

Debonnaire, P. *et al.* (2017) 'Left atrial size and function in hypertrophic

cardiomyopathy patients and risk of new-onset atrial fibrillation', *Circulation: Arrhythmia and Electrophysiology*, 10(2). doi: 10.1161/CIRCEP.116.004052.

Desai, R. *et al.* (2017) 'Burden of Arrhythmias in Epilepsy Patients: A Nationwide Inpatient Analysis of 1.4 Million Hospitalizations in the United States', *Cureus*, 9(8). doi: 10.7759/CUREUS.1550.

Do, D. H. *et al.* (2017) 'Thoracic epidural anesthesia can be effective for the short-term management of ventricular tachycardia storm', *Journal of the American Heart Association*, 6(11). doi: 10.1161/JAHA.117.007080.

Doesch, C. *et al.* (2013) 'Epicardial adipose tissue assessed by cardiac magnetic resonance imaging in patients with heart failure due to dilated cardiomyopathy', *Obesity (Silver Spring, Md.)*, 21(3). doi: 10.1002/OBY.20149.

Dusi, V. *et al.* (2019) 'Cardiac Sympathetic Denervation in Channelopathies', *Frontiers in Cardiovascular Medicine*. doi: 10.3389/fcvm.2019.00027.

Eckart, R. E. *et al.* (2011) 'Sudden death in young adults: an autopsy-based series of a population undergoing active surveillance', *Journal of the American College of Cardiology*, 58(12), pp. 1254–1261. doi: 10.1016/J.JACC.2011.01.049.

Ellestad, M. H. (1996) 'Chronotropic incompetence: The implications of heart rate response to exercise (compensatory parasympathetic hyperactivity?)', *Circulation*. Circulation, pp. 1485–1487. doi: 10.1161/01.CIR.93.8.1485.

Elliott, P. M. *et al.* (2006) 'Historical trends in reported survival rates in patients with hypertrophic cardiomyopathy', *Heart*. doi: 10.1136/hrt.2005.068577.

Erol, C. and Seker, M. (2012) 'The prevalence of coronary artery variations on coronary computed tomography angiography', *Acta Radiologica*, 53(3), pp. 278–284. doi: 10.1258/ar.2011.110394.

Evranos, B. *et al.* (2016) 'Role of Adjuvant Renal Sympathetic Denervation in the

Treatment of Ventricular Arrhythmias', *American Journal of Cardiology*. doi: 10.1016/j.amjcard.2016.07.036.

Fabre, A. and Sheppard, M. N. (2006) 'Sudden adult death syndrome and other non-ischaemic causes of sudden cardiac death', *Heart*. Heart, pp. 316–320. doi: 10.1136/hrt.2004.045518.

Fallavollita, J. A. *et al.* (2014) 'Regional myocardial sympathetic denervation predicts the risk of sudden cardiac arrest in ischemic cardiomyopathy', *Journal of the American College of Cardiology*. doi: 10.1016/j.jacc.2013.07.096.

De Ferrari, G. M. *et al.* (2015) 'Clinical Management of Catecholaminergic Polymorphic Ventricular Tachycardia: The Role of Left Cardiac Sympathetic Denervation', *Circulation*, 131(25), pp. 2185–2193. doi: 10.1161/CIRCULATIONAHA.115.015731.

Finocchiaro, G. *et al.* (2019) 'Sudden Death Can Be the First Manifestation of Hypertrophic Cardiomyopathy: Data From a United Kingdom Pathology Registry', *JACC: Clinical Electrophysiology*. Elsevier Inc, pp. 252–254. doi: 10.1016/j.jacep.2018.11.004.

Finocchiaro, G. *et al.* (2020) 'Diagnostic yield of hypertrophic cardiomyopathy in first-degree relatives of decedents with idiopathic left ventricular hypertrophy', *Europace*. doi: 10.1093/europace/euaa012.

Foà, A. *et al.* (2019) 'Histopathological comparison of intramural coronary artery remodeling and myocardial fibrosis in obstructive versus end-stage hypertrophic cardiomyopathy', *International Journal of Cardiology*, 291, pp. 77–82. doi: 10.1016/J.IJCARD.2019.03.060.

Folino, A. F. *et al.* (2002) 'Heart rate variability in arrhythmogenic right ventricular cardiomyopathy correlation with clinical and prognostic features', *PACE - Pacing and*

Clinical Electrophysiology, 25(9), pp. 1285–1292. doi: 10.1046/j.1460-9592.2002.01285.x.

Franciosi, S. *et al.* (2017) 'The role of the autonomic nervous system in arrhythmias and sudden cardiac death', *Autonomic Neuroscience: Basic and Clinical*. doi: 10.1016/j.autneu.2017.03.005.

Fukuda, K. *et al.* (2015) 'Cardiac Innervation and Sudden Cardiac Death', *Circulation Research*. doi: 10.1161/CIRCRESAHA.116.304679.

Fuller, B. *et al.* (2017) 'Increased Epicardial Fat Thickness in Sudden Death From Stable Coronary Artery Atherosclerosis', *The American journal of forensic medicine and pathology*, 38(2), pp. 162–166. doi: 10.1097/PAF.0000000000000310.

Gaitskell, K., Perera, R. and Soilleux, E. J. (2011) 'Derivation of new reference tables for human heart weights in light of increasing body mass index', *Journal of Clinical Pathology*, 64(4), pp. 358–362. doi: 10.1136/JCP.2010.084574.

Galati, G. *et al.* (2016) 'Histological and histometric characterization of myocardial fibrosis in end-stage hypertrophic cardiomyopathy', *Circulation: Heart Failure*, 9(9). doi: 10.1161/CIRCHEARTFAILURE.116.003090.

Gallo, P, D'Amati, G. (2001) 'Cardiomyopathies', in *Silver M, Gotlieb A, Schoen F, eds. Cardiovascular Pathology.* Churchill Livingstone, pp. 285–325. Available at: https://www.google.com/search?q=+Gallo+P%2C+D%27Amati+G.+Cardiomyopathies.+In%3A+Silver+M%2C+Gotlieb+A%2C+Schoen+F%2C+eds.+Cardiovascular+Pathology.+New+York%2C+NY%3A+Churchill+Livingstone%3B+2001%3A+285–325.&rlz=1C1GCEB_enGB917GB917&biw=1920&bih=1089&ei= (Accessed: 23 February 2022).

Gandjbakhch, E. *et al.* (2018) 'Clinical Diagnosis, Imaging, and Genetics of Arrhythmogenic Right Ventricular Cardiomyopathy/Dysplasia: JACC State-of-the-Art

Review', *Journal of the American College of Cardiology*. doi: 10.1016/j.jacc.2018.05.065.

Gao, D. and Sapp, J. L. (2013) 'Electrical storm: Definitions, clinical importance, and treatment', *Current Opinion in Cardiology*. doi: 10.1097/HCO.0b013e32835b59db.

Garbi, M., Lancellotti, P. and Sheppard, M. N. (2018) 'Mitral valve and left ventricular features in malignant mitral valve prolapse', *Open Heart*, 5(2), p. 925. doi: 10.1136/openhrt-2018-000925.

Garcia, F. C. *et al.* (2009) 'Epicardial substrate and outcome with epicardial ablation of ventricular tachycardia in arrhythmogenic right ventricular cardiomyopathy/dysplasia', *Circulation*, 120(5), pp. 366–375. doi: 10.1161/CIRCULATIONAHA.108.834903.

Gardner, R. T. *et al.* (2015) 'Targeting protein tyrosine phosphatase σ after myocardial infarction restores cardiac sympathetic innervation and prevents arrhythmias', *Nature Communications*. doi: 10.1038/ncomms7235.

La Gerche, A. *et al.* (2011) 'Disproportionate exercise load and remodeling of the athlete's right ventricle', *Medicine and science in sports and exercise*, 43(6), pp. 974–981. doi: 10.1249/MSS.0B013E31820607A3.

Gilligan, D. M. *et al.* (1993) 'Autonomic function in hypertrophic cardiomyopathy', *British heart journal*, 69(6), pp. 525–529. doi: 10.1136/HRT.69.6.525.

Gjerløff, T. *et al.* (2014) 'In Vivo Imaging of Human Acetylcholinesterase Density in Peripheral Organs Using 11C-Donepezil: Dosimetry, Biodistribution, and Kinetic Analyses', *Journal of Nuclear Medicine*, 55(11), pp. 1818–1824. doi: 10.2967/JNUMED.114.143859.

Glennon, P. E., Petersen, M. E. and Sheppard, M. N. (1996) 'Fatal giant cell myocarditis after resection of thymoma.', *Heart*, 75(5), p. 531. doi:

10.1136/HRT.75.5.531.

Gordon, L. *et al.* (1993) ‘Development of the peptidergic innervation of human heart.’, *Journal of anatomy*, 183 (Pt 1, pp. 131–40. Available at: https://www.ncbi.nlm.nih.gov/pmc/articles/pmc1259861/ (Accessed: 21 March 2022).

Greulich, S. *et al.* (2012) ‘Secretory products from epicardial adipose tissue of patients with type 2 diabetes mellitus induce cardiomyocyte dysfunction’, *Circulation*, 126(19), pp. 2324–2334. doi: 10.1161/CIRCULATIONAHA.111.039586.

Grimm, W. and Maisch, B. (2002) ‘Sudden cardiac death in dilated cardiomyopathy - Therapeutic options’, *Herz*. doi: 10.1007/s00059-002-2425-0.

Groeneweg, J. A. *et al.* (2015) ‘Clinical Presentation, Long-Term Follow-Up, and Outcomes of 1001 Arrhythmogenic Right Ventricular Dysplasia/Cardiomyopathy Patients and Family Members’, *Circulation: Cardiovascular Genetics*. doi: 10.1161/CIRCGENETICS.114.001003.

Le Guludec, D. *et al.* (1997) ‘Increased Myocardial Muscarinic Receptor Density in Idiopathic Dilated Cardiomyopathy’, *Circulation*, 96(10), pp. 3416–3422. doi: 10.1161/01.CIR.96.10.3416.

Hagen, P., Scholz, D. and Edwards, W. (1984) ‘Incidence and size of patent foramen ovale during the first 10 decades of life: an autopsy study of 965 normal hearts’, *Mayo Clinic proceedings*, 59(1), pp. 17–20. doi: 10.1016/S0025-6196(12)60336-X.

Haider, A. W. *et al.* (1998) ‘Increased left ventricular mass and hypertrophy are associated with increased risk for sudden death’, *Journal of the American College of Cardiology*. doi: 10.1016/S0735-1097(98)00407-0.

Haissaguerre, M. *et al.* (2022) ‘Purkinje network and myocardial substrate at the onset of human ventricular fibrillation: implications for catheter ablation’, *European Heart Journal*, 43(12), pp. 1234–1247. doi: 10.1093/EURHEARTJ/EHAB893.

Haïssaguerre, M. *et al.* (2003) ‘Mapping and Ablation of Ventricular Fibrillation Associated With Long-QT and Brugada Syndromes’. doi: 10.1161/01.CIR.0000088781.99943.95.

Halliday, B. P. *et al.* (2019) ‘Outcome in Dilated Cardiomyopathy Related to the Extent, Location, and Pattern of Late Gadolinium Enhancement’, *JACC: Cardiovascular Imaging*, 12(8P2), pp. 1645–1655. doi: 10.1016/J.JCMG.2018.07.015.

Halushka, M. K. *et al.* (2016) ‘Consensus statement on surgical pathology of the aorta from the Society for Cardiovascular Pathology and the Association For European Cardiovascular Pathology: II. Noninflammatory degenerative diseases — nomenclature and diagnostic criteria’, *Cardiovascular Pathology*, 25(3), pp. 247–257. doi: 10.1016/J.CARPATH.2016.03.002.

Han, J. and Moe, G. K. (1964) ‘Nonuniform recovery of excitability in ventricular muscle.’, *Circulation research*, 14, pp. 44–60. doi: 10.1161/01.RES.14.1.44.

Hanna, P., Shivkumar, K. and Ardell, J. L. (2018) ‘Calming the Nervous Heart: Autonomic Therapies in Heart Failure’, *Cardiac Failure Review*. doi: 10.15420/cfr.2018.20.2.

Hasan, W. *et al.* (2006) ‘Sympathetic hyperinnervation and inflammatory cell NGF synthesis following myocardial infarction in rats’, *Brain Research*. doi: 10.1016/j.brainres.2006.09.054.

Hatem, S. N. and Sanders, P. (2014) ‘Epicardial adipose tissue and atrial fibrillation’, *Cardiovascular Research*. Oxford University Press, pp. 205–213. doi: 10.1093/cvr/cvu045.

Hayashi, M., Shimizu, W. and Albert, C. M. (2015) ‘The Spectrum of Epidemiology Underlying Sudden Cardiac Death’, *Circulation Research*, 116(12), p. 1887. doi:

10.1161/CIRCRESAHA.116.304521.

Henderson, A. (1996) ‘Coronary heart disease: Overview’, *The Lancet*, 348(SUPPL.1), pp. S1–S4. doi: 10.1016/S0140-6736(96)98001-0.

Henning, R. J. and Sawmiller, D. R. (2001) ‘Vasoactive intestinal peptide: cardiovascular effects’, *Cardiovascular research*, 49(1), pp. 27–37. doi: 10.1016/S0008-6363(00)00229-7.

Hill, S. F. and Sheppard, M. N. (2010) ‘Non-atherosclerotic coronary artery disease associated with sudden cardiac death’, *Heart*, 96(14), pp. 1119–1125. doi: 10.1136/HRT.2009.185157.

Homma, S. and Sacco, R. L. (2005) ‘Patent foramen ovale and stroke’, *Circulation*, 112(7), pp. 1063–1072. doi: 10.1161/CIRCULATIONAHA.104.524371.

Hookana, E. *et al.* (2011) ‘Causes of nonischemic sudden cardiac death in the current era’, *Heart rhythm*, 8(10), pp. 1570–1575. doi: 10.1016/J.HRTHM.2011.06.031.

Hoover, D. B. *et al.* (2009) ‘Localization of multiple neurotransmitters in surgically derived specimens of human atrial ganglia’, *Neuroscience*, 164(3), pp. 1170–1179. doi: 10.1016/J.NEUROSCIENCE.2009.09.001.

Horckmans, M. *et al.* (2018) ‘Pericardial adipose tissue regulates granulopoiesis, fibrosis, and cardiac function after myocardial infarction’, *Circulation*, 137(9), pp. 948–960. doi: 10.1161/CIRCULATIONAHA.117.028833.

Houlton, J. *et al.* (2019) ‘Therapeutic potential of neurotrophins for repair after brain injury: A helping hand from biomaterials’, *Frontiers in Genetics*, 10(JUL), p. 790. doi: 10.3389/FNINS.2019.00790/BIBTEX.

Huang, Y. *et al.* (2013) ‘Image analysis of liver collagen using sirius red is more accurate and correlates better with serum fibrosis markers than trichrome’, *Liver*

International, 33(8), pp. 1249–1256. doi: 10.1111/LIV.12184.

Hucker, W. J., Nikolski, V. P. and Efimov, I. R. (2007) 'Autonomic control and innervation of the atrioventricular junctional pacemaker', *Heart Rhythm*. doi: 10.1016/j.hrthm.2007.06.011.

Ieda, M. *et al.* (2007) 'Sema3a maintains normal heart rhythm through sympathetic innervation patterning', *Nature medicine*, 13(5), pp. 604–612. doi: 10.1038/NM1570.

Ihdayhid, A. R. *et al.* (2020) 'Ethnic differences in coronary anatomy, left ventricular mass and CT-derived fractional flow reserve', *Journal of Cardiovascular Computed Tomography*. doi: 10.1016/j.jcct.2020.09.004.

Irie, T. *et al.* (2017) 'Cardiac sympathetic innervation via middle cervical and stellate ganglia and antiarrhythmic mechanism of bilateral stellectomy', *American Journal of Physiology - Heart and Circulatory Physiology*. doi: 10.1152/ajpheart.00644.2016.

James, W. P. T. (2009) 'WHO recognition of the global obesity epidemic', *International Journal of Obesity 2008 32:7*, 32(7), pp. S120–S126. doi: 10.1038/ijo.2008.247.

Janes, R. D. *et al.* (1986) 'Anatomy of human extrinsic cardiac nerves and ganglia', *The American Journal of Cardiology*, 57(4), pp. 299–309. doi: 10.1016/0002-9149(86)90908-2.

Japp, A. G. *et al.* (2016) 'The Diagnosis and Evaluation of Dilated Cardiomyopathy', *Journal of the American College of Cardiology*. doi: 10.1016/j.jacc.2016.03.590.

Jugdutt, B. I. *et al.* (2003) 'Ventricular Remodeling After Infarction and the Extracellular Collagen Matrix When Is Enough Enough? Review: Current Perspective', *Circulation*, 108, pp. 1395–1403. doi: 10.1161/01.CIR.0000085658.98621.49.

Julian, K. *et al.* (2022) 'A review of cardiac autonomics: from pathophysiology to

therapy.', *Future cardiology*, 18(2), pp. 125–133. doi: 10.2217/fca-2021-0041.

Kadish, A. *et al.* (2004) 'Prophylactic Defibrillator Implantation in Patients with Nonischemic Dilated Cardiomyopathy', *New England Journal of Medicine*. doi: 10.1056/NEJMoa033088.

Kallmünzer, B. *et al.* (2012) 'Serious cardiac arrhythmias after stroke: Incidence, time course, and predictors-a systematic, prospective analysis', *Stroke*, 43(11), pp. 2892–2897. doi: 10.1161/STROKEAHA.112.664318.

Kapur, R. P. *et al.* (2017) 'Choline Transporter Immunohistochemistry', *undefined*, 20(4), pp. 308–320. doi: 10.1177/1093526617697060.

Kasama, S. *et al.* (2007) 'Evaluation of cardiac sympathetic nerve activity and left ventricular remodelling in patients with dilated cardiomyopathy on the treatment containing carvedilol', *European Heart Journal*, 28(8), pp. 989–995. doi: 10.1093/eurheartj/ehm048.

Kasama, S. *et al.* (2012) 'Relationship between late ventricular potentials and myocardial 123I-metaiodobenzylguanidine scintigraphy in patients with dilated cardiomyopathy with mild to moderate heart failure: Results of a prospective study of sudden death events', *European Journal of Nuclear Medicine and Molecular Imaging*, 39(6), pp. 1056–1064. doi: 10.1007/s00259-012-2092-1.

Katritsis, D. G., Gersh, B. J. and Camm, A. J. (2016) 'A Clinical Perspective on Sudden Cardiac Death', *Arrhythmia & Electrophysiology Review*, 5(3), p. 177. doi: 10.15420/AER.2016:11:2.

Kawano, H., Okada, R. and Yano, K. (2003) 'Histological study on the distribution of autonomic nerves in the human heart', *Heart and Vessels*, 18(1), pp. 32–39. doi: 10.1007/s003800300005.

Kawut, S. M. *et al.* (2011) 'Sex and race differences in right ventricular structure and

function: The multi-ethnic study of atherosclerosis-right ventricle study', *Circulation*, 123(22), pp. 2542–2551. doi: 10.1161/CIRCULATIONAHA.110.985515.

Keilson, M. J., Allen Hauser, W. A. and Magrill, J. P. (1989) 'Electrocardiographic changes during electrographic seizures', *Archives of neurology*, 46(11), pp. 1169–1170. doi: 10.1001/ARCHNEUR.1989.00520470023018.

Kienzle, M. G. *et al.* (1992) 'Effect of direct, reflex and exercise-provoked increases in sympathetic tone on idiopathic ventricular tachycardia', *The American Journal of Cardiology*, 69(17), pp. 1433–1438. doi: 10.1016/0002-9149(92)90896-7.

Kiernan, J. A. (2013) 'Sirius Red Staining Protocol for Collagen', *med.emory.edu*, pp. 1–3. Available at: https://med.emory.edu/departments/medicine/divisions/cardiology/research/labs/microscopy-in-medicine/_documents/sirius-red-collagen-staining-protocol.pdf (Accessed: 26 February 2022).

Kiernan, J. A. (2015) 'Methods for connective tissue', in *Histological and Histochemical Methods: Theory and Practice*, pp. 184–205. doi: 10.1016/0014-5793(83)80096-9.

Kim, M. N. *et al.* (2018) 'The relationship between epicardial adipose tissue and coronary artery stenosis by sex and menopausal status in patients with suspected angina', *Biology of Sex Differences*, 9(1). doi: 10.1186/s13293-018-0212-8.

Kim, S. A. *et al.* (2017) 'Epicardial adipose tissue is related to cardiac function in elderly women, but not in men', *Nutrition, Metabolism and Cardiovascular Diseases*, 27(1), pp. 41–47. doi: 10.1016/j.numecd.2016.11.001.

Kitzman, D. w. *et al.* (1988) 'Age-Related Changes in Normal Human Hearts During the First 10 Decades of Life. Part II (Maturity): A Quantitative Anatomic Study of 765 Specimens From Subjects 20 to 99 Years Old', *Mayo Clinic Proceedings*, 63(2), pp.

137–146. doi: 10.1016/S0025-6196(12)64946-5.

Klabunde, R. E. (2021) ‘Cardiovascular Physiology Concepts’, in, p. 265. Available at: http://www.cvphysiology.com/index.html (Accessed: 16 March 2022).

Knaapen, M. *et al.* (2013) ‘Prevalence of left and balanced coronary arterial dominance decreases with increasing age of patients at autopsy. A postmortem coronary angiograms study’, *Cardiovascular Pathology*, 22(1), pp. 49–53. doi: 10.1016/J.CARPATH.2012.02.012.

Kong, M. H. *et al.* (2011) ‘Systematic review of the incidence of sudden cardiac death in the United States’, *Journal of the American College of Cardiology*, 57(7), pp. 794–801. doi: 10.1016/J.JACC.2010.09.064.

Kou, S. *et al.* (2014) ‘Echocardiographic reference ranges for normal cardiac chamber size: Results from the NORRE study’, *European Heart Journal Cardiovascular Imaging*, 15(6), pp. 680–690. doi: 10.1093/ehjci/jet284.

Kyösola, K. *et al.* (1976) ‘Fluorescence histochemical and electron-microscopical observations on the innervation of the atrial myocardium of the adult human heart’, *Virchows Archiv. A, Pathological anatomy and histology*, 371(2), pp. 101–119. doi: 10.1007/BF00444927.

De La Grandmaison, G. L., Clairand, I. and Durigon, M. (2001) ‘Organ weight in 684 adult autopsies: New tables for a Caucasoid population’, *Forensic Science International*, 119(2), pp. 149–154. doi: 10.1016/S0379-0738(00)00401-1.

Lahrouchi, N. *et al.* (2017) ‘Utility of Post-Mortem Genetic Testing in Cases of Sudden Arrhythmic Death Syndrome’, *Journal of the American College of Cardiology*, 69(17), pp. 2134–2145. doi: 10.1016/j.jacc.2017.02.046.

Lauer, M. S. *et al.* (1996) ‘Impaired Heart Rate Response to Graded Exercise Prognostic Implications of Chronotropic Incompetence in the Framingham Heart

Study', *Circulation*, 93(8), pp. 1520–1526. doi: 10.1161/01.CIR.93.8.1520.

Leeuw, N. *et al.* (2001) 'Histopathologic findings in explanted heart tissue from patients with end-stage idiopathic dilated cardiomyopathy', *Transplant International*, 14(5), pp. 299–306. doi: 10.1111/J.1432-2277.2001.TB00063.X.

Lenkiewicz, J. E., Davies, M. J. and Rosen, D. (1972) 'Collagen in human myocardium as a function of age', *Cardiovascular Research*, 6(5), pp. 549–555. doi: 10.1093/CVR/6.5.549.

Leone, O. *et al.* (2012) 'New pathological insights into cardiac amyloidosis: implications for non-invasive diagnosis', *https://doi.org/10.3109/13506129.2012.684810*, 19(2), pp. 99–105. doi: 10.3109/13506129.2012.684810.

Li, S. T. *et al.* (2000) 'Myocardial perfusion and sympathetic innervation in patients with hypertrophic cardiomyopathy', *Journal of the American College of Cardiology*, 35(7), pp. 1867–1873. doi: 10.1016/S0735-1097(00)00626-4.

Liang, C. (2007) 'Cardiac sympathetic nerve terminal function in congestive heart failure.', *Acta pharmacologica Sinica*, 28(7), pp. 921–927. doi: 10.1111/j.1745-7254.2007.00585.x.

Limbruno, U. *et al.* (1998) 'Altered autonomic cardiac control in hypertrophic cardiomyopathy. Role of outflow tract obstruction and myocardial hypertrophy', *European heart journal*, 19(1), pp. 146–153. doi: 10.1053/EUHJ.1997.0743.

Litwin, S. E. *et al.* (2020) 'Longitudinal Changes in Cardiac Structure and Function in Severe Obesity: 11-Year Follow-Up in the Utah Obesity Study', *Journal of the American Heart Association*. doi: 10.1161/JAHA.119.014542.

Liu, L. and Nattel, S. (1997) 'Differing sympathetic and vagal effects on atrial fibrillation in dogs: Role of refractoriness heterogeneity', *American Journal of*

Physiology - Heart and Circulatory Physiology, 273(2 42-2). doi: 10.1152/ajpheart.1997.273.2.h805.

Von Lüdinghausen, M. (2003) 'The Clinical Anatomy of the Coronary Arteries.', in *dvances in Anatomy Embryology and Cell Biology.* Available at: https://scholar.google.com/scholar?hl=en&as_sdt=0%2C5&q=Von+Lüdinghausen%2C+M.+%282003%29+The+Clinical+Anatomy+of+the+Coronary+Arteries.+Advances+in+Anatomy+Embryology+and+Cell+Biology.+Berlin%2C+Springer%2C+vol+167%2C+pp+45–52.&btnG= (Accessed: 19 March 2022).

Lynge, T. H. *et al.* (2019) 'Sudden cardiac death caused by myocarditis in persons aged 1–49 years: a nationwide study of 14 294 deaths in Denmark', *Forensic Sciences Research*, 4(3), p. 247. doi: 10.1080/20961790.2019.1595352.

Lynge, T. H. *et al.* (2021) 'Nationwide burden of sudden cardiac death: A study of 54,028 deaths in Denmark', *Heart Rhythm*, 18(10), pp. 1657–1665. doi: 10.1016/j.hrthm.2021.05.005.

Machado, C. R. S. *et al.* (2000) 'Cardiac autonomic denervation in congestive heart failure: Comparison of Chagas' heart disease with other dilated cardiomyopathy', *Human Pathology*, 31(1), pp. 3–10. doi: 10.1016/S0046-8177(00)80191-4.

Mancio, J. *et al.* (2017) 'Gender differences in the association of epicardial adipose tissue and coronary artery calcification: EPICHEART study: EAT and coronary calcification by gender', *International Journal of Cardiology*, 249, pp. 419–425. doi: 10.1016/j.ijcard.2017.09.178.

Marcus, F. I. *et al.* (1982) 'Right ventricular dysplasia: a report of 24 adult cases', *Circulation*, 65(2), pp. 384–398. doi: 10.1161/01.CIR.65.2.384.

Marcus, F. I. *et al.* (2010) 'Diagnosis of arrhythmogenic right ventricular cardiomyopathy/Dysplasia: Proposed modification of the task force criteria',

Circulation, 121(13), pp. 1533–1541. doi: 10.1161/CIRCULATIONAHA.108.840827.

Margey, R. *et al.* (2011) 'Sudden cardiac death in 14- to 35-year olds in Ireland from 2005 to 2007: A retrospective registry', *Europace*, 13(10), pp. 1411–1418. doi: 10.1093/europace/eur161.

Marieb, E. N. (2004) *Human anatomy & physiology*. San Francisco Calif.: Pearson Benjamin Cummings.

Maron, B. J. *et al.* (1995) 'Prevalence of hypertrophic cardiomyopathy in a general population of young adults: Echocardiographic analysis of 4111 subjects in the CARDIA study', *Circulation*. doi: 10.1161/01.CIR.92.4.785.

Maron, B. J. *et al.* (2016) 'Demographics and Epidemiology of Sudden Deaths in Young Competitive Athletes: From the United States National Registry', *The American journal of medicine*, 129(11), pp. 1170–1177. doi: 10.1016/J.AMJMED.2016.02.031.

Maron, B. J. *et al.* (2020) 'Hypertrophic Cardiomyopathy and Sudden Death Initially Identified at Autopsy', *The American Journal of Cardiology*, 127, pp. 139–141. doi: 10.1016/J.AMJCARD.2020.04.021.

Maron, B. J., Roberts, W. C. and Epstein, S. E. (1982) 'Sudden death in hypertrophic cardiomyopathy: A profile of 78 patients', *Circulation*, 65(7 I), pp. 1388–1394. doi: 10.1161/01.CIR.65.7.1388.

Marron, K. *et al.* (1994) 'Human endocardial innervation and its relationship to the endothelium: An immunohistochemical, histochemical, and quantitative study', *Cardiovascular Research*, 28(10), pp. 1490–1499. doi: 10.1093/cvr/28.10.1490.

Marron, K. *et al.* (1995) 'Distribution, Morphology, and Neurochemistry of Endocardial and Epicardial Nerve Terminal Arborizations in the Human Heart', *Circulation*, 92(8), pp. 2343–2351. doi: 10.1161/01.CIR.92.8.2343.

Marron, K. *et al.* (1996) ‘Innervation of Human Atrioventricular and Arterial Valves’, *Circulation*, 94(3), pp. 368–375. doi: 10.1161/01.CIR.94.3.368.

Martin, R. *et al.* (2018) ‘Characteristics of Scar-Related Ventricular Tachycardia Circuits Using Ultra-High-Density Mapping’, *Circulation. Arrhythmia and electrophysiology*, 11(10), p. e006569. doi: 10.1161/CIRCEP.118.006569.

Maury, P. (2011) ‘Why is the right ventricular outflow tract so arrhythmogenic? (... or is it really?...)’, *Heart*, pp. 1361–1633. doi: 10.1136/heartjnl-2011-300465.

Mauvais-Jarvis, F. *et al.* (2020) ‘Sex and gender: modifiers of health, disease, and medicine’, *The Lancet*. Lancet Publishing Group, pp. 565–582. doi: 10.1016/S0140-6736(20)31561-0.

Mazurek, T. *et al.* (2003) ‘Human Epicardial Adipose Tissue Is a Source of Inflammatory Mediators’, *Circulation*, 108(20), pp. 2460–2466. doi: 10.1161/01.CIR.0000099542.57313.C5.

McKenna, W. J., Maron, B. J. and Thiene, G. (2017) ‘Classification, epidemiology, and global burden of cardiomyopathies’, *Circulation Research*. doi: 10.1161/CIRCRESAHA.117.309711.

McMurray, J. J. V. *et al.* (2012) ‘ESC Guidelines for the diagnosis and treatment of acute and chronic heart failure 2012: The Task Force for the Diagnosis and Treatment of Acute and Chronic Heart Failure 2012 of the European Society of Cardiology. Developed in collaboration with the Heart’, *European heart journal*. doi: 10.1093/eurheartj/ehs104.

Mellor, G. *et al.* (2014) ‘Clinical characteristics and circumstances of death in the sudden arrhythmic death syndrome’, *Circulation: Arrhythmia and Electrophysiology*, 7(6), pp. 1078–1083. doi: 10.1161/CIRCEP.114.001854.

Meng, L. *et al.* (2017) ‘Efficacy of Stellate Ganglion Blockade in Managing Electrical

Storm: A Systematic Review', *JACC: Clinical Electrophysiology*. doi: 10.1016/j.jacep.2017.06.006.

Merlo, M. *et al.* (2018) 'Reverse remodeling in Dilated Cardiomyopathy: Insights and future perspectives', *IJC Heart and Vasculature*. doi: 10.1016/j.ijcha.2018.02.005.

Miles, C. *et al.* (2019) 'Sudden Death and Left Ventricular Involvement in Arrhythmogenic Cardiomyopathy', *Circulation*, 139(15). doi: 10.1161/CIRCULATIONAHA.118.037230.

Miles, C. *et al.* (2020) 'Morphometric characterization of collagen and fat in normal ventricular myocardium', *Cardiovascular Pathology*. doi: 10.1016/j.carpath.2020.107224.

Mills, P. and Hall, R. (2003) 'Professor Michael Davies, British Heart Foundation Professor of Cardiac Pathology, Editor of Heart 1992–1999', *Heart*, 89(5), pp. 473–473. doi: 10.1136/HEART.89.5.473.

Misawa, H. *et al.* (2001) 'Distribution of the high-affinity choline transporter in the central nervous system of the rat', *Neuroscience*, 105(1), pp. 87–98. doi: 10.1016/S0306-4522(01)00147-6.

Mistrova, E., Kruzliak, P. and Chottova Dvorakova, M. (2016) 'Role of substance P in the cardiovascular system', *Neuropeptides*, 58, pp. 41–51. doi: 10.1016/J.NPEP.2015.12.005.

Miyazawa, I. *et al.* (2018) 'Change in pericardial fat volume and cardiovascular risk factors in a general population of Japanese men', *Circulation Journal*, 82(10), pp. 2542–2548. doi: 10.1253/circj.CJ-18-0153.

Modena, M. G. *et al.* (1997) 'Left atrial size is the major predictor of cardiac death and overall clinical outcome in patients with dilated cardiomyopathy: A long-term follow-up study', *Clinical Cardiology*, 20(6), pp. 553–560. doi:

10.1002/CLC.4960200609.

Molina, C. E. *et al.* (2014) ‘Interventricular differences in β-adrenergic responses in the canine heart: Role of phosphodiesterases’, *Journal of the American Heart Association*, 3(3). doi: 10.1161/JAHA.114.000858.

Moon, J. C. *et al.* (2013) ‘Myocardial T1 mapping and extracellular volume quantification: a Society for Cardiovascular Magnetic Resonance (SCMR) and CMR Working Group of the European Society of Cardiology consensus statement’, *Journal of Cardiovascular Magnetic Resonance*, 15(1), p. 92. doi: 10.1186/1532-429X-15-92.

Morentin, B., Suárez-Mier, M. P. and Aguilera, B. (2003) ‘Sudden unexplained death among persons 1-35 years old’, *Forensic Science International*, 135(3), pp. 213–217. doi: 10.1016/S0379-0738(03)00212-3.

Mörner, S. *et al.* (2005) ‘Parasympathetic dysfunction in hypertrophic cardiomyopathy assessed by heart rate variability: comparison between short-term and 24-h measurements’, *Clinical physiology and functional imaging*, 25(2), pp. 90–99. doi: 10.1111/J.1475-097X.2004.00595.X.

Mosteller, R. (1987) ‘Simplified Calculation of Body-Surface Area’, *New England Journal of Medicine*, 317(17), pp. 1098–1098. doi: 10.1056/nejm198710223171717.

Myerburg, R. J. and Junttila, M. J. (2012) ‘Sudden cardiac death caused by coronary heart disease’, *Circulation*, 125(8), pp. 1043–1052. doi: 10.1161/CIRCULATIONAHA.111.023846.

Nademanee, K. *et al.* (2015) ‘Fibrosis, Connexin-43, and Conduction Abnormalities in the Brugada Syndrome’, *Journal of the American College of Cardiology*, 66(18), pp. 1976–1986. doi: 10.1016/J.JACC.2015.08.862.

Nag, A. C. (1980) ‘Study of non-muscle cells of the adult mammalian heart: a fine

structural analysis and distribution.', *Cytobios*, 28(109), pp. 41–61. Available at: https://europepmc.org/article/med/7428441 (Accessed: 18 February 2022).

Nagaoka, H. *et al.* (1996) 'Relation between depressed cardiac response to exercise and autonomic nervous activity in mildly symptomatic patients with idiopathic dilated cardiomyopathy', *Chest*, 109(4), pp. 925–932. doi: 10.1378/CHEST.109.4.925.

Nakanishi, K. *et al.* (2014) 'Persistent epicardial adipose tissue accumulation is associated with coronary plaque vulnerability and future acute coronary syndrome in non-obese subjects with coronary artery disease', *Atherosclerosis*, 237(1), pp. 353–360. doi: 10.1016/j.atherosclerosis.2014.09.015.

Nascimento Matos, D. *et al.* (2020) 'Epicardial fat volume outperforms classic clinical scores for predicting atrial fibrillation relapse after pulmonary vein isolation', *European Heart Journal*, 41(Supplement_2). doi: 10.1093/ehjci/ehaa946.0587.

Nashelsky, M. B. and Lawrence, C. H. (2003) 'Accuracy of Cause of Death Determination Without Forensic Autopsy Examination', *American Journal of Forensic Medicine and Pathology*. doi: 10.1097/01.paf.0000097857.50734.c3.

National Institute for Health and Care Excellence (2014) *Implantable cardioverter defibrillators and cardiac resynchronisation therapy for arrhythmias and heart failure*. Available at: www.nice.org.uk/guidance/ta314 (Accessed: 14 December 2021).

Neri, R. *et al.* (1986) 'Arrhythmias in dilated cardiomyopathy', *Postgraduate Medical Journal*. doi: 10.1136/pgmj.62.728.593.

Netter, F. (2014) *Atlas of human anatomy, Professional Edition E-Book: including NetterReference. com Access with full downloadable image Bank*. Available at: https://books.google.com/books?hl=en&lr=&id=grIBCgAAQBAJ&oi=fnd&pg=PA1&dq=F.+Netter:+Atlas+of+Human+Anatomy,+6th+Edition,+Elsevier+Saunders+(2014).&ots=NveVMhIFxo&sig=hInBJvd1zdgsPpOjshyfABsb9LI (Accessed: 18 January

2022).

Ng, G. A. (2014) ‘Vagal modulation of cardiac ventricular arrhythmia’, *Experimental Physiology*. doi: 10.1113/expphysiol.2013.072652.

Nishisato, K. *et al.* (2010) ‘Impaired cardiac sympathetic innervation and myocardial perfusion are related to lethal arrhythmia: Quantification of cardiac tracers in patients with ICDs’, *Journal of Nuclear Medicine*. doi: 10.2967/jnumed.110.074971.

Noor, B. *et al.* (2020) ‘Quantitative assessment of cardiovascular autonomic impairment in cancer survivors: a single center case series’, *Cardio-oncology*, 6(1). doi: 10.1186/S40959-020-00065-9.

Norita, K., De Noronha, S. V. and Sheppard, M. N. (2012) ‘Sudden cardiac death caused by coronary vasculitis’, *Virchows Archiv*, 460(3), pp. 309–318. doi: 10.1007/S00428-011-1173-Z/FIGURES/8.

De Noronha, S. V. *et al.* (2014) ‘The importance of specialist cardiac histopathological examination in the investigation of young sudden cardiac deaths’, *Europace*. doi: 10.1093/europace/eut329.

Nuzzi, V. *et al.* (no date) ‘Atrial fibrillation in dilated cardiomyopathy: Outcome prediction from an observational registry’, *Elsevier*. Available at: https://www.sciencedirect.com/science/article/pii/S0167527320336457 (Accessed: 24 March 2022).

O’Mahony, C. *et al.* (2014) ‘A novel clinical risk prediction model for sudden cardiac death in hypertrophic cardiomyopathy (HCM Risk-SCD)’, *European Heart Journal*, 35(30), pp. 2010–2020. doi: 10.1093/eurheartj/eht439.

Obokata, M. *et al.* (2017) ‘Evidence Supporting the Existence of a Distinct Obese Phenotype of Heart Failure with Preserved Ejection Fraction’, *Circulation*, 136(1), pp. 6–19. doi: 10.1161/CIRCULATIONAHA.116.026807.

Oh, Y. S. *et al.* (2006) ‘Spatial distribution of nerve sprouting after myocardial infarction in mice’, *Heart Rhythm*. doi: 10.1016/j.hrthm.2006.02.005.

Oken, D. E. and Boucek, R. J. (1957) ‘Quantitation of collagen in human myocardium.’, *Circulation research*, 5(4), pp. 357–361. doi: 10.1161/01.RES.5.4.357.

Oki, H. *et al.* (1994) ‘Cardiac Sympathetic Innervation in Patients With Dilated Cardiomyopathy-Immunohistochemical Study Using Anti-Tyrosine Hydroxylase Antibody-’, *JAPANESE CIRCULATION JOURNAL*, 58(6), pp. 389–394. doi: 10.1253/jcj.58.389.

Olivetti, G. *et al.* (1997) ‘Apoptosis in the Failing Human Heart’, *New England Journal of Medicine*, 336(16), pp. 1131–1141. doi: 10.1056/nejm199704173361603.

Onicescu, D. and Vidulescu, C. (1989) ‘Cholinergic innervation of the ventricular myocardium in the human fetal heart.’, *Morphologie et embryologie*, 35(4), pp. 245–248.

Pandat, S. *et al.* (2020) ‘An association between right ventricular dysfunction and sudden cardiac death’, *Heart rhythm*, 17(2), pp. 169–174. doi: 10.1016/J.HRTHM.2019.10.021.

Parisi, V. *et al.* (2020) ‘Echocardiographic Epicardial Adipose Tissue Thickness for Risk Stratification of Patients With Heart Failure’, *Frontiers in Physiology*, 11, p. 43. doi: 10.3389/FPHYS.2020.00043/BIBTEX.

Paul, M. *et al.* (2011) ‘Cardiac sympathetic dysfunction in genotyped patients with arrhythmogenic right ventricular cardiomyopathy and risk of recurrent ventricular tachyarrhythmias’, *Journal of Nuclear Medicine*, 52(10), pp. 1559–1565. doi: 10.2967/jnumed.111.088997.

Paul, M. *et al.* (2014) ‘Autonomic Dysfunction in Patients with Arrhythmogenic Right Ventricular Cardiomyopathy: Biochemical Evidence of Altered Signaling Pathways’,

Pacing and Clinical Electrophysiology, 37(2), pp. 173–178. doi: 10.1111/PACE.12237.

Paulsen, S. and Vetner, M. (1973) 'Anatomical variations of the coronary arteries and origin of blood supply to sinoauricular and atrioventricular nodes determined on the basis of postmortem coronary angiography.', *Acta Pathologica Microbiologica Scandinavica Section A Pathology*, 81 A(6), pp. 784–790. doi: 10.1111/j.1699-0463.1973.tb03572.x.

Pauza, D. H. *et al.* (2000) 'Morphology, distribution, and variability of the epicardiac neural ganglionated subplexuses in the human heart', *Anatomical Record*, 259(4), pp. 353–382. doi: 10.1002/1097-0185(20000801)259:4<353::AID-AR10>3.0.CO;2-R.

Pauziene, N., Pauza, D. H. and Stropus, R. (2000) 'Morphology of human intracardiac nerves : an electron microscope study', *J. Anat*, 197, pp. 437–459.

Pelà, G. *et al.* (2016) 'Sex-related differences in left ventricular structure in early adolescent non-professional athletes', *European Journal of Preventive Cardiology*, 23(7), pp. 777–784. doi: 10.1177/2047487315608826.

Petraitiene, V., Pauza, D. H. and Benetis, R. (2014) 'Distribution of adrenergic and cholinergic nerve fibres within intrinsic nerves at the level of the human heart hilum', *European Journal of Cardio-Thoracic Surgery*, 45(6), pp. 1097–1105. doi: 10.1093/EJCTS/EZT575.

Pfaffenberger, S. *et al.* (2013) 'Size matters! Impact of age, sex, height, and weight on the normal heart size', *Circulation: Cardiovascular Imaging*, 6(6), pp. 1073–1079. doi: 10.1161/CIRCIMAGING.113.000690.

Pianca, N. *et al.* (2019) 'Cardiac sympathetic innervation network shapes the myocardium by locally controlling cardiomyocyte size through the cellular proteolytic machinery', *The Journal of Physiology*, 597(14), pp. 3639–3656. doi:

10.1113/JP276200.

Pinto, Y. M. *et al.* (2016) ‘Proposal for a revised definition of dilated cardiomyopathy, hypokinetic non-dilated cardiomyopathy, and its implications for clinical practice: A position statement of the ESC working group on myocardial and pericardial diseases’, *European Heart Journal*, 37(23), pp. 1850–1858. doi: 10.1093/eurheartj/ehv727.

Priori, S. G. *et al.* (2002) ‘TASK FORCE ON SUDDEN CARDIAC DEATH, EUROPEAN SOCIETY OF CARDIOLOGYSummary of Recommendations’, *EP Europace*, 4(1), pp. 3–18. doi: 10.1053/EUPC.2001.0214.

Rechardt, L. *et al.* (1986) ‘Peptidergic innervation of human atrial myocardium: an electron microscopical and immunocytochemical study.’, *Journal of the autonomic nervous system*, 17(1), pp. 21–32. doi: 10.1016/0165-1838(86)90041-x.

Reichenbach, D. D., Moss, N. S. and Meyer, E. (1977) ‘Pathology of the heart in sudden cardiac death’, *The American journal of cardiology*, 39(6), pp. 865–872. doi: 10.1016/S0002-9149(77)80041-6.

Reinier, K. *et al.* (2014) ‘The Association Between Atrial Fibrillation and Sudden Cardiac Death: The Relevance of Heart Failure’, *JACC: Heart Failure*, 2(3), pp. 221–227. doi: 10.1016/J.JCHF.2013.12.006.

Rich, L. and Whittaker, P. (2005) ‘Collagen and picrosirius red staining: a polarized light assessment of fibrillar hue and spatial distribution’, *Journal of Morphological Sciences*, 22(2), pp. 97–104. Available at: http://www.jms.periodikos.com.br/article/587cb4587f8c9d0d058b460c (Accessed: 20 December 2021).

Van Rijsingen, I. A. W. *et al.* (2012) ‘Risk factors for malignant ventricular arrhythmias in lamin a/c mutation carriers a European cohort study’, *Journal of the*

American College of Cardiology, 59(5), pp. 493–500. doi: 10.1016/J.JACC.2011.08.078.

Risgaard, B. *et al.* (2014) 'Burden of sudden cardiac death in persons aged 1 to 49 years: nationwide study in Denmark', *Circulation. Arrhythmia and electrophysiology*, 7(2), pp. 205–211. doi: 10.1161/CIRCEP.113.001421.

Risgaard, B. *et al.* (2015) 'Risk factors and causes of sudden noncardiac death: A nationwide cohort study in Denmark', *Heart Rhythm*. doi: 10.1016/j.hrthm.2015.01.024.

Robertson, J. *et al.* (2019) 'Higher Body Mass Index in Adolescence Predicts Cardiomyopathy Risk in Midlife: Long-Term Follow-Up among Swedish Men', *Circulation*, 140(2), pp. 117–125. doi: 10.1161/CIRCULATIONAHA.118.039132.

Robertson, J. *et al.* (2020) 'Body mass index in young women and risk of cardiomyopathy: A long-term follow-up study in sweden', *Circulation*. doi: 10.1161/CIRCULATIONAHA.119.044056.

Sabater-Molina, M. *et al.* (2018) 'Genetics of hypertrophic cardiomyopathy: A review of current state', *Clinical Genetics*. doi: 10.1111/cge.13027.

Salton, C. J. *et al.* (2002) 'Gender differences and normal left ventricular anatomy in an adult population free of hypertension: A cardiovascular magnetic resonance study of the Framingham Heart Study Offspring cohort', *Journal of the American College of Cardiology*, 39(6), pp. 1055–1060. doi: 10.1016/S0735-1097(02)01712-6.

Sasaki, T. *et al.* (2013) 'Impact of nonischemic scar features on local ventricular electrograms and scar-related ventricular tachycardia circuits in patients with nonischemic cardiomyopathy', *Circulation: Arrhythmia and Electrophysiology*, 6(6), pp. 1139–1147. doi: 10.1161/CIRCEP.113.000159/-/DC1.

Schejbal, V. (1989) 'EPIKARDIALES FETTGEWEBE DER RECHTEN

HERZKAMMER - MORPHOLOGIE, MORPHOMETRIE UND FUNKTIONELLE BEDEUTUNG', *Pneumologie*, 43(9), pp. 490–499. Available at: https://europepmc.org/article/med/2813303 (Accessed: 11 May 2021).

Schlesinger, M. J. (1940) 'Significant Variations in the Anatomic Pattern of the Coronary Vessels', in Schlesinger, M. J. (ed.) *Blood, Heart and Circulation*. 4th edn. American Association for the Advancement of Science Publication . Available at: https://scholar.google.com/scholar_lookup?title=Significant Variations in the Anatomic Pattern of the Coronary Vessels. Blood%2C Heart and Circulation&publication_year=1940&author=M.J. Schlesinger (Accessed: 19 March 2022).

Schwartz, C. J. and Gerrity, R. G. (1975) 'Anatomical pathology of sudden unexpected cardiac death.', *Circulation*, 52(6 Suppl), pp. III18-26. Available at: https://europepmc.org/article/med/1182972 (Accessed: 14 December 2021).

Schwartz, P. J. *et al.* (2004) 'Left Cardiac Sympathetic Denervation in the Management of High-Risk Patients Affected by the Long-QT Syndrome', *Circulation*. doi: 10.1161/01.CIR.0000125523.14403.1E.

Schwartz, P. J. (2014) 'Cardiac sympathetic denervation to prevent life-threatening arrhythmias', *Nature Reviews Cardiology*. doi: 10.1038/nrcardio.2014.19.

Seib, G. A. (1934) 'Incidence of the patent foramen ovale cordis in adult american whites and american negroes', *American Journal of Anatomy*, 55(3), pp. 511–525. doi: 10.1002/AJA.1000550306.

Semsarian, C. *et al.* (2015) 'New perspectives on the prevalence of hypertrophic cardiomyopathy', *Journal of the American College of Cardiology*. doi: 10.1016/j.jacc.2015.01.019.

Sepehrkhouy, S. *et al.* (2017) 'Distinct fibrosis pattern in desmosomal and

phospholamban mutation carriers in hereditary cardiomyopathies', *Heart Rhythm*, 14(7), pp. 1024–1032. doi: 10.1016/j.hrthm.2017.03.034.

Sheppard, M. (2022) *Practical Cardiovascular Pathology, 3rd edition*, *Practical Cardiovascular Pathology, 2nd edition*. PRODUCTIVITY Press. doi: 10.1201/b13327.

Sheppard, M. and Survana, K. (2015) 'Guidelines on autopsy practice: Sudden death with likely cardiac pathology', *Royal college of Pathologists*. Available at: www.rcpath.org (Accessed: 18 January 2022).

Shimizu, M. *et al.* (2001) 'Increased QT dispersion does not reflect the increased regional variation of cardiac sympathetic nervous activity in hypertrophic cardiomyopathy', *American heart journal*, 142(2), pp. 358–362. doi: 10.1067/MHJ.2001.116765.

Shivkumar, K. *et al.* (2016) 'Clinical neurocardiology defining the value of neuroscience-based cardiovascular therapeutics', *Journal of Physiology*. doi: 10.1113/JP271870.

Shriki, J. E. *et al.* (2012) 'Identifying, characterizing, and classifying congenital anomalies of the coronary arteries', *Radiographics*, 32(2), pp. 453–468. doi: 10.1148/rg.322115097.

Shvalev, V. N., Zhuchkova, N. I. and Vikhert, A. M. (1980) '[Changes in the intracardiac nerve plexuses in sudden death].', *Kardiologiia*, 20(7), pp. 80–83.

Singh, S. *et al.* (1996) 'Topography of cardiac ganglia in the adult human heart', *The Journal of thoracic and cardiovascular surgery*, 112(4), pp. 943–953. doi: 10.1016/S0022-5223(96)70094-6.

Singh, S. *et al.* (1999) 'Monoamine- and histamine-synthesizing enzymes and neurotransmitters within neurons of adult human cardiac ganglia', *Circulation*, 99(3),

pp. 411–419. doi: 10.1161/01.CIR.99.3.411/FORMAT/EPUB.

Skurdal, A. C. and Nordrum, I. S. (2016) 'A retrospective study of postmortem heart weight in an adult Norwegian population', *Cardiovascular Pathology*, 25(6), pp. 461–467. doi: 10.1016/j.carpath.2016.07.003.

Slart, R. H. J. A. *et al.* (2019) 'Imaging cardiac innervation in amyloidosis.', *Journal of nuclear cardiology : official publication of the American Society of Nuclear Cardiology*, 26(1), pp. 174–187. doi: 10.1007/s12350-017-1059-9.

Srinivasan, N. T. and Schilling, R. J. (2018) 'Sudden cardiac death and arrhythmias', *Arrhythmia & Electrophysiology Review*. doi: 10.15420/aer.2018.15.2.

Standring, S. (2021) 'Gray's Anatomy: 42nd edition | | ISBN: 9780702077050 | ANZ Elsevier Health Bookshop : Books', *Gray's Anatomy*. Edited by Elsevier, pp. 955–985. Available at: https://www.elsevierhealth.com.au/grays-anatomy-9780702077050.html (Accessed: 13 December 2021).

Stavrakis, S. *et al.* (2015) 'Low-level transcutaneous electrical vagus nerve stimulation suppresses atrial fibrillation', *Journal of the American College of Cardiology*. doi: 10.1016/j.jacc.2014.12.026.

Stavrakis, S. *et al.* (2017) 'Low-Level Vagus Nerve Stimulation Suppresses Post-Operative Atrial Fibrillation and Inflammation: A Randomized Study', *JACC: Clinical Electrophysiology*. doi: 10.1016/j.jacep.2017.02.019.

Stecker, E. C. *et al.* (2014) 'Public health burden of sudden cardiac death in the United States', *Circulation: Arrhythmia and Electrophysiology*, 7(2), pp. 212–217. doi: 10.1161/CIRCEP.113.001034.

Stevens, S. M., Reinier, K. and Chugh, S. S. (2013) 'Increased Left Ventricular Mass as a Predictor of Sudden Cardiac Death: Is it Time to put it to the Test?', *Circulation. Arrhythmia and electrophysiology*, 6(1), p. 212. doi: 10.1161/CIRCEP.112.974931.

Still, W. J. S. (1961) ‘Endocardial fibroelastosis’, *American Heart Journal*, 61(5), pp. 579–585. doi: 10.1016/0002-8703(61)90628-7.

‘Sudden cardiac death. Report of a WHO Scientific Group’ (1985) *World Health Organization technical report series*, 726, pp. 5–25. Available at: https://pubmed.ncbi.nlm.nih.gov/3936284/ (Accessed: 23 August 2021).

Sugihara, N. *et al.* (1988) ‘Quantitation of myocardial fibrosis and its relation to function in essential hypertension and hypertrophic cardiomyopathy’, *Clinical Cardiology*, 11(11), pp. 771–778. doi: 10.1002/CLC.4960111109.

Van Suylen, R. J. *et al.* (1996) ‘Collagen content and distribution in the normal and transplanted human heart: A postmortem quantitative light microscopic analysis’, *Cardiovascular Pathology*, 5(2), pp. 61–68. doi: 10.1016/1054-8807(95)00087-9.

Tan, C. M. J. *et al.* (2018) ‘The role of neuropeptide Y in cardiovascular health and disease’, *Frontiers in Physiology*, 9(SEP), p. 1281. doi: 10.3389/FPHYS.2018.01281/BIBTEX.

Tanaka, M. *et al.* (1986) ‘Quantitative analysis of myocardial fibrosis in normals, hypertensive hearts, and hypertrophic cardiomyopathy.’, *Heart*, 55(6), pp. 575–581. doi: 10.1136/HRT.55.6.575.

Tansey, D. K., Aly, Z. and Sheppard, M. N. (2005) ‘Fat in the right ventricle of the normal heart’, *Histopathology*, 46(1), pp. 98–104. Available at: https://onlinelibrary.wiley.com/doi/full/10.1111/j.1365-2559.2005.02054.x (Accessed: 28 April 2021).

Teare, D. (1958) ‘Asymmetrical hypertrophy of the heart in young adults.’, *British heart journal*, 20(1), pp. 1–8. doi: 10.1136/hrt.20.1.1.

Terai, H. *et al.* (2003) ‘Changes in Cardiac Sympathetic Nerve Innervation and Activity in Pathophysiologic Transition from Typical to End-Stage Hypertrophic

Cardiomyopathy', *Journal of Nuclear Medicine*, 44(10).

Thanassoulis, G. *et al.* (2010) 'Pericardial fat is associated with prevalent atrial fibrillation: The framingham heart study', *Circulation: Arrhythmia and Electrophysiology*, 3(4), pp. 345–350. doi: 10.1161/CIRCEP.109.912055.

Thompson, T. and Evans, W. (1930) 'Paradoxical Embolism', *QJM: An International Journal of Medicine*, os-23(90), pp. 135–150. Available at: https://academic.oup.com/qjmed/article/os-23/90/135/1589199 (Accessed: 25 January 2022).

Unverferth, D. V. *et al.* (1986) 'Extent of myocardial fibrosis and cellular hypertrophy in dilated cardiomyopathy', *The American Journal of Cardiology*, 57(10), pp. 816–820. doi: 10.1016/0002-9149(86)90620-X.

Varnava, A. M. *et al.* (2000) 'Hypertrophic cardiomyopathy: the interrelation of disarray, fibrosis, and small vessel disease', *Heart*, 84, pp. 476–482. Available at: www.heartjnl.com (Accessed: 21 December 2021).

Vaseghi, M. and Shivkumar, K. (2008) 'The Role of the Autonomic Nervous System in Sudden Cardiac Death', *Progress in Cardiovascular Diseases*. doi: 10.1016/j.pcad.2008.01.003.

Veltman, C. E. *et al.* (2012) 'Prognostic value of coronary vessel dominance in relation to significant coronary artery disease determined with non-invasive computed tomography coronary angiography', *European Heart Journal*, 33(11), pp. 1367–1377. doi: 10.1093/EURHEARTJ/EHS034.

Veselka, J., Anavekar, N. S. and Charron, P. (2017) 'Hypertrophic obstructive cardiomyopathy', *The Lancet*. doi: 10.1016/S0140-6736(16)31321-6.

Vliegen, H. W. *et al.* (1991) 'Myocardial changes in pressure overload-induced left ventricular hypertrophy. A study on tissue composition, polyploidization and

multinucleation', *European heart journal*, 12(4), pp. 488–494. doi: 10.1093/OXFORDJOURNALS.EURHEARTJ.A059928.

Voigt, J. (1976) 'The forensic problem of post-mortem diagnosis of sudden cardiac death', *Forensic Science*, 8(C), pp. 73–76. doi: 10.1016/0300-9432(76)90049-2.

Vormbrock, J. *et al.* (2014) 'Determinants of Right Ventricular Muscle Mass in Idiopathic Dilated Cardiomyopathy: Impact of Left Ventricular Muscle Mass and Pulmonary Hypertension', *Int. J. Med. Sci*, 11(8), pp. 834–840. doi: 10.7150/ijms.6961.

Vracko, R., Thorning, D. and Frederickson, R. G. (1991) 'Nerve fibers in human myocardial scars', *Human Pathology*, 22(2), pp. 138–146. doi: 10.1016/0046-8177(91)90035-N.

Waller, B. F. *et al.* (1995) 'Intracardiac thrombi: Frequency, location, etiology, and complications: A morphologic review—Part I', *Clinical Cardiology*, 18(8), pp. 477–479. doi: 10.1002/CLC.4960180811.

Wang, T. J. *et al.* (2004) 'Obesity and the risk of new-onset atrial fibrillation', *Journal of the American Medical Association*. doi: 10.1001/jama.292.20.2471.

Weintraub, R. G., Semsarian, C. and Macdonald, P. (2017) 'Dilated cardiomyopathy', *The Lancet*. doi: 10.1016/S0140-6736(16)31713-5.

van Weperen, V. Y. H., Vos, M. A. and Ajijola, O. A. (2021) 'Autonomic modulation of ventricular electrical activity: recent developments and clinical implications', *Clinical Autonomic Research*, 31(6), pp. 659–676. doi: 10.1007/S10286-021-00823-4/TABLES/1.

Westaby, J. D. *et al.* (2019) 'Insights from examination of hearts from adults dying suddenly to the understanding of congenital cardiac malformations', *Clinical Anatomy*. doi: 10.1002/ca.23531.

Westaby, J. D. *et al.* (2021) ‘Characterisation of hypertensive heart disease: pathological insights from a sudden cardiac death cohort to inform clinical practice.’, *Journal of human hypertension*. doi: 10.1038/s41371-021-00507-6.

Westaby, J. D. and Sheppard, M. N. (2021) ‘Mitral Valve Pathology’, in *Mitral Valve Disease*. Cham: Springer International Publishing, pp. 97–111. doi: 10.1007/978-3-030-67947-7_8.

Westaby, S. *et al.* (1984) ‘Adult human valve dimensions and their surgical significance’, *The American Journal of Cardiology*, 53(4), pp. 552–556. doi: 10.1016/0002-9149(84)90029-8.

Wharton, J. *et al.* (1990) ‘Immunohistochemical demonstration of human cardiac innervation before and after transplantation.’, *Circulation Research*, 66(4), pp. 900–912. doi: 10.1161/01.RES.66.4.900.

Whitaker, R. H. (Robert H. . (2020) ‘Heart and pericardium’, in Robert H Whitaker (ed.) *A visual guide to clinical anatomy*. 1st edn. Wiley Blackwell, pp. 166–186.

Wichter, T. *et al.* (2000) ‘Abnormalities of cardiac sympathetic innervation in arrhythmogenic right ventricular cardiomyopathy : quantitative assessment of presynaptic norepinephrine reuptake and postsynaptic beta-adrenergic receptor density with positron emission tomography’, *Circulation*, 101(13), pp. 1552–1558. doi: 10.1161/01.CIR.101.13.1552.

Wingren, C. J. and Ottosson, A. (2015) ‘Postmortem heart weight modelled using piecewise linear regression in 27,645 medicolegal autopsy cases’, *Forensic Science International*, 252, pp. 157–162. doi: 10.1016/j.forsciint.2015.04.036.

Winkel, B. G. *et al.* (2011) ‘Nationwide study of sudden cardiac death in persons aged 1-35 years’, *European Heart Journal*, 32(8), pp. 983–990. doi: 10.1093/eurheartj/ehq428.

Wong, C. X. *et al.* (2019) *Epidemiology of Sudden Cardiac Death: Global and Regional Perspectives*, *Heart Lung and Circulation*. Elsevier Ltd. doi: 10.1016/j.hlc.2018.08.026.

Xiao, Y. *et al.* (2018) 'The Association Between Myocardial Fibrosis and Depressed Capillary Density in Rat Model of Left Ventricular Hypertrophy', *Cardiovascular toxicology*, 18(4), pp. 304–311. doi: 10.1007/S12012-017-9438-7.

Zandstra, T. E. *et al.* (2021) 'Asymmetry and Heterogeneity: Part and Parcel in Cardiac Autonomic Innervation and Function', *Frontiers in Physiology*. Front Physiol. doi: 10.3389/fphys.2021.665298.

Zannad, F. *et al.* (2015) 'Chronic vagal stimulation for the treatment of low ejection fraction heart failure: Results of the NEural Cardiac TherApy for Heart Failure (NECTAR-HF) randomized controlled trial', *European Heart Journal*, 36(7), pp. 425–433. doi: 10.1093/eurheartj/ehu345.

Zhu, C. *et al.* (2019) 'Neuromodulation for Ventricular Tachycardia and Atrial Fibrillation: A Clinical Scenario-Based Review', *JACC: Clinical Electrophysiology*. doi: 10.1016/j.jacep.2019.06.009.

Zipse, M. M. *et al.* (2020) 'Impact of epicardial adipose tissue and catheter ablation strategy on biophysical parameters and ablation lesion characteristics', *Journal of Cardiovascular Electrophysiology*, 31(5), pp. 1114–1124. doi: 10.1111/jce.14383.

Supplementary Material

The following are the forms that are required to be filled in and sent with heart referrals.

Form A

MAKE SURE ALL HEARTS ARE DELIVERED BETWEEN 9AM -4.30PM

Address for delivery:	Address for correspondence:
Prof M N Sheppard Site Services, Goods In St George's, University of London Cranmer Terrace, London SW17 0RE Prof. M. N. Sheppard PA: 020 8725 5112/5959 Fax: 020 8725 5139	Cardiovascular Pathology Cardiovascular Sciences Research Centre St George's University of London Cranmer Terrace, London SW17 0RE

REFERRAL OF HEART REQUEST

Name of Patient:

DOB:	**DOD:**
☐**Coroner case** **OR**	☐**Hospital Post mortem**
(Coroner's Officer)	
(Coroner)	
(Pathologist)	
Referral Centre:	**Urgent:**
Phone No:	**Fax No:**
Email address:	**Date expected:**
Spleen to be sent Y/N	**Have you RNAse later tubes for Spleen Y/N**

IMPORTANT

Please note the following:

- **Consent Forms B (pages 1-2)**
- **Confirmation of receipt Form C**
- **Packing instructions Form D (2 pages)**
- **UK SUDDEN CARDIAC DEATH (SCD) DATABASE case Inclusion Criteria**
- **Family Questionnaire**
- **Map of Location to deliver heart and spleen at St George's Medical School**

PLEASE INCLUDE THE PRELIMINARY POST-MORTEM REPORT INCLUDING THE HEIGHT, WEIGHT AND BMI OF THE PATIENT.

NUMBER OF PAGES INCLUDING COVER SHEET: _____10_____
SIGNED: **DATE:**

The information contained in this facsimile message is privileged and confidential information intended only for the use of the individual or entity named above. If the receiver of this message is not the intended recipient, you are hereby notified that any dissemination, distribution, or copying of this telecopy is strictly prohibited. If you have received this telecopy in error, please immediately notify us by telephone: 020 8725 5112 or fax: 020 8725 5139.

FORM B –CONSENT FORM 1/2

CORONER'S REFERRALS – RETURNING / RETENTION / RESEARCH & TEACHING

NAME OF DECEASED	
DATE OF BIRTH	
DATE OF DEATH	
PATHOLOGIST NAME	
MORTUARY	
CORONER OFFICER AND TELEPHONE NOS	
CORONER & AREA	
GP NAME, CONTACT AND POSTCODE	

The heart of the patient named above is referred to Professor Mary Sheppard for specialist analysis to help determine the cause of death. This will involve analysis of the whole heart as well as generating blocks and slides.

We routinely ask for consent to retain the heart, blocks and slides we generate in the laboratory for present and future ethically approved research and teaching. All material will be respectfully disposed of at the discretion of health professionals when no longer needed.

Both pages of Form B are for recording the family wishes concerning the heart, blocks and slides generated and must be filled in in order for us to comply with HTA rules including NOK details.

A very small piece of spleen is taken for possible future genetic testing. **Family will be contacted to give their informed consent at a future date if genetic testing is required.**

PLEASE TICK THE APPROPRIATE BOXES RECORDING THE FAMILY WISHES, CONCERNING THE HEART, BLOCKS , SLIDES AND SPLEEN*:*

BOTH SIDES OF THIS SHEET MUST BE COMPLETED IN FULL.

PERMISSION FOR SPECIMENS LISTED BELOW:	TO RETAIN FOR RESEARCH AND TEACHING	TO RETURN
HEART		
BLOCKS & SLIDES GENERATED BY CRY LAB		
SMALL PIECE OF SPLEEN		

PLEASE NOTE IF NOK CHANGE THEIR MIND AT ANY TIME, THE NEW DECISION SHOULD BE EMAILED TO CRYPATHOLOGY@SGUL.AC.UK AND THEIR WISHES WILL BE CARRIED OUT APPROPRIATELY

FORM B –CONSENT FORM 2/2

NAME OF PERSON COMPLETING FORM B ……..……

POSITION OF PERSON ……..……

PHONE NUMBER…..…… EMAIL: ……

SIGNATURE……DATE……..……

FAMILY MEMBER CONSENTING ……..

RELATION TO DECEASED……

PHONE NUMBER……EMAIL……

HOME ADDRESS……

DETAILS ABOVE UNDER GDPR WILL ONLY BE USED FOR OBTAINING CONSENT FOR GENETIC TESTING WHERE APPROPRIATE AND AS A RECORD OF NEXT OF KIN WISHES

RETURN OF SPECIMEN

We routinely request that the referring mortuary arranges for return of the heart. When that is next of kin wishes.

PLEASE GIVE CONTACT DETAILS OF THE MORTAURY / THE PERSON ORGANISING COLLECTION, AND THE RETURN ADDRESS FOR THE ORGAN:

NAME: _____

ADDRESS: _____

TELEPHONE NO: _____ EMAIL: _____.

We aim to complete examination and issue a report within 2 weeks of the date of receipt, however in certain circumstances this may be longer.
If there is an urgency in returning the heart for funeral arrangements please inform us immediately so we can speed up the investigation.

FORM C

CONFIRMATION OF RECEIPT OF SPECIMEN

CRY Cardiovascular Pathology Research Centre

Patient's Name:

D.O.B.:

Your Lab/PM No: **CRY ID No:**

SPECIMENS SENT:

Heart: ☐ **Spleen:** ☐ **No. of Slides:** ☐ **No. of Blocks:** ☐

Mortuary Manager Name:
Mortuary Address:

Fax No/Email: **Tel No:**

PACKAGE incorrectly labelled:

Patient Information on Outer Box ☐ Formalin in leak Proof Container ☐ No Outer Box ☐ No UN/Diagnostic/Pathology Specimen Label ☐

SPECIMENS RECEIVED:

Heart: ☐ **Spleen:** ☐ **No. of Slides:** ☐ **No. of Blocks:** ☐

Person receiving the specimen (Please Print):

Signature: **Date:**
(Person receiving the specimen)

This is confirmation that we have received this specimen.

For office use only:

Confirmation sent: Fax / Email / Post **Date sent:**

Scan done: **Date scanned:**

WHAT TO SEND

FULL POST MORTEM REPORT

HEART sliced at mid-ventricle level with blood clot removed and fixed in formalin FOR 24-48hrs HOURS

Heart removed from formalin and packaged according to instructions provided

BLOCKS/SLIDES OF HEART if available

A small 1cm square of fresh spleen put into RNASelater fluid tubes supplied by

us: This can be included with the heart container addressed to:

POSTAL ADDRESS

Professor Mary Sheppard

Goods Inwards
Department of Cardiovascular Pathology

St George's University of London Cranmer Terrace

London SW17 ORE

Mobile 07577311498

Phone 02087255112/02087255959

Fax 02087255139

POST MORTEM REPORT can be emailed to [redacted]@nhs.net which is secure for patient details

The coroner's officer and coroner are in direct contact with the family and are the most important people in obtaining consent to send the heart and spleen for examination and testing which will be invaluable for the family in future screening. **The heart with a small piece of fresh spleen should be retained in discussion with the pathologist in the situations outlined below.** Age range 1-no limit,

CIRCUMSTANCES OF DEATH

- Found dead in bed, at home or in the community with no previous significant heart disease history
- Found collapsed in community and brought in dead or died shortly after admission to local hospital
- Witnessed or unwitnessed collapse with failure to resuscitate at home or in the community
- Collapse during or after sport event
- Cardiac arrest with resuscitation and survival to hospital admission but died with hypoxic brain damage
- Drowning where circumstances are not clear. Found dead at bottom of pool with no struggle.
- Road traffic accident where circumstances indicate driver collapsed before accident or car veered off road before impact. Found dead at wheel of car that is stationary
- Toxicology is negative or non-toxic levels of drugs are found

AUTOPSY FINDINGS

- Normal heart and no cause identified after full autopsy and toxicology
- Heavy dilated heart with normal coronary arteries,
- Right or left ventricle with dilation/ fatty infiltration / scarring
- Ventricular hypertrophy with no reported history of hypertension or aortic valve disease
- Scarring in right or left ventricle with normal coronary arteries
- Subendocardial scarring with normal coronary arteries
- Anomalous coronary arteries/ coronary artery dissection/ vasculitis /aneurysm
- Coronary arteries with obstruction/dilatation not due to atheroma
- Coronary artery atheroma in under 40 age group
- Aortic dissection in under 40 years with no history of hypertension
- Significant congenital heart abnormality with or without surgery
- Any unusual valve disease such as mitral valve prolapse or endocarditis
- Any complex post cardiac surgical/procedure case

FAMILY QUESTIONAIRE

Circumstances of death

Was the patient previously well

Did patient have symptoms prior to the sudden death

Had patient a previous history of heart disease or attended a heart clinic.

Had patient a history of chest pain, blackouts, or other symptoms prior to death

Had patient a previous history of other disease

Was patient on any medication

Had patient a history of cardiac arrhythmias (irregular heart beat)

Had patient a previous ECG

Was there a history of epilepsy

Was there a history of asthma or shortness of breath

Is there a family history of heart disease

Is there a previous family history of sudden premature death or infant death

Was patient a smoker

Was patient a regular drinker

FORM D REFERRAL PACKING INSTRUCTIONS

A. HEART Specimen B. Spleen

Specimen to be sent to:
Professor M Sheppard
Site Services
Goods Inwards
St George's, University of London
Cranmer Terrace
London SW17 0RE

To ensure compliance with guidelines issued by the Human Tissue Authority (HTA) please follow the following protocol which is designed to provide us with the requisite information to deal sensitively and appropriately with human tissue specimens, and to comply with relatives' wishes.

After examination is complete, we will contact you regarding collection of the specimen.
NOTE: The referring hospital is responsible for organising both delivery and return of material.

A. HEART SAMPLES:
SPECIMENS REFERRED TO US MUST BE FIXED IN 10% FORMALIN FOR 24-48 hours PRIOR TO DESPATCH. ALL FORMALIN MUST BE DRAINED BEFORE SENDING

1. Place a label with the following information into either a ziplock or sealable bag:
   - Patients Name, DOB
     Your Reference Number
     Height and Weight of patient
     Formalin hazard label

2. Fix the label to the HEART

3. Wrap specimen in absorbent material dampened with formalin

4. Seal specimen in the ziplock/sealable bag expelling as much air as possible.

5. **Place in a leak proof plastic container surrounded by absorbent material, large enough to contain the heart without squeezing or distorting the heart. See pictures below.**

6. Affix addressee, address of Mortuary, Name of the patient, 'Diagnostic Specimen UN3373' label, and 10% Formalin Hazard label to leak proof container.





1. Pack leak proof container into an outer box.

2. In the outer box include the following:
   - Completed consent form detailing relatives' permission to return/retain the blocks and slides (**Form B**)
   - Completed confirmation of receipt of specimen form (**Form C**)
   - Letter of referral with clinical details and any points of interest for investigation
   - Provide preliminary post-mortem report if available

3. Seal the box with tape

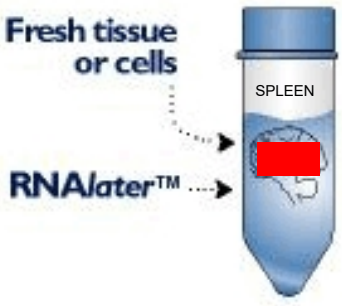
4. Affix Addressee (top of page 1), return address and 'Diagnostic Specimen UN3373 label to the outer box. **NOTE: NO PATIENT INFORMATION OR DETAILS ARE TO BE INCLUDED ON THE OUTER BOX.**

5. Arrange a courier to deliver the specimen to us between the hours of **9am – 4.30pm Monday - Friday**.

Note: The specimen should be transported by courier ONLY.

A. Spleen to be put in RNAselater tube

1. If you do not have a CRY RNAaselater sample tube kit, please contact us on 020 8725 5112 and we will supply you with 3 samples.
2. Cut a **small fresh** piece of spleen tissue (0.5cm x 0.5cm x 0.5cm) The RNAaselater solution **cannot penetrate large samples**.
3. Place tissue into pre-filled 3ml RNAaselater container with lid.
4. Label side of tube with patient name and date of birth using pen, or sticky label.
5. Place 3ml tube in large 50ml clear tube.
6. Store at room temperature (or preferably in refrigerator) until sent by courier with specimen.
7. Do not put frozen material in RNAse later. If sample is frozen, thaw first and then place in RNAse later



NOTE: RNAlater solution can be stored indefinitely at room temperature and does not expire.